
**STRUCTURAL SYSTEMS**
**RESEARCH PROJECT**

Report No.
SSRP–2001/24
**FINAL**

# SEISMIC PERFORMANCE OF PRECAST SEGMENTAL BRIDGE SUPERSTRUCTURES

**by**

**SAMI HANNA MEGALLY**
**MANU GARG**
**FRIEDER SEIBLE**
**ROBERT K. DOWELL**

Final Report Submitted to Caltrans under Contract No. 59A0051

May 2002

Department of Structural Engineering
University of California, San Diego
La Jolla, California 92093-0085

University of California, San Diego
Department of Structural Engineering
Structural Systems Research Project

Report No. SSRR-2001/24

**FINAL REPORT**

# Seismic Performance of Precast Segmental Bridge Superstructures

by

**Sami Hanna Megally**
*Assistant Project Scientist*

**Manu Garg**
*Graduate Research Assistant*

**Frieder Seible**
*Professor of Structural Engineering*

**Robert K. Dowell**
*Principal, Dowell-Holombo Engineering, Inc.*

Final Report Submitted to Caltrans under Contract No. 59A0051

Department of Structural Engineering
University of California, San Diego
La Jolla, California 92093-0085

May 2002

# Technical Report Documentation Page

| 1. Report No. | 2. Government Accession No. | 3. Recipient's Catalog No. |
|---|---|---|
| SSRP-2001/24 | | |

| 4. Title and Subtitle | 5. Report Date |
|---|---|
| Seismic Performance of Precast Segmental Bridge Superstructures | December 2001 |
| | 6. Performing Organization Code |

| 7. Author(s) | 8. Performing Organization Report No. |
|---|---|
| Sami Hanna Megally, Manu Garg, Frieder Seible, Robert K. Dowell | UCSD / SSRP-2001/24 |

| 9. Performing Organization Name and Address | 10. Work Unit No. (TRAIS) |
|---|---|
| Department of Structural Engineering<br>School of Engineering<br>University of California, San Diego<br>La Jolla, California 92093-0085 | 11. Contract or Grant No.<br>59A0051 |

| 12. Sponsoring Agency Name and Address | 13. Type of Report and Period Covered |
|---|---|
| California Department of Transportation<br>Division of Engineering Services<br>1801 30th St., West Building MS-9<br>Sacramento, California 95807 | Final Report – July 1997 / December 2001 |
| | 14. Sponsoring Agency Code |

15. Supplementary Notes

Prepared in cooperation with the State of California Department of Transportation.

16. Abstract


Precast segmental bridges have well-known advantages over conventional cast-in-place bridge construction. Popularity of precast segmental bridges is hampered in high seismic zones because of lack of information on their seismic performance. Also, little design guidelines are currently available for design of precast segmental bridges in high seismic zones. A large-scale experimental research project is currently in progress at the University of California, San Diego (UCSD). This research project consists of three phases. The research objective of the first and second research phases was to investigate the seismic performance of the precast superstructure segment-to-segment joints. A system test will be performed in the third phase to investigate the seismic performance of superstructure-pier systems subjected to gravity loads combined with seismic forces. This report presents the results of the first two phases of the research program.

The objective of the first phase was to investigate the seismic performance of segment-to-segment joints close to midspan in regions with high positive moments and low shearing forces. The second phase was concerned with the seismic performance of joints close to the piers with high negative bending moments and high shearing forces.

In each of the two research phases, four test units were built at 2/3-scale with respect to a prototype structure. The test variables were: (1) ratio of internal to external post-tensioning of the superstructure, and (2) presence of cast-in-place deck closure joints at locations of the segment-to-segment joints. The precast segments were bonded by slow-set Segmental Bridge Adhesive (epoxy). In each of the two phases, the entire joint surfaces of all test units were epoxy bonded with no mild reinforcement crossing the joints, except for one test unit, which had a reinforced cast-in-place deck closure at the location of each joint, with the web and bottom soffit of the segments epoxy bonded. The test units with cast-in-place deck closure joints had similar details to those proposed originally for the new East Span Skyway Structure of the San Francisco-Oakland Bay Bridge. Three-dimensional finite element models of the test units were developed.

The experiments showed that the superstructure segment-to-segment joints could undergo significant joint openings without failure. In the first phase, test units with internally bonded tendons experienced explosive failure by rupture of the tendons or concrete crushing. All test units of the second phase failed by compression in the bottom slab of the superstructure. In both research phases, 100 percent external post-tensioning proved to result in the highest ductility, highest displacement capacity and minimum permanent residual displacements after earthquakes. Cast-in-place deck closure joints substantially enhance the energy dissipation capability of the superstructure.


| 17. Key Words | 18. Distribution Statement |
|---|---|
| epoxy bonding, post-tensioning, precast, prestressed concrete, segmental, seismic, superstructures | Unlimited |

| 19. Security Classification (of this report) | 20. Security Classification (of this page) | 21. No. of Pages | 22. Price |
|---|---|---|---|
| Unclassified | Unclassified | ~317 | |

## Disclaimer

The contents of this report reflect the views of the authors who are responsible for the facts and accuracy of the data presented herein. The contents do not necessarily reflect the official views or policies of the California Department of Transportation. This report does not constitute a standard, specification or regulation.

# Abstract

Precast segmental bridges have well-known advantages over conventional cast-in-place bridge construction. Popularity of precast segmental bridges is hampered in high seismic zones because of lack of information on their seismic performance. Also, little design guidelines are currently available for design of precast segmental bridges in high seismic zones. A large-scale experimental research project is currently in progress at the University of California, San Diego (UCSD). This research project consists of three phases. The research objective of the first and second research phases was to investigate the seismic performance of the precast superstructure segment-to-segment joints. A system test will be performed in the third phase to investigate the seismic performance of superstructure-pier systems subjected to gravity loads combined with seismic forces. This report presents the results of the first two phases of the research program.

The objective of the first phase was to investigate the seismic performance of segment-to-segment joints close to midspan in regions with high positive moments and low shearing forces. The second phase was concerned with the seismic performance of joints close to the piers with high negative bending moments and high shearing forces.

In each of the two research phases, four test units were built at 2/3-scale with respect to a prototype structure. The test variables were: (1) ratio of internal to external post-tensioning of the superstructure, and (2) presence of cast-in-place deck closure joints at locations of the segment-to-segment joints. The precast segments were bonded by slow-set Segmental Bridge Adhesive (epoxy). In each of the two phases, the entire joint surfaces of all test units were epoxy bonded with no mild reinforcement crossing the joints, except for one test unit, which had a reinforced cast-in-place deck closure at the location of each joint, with the web and bottom soffit of the segments epoxy bonded. The test units with cast-in-place deck closure joints had similar details to those proposed originally for the new East Span Skyway Structure of the San Francisco-Oakland Bay Bridge. Three-dimensional finite element models of the test units were developed.

The experiments showed that the superstructure segment-to-segment joints could undergo significant joint openings without failure. In the first phase, test units with internally bonded tendons experienced explosive failure by rupture of the tendons or

concrete crushing. All test units of the second phase failed by compression in the bottom slab of the superstructure. In both research phases, 100 percent external post-tensioning proved to result in the highest ductility, highest displacement capacity and minimum permanent residual displacements after earthquakes. Cast-in-place deck closure joints substantially enhance the energy dissipation capability of the superstructure.

# Acknowledgments

This study was made possible by funding from the California Department of Transportation under contract No. 59A0051.

The experiments presented in this report were tested at the Charles Lee Powell Laboratory of the University of California-San Diego (UCSD). A number of technical personnel of UCSD assisted in the experimental investigation. Among them L. Berman and C. Latham deserve special mention for their contribution in construction and testing of the precast segmental Units. Thanks are also due to P. Nelson, J. Ward, S. Sherritt, M. Dyson, F. Ho, C. Stearns, A. Sherman, and the invaluable undergraduate staff for their assistance.

We would like to acknowledge members of the AASHTO-PCI-ASBI Technical Research Committee for reviewing the design of the experimental program. Members of the American Segmental Bridge Institute (ASBI) are also acknowledged for their comments and guidance during design of the Phase II test units. We would like to acknowledge J. Muller International, San Diego, for preparation of construction drawings of the Phase I test units. Dywidag-Systems International, USA (DSI) is gratefully acknowledged for donation of the prestressing strands, post-tensioning hardware and technical assistance in post-tensioning and duct grouting of the test units. Sika Corporation is also acknowledged for donation of the epoxy used in bonding of the precast segments. Headed reinforcing bars incorporated in two of test units were donated by the Headed Reinforcement Corporation, California, which is gratefully acknowledged.

# TABLE OF CONTENTS

# LIST OF FIGURES

# LIST OF TABLES

# 1 Introduction

## 1.1 General

Precast segmental construction has evolved over the last fifty years to cope with construction difficulties such as: deep valleys and irregular landscapes that prohibit conventional falsework erection, the desire for shorter construction times, and the ever-present need for higher quality and more efficient construction. Precast segmental construction, as we know it today began in Western Europe in the 1950s and was first implemented in the United States near Corpus Christi, Texas in the 1970s. Since then the use of segmental construction has steadily increased, however there is still marked apprehension in certain areas, specifically in seismic zones.

The precast construction process involves the segmental manufacturing of bridge components in precast yards or plants. These segments are then transported to the job site and assembled. The two common assembly procedures for precast segmental superstructures are the span-by-span method and the balanced cantilever method. In the span-by-span method entire spans are segmentally constructed and then lifted into place or constructed in place on a temporary steel truss, while in the balanced cantilever method segments are installed one at a time on either side of the piers. Both methods offer many advantages to the cast-in-place method.

Precast segmental construction allows for the elimination of conventional falsework. Without falsework the surrounding environment is not disturbed and construction can take place high above valley floors. This is an appealing benefit in California with its busy freeway and highway systems where existing traffic flow can

continue virtually unabated while construction is underway. The absence of falsework also translates in reduced construction traffic and materials, in and around the site, minimizing the need for lane closures and the blockage of traffic.

The time in which precast segmental bridges are constructed can be substantially less than their cast-in-place counterparts as construction tasks can be completed simultaneously; superstructure segments can be manufactured off site while piers are constructed on site. Construction processes are more refined and efficient at established precast yards/plants than with the cast-in-place method. The quality of precast components is higher than cast-in-place components as precast yards/plants operate in a controlled environment with closely monitored control mix designs and curing conditions.

Given all of the benefits of precast segmental construction and its advantages over cast-in-place construction there is still apprehension in utilizing this construction practice in seismic zones. The reason for this apprehension is the lack of information on the seismic response of segmentally constructed precast bridges. The AASHTO Guide Specifications for Design and Construction of Segmental Concrete Bridges[1] permits the use of precast segmental construction in high seismic zones (Zones 3 and 4) provided that segment-to-segment joints are bonded by segmental bridge adhesive (epoxy). The same AASHTO specification also requires that external tendons should account for no more than 50 percent of the superstructure post-tensioning. Additional recommendations in seismic areas such as California suggest that mild reinforcement should cross the segment-to-segment joints of precast segmental bridge superstructures. These

recommendations are intended to be conservative but are based on little if any research investigating the seismic response of precast segmental bridges.

Research at the University of California, San Diego looks to increase the knowledge of how precast segmental bridges respond to seismic events and to show that precast construction is a feasible option for bridge construction in high seismic zones. A three-phase project has been initiated by the American Segmental Bridge Institute (ASBI) and funded by the California Department of Transportation (Caltrans) for this study. Phase I focuses on the seismic response of segment-to-segment joints in precast segmental superstructures with different ratios of internal to external post-tensioning under simulated seismic fully reversed cyclic loading. Phase II will also vary the ratio of internal to external post-tensioning but will focus on segment-to-segment joints in regions with high negative moments and high shears. Both Phase I and Phase II also look at the effect of mild steel reinforcement across the joints in precast segmental superstructures with internally bonded tendons. Phase III will study the performance of segmental superstructure and columns under the combined effect of gravity loads and longitudinal and vertical seismic forces.

The concern with precast segmental bridges is that under seismic motions the superstructure would undergo large deflections resulting in significant joint openings. There is added concern of the behavior of segmental superstructures in regions with both high moments and shears when joint opening is coupled with the possibility of vertical sliding between segments.

Precast segmental construction utilizes post-tensioning tendons, most commonly steel, to act as the continuous reinforcement. These tendons can either be internally

bonded or external to the stem walls of the concrete box girder. With internally bonded tendons the duct through which the tendon runs is grouted following post-tensioning. External tendons, typically, are not embedded in the bridge superstructure concrete. Rather, they run along side the superstructure, inside the superstructure in the case of box girders, through deviators that provide the desired profile. Under seismic motions the internal and external tendons display very different characteristics. With bonded tendons when a crack appears or a joint opens the tendon experiences localized strains at the location of the opening, this strain is transferred through the bond between the tendon and grout. In the unbonded case because the tendon is restrained only at the ends and deviation points any strains induced are constant along any segment of the tendon. A tendon segment is the portion of the tendon between two successive deviators or between the anchor end and the first deviator.

Superstructure segments utilize shear and alignment keys at each joint. Shear keys prevent relative vertical sliding between segments. Alignment keys are generally fewer in number than shear keys but assure the proper positioning of segments with each other. Segments are normally match-cast, thus establishing a proper fit between segments.

## 1.2 Research Objectives

The goal of this project was to study the performance of segment-to-segment joints in bridge superstructures under simulated seismic fully reversed cyclic loading for varying ratios of internal to external post-tensioning. An additional objective was to study the seismic performance of segment-to-segment joints that have cast-in-place deck closures with mild reinforcement crossing the segment-to-segment joints, similar to the

design proposed originally for the new East Span Skyway Structure of the San Francisco-Oakland Bay Bridge. The study of Phase I focused on superstructure joints close to midspan where high moments and low shears are induced. The study of Phase II focused on superstructure joints close to the bent cap where high negative moments and high shears are induced. The major objectives of this research are to investigate: (1) seismic behavior with respect to the opening and closing of joints under cyclic seismic loading, (2) crack development and propagation, and (3) failure modes.

**Table 1-1 Test Matrix for Phase I and Phase II**

| Unit No. | Description | Nomenclature |
|---|---|---|
| 1 | 100% Internal Post-Tensioning | 100-INT |
| 2 | 100% Internal Post-Tensioning with Cast-in-Place Deck Closure Joints | 100-INT-CIP |
| 3 | 100% External Post-Tensioning | 100-EXT |
| 4 | 50% Internal and 50% External Post-Tensioning | 50-INT/50-EXT |

A prototype precast segmental bridge structure was designed. Four test units were designed and constructed for each phase of this study at a 2/3-scale of the prototype structure. The four test units of the two phases were organized in an identical manner. Two test units utilized 100% internal tendons; one of these units had cast-in-place closure joints with mild reinforcement crossing the segment-to-segment joints. A third test unit utilized 100% external tendons and the final unit used a combination of 50% internal tendons and 50% external tendons, neither of these units had any mild reinforcement across the joints. The external tendons used in the third and fourth test units in each phase were protected in transparent poly-carbon tubes that were not grouted. The pipes were not grouted so the external tendons can be visualized during the tests and to simplify

construction of the test units; grouting of the external tendons would not have any influence on the experimental results. Table 1-1 shows a summary of the test unit configuration. From herein Units 1 through 4 shall be referred to as 100-INT, 100-INT-CIP, 100-EXT, and 50-INT/50-EXT, respectively.

## 1.3 Previous Research

To the author's knowledge there has not been any significant research with respect to the seismic response of precast segmentally constructed superstructures. Researchers at the University of Texas at Austin investigated the response of segmental box girders using external tendons, but not for use in seismic regions[2]. The research at the University of Texas focused mainly on the behavior of segmentally constructed bridges with external tendons; only monotonic tests were performed. Both dry joints and epoxy joints were investigated with good results as both designs displayed considerable ductility during testing.

Additional testing at the University of Texas at Austin looked at the same segmental bridge structure as in previous tests with the addition of bonded deviators with external tendons and supplemental, grouted internal tendons[3]. The supplemental internal tendons accounted for only an eleven percent increase in the total prestressing steel area and were utilized when the external tendons were bonded at each deviator. Results of this testing showed that discrete bonding of external tendons and the addition of supplemental internal tendons improved the strength and ductility of segmental bridge superstructures[3].

## 1.4 Report Layout

The test units of Phases I and II were designed at a 2/3-scale of a prototype structure. The prototype structure is described in Chapter 2 of this report. The experimental program of Phase I is also described in Chapter 2. The experimental and analytical results of Phase I are presented in Chapters 3 and 4, respectively. Chapter 4 also briefly describes the finite element model developed for Phase I.

The experimental program of the second phase is described in Chapter 5. Chapter 6 and Chapter 7 contain the experimental and analytical results of Phase II, respectively.

A summary of both Phase I and Phase II along with conclusions is presented in Chapter 8. Additional experimental data for both phases is presented in Appendices A and B.

# 2 Experimental Program of Segment-to-Segment Joints subjected to High Moment and Low Shear (Phase I)

## 2.1 Prototype Structure

The prototype structure used for the design of the test units in Phase I is a single cell box girder bridge that consists of five spans with three interior spans of 100 ft (30.48 m) and exterior spans of 75 ft (22.86 m) for a total length of 450 ft (137.2 m) (see Figure 2-1). Each span of the prototype structure is post-tensioned with a harped shape tendon. Due to the short span lengths it is assumed that the prototype structure is constructed by the span-by-span method.

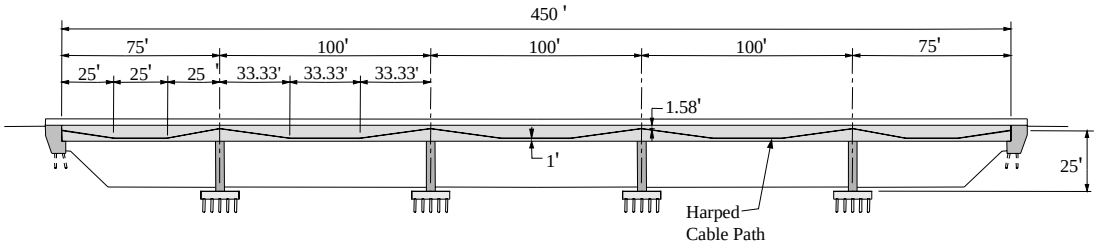


(a) Elevation

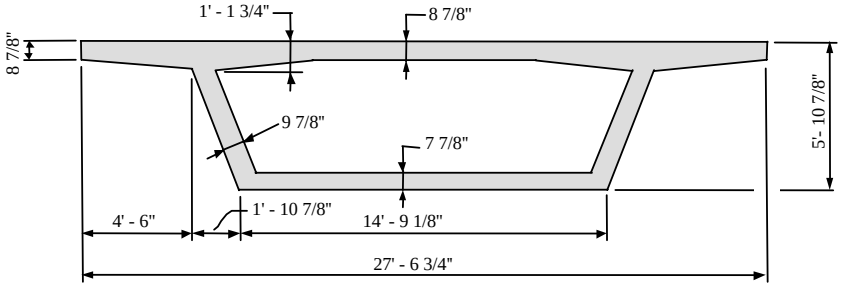


(b) Cross section

**Figure 2-1 Prototype Structure**

The prototype structure was designed according to the AASHTO Guide Specifications for Design and Construction of Segmental Concrete Bridges[1], the AASHTO-PCI-ASBI Segmental Box Girder Standards for Span-by-Span and Balanced Cantilever Construction[4], and the AASHTO Standard Specifications for Highway Bridges[5]. Full gravity, thermal, and seismic analyses were performed on the prototype structure shown in Figure 2-1. Section and material properties used for the design of the prototype structure are shown in Table 2-1.

**Table 2-1 Prototype Section and Material Properties**

| Properties | Symbol | Value |
|---|---|---|
| Gross Section Area | A | 6,076 in.$^2$ (3.92 m$^2$) |
| Moment of Inertia | I | 4.29E6 in.$^4$ (1.79 m$^4$) |
| Section Centroid from Bottom Surface | $c_b$ | 45.2 in. (1.15 m) |
| Section Centroid from Top Surface | $c_t$ | 25.7 in. (0.65 m) |
| Tendon Eccentricity at Midspan | $e_b$ | 33.2 in. (0.84 m) |
| Tendon Eccentricity at Pier Centerline | $e_t$ | 6.7 in. (0.17 m) |
| Concrete Strength | $f'_c$ | 5 ksi (34.5 MPa) |
| Concrete Modulus of Elasticity | $E_c$ | 4,030 ksi (27.8 GPa) |
| Prestressing steel Ultimate Strength | $f_{pu}$ | 270 ksi (1860 MPa) |

### 2.1.1 Design Criteria

#### 2.1.1.1 Dead Load

The dead load on the prototype structure includes the self-weight, two barriers and future AC surfacing or overlay (assumed to be 35 psf). These loads are tabulated in Table 2-2. The total dead load is $\omega_{DL}$ = 8.08 kip/ft (118 kN/m).

Dead load moments were calculated for a single 100 ft span (30.48 m) because with equal interior spans, ¾ length end spans and an evenly distributed load across all spans, no superstructure joint rotations would occur at the interior piers. The resulting end moments are 6,733 kip-ft (9,129 kN-m) and mid-span moments are 3,367 kip-ft (4,565 kN-m).

**Table 2-2 Dead Loads on the prototype structure**

| Description | Load |
|---|---|
| Self-weight | 6.33 kip/ft (92.4 kN/m) |
| Barriers (2) | 0.78 kip/ft (11.4 kN/m) |
| Future AC surfacing or overlay | 0.97 kip/ft (14.2 kN/m) |
| **Total Dead Load** | **8.08 kip/ft (118 kN/m)** |

#### 2.1.1.2 Live Load

The number of live load lanes was found from the AASHTO specifications. For a box-girder bridge type the AASHTO specification calculates the number of design live load lanes by dividing the deck width (in feet) by fourteen (=27.56/14). The number of live load lanes for the prototype structure was 2.

Live load moments were found using the Caltrans Bridge Design Aides[6] using the more critical of:

i. Two lanes of 0.64 kip/ft and moment rider of 18 kips.

ii. Two HS20-44 trucks with loads of 32 kips at the second and third axles with variable spacing between 14 ft and 30 ft and front axle of 8 kips spaced 14 ft in front of the second axle. The truck loads were positioned along the structure to obtain the most critical loading.

Both live load and dead load moments were calculated at each 1/10-point, these are presented in Table 2-3 and **Error! Reference source not found.**, the combinations of dead load and live load moments are also shown. Live load moments include the effect of an impact coefficient that was determined to be 0.22.

**Table 2-3 Dead Load and Live Load Moments**

| Location (x/L) | $M_{DL}$ | | $M_{LL}$ – Max. Positive | | $M_{LL}$ – Max. Negative | | $M_{DL}+M_{LL}$ Max. Pos. | | $M_{DL}+M_{LL}$ Max. Neg. | |
|---|---|---|---|---|---|---|---|---|---|---|
| | kip-ft | kN-m | kip-ft | kN-m | kip-ft | kN-m | kip-ft | kN-m | kip-ft | kN-m |
| 0.0 | -6733 | -9129 | 452 | 613 | -2416 | -3276 | --- | --- | -9149 | -12405 |
| 0.1 | -3097 | -4199 | 534 | 724 | -1352 | -1833 | --- | --- | -4449 | -6032 |
| 0.2 | -269 | -365 | 1212 | 1643 | -1024 | -1388 | 943 | 1279 | -1293 | -1753 |
| 0.3 | 1751 | 2374 | 1852 | 2511 | -862 | -1169 | 3603 | 4885 | --- | --- |
| 0.4 | 2963 | 4017 | 2240 | 3037 | -862 | -1169 | 3603 | 4885 | --- | --- |
| 0.5 | 3367 | 4565 | 2340 | 3173 | -858 | -1163 | 5707 | 7738 | --- | --- |
| 0.6 | 2963 | 4017 | 2240 | 3037 | -862 | -1169 | 3603 | 4885 | --- | --- |
| 0.7 | 1751 | 2374 | 1852 | 2511 | -862 | -1169 | 3603 | 4885 | --- | --- |
| 0.8 | -269 | -365 | 1212 | 1643 | -1024 | -1388 | 943 | 1279 | -1293 | -1753 |
| 0.9 | -3097 | -4199 | 534 | 724 | -1352 | -1833 | --- | --- | -4449 | -6032 |
| 1.0 | -6733 | -9129 | 452 | 613 | -2416 | -3276 | --- | --- | -9149 | -12405 |

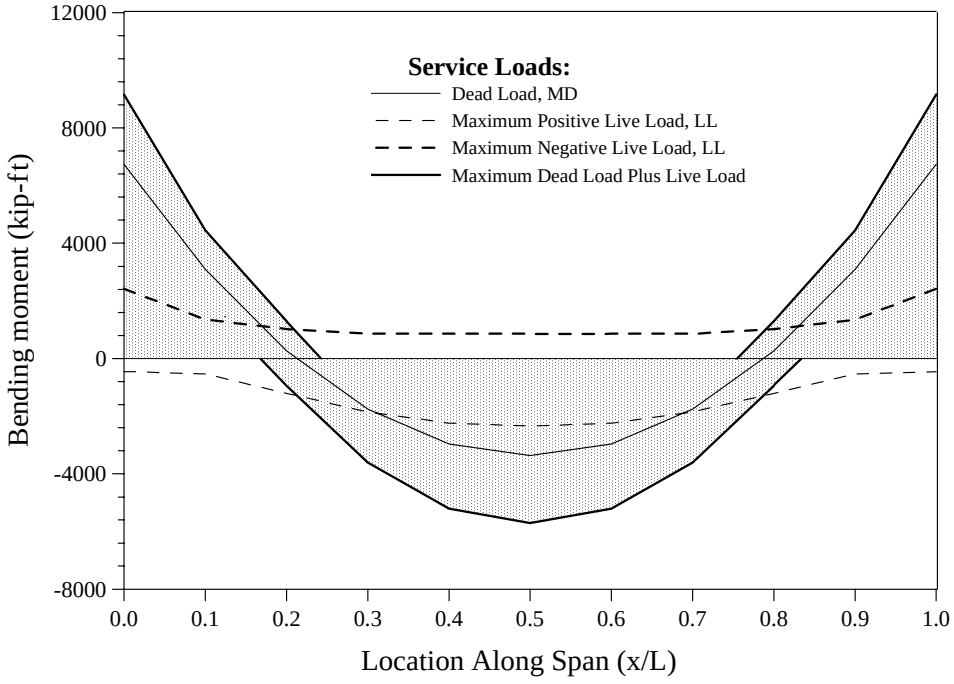


**Figure 2- 1 Dead and Live Load Moment Demands**

### 2.1.1.3 Thermal Stresses

AASHTO design standards stipulate that in addition to dead and live load demands, half of the temperature stress values need to be incorporated in design. The non-linear temperature gradient was applied based on the AASHTO-PCI-ASBI Standards[4]; this gradient is shown in Figure 2-2 (also according to Section 6.4.4 of the AASHTO Guide Specifications for Design and Construction of Segmental Concrete Bridges[1]). For the central span the bottom and top fiber stresses due to the temperature gradient were found to be 230 psi and 830 psi, respectively[7]. According to Section 7.2.2.1 of the AASHTO Guide Specifications for Design and Construction of Segmental Concrete Bridges[1], referred to as the AASHTO Guide Specifications throughout this report, only one half of the thermal stresses in concrete should be combined with the concrete stresses resulting from dead and live loads. Thus the stresses considered in design due to the temperature gradient were 415 psi compression in the top fibers and 115 psi tension in the bottom fibers.

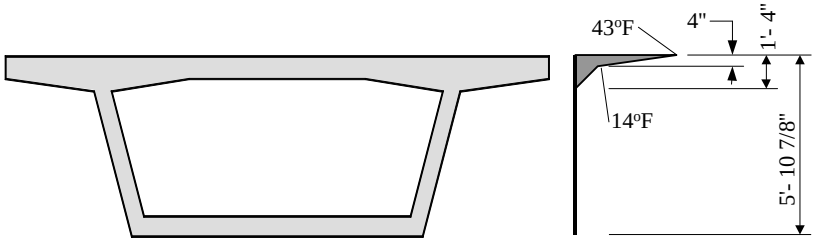


**Figure 2-2 Non-linear Temperature Gradient**

### 2.1.2 Prestressing Steel Design

The cable path for the prototype structure was assumed to be harped at the 1/3 location with the maximum offsets from the bridge soffit to the center of gravity of the tendon of 1 ft (0.305 m) and from the top of the bridge deck to the CG of the tendon of

1.58 ft (0.482 m). The prestressing force was designed for the moment due to dead load plus live load of 5,707 kip-ft (7,738 kN-m); additional stresses due to the temperature gradient were also included. The design criterion was to not allow tensile stresses at the segment-to-segment joints under extreme service loading. For the prototype structure it was found that the required prestressing force was P = 2,744 kips (12.21 MN) and to satisfy this requirement, assuming the stress in the prestressing steel is 60 percent of ultimate, 80 strands were needed (strands were assumed to be Grade 270, 0.6 inch diameter 7-wire strand). Forty strands were provided in each web of the single cell box girder.

The above indicates that the superstructure was not designed based on seismic forces, but rather based on service loads. Cross section of the prototype superstructure was selected based on the AASHTO-PCI-ASBI Segmental Box Girder Standards[4] and the prestressing steel was designed such that no tensile stresses would occur in the superstructure under extreme service load combinations. Seismic capacity of the superstructure under combined longitudinal and vertical seismic forces was then checked (Section 2.1.3 of this report).

To verify the design maximum and minimum stresses were calculated at each 1/10 point along the span. The results in Figure 2-3 show that the given design is adequate at all locations. No tensile stresses are developed and maximum compressive stresses are well below the allowable $0.6f_c'$ or 3 ksi (20.7 MPa). The figure also shows that the segment-to-segment joint at midspan is the most critical for design.

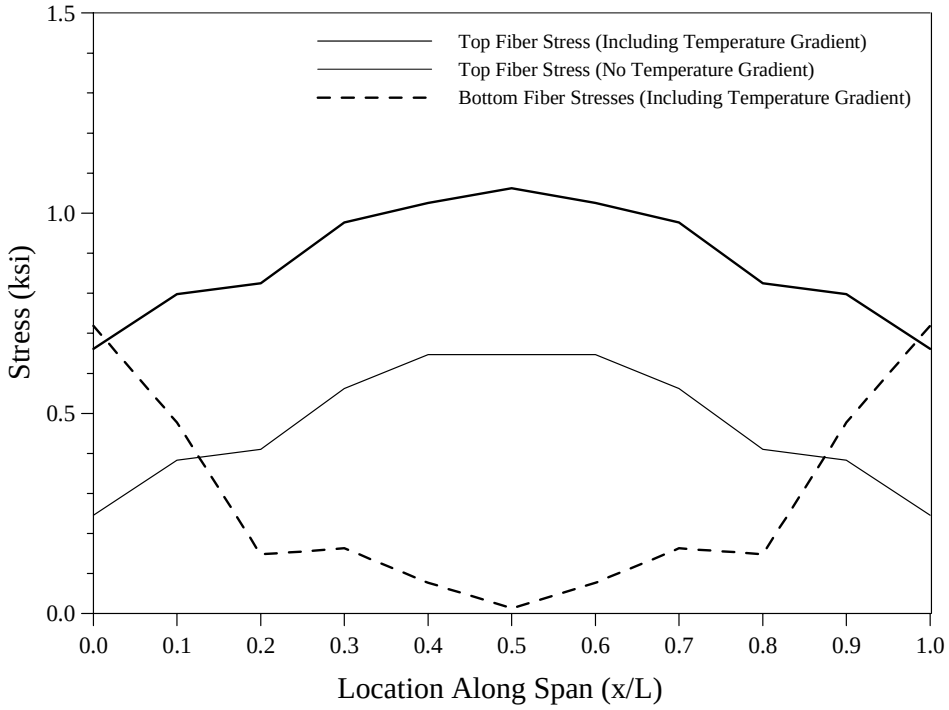


**Figure 2-3 Top and bottom fiber concrete compressive stresses from dead load, live load, temperature gradient and prestressing**

### 2.1.3 Seismic Analysis

Seismic analysis of the prototype structure was carried out to determine the longitudinal seismic moment demands on the superstructure. The approximate column plastic moment and shear demands were calculated. Superstructure moment and shear demands were then obtained from the column capacity taken at the centroid of the superstructure section, 25 ft (7.62 m) from the top of the footing.

The axial load due to dead load on the column was comprised of the tributary weight of the superstructure plus the weight of the bent cap. The bent cap weighs approximately 22.5 kips (100 kN) and the total dead load, $\omega_{DL}$, is 8.08 kip/ft (118 kN/m).

$$W_{column} = 8.08 \times 100 + 22.5 = 831 \text{ kips } (3697 \text{ kN}) \qquad (2\text{-}1)$$

Assuming that the structure acceleration is 2g (from an ARS curve with peak ground acceleration of 0.7g) the elastic column moment demand is found as:

$$M_E = (831 \times 2) \times (25 / 2) = 20{,}800 \text{ kip-ft } (28{,}202 \text{ kN-m}) \quad (2\text{-}2)$$

Using a strength reduction factor Z of 4, the required nominal moment was:

$$M_N = M_E / Z = 20{,}800 / 4 = 5{,}200 \text{ kip-ft } (7050 \text{ kN-m}) \quad (2\text{-}3)$$

For this analysis it was assumed that the plastic moment was 1.3 times the nominal moment. Thus the plastic moment, $M_p$, becomes 6,760 kip-ft (9166 kN-m). The plastic shear, $V_p$, was calculated as:

$$V_p = 2 \times M_p / L_c = 2 \times 6{,}760 / (25 - 45.2 / 12) = 637 \text{ kips } (2834 \text{ kN}) \quad (2\text{-}4)$$

Where $L_c$ is the clear column height.

The moment induced by the column at the centroid of the superstructure is the plastic moment plus the plastic shear multiplied by the distance from the top of the column to the centroid of the superstructure:

$$M_p + V_p \times c = 6{,}760 + 637 \times 45.2 / 12 = 9{,}159 \text{ kip-ft } (12{,}418 \text{ kN-m}) \quad (2\text{-}5)$$

Assuming that one half of this moment goes to each span, the seismic moment demand at the column centerline is $\pm$ 4,580 kip-ft (6210 kN-m) at the end of each span. With these end moments the moment demands are determined at each 1/10 point along the span. The longitudinal seismic moment demands on the superstructure vary linearly between bents and are added to the dead load moments. Moments and shears due to dead load and longitudinal seismic forces are shown in Table 2-4.

**Table 2-4 Longitudinal seismic and dead load moments and shears**

| Location (x/L) | $M_{DL}$ kip-ft (kN-m) | $M_{EQ}$ kip-ft (kN-m) | $M_{DL} + M_{EQ}$ kip-ft (kN-m) | $V_{DL}$ kip (kN) | $V_{EQ}$ kip (kN) | $V_{DL} + V_{EQ}$ kip (kN) |
|---|---|---|---|---|---|---|
| 0.0 | -6733 (-9129) | 4580 (6210) | -2153 (-2919) | 404 (1797) | -92 (-409) | 312 (1388) |
| 0.1 | -3097 (-4199) | 3664 (4968) | 567 (769) | 323 (1437) | -92 (-409) | 231 (1028) |
| 0.2 | -269 (-365) | 2748 (3725) | 2479 (3361) | 242 (1076) | -92 (-409) | 150 (667) |
| 0.3 | 1751 (2374) | 1832 (2484) | 3583 (4858) | 162 (721) | -92 (-409) | 70 (311) |
| 0.4 | 2963 (4017) | 916 (1242) | 3879 (5259) | 81 (360) | -92 (-409) | -11 (-49) |
| 0.5 | 3367 (4565) | 0 | 3367 (4565) | 0 | -92 (-409) | -92 (-409) |
| 0.6 | 2963 (4017) | -916 (-1242) | 2047 (2775) | -81 (-360) | -92 (-409) | -173 (-770) |
| 0.7 | 1751 (2374) | -1832 (-2484) | -81 (-110) | -162 (-721) | -92 (-409) | -254 (-1130) |
| 0.8 | -269 (-365) | -2748 (-3725) | -3017 (-4091) | -242 (-1076) | -92 (-409) | -334 (-1486) |
| 0.9 | -3097 (-4199) | -3664 (-4968) | -6761 (-9167) | -323 (-1437) | -92 (-409) | -415 (-1846) |
| 1.0 | -6733 (-9129) | -4580 (-6210) | -11313 (-15339) | -404 (-1797) | -92 (-409) | -496 (-2206) |

In addition to longitudinal seismic loading the seismic analysis of the prototype structure also considered vertical loading due to vertical ground accelerations. Moment demands from dead load, two times dead load, three times dead load and minus dead load representing vertical accelerations of 0, 1, 2, and –2 g's, respectively, are shown in Figure 2-4. The figure also shows the moment capacity of the section, reserve moment capacity (section moment capacity minus the secondary prestressing moment) and decompression moment (moment required to develop zero tensile stress in the bottom or top section fibers for positive and negative bending).

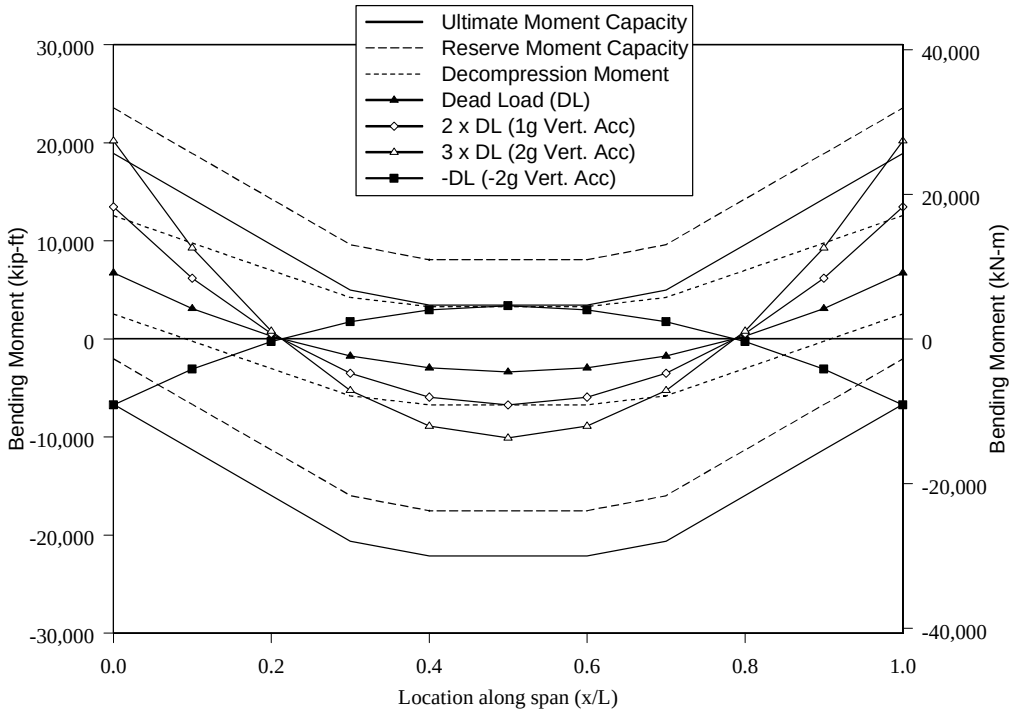


**Figure 2-4 Moment demands with vertical accelerations**

With 1g vertical acceleration downward the bottom of the section at midspan reached zero tension/compression (decompression) and the top of the section near the bent develops tensile stresses. With 2g vertical upward acceleration, the top of the section at midspan reached decompression, without top reinforcement crossing the segment-to-segment joints, the ultimate section capacity was reached; while at the bents the ultimate moment capacity was reached. With 2g vertical downward acceleration, the decompression range increased to 40 ft (12.2 m) and the moment at the bent exceeded the section capacity but not the reserve moment capacity.

Figure 2-5 shows the results for longitudinal seismic loading based on column plastic hinging, dead load and vertical seismic motions. The moment capacity curves are the same as presented above. The results demonstrate that the longitudinal seismic

loading tends to move the critical location for potential joint opening from midspan to the 0.4 to 0.6 span locations for 1g and -2g vertical accelerations. With no vertical acceleration the critical location for bottom joint opening was at midspan. The critical location for top joint opening with 2g vertical acceleration upward moved to 0.6 span locations. With 2g vertical acceleration downward the range of soffit tension stress increased to 40 ft (12.2 m) about the 0.4 span location; negative moment demand at the bent exceeded the section reserve and ultimate moment capacity. Concrete stresses plotted in Figure 2-3 and the moments plotted in Figure 2-4 indicate that under vertical acceleration the highest potential for joint opening is at midspan. For this reason it was decided to model the middle 1/3 portion of the prototype superstructure in the experiments of the first phase of this research program.

It should be remembered that the prestressing steel was designed such that no concrete tensile stresses would occur in the superstructure under extreme combinations of service loads (Section 2.1.2). Thus the amount of prestressing steel was not determined based on seismic forces such that plastic hinging occurs in the columns without opening of the joints between the precast superstructure segments. It will be shown in this report that the superstructure joints could undergo significant opening without failure or drop of the load carrying capacity. It will also be shown that the superstructure would be restored to its original undeformed shape before earthquake occurrence if it was post-tensioned by external (unbonded) tendons; in this case the joints between precast segments may be allowed to open during major seismic events. If the superstructure joints are designed to remain closed during extreme seismic events, the required amount of prestressing steel may be significant and uneconomic.

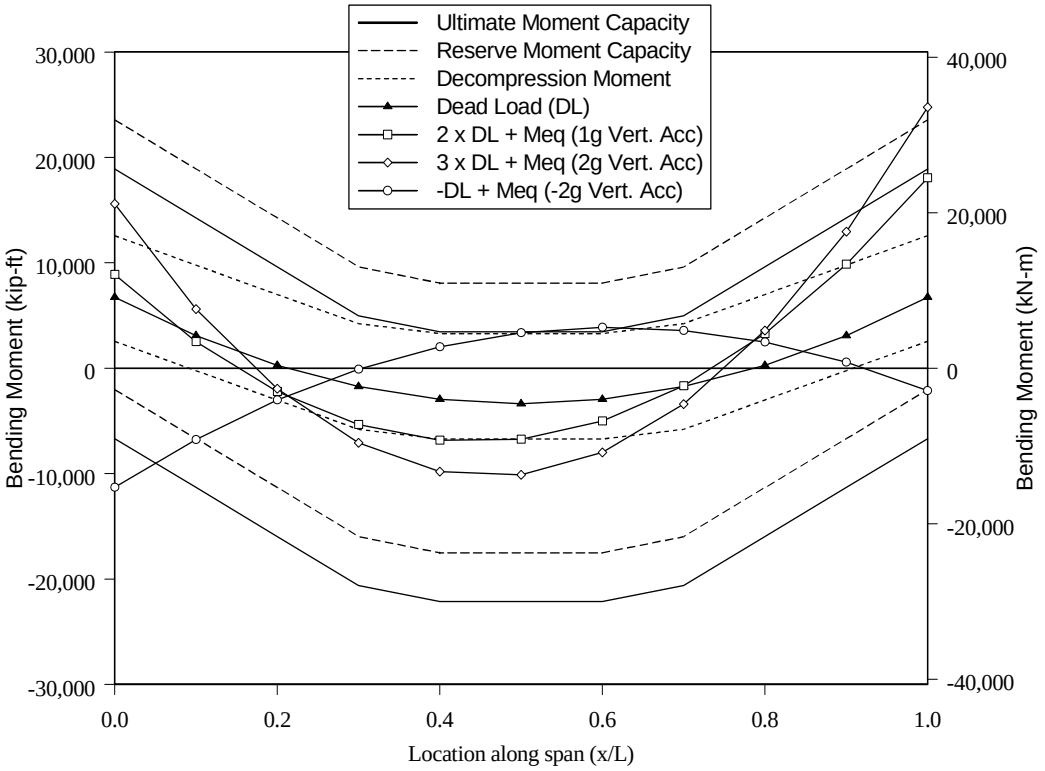


**Figure 2-5 Moment demands with vertical accelerations and column hinging**

## 2.2 Development of Test Units

### 2.2.1 Design

The test units were designed at 2/3-scale of the prototype design dimensions. The test units of Phase I represented the center 1/3 of the prototype span where moments are most critical and the segment-to-segment joints have the highest potential to open. The test zone of each unit was 24 ft (7.32 m) long and was made up of four 6 ft (1.83 m) segments. The complete test unit was comprised of the four segments of the test zone as well as two 5 ft (1.52 m) end segments (see Figure 2-6). From herein the joints between segments are referred to J1 through J5, respectively.

To simplify construction and reduce the overall size and the required force levels a simplified I-section was developed for the test Units. The widths of the top and bottom

slabs were equal to the scaled half widths of the deck and soffit of the prototype box-section design. The typical cross-section of the test units is shown in Figure 2-7. The test units were designed such that at service load level the stresses in the test unit match those of the prototype structure.

Unit 100-INT-CIP utilized cast-in-place closure joints in the top deck. The mild reinforcement crossing the joint in this design was in two different configurations. The longitudinal deck reinforcement on one half of the test unit consisted of hairpin bars, whereas on the other half headed bars were used (see Figure 2-8). Both reinforcement details provided adequate anchorage of the reinforcing bars in the cast-in-place deck joints so their full yield strength could be mobilized. The reinforced cast-in-place deck detail across each joint in Unit 100-INT-CIP was similar to the detail proposed originally for the new East Bay Skyway Structure of the San Francisco-Oakland Bay Bridge.

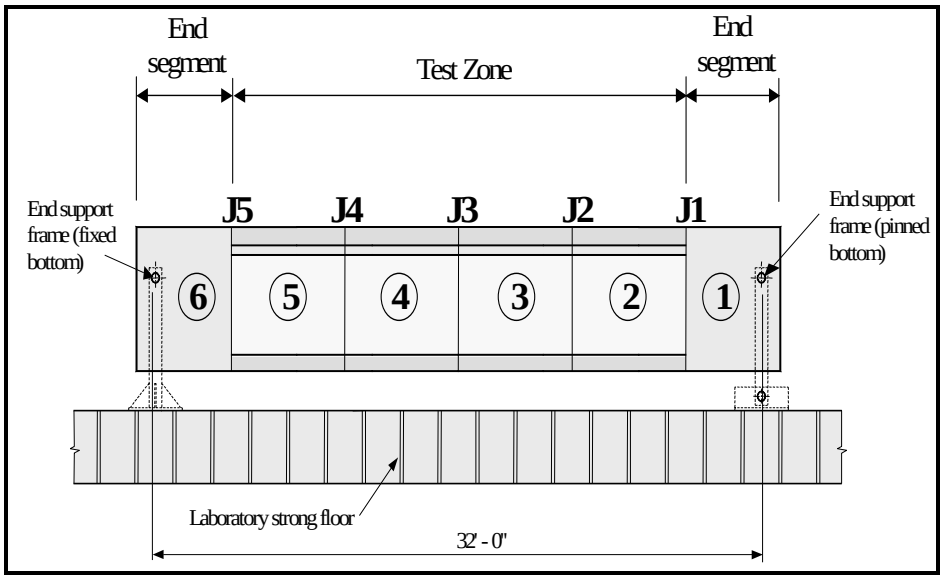


**Figure 2-6 Typical test unit elevation**

The number of 0.6 in (15 mm) ϕ post-tensioning strands and their location were scaled from the prototype structure. Sixteen strands were placed at 8 in. (203 mm) from

the bottom surface of the test unit (See Figure 2-7). Auxiliary post-tensioning steel was provided in the top and bottom slabs to properly clamp the joints together after the application of epoxy.

It should be remembered that the external tendons in Units 100-EXT and 50-INT/50-EXT (See Figure 2-7) were placed inside transparent poly-carbon tubes, which were not grouted after post-tensioning. Ducts of the external tendons, or the poly-carbon tubes, were not grouted because of the following reasons: (1) to visualize strands of the external tendons during the tests and to inspect for failure of the strands or strand wires, (2) to protect the electrical resistance strain gages placed on the external tendons from possible damage caused by grouting, and (3) to simplify the construction of test units.

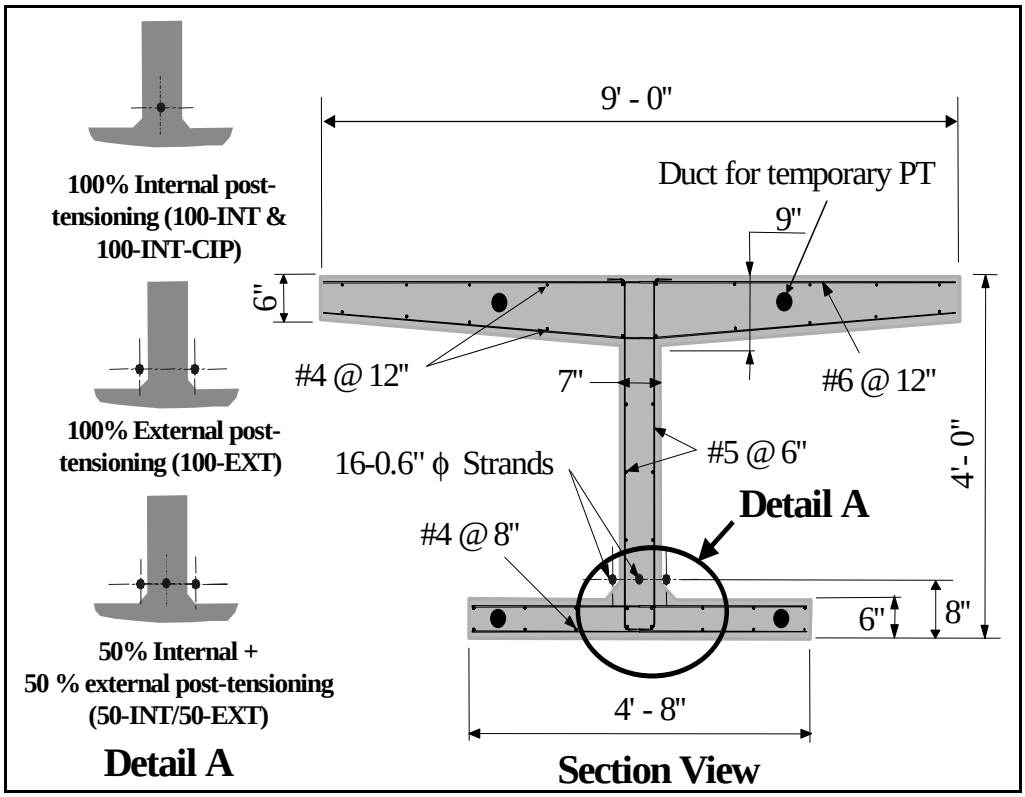


**Figure 2-7 Test unit cross-section**

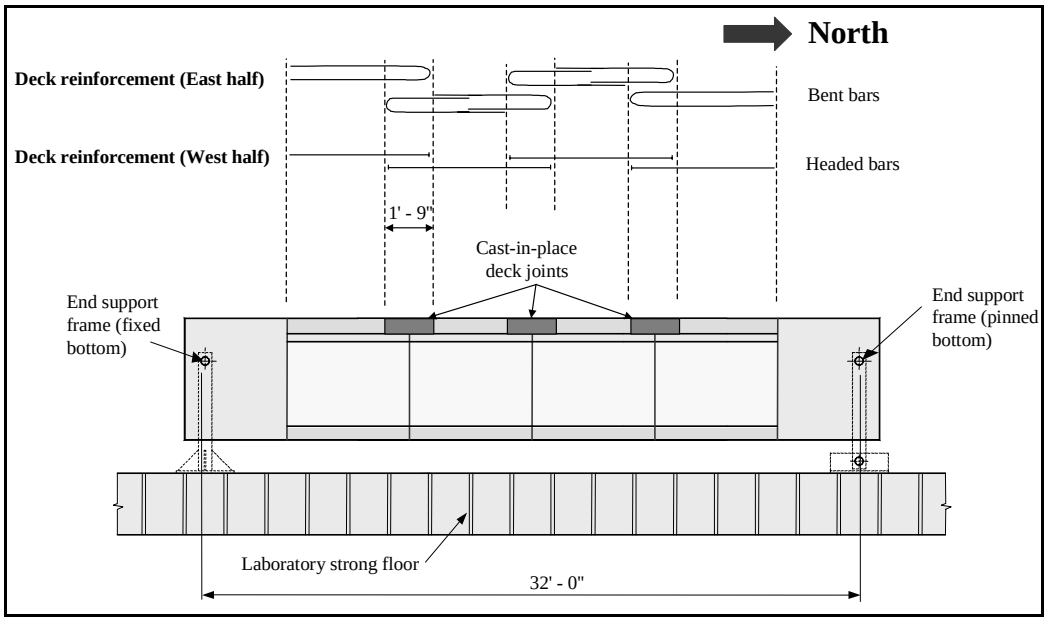


**Figure 2-8 Reinforced cast-in-place deck joints of Test Unit 100-INT-CIP**

Most of the strain gages that were placed on the prestressing steel strands could survive during stressing of the tendons and also during grouting of the ducts of internal tendons. However, within 24 to 48 hours after grouting a significant number of strain gages started to malfunction most likely as a result of moisture of the grout; the malfunctioned gages could still provide strain measurements but it was believed that these measurements were not reliable. Some other strain gages could survive and were damaged during the seismic test. Ducts of the external tendons were not grouted, thus the number of damaged strain gages placed on the external tendons could be minimized. Ducts of the external tendons in the Phase II test units were also not grouted for the same above-mentioned reasons. A better method of sealing the strain gages against moisture of the grout should be investigated and used in future experiments with internally bonded tendons that are monitored by electrical resistance strain gages.

The external tendons in actual bridges are placed inside ducts, which are grouted after post-tensioning to protect the strands from corrosion in the long term. It is strongly believed that grouting of the ducts that housed the external tendons in Units 100-EXT and 50-INT/50-EXT would have had no influence on the experimental results and the results of the experiments would be applicable to structures with grouted external tendons. This is justified by the fact that grout of the external tendons is never counted upon for any structural capacity. Since the external tendons are grouted after the strands have been stressed and locked off, there is no precompression in the grout. Therefore the grout would crack with stress increase in the external tendons. This, for all practical purposes, would eliminate any load carrying capacity or stiffening effect from presence of the grout in the external tendons. For the test units it can be shown that if the external tendons were grouted, the grout would have been fully cracked during the early stage of the test and before application of fully reversed cyclic displacements to the test unit, which simulated the effects of earthquake forces.

As mentioned earlier, the test units of Phase I represented the middle 1/3 portion of the prototype superstructure in which the tendons were horizontal. It means that Units 100-EXT and 50-INT/50-EXT modeled the superstructure between deviators of the external tendons. The external tendons may be fully bonded at the deviator locations, which was considered in the Phase I test units since the external tendons were fully bonded inside Segments 1 and 6 (see Figure 2-6). In a more realistic representation of actual bridge superstructures with external tendons, the deviators and anchorage blocks should be modeled in experiments that represent a complete span of the superstructure. This will be done in the third phase of this research program, which is not part of this

report. In the third phase of this program, a complete span superstructure-column system will be tested under the combined effects of dead load, longitudinal and vertical seismic forces. The external tendons will be placed in ducts that can be grouted after post-tensioning to represent actual bridge practice.

### 2.2.2 Construction

A casting bed was built for construction of all test units. Segments 1, 3 and 5 were cast, and then Segments 2, 4 and 6 were match cast against the first group of segments. Figure 2-9 shows a typical test unit before the second casting. A mixture of soap and talc was used as a bond breaker at the interface of segments. Within 48 hours of the final pour the six segments were separated from one another (see Figure 2-10). After the concrete cured sufficiently the segments were shipped to the Charles Lee Powell Structural Research Laboratories at the University of California, San Diego.

**Figure 2-9 Typical test unit after first segment casting**

**Figure 2-10 Typical test unit after construction with segments separated**

A wooden platform was built to support the segments for assembly (see Figure 2-11 Figure 2-12). The segments were placed on the wooden platform with enough space for men to work between segments. The first segment was positioned in the end support frame with the pinned boundary condition as well as on the platform. Segmental Bridge Adhesive (epoxy) typically used in span-by-span construction of precast segmental bridges was applied on the joint surfaces of each segment. For three of the test units, epoxy was applied on the entire joint surface (see Figure 2-13). In Unit 100-INT-CIP there was a gap in the top slab at each joint which was closed later by a cast-in-place concrete slab strip; for this unit epoxy was applied to the remaining joint surface: the web and bottom slab (see Figure 2-14). Working from the first segment already in the pinned support frame each segment was epoxied and mated with its corresponding segment. Numerous sheets of plastic were used between the segments and the wooden platform to act as a low-friction surface on which the segments could slide. To mate the segments one segment was first lifted and moved by crane close to its final position. At this point Come-Alongs (hand operated winch) were attached to the segment and it was winched into place, sliding on the plastic sheets until contact was made between both epoxied surfaces.

After the application of epoxy and the final positioning of the segments, the test units were temporarily post-tensioned with four 1-inch (25.4 mm) diameter high strength ASTM A 722 steel bars. Two bars were placed in the top slab and two bars in the bottom slab (see Figure 2-15). The temporary prestressing forces in the high-strength bars were determined such that the entire segment-to-segment joints surfaces would have a minimum compressive stress of 40 psi[8].

After epoxy bonding of the precast segments, each test unit was post-tensioned such that the effective post-tensioning force at the time of testing was approximately 600 kips (2,669 kN). The jacking force in each operation was calculated taking into account the effect of losses due to anchor set, elastic shortening, concrete creep and shrinkage, and relaxation of the prestressing steel. Figure 2-15 shows a typical test unit during post-tensioning, also shown are the temporary post-tensioning bars. After the permanent post-tensioning of the test units the temporary bars in the bottom slab were removed. The temporary bars in the top slab were not removed until the addition of vertical load on the test unit to simulate the prototype dead load stresses. This sequence was followed to ensure the test units did not crack before testing. The wooden platform was removed following the permanent post-tensioning and the test unit was mounted on the remaining end support.

**Figure 2-11 End Segment No. 6 and Segment No. 5 on Wooden Platform**


**Figure 2-12 Unit 100-INT on wooden platform (without epoxy)**

**Figure 2-13 Application of epoxy on Unit 100-INT**

**Figure 2-14 Application of epoxy on Unit 100-INT-CIP with CIP joint reinforcement**

**Figure 2-15 Post-tensioning of unit 100-INT**

## 2.3 Materials Testing

Tests were conducted at the UCSD Powell Structural Laboratories to determine the material properties of the concrete used in all four Units and the steel used in the cast-in-place deck joints of Unit 100-INT-CIP. Compression tests were performed on unconfined concrete cylinders from each batch of concrete. The compressive strengths of concrete on the day of testing for each Unit are shown in Table 2-5. The results for each Unit are separated into two groups, the first for Segments 1, 3, and 5 and the second group for Segments 2, 4, and 6 because the latter group was match cast against the first one. For Unit 100-INT Segment 3, although match cast, was cast at a different time than the other segments due to construction difficulties. For Unit 100-INT-CIP the concrete compressive strength is also shown for the cast-in-place deck closure, the yield strength of the reinforcing steel in the CIP deck closure is listed in Table 2-6. The expected 28-days compressive strength of the grout used was 5,560 psi (38.4 MPa).

The adhesive used to join the segments was Sikadur 31 SBA, Slow-Set. It is a two-component moisture tolerant, high-modulus, high strength structural epoxy paste used specifically to bond hardened concrete in segmental bridge construction. The expected properties of this material were a compressive strength within 72 hours of 2,000 psi (13.8 MPa) and within 14 days a contact strength and bond strength of 1,000 psi (6.9 MPa) each. No information was available on long-term material properties of the epoxy, but the long-term properties of the epoxy will not contribute to the long-term structural performance of the precast segmental bridges since the thickness of epoxy layers between the precast segments is extremely small. Most of the epoxy applied on the joint surfaces before bonding of the precast segments is squeezed out after temporary post-tensioning of

the segments that follows the epoxy bonding process. Thus the major function of the epoxy is to seal the joints. Based on the information obtained from the American Segmental Bridge Institute (ASBI) as well as from well-known precast segmental bridge design engineering firms, no structural problems have been reported in precast segmental bridges as a result of long-term performance of the epoxy. Investigation of the long-term performance of precast segmental bridges was not in the scope of the research work presented in this report; thus no attempt was made to investigate the long-term properties of epoxy and their effects on the overall long-term performance of precast segmental bridges.

**Table 2-5 Concrete compressive strength**

| Unit | | Day of Test ksi (MPa) |
|---|---|---|
| 100-INT | Seg. 1 and 5 | 5.11 (35.2) |
| | Seg. 3 | 7.21 (49.7) |
| | Seg. 2, 4, 6 | 6.96 (48.0) |
| 100-INT-CIP | Seg. 1, 3, 5 | 7.25 (50.0) |
| | Seg. 2, 4, 6 | 5.74 (39.6) |
| | CIP Deck Closure | 5.87 (40.5) |
| 100-EXT | Seg. 1, 3, 5 | 5.92 (40.8) |
| | Seg. 2, 4, 6 | 6.79 (46.8) |
| 50-INT/50-EXT | Seg. 1, 3, 5 | 8.01 (55.3) |
| | Seg. 2, 4, 6 | 6.17 (42.6) |

**Table 2-6 Yield strength of reinforcing steel**

| Unit | | Yield Strength ksi (MPa) |
|---|---|---|
| 100-INT-CIP | Headed Bars | 67.7 (467) |
| | Bent Bars | 75.6 (521) |

## 2.4 Test Setup

Representations of the test set-up are shown in Figure 2-16 through Figure 2-18. Each test unit was simply supported by means of steel pins and links at the ends. At one end a single pin through a fixed frame supported the test unit; this end support restricted horizontal and vertical motion while allowing rotation. A single steel pin through two rocker links supported the other end of the test unit. These rocker links restricted vertical motion while allowing horizontal motion and rotation about the pin.

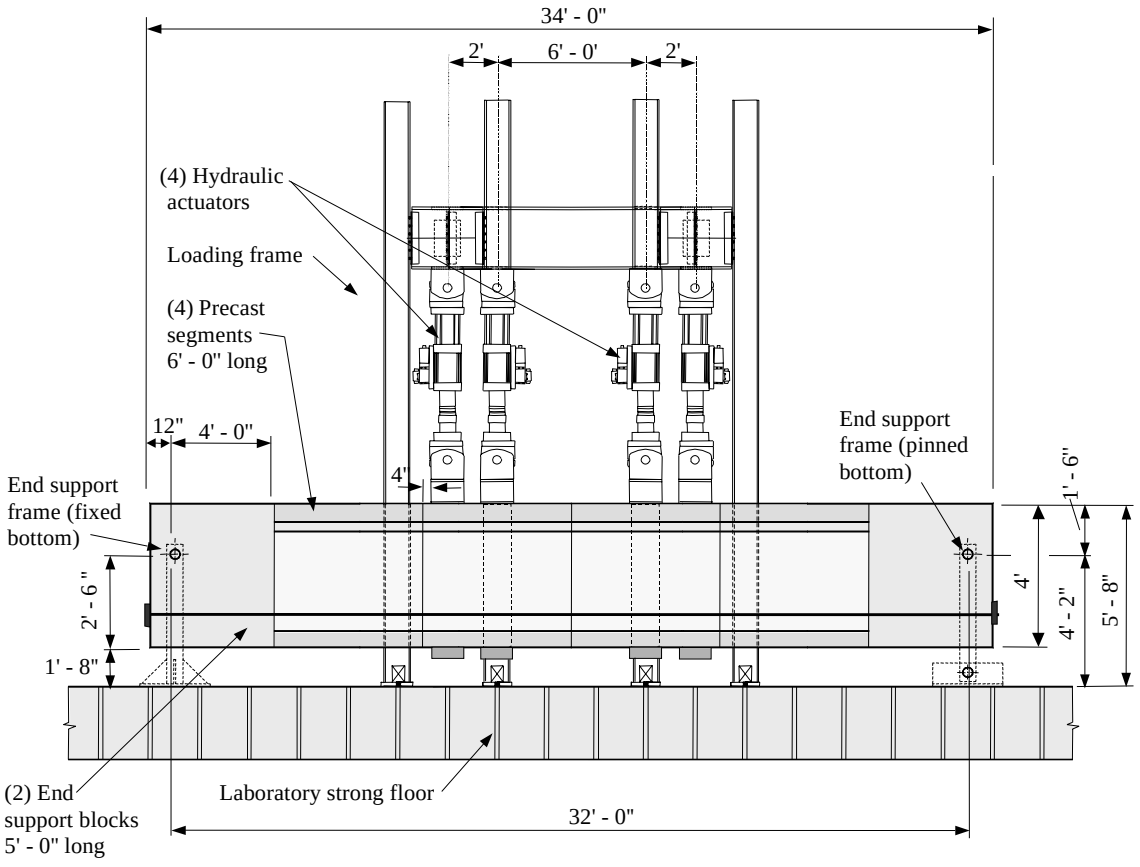


**Figure 2-16 Test setup elevation**

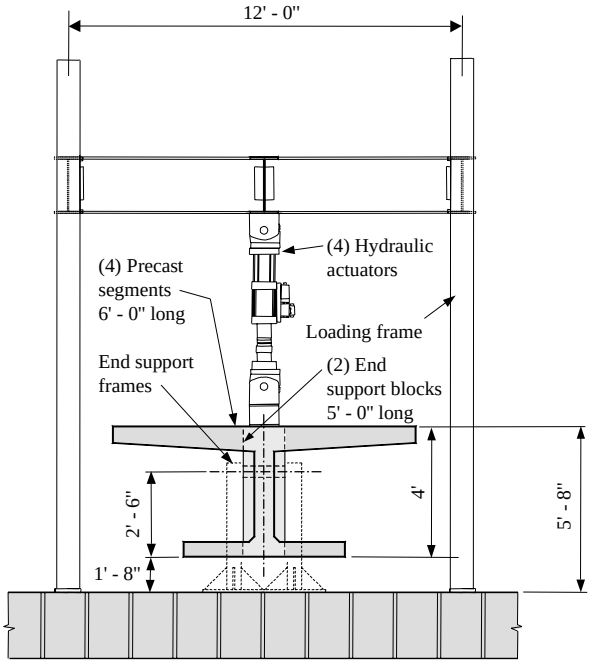


**Figure 2-17 Test setup side view**

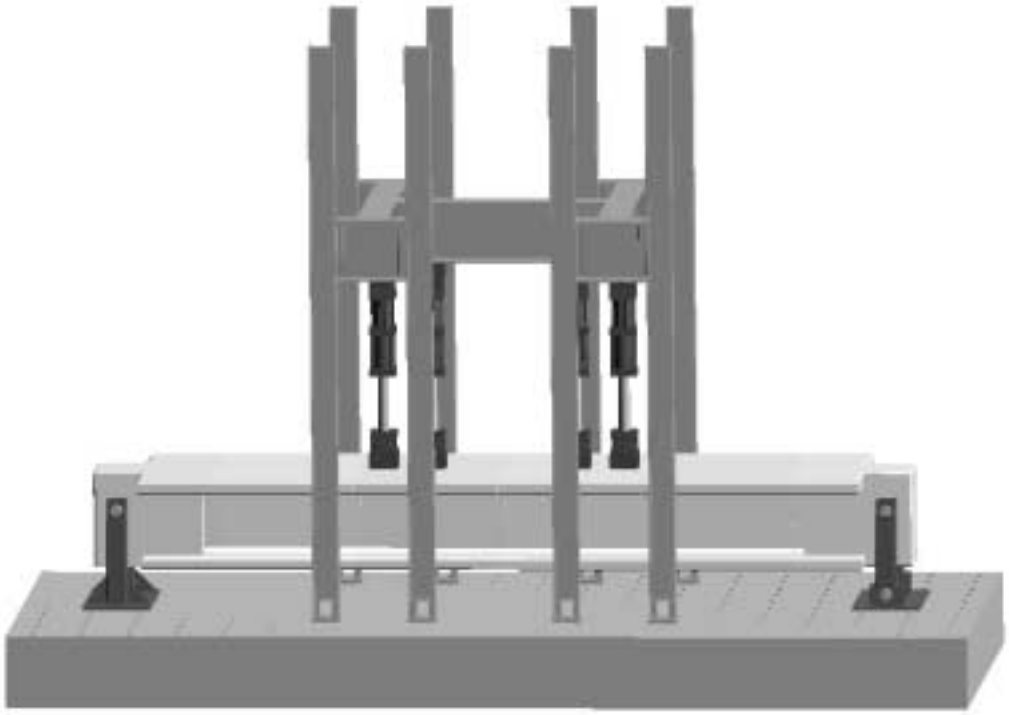

**Figure 2-18 Three dimensional view of test setup**

Each end support was post-tensioned to the lab strong-floor with six high strength steel bars. The steel pins were machined to 6 in. (152 mm) and inserted into steel sleeves that were cast into the end segments of the test units. The centers of the pins were located at the neutral axis of the test unit.

Servo-controlled hydraulic actuators were used to apply external loads to each test unit to simulate service loads and vertical seismic loading. Structural steel pieces were used to connect the actuators with the test units. The mid-span joint of the test units, like the mid-span joint of the prototype structure, was the location of the maximum bending moment and zero shear. To properly represent the stresses at midspan of the prototype structure under combined dead load, superimposed dead load, and primary and secondary prestressing moment effects, additional vertical downward load was required on the test unit. This load, referred to as the reference load from herein, was applied at the beginning of each test.

## 2.5 Instrumentation

Each test Unit was instrumented with 40 linear potentiometers to measure relative vertical and horizontal displacements between segments, 30 concrete strain gages, 24 steel strain gages to measure strains in the post-tensioning steel, and 2 inclinometers to measure the rotation of the end segments. Schematics showing the location of instrumentation are shown in Figure 2-19 (a) and (b).

These horizontal displacement transducers were placed at each joint to measure the joint opening. Vertical transducers on the web of each Unit monitored relative vertical sliding between adjacent segments. Linear potentiometers were placed 6 in. (152 mm) from each joint to measure vertical deflections and under the supports to monitor any

uplift. Six strain gages were put on four steel strands; three gages were put near the center joint and three gages near joint J4 (see Figure 2-6).

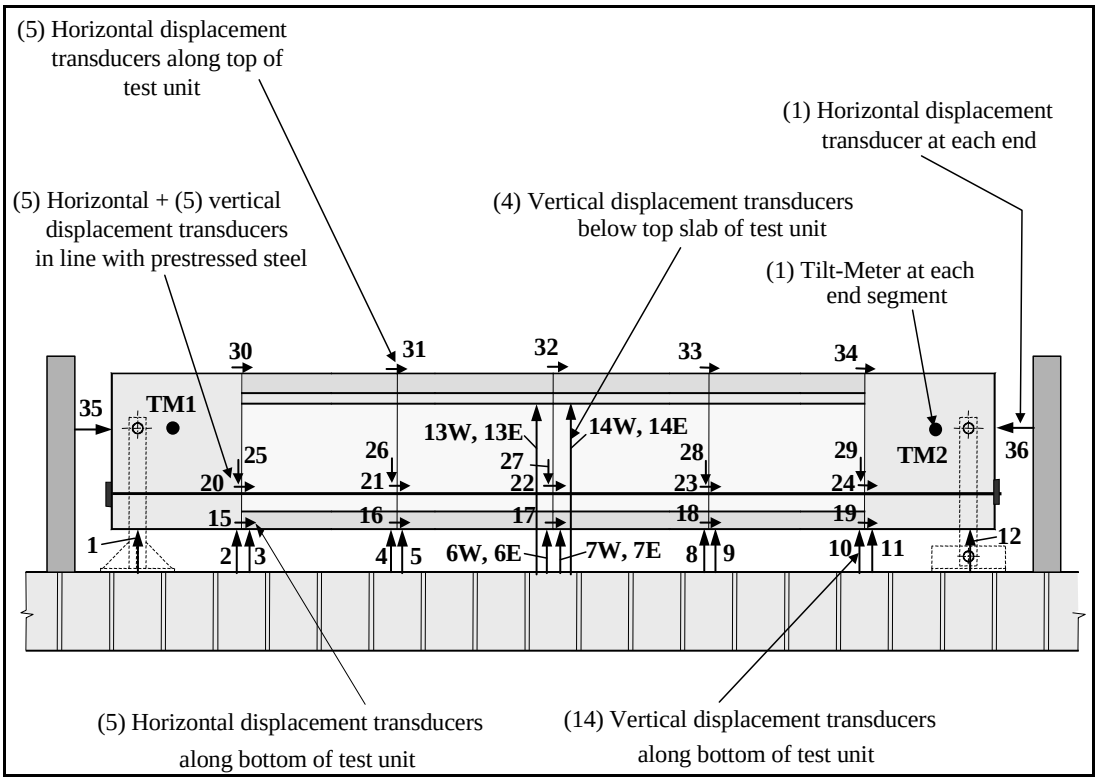


(a) Elevation

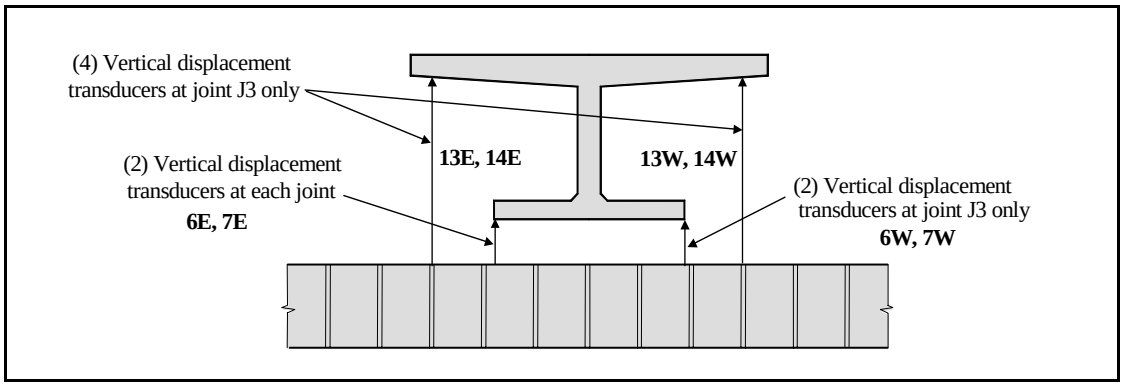


(b) Side View

**Figure 2-19 Displacement transducer layout**

## 2.6 Loading Sequence

Testing of each unit was divided into two stages. Stage 1 was the Service Load Conditioning and Stage 2 was the Seismic Test. In Service Load Conditioning only the two interior actuators were used; both actuators were in load control. Each test Unit underwent load conditioning where the load was cycled, beginning at the reference load, between maximum and minimum service load conditions. A total of 100,000 cycles were completed for each test unit at a rate of 2.0 Hz for Units 100-INT and 100-INT-CIP. The 100,000 loading cycles were completed at a rate of 2.5 Hz for Units 100-EXT and 50-INT/50-EXT to accelerate the test. At the reference load the force in each actuator was 74.5 kips (331 kN) and was cycled between 112 kips (498 kN) and 65 kips (289 kN).

In the Seismic Test all four actuators were used. One interior actuator was placed in displacement control based on the vertical displacement transducer 6 in. (152 mm) from the center joint. The remaining actuators were then slaved to the first actuator in force control. Thus, the forces in all four actuators were equal. Each test unit was subjected to fully reversed loading cycles with increasing displacement amplitude. The loading sequence utilized for the Seismic Test is shown in Figure 2-20. Three cycles were performed at each displacement level through the 4 in. (102 mm) cycles; beyond the 4 in. cycle only one cycle was performed at each displacement level. Each Unit was loaded until failure.

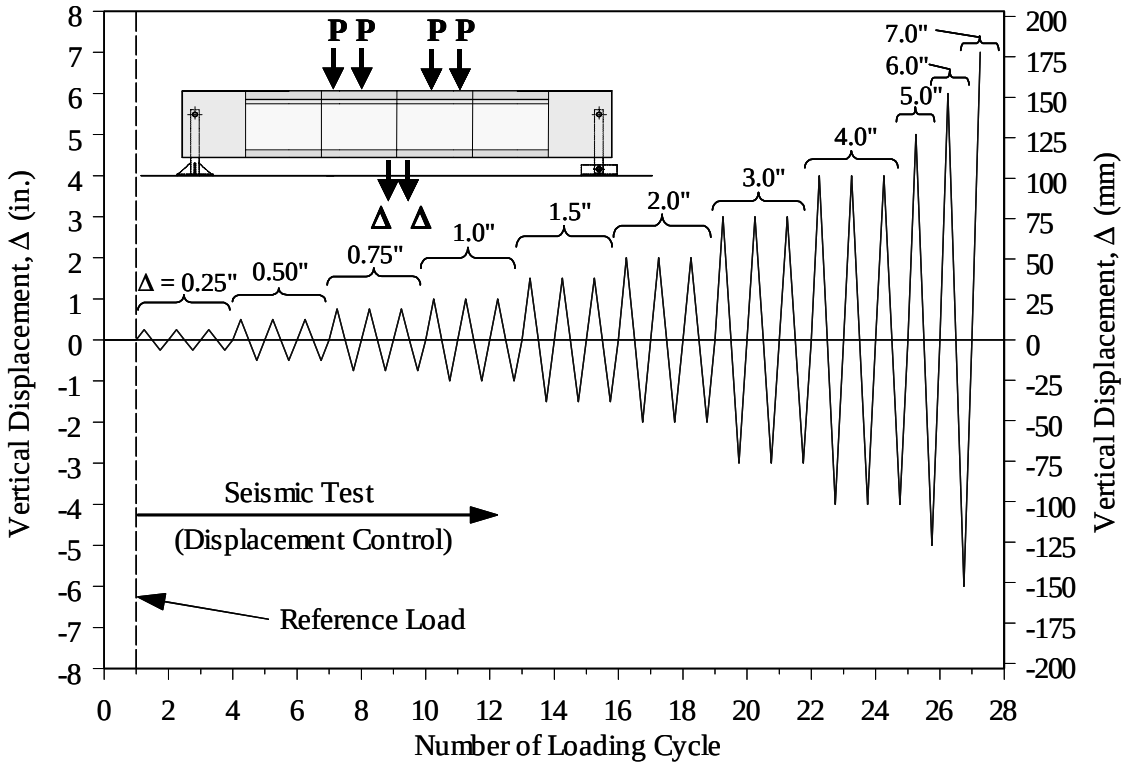


**Figure 2-20 Vertical loading sequence**

# 3 Experimental Results for Segment-to-Segment Joints Subjected to High Bending Moments and Low Shears (Phase I)

## 3.1 General Observations

### 3.1.1 Test Unit 100-INT

**Service Load Conditioning**

To begin testing the unit was loaded to the reference load, P = 74.5 kips (331 kN), and the remaining temporary prestressing was released. One quasi-static cycle between the maximum and minimum service load levels, $P_{max}$ = 112 kips (489 kN), $P_{min}$ = 65 kips (289 kN), was completed. No cracking was observed during this cycle. A total of 100,000 cycles was then completed at 2.0 Hz, again, cycling between the maximum and minimum service load levels. No cracking was evident upon completion of this conditioning.

**Seismic Test**

Flexural cracking was observed in the first downward displacement cycle at +0.25 in. (6.35 mm). Joints J3 (midspan) and J4 began opening during this cycle and additional flexural cracking was observed within Segments 3 and 4. The crack at midspan occurred in the cover concrete adjacent to the epoxy bonded joint. Shear cracks were observed in the web between the exterior load points and supports. Joint J2 did not open until the 0.75 in. (19.1 mm) downward displacement cycle. Shear cracks continued to develop and extend with subsequent cycles. Flexural cracks developed with less frequency than shear cracks once the three middle joints opened. There was a fairly even distribution of shear cracks across the Unit. The midspan joint J3 is shown at displacement peaks of the 1.0 in. (25.4 mm) cycle in Figure 3-1 and Figure 3-2. Shear cracks in the web traveled at

nearly 45 degrees traversing over joints without deviation as seen in Figure 3-3. Beyond the 2.0 in. (50.8 mm) displacement cycle increasing joint opening seemed focused on the center joint J3. The negative peak of the 2.0 in. (50.8 mm) cycle is shown in Figure 3-4. The sign convention used throughout this chapter is positive for downward load and displacement. Joint J3 would open widely while joints J2 and J4 overall opening did not increase significantly. All of the joint openings, however, were able to close and virtually disappear with a reversal in loading. At the reference load all of the openings were reduced to hairline cracks at the joints. The first signs of spalling in the top deck concrete were observed at joint J3 in the first 4.0 in. (102 mm) downward displacement cycle. In these cycles horizontal cracks were observed near the C.G. of the post-tensioning steel. These cracks extended approximately 4.5 in. (114 mm) in each direction from midspan. Following the completion of three cycles at 4.0 in. (102 mm) (see Figure 3-5) the test unit was loaded to what would have been the first cycle at 5.0 in. (127 mm) but fourteen of the sixteen post-tensioning strands fractured at a peak displacement of 4.8 in. (122 mm), the maximum load was 490 kips (2,180 kN) (see Figure 3-6).

The -0.5 in. (-12.7 mm) displacement cycles brought the first opening of joint J3 in the upward loading direction. No other joints opened during upward loading. Few shear cracks developed before the opening of joint J3. Without reinforcement crossing the joints in the top deck the midspan joint was free to widen with subsequent cycling. Again, the opening at J3, although wide, was able to completely close on each cycle. The first upward -3 in. (-76.2 mm) displacement cycle brought the beginning of concrete spalling on the bottom surface.

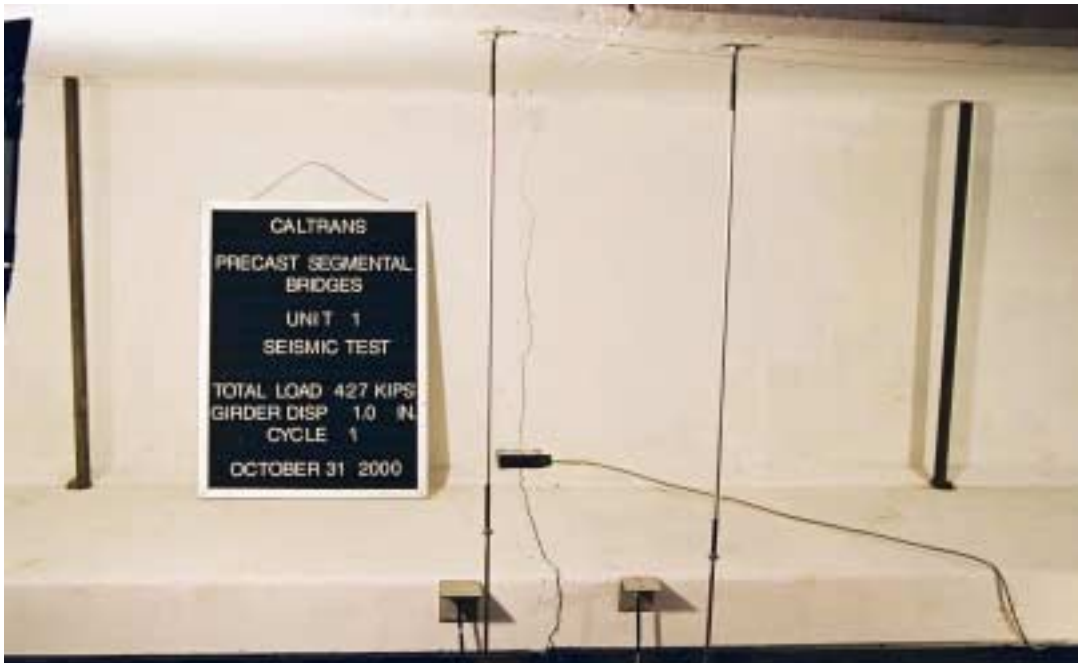


**Figure 3-1 West side of Unit 100-INT, joint J3; Δ=+1.0 in. (25.4 mm)**


**Figure 3-2 West side of Unit 100-INT, joint J3; Δ=-1.0 in. (-25.4 mm)**

**Figure 3-3 Unit 100-INT, East side of joint J4; Δ=+1.5 in. (38.1 mm)**

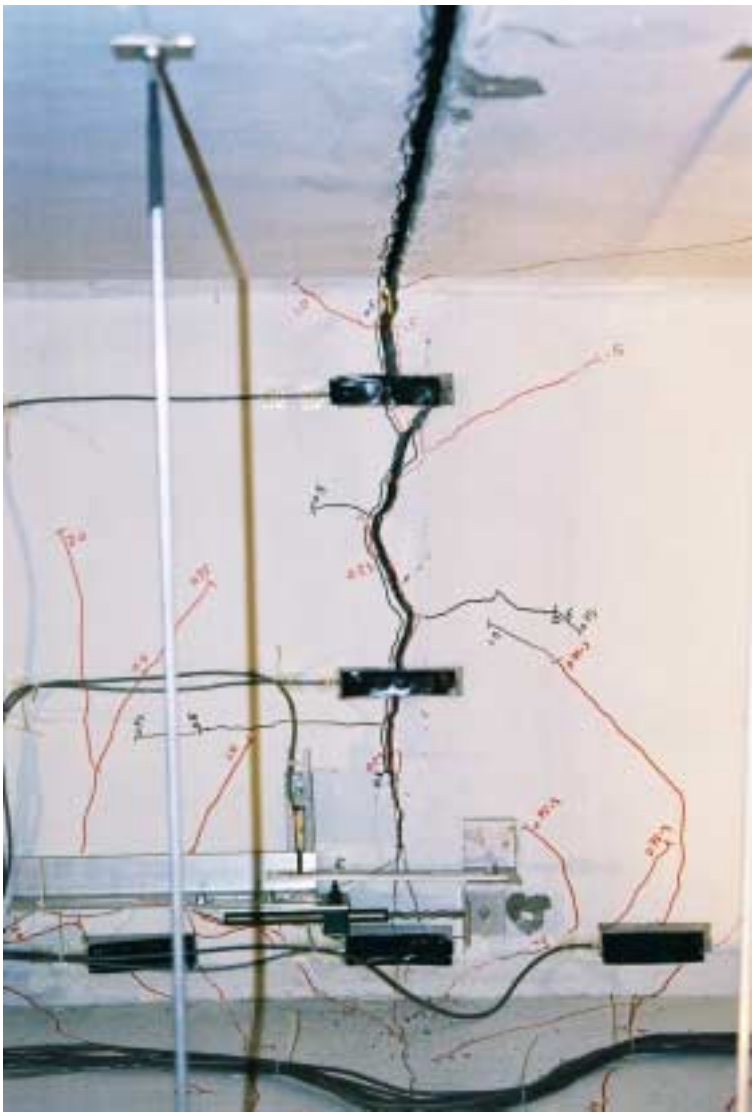

**Figure 3-4 Unit 100-INT, East side of joint J3; Δ=-2 in. (-50.8 mm)**


**Figure 3-5 Unit 100-INT, West side of joint J3; Δ=+4.0 in. (102 mm)**

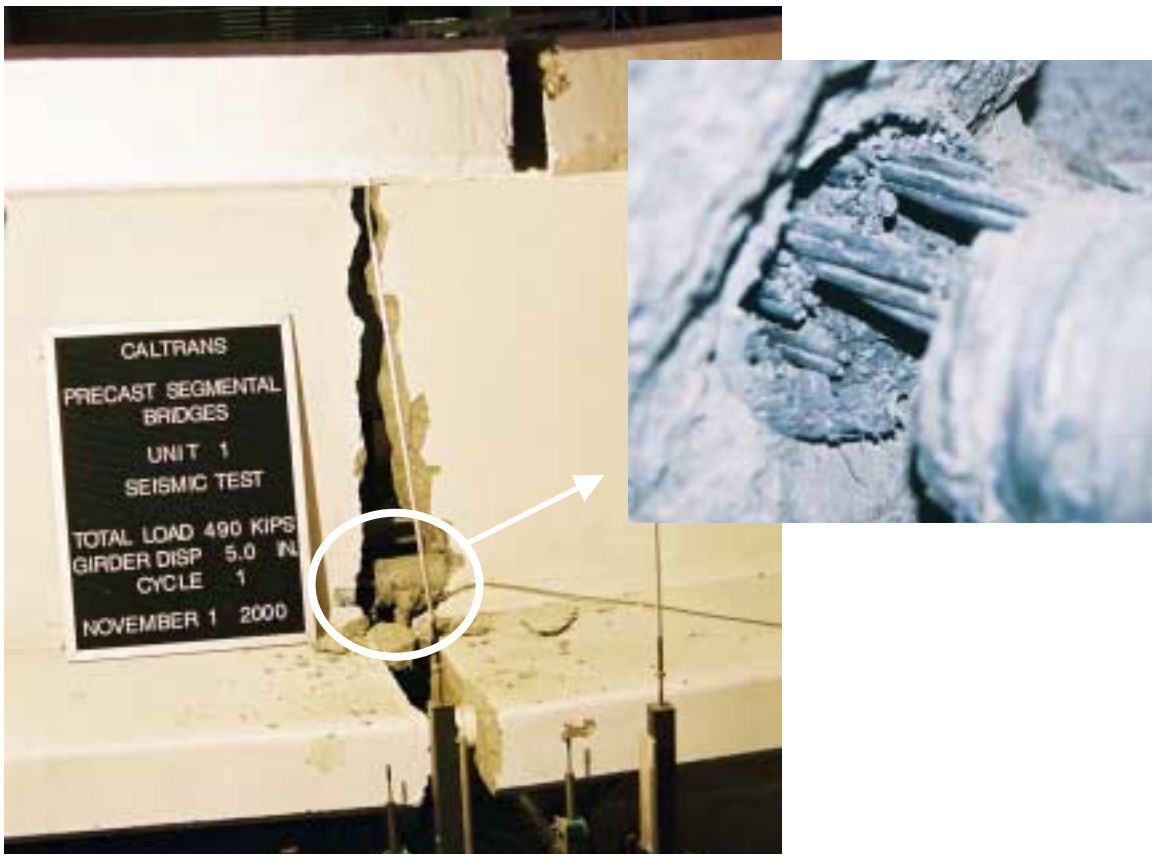


**Figure 3-6 Unit 100-INT, West side of joint J3 after failure with tendon close-up**

### 3.1.2 Test Unit 100-INT-CIP

**Service Load Conditioning**

The test unit was loaded to the reference load with two actuators each to a load of P = 74.5 kips (331 kN) and the temporary post-tensioning was removed. One quasi-static cycle between maximum and minimum service load levels was completed. The Unit underwent 100,000 cycles of the maximum and minimum service load conditions at 2.0 Hz. No cracking was observed upon completion of this stage of testing.

**Seismic Test**

Flexural joint opening was first observed at joint J3 in the first +0.25 in. (6.35 mm) downward displacement cycle. Some flexural cracks developed within the center two segments and shear cracks developed in the web in similar fashion to Unit 100-INT. Joints J2 and J4 adjacent to midspan began opening in the first downward cycle of +0.5 in. (12.7 mm). The opening of joints J2 and J4 did not increase significantly with increasing displacements as did joint J3. However, due to the cast-in-place closure joint the opening at J3 was not able to travel up through the entire joint surface. Instead, there was a bifurcation of the crack at joint J3 in the web approximately 8 in. (203 mm) from the underside of the top deck. This crack pattern is visible in its initial stages in Figure 3-7. With continued cycling these cracks propagated towards the interface of the cast-in-place joint closure and the precast concrete. The crack at joint J3 in downward cycle closed completely with a reversal of load (see Figure 3-8). Like the previous Unit, Unit 100-INT-CIP exhibited an even distribution of shear cracking across the test zone (see Figure 3-9). Cyclic loading caused longitudinal cracks to form in the closure joint at midspan preceding the buckling of longitudinal reinforcement in this joint. The

longitudinal cracks were observed during the +2.0 in. (50.8 mm) displacement cycle. Concrete spalling was observed in the top deck during the +3 in. (76.2 mm) displacement cycle. The longitudinal reinforcement in the closure joint buckled during the +4 in. (102 mm) cycle, both the positive and negative peaks are shown in Figure 3-10 and Figure 3-11, respectively. Compression failure of the top deck finally occurred at a displacement of 5.85 in. (149 mm) and a peak load P = 480 kip (2,135 kN) (see Figure 3-12). The compression failure was initiated by buckling of the closure joint reinforcement, which pushed against the concrete cover. Buckling of the cast-in-place deck reinforcing bars could be prevented if closed stirrups are provided inside the cast-in-place deck closure joints to enclose the top and bottom layers of longitudinal mild steel reinforcement of the deck.

The first flexural crack in the upward loading direction was observed during the -0.75 in. (-19.1 mm) displacement cycle. This cracking was observed, not at the segment joint location, but at the interface of the precast concrete of the top deck and the cast-in-place closure joint. Several closely spaced, narrow, flexural cracks appeared in the top deck under upward loading, rather than the single, wide crack at midspan. At the maximum upward displacement, however, the largest cracks were observed at the interface of the CIP concrete and the precast concrete. The cracks at the interface of joint J3 propagated through the web angling towards the crack that formed at midspan during the downward cycles.

Much of the behavioral characteristics of Unit 100-INT-CIP were initially attributed to debonding of the post-tensioned tendon. However, after thorough investigation of the tendon no conclusive signs of debonding were present. The investigative approach

included taking 12 in. (305 mm) slices of the tendon starting from midspan. These slices were then visually inspected but no obvious signs of tendon debonding were apparent. Additional tests were conducted on the slices; a SATEC compression-testing machine was used to perform punching tests. The force required to push the tendon section through was recorded; the results, which also showed no conclusive sign of debonding, are presented in Appendix A.

No difference was observed in performance of the two halves of Test Unit 100-INT-CIP in which bent hairpin bars and headed bars were used for longitudinal mild steel reinforcement in the cast-in-place deck closure joints (see Figure 2-8). However headed bars are recommended for construction reasons, especially if closed stirrups are provided in the cast-in-place deck to enclose the top and bottom layers of deck reinforcement.


**Figure 3-7 Unit 100-INT-CIP joint J3, West side; Δ=+1.5 in. (38.1 mm)**


**Figure 3-8 Unit 100-INT-CIP joint J3 West side; Δ=-1.5 in. (-38.1 mm)**

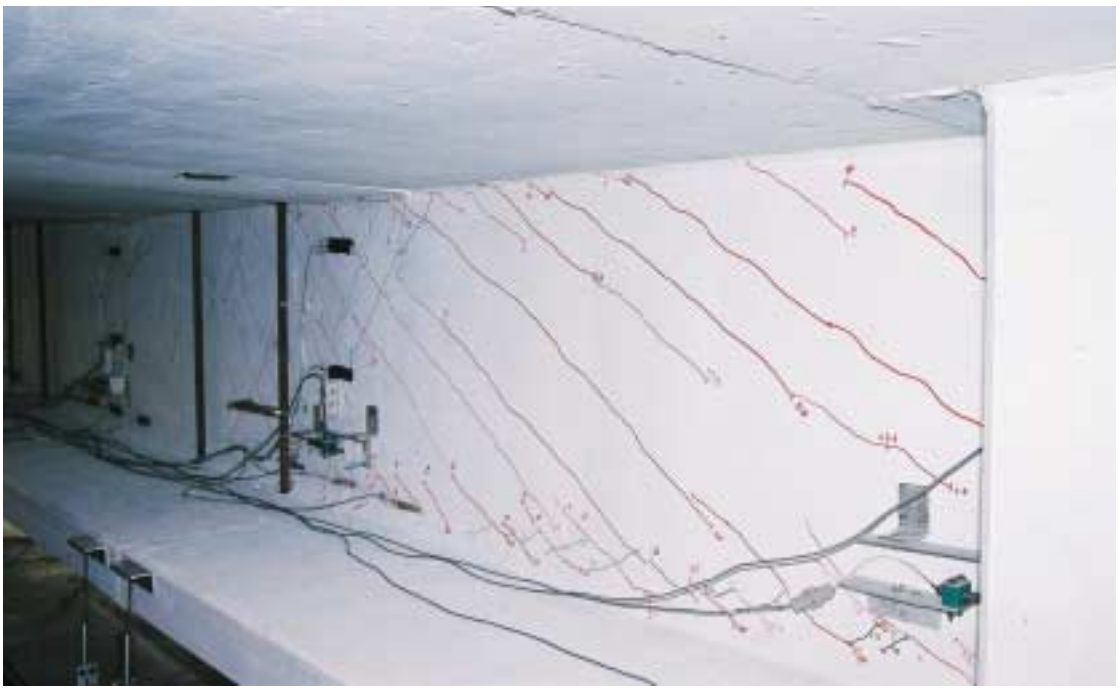

**Figure 3-9 Unit 100-INT-CIP, East side web from north end; Δ=+1.5 in. (38.1 mm)**


**Figure 3-10 Unit 100-INT-CIP, West side of joint J3; Δ=+4.0 in. (102 mm)**


**Figure 3-11 Unit 100-INT-CIP joint J3; Δ=-4.0 in. (-102 mm)**

**Figure 3-12 Unit 100-INT-CIP joint J3 after failure**

### 3.1.3 Test Unit 100-EXT

**Service Load Conditioning**

Similar to the previous Units the temporary post-tensioning was removed at the reference load of P = 74.5 kips (331 kN). Beginning at the reference load one quasi-static cycle was performed between the maximum and minimum service load levels. Uncharacteristic of the previous two test units, minor hairline shear cracks were observed in the web at the maximum service load level of P = 112 kips (498 kN). Load conditioning followed this first cycle, 100,000 cycles were completed at 2.5 Hz. No new cracks were observed upon the completion of these cycles and there was minor extension of the few existing shear cracks in the web.

**Seismic Test**

During downward loading flexural cracking was first observed during the first cycle at +0.25 in. (6.35 mm). Joint J3 is shown in Figure 3-13 at +1.0 in. (25.4 mm), this figure clearly shows that the joint opening occurred in the cover concrete, in this case near the termination point of longitudinal bars, not in the epoxy. Figure 3-14 shows joint J3 at -1.0 in. (-25.4 mm) displacement, the crack at midspan from downward loading all but disappeared when the loading was reversed. A single crack occurred 3.0 in. (76.2 mm) from joint J3 and shear cracks were observed in the web. During subsequent cycles widening of the opening at joint J3 was observed as well as the extension of shear cracks in the web, however, there were significantly fewer shear cracks than in the previous two test units; no shear cracks were observed in either segment 3 or 4. Few cracks developed once joint J3 opened. No flexural opening was observed in any joint other than joint J3; not many flexural cracks were observed away from the center joint. The deck slab began

showing signs of spalling during the +3.0 in. (76.2 mm) downward displacement cycle. Degradation of the deck concrete under compression began much sooner than in Units 100-INT and 100-INT-CIP due, in part, to the fact that as the structure deflected downward the external tendon stayed at a nearly constant elevation between the harping points. Subsequently, the moment arm between the compression and tension resultant forces was greatly reduced thus lowering the overall capacity. A peak load of 417 kips (1,855 kN) was attained at a displacement of 3.53 in. (89.7 mm), joint J3 is shown in Figure 3-15 at the completion of the +4.0 in. (102 mm) displacement cycle. Unit 100-EXT was able to undergo increased displacements but the load carrying capacity gradually dropped with each cycle beyond the peak load. Figure 3-16 and Figure 3-17 show joint J3 at the maximum displacement of +7.0 in. (178 mm), the latter figure shows the deteriorated state of the top deck at this displacement. Figure 3-18, taken after the end of testing, illustrates the fact that with external tendons shear crack development is not distributed across the entire section, the few shear cracks that were observed occurred only near the ends of the test zone.

In the upward loading direction joint J3 began cracking during the -0.5 in. (-12.7 mm) cycle. A fairly small number of shear cracks developed during this cycle. There was a drop in overall load during the first -0.75 in. (-19.1 mm) cycle as the opening at J3 continued to widen. During the –2.0 in. (-50.8 mm) displacement cycle the bottom deck began to come in contact with the post-tensioning tendon. The peak load increased in the -3.0 in. (-76.2 mm) cycle due to this contact. There seemed to be no other adverse effect of the bottom deck bearing up on the tendon. Concrete began spalling on the bottom surface during the -4.0 in. (-102 mm) cycle and longitudinal cracks developed on the side

of the bottom slab. Testing continued to maximum displacement of -6.0 in. (-152 mm), at which point the actuator limitations were met. All opening was restricted to joint J3 and the compression concrete at the bottom deck remained intact.

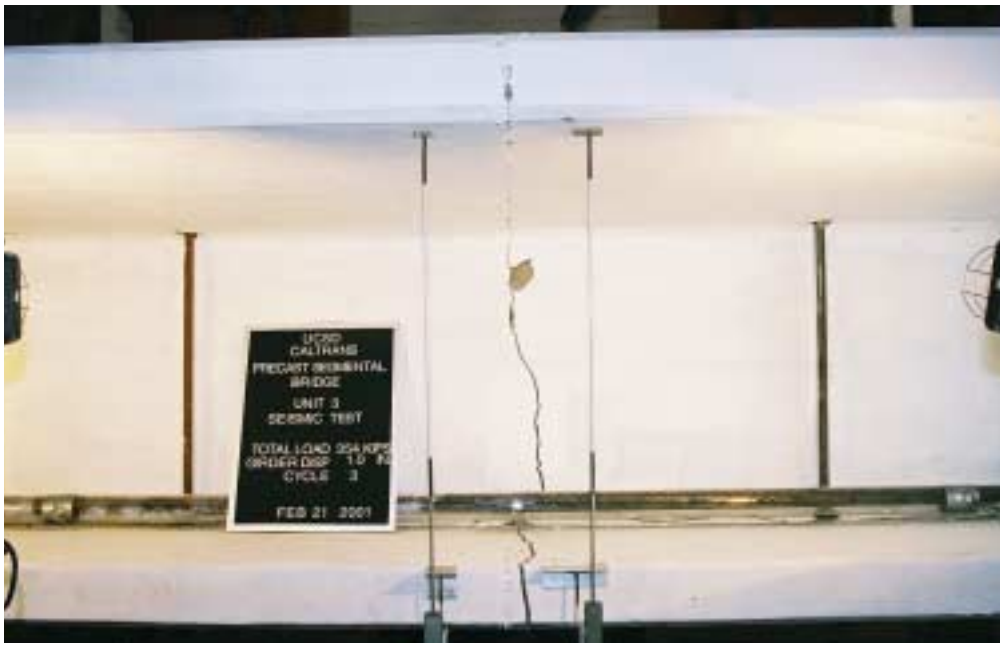


**Figure 3-13 Unit 100-EXT, West side of joint J3, Δ=+1.0 in. (25.4 mm)**


**Figure 3-14 Unit 100-EXT, West side of joint J3, Δ=-1.0 in. (-25.4 mm)**

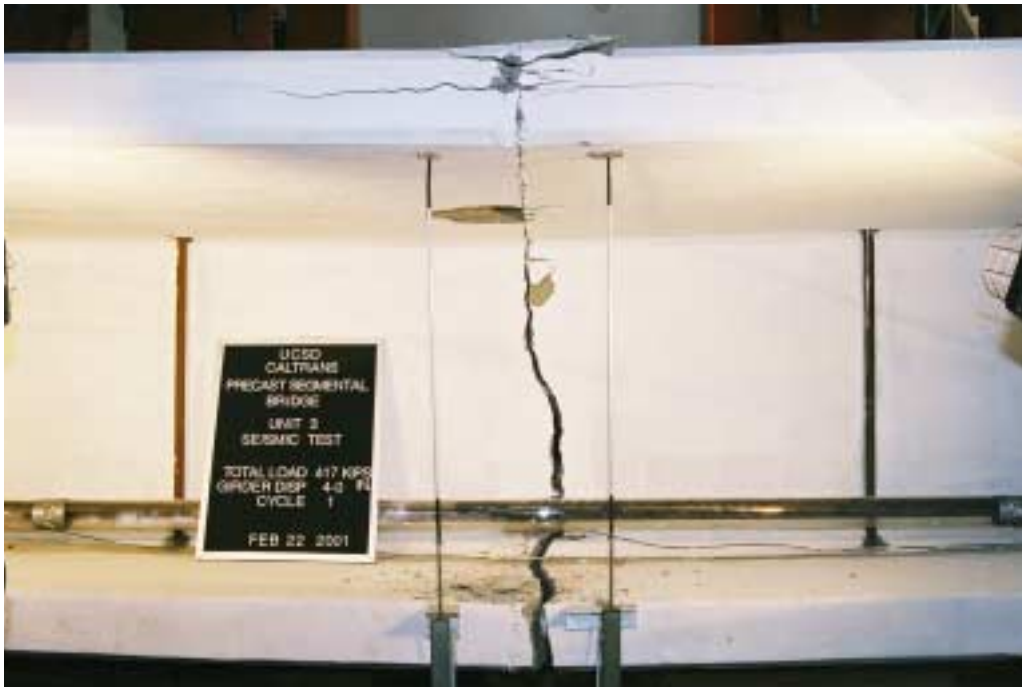


**Figure 3-15 West side of joint J3 of Unit 100-EXT, Δ=+4.0 in. (102 mm)**

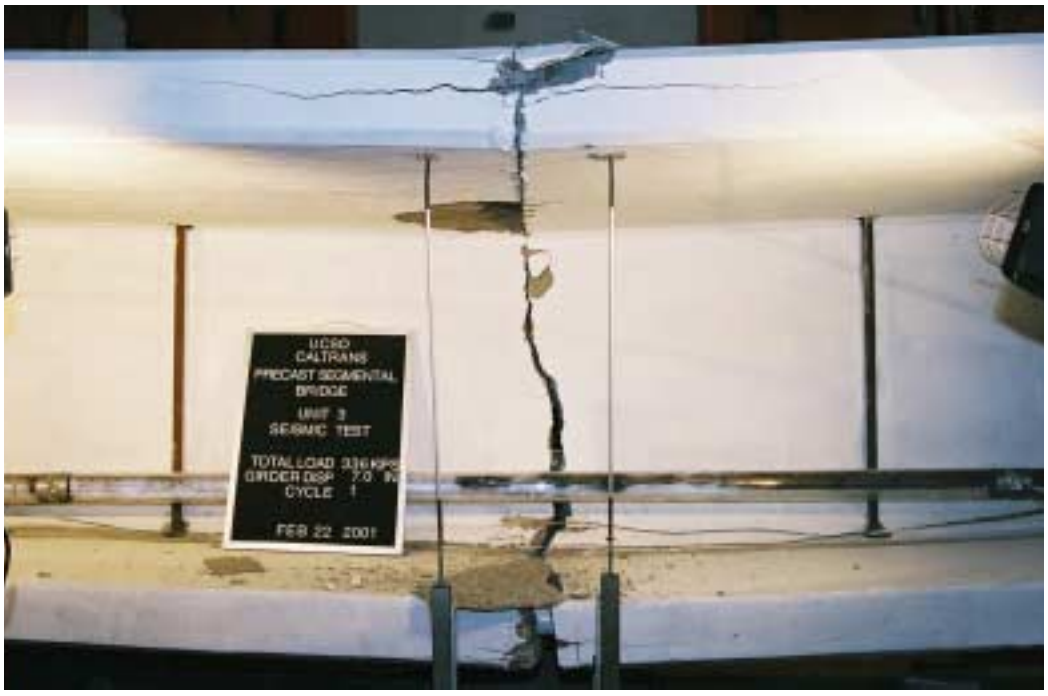


**Figure 3-16 West side of joint J3 of Unit 100-EXT, Δ=+7.0 in. (178 mm)**


**Figure 3-17 View of deck at joint J3 of Unit 100-EXT, Δ=+7.0 in. (178 mm)**

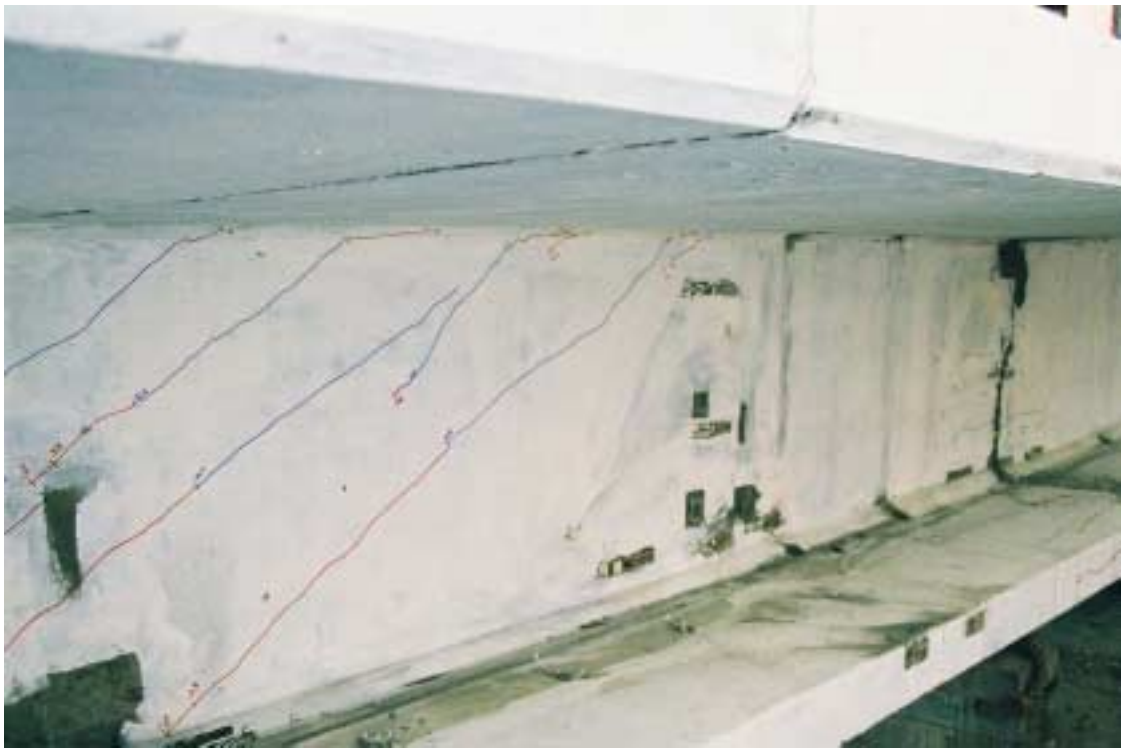

**Figure 3-18 East side of web looking north at joints J4 and J3, post-test**

### 3.1.4 Test Unit 50-INT/50-EXT

**Service Load Conditioning**

No cracking was observed upon the release of the temporary post-tensioning and with an applied load of P = 74.5 kips (331 kN). Minor hairline shear cracks were observed in the web at the maximum service load level of P = 112 kips. These cracks occurred only in segments 4 and 5. No additional cracking occurred with the completion of 100,000 cycles at 2.5 Hz.

**Seismic Test**

In the downward loading direction flexural cracking was first observed during the +0.25 in. (6.35 mm) displacement cycle. This cracking did not, however, occur at midspan joint J3 but approximately 15 in. (381 mm) away from midspan. New shear cracks were observed between the load points and end supports. Joint J3 opened in the first +0.5 in. (12.7 mm) displacement cycle. Very few additional flexural cracks were observed once the midspan joint opened. Shear cracks did, however, continue to occur and propagate during subsequent cycles.

During the 2.0 in. (50.8 mm) downward displacement cycle (see Figure 3-19) a drop in load was observed but there was no visible sign of structural weakening. Signs of concrete spalling were observed on the top surface during the 3.0 in. (76.2 mm) displacement cycle. The peak load for Unit 50-INT/50-EXT, 452 kips (2,011 kN) was attained during the +4.0 in. (102 mm) cycle at a displacement of +3.8 in. (96.5 mm), joint J3 is shown in Figure 3-20 at 4.0 in. (102 mm) displacement. Popping sounds were audible at the peak load and were attributed to the fracturing of internal post-tensioning strands. In the +5.0 in. (127 mm) displacement cycle the sound of fracturing strands was

heard and again there was a drop in overall load, it seems that all of the remaining internal strands fractured during this cycle. The test continued for two cycles, with only the external tendons intact, with a load that was less than 50% of the peak load. Figure 3-21 shows the distribution of shear cracks on the web at joint J4. A fewer number of shear cracks were observed than Unit 100-INT, but there was a better distribution of shear cracks than Unit 100-EXT.

In the upward loading direction cracking at J3 occurred during the -0.5 in. (-12.7 mm) displacement cycle. Spalling of the bottom surface was observed during the -3.0 in. (-76.2 mm) displacement cycle. Joint J3 was the only one to open and opened widely in the upward direction, similar to the previous test units.

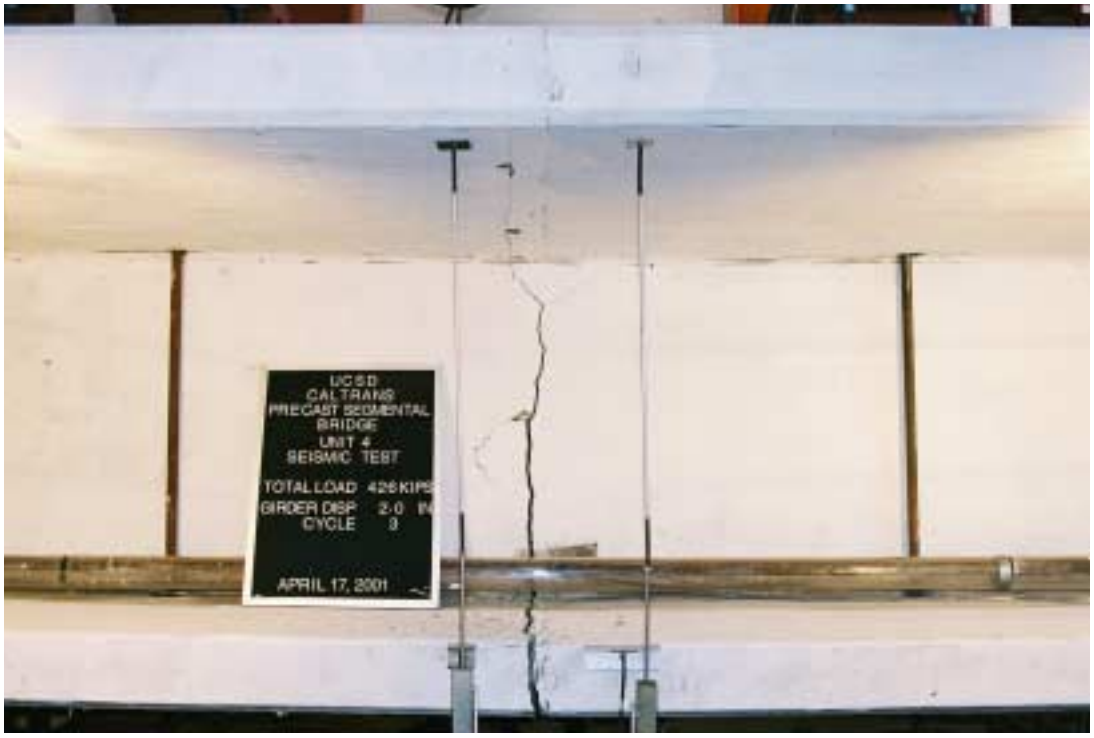


**Figure 3-19 West side of joint J3 of Unit 50-INT/50-EXT, Δ=+2.0 (50.8 mm)**


**Figure 3-20 West side of joint J3 of Unit 50-INT/50-EXT, Δ=+4.0 in. (102 mm)**

**Figure 3-21 East web of Unit 50-INT/50-EXT at joint J4, post-test**

## 3.2 Load-Displacement Response

The vertical displacement was measured at 6 in. (152 mm) from midspan and the sign convention is positive in the downward direction. This displacement is plotted against the total load applied to the test units in the figures that will follow; a dashed line represents the reference load in these figures. The residual displacement of the test units corresponds to the reference load. The equivalent viscous damping ratio was calculated for all test units based on the 3 in. (76.2 mm) load-displacement cycle because one of the test units (50-INT/50-EXT) failed during the 4.0 in. (102 mm) displacement cycle. The hysteretic damping was converted to equivalent viscous damping using the following equation[9]:

$$\zeta_{eff} = \frac{A_h}{2\pi F \Delta} \tag{3-1}$$

Where $A_h$ is the area of the hysteresis loop, F is the total load and $\Delta$ is the corresponding displacement.

### 3.2.1 Test Unit 100-INT

The history of total applied load versus vertical displacement is shown in Figure 3-22. The figure reflects increasing strength in the downward direction until the tendon ruptured at $\Delta$=+4.8 in. (122 mm) and a load of 490 kips (2,180 kN). In the upward loading direction the maximum load of -93 kips (-414 kN) was reached at a relatively small displacement of $\Delta$=-0.5 in. (-12.7 mm), this occurred because there was no reinforcement crossing the joints in the deck slab. Almost no hysteretic response was observed in the upward loading cycles. The damping ratio of the complete cycle of testing at the 3 in. (76.2 mm) displacement was determined to be 4.21 percent. The

residual displacement remained relatively low through the 2.0 in. (50.8 mm) displacement cycle at approximately 0.5 in. (12.7 mm) but increased to a maximum of 1.96 in. (49.8 mm).

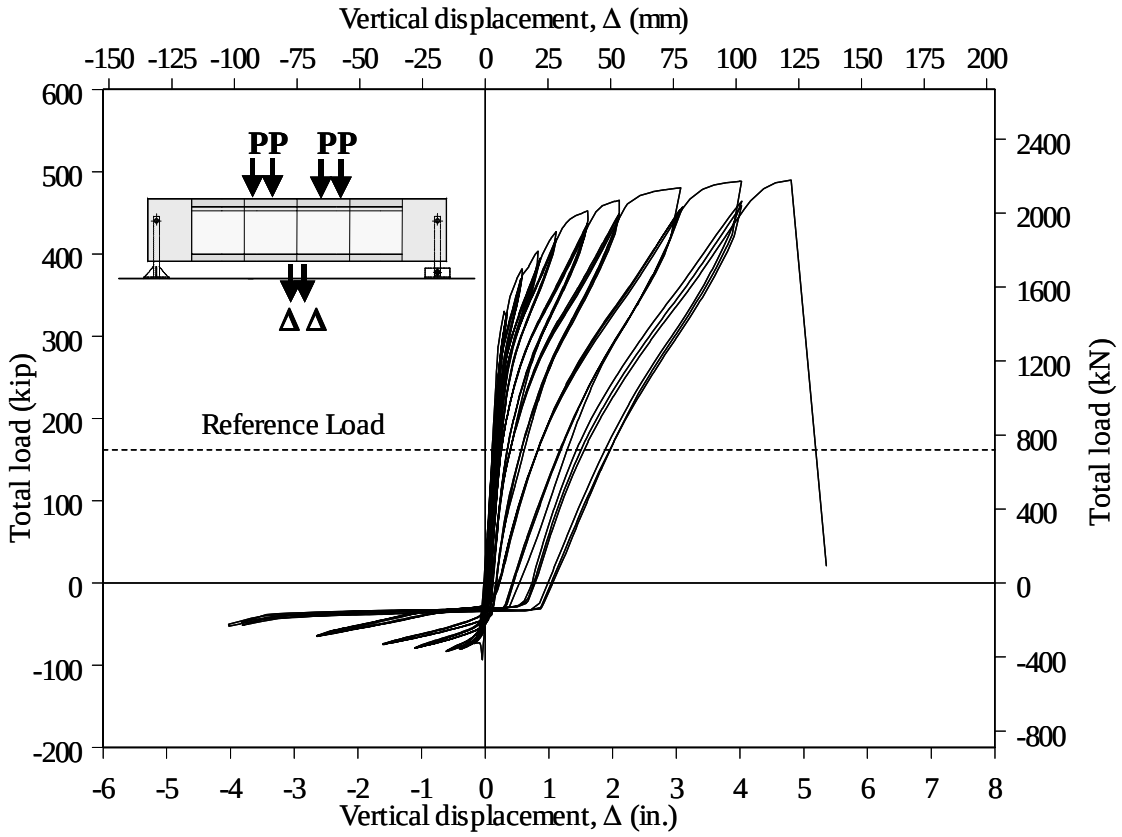


**Figure 3-22 History of total load versus displacement, Unit 100-INT**

### 3.2.2 Test Unit 100-INT-CIP

The load-displacement response for Unit 100-INT-CIP is displayed in Figure 3-23. The response in the downward loading direction is similar to that of Unit 100-INT. Major nonlinear response began at a load of approximately 380 kips (1,690 kN) until the compression failure of the deck. In the upward loading direction the test unit displayed stable hysteretic response. The strength of the CIP reinforcing bars was able to be

developed translating to a maximum upward load of -327 kips (-1,455 kN). The yielding of the continuous deck reinforcement along with the inelastic response of the post-tensioning tendon accounted for a damping ratio of 8.75 percent for the complete cycle at 3 in. (76.2 mm) displacement. The residual displacement at the reference load level reached a maximum of 0.93 in. (23.6 mm).

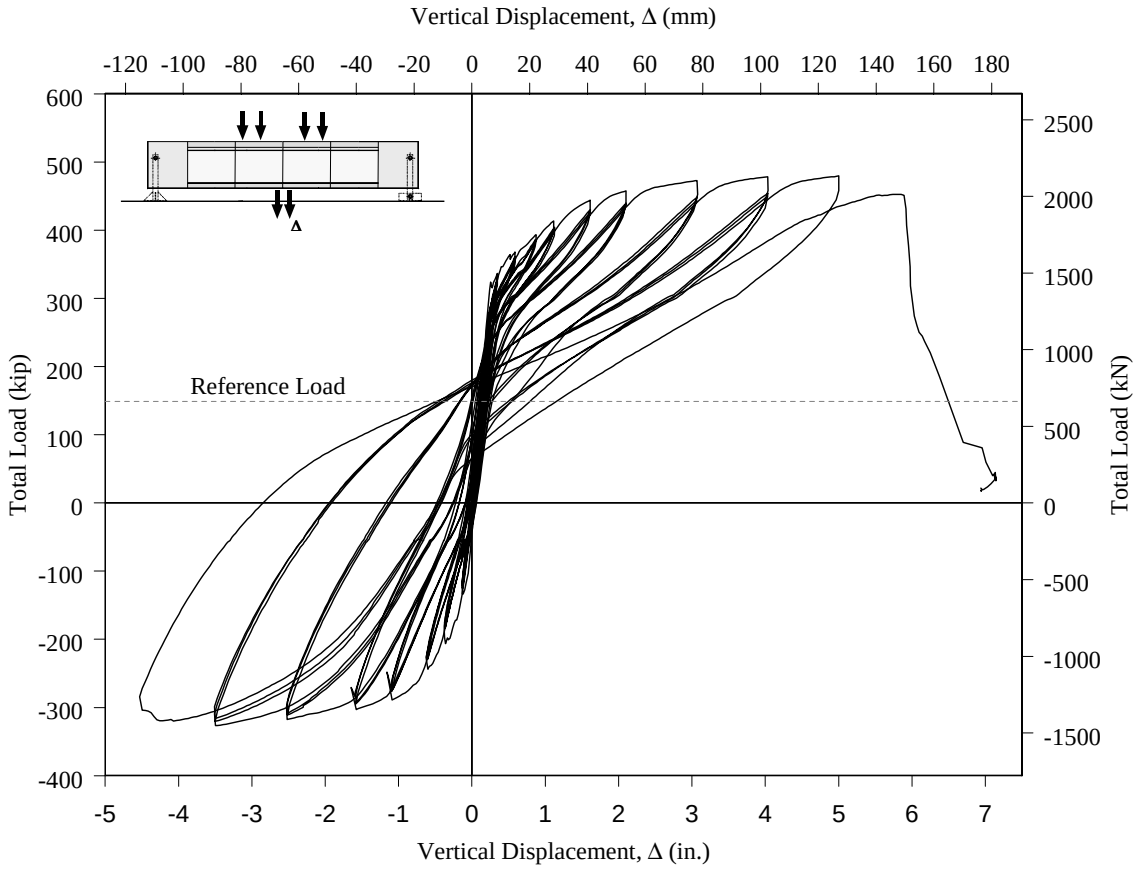


**Figure 3-23 History of total load versus displacement, Unit 100-INT-CIP**

### 3.2.3 Test Unit 100-EXT

The force-displacement response for Unit 100-EXT is shown in Figure 3-24. Nonlinear response in the downward direction began at about 300 kips (1,335 kN), most of the inelastic behavior occurred in the concrete. Most of the energy dissipated in the

final displacement cycles was through the crushing of concrete; the equivalent viscous damping of the complete cycle at 3 in. (76.2 mm) displacement was 2.63 percent. The residual displacement through the +4.0 in. (102 mm) cycle remained small, in the order of 0.4 in. (10.2 mm); the external tendons were able to apply a restoring force to return the test unit to near zero residual displacement. The maximum force, 417 kips (1,855 kN) was attained during the 4.0 in. (102 mm) cycle at a displacement of 3.53 in. (89.7 mm). There was a drop in load following this and the gradual decrease of the load carrying capacity continued in subsequent cycles.

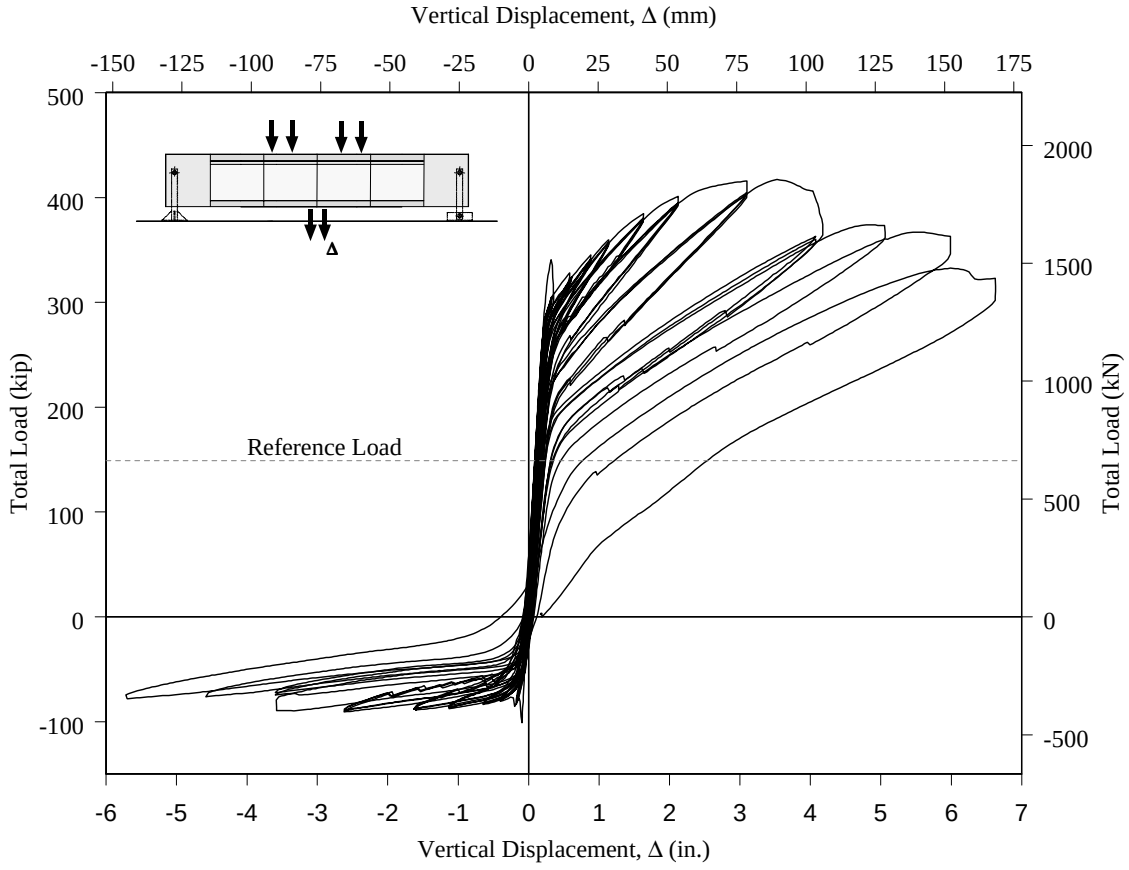


**Figure 3-24 History of total load versus displacement, Unit 100-EXT**

### 3.2.4 Test Unit 50-INT/50-EXT

The load-displacement response for Unit 50-INT/50-EXT is shown in Figure 3-25. In the downward direction the response was similar to the previous test units with internal tendons through the 4.0 in (102 mm) displacement cycle. Nonlinear response began around 360 kips (1,601 kN). The response in the upward loading direction was typical of test units without continuous reinforcement crossing the joints: little to no dissipation of energy and low load capacity. The equivalent viscous damping during the 3 in. (76.2 mm) displacement cycle was 3.87 percent. After the failure of the internal tendons the load was significantly lower and the displacements relatively large.

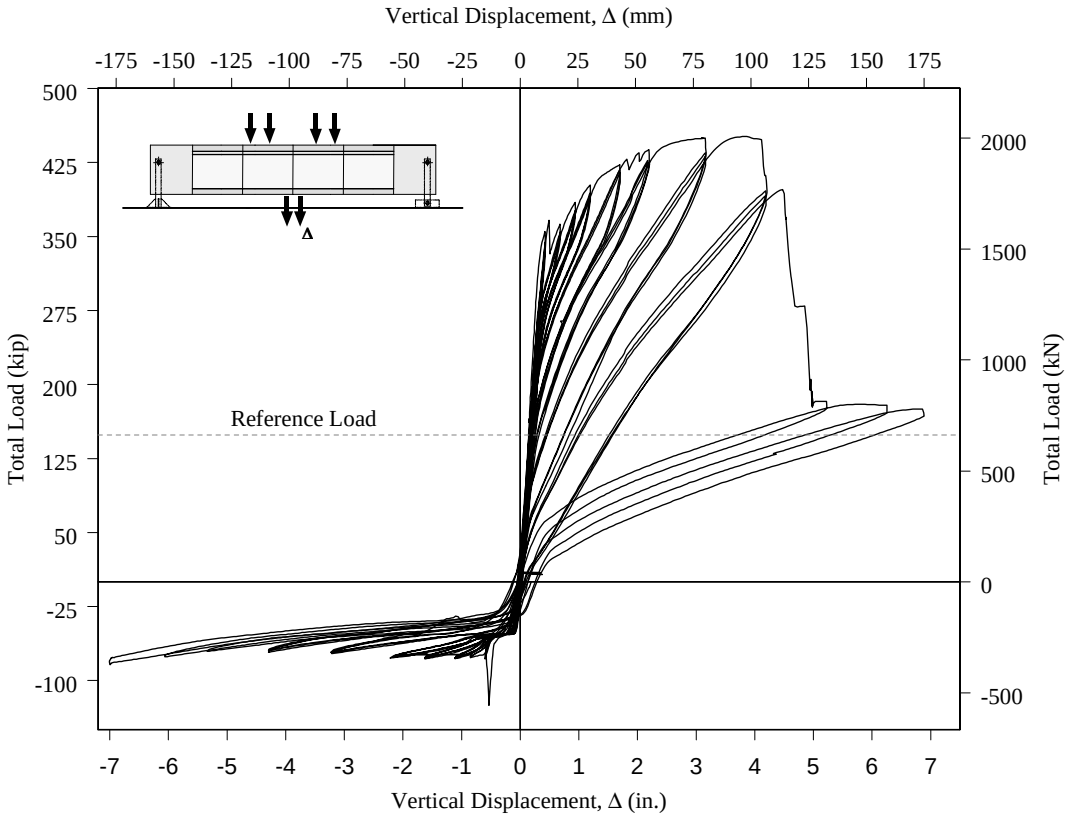


**Figure 3-25 History of total load versus displacement, Unit 50-INT/50-EXT**

## 3.3 Test Data

A selection of the test data is presented here for conciseness. The remaining data can be found in Appendix A.

### 3.3.1 Deflection Profiles

Deflection profiles for downward loading are shown below for all four units. Profiles for upward loading are shown at the –3.0 in. (-76.2 mm) displacement in Figure 3-26. The 3.0 in. (76.2 mm) displacement cycle was the last cycle for which there was deflection data for all units in the upward direction due to instrument malfunction. In all of the units except for 100-INT-CIP, only the center joint J3 opened during upward loading. As shown earlier linear potentiometers were placed six inches from either side of each joint to measure the vertical deflection at each point (see Figure 2-19).

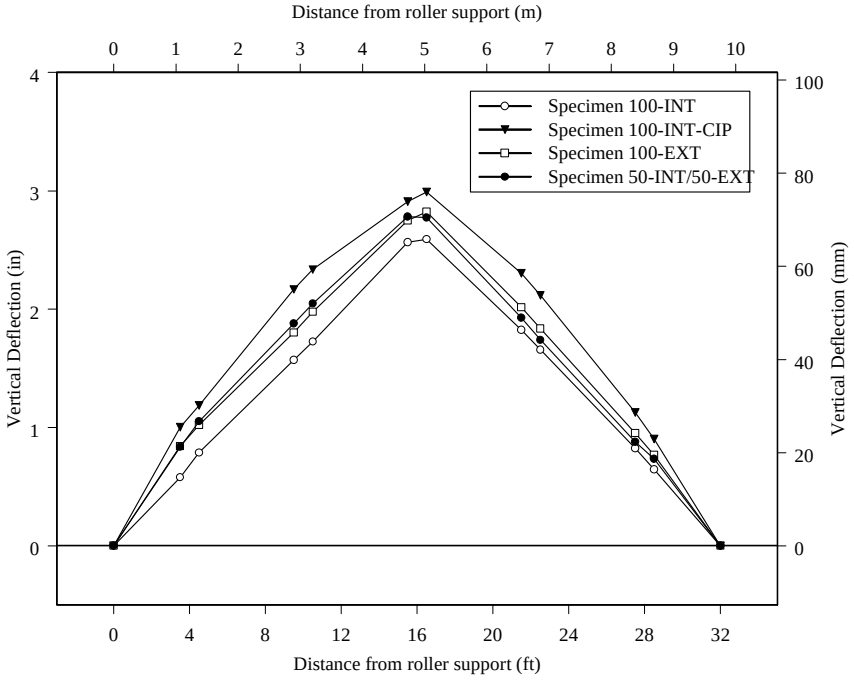


**Figure 3-26 Deflection profile during upward loading for all test units at -3.0 in. (-76.2 mm)**

**Test Unit 100-INT**

The deflection profile of downward loading for Unit 100-INT is shown in Figure 3-27. Opening of the three center joints J2, J3, and J4 is clearly evident in the deflection profile at 1.0 in. (25.4 mm) midspan displacement with a clear change in slope between segments. However, with the larger deflections much of the joint opening was focused at the center joint.

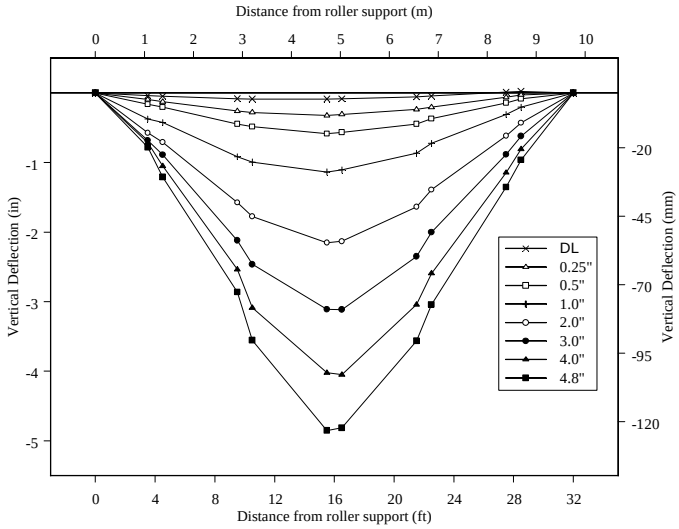


**Figure 3-27 Downward loading displacement profiles, Unit 100-INT**

**Test Unit 100-INT-CIP**

The displacement profiles for downward loading through the 4.0 in. (102 mm) displacement cycle are shown in Figure 3-28. Similar to Test Unit 100-INT, Figure 3-28 shows that at larger displacements joint J3 underwent significantly larger increases in opening compared to joints J2 and J4.

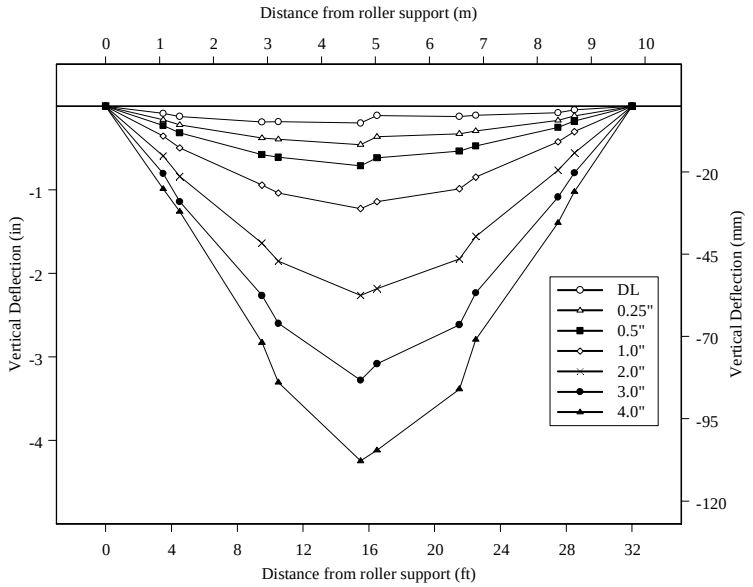


**Figure 3-28 Downward loading displacement profiles, Unit 100-INT-CIP**

**Test Unit 100-EXT**

The displacement profiles for downward loading are shown in Figure 3-29. The figure reflects the fact that only the center joint J3 opened during testing.

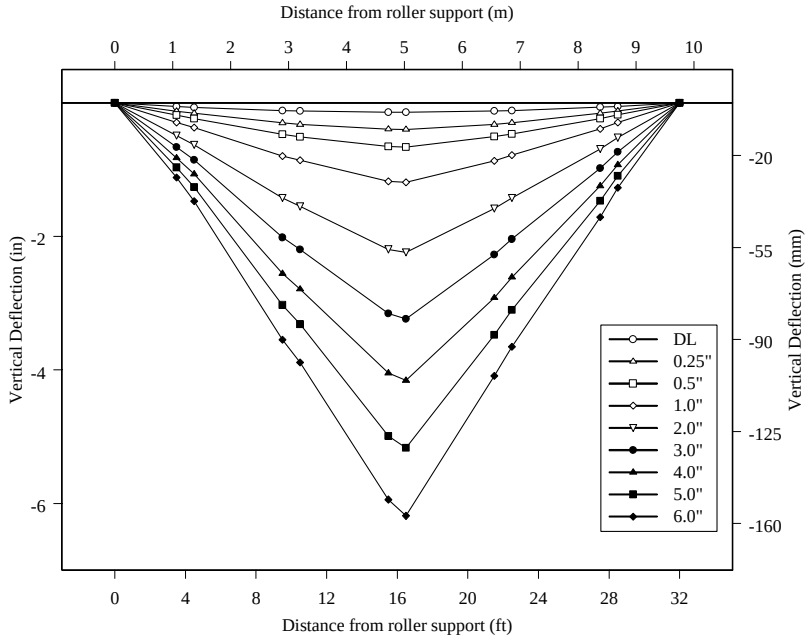


**Figure 3-29 Downward loading displacement profiles, Unit 100-EXT**

**Test Unit 50-INT/50-EXT**

The displacement profile for downward loading is shown in Figure 3-30. It is clear in the figure that the center joint J3 had the most significant opening compared to joints J2 and J4.

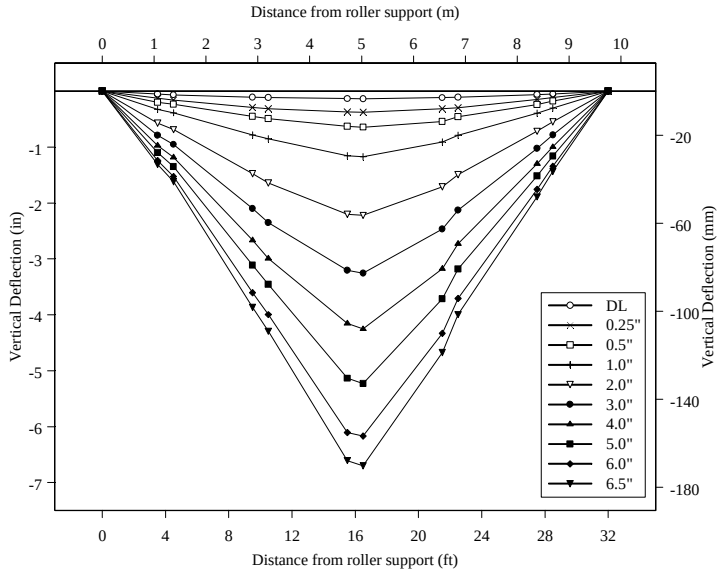


**Figure 3-30 Downward loading displacement profile, Unit 50-INT/50-EXT**

### 3.3.2 Joint Rotation

Joint rotations were measured by means of linear potentiometers on the top and bottom surface at each joint. The rotation at each joint was calculated by taking the difference between the horizontal potentiometers' readings; the difference in readings was then by the distance between them. In the event that one of the two potentiometers was damaged the measurement of the horizontal potentiometer that was attached to the web at the joints was used. In the case of Unit 100-EXT joint rotations were not available past the 5 in (127 mm) displacement cycle, but they could be determined from measurements of the vertical potentiometers placed below the bottom slab.

**Test Unit 100-INT**

Figure 3-31 shows the joint rotation in radians of joint 3 plotted versus the bending moment. The maximum rotation with downward loading, before failure, was 0.035 radians. With upward loading the maximum rotation was 0.044 radians.

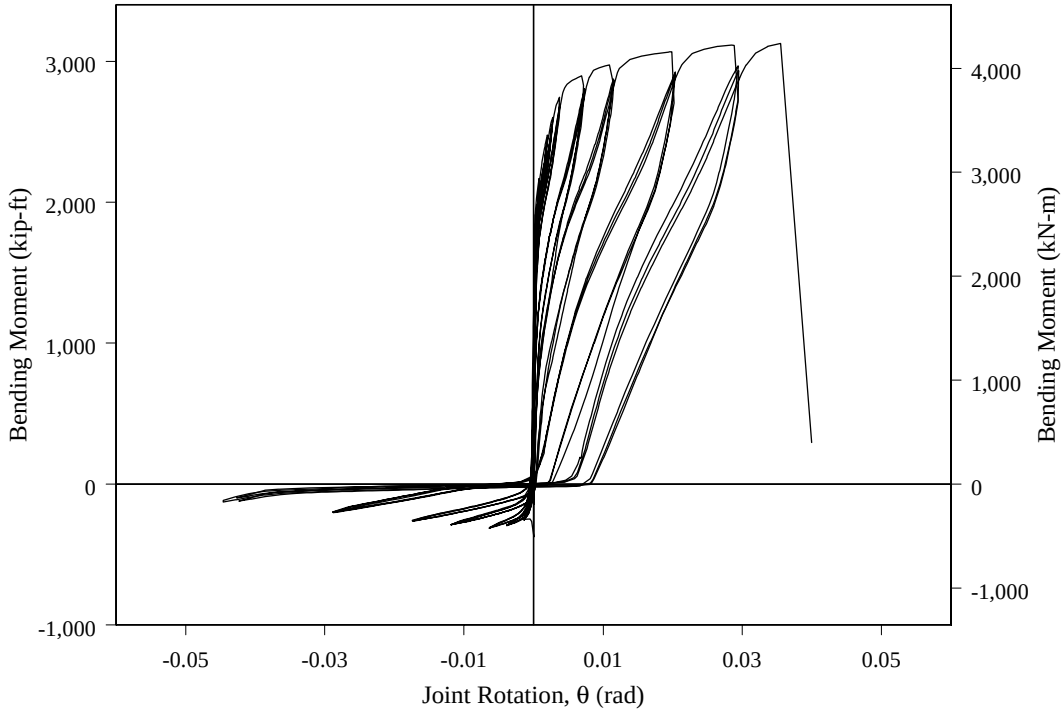


**Figure 3-31 Joint J3 rotation versus moment, Unit 100-INT**

Joint rotation for joint J2 is shown in Figure 3-32 plotted against bending moment. The figure reflects the fact that there was no opening of joint J2 in the upward direction and the maximum rotations in the downward direction were relatively small compared to joint J3. Joint J4 exhibited similar behavior to joint J2, the plot of J4 rotation can be found in Appendix A.

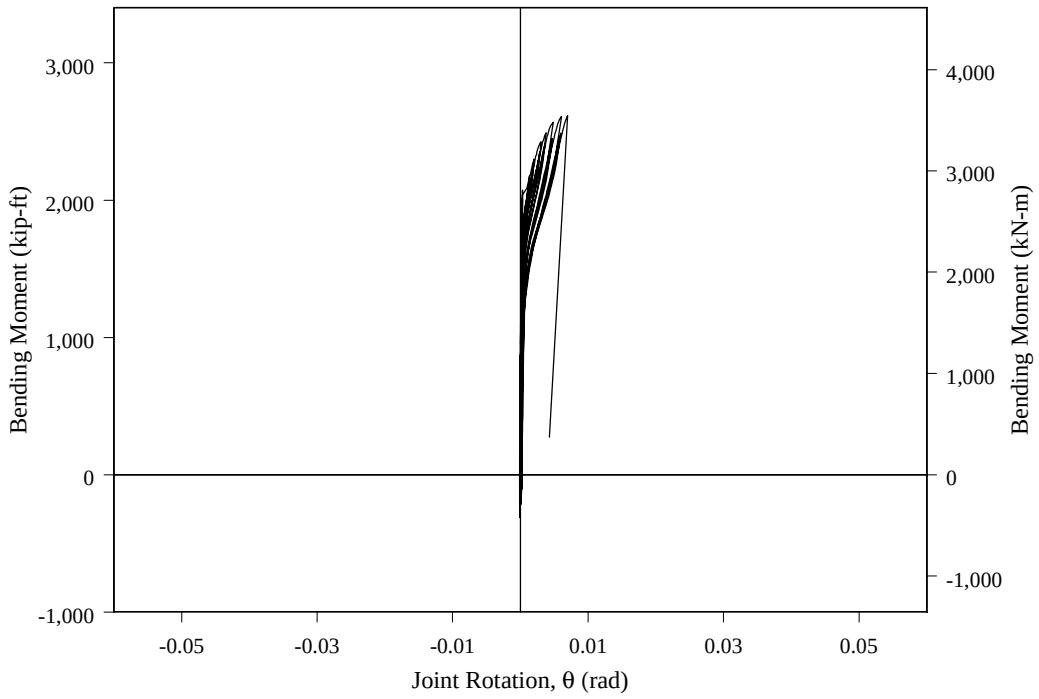


**Figure 3-32 Joint J2 rotation versus moment, Unit 100-INT**

**Test Unit 100-INT-CIP**

Joint J3 rotation versus bending moment is shown in Figure 3-33. The maximum rotation before failure in the downward direction was 0.039 rad. and in the upward direction 0.026 rad. The joint rotation under upward loading was significantly less than the maximum joint rotation of Unit 100-INT because of the reinforced cast-in-place deck closure joint in Unit 100-INT-CIP. The cast-in-place closure prevented wide opening of joint J3 under upward loading. The maximum rotation of joint J2 and J4 in the downward direction was 0.006 rad. and 0.008 rad., respectively; the minimum rotation was -0.004 rad. for both joints. The plot of J4 rotation versus moment is shown in Figure 3-34; the figure for J2 was very similar to that of J4 and can be found in Appendix A.

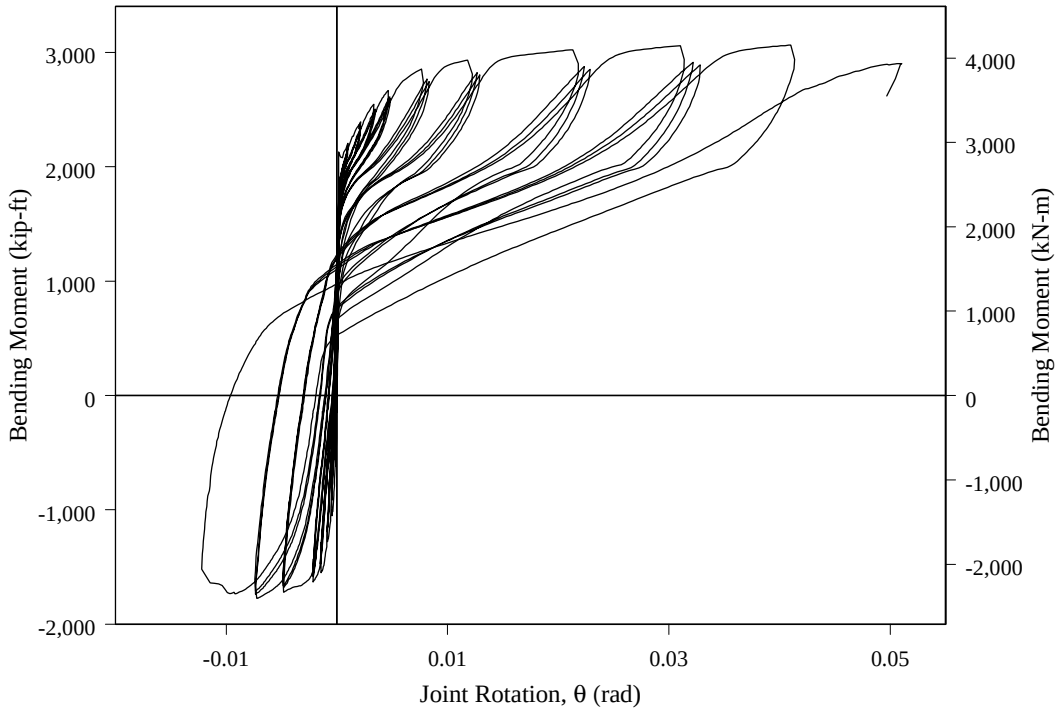


**Figure 3-33 Joint J3 rotation versus moment, Unit 100-INT-CIP**

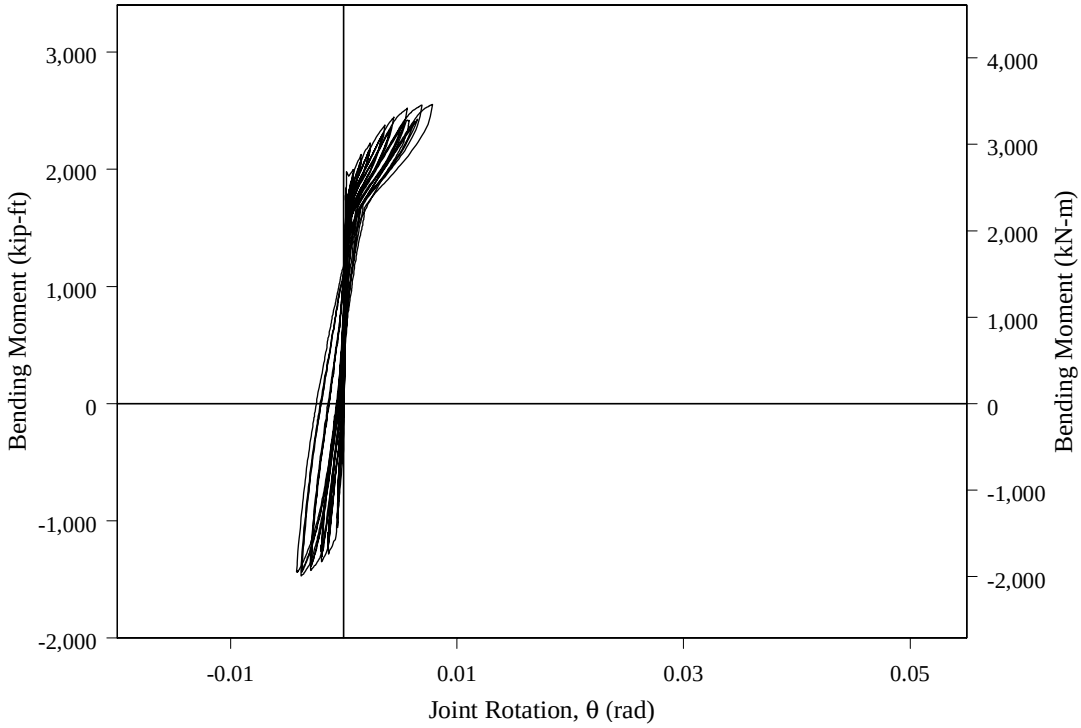


**Figure 3-34 Joint J4 rotation versus moment, Unit 100-INT-CIP**

**Test Unit 100-EXT**

Only joint J3 exhibited opening in Unit 100-EXT; joint rotation versus moment is shown in Figure 3-35. The maximum rotation measured during the 5.0 in. (127 mm) displacement cycle for the downward direction was 0.05 rad. and –0.047 rad. in the upward direction; all of the horizontal potentiometers were removed beyond this displacement. The large peak in the plot in the upward loading direction is a result of the instruments' removal. The maximum joint rotation was measured from the vertical potentiometers under the Unit, for downward loading this value was 0.065 rad. and –0.068 rad. for upward loading.

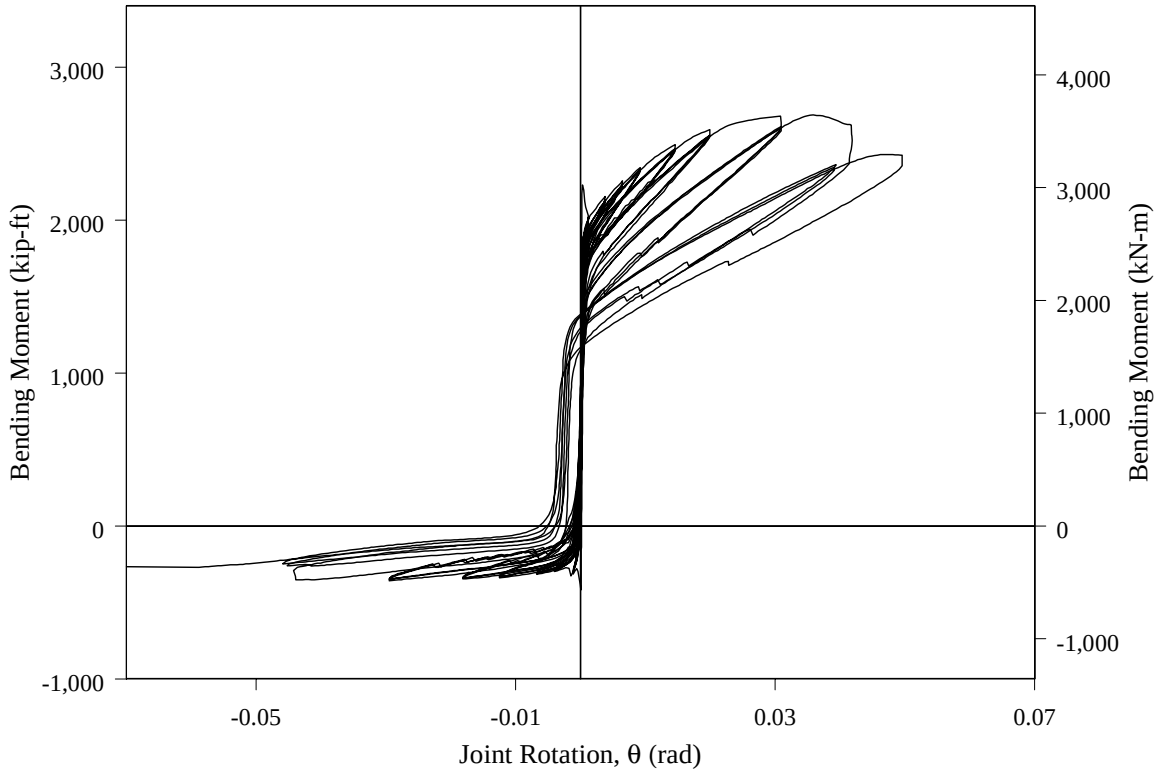


**Figure 3-35 Joint J3 rotation versus moment, Unit 100-EXT**

**Test Unit 50-INT/50-EXT**

The rotation of joint J3 plotted versus bending moment is shown in Figure 3-36. The maximum rotation under downward loading before the failure of the internal tendon was 0.04 rad. The maximum rotation under upward loading before failure of the internal tendon was -0.033 rad. The figure shows that the joint was able to undergo large rotations with only the external tendons intact.

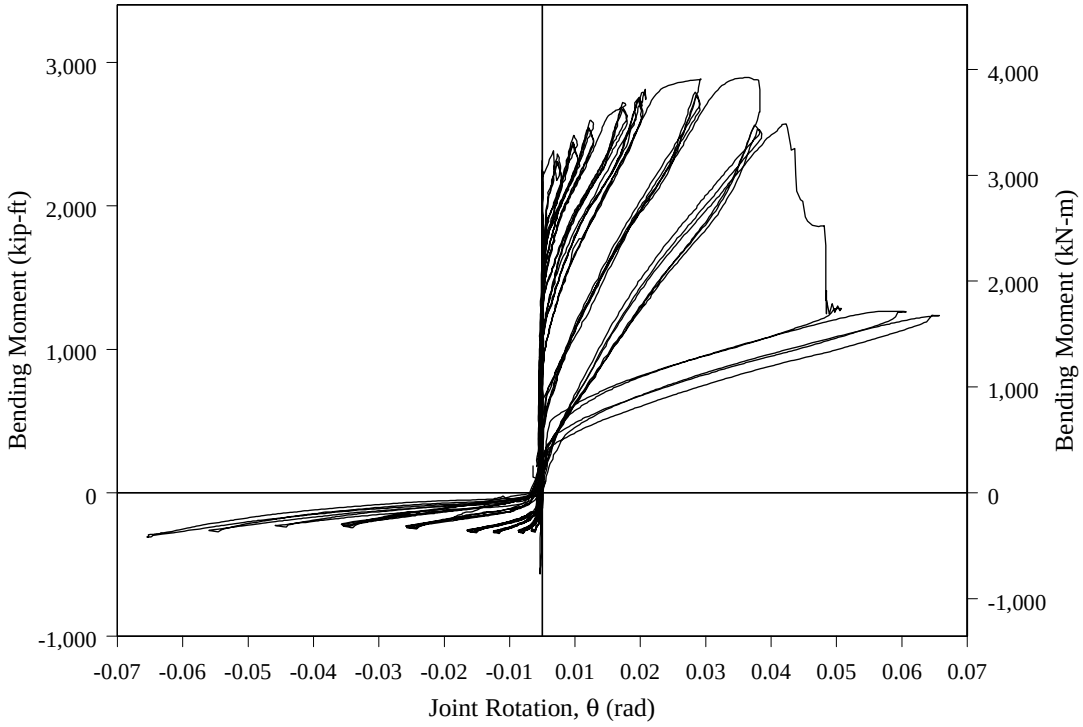


**Figure 3-36 Joint J3 rotation versus moment, Unit 50-INT/50-EXT**

## 3.4 Comparisons of Experimental Results of Different Test Units

Test data comparing the performance of the four test units is presented below.

### 3.4.1 Load-Displacement Comparisons

The load displacement envelopes for downward loading are shown in Figure 3-37 for all test Units. Unit 100-EXT exhibited superior ductility and a higher maximum displacement. The load carrying capacity of Unit 50-INT/50-EXT was nearly halfway between the capacities of Test Units 100-EXT and 100-INT. Table 3-1 summarizes the peak loads and maximum displacements before the failure of all four units.

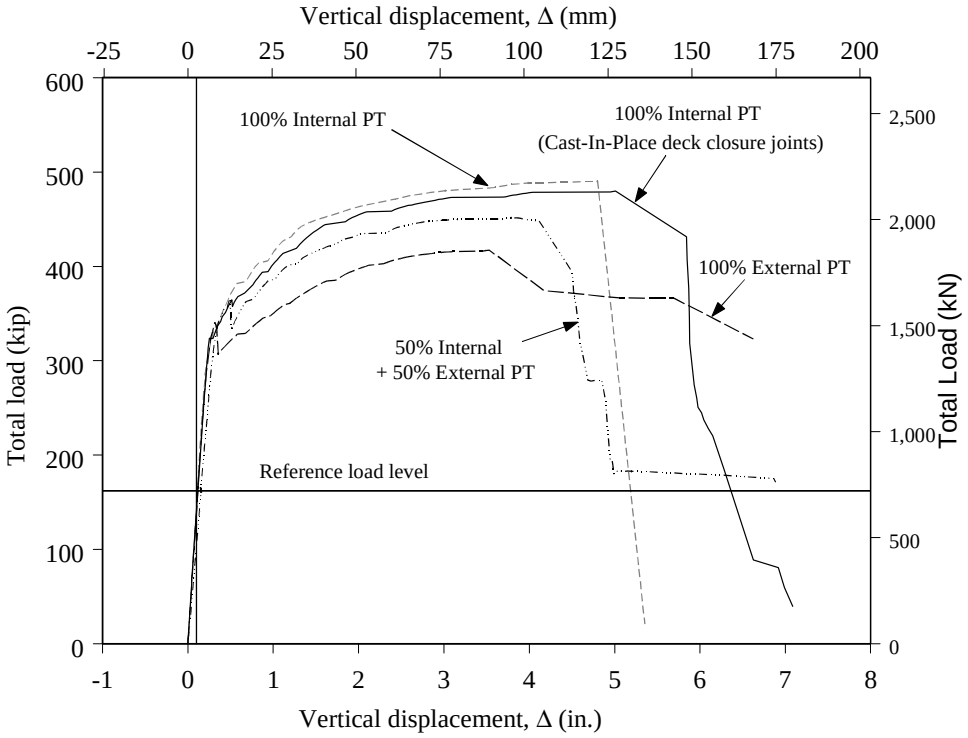


**Figure 3-37 Envelopes of load versus displacement for downward loading**

**Table 3-1 Peak loads and displacements (downward loading)**

| Unit | Peak Load | | Maximum Displacement | |
|---|---|---|---|---|
| | kip | kN | in | mm |
| 100-INT | 490 | 2180 | 4.8 | 122 |
| 100-INT-CIP | 480 | 2135 | 5.9 | 150 |
| 100-EXT | 417 | 1855 | 6.6 | 168 |
| 50-INT/50-EXT | 451 | 2006 | 3.8 | 97 |

Figure 3-38 shows the history of total load for Units 100-INT and 100-INT-CIP versus displacement. The variable of these two tests was the presence of mild reinforcement in the deck across the segment-to-segment joints. The maximum load capacity in the upward direction greatly increased from 93 kips (414 kN) for Unit 100-INT to 327 kips (1,455 kN) for Unit 100-INT-CIP. The figure reflects the effect on the hysteretic behavior by the addition of longitudinal reinforcement across the joints. As mentioned earlier the energy dissipation ability of Unit 100-INT-CIP was much greater than 100-INT. However the cast-in-place deck closure joints similar to the ones in Unit 100-INT-CIP complicate the precast segmental construction concept and slow down the construction; the construction costs are consequently increased. The equivalent damping coefficients at the 3 in. (76.2 mm) displacement cycle for Units 100-INT and 100-INT-CIP were 8.75 and 4.21 percent, respectively.

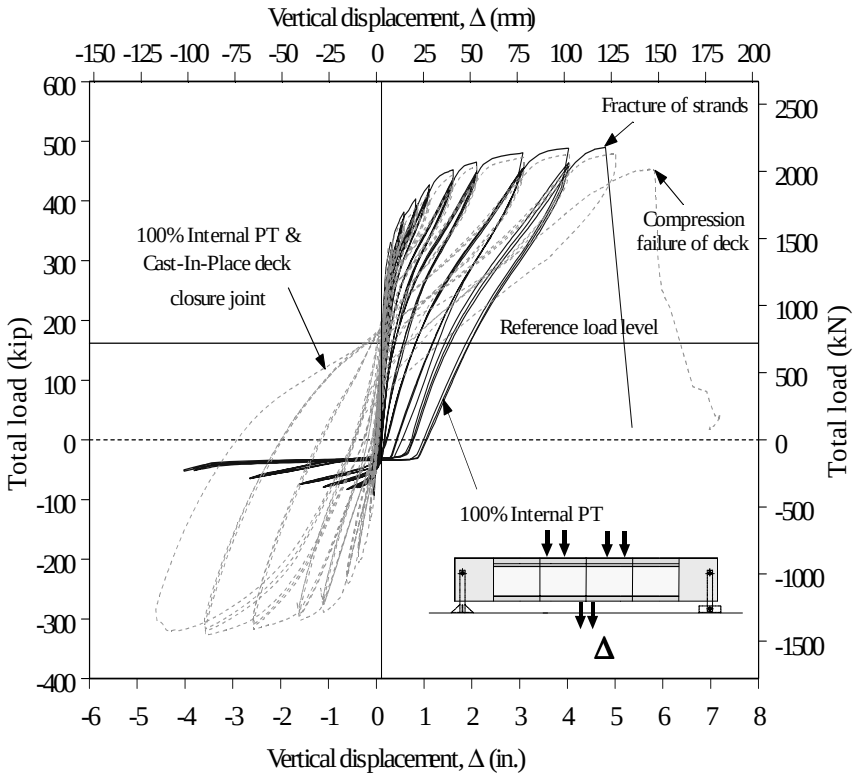


**Figure 3-38 History of total load versus displacement, Units 100-INT and 100-INT-CIP**

The plots of the load-displacement histories for Units 100-INT, 100-EXT, and 50-INT/50-EXT are shown in Figure 3-39. The test variable in these units was the ratio of internal to external post-tensioning. Again, Unit 100-EXT showed a more ductile response and larger displacement capacity than its counterparts with internal tendons. Unit 50-INT/50-EXT had a lower load capacity and lower displacement capacity than 100-INT. The internally bonded tendon in Unit 50-INT/50-EXT picked up high forces with respect to the internally bonded tendons in Units 100-INT and 100-INT-CIP; thus the internally bonded tendon in Unit 50-INT/50-EXT failed at lower displacement compared to the other test units.

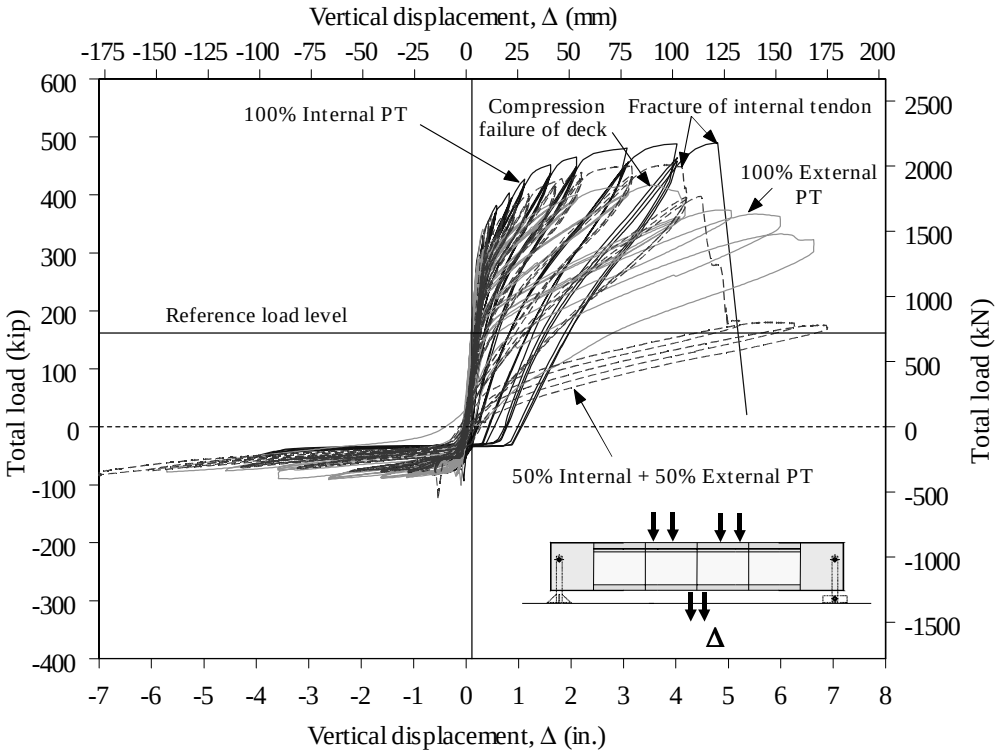


**Figure 3-39 Load versus displacement for Units 100-INT, 100-EXT and 50-INT/50-EXT**

### 3.4.2 Permanent Residual Displacements

One of the important seismic performance issues is the permanent residual displacement of the superstructure after earthquake occurrence. Residual displacement, $\Delta_r$, were measured for all Phase I test units during the displacement cycle to $\Delta$ = +3.0 in. (76.2 mm). Figure 3-40 shows the seismic load versus displacement, $\Delta$, during the downward loading portion of the 3.0 in. (76.2 mm) displacement cycle for all test units. The midspan joint of the four units is shown at the peak of the 3 in. (76.2 mm) downward displacement cycle in Figure 3-41 to Figure 3-44. The horizontal solid line shown in Figure 3-40 represents the reference load level, or zero seismic loads. The displacement measured during the unloading portion, of any of the curves shown in Figure 3-40, at zero seismic load (i.e. at the reference load level) represents the permanent residual

displacement, $\Delta_r$. Values of $\Delta_r$ measured after 3.0 in. (76.2 mm) maximum displacement of all test units are also given in Table 3-2. The values of $\Delta_r$ for all test units are normalized to the residual displacement of Unit 100-EXT, $\Delta_{ref}$ (= 0.14 in. = 3.56 mm). The ratio $\Delta_r/\Delta_{ref}$ is given in Table 3-2 for all test units.

Comparison of the $\Delta_r/\Delta_{ref}$ values given in the table indicates that permanent residual displacements can be minimized by use of 100 external post-tensioning. This is because the strains in external tendon are significantly less than the corresponding strains in internally bonded tendons. Inelastic strains in internally bonded tendons result in loss of the prestressing force, large permanent displacements and joint openings. Comparison of $\Delta_r/\Delta_{ref}$ values given in Table 3-2 for Units 100-INT and 100-INT-CIP also indicates that use of cast-in-place deck closure in segment-to-segment joints will reduce the permanent residual displacements.

### 3.4.3 Energy Dissipation and Damping Coefficients

Viscous damping coefficient, ., can be considered as a measure of energy dissipation capability of the test units. The viscous damping coefficient is determined by Eq. (3-1) that relates the area within the hysteresis loop of the 3.0 in. (76.2 mm) displacement cycle to that of the elastic strain energy. The values of . are given in Table 3-2. The viscous damping coefficient for all test units is normalized to the damping coefficient of Unit 100-EXT, $._{Ref}$ ($._{Ref}$ = 2.63%). The values of ($./._{Ref}$) given in the table indicate that cast-in-place deck closure joints result in highest energy dissipation capability and damping coefficient among all test unit. The lowest energy dissipation

capability and damping coefficient was observed for Unit 100-EXT with only external tendons. High-energy dissipation capability of the superstructure may not be a design target since plastic hinging is anticipated in the columns, rather than in the superstructure.

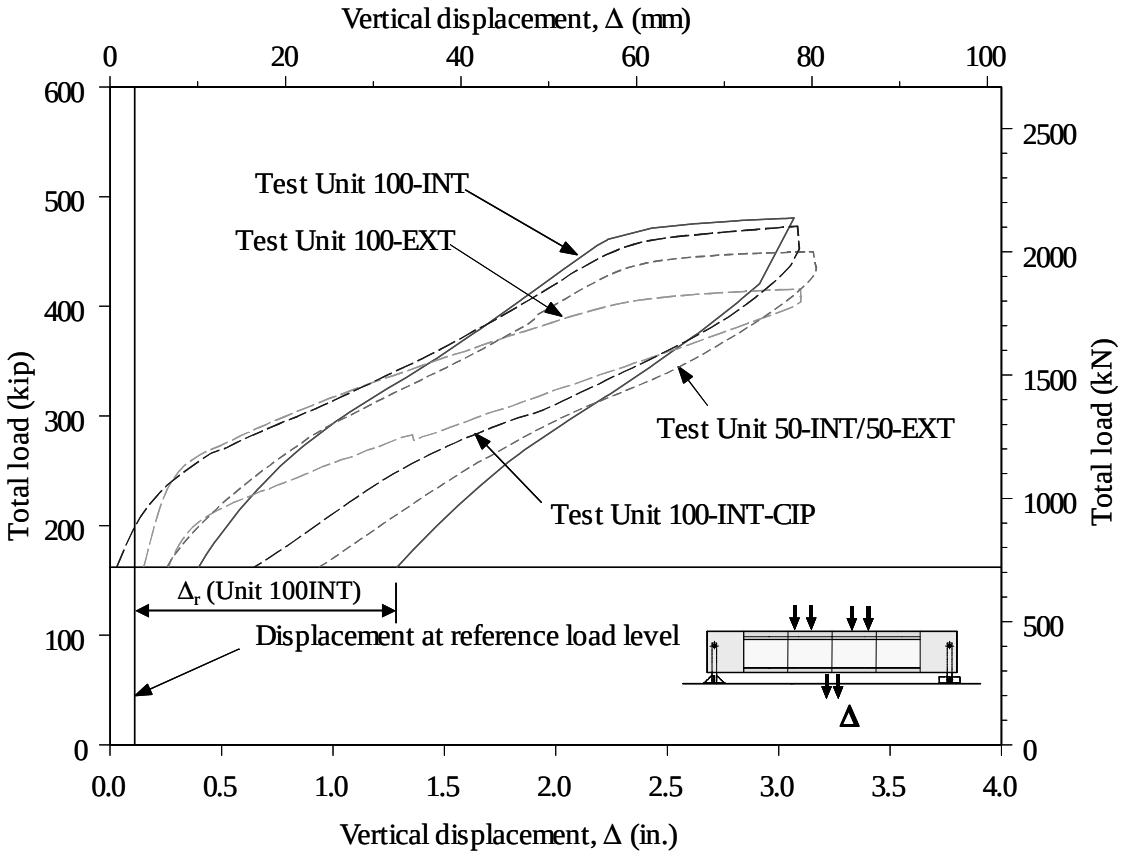


**Figure 3- 40 Downward load versus displacement, 3 in. (76.2 mm) cycle only**

**Table 3-2 Residual displacements and damping coefficients, 3 in. (76.2 mm) cycle**

| Unit | $\Delta_r$ in | $\Delta_r$ mm | $\Delta_r/\Delta_{ref}$ | $\zeta$ | $\zeta/\zeta_{ref}$ |
|---|---|---|---|---|---|
| 100-INT | 1.17 | 29.7 | 8.36 | 4.21 | 1.60 |
| 100-INT-CIP | 0.53 | 13.5 | 3.79 | 8.75 | 3.33 |
| 100-EXT | 0.14 | 3.56 | 1.00 | 2.63 | 1.00 |
| 50-INT/50-EXT | 0.82 | 20.8 | 5.86 | 3.87 | 1.47 |


**Figure 3-41 Joint J3 in Unit 100-INT at Δ =+3 in. (76.2 mm)**

**Figure 3-42 Joint J3 in Unit 100-INT-CIP at Δ =+3 in. (76.2 mm)**

**Figure 3-43 Joint J3 in Unit 100-EXT at Δ =+3 in. (76.2 mm)**

**Figure 3-44 Joint J3 in Unit 50-INT/50-EXT at Δ =+3 in. (76.2 mm)**

### 3.4.4 Tendon Strains

There was a marked difference in behavior between internal and external tendons. Internal tendons exhibited much higher strains than their external counterparts. Unit 50-INT/50-EXT adheres to the current guidelines that allow combining both internal and external tendons. Results of Unit 50-INT/50-EXT demonstrated that the strains in the internally bonded tendons are much higher than those of 100% internal or 100% external post-tensioning. This is illustrated in the following two figures. A dashed line represents the yield strain; this strain corresponds to the stress level at which a permanent inelastic strain of 0.2 percent occurs upon unloading of the tendon. Figure 3-45 compares the strain data available for the internal tendons in Units 100-INT-CIP and 50-INT/50-EXT.

Unfortunately, the strain gages placed on the internal tendon of Unit 100-INT were damaged; however the strains in the internal tendons in Units 100-INT and 100-INT-CIP were very similar as evidenced by the experimental failure load of both test units and by the finite element analyses results (Chapter 4). The strain in the internal tendon in Unit 50-INT/50-EXT reached the yield strain of approximately 10,430 micro strain during the 1.0 in. (25.4 mm) displacement cycle, while the tendon of Unit 100-INT-CIP didn't reach yield until the 2.0 in. (50.8 mm) cycle. The increased strain led Unit 50-INT/50-EXT to fail by rupture of the internal tendon well before the units with 100% internal tendons. High inelastic strains in internally bonded tendons resulted in a loss of prestressing force and large displacements and joint openings.

Figure 3-46 shows the comparison between the external tendons in Units 100-EXT and 50-INT/50-EXT. The external tendons in both Units remained intact through the completion of testing. It should be remembered that the external tendons in Test Units

100-EXT and 50-INT/50-EXT were not grouted. However as mentioned earlier, grouting of the external tendons in the test units would have had no influence on the experimental results. The change in external tendon stresses during the first stage of the test, i.e. up to reference load level and before application of fully reversed cyclic displacements in the seismic test, exceeded 3 ksi (20.7 MPa), which would be sufficient to fully crack the grout if the external tendons were grouted.

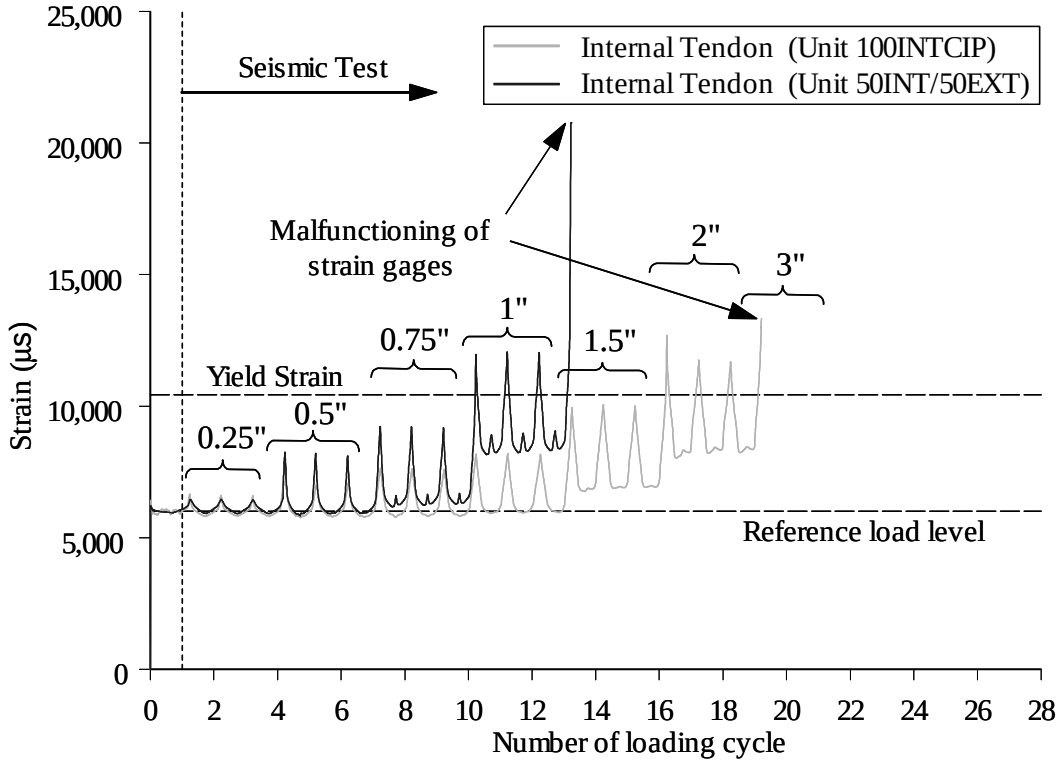


**Figure 3-45 Strain history of internal tendons in Units 100-INT-CIP and 50-INT/50-EXT**

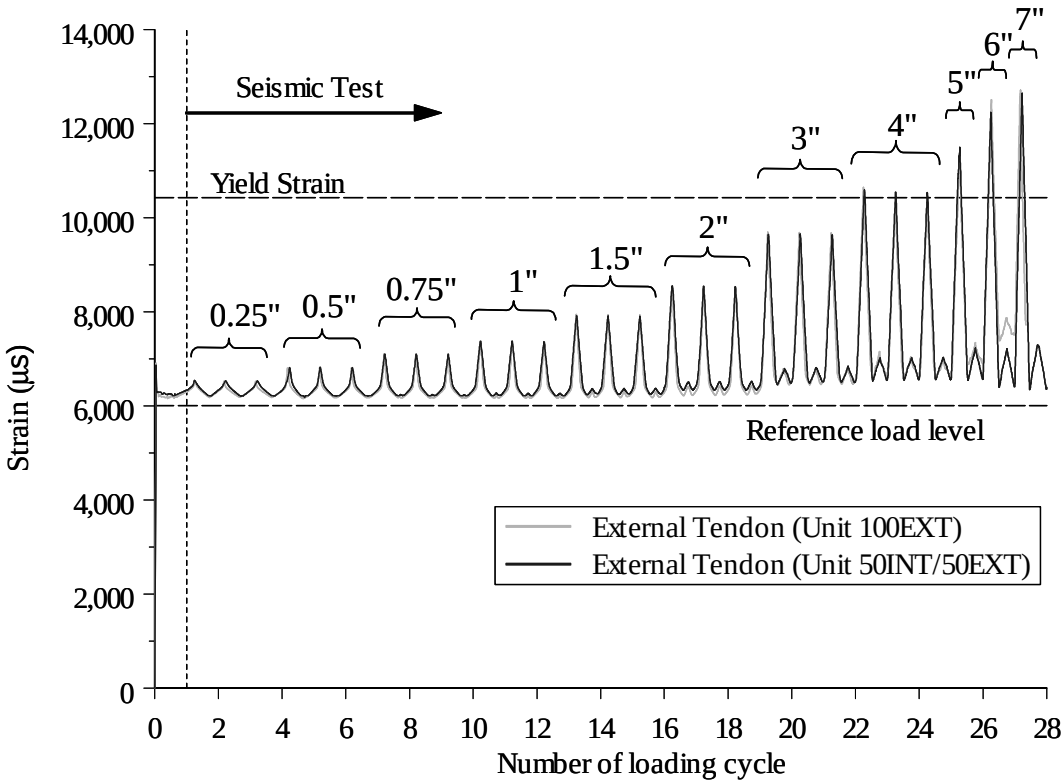


**Figure 3-46 Strain history of external tendons in Units 100-EXT and 50-INT/50-EXT**

### 3.4.5 Cracking Strength

The concrete cracking strength at joint locations was determined using the known section properties of the test units, the experimental flexural moments at onset of cracking, or joint opening, and the measured effective prestressing force. The midspan Joint J3 in Unit 100-INT opened under downward loading when the concrete reached a tensile stress of 3.25 $\sqrt{f_c'}$ (psi) [= 0.27 $\sqrt{f_c'}$ (MPa)]. Opening of the joint occurred by cracking in the concrete cover adjacent to the segment-to-segment joint, rather than by opening of the epoxy bonded joint itself. This indicates that the slow-set segmental bridge

adhesive (epoxy) used in construction of the test units, and in construction of precast segmental bridges, has higher tensile strength than the relatively weak adjacent concrete cover. Joint J3 in Unit 100-INT-CIP opened at a concrete tensile stress of 5.61 $\sqrt{f_c'}$ (psi) [= 0.47 $\sqrt{f_c'}$ (MPa)]. It should be mentioned that no tensile stresses are allowed to occur under service loads according to Section 9.2.2.2 of the AASHTO Guide Specifications for Design and Construction of Segmental Concrete Bridges.[1] Cracking of the top surface in Unit 100-INT-CIP occurred at a concrete tensile stress of about 4.00 $\sqrt{f_c'}$ (psi ) [= 0.33 $\sqrt{f_c'}$ (MPa)], which was relatively low considering the continuity of the deck. The onset of cracking occurred in the deck at the interface between the precast concrete and that of the cast-in-place deck closure joint. The relatively weak interface between the precast and cast-in-place concretes resulted in this relatively low cracking strength.

The midspan Joint J3 in Unit 100-EXT opened when the concrete reached tensile stresses of 4.50 $\sqrt{f_c'}$ (psi) [= 0.37 $\sqrt{f_c'}$ (MPa)] and 3.92 $\sqrt{f_c'}$ (psi) [= 0.33 $\sqrt{f_c'}$ (MPa)] under downward and upward loading, respectively. The midspan Joint J3 in Unit 50-INT/50-EXT opened when the concrete reached tensile stresses of 7.33 $\sqrt{f_c'}$ (psi) [= 0.61 $\sqrt{f_c'}$ (MPa)] and 4.73 $\sqrt{f_c'}$ (psi) [= 0.39 $\sqrt{f_c'}$ (MPa)] under downward and upward loading, respectively.

There is considerable scatter in the concrete tensile strength determined as described above for all test units. However the above-mentioned results indicate that a tensile strength of 3.00 $\sqrt{f_c'}$ (psi) [= 0.25 $\sqrt{f_c'}$ (MPa)] should be used in design. For precast segmental bridges with cast-in-place deck closure joints, potential cracks may

occur at the interface between concrete of the precast segments and concrete of the CIP deck closure because of the relatively weak interface between the precast and CIP concretes. Based on the experimental results of Unit 100-INT-CIP, a concrete cracking strength of 4.00 $\sqrt{f_c'}$ (psi ) [= 0.33 $\sqrt{f_c'}$ (MPa)] is recommended for design in this case.

### 3.4.6 Flexural Moment Capacity

According to the AASHTO Guide Specifications[1], the flexural moment capacity of precast segmental bridges should be calculated using provisions of Section 9.17 of the AASHTO Standard Specifications[5] in addition to provisions of Section 11.2 of the AASHTO Guide Specifications[1]. According to the AASHTO Standards[5], the design flexural strength of rectangular or flanged section in which the neutral axis lies within the flange shall be calculated using the following equation:

$$M_n = \phi \left[ A_{ps}\ f_{su}\ d_p \left( 1 - 0.6 \frac{A_{ps}\ f_{su}}{b\ d_p\ f_c'} \right) \right] \qquad (3\text{-}2)$$

in which $M_n$ is the flexural moment capacity; $\phi$ is the strength-reduction factor ($\phi$ = 1.00 for evaluation of experimental results); $A_{ps}$ is the total area of prestressing steel ($A_{ps}$ = 3.47 in.$^2$ = 2,240 mm$^2$ for all test units); $f_{su}$ is the average stress in prestressing steel at ultimate load; $d_p$ is the distance from extreme compressive fiber to centroid of the prestressing force ($d_p$ = 40 in. = 1.02 m in all test units); $b$ is width of section ($b$ = 108 in. = 2.74 m in all test units); and $f_c'$ is the concrete compressive strength (see Table 2-5). The average stress in internally bonded tendons (Test Units 100-INT, 100-INT-CIP and 50-INT/50-EXT) is calculated by the following equation[5]:

$$f_{su} = f_{pu}\left(1 - 0.5\frac{A_{ps}\ f_{pu}}{b\ d_p\ f_c'}\right) \qquad (3\text{-}3)$$

in which $f_{pu}$ is the ultimate tensile strength ($f_{pu}$ = 270 ksi = 1,862 MPa). The average stress in external (unbonded) tendons is calculated by the following equation:

$$f_{su} = f_{se} + 900\left(\frac{d_p - c_y}{\left(l_i\ /\left[1 + 0.5\ N_s\right]\right)}\right) \ \leq\ f_{py} \qquad (3\text{-}4)$$

in which $f_{se}$ is the effective prestressing steel stress after losses; $c_y$ is neutral axis depth from the extreme compressive fiber; $l_i$ is length of the tendon between anchorages ($l_i$ = 25 ft = 7.62 m for the external tendons in Units 100-EXT and 50-INT/50-EXT); $N_s$ is the number of support hinges crossed by the external tendons ($N_s$ = 0 for Units 100-EXT and 50-INT/50-EXT); and $f_{py}$ is the yield stress of the strands ($f_{py}$ = 0.90 $f_{pu}$ = 243 ksi = 1676 MPa).

The calculated flexural moment capacity of all test units, $M_n$, is given in Table 3-3. The experimental peak flexural moment at midspan, $M_{Test}$, as well as the ratio ($M_{Test}/M_n$) are also given in Table 3 for all test units. The flexural moment capacity, $M_n$, was calculated using Eqs. (3-2) to (3-4). Values of the ratio ($M_{Test}/M_n$) were close to 1.00 for all test units, indicating that the flexural moment capacity of precast segmental bridge superstructures can be reasonably estimated using provisions of the AASHTO Standard Specifications[5] and the AASHTO Guide Specifications[1] (Eqs. 3-2 to 3-4).

The ratio ($M_{Test}/M_n$) was slightly less than 1.00 for Unit 100-EXT with external tendons only. This slightly low value of ($M_{Test}/M_n$) for this test unit was due to the change in geometry of the cross section as the test unit experienced vertical deflection whereas the external tendons essentially remained horizontal. This resulted in reduction of the

internal moment arm between the tendons and centroid of the compressive stress block at the midspan section; this reduction in the internal moment arm was not considered in calculation of $M_n$ for Unit 100-EXT.

**Table 3-3 Experimental and calculated flexural moment capacity of test units (Phase I)**

| Unit | $M_{Test}$ kip-ft (kN-m) | $M_n$ kip-ft (kN-m) | $M_{Test} / M_n$ |
|---|---|---|---|
| 100-INT | 3126 (4238) | 2993 (4057) | 1.04 |
| 100-INT-CIP | 3062 (4152) | 2974 (4032) | 1.03 |
| 100-EXT | 2688 (3644) | 2732 (3704) | 0.98 |
| 50-INT/50-EXT | 2894 (3924) | 2867 (3888) | 1.01 |

# 4 Analytical Research of Segment-to-Segment Joints Subjected to High Bending Moments and Low Shears (Phase I)

## 4.1 Finite Element Models

In addition to the experimental testing two analytical models were developed for each test Unit[10]. These models were developed to better understand the behavior of precast segmental bridges so they could later be used to predict the response of these bridges.

A two-dimensional model was used to determine the seismic demands on the segment-to-segment joints in the prototype structure. The models were subjected to various vertical component time histories, which have been used in design of the Benecia-Martinez Bridge in California, to obtain joint displacements, joint rotations, and tendon behavior. These input motions were obtained from TYLIN International, San Francisco, California. Results of the time-history analyses showed very small demands on openings of the segment-to-segment joints. The maximum joint rotations from the experiments were in the order of 30 times the demands obtained from the time-history analyses. The analyses were performed for the prototype structure, which had short spans, under the effect of vertical earthquake acceleration only. It is believed that higher demands on joint rotations would be expected if time-history analyses were performed for long-span bridges under combined longitudinal and vertical seismic input motions. However, the maximum demands on joint rotations will never exceed the joints' rotational capacities determined from the experiments. In the third phase of the research project on seismic performance of precast segmental bridges, extensive nonlinear time-

history analyses will be performed under the combined effects of gravity load, longitudinal and vertical seismic input motions. Several prototype precast segmental bridges with different geometry and post-tensioning layout, constructed using both the span-by-span and the balanced cantilever methods, will be designed and analyzed to obtain accurate information on the seismic demands on joint displacements and rotations.

Three-dimensional finite element models were developed to predict the response of the Phase I test units; the loading application and boundary conditions for the 3-D model are shown in Figure 4-1. Detailed finite element models were developed for all test units. Analyses were performed using the general-purpose finite element program ABAQUS,[11] interfaced with the ANACAP[12] concrete material model.

The concrete was modeled as 3-D, 8-node, solid brick elements with strain-hardening and strain-softening capabilities in compression, and tension cutoff with cracks that do not heal upon closure[12]. Confinement effects were assumed to be negligible and the unconfined concrete strength was taken as 7.5 ksi (51.7 MPa). The model was developed in a similar way to the test units, with no solid elements crossing the joints between the precast segments and no connection between solid elements on either side of the joints. The joints were free to open by providing double nodes and compression-only springs at all nodes in the cross-section at locations of joints. Prestressing steel was modeled by truss elements and connected to the concrete nodes at each 12-in. (305 mm) cross section, representing bonded strands.

External tendons were also modeled by truss elements connected to the solid blocks in the precast end segments (Segments 1 and 6 in Figure 2-6). Beyond 2.0 in. (50.8 mm) displacement in the upward loading direction, the bottom slab of Test Units 100-EXT and

50-INT/50-EXT started to come in contact with the external tendons; this contact was achieved by gap elements in the finite element models. The ultimate tensile strength of the prestressing steel was assumed to be 270 ksi (1,862 MPa) and the corresponding ultimate strain was assumed to be 0.04. The following stress-strain relationship[13] was adopted in the finite element analyses:

$$f_{ps} = E_{ps}\,\varepsilon_{ps}\left\{0.025 + \frac{0.975}{\left[1 + \left(118\,\varepsilon_{ps}\right)^{10}\right]^{0.1}}\right\} \qquad (4\text{-}1)$$

Where $\varepsilon_{ps}$ is the tendon strain, $f_{ps}$ is the tendon stress and $E_{ps}$ is the elastic modulus of the strands.

All mild steel reinforcement was modeled as 1-D sub-elements in the solid concrete elements. No mild steel reinforcement crossed the joints of Unit 100-INT. Test Unit 100-INT-CIP with the cast-in-place deck joint, required mild steel reinforcing bars to be placed across the joints at the deck level; these mild steel bars were activated and yielded under upward loading of the test unit. At the joints, the prestressing steel was not connected to the center nodes, but to nodes at sections 12 in. (305 mm) on either side of the centerline. This represented an idealized unbonded length at the joints of 24 in. (610 mm). Loading was applied to the models in displacement control as shown in Figure 2-20.

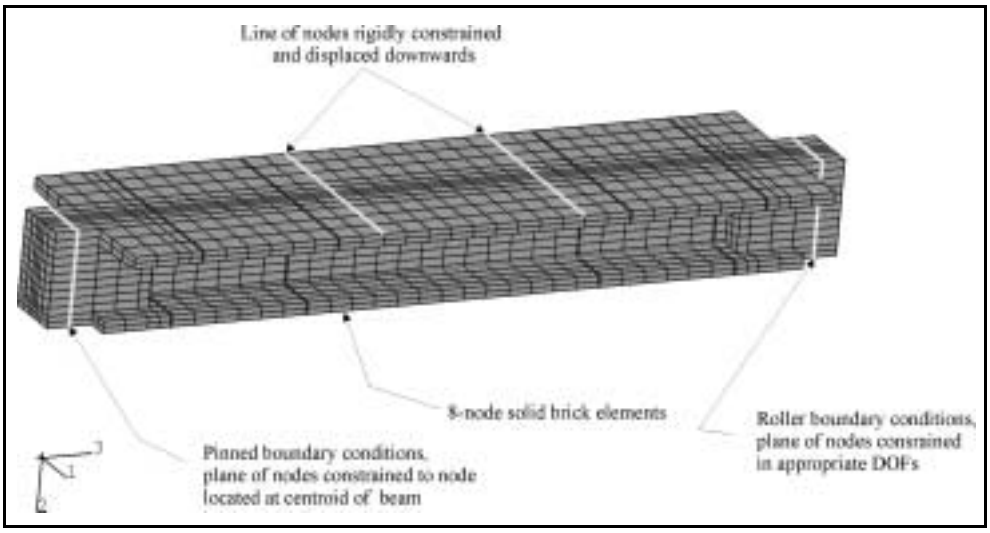


**Figure 4-1 Boundary conditions and loading application for 3-D model**

## 4.2 Results

Below are the results of the finite element analyses; additional strain contour plots for all test units can be found in Appendix A.

### 4.2.1 Test Unit 100-INT

The finite element model for Test Unit 100-INT was able to closely match the experimental behavior of the test unit as evidenced in Figure 4-2. The predicted failure displacement was 4.5 in. (114 mm) compared to the experimental value of 4.8 in. (122 mm), while the predicted ultimate load was 460 kips (2,046 kN) compared to the actual value of 490 kips (2,180 kN).

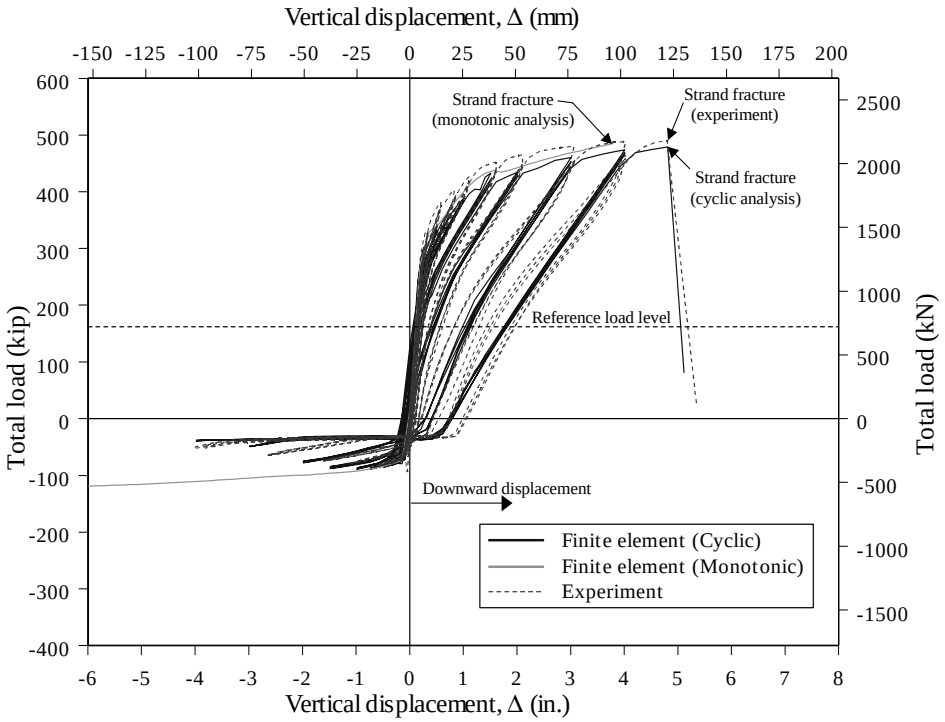


**Figure 4-2 Load versus displacement analysis results for Unit 100-INT**

A very useful feature of the analytical modeling is the ability to predict the behavior of the post-tensioning steel. In the case of Unit 100-INT all the steel tendon strain gages were lost before the start of testing so the analytical predictions became especially valuable. The post-tensioning steel strain and stress histories at joint J3 from the finite element analyses are shown in Figure 4-3 and Figure 4-4, respectively. Figure 4-3 shows that the tendon exhibits elastic behavior through the 1.0 in. (25.4 mm) cycles as the strain returns to its initial state upon unloading. Beyond the 1.0 in. (25.4 mm) displacement cycle, however, the tendon begins to exhibit inelastic behavior; the tendon elongates and undergoes permanent deformation. As this plastic elongation increases with each displacement cycle the prestressing force in the tendon decreases, reducing to zero by the 4 in. (102 mm) cycles (see Figure 4-4).

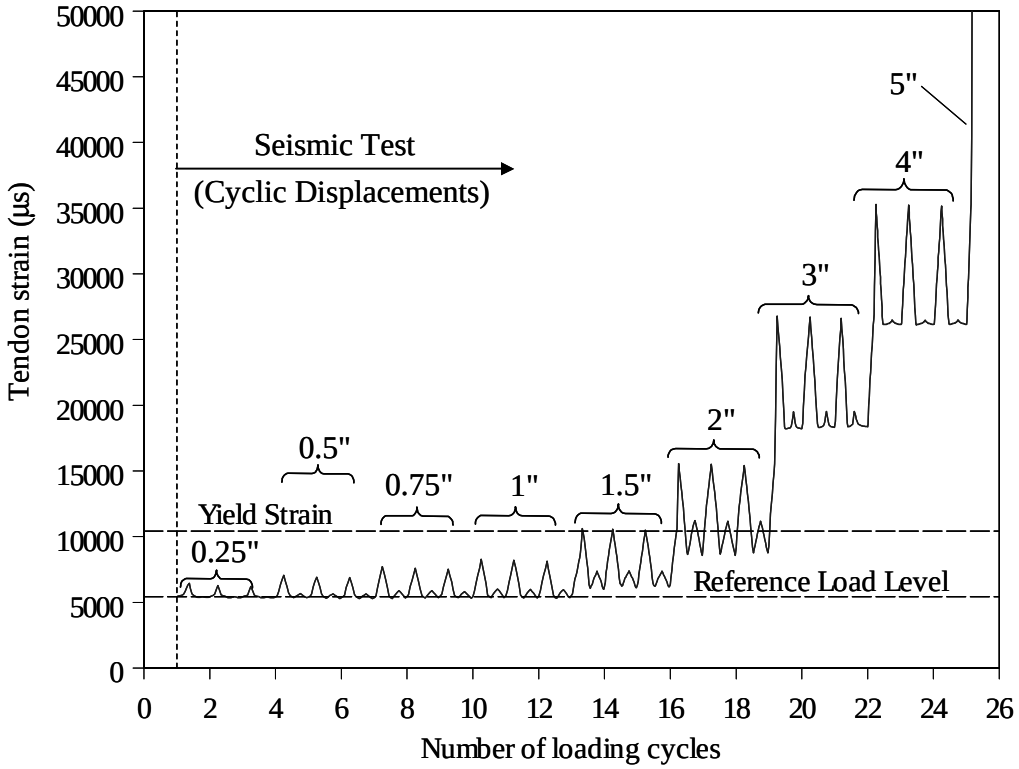


**Figure 4-3 Prestressing steel strain history at midspan of Unit 100-INT**

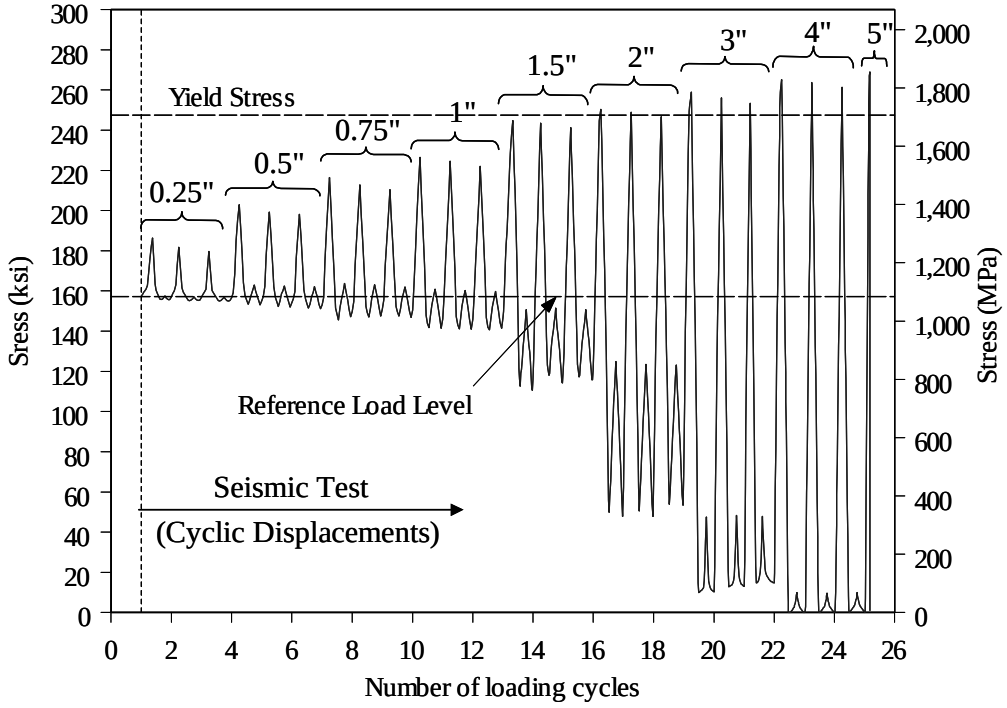


**Figure 4-4 Prestressing steel stress history at midspan of Unit 100-INT**

### 4.2.2 Test Unit 100-INT-CIP

The load displacement response developed with analytical models for Test Unit 100-INT-CIP is shown in Figure 4-5, they have been plotted against the actual load displacement curve from the experiment. The monotonic analysis results were able to more closely match the actual experiment than was the cyclic analysis. Both of the analytical results were unable to predict the actual deck compression failure and the buckling of the steel closure ties. This was due in part to the nature of the model as the closure tie steel reinforcement was modeled using 1-D truss elements, which do not have the ability to buckle[10]. It was hypothesized that a revision of the material models used in the analysis could improve the model. There is confidence, however, based on the monotonic result that the basic analytical model is correct[10].

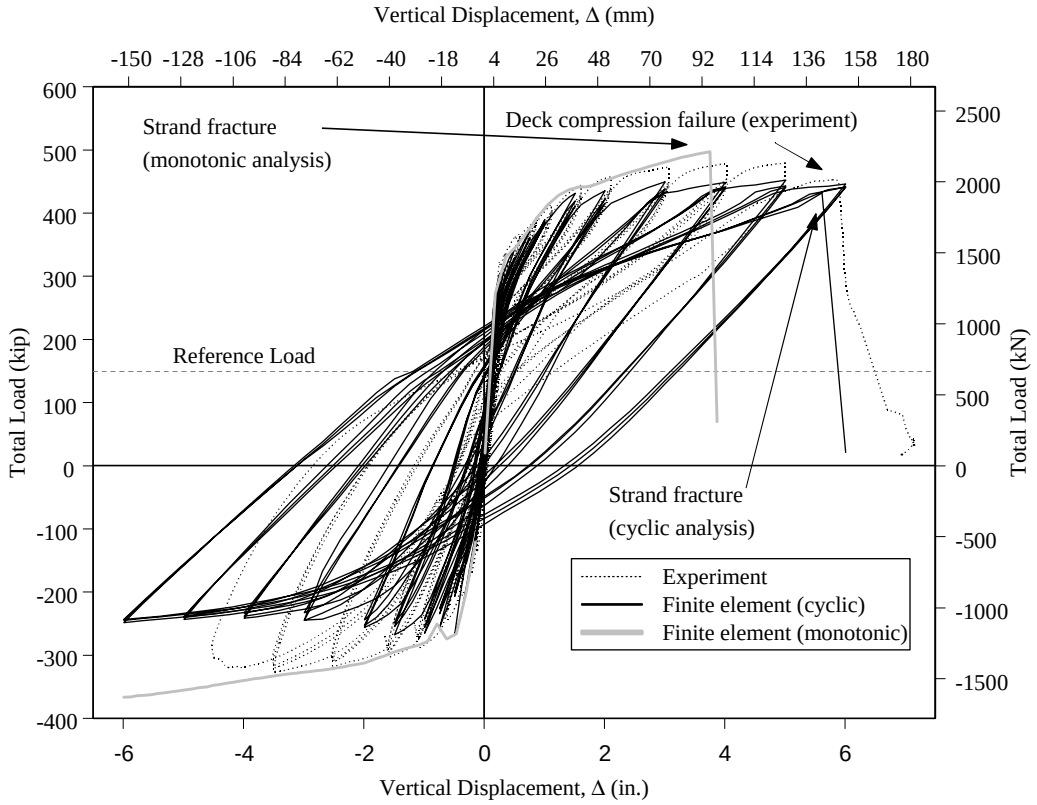


**Figure 4-5 Load versus displacement analysis results of Unit 100-INT-CIP**

The strain history of the steel tendon in the finite element model is shown along with the available experimental strain history in Figure 4-6. There is good correlation between the two plots while the strain gage was still functioning. The experimental and analytical results from this Unit confirm the findings of the analysis for Unit 100-INT that the tendon was strained beyond yield during early displacement cycles. Subsequently, the prestressing force was indeed reduced during further cycling, as evidenced in Figure 4-7.

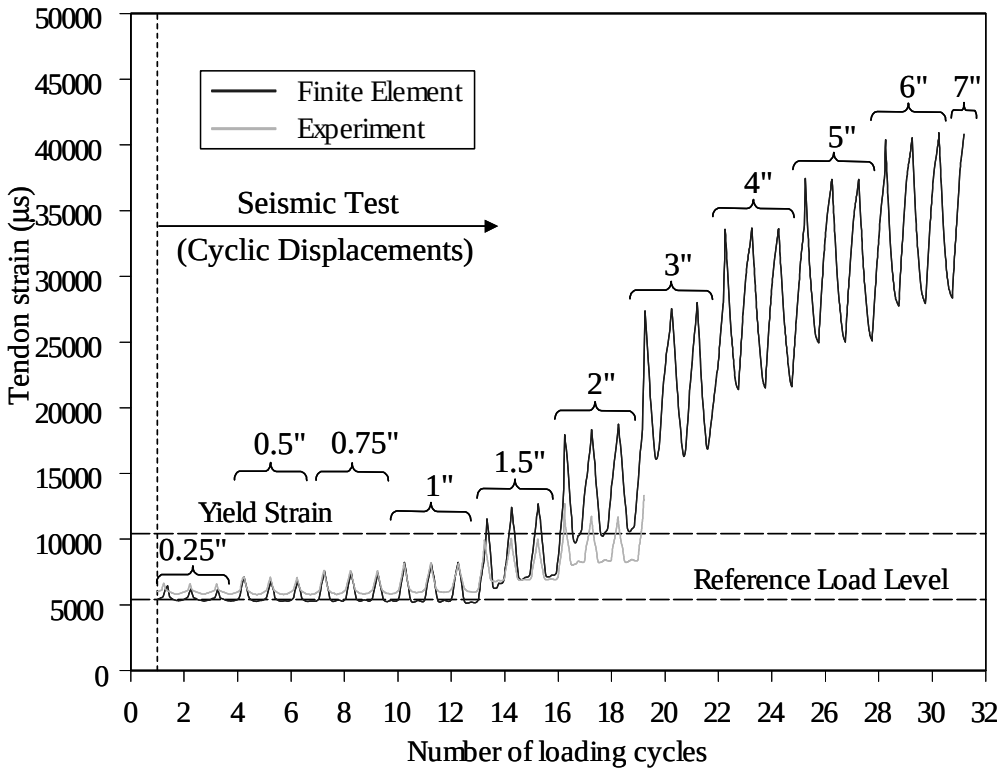


**Figure 4-6 Analytical strain history of steel tendon for Unit 100-INT-CIP**

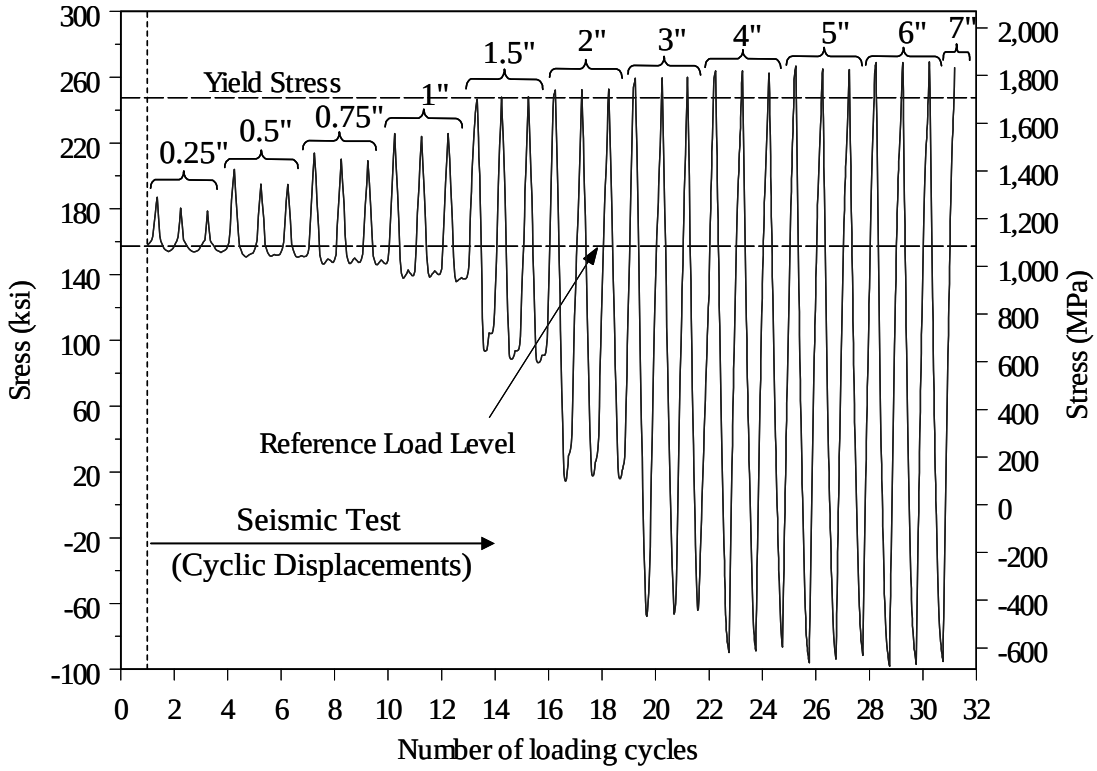


**Figure 4-7 Analytical stress history of steel tendon for Unit 100-INT-CIP**

### 4.2.3 Test Unit 100-EXT

The analytical load displacement response for Test Unit 100-EXT is shown in Figure 4-8. The analytical model was unable to capture the reduction of concrete stiffness so the analytical failure mode was determined assuming a failure strain of 0.003[10]. This strain was attained in the analytical model between 6 and 9 in. (152 and 229 mm). The strain contour for Unit 100-EXT is shown in Appendix A.

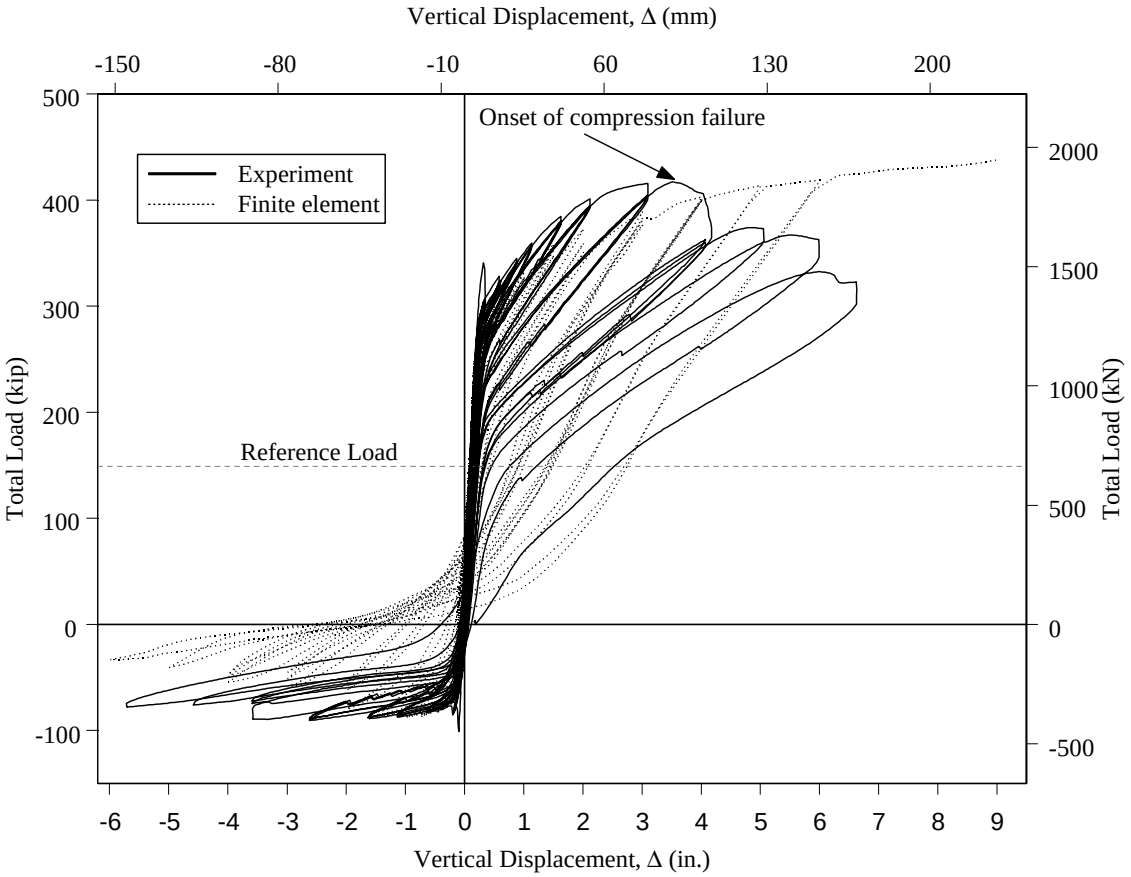


**Figure 4-8 Load versus displacement analysis results for Unit 100-EXT**

The strain and stress history for the steel tendon of Unit 100-EXT are shown in Figure 4-9 and Figure 4-10, respectively. As expected the plots indicate that the strains in this Unit with the external unbonded tendon are lower than the previous units with bonded tendons. A loss in the initial prestressing force was observed following yielding of the tendons as can be seen in Figure 4-10. However loss in the initial prestressing force in the external tendons was not significant as loss of initial prestressing force in the internally bonded tendons (see Figure 4-4 and Figure 4-7).

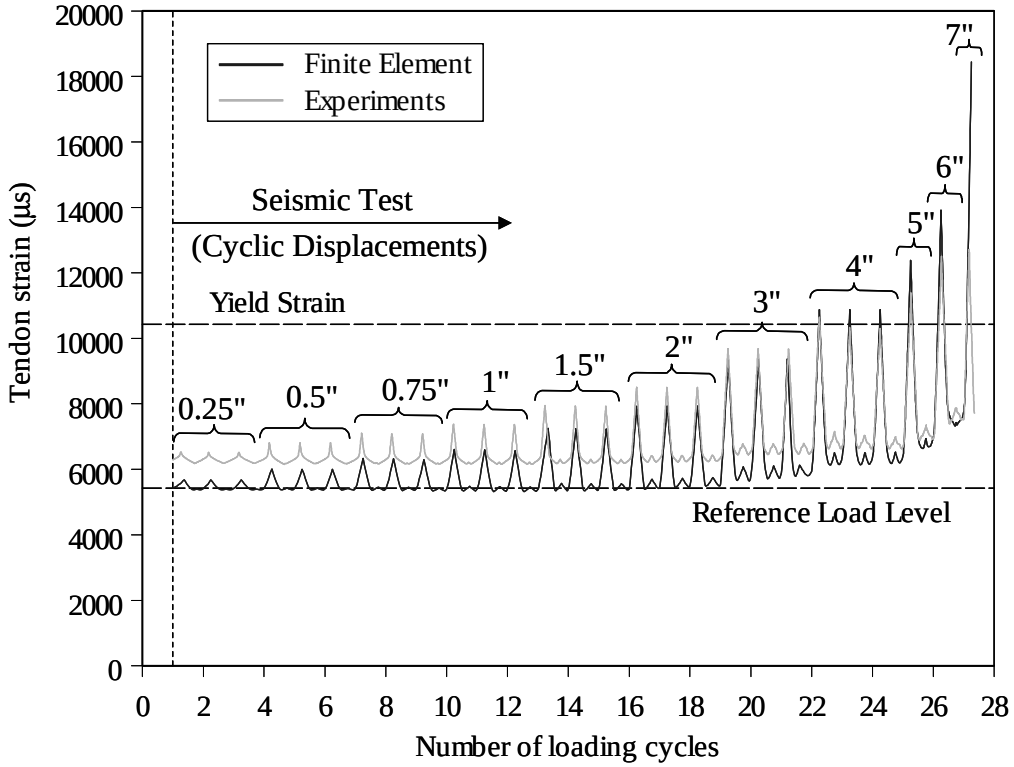


**Figure 4-9 Analytical strain history results in tendon at midspan of Unit 100-EXT**

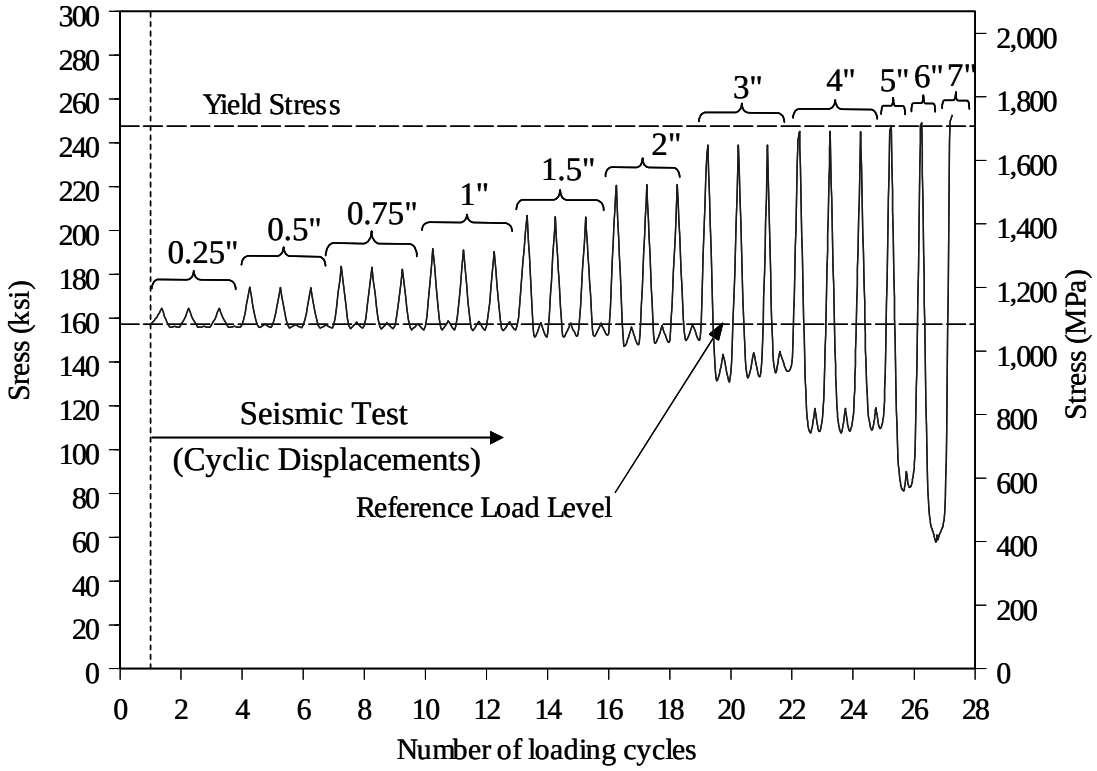


**Figure 4-10 Analytical stress history results in tendon at midspan of Unit 100-EXT**

### 4.2.4 Test Unit 50-INT/50-EXT

The analytical load displacement response for Test Unit 50-INT/50-EXT is shown along with the experimental result in Figure 4-11. The analytical model was able to match the experiment fairly closely; in both models failure occurred in the bonded tendon, the analytical model at 3.4 in. (86.4 mm) at a load level of 442 kips (1,966 kN) and at 3.8 in. (96.5 mm) and a load level of 452 kips (2,011 kN) for the experimental test unit. The analytical model also captured the further cycling with only the external tendons intact.

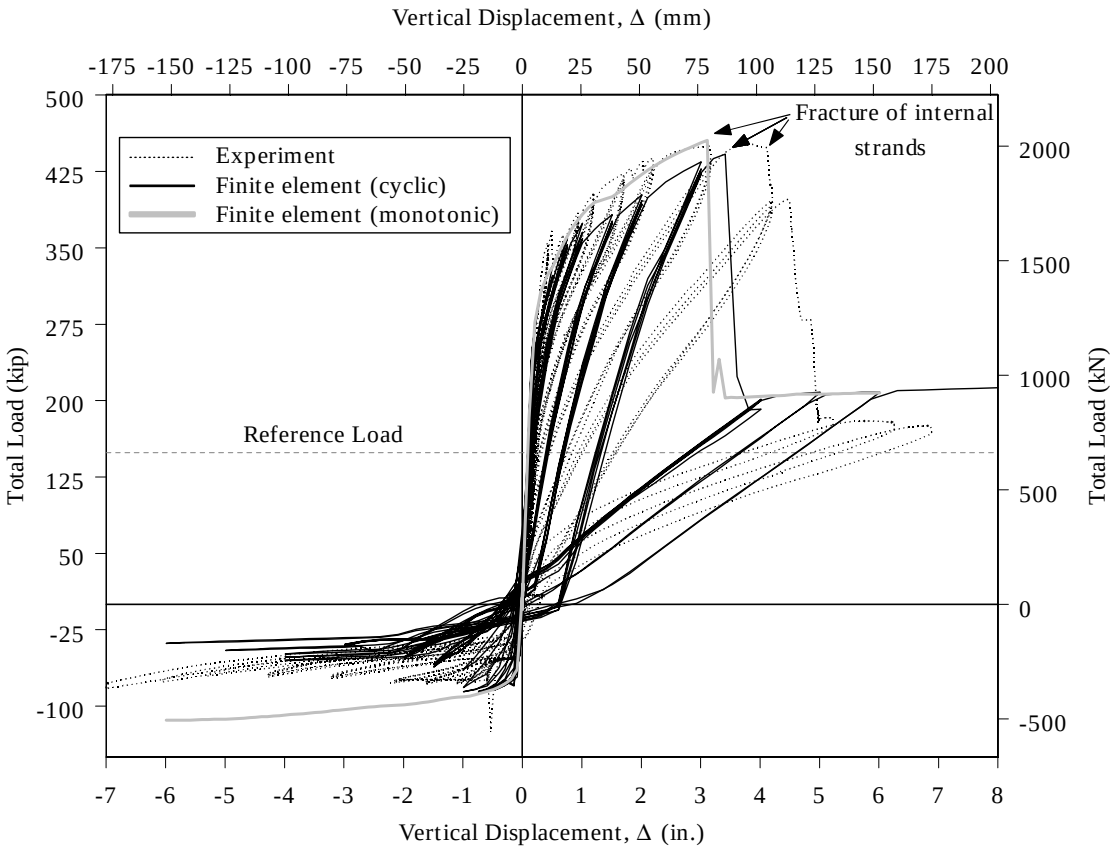


**Figure 4-11 Load versus displacement analysis results for Unit 50-INT/50-EXT**

Consistent with previous findings the strains in the bonded tendons were much higher than in the unbonded tendons even when used together as they were in Unit 50-INT/50-EXT. In fact, the strains in the bonded tendon in Test Unit 50-INT/50-EXT increased at a faster rate than the strains in the bonded tendons from either Unit 100-INT or Unit 100-INT-CIP. These high strains led to early rupture of the internal tendon in both the analytical model and the experiment. The analytical strain and stress histories are shown in Figure 4-12 and Figure 4-13, respectively. The stress history shown in Figure 4-13 indicates that because of the relatively early yielding of the internal tendon in Unit 50-INT/50-EXT, loss of the initial prestressing force started to occur at relatively low displacement compared to Unit 100-INT with 100% internal post-tensioning (compare

the results shown in Figure 4-4 and Figure 4-13). In Unit 100-INT, the initial prestressing force was completely lost following midspan deflection in the test unit of 4 in. (102 mm) as can be seen in Figure 4-4; whereas the initial prestressing force in the internal tendon in Unit 50-INT/50-EXT was completely lost after 1.5 in. (38.1 mm) of midspan displacement as shown in Figure 4-13. The results shown in Figure 4-10 indicate that there is also some loss of the initial prestressing force with 100% external post-tensioning; however the loss in the initial prestressing force is not significant compared to the loss in prestressing force in bonded tendons. The above indicates that the worst case would result from combination of the internally bonded tendons with external tendons.

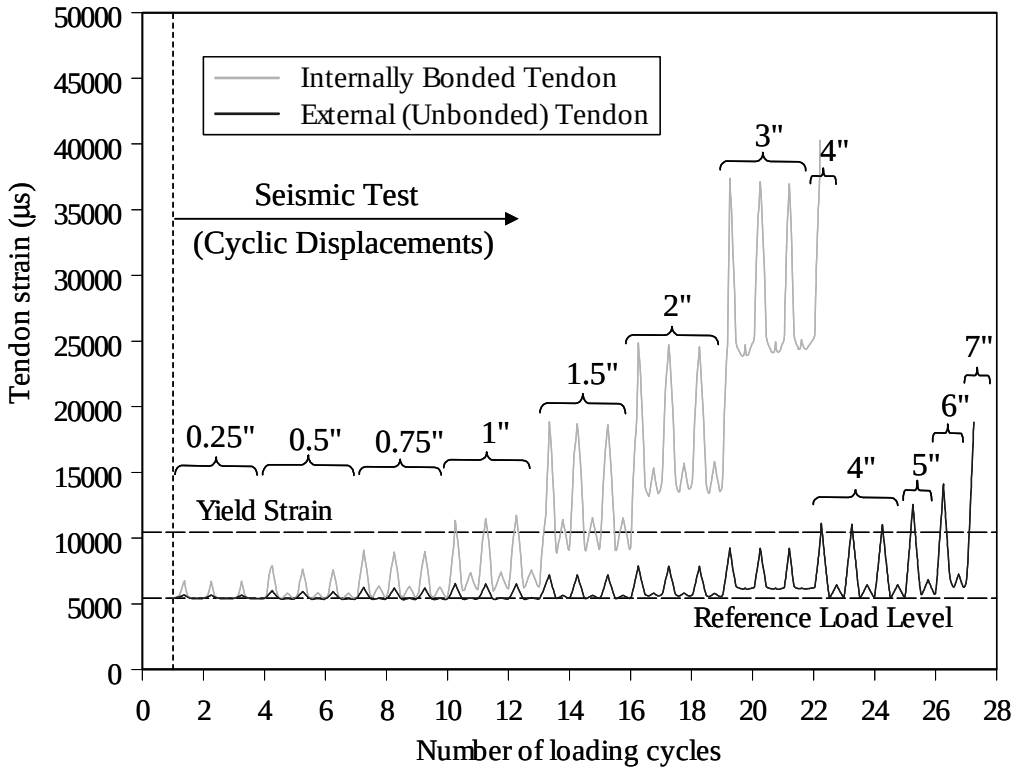


**Figure 4-12 Analytical tendon strain history for Unit 50-INT/50-EXT**

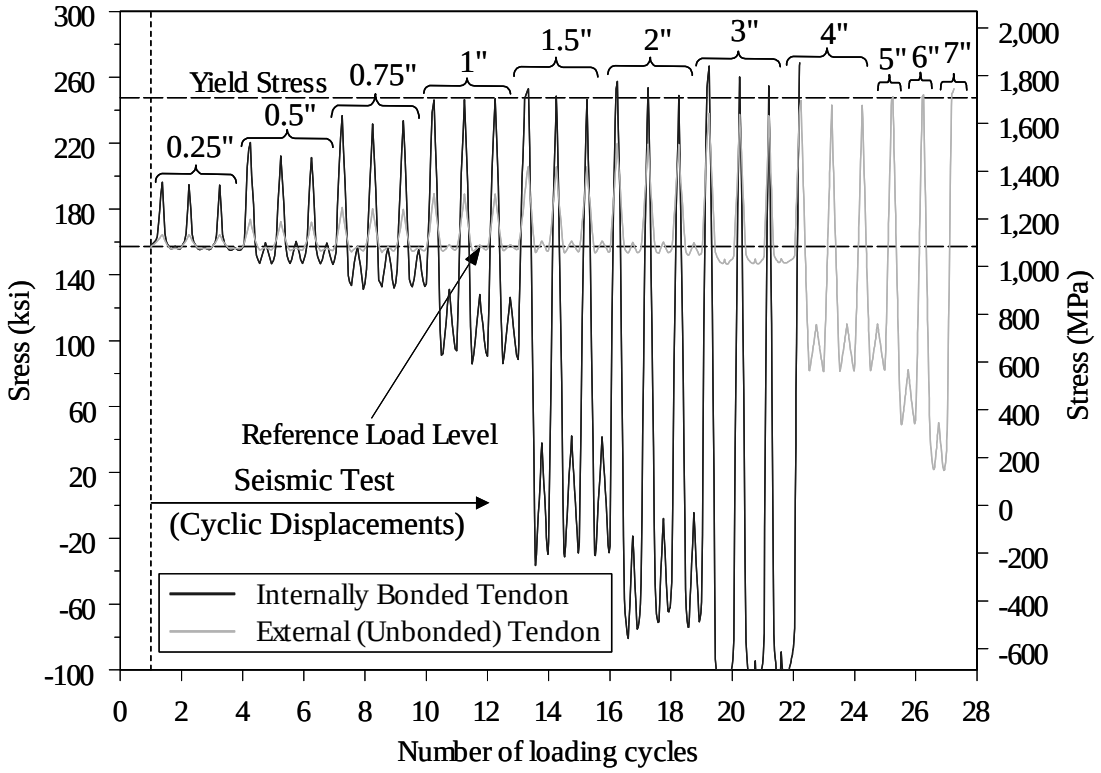


**Figure 4-13 Analytical tendon stress history for Unit 50-INT/50-EXT**

Shown below in Figure 4-14 and Figure 4-15 are the plots of the analytical and experimental tendon strain histories of both the bonded and unbonded tendons, respectively, for Unit 50-INT/50-EXT. The good correlation of strains, as shown in these plots, supports the earlier findings regarding tendon behavior. The strains in the bonded tendon in Test Unit 50-INT/50-EXT reached values well past yield, again at a much faster rate than either of the first two Units. Subsequently, the initial stress in the tendon reduced to zero in the bonded tendon case.

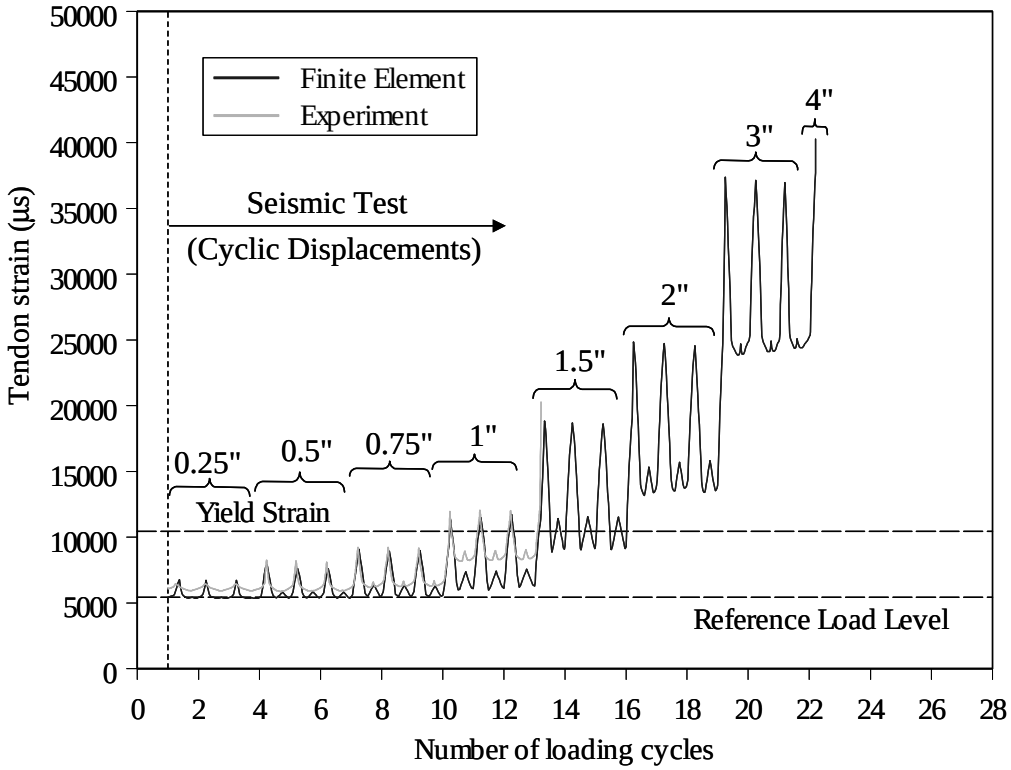


**Figure 4-14 Analytical and experimental internally bonded tendon strain history for Unit 50-INT/50-EXT**

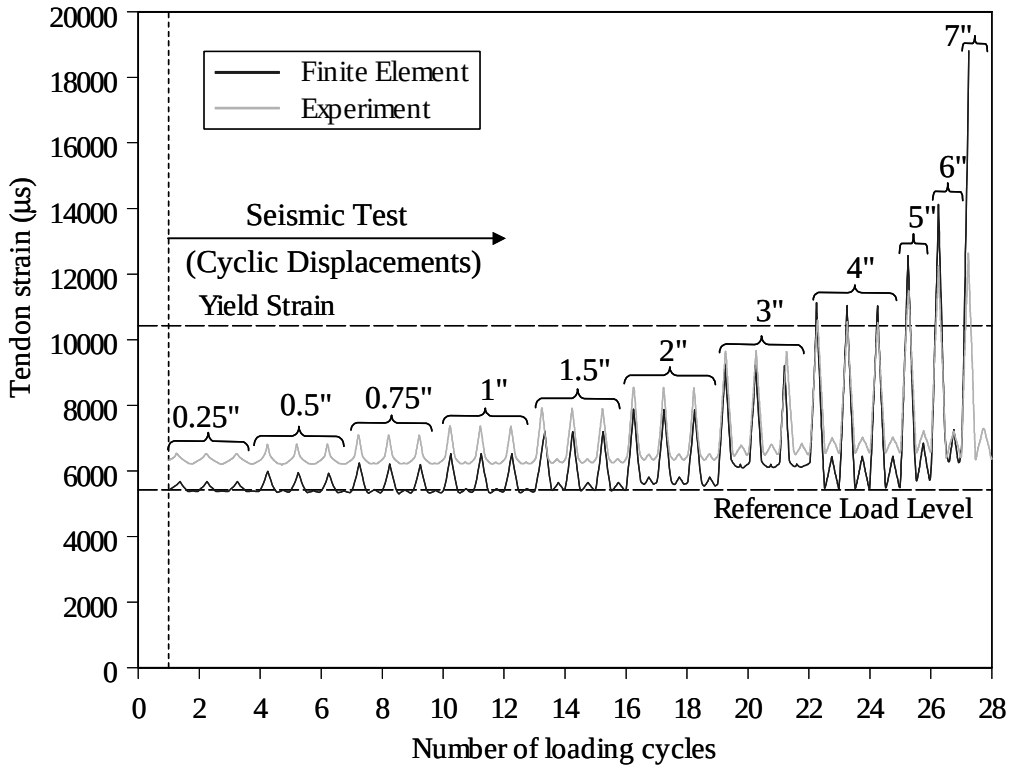


**Figure 4-15 Analytical and experimental external (unbonded) tendon strain history for Unit 50-INT/50-EXT**

# 5 Experimental Program of Segment-to-Segment Joints Subjected to High Bending Moments Combined with High Shears (Phase II)

## 5.1 Prototype Structure

The prototype structure used for the design of the test units in Phase II of the experimental program is the same prototype structure used in design of Phase I test units. Design of the prototype structure is presented in Section 2.1 of this report. Each span of the prototype structure is post-tensioned with a harped shape tendon. In addition to the harped-shape tendon, it is assumed that the prototype superstructure, used in design of Phase II test units, is post-tensioned by horizontal continuity tendons, which are close to the bottom soffit of the superstructure. It should be mentioned that the prototype structure used in design of Phase I test units did not have horizontal continuity tendons. The horizontal tendon was included in design of the test units of Phase II based on the recommendation of the Seismic Research Committee of the American Segmental Bridge Institute (ASBI). It should be mentioned that seismic design of the bridge superstructure at the location of the pier might show that no horizontal continuity tendons are needed in the superstructure close to its bottom soffit. This is because of the high flexural moments in the superstructure close to pier locations that result in high compressive stresses in the superstructure's bottom soffit under gravity loads. The segment-to-segment joints near the pier locations will not open at the bottom soffit unless the bending moments resulting from the seismic forces are significantly higher than the dead load moments. Figure 5-1a shows an elevation view of the prototype structure. The horizontal continuity tendon is also shown in the figure. It should be remembered that cross section of the prototype

superstructure consists of a single cell box girder as shown in Figure 5-1b. Due to the short span lengths it is assumed that the prototype structure is constructed using the span-by-span method. The objective of Phase II of the experimental program was to investigate the seismic performance of superstructure segment-to-segment joints subjected to high bending moments combined with high shear, or in other words segment-to-segment joints close to locations of the piers (see Figure 5-1).

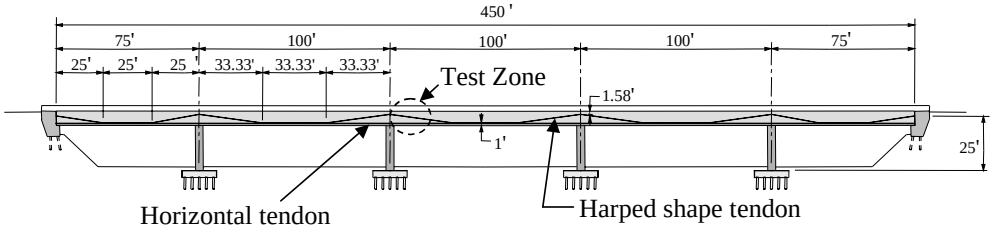


(a) Elevation

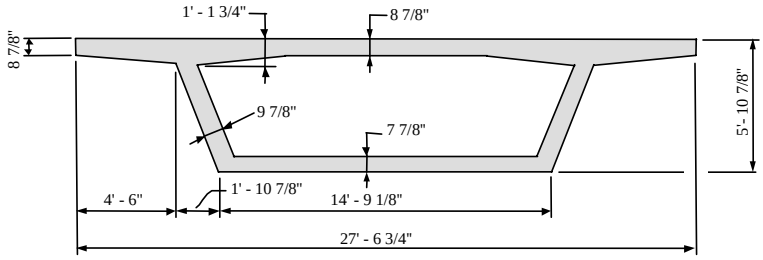


(b) Cross section

**Figure 5-1 Prototype structure used for design of Phase II test units**

The prototype structure was designed according to the AASHTO Guide Specifications for Design and Construction of Segmental Concrete Bridges[1], the AASHTO-PCI-ASBI Segmental Box Girder Standards for Span-by-Span and Balanced Cantilever Construction[4], and the AASHTO Standard Specifications for Highway Bridges[5]. Full gravity, thermal, and seismic analyses were performed on the prototype

structure. Section and material properties used for the design of the prototype structure are given in Table 2-1.

Design loads of the prototype structure are presented in Section 2.1.1 of this report. However, the design of prestressing steel in the prototype structure used in design of Phase II test units (Figure 5-1) is different than design of the prestressing steel in the prototype structure used in design of Phase I test units (Section 2.1.2). As for the prototype structure of Phase I of this research program, the section at midspan is critical for design under service load. The design criterion is not to allow any tensile stresses at the midspan joint of the prototype superstructure.

The secondary bending moments at midspan due to prestressing steel in the prototype structure of Phase I is 1.66P (in kips and ft units), where P is the total prestressing force in the prototype superstructure after all losses. However, the prestressing secondary moment at midspan in the prototype structure of Phase II is 1.88P (in kips and ft units) because of the additional horizontal continuity tendon considered in Phase II prototype superstructure. To prevent occurrence of tensile stresses at the mid-span joint under extreme service load combinations, a total prestressing force of 3,029 kips (13,474 kN) is required. Assuming that the stress in the prestressing steel is 60 percent of its ultimate strength, 87 strands are needed in the prototype superstructure (Grade 270 7-wire strands with 0.6 in. diameter). Forty-five strands are provided in each web of the single cell box girder making a total of 90 strands. In each of the two webs of the prototype box section, the harped-shape tendon consists of 36 strands, whereas the horizontal continuity tendon consists of 9 strands. Stresses in the superstructure at face of the pier were all compressive under extreme service load combinations. At location of the

first superstructure segment-to-segment joint, the shearing force under dead loads and superimposed dead load is 364 kips (1,619 kN); the stresses at the top and bottom concrete surfaces are -480 psi (-3.3 MPa) and -579 psi (-4 MPa), respectively. The sign convention is positive for tensile stresses. The total prestressing force in the harped-shape and the horizontal tendons are 2,508 kips (11,157 kN) and 627 kips (2,789 kN), respectively.

Seismic performance of an assembly of segment-to-segment joints at the midspan zone was investigated in Phase I of this research program. In Phase II, it was decided to investigate the seismic performance of only one joint, which is the closest to the pier. The first segment-to-segment joint is the one that connects the precast superstructure first segment with the precast pier segment. The term pier segment refers to the precast segment of the superstructure that is placed on top of the pier. Precast pier segments are used when the pier consists of precast segments. Thus if the prototype structure piers consist of precast segments, the joint modeled in the experiments of Phase II represents the superstructure segment-to-segment joint closest to the pier. However, it is common especially in high seismic zones that the pier is made of cast-in-place concrete and the pier segment is built monolithically with the pier. In this case, the first precast segment of the superstructure cannot be match cast against the pier segment, and a gap exists between the pier segment and the first precast segment of the superstructure. The length of this gap is usually 6 in. (152 mm) or more and it is closed by cast-in-place concrete. The cast-in-place segment closure gap is not modeled in any of the test units of Phase II. This means that Phase II test units represent the joint between the pier segment and the first precast segment of the superstructure in case of precast pier and pier segment. If the

pier segment is built monolithically with the cast-in-place pier, the test units represent the joint between the first and second precast segments of the superstructure. The objective of the Phase II experimental program is to investigate the seismic performance of segment-to-segment joints subjected to high bending moments combined with high shears. Transfer of the bending moments and shearing forces between the superstructure and the pier is not investigated in the Phase II experiments. Thus, the fact that the pier is made of cast-in-place or precast concrete does not affect the design of the test units of Phase II.

## 5.2 Description of Test Units

### 5.2.1 Design of Test Units

As in Phase I, the test units of Phase II were designed at 2/3-scale of the prototype structure. As mentioned in the previous section, the test units represented the joint between the precast pier segment and the first precast segment of the superstructure. This segment-to-segment joint is subjected to high bending moments from gravity loads and longitudinal seismic motions combined with high shearing forces. As seen in Chapter 3, segment-to-segment joints, subjected to high bending moments and low shears, could undergo significant opening without failure. The main objective of the Phase II experiments was to investigate opening and closure of the joints in presence of high shearing forces. Each test unit was 19 ft and 4 in. (5.89 m) long and was made up of three precast concrete segments.

The experimental program of Phase II consisted of testing four units with the main variable being the ratio of internal to external post-tensioning of the superstructure. The test matrix of Phase II experiments is identical to the test matrix of Phase I experiments and is given in Table 5-1. The joints of the first, third and fourth test units were epoxy bonded with no reinforcement crossing the joints other than the prestressing steel. The second test unit had a reinforced cast-in-place deck closure with the remaining portions of the joint connected by epoxy. The first and second test units were post-tensioned by internally bonded tendons, whereas the third test unit was post-tensioned by external tendons. Internally bonded tendons achieved one half of the post-tensioning of the fourth test unit, whereas external tendons achieved the other half. Test Units 100-INT, 100-EXT and 50-INT/50-EXT together form the first test series in which the test variable was the ratio of internal to external post-tensioning. Units 100-INT and 100-INT-CIP together form the second test series in which the test variable was the construction of cast-in-place deck closure joint.

**Table 5-1 Test Matrix**

| Unit No. | Description | Nomenclature |
|---|---|---|
| 1 | 100% Internal Post-Tensioning | 100-INT |
| 2 | 100% Internal Post-Tensioning with Cast-in-Place Deck Closure Joint | 100-INT-CIP |
| 3 | 100% External Post-Tensioning | 100-EXT |
| 4 | 50% Internal and 50% External Post-Tensioning | 50-INT/50-EXT |

The complete test unit was comprised of the three precast segments as shown in Figure 5-2. The label numbers used throughout Chapters 5 and 6 of this report for the precast segments and the joints are also shown in Figure 5-2. Seismic performance of

Joint $J_1$, between Segments 1 and 2 (see Figure 5-2) was the focus of the Phase II experiments. Joint $J_1$ had shear keys and alignment keys, as will be shown later, and Segments 1 and 2 were epoxy bonded at Joint $J_1$. Segment 1 represents the first precast segment of the superstructure, whereas Segment 2 represents the pier segment. The test unit was supported on two precast concrete footing segments. The test unit was loaded at the cantilever tip of Segment 1 and was tied down to the laboratory strong floor by means of vertical high-strength bars. It was necessary to have an additional precast segment (Segment 3 in Figure 5-2) to provide sufficient tie down of the test unit to the laboratory floor. It will be shown later that Segments 2 and 3 were tied together by prestressed high-strength bars so that the two segments act as one piece. Joint $J_2$ between Segments 2 and 3 did not have any shear keys and the two segments were not epoxy-bonded. Only Joint $J_1$ is located in the test zone shown in Figure 5-2.

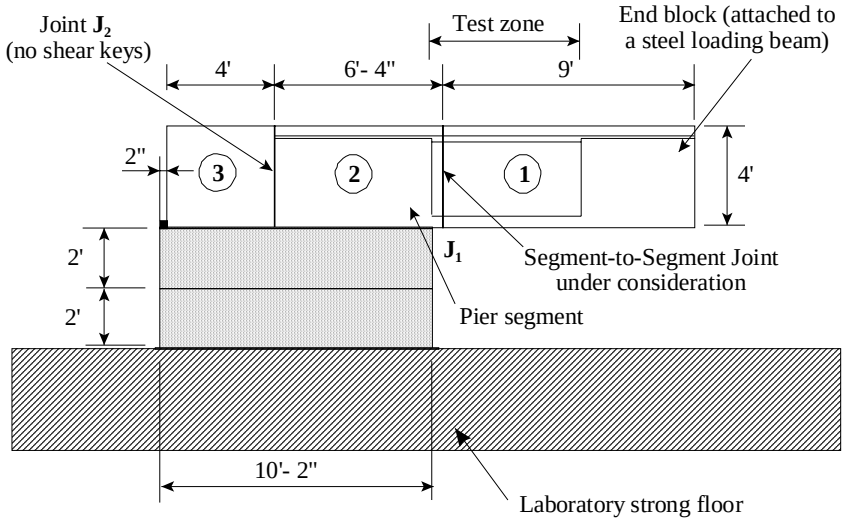


**Figure 5-2 A Typical test unit of Phase II**

To simplify construction and reduce the overall size, the test setup and the required force levels, it was decided to model only one half of the prototype cross section in the

Phase II experiments. As for Phase I test units, this resulted in a simplified I-section for the test units. The widths of the top and bottom slabs equal the scaled half widths of the deck and soffit of the prototype box-section design. The typical cross-section of the test units is shown in Figure 5-3.

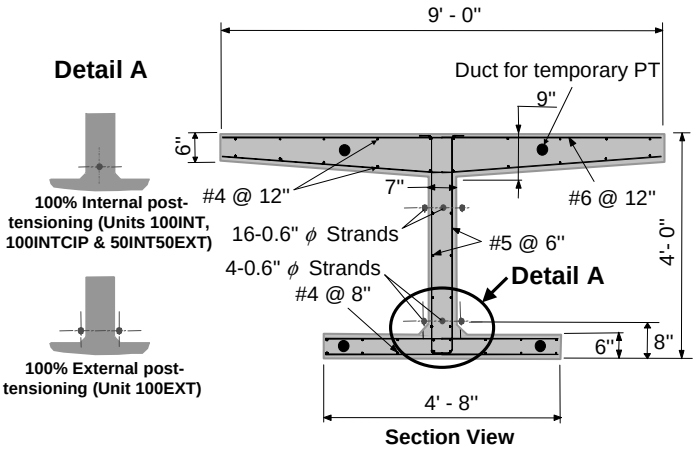


a) Cross Section of the Test Zone and the Horizontal Tendon

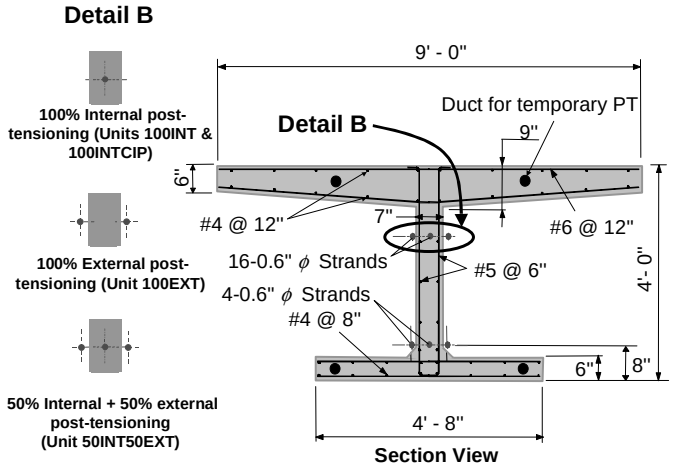


b) Cross Section of the Test Zone and the Harped-Shape Tendon

**Figure 5-3 Cross section of the test zone of Phase II test units**

Only the test zone of each test unit had the I-shape cross-section shown in Figure 5-3. The test zone is shown in Figure 5-2 and it consisted of the first 5 ft (1.52m) of

Segment 1, and 4 in. (0.10 m) of Segment 2. The last 4 ft (1.22 m) nearest the cantilever tip of the test unit had a 4 ft and 8 in. (1.42 m) wide solid block. This end block utilized PVC ducts for high-strength bars, which were used to extend the length of the test unit by a loading steel beam as will be shown later. The end block also accommodated the anchor heads for the prestressing tendons. Only 4 in. (0.10 m) of Segment 2 had the I-shape cross-section shown in Figure 5-3; the remaining portion of Segment 2 had a solid block of 4 ft and 8 in. (1.42 m) width. The solid block of Segment 2 represented the pier segment diaphragm in typical bridges; it also utilized horizontal and vertical PVC ducts required for the high-strength bars used, respectively, in tying of Segments 2 and 3 together and in vertical tie down of the test unit to the laboratory floor.

As mentioned earlier, the prototype superstructure was post-tensioned by a harped-shape tendon and a horizontal continuity tendon. Both tendons were modeled in the Phase II test units. Figure 5-4 shows a schematic drawing of a typical test unit with the layout of the two tendons. The prototype structure had two horizontal continuity tendons, one on each of the two webs of the box girder; each tendon consisted of 9-0.6″ ϕ strands. The continuity tendon was modeled in the test units by the horizontal tendon shown in Figure 5-4, which consisted of 4-0.6″ ϕ strands. The horizontal tendon was located at 8 in. (0.20 m) above the soffit of the test unit; which represented a 2/3-scale of the 1 ft (0.30 m) eccentricity in the prototype structure. The prototype structure had two harped-shape tendons each of 36-0.6″ ϕ strands. Because only one half of the box girder was modeled in the experiments, only one of the harped-shape tendons was represented in the test unit by the inclined tendon shown in Figure 5-4; this inclined tendon consisted of 16-0.6″ ϕ strands. The inclined, or upper, tendon had a straight-line profile in Zone I of the test unit

(see Figure 5-4). The eccentricities and the slope of the upper tendon in Zone I represented the scaled harped-shape tendon profile in the prototype structure. Zone I ends at 3 ft and 4 in. (1.02 m) from Joint $J_1$, or in other words at the location of the pier centerline. The upper tendon had a parabolic profile in Zone II; the parabolic tendon profile does not affect the results of the experiments since the focus of the tests was the performance of Joint $J_1$ only. Again, the transfer of the shearing force and bending moments from the superstructure to the pier, or the footing in the test units, was beyond the scope of this research.

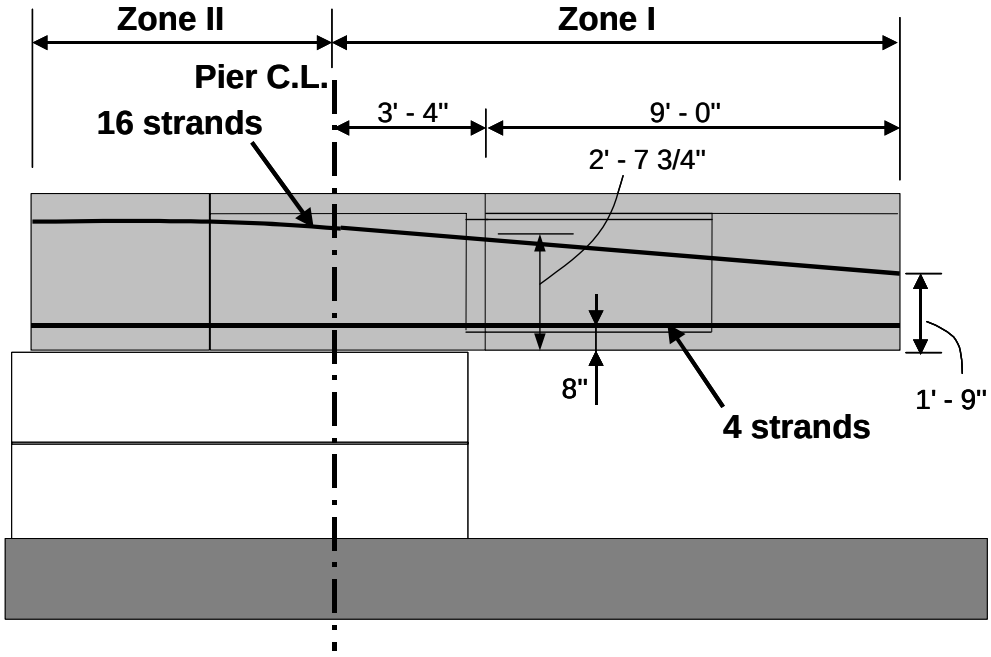


**Figure 5-4 Layout of post-tensioning tendons of Phase II test units**

Figure 5-3a shows the location of the horizontal, or lower, tendon in different test units. The tendon consisted of 4-0.6″ ϕ strands as mentioned earlier. For Test Units 100-INT, 100-INT-CIP and 50-INT/50-EXT, the tendon was internally bonded as shown

schematically in Figure 5-3a. In Unit 100-EXT, two exterior tendons each of 2-0.6″ ϕ strands were used in lieu of one internally bonded tendon. This was done to represent the common practice when the superstructure is post-tensioned externally. Figure 5-3b shows the location of the inclined, or upper, tendon in different test units. The tendon consisted of Grade 270 16-0.6″ ϕ strands as mentioned earlier. For Test Units 100-INT and 100-INT-CIP, the tendon was internally bonded. In Unit 100-EXT, two exterior tendons each of 8-0.6″ ϕ strands were used in lieu of one internally bonded tendon. In Unit 50-INT/50-EXT, an internally bonded tendon achieved one half of the post-tensioning. Thus, the internally bonded tendon of Unit 50-INT/50-EXT consisted of 8-0.6″ ϕ. Two external tendons, each of 4-0.6″ ϕ strands, achieved the other half of post-tensioning (see Figure 5-3b). The external upper and lower tendons in Units 100-EXT and 50-INT/50-EXT were grouted only inside the solid blocks of Segments 2 and 3. The external tendons were not grouted in the test zone or the solid block in Segment 1 at the cantilever tip. In actual precast segmental bridges, external tendons are placed inside ducts that are grouted after stressing of the external tendons. However, as mentioned before in Section 2.2.1, grouting of the external tendons would have had no influence on the performance of the test units with external tendons. Thus it was decided to place the external tendons inside non-grouted transparent poly-carbon pipes. Based on discussions with bridge design engineering consultants and the American Segmental Bridge Institute (ASBI), the results of Test Units 100-EXT and 50-INT/50-EXT with ungrouted external tendons are also applicable to precast segmental bridges with grouted external tendons.

The prestressing force in the upper and lower tendons of the test units were chosen such that the concrete stresses at Joint $J_1$ in the test units would match the concrete

stresses at the corresponding segment-to-segment joint in the prototype structure. Based on the prototype design, the required effective prestressing forces in the upper and lower tendons of the test units were 560 kips (2,491 kN) and 140 kips (623 kN), respectively. Prestress losses due to anchor set, elastic shortening and time-dependent effects were estimated and the jacking forces were determined. The recorded strains in the strands ranged between 5500 μs to about 6100 μs with an average of about 5800 μs. The corresponding average stress in the strands was about 162 ksi (1,117 MPa). The corresponding forces in the upper and lower tendons of the test units were 557 kips (2,478 kN) and 139 kips (618 kN), respectively. Thus, the actual prestressing forces at the time of testing were very close to the required forces after all losses. In other words, the concrete stresses at Joint $J_1$ in the test units due to prestressing effects matched the corresponding concrete stresses in the prototype structure.

Test Unit 100-INT-CIP utilized cast-in-place closure joint in the deck at location of Joint $J_1$. Both hairpin bars and headed bars were used for longitudinal reinforcement of the deck in Test Unit 100-INT-CIP of Phase I. The structural performance was very similar of the cast-in-place closure joint with both reinforcement types. Thus, it was decided to use headed bars only for the longitudinal deck reinforcement in Phase II. Figure 5-5 shows a schematic drawing of Test Unit 100-INT-CIP and the deck longitudinal reinforcing bars in the deck closure joint. Top and bottom headed bars were used in the deck in Segments 1 and 2; these headed bars overlapped inside the cast-in-place deck closure joint as shown in Figure 5-5. The heads welded to the bar ends achieves the mechanical anchorage of headed bars, thus the full yield strength of the headed bars could be mobilized. The reinforced cast-in-place deck closure detail across

Joint $J_1$ in Test Unit 100-INT-CIP was similar to the detail proposed originally for the new East Bay Skyway Structure of the San Francisco-Oakland Bay Bridge (SFOBB). Width of the cast-in-place deck closure joint in the SFOBB superstructure is 31.5 in. (0.80 m); width of the closure joint was scaled in the test units by a factor of 2/3.

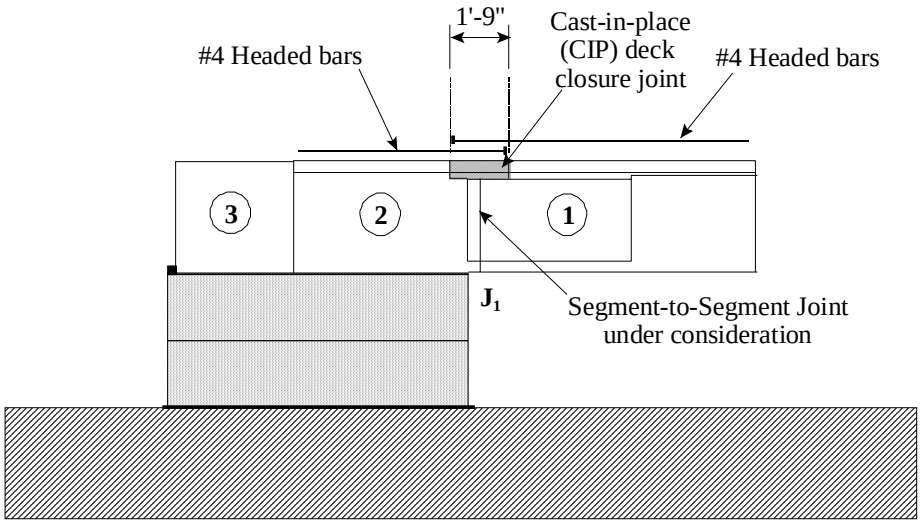


**Figure 5-5 Reinforced cast-in-place deck joint of Test Unit 100-INT-CIP (Phase II)**

### 5.2.2 Construction

The two precast footing segments were cast before construction of Segments 1 to 3 of the test units. Figure 5-6 shows the reinforcement of one of the two identical precast footing segments, which were used to support the test units.

**Figure 5-6 Reinforcement of one of the precast footing segments for test units**

The precast segments were built on a steel casting bed. For each test unit, Segment 1 was built first. The reinforcement of the segment is shown in Figure 5-3 for the test zone (I-shaped cross section portion). Figure 5-7 shows the deck reinforcement in Segment 1 in the test zone of Unit 100-INT. Figure 5-8 shows the reinforcing cage of Segment 1 of Unit 100-EXT. The reinforcement of the web and the bottom slab of the I-shaped portion of the segment are shown in Figure 5-8. The figure also shows the reinforcement cage of the end block (at cantilever tip) of Segment 1.

**Figure 5-7 Reinforcement of the deck in the test zone**

**Figure 5-8 Reinforcement of Segment 1**

As mentioned earlier, the test unit was extended by a steel loading beam, which was attached to the test unit at its cantilever tip (i.e. at the end block of Segment 1). Figure 5-8 shows the horizontal PVC ducts which accommodated high-strength prestressing bars; these prestressing bars were used to connect the steel loading beam to the concrete test unit. The horizontal bars were post-tensioned at high force levels. The end block of Segment 1 also accommodated the anchor heads of the prestressing tendons. The total axial force in the solid block of Segment 1 was about 5,000 kips (22,242 kN). Thus heavy confinement of the end block was required. Confinement of the end block was achieved by provision of stirrups, vertical headed bars and horizontal headed bars as shown in Figure 5-8 to Figure 5-10.

**Figure 5-9 Reinforcement of the end block of Segment 1**

**Figure 5-10 Reinforcement of Segment 1 at the cantilever tip**

Segment 1 was constructed first followed by construction of Segment 2. After hardening of concrete in Segment 1, a bond-breaker was applied on the surface of Joint $J_1$ and Segment 2 was match cast against Segment 1. Figure 5-11 shows the reinforcement of Segment 2; the figure also shows that Segment 2 was match cast against Segment 1. Finally, Segment 3 was match cast against Segment 2.

**Figure 5-11 Reinforcement of Segment 2**

After the concrete cured sufficiently the segments were shipped to the Charles Lee Powell Structural Research Laboratories at the University of California, San Diego. Figure 5-12 shows the precast Segment No. 1 of Test Unit 100-INT with 100% internal post-tensioning. The figure shows the I-shaped cross section of the test unit in the test zone and the surface of Joint $J_1$. Figure 5-12 also shows the shear keys in the web as well as the alignment keys in the deck and bottom slab. The figure also shows the ducts in the

web for the upper and lower prestressing tendons of the test unit. Four ducts in the deck and bottom slab are also shown in Figure 5-12; high-strength bars were placed inside these ducts to provide temporary clamping forces on the test units after epoxy bonding of Segments 1 and 2.

**Figure 5-12 Precast Segment No. 1 of Test Unit 100-INT**

The footing segments were placed on the laboratory floor followed by placement of the precast Segments No. 2 and 3 on top of the footing. Segments 2 and 3 were post-tensioned together by 1 3/4″ (44.5 mm) ϕ high-strength bars as shown in Figure 5-13. Segment 2 and 3 were joined together by means of eight high-strength bars in Units 100-INT, 100-EXT and 50-INT/50-EXT. Because of the relatively high forces transferred from the test unit to the footing, Segments 2 and 3 of Test Unit 100-INT-CIP were

connected together by post-tensioning of twelve 1 3/4″ (44.5 mm) ϕ high-strength bars. The prestressing force in each of these bars was selected such that no vertical slip or joint opening occurs at Joint $J_2$ between the two segments. Segments 2 and 3 were then tied down to the laboratory strong floor by means of 10-1 3/4″ (44.5 mm) ϕ high-strength bars as shown in Figure 5-14.

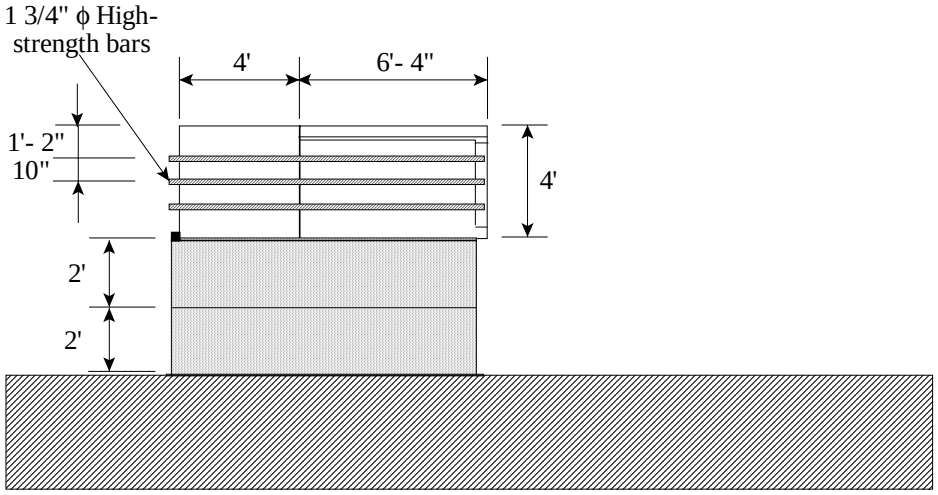


**Figure 5-13 Assembly of Segments 2 and 3 of the test units**

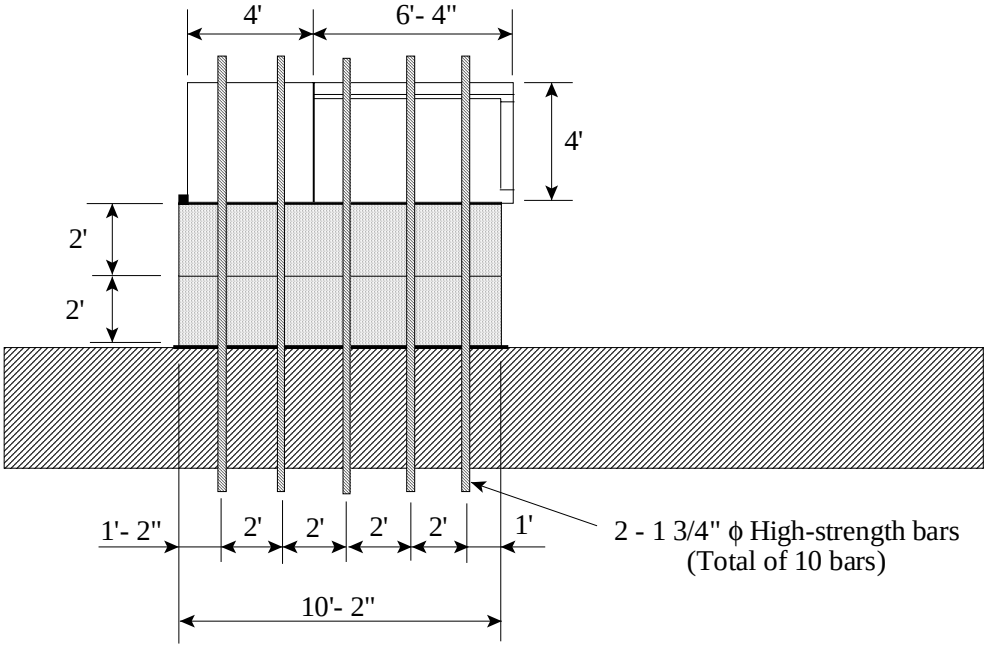


**Figure 5-14 Vertical tie-down of Segments 2 and 3**

A wooden platform was built to support Segment 1 before its assembly with Segments 2 and 3 of the test unit. Segment No. 1 was placed on the wooden platform with enough space for men to work between the segments. Slow-Set Segmental Bridge Adhesive (epoxy) typically used in span-by-span construction of precast segmental bridges was applied on the surface of Joint $J_1$ in Segments 1 and 2. The epoxy was applied on the entire joint surface (shown in Figure 5-3) in Units 100-INT, 100-EXT and 50-INT/50-EXT. Figure 5-15 shows application of the epoxy on surface of Joint $J_1$ in Test Unit 100-INT.

**Figure 5-15 Application of epoxy on surface of Joint $J_1$ in Test Unit 100-INT**

There was a gap in the top slab at the location of Joint $J_1$ in Test Unit 100-INT-CIP (see Figure 5-5). A cast-in-place concrete slab strip closed this gap later. Thus in Test Unit 100-INT-CIP the epoxy was applied to the remaining joint surface; it means the web and bottom slab (see Figure 5-16). Epoxy was applied on the surface of Joint $J_1$ and Segment 1 was mated with Segment 2. Numerous sheets of plastic were used between the Segment 1 and the wooden platform to act as a low-friction surface on which the

segment could slide. To mate the segments, Segment No. 1 was first lifted and moved by crane close to its final position. At this point Come-Alongs (hand operated winch) were attached to the segment and it was winched into place, sliding on the plastic sheets until contact was made between the two precast segments. Figure 5-17 shows Test Unit 100-INT after assembly of the precast segments. The wooden platform (shown in Figure 5-17) was removed after post-tensioning of the test unit.

**Figure 5-16 Application of epoxy on surface of Joint $J_1$ in Test Unit 100-INT-CIP**

**Figure 5-17 Test Unit 100-INT after epoxy bonding**

After the application of epoxy and the final assembly of the segments, each test unit was temporarily post-tensioned with four 1-inch (25.4 mm) diameter high-strength ASTM A 722 steel bars. Two bars were placed in the top slab and two bars in the bottom slab. The bars were prestressed by means of hollow jacks placed against the surface of Segment 3 (see Figure 5-18); these hollow jacks remained on the test units until release of the temporary prestressing forces provided by the high-strength bars. The temporary prestressing forces in the high-strength bars were determined such that the entire surface of segment-to-segment Joint $J_1$ would have a minimum compressive stress of 40 psi[8]. Figure 5-18 shows Segment 3 with the four high-strength bars used for temporary prestressing after epoxy bonding. This temporary prestressing was removed just after permanent post-tensioning of the test units. Figure 5-18 also shows the horizontal high-strength bars used in connecting Segments 2 and 3 together (see Figure 5-13).

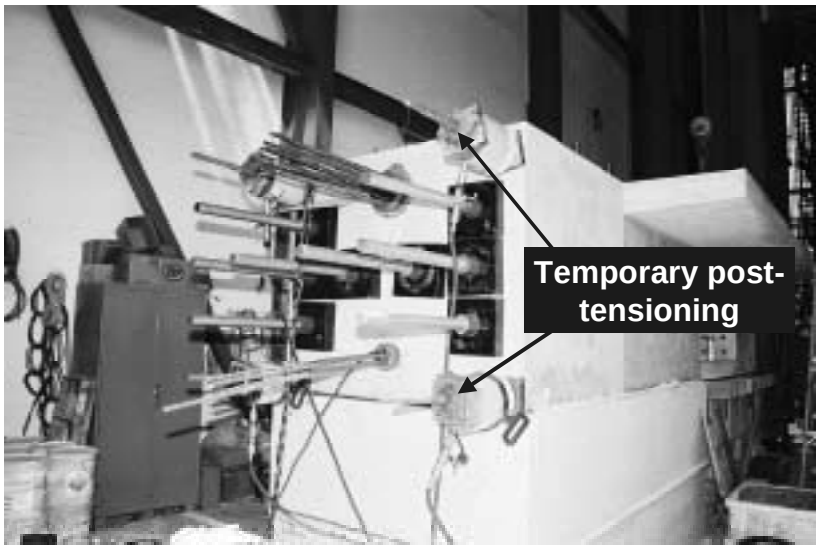


**Figure 5-18 End face of Segment 3 in Test Unit 100-INT**

After epoxy bonding of Test Unit 100-INT-CIP, the gap in the deck at location of Joint $J_1$ was closed by cast-in-place concrete. Figure 5-19 shows the deck gap in Unit

100-INT-CIP. The Overlapping headed reinforcing bars are shown in the figure. The concrete surface of the precast segments was roughly finished at the location of the deck gap to improve the interface between the precast concrete segments and the cast-in-place deck closure concrete.

**Figure 5-19 Gap in the deck of Test Unit 100-INT-CIP which was filled with cast-in-place concrete**

Each test unit was post-tensioned such that the effective post-tensioning forces at the time of testing were approximately 560 kips (2,491 kN) and 140 kips (623 kN) in the upper and lower tendons, respectively, as mentioned earlier. Figure 5-20 shows Test Unit 100-INT during post-tensioning of the upper tendon. The upper (top) and lower (bottom) tendons were post-tensioned from one end at the tip of Segment 1 (see Figure 5-20). The figure also shows the lower tendon. Figure 5-21 shows Joint $J_1$ of Unit 100-EXT during early stages of the test. Figure 5-21 shows the upper and lower external tendons. Figure

5-22 is similar to Figure 5-21, but it shows the exterior upper tendon in Unit 50-INT/50-EXT. After permanent post-tensioning of the test units the temporary bars in the deck and the bottom slab were removed. The wooden platform was removed following the permanent post-tensioning.

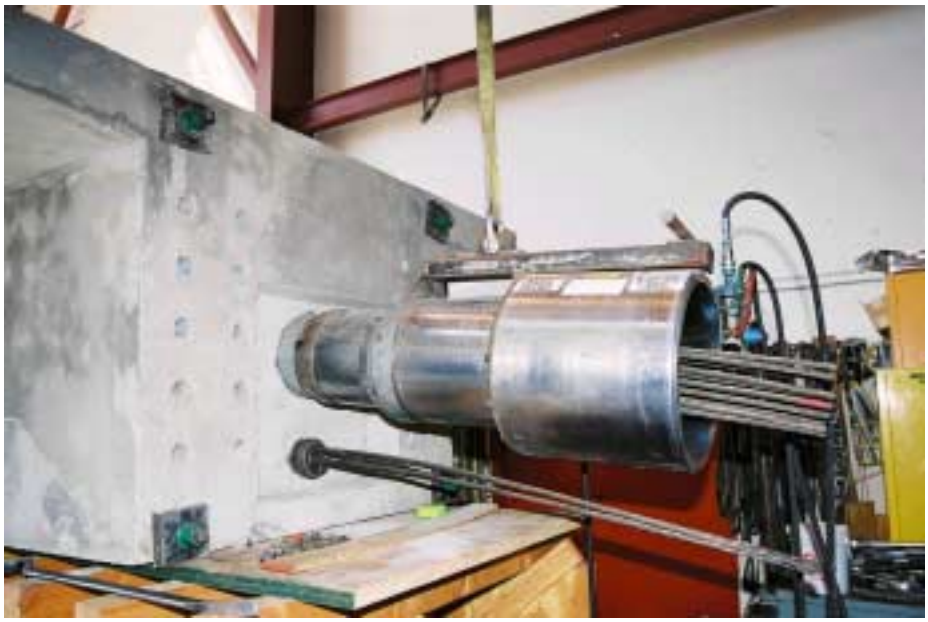

**Figure 5-20 Post-tensioning of Test Unit 100-INT**


**Figure 5-21 External Tendons in Test Unit 100-EXT**

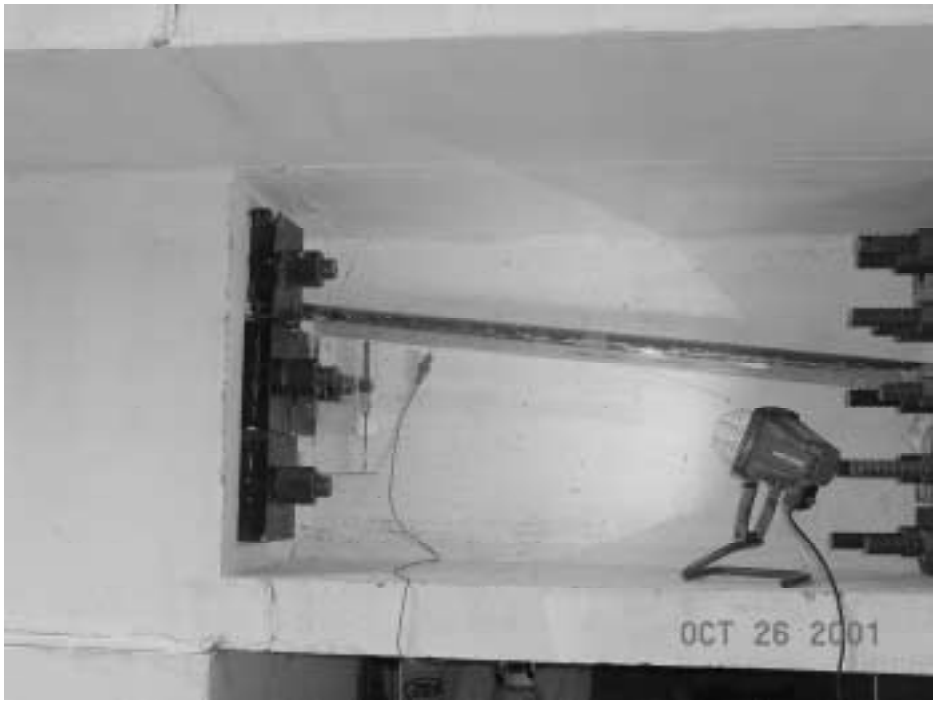


**Figure 5-22 External tendon in Test Unit 50-INT/50-EXT**

## 5.3 Materials Testing

Tests were conducted at the UCSD Powell Structural Laboratories to determine the material properties of the concrete used in all test units and the headed reinforcement used in the cast-in-place deck joints of Test Unit 100-INT-CIP. Compression tests were performed on unconfined concrete cylinders from each concrete batch. The day-of-test compressive strength of concrete for each test unit is given in Table 5-2. For Test Unit 100-INT-CIP the concrete compressive strength is also shown for the cast-in-place deck closure. Table 5-2 also gives the day-of-test compressive strength of the grout. The yield strength of the reinforcing steel in the cast-in-place deck closure joint of Unit 100-INT-CIP was 76.2 ksi (526 MPa); the measured ultimate strength of the headed bars was 100.7 ksi (694 MPa).

The adhesive used to join the segments was Sikadur 31 SBA (Segmental Bridge Adhesive), Slow-Set. It is a two-component moisture tolerant, high-modulus, high strength structural epoxy paste used specifically to bond hardened concrete in segmental bridge construction. The expected properties of this material were a compressive strength within 72 hours of 2,000 psi (13.8 MPa) and within 14 days a contact strength and bond strength of 1,000 psi (6.9 MPa) each.

**Table 5-2 Compressive strength of the concrete and the grout**

| Test Unit | | Day-of-Test compressive strength ksi (MPa) |
|---|---|---|
| 100-INT | Segment 1 | 5.02 (34.6) |
| | Segment 2 | 4.96 (34.2) |
| | Segment 3 | 5.79 (39.9) |
| | Grout | 4.66 (32.1) |
| 100-INT-CIP | Segment 1 | 6.02 (41.5) |
| | Segment 2 | 6.10 (42.1) |
| | Segment 3 | 7.15 (49.3) |
| | CIP Deck Closure | 4.46 (30.8) |
| | Grout | 2.17 (15.0) |
| 100-EXT | Segment 1 | 5.10 (35.2) |
| | Segment 2 | 5.89 (40.6) |
| | Segment 3 | 5.02 (34.6) |
| 50-INT/50-EXT | Segment 1 | 4.59 (31.7) |
| | Segment 2 | 5.00 (34.5) |
| | Segment 3 | 4.58 (31.6) |
| | Grout | 3.89 (26.8) |

## 5.4 Test Setup

A steel beam (steel nose) extended each test unit as shown in Figure 5-23. The external loads were applied on the steel beam and transferred to the concrete test unit through a moment connection between the steel beam and the end block of Segment No. 1 (see Figure 5-2). Up to 30-1 3/8″ (34.9 mm) ϕ ASTM A 722 high-strength bars were used to connect the steel beam to the concrete test unit. The post-tensioning forces of these high-strength bars were determined such that no joint opening occurs between the steel beam and the test unit. The connection was also designed to transfer high shearing forces without vertical slip between the steel beam and the test unit.

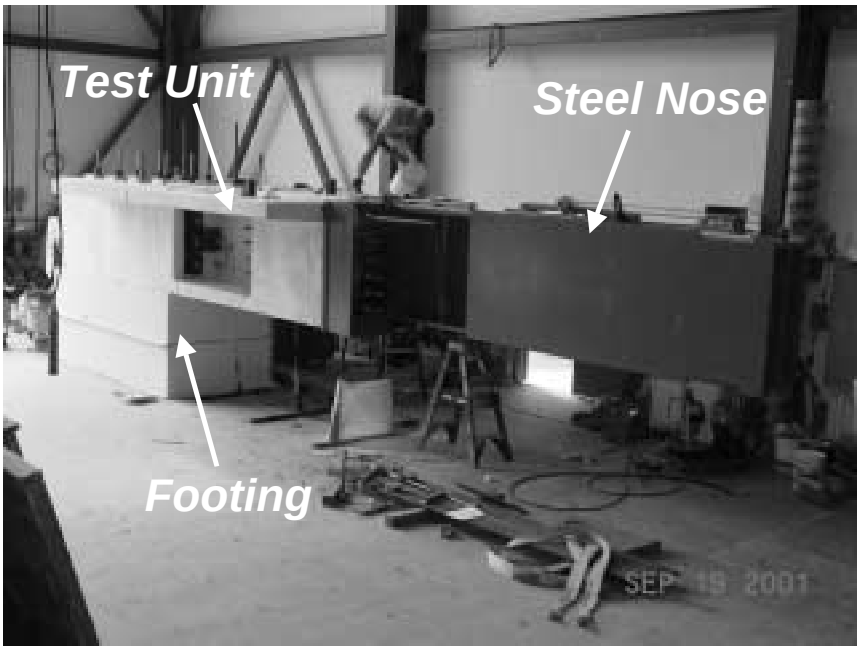


**Figure 5-23 One of the test units with the steel loading beam (steel nose)**

The test setup is shown in Figure 5-24 and Figure 5-25. Each test unit was simply supported on one side on precast concrete footing, simulating a fixed support. Two servo-controlled hydraulic actuators were used to apply external loads to the steel beam. The loads in the two actuators followed a prescribed function such that the correct simultaneous values of bending moment and shearing force would be applied at Joint $J_1$ of the test unit. It should be remembered that the objective of the Phase II experimental program was to investigate the seismic performance of Joint $J_1$ only. Simultaneous values of the shearing force that would be transferred with the bending moment at Joint $J_1$ were determined from analysis of the superstructure under gravity loads and longitudinal seismic loading. Each test was conducted in two stages as will be described in Section 5.6.

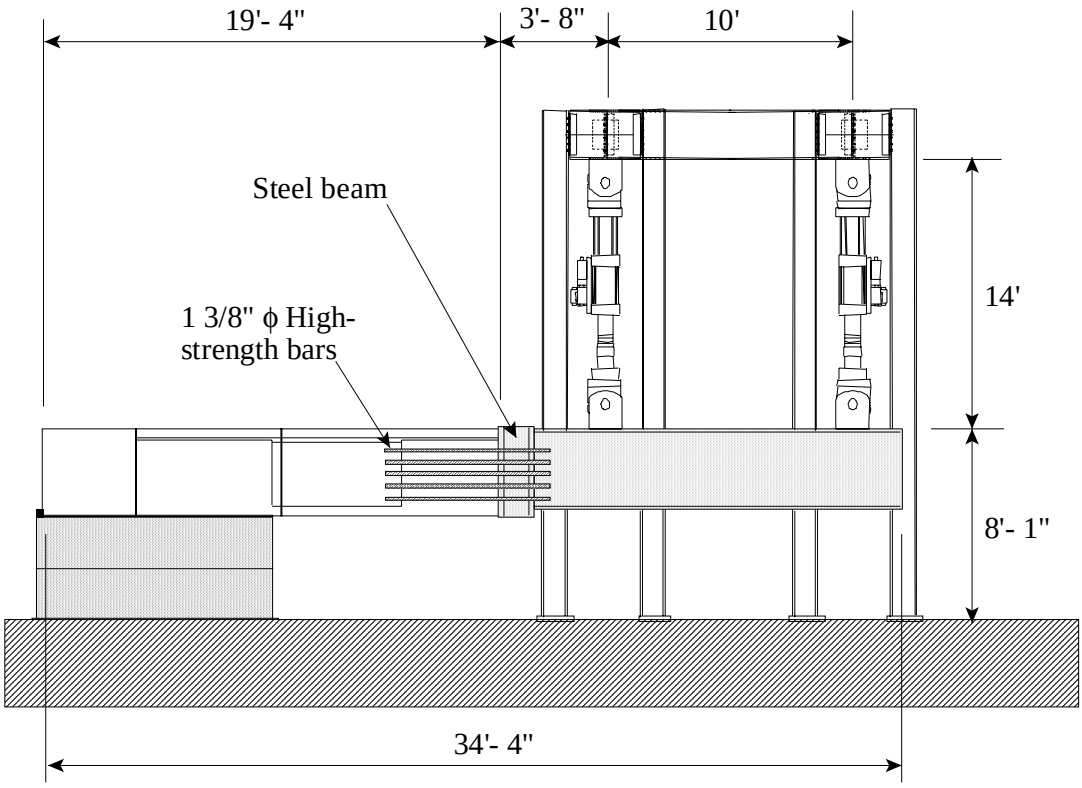


**Figure 5-24 Schematic drawing of the test setup**

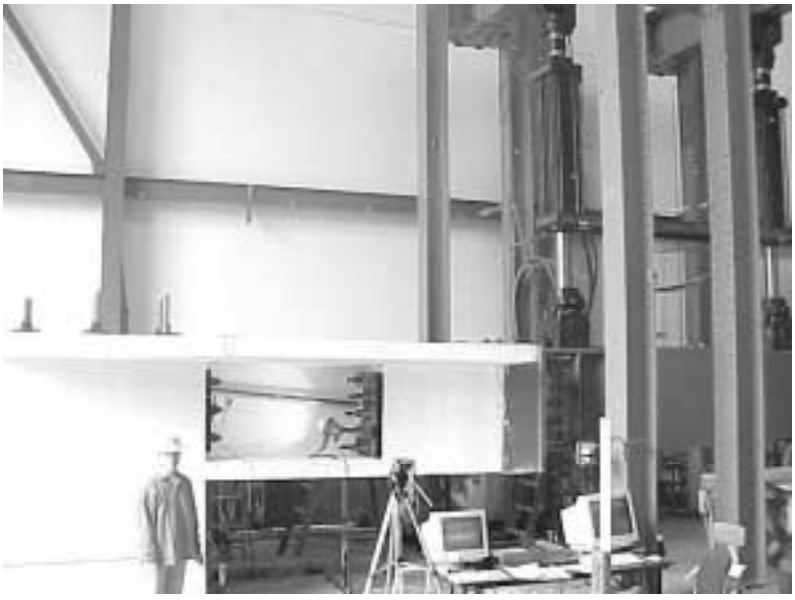

**Figure 5-25 Test setup (Test Unit 50-INT/50-EXT)**

## 5.5 Instrumentation

Each test unit was instrumented with 17 linear potentiometers to measure vertical displacements, relative vertical and horizontal displacements, up to 34 electrical resistance strain gages to measure strains in the post-tensioning steel, and 2 inclinometers to measure the rotation of Segments 1 and 2 in the vicinity of Joint $J_1$. Two electrical resistance strain gages were used to measure concrete strains at top and bottom surfaces of joint $J_1$. The results obtained from the concrete strain gages will be presented. Thirty-four electrical resistance strain gages were used to measure the strains in the headed bars of the cast-in-place deck closure joint in Test Unit 100-INT-CIP.

Figure 5-26 shows an elevation view of the potentiometers used to measure displacements during testing of each test unit. Figure 5-27 shows the potentiometers used to monitor the relative displacements between Segments 1 and 2 at Joint $J_1$. Potentiometers LPT-W and LPT-E shown in Figure 5-27 (Potentiometers LPT in Figure 5-26) were provided to measure the opening of Joint $J_1$ at the top surface of the test unit due to the applied bending moments. Similarly, potentiometers LPB-E and LPB-W (Figure 5-27) were provided to measure the joint opening at the bottom surface of the test unit. Opening of Joint $J_1$ was also measured at the elevation of the upper and lower tendons by potentiometers LPWH-T and LPWH-B (see Figure 5-27), respectively. Two vertical potentiometers were placed on the web of each test unit at the location of Joint $J_1$ to measure the relative vertical sliding between Segments 1 and 2 (see Figure 5-2 for segment numbers). These vertical potentiometers are labeled LPWV-E and LPWV-W and they are shown in Figure 5-27 (also designated as LPWV in Figure 5-26).

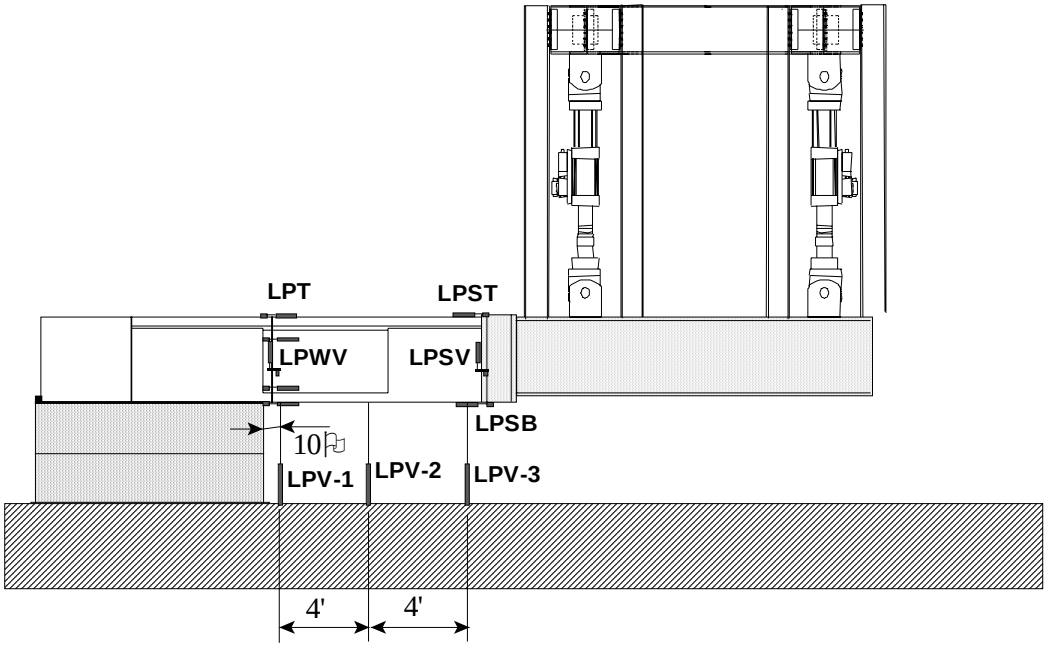


**Figure 5-26 Elevation of potentiometers used to monitor displacement of test units**

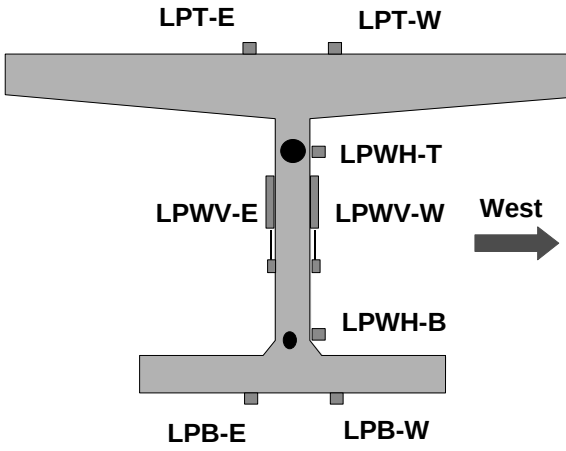


**Figure 5-27 Potentiometers used at the segment-to-segment joint $J_1$**

Potentiometers LPSV (one on each side of the test unit) were used to measure any relative vertical slip between the steel beam and the test unit (see Figure 5-26). Two other potentiometers were used to measure the joint opening between the steel beam and the test unit; these potentiometers were named LPST and LPSB (see Figure 5-26). The potentiometers mounted on the web of the test unit at location of Joint $J_1$ and are shown

in Figure 5-28a. Potentiometer LPSV used to measure the vertical slip between the steel beam and the test unit is shown in Figure 5-28b.

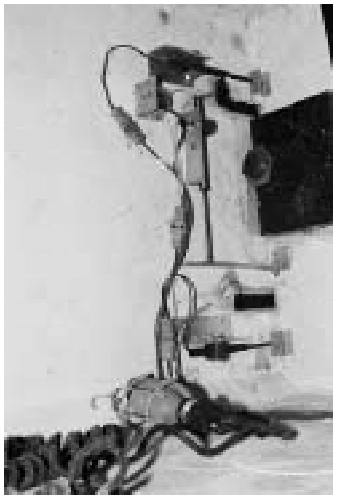

a) Instrumentation at web

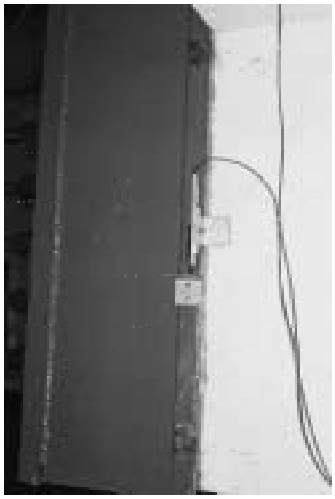

b) Instrumentation at steel beam

**Figure 5-28 Potentiometers to measure relative displacements**

As mentioned earlier, two inclinometers were mounted on the web of each test unit adjacent to Joint $J_1$ to measure joint rotations. The first inclinometer was mounted on Segment 1 and the second one was mounted on Segment 2. The difference between the readings of the two inclinometers gives the rotation of Joint $J_1$.

Figure 5-29 shows the locations of electrical resistance strain gages used to measure the strains in prestressing tendons of internally bonded tendons. Only one gage was placed on each strand of the external tendons since each strand would have a constant strain along its length in the test zone (test zone is shown in Figure 5-2).

Figure 5-30 shows the locations of electrical resistance gages used to measure the strains in the headed reinforcement bars in the cast-in-place deck closure joint of Test Unit 100-INT-CIP. Strains were measured in the bars only in one half of the test unit.

Strains were measured at the interface between the precast concrete and the cast-in-place concrete; the strains were also measured at location of Joint $J_1$ as shown in Figure 5-30.

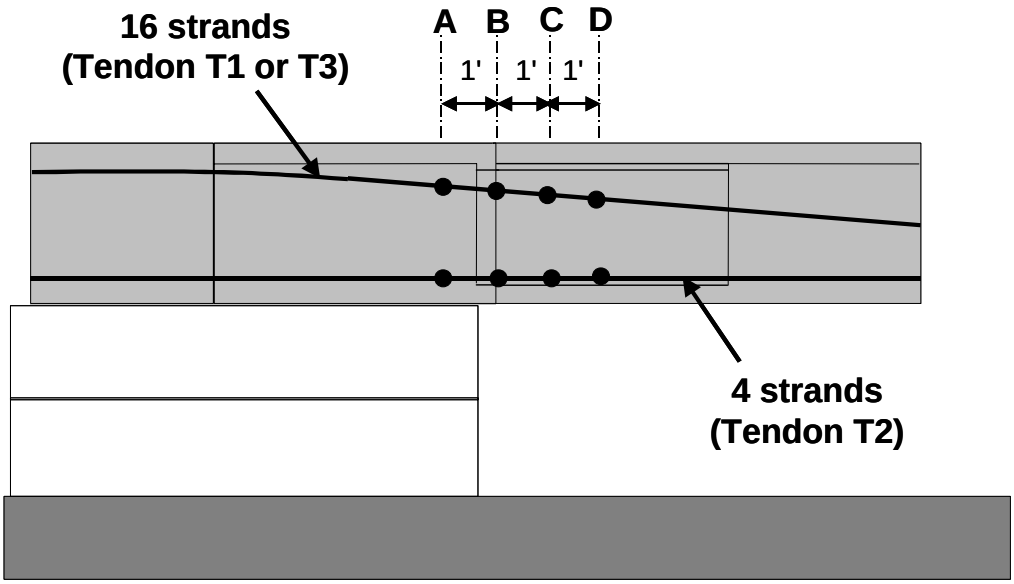


**Figure 5-29 Locations of strain gages in internally bonded tendons**

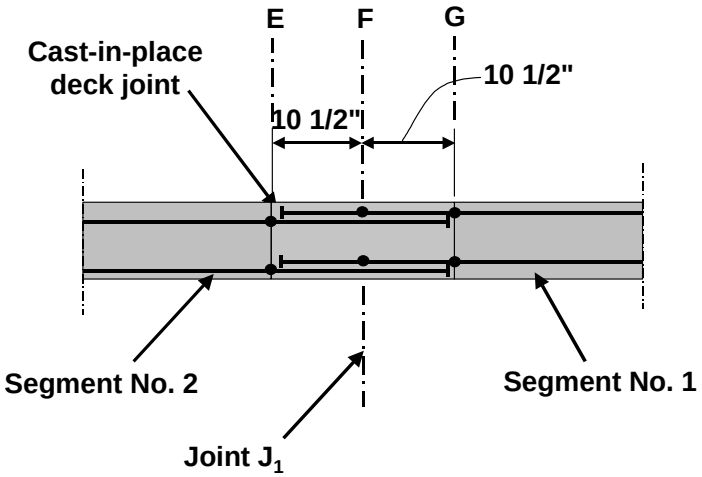


**Figure 5-30 Strain gages in longitudinal reinforcement in the cast-in-place deck closure joint of Test Unit 100-INT-CIP**

## 5.6 Loading Sequence

Unlike Phase I experiments, service load conditioning was not performed for the Phase II experiments. The test units of Phase I had linear elastic behavior under service load conditioning, thus it was decided to eliminate the service load conditioning stage from the tests of Phase II. The bottom soffit at midspan (modeled in Phase I tests) was subjected to zero concrete stress under extreme service load combination; whereas the joints close to the columns (modeled in Phase II tests) were subjected to higher residual compressive stresses under service loads. Thus likelihood of joint opening, or cracking at joint location, was higher at midspan of the prototype structure. Since no joints opened during service load conditioning of the Phase I test units, joint opening was not likely to occur under service load conditioning of the Phase II experiments. To simplify the test procedure, reduce the testing time and since service load conditioning will not affect results of the seismic test, it was decided not to perform service load conditioning in the Phase II experiments.

The seismic test of Phase II units was done in two stages. Additional loads were applied to each test unit in the first stage so that the concrete stresses at Joint $J_1$ of the test unit would match the concrete stresses in the corresponding joint in the prototype structure under dead load and superimposed dead loads. These additional loads were required because of the reduced scale of the test unit (2/3-scale) and also because of the superimposed dead loads in the superstructure.

Under the effect of dead load and superimposed dead loads, the concrete stresses in the prototype structure at top and bottom surfaces of the joint were -480 psi (-3.3 MPa) and –579 psi (-4 MPa), respectively. Finite element analyses of the Phase I test units

showed that the prestressing force is reduced with increased reversed cyclic displacements, especially in internally bonded tendons (Sections 4.2.1 and 4.2.4). In design of the loading protocol of the Phase II test units and based on the analytical observations of Phase I, it was decided not to simulate the concrete stresses resulting from secondary prestressing effects in the prototype structure. This is because the prestressing force can be reduced with cyclic loading (see Figure 4-4 and Figure 4-13) and also to keep the maximum actuator forces expected during the seismic test below the actuators' force capacity. Ignoring the secondary effects of prestressing on the reference load values would affect the flexural moment at onset of joint opening, but would not affect performance of the segment-to-segment joint after cracking, or the failure mode and displacement capacity of the test units. This resulted in concrete stresses of -56 psi (-0.4 MPa) and –1,325 psi (-9.1 MPa) at top and bottom surfaces, respectively. The applied loads at the test unit to match these stresses are shown in Figure 5-31. The loads shown in Figure 5-31 resulted in concrete stresses of –56 psi (-0.4 MPa) and –1,323 psi (-9.1 MPa) at top and bottom surfaces, respectively at location of Joint $J_1$. The concrete stresses in each test unit were very close to the corresponding concrete stresses in the prototype structure. The shearing force transferred at the first segment-to-segment joint in the prototype structure was 364 kips (1,619 kN). The corresponding shearing force at Joint $J_1$ in the test units (2/3-scale) = 0.5 x (364) x $(2/3)^2$ = 80.9 kips (360 kN). The applied loads shown in Figure 5-31, in addition to self-weight of the steel beam and the test unit resulted in a shearing force of 81.5 kips (363 kN) at the location of Joint $J_1$. The above indicates the accurate simulation in the test units of the bending moments and the

simultaneous shearing forces in the prototype structure. The loads shown in Figure 5-31 are referred to as the reference load level throughout Chapter 6 of this report.

The second stage of testing represented the seismic test. Starting from the reference load level, each test unit was subjected to fully reversed cyclic vertical displacements applied at the location of the actuator closest to the steel beam cantilever tip as shown in Figure 5-32. The actuator closest to the cantilever tip was the master actuator and the test unit was loaded in displacement control.

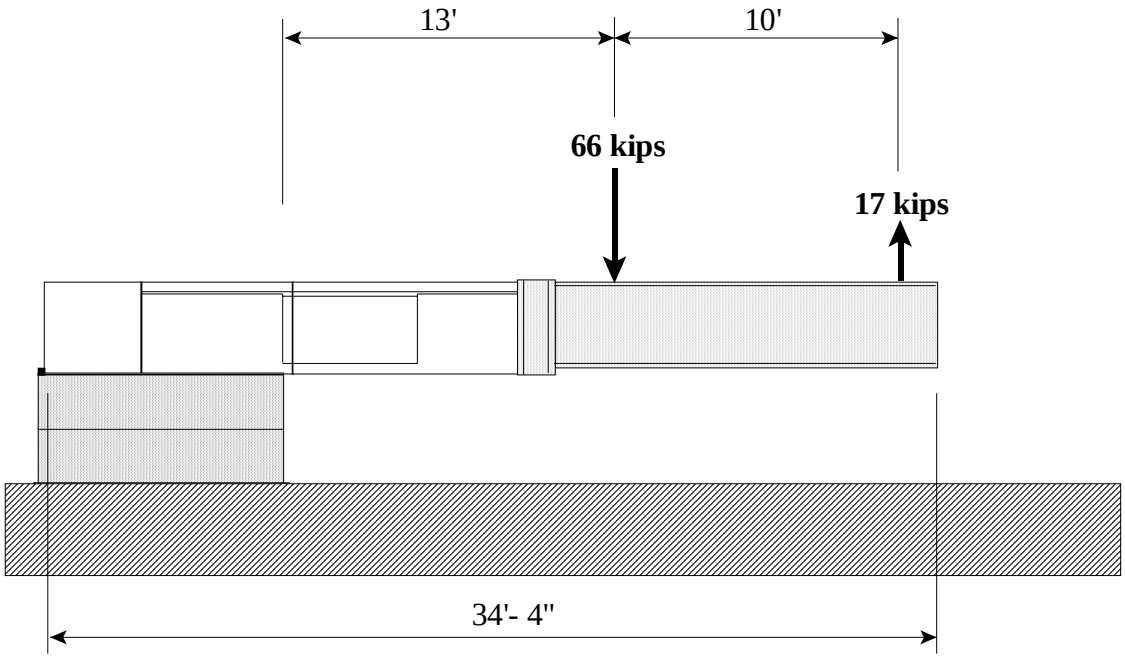


**Figure 5-31 Applied Loads on the test unit before the seismic test**

**(Reference Load Level)**

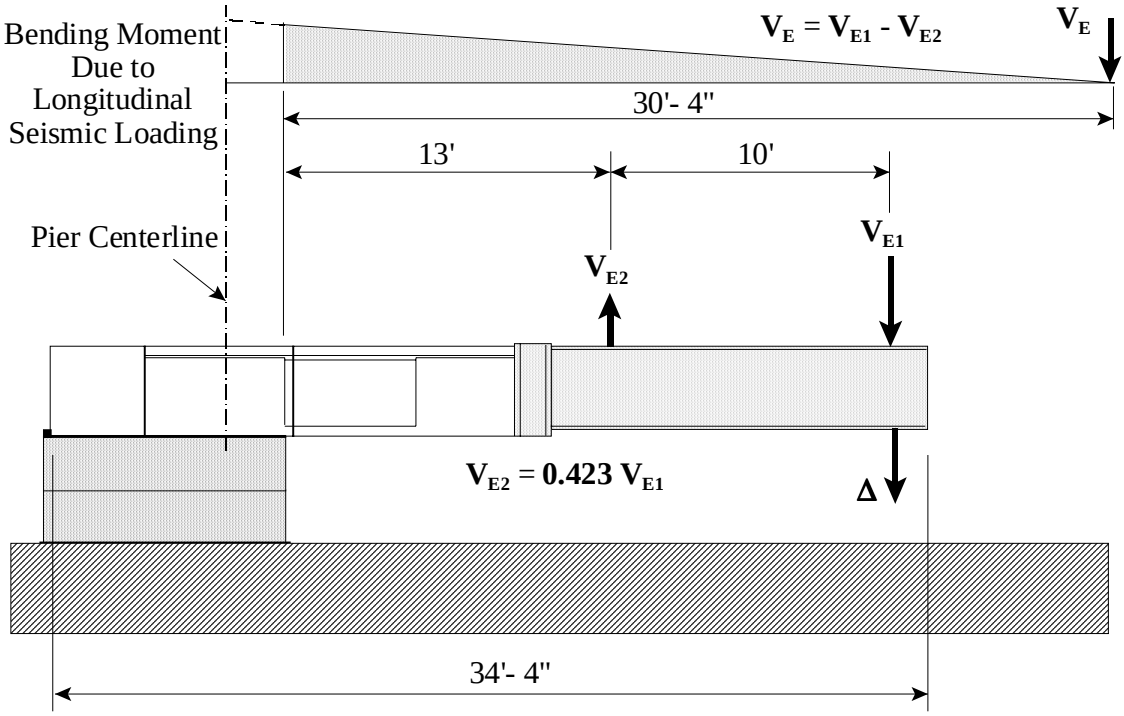


**Figure 5-32 Loading procedure during the seismic test**

The second actuator was loaded in force control. The force in the second actuator was related to the force in the master actuator by a prescribed function. The prescribed function of the force in the second actuator, $V_{E2}$, is given in Figure 5-32. It should be mentioned that $V_{E1}$ and $V_{E2}$ in Figure 5-32 are the change in actuator forces during the seismic test only. It means the actuator forces at the reference load level (shown in Figure 5-31) must be added to $V_{E1}$ and $V_{E2}$ in order to determine the total force in each of the two actuators. The prescribed function relating $V_{E2}$ to $V_{E1}$ was obtained from the bending moment diagram in the prototype structure due to longitudinal seismic forces, which is schematically shown in Figure 5-32. The prescribed function of the actuator forces was determined such that the correct combination of bending moments and the corresponding shearing forces are transferred at Joint $J_1$ throughout the test.

Each test unit was subjected to fully reversed loading cycles with increasing displacement amplitude. The control displacement was that below the master actuator and is denoted as Δ in Figure 5-32. The displacement Δ was applied in increasing amplitude according to the loading protocol shown in Figure 5-33. Three cycles were performed at each displacement level until failure.

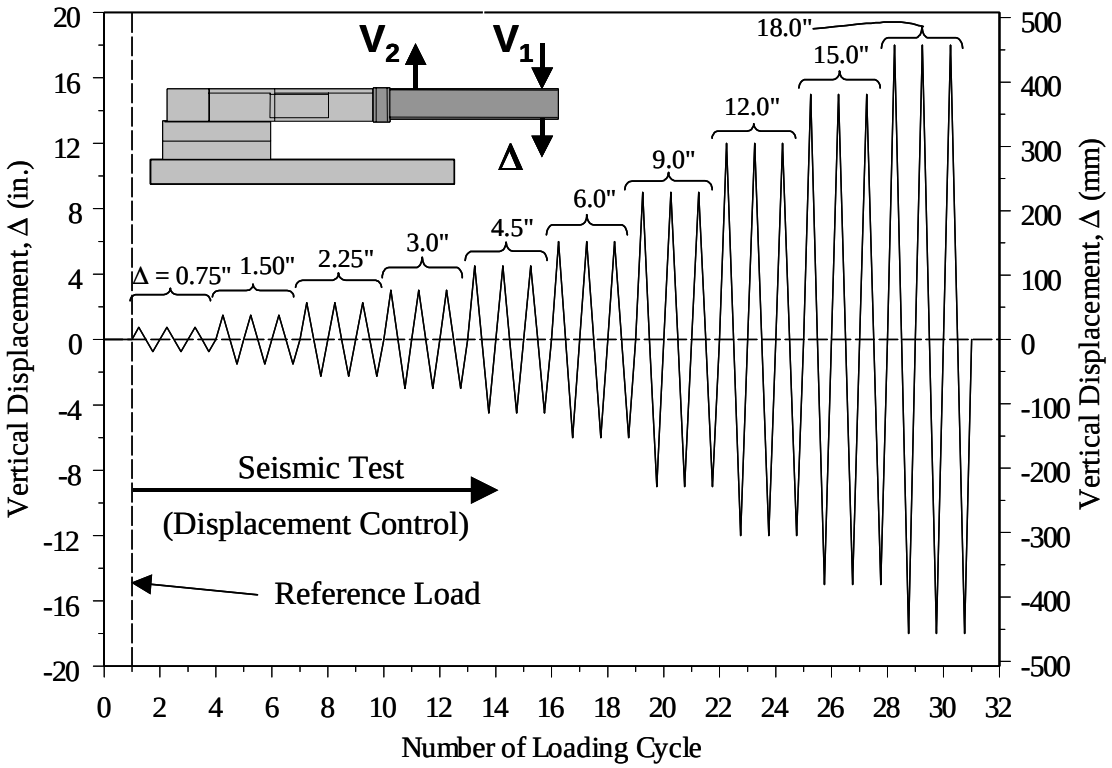


**Figure 5-33 Loading protocol for the seismic test (Phase II)**

# 6 Experimental Results of Segment-to-Segment Joints Subjected to High Bending Moments Combined With High Shears (Phase II)

The experimental results of the Phase II test units are presented in this chapter. The major objectives of the experimental program of Phase II were to investigate the seismic performance of the segment-to-segment joints subjected to high bending moments combined with high shears in terms of: (1) opening and closure of the joints under repeated reversed cyclic displacements, (2) crack development and propagation, and (3) modes of failure.

## 6.1 General Observations

### 6.1.1 Test Unit 100-INT

No cracks occurred during the first stage of the test, or in other words when the test unit was loaded to the reference load level. The seismic test (Stage II of the test) started from the reference load level with downward loading of the test unit up to $\Delta$ = 0.75 in. (19 mm) (see Section 5.6). As expected, the first crack occurred at the location of Joint $J_1$ during this loading cycle. The total seismic force of the actuators at onset of cracking was about 45 kips (200 kN). The term seismic force referred to throughout this chapter is the summation of the two actuator forces during the seismic testing stage; thus the seismic force = $V_E = V_{E1} - V_{E2}$ (because the forces in the two actuators were applied in opposite directions). In addition to the seismic force on the test unit (= $V_{E1} - V_{E2}$), the shearing

force resulting from the reference loads was, $V_{ref}$ = 66 – 17 = 49 kips (218 kN). A shearing force of about 32 kips (142 kN), resulting from the self-weights of the test unit and the steel beam, should also be added to $V_{ref}$ and $V_E$ to obtain the total shearing force transferred at Joint $J_1$. Thus, the onset of cracking occurred when the shearing force transferred at Joint $J_1$ was about 126 kips (560 kN). The first crack occurred at the top surface of the test unit and adjacent to the location of the epoxy bonded joint surface. Figure 6-1 shows Joint $J_1$ of Test Unit 100-INT at 0.75 in. (19 mm) downward displacement. Onset of cracking under upward loading occurred at Joint $J_1$ in the bottom surface of the test unit during the first cycle to 0.75 in. (19 mm) upward displacement. Unit 100-INT at 0.75 in. (19 mm) upward displacement is shown in Figure 6-2.

The crack propagated adjacent to the epoxy-bonded joint in the web of Segment 1. Under upward loading, Joint $J_1$ opened at the bottom surface of the test unit and longitudinal reinforcing bars could be seen sticking out of the bottom slab of Segment 1. As the joint closed during the following downward loading cycles, these bars (protruding from Segment 1) came in contact with the concrete surface of Segment 2 (pier segment).

**Figure 6-1 Test Unit 100-INT at 0.75 in. (19 mm) downward displacement**

**Figure 6-2 Test Unit 100-INT at 0.75 in. (19 mm) upward displacement**

With repeated opening and closure of the joint, these reinforcing bars started to buckle. It appeared that there was some concrete segregation in the bottom slab of Unit 100-INT. The top concrete cover of the bottom slab was relatively weak and it could not prevent buckling of the bottom slab longitudinal reinforcement. As a result of this, the bars buckled and pushed the concrete cover resulting in crushing of the bottom slab concrete at 3 in. (76 mm) of downward displacement (see Figure 6-3).

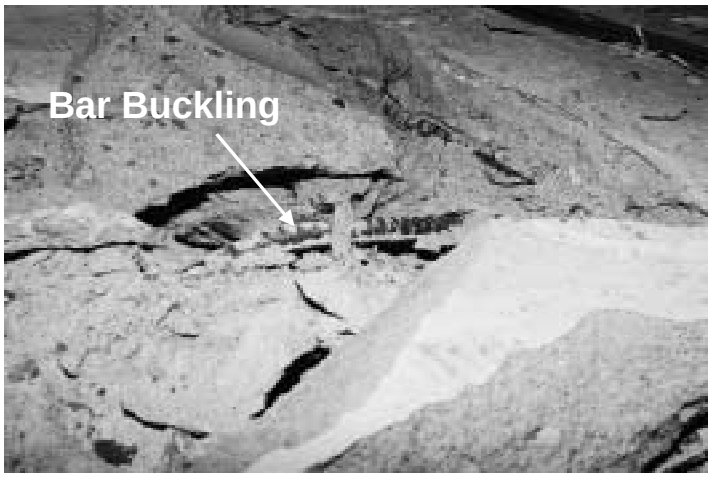


**Figure 6-3 Bottom slab of Unit 100-INT at 3 in. (76 mm) downward displacement**

With increased displacements, other cracks occurred in Segments 1 and Segment 2 in the vicinity of Joint $J_1$. Figure 6-4 shows Unit 100-INT at 3 in. (76 mm) upward displacement; the figure shows the cracks in the web of Segment 1. Despite the few cracks that occurred in the joint vicinity, the major crack was the first one, which occurred just outside the joint interface. The joint opening increased significantly with increased applied displacements. Performance of the test unit was dominated by flexure.

The test was continued until compression failure of the bottom slab under downward loading at 6 in. (152 mm) displacement. Figure 6-5a shows the joint of Test Unit 100-INT at 6 in. (152 mm) displacement. Immediately after the photo shown in Figure 6-5a was taken, concrete compression failure occurred in the bottom slab at location of the joint as shown in Figure 6-5b. The total applied seismic force was reduced as a result of this compression failure by about 19 kips (85 kN). The test could be continued until an explosive compression failure occurred in the bottom slab and the web during the second loading cycle at 6 in. (152 mm) displacement (see Figure 6-6). The seismic load carrying capacity was lost, but the test unit could sustain the applied reference loads. After this explosive failure, relative vertical slip was observed between the segments adjacent to Joint $J_1$ as can be seen in Figure 6-6.


**Figure 6-4 Cracks in Unit 100-INT at 3 in. (76 mm) upward displacement**

After failure of the test unit under downward loading, it was decided to load the test unit in the upward direction only up to failure. The upward displacement, Δ, was applied with increasing amplitudes up to failure. Three cycles were performed at each displacement level. The test unit failed by compression in the deck at about 12 in. (305 mm) of upward displacement as shown in Figure 6-7 and Figure 6-8.

a) Just before concrete crushing

b) Just after concrete crushing

**Figure 6-5 Test Unit 100-INT at 6 in. (152 mm) downward displacement**

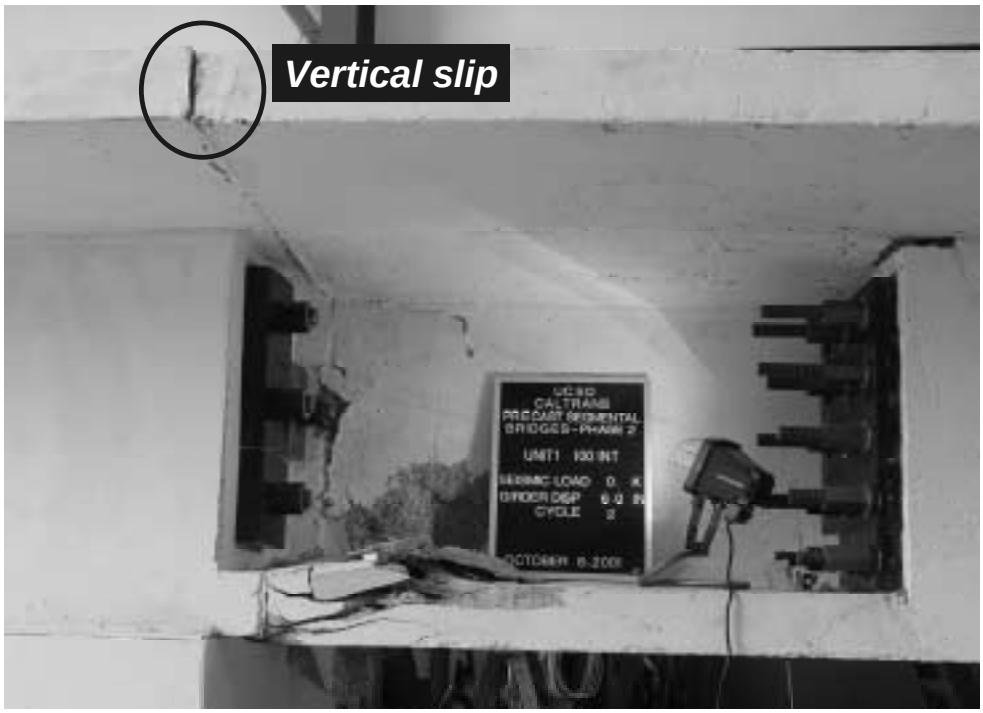


**Figure 6-6 Compression failure of Test Unit 100-INT under downward loading**

**Figure 6-7 Compression failure of Test Unit 100-INT under upward loading**


**Figure 6-8 Compression failure of the deck in Test Unit 100-INT**

The prestressing tendons were inspected after the test to see if any strands fractured. No signs of strand fracture could be found in the upper tendon as can be seen in Figure 6-9a. The lower (horizontal) tendon also did not fracture. However, Figure 6-9b shows signs of buckling of the lower tendon as it was subjected to compressive stresses under downward loading at high displacement levels.

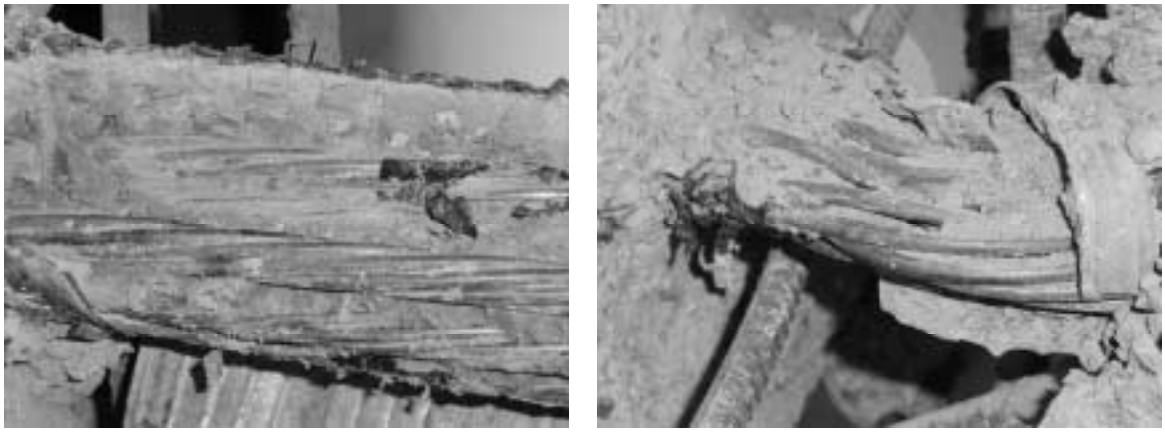

a) Upper tendon b) Lower tendon

**Figure 6-9 Prestressing steel after failure of Test Unit 100-INT**

Figure 6-10 shows a portion of the web of the I-shaped cross section after failure of Unit 100-INT. The shear keys and the epoxy layer at Joint $J_1$, between Segments 1 and 2, can be seen in the figure. As in the Phase I experiments, the crack occurred in the concrete cover of the precast segment rather than at the joint interface, as can be seen in Figure 6-10.

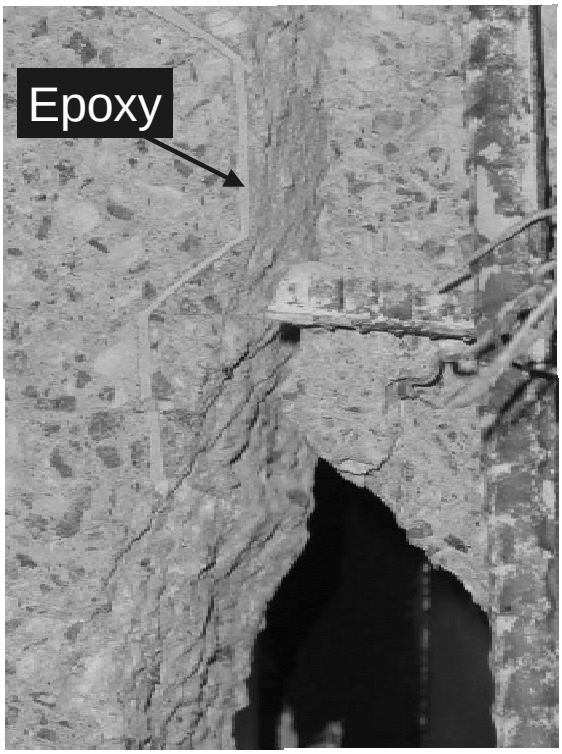


**Figure 6-10 Segment-to-segment joint after failure of Test Unit 100-INT**

The above indicates that performance of Test Unit 100-INT was dominated by flexure. The test unit failed in compression under both loading directions. Despite the high shearing force transferred at Joint $J_1$, relative vertical slip between the adjacent precast segments occurred only after compression failure in the bottom slab.

### 6.1.2 Test Unit 100-INT-CIP

As in Unit 100-INT, no cracks occurred during the first stage of the test, or in other words when the test unit was loaded to the reference load level. The first crack occurred at the location of Joint $J_1$ during the first loading cycle to $\Delta$ = +0.75 in. (19 mm); the positive sign convention is for downward displacement or load. The total seismic force of the actuators at onset of cracking was about 15 kips (67 kN). Thus, at onset of cracking the shearing force transferred at Joint $J_1$ was about 96 kips (427 kN). The first crack occurred at the top surface of the test unit at the construction joint between the precast Segment No. 1 and the cast-in-place deck closure joint. Another crack occurred simultaneously at the construction joint between Segment No. 2 and the cast-in-place deck closure joint. Figure 6-11 shows Joint $J_1$ of Test Unit 100-INT-CIP at 0.75 in. (19 mm) downward displacement. The figure shows the two cracks that occurred at the interface between the cast-in-place deck closure joint and the precast concrete of Segments 1 and 2. It should be remembered that longitudinal deck reinforcing bars of the precast Segments 1 and 2 overlapped within the cast-in-place joint. Thus the interior portion of the cast-in-place joint was heavily reinforced, whereas less reinforcement existed at the construction joint. Thus, the first cracks occurred at the interface between the cast-in-place joint and the precast segments. Other cracks also occurred in the deck along the length of the precast Segment No. 1.

Onset of cracking under upward loading occurred at the bottom surface of Joint $J_1$ during the first cycle to 0.75 in. (19 mm) upward displacement. Unit 100-INT-CIP at 0.75 in. (19 mm) upward displacement is shown in Figure 6-12. The crack occurred in the concrete cover of Segment No. 2 (pier segment) adjacent to the epoxy bonded Joint $J_1$.

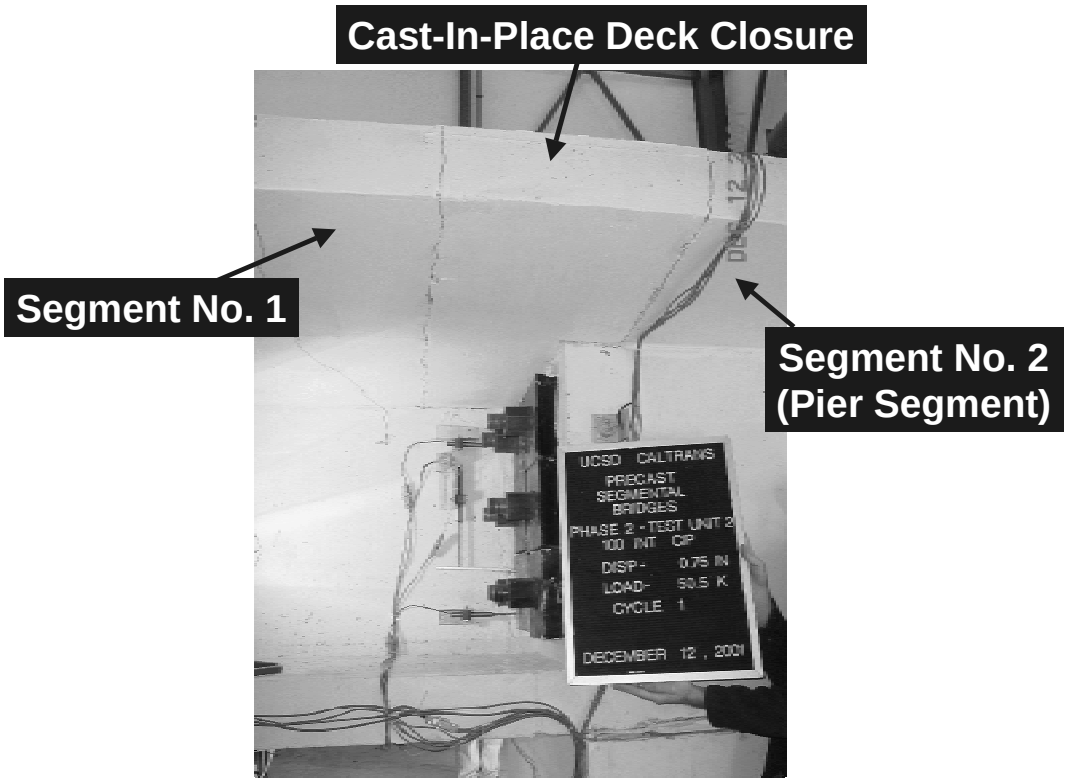


**Figure 6-11 Test Unit 100-INT-CIP at 0.75 in. (19 mm) downward displacement**

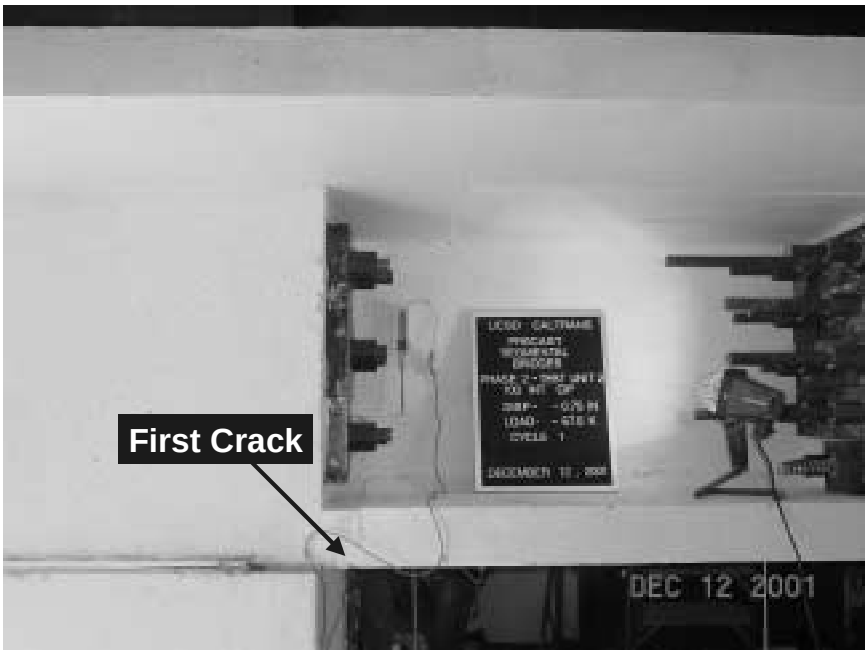


**Figure 6-12 Test Unit 100-INT-CIP at 0.75 in. (19 mm) upward displacement**

With increased displacements, other cracks occurred in Segments 1 and Segment 2 in the vicinity of Joint $J_1$. Figure 6-13 shows the deck of Unit 100-INT-CIP at 3 in. (76 mm) downward displacement. Figure 6-13 shows that instead of one wide crack at the location of Joint $J_1$ in Unit 100-INT, several closely spaced cracks with small widths occurred in the deck of Unit 100-INT-CIP. The reason for different crack development under downward loading of Unit 100-INT-CIP was the continuity of the deck and the mild steel reinforcement crossing the segment-to-segment joints. This mild steel reinforcement controlled the widths of cracks in the deck of Unit 100-INT-CIP.

Figure 6-14 shows Segment No. 1 under 3.0 in. (76 mm) downward displacement. It will be shown later that Test Unit 100-INT-CIP was subjected to the highest downward loads among all test units because of the mild reinforcement crossing Joint $J_1$. Thus, Unit 100-INT-CIP was subjected to the highest shearing forces. Shear cracks occurred in the web of Segment 1 as a result of the high shearing forces (see Figure 6-14), however no vertical slip occurred between Segments 1 and 2 before flexural failure of the test unit.

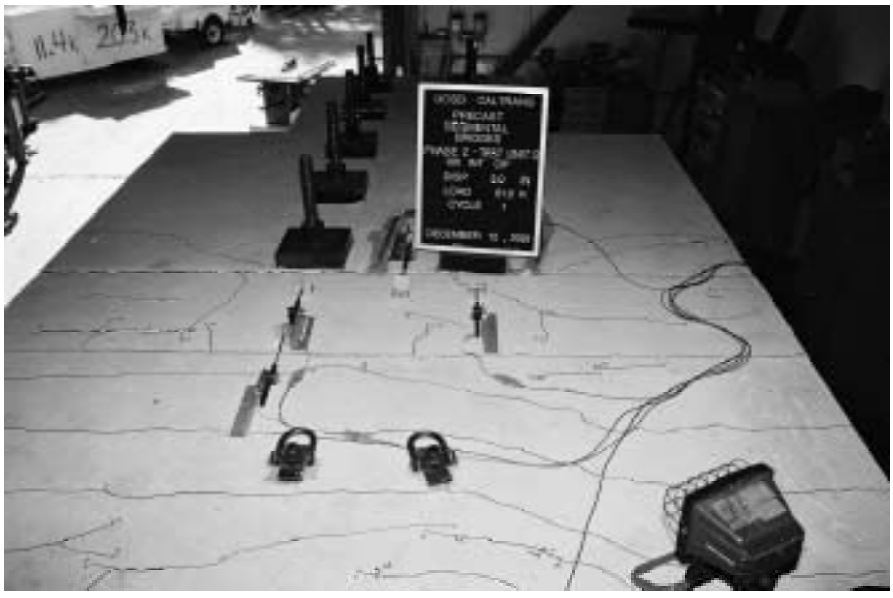

**Figure 6-13 Cracking in the deck of Unit 100-INT-CIP**

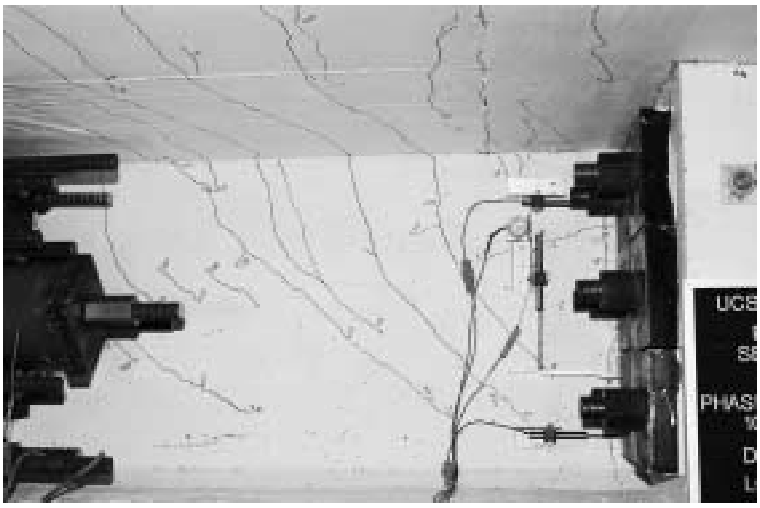

**Figure 6-14 Shear cracks in Unit 100-INT-CIP**

Widths of the closely spaced cracks shown in Figure 6-13 increased at higher displacements in the downward direction. The two cracks, which occurred between the cast-in-place deck closure joint and the deck of Segments 1 and 2 had the highest crack widths. Other cracks, which occurred along the length of Segment 1 had small widths throughout the test. Figure 6-15 shows Test Unit 100-INT-CIP at $\Delta$ = +6.0 in. (152 mm); signs of compression failure in the bottom slab were observed at this displacement level.


**Figure 6-15 Test Unit 100-INT-CIP at 6 in. (152 mm) downward displacement**

The dominant crack at the bottom surface of Unit 100-INT-CIP was the first crack, which occurred under upward loading in the concrete cover adjacent to Joint $J_1$. Unlike the deck, there was no mild reinforcement crossing Joint $J_1$ in the bottom slab of Unit 100-INT-CIP. Thus, this single crack opened significantly under upward loading at high displacement levels.

As mentioned earlier, signs of compression failure were observed in the bottom slab at 6 in. (152 mm) downward displacement. Immediately after reaching $\Delta$ = +6.0 in. (152 mm) the load carrying capacity of Unit 100-INT-CIP dropped by about 27 kips (120 kN). However, the test was continued until severe concrete crushing of the bottom slab and the web, which occurred at about 6.4 in. (163 mm) displacement. A maximum downward displacement, $\Delta$ = +9.0 in. (229 mm) was reached during the test and the seismic load carrying capacity of the test unit at this displacement level was about 5 kips (22 kN) only. However despite the severe damage at this displacement level, the test unit was still able to carry the reference loads, which represented the dead loads and superimposed dead loads of the prototype structure. Figure 6-16 shows Test Unit 100-INT-CIP at 9 in. (229 mm) displacement.

After failure of the test unit under downward loading, it was decided to apply upward displacements only until failure of the test unit in the upward loading direction. The displacement, $\Delta$, was applied in upward direction with increasing amplitudes up to failure. Three cycles were performed at each displacement level with no reversal of the applied displacement. Failure of the test unit occurred at about $\Delta$ = -14.3 in. (-363 mm) when the strands in the lower (horizontal) tendon fractured. Figure 6-17 shows Unit 100-INT-CIP at the maximum reached displacement, $\Delta$ = -15.0 in. (-381 mm). The concrete

around the lower tendon was removed after the test. Figure 6-18 shows the lower tendon after removal of the surrounding concrete; the figure shows fracture of the strands.


**Figure 6-16 Compression failure of Test Unit 100-INT-CIP under downward loading at 9 in. (229 mm)**


**Figure 6-17 Test Unit 100-INT-CIP at 15 in. (381 mm) upward displacement**

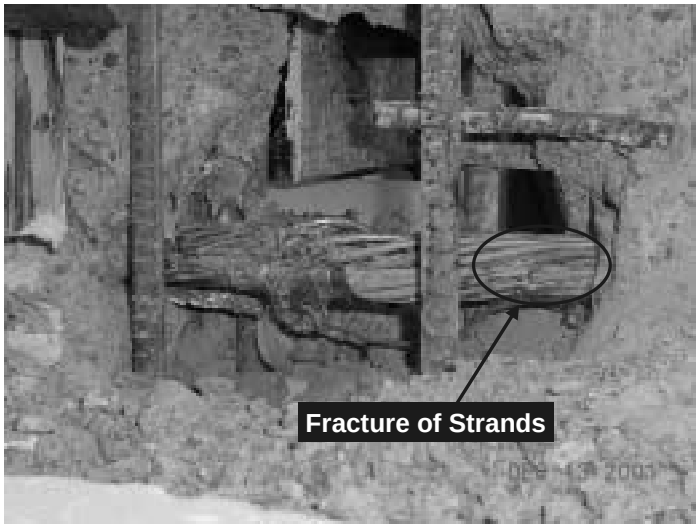


**Figure 6-18 Fracture of the lower tendon in Test Unit 100-INT-CIP**

### 6.1.3 Test Unit 100-EXT

No cracks occurred during the first stage of the test, or in other words when the test unit was loaded to the reference load level (reference load values given in Figure 5-31). As for Unit 100-INT, the first crack occurred at the location of Joint $J_1$ during the first loading cycle to a downward displacement of $\Delta$ = +0.75 in. (19 mm) (see Figure 5-33). The total seismic force of the actuators at onset of cracking was about 34 kips (151 kN). Thus, the onset of cracking occurred when the shearing force transferred at Joint $J_1$ was about 115 kips (512 kN). The first crack occurred at the top surface of the test unit and adjacent to location of the joint. Figure 6-19 shows Joint $J_1$ of Test Unit 100-EXT at 0.75 in. (19 mm) downward displacement. Onset of cracking under upward loading occurred at the bottom surface of Joint $J_1$ during the first cycle to 0.75 in. (19 mm) displacement. Unit 100-EXT at 0.75 in. (19 mm) upward displacement is shown in Figure 6-20.

**Figure 6-19 Test Unit 100-EXT at 0.75 in. (19 mm) downward displacement**


**Figure 6-20 Test Unit 100-EXT at 0.75 in. (19 mm) upward displacement**

With increased displacements, other cracks occurred in Segments 1 and 2 in the vicinity of Joint $J_1$. The major crack was the first one, which occurred just outside the joint interface. This crack opened significantly with increased applied displacements. Performance of the test unit was dominated by flexure.

The test was continued until concrete softening of the bottom slab under downward loading at 6 in. (152 mm) displacement. Figure 6-21 shows the joint of Test Unit 100-EXT at 6 in. (152 mm) displacement. The figure shows horizontal cracks at the side of the bottom slab. Signs of concrete spalling at the bottom surface of Unit 100-EXT were also observed at 6 in. (152 mm) downward displacement, and it can be seen in Figure 6-22.


**Figure 6-21 Compression softening of the bottom slab of Unit 100-EXT at 6 in. (152 mm) downward displacement**

**Figure 6-22 Bottom surface of Test Unit 100-EXT at**

**6 in. (152 mm) downward displacement**

Despite the signs of compression failure observed at 6 in. (152 mm) downward displacement, the test could be continued to a much higher displacement level with insignificant reduction in the load carrying capacity of the test unit. Joint $J_1$ experienced repeated opening and closure and significant joint openings were measured. The significant joint opening can be seen in Figure 6-23, which shows Test Unit 100-EXT at 12 in. (305 mm) downward displacement. Despite the significant joint openings, the joint had the capability to transfer high bending moments combined with high shearing forces.


**Figure 6-23 Test Unit 100-EXT at 12 in. (305 mm) downward displacement**

Compression softening and strength degradation of the test unit occurred with further cyclic loading. Figure 6-24 shows the test unit at 12 in. (305 mm) upward displacement, which was the last loading cycle before termination of the test. The figure shows relative vertical slip between the precast segments adjacent to Joint $J_1$. Figure 6-25 shows concrete crushing in the deck of the test unit. Some of the strand wires in the upper tendon (inclined tendon) fractured during downward loading of the test unit at high displacement levels. Some of the fractured strands in the upper tendon are shown in

Figure 6-26. Some of the strand wires of the lower (horizontal) tendon also fractured under upward loading at high displacement levels.

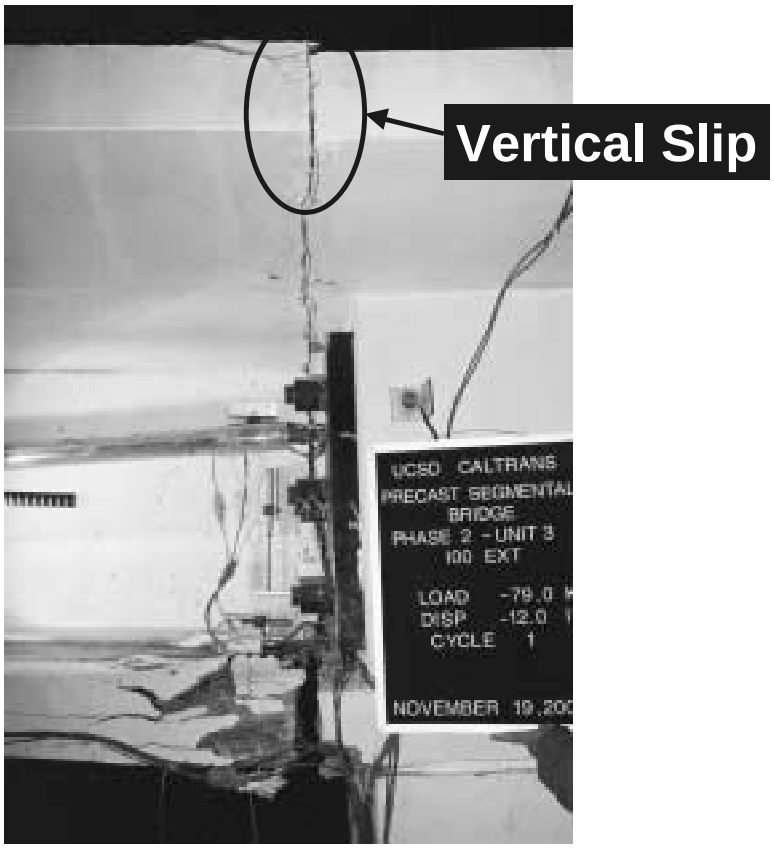


**Figure 6-24 Test Unit 100-EXT at 12 in. (305 mm) upward displacement**

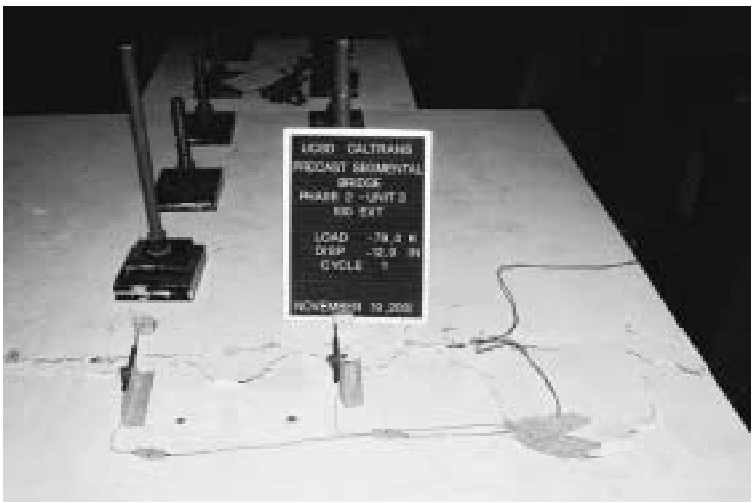

**Figure 6-25 Concrete spalling in the deck in Test Unit 100-EXT**

**Figure 6-26 Fracture of strand wires in the upper tendon of Test Unit 100-EXT**

The test was terminated at about 13.2 in. (335 mm) downward displacement when the bottom slab and bottom portion of the web experienced explosive compression failure at location of Joint $J_1$ (see Figure 6-27). The seismic load carrying capacity was lost after occurrence of this explosive compression failure. Buckling of the lower (horizontal) tendon was observed during the last downward loading cycle just before termination of the test as shown in Figure 6-28.


**Figure 6-27 Compression failure of Test Unit 100-EXT**


**Figure 6-28 Buckling of the lower tendon of Test Unit 100-EXT**

### 6.1.4 Test Unit 50-INT/50-EXT

As in all other test unit, no cracks occurred in Unit 50-INT/50-EXT during the first stage of the test up to application of the reference loads. The first crack occurred at the location of Joint $J_1$ under downward loading during the first displacement cycle of $\Delta$ = +0.75 in. (19 mm). The total seismic force of the actuators at onset of cracking was about 29 kips (129 kN). Thus at onset of cracking, the shearing force transferred at Joint $J_1$ was about 110 kips (489 kN). The first crack occurred at the top surface of the test unit and adjacent to the location of the epoxy bonded joint surface. Figure 6-29 shows Joint $J_1$ of Test Unit 50-INT/50-EXT at 0.75 in. (19 mm) downward displacement. Onset of cracking under upward loading occurred at the bottom surface of Joint $J_1$ during the first cycle to 0.75 in. (19 mm) upward displacement. Figure 6-30 shows Unit 50-INT/50-EXT at 0.75 in. (19 mm) upward displacement.


**Figure 6-29 Test Unit 50-INT/50-EXT at 0.75 in. (19 mm) downward displacement**


**Figure 6-30 Test Unit 50-INT/50-EXT at 0.75 in. (19 mm) upward displacement**

With increased displacements, other cracks occurred in Segments 1 and 2 in the vicinity of Joint $J_1$. The major crack was the first one, which occurred adjacent to the joint. This crack opened significantly with increased applied displacements. Performance of the test unit was dominated by flexure.

The test was continued until concrete crushing of the bottom slab under downward loading at 6 in. (152 mm) displacement. Figure 6-31 shows Joint $J_1$ of Unit 50-INT/50-EXT at 6 in. (152 mm) downward displacement. The figure shows concrete crushing of the bottom slab.


**Figure 6-31 Compression softening of the bottom slab of Test Unit 50-INT/50-EXT at 6 in. (152 mm) downward displacement**

Despite the compression failure observed at 6 in. (152 mm) downward displacement, the test could be continued to a higher displacement level. An explosive compression failure of the bottom slab occurred at about 7.2 in. (183 mm) downward displacement. Figure 6-32 shows Unit 50-INT/50-EXT at about 8.0 in. (203 mm) downward displacement; it means shortly after occurrence of the explosive compression failure. Buckling of the longitudinal reinforcement of the bottom slab was also observed as can be seen in Figure 6-33. Figure 6-34 shows the concrete crushing at the bottom surface of Test Unit 50-INT/50-EXT.

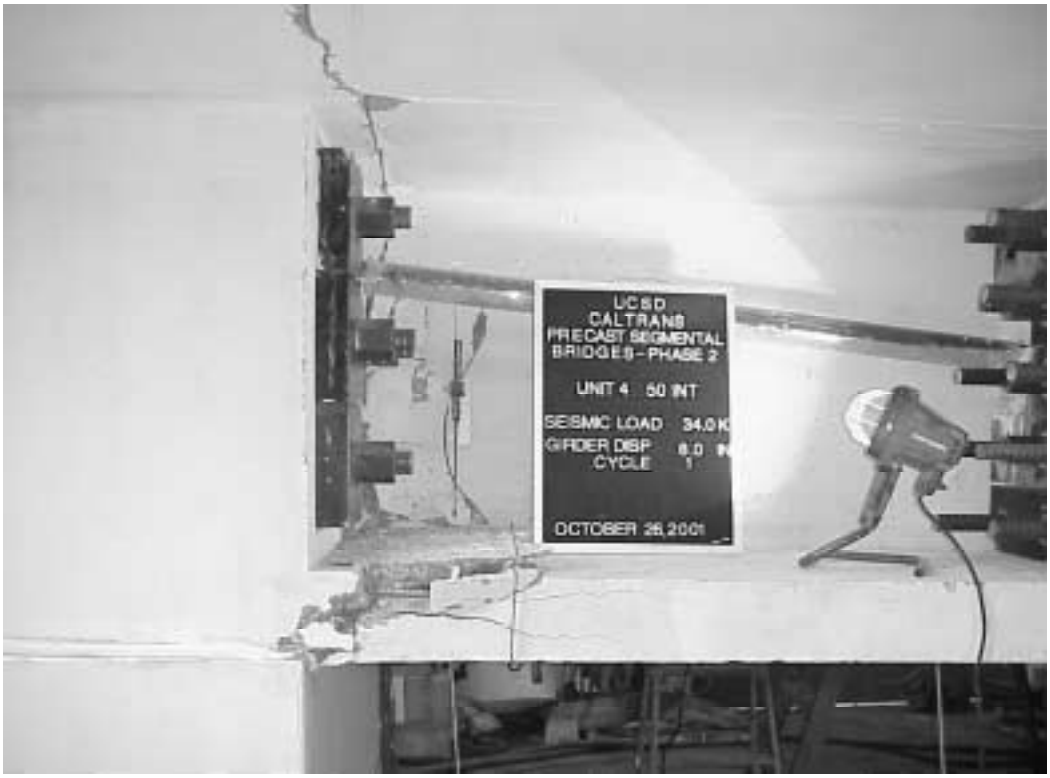


**Figure 6-32 Test Unit 50-INT/50-EXT at 8 in. (203 mm) downward displacement**


**Figure 6-33 Close-up of the compression failure of Unit 50-INT/50-EXT**

**Figure 6-34 Compression failure at the bottom slab of Test Unit 50-INT/50-EXT**

After compression failure of Unit 50-INT/50-EXT under downward loading, the test unit was loaded in the upward direction. Noise was heard during upward loading of the test unit. A sudden drop in the load carrying capacity accompanied the noise. This noise was due to fracture of the strands of the lower (horizontal) prestressing tendon. Failure of individual strands occurred simultaneously with concrete crushing in the deck. The test was stopped after an upward displacement of about 7.3 in. (185 mm) was reached. Figure 6-35 shows the test unit at the highest displacement level reached in the upward direction and just before end of the test.

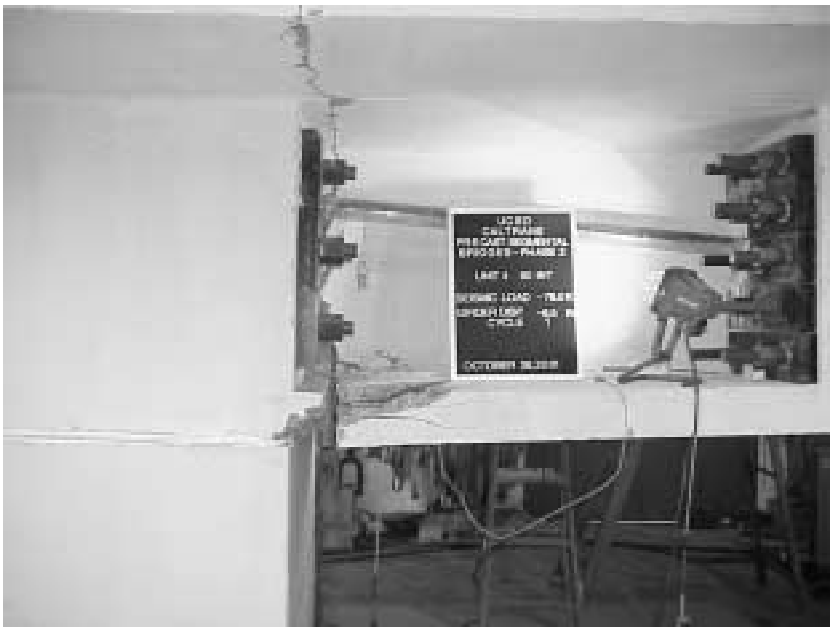

**Figure 6-35 Unit 50-INT/50-EXT at an upward displacement of 7.3 in. (185 mm)**

## 6.2 Load-Displacement Response

The vertical displacement, Δ, which controlled the test loading protocol, was measured below the master actuator (actuator nearest to the cantilever tip). The vertical displacement, Δ, was plotted versus the total applied load and the results are shown in

this section. The sign convention is positive for downward total applied load and displacement, Δ. The total load is the sum of the forces in the two actuators. A shearing force of about 32 kips (142 kN) should be added to the total applied load in order to determine the total shearing force transferred at Joint $J_1$. The 32 kips (142 kN) shearing force resulted from the self-weights of the test unit and the steel beam. It should be remembered that the reference load level represents the loads required to obtain the correct concrete normal stresses and shearing force in the prototype structure under dead load and superimposed dead loads.

The maximum load carrying capacities under downward and upward loading are given in Table 6-1 for all test units. The table also gives the downward displacement, Δ (Figure 5-33) just before complete failure of the test units. The maximum displacements, given in Table 6-1, correspond to the load levels indicated by the solid circles in the load-displacement curves, which are presented in this section.

**Table 6-1 Peak loads and displacements of Phase II test units**

| Test Unit | Peak Load kips (kN) | | Displacement at Failure in. (mm) | |
|---|---|---|---|---|
| | Downward | Upward | Downward | Upward |
| 100-INT | 94.2 (419) | -40.1 (-178) | 6.0 (152) | -10.8 (-274) |
| 100-INT-CIP | 141.3 (629) | -39.0 (-173) | 6.4 (163) | -14.3 (-363) |
| 100-EXT | 95.6 (425) | -30.0 (-133) | 12.9 (328) | -11.9 (-302) |
| 50-INT/50-EXT | 96.0 (427) | -32.7 (-145) | 7.2 (183) | -6.1 (-155) |

### 6.2.1 Test Unit 100-INT

The total load versus the vertical displacement, Δ, of Test Unit 100-INT is shown in Figure 6-36. The horizontal dashed line shown in the figure represents the reference load. As mentioned earlier in Section 6.1.1, onset of cracking occurred during loading of the test unit to Δ = +0.75 in. (19 mm). Onset of cracking was accompanied by sudden drop in the applied load as can be seen in Figure 6-36. The figure also shows a drop in the applied load at Δ = +3.0 in. (76 mm); this was caused by the premature local concrete crushing of the bottom slab (see Figure 6-3). Compression failure occurred in the bottom slab during the first cycle at Δ = +6.0 in. (152 mm) (downward loading). Explosive compression failure occurred also in the web during the second cycle at Δ = +6.0 in. (152 mm).

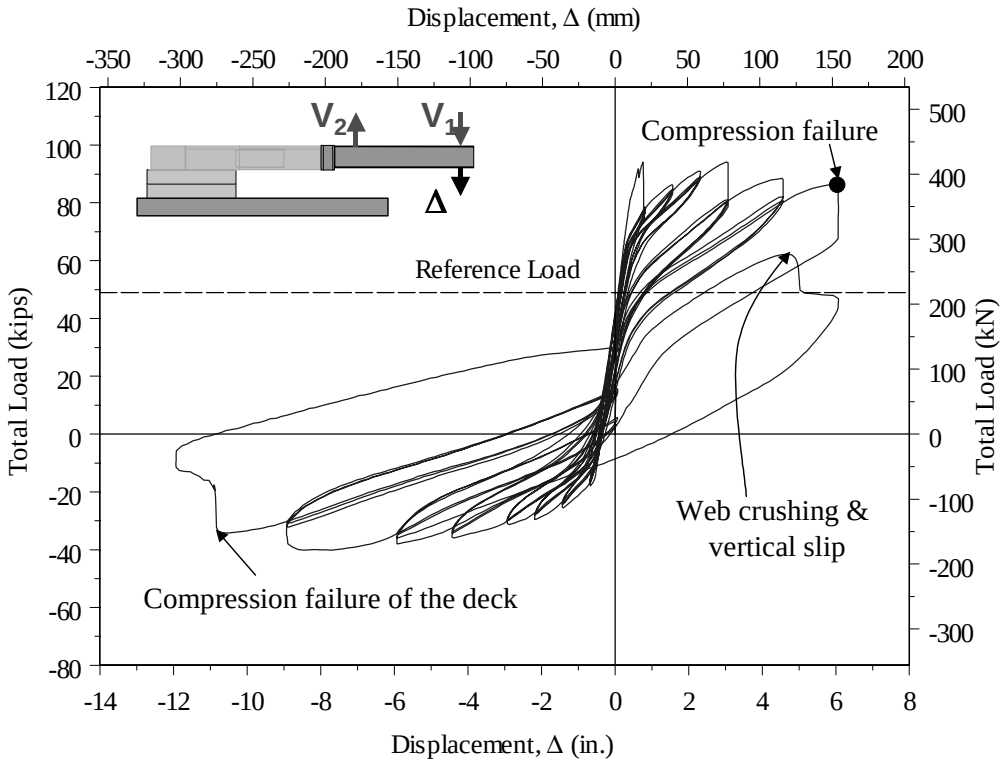


**Figure 6-36 Total load versus displacement of Test Unit 100-INT**

Vertical slip between the segments adjacent to Joint $J_1$ (Segments 1 and 2) was also observed after the explosive compression failure that occurred at $\Delta$ = +6.0 in. (152 mm). Figure 6-36 indicates that the load carrying capacity dropped approximately to the reference load value after compression failure of the bottom slab. Unit 100-INT failed also in compression under upward loading at a displacement of about 12 in. (305 mm).

### 6.2.2 Test Unit 100-INT-CIP

The total load versus the vertical displacement, $\Delta$, of Test Unit 100-INT-CIP is shown in Figure 6-37. The horizontal dashed line shown in the figure represents the reference load. As mentioned earlier in Section 6.1.2, onset of cracking occurred during loading of the test unit to $\Delta$ = +0.75 in. (19 mm). Deck mild reinforcement crossed the segment-to-segment joint in Unit 100-INT-CIP. Thus instead of one wide crack at the joint, several closely spaced cracks with small widths occurred along the length of Segment No. 1. As a result of the relatively uniform crack distribution in Unit 100-INT-CIP under downward loading, no drop in the applied load was observed in this test unit. Compression failure occurred in the bottom slab at $\Delta$ = +6.0 in. (152 mm) (downward loading). Compression failure occurred also in the web at $\Delta$ = +6.4 in. (163 mm). Figure 6-37 shows that at $\Delta$ = +9.0 in. (229 mm), the load carrying capacity of the test unit dropped significantly, but the test unit was still able to carry the reference load.

Figure 6-37 shows that Unit 100-INT-CIP had a significantly higher capacity with respect to the other test units because of the deck mild reinforcement crossing the segment-to-segment joint. Figure 6-37 also shows the relatively high-energy dissipation

capability of Unit 100-INT-CIP under downward loading because of yielding of the deck mild steel in the cast-in-place deck closure joint as will be shown later.

Test Unit 100-INT had ductile performance under upward loading as can be seen in Figure 6-37. The test unit could undergo significant upward displacement before failure. The test unit failed at about Δ = -14.3 in. (-363 mm) by fracture of the strands in the lower tendon.

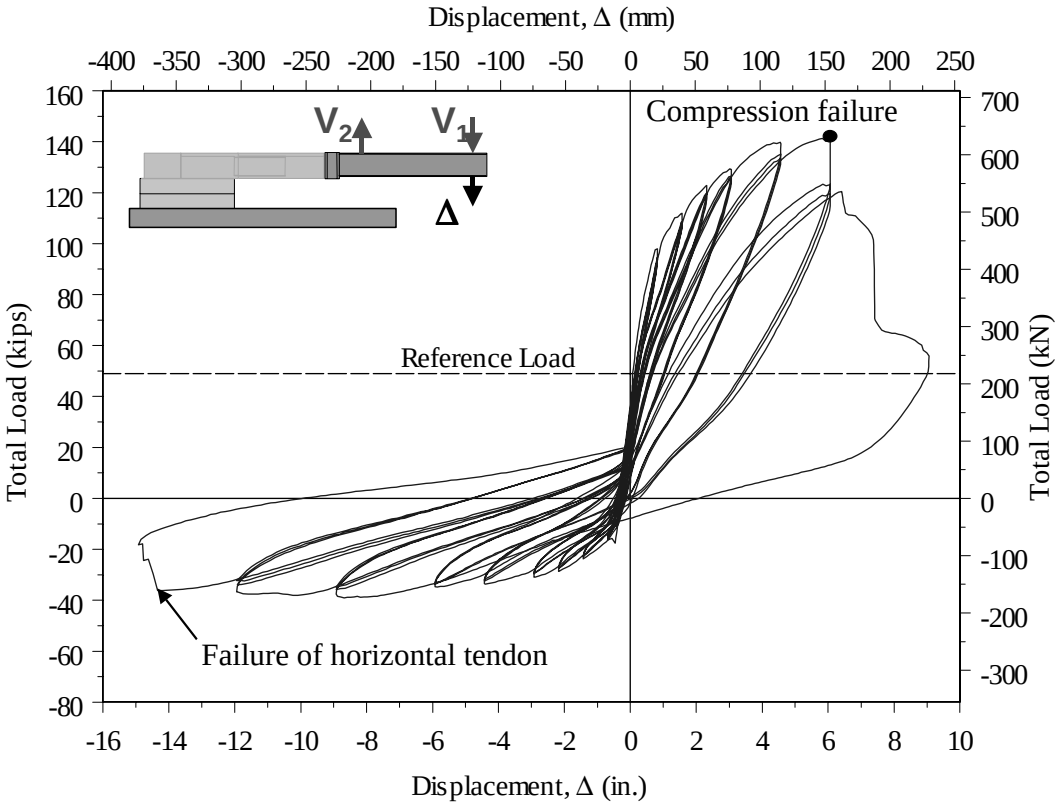


**Figure 6-37 Total load versus displacement of Test Unit 100-INT-CIP**

### 6.2.3 Test Unit 100-EXT

The total load versus the vertical displacement, Δ, of Test Unit 100-EXT is shown in Figure 6-38. The horizontal dashed line shown in the figure represents the reference

load. As mentioned earlier in Section 6.1.3, onset of cracking occurred during loading of the test unit to Δ = +0.75 in. (19 mm). Onset of cracking was accompanied by sudden drop in the applied load as can be seen in Figure 6-38. Onset of concrete crushing was observed in the bottom slab under downward loading of the test unit to Δ = +6.0 in. (152 mm). However, Figure 6-38 shows that unlike the explosive failure of Units 100-INT and 50-INT/50-EXT, Unit 100-EXT had a gradual drop in its load carrying capacity with increasing displacement, Δ. The test unit failed at relatively high downward displacement (see Table 6-1) compared to the other test units. Test Unit 100-EXT had an explosive failure at about 13.0 in. (330 mm) and the load carrying capacity just after failure was reduced below the reference load value.

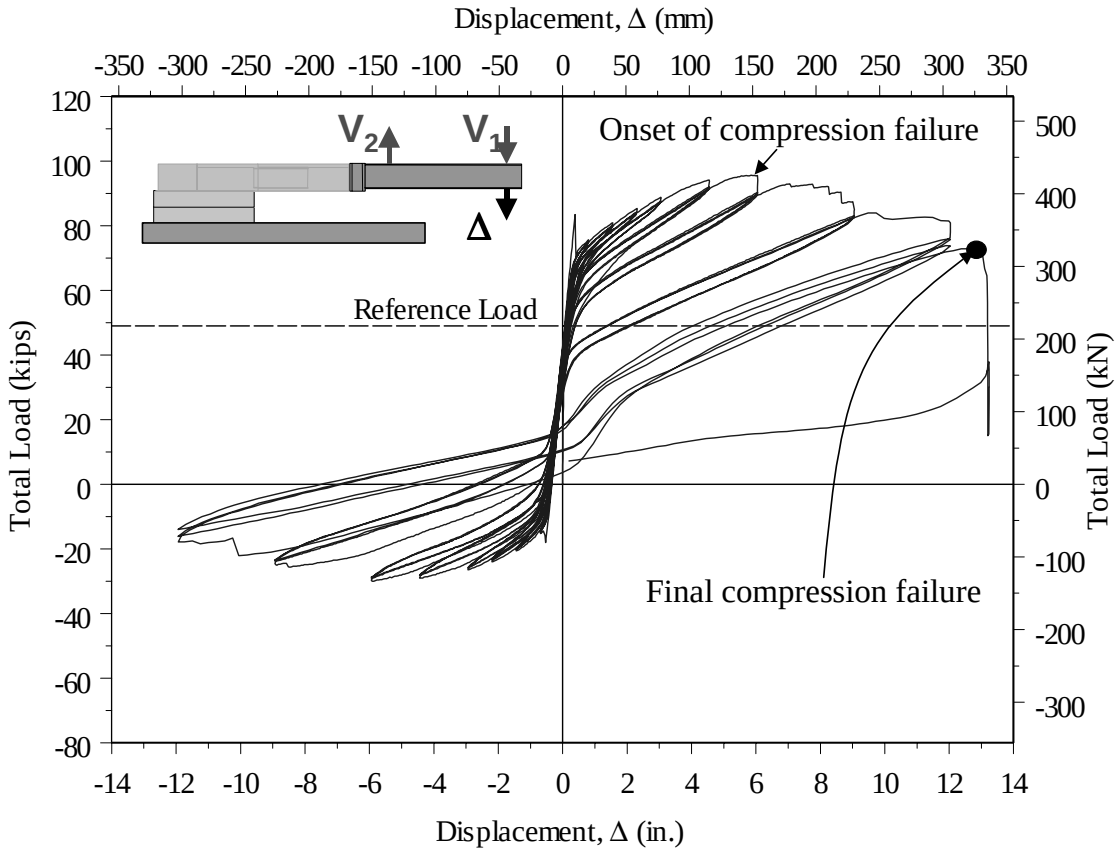


**Figure 6-38 Total load versus displacement of Test Unit 100-EXT**

### 6.2.4 Test Unit 50-INT/50-EXT

The total load versus the vertical displacement, Δ, of Test Unit 50-INT/50-EXT is shown in Figure 6-39. The horizontal dashed line shown in the figure represents the reference load. Onset of cracking occurred during loading of the test unit to Δ = +0.75 in. (19 mm). Onset of cracking was accompanied by sudden drop in the applied load as can be seen in Figure 6-39. Onset of concrete crushing was observed in the bottom slab under downward loading of the test unit to Δ = +6.0 in. (152 mm). Full compression failure occurred in the bottom slab at a downward displacement of about Δ = +7.2 in. (183 mm). The downward load carrying capacity of the test unit dropped to a value less than the reference load level. After failure under downward loading, Unit 50-INT/50-EXT was loaded in the upward direction. At about Δ = -6.1 in. (-155 mm), strands of the lower (horizontal tendon) prestressing tendon fractured and the test was stopped at about Δ = -7.2 in. (-183 mm).

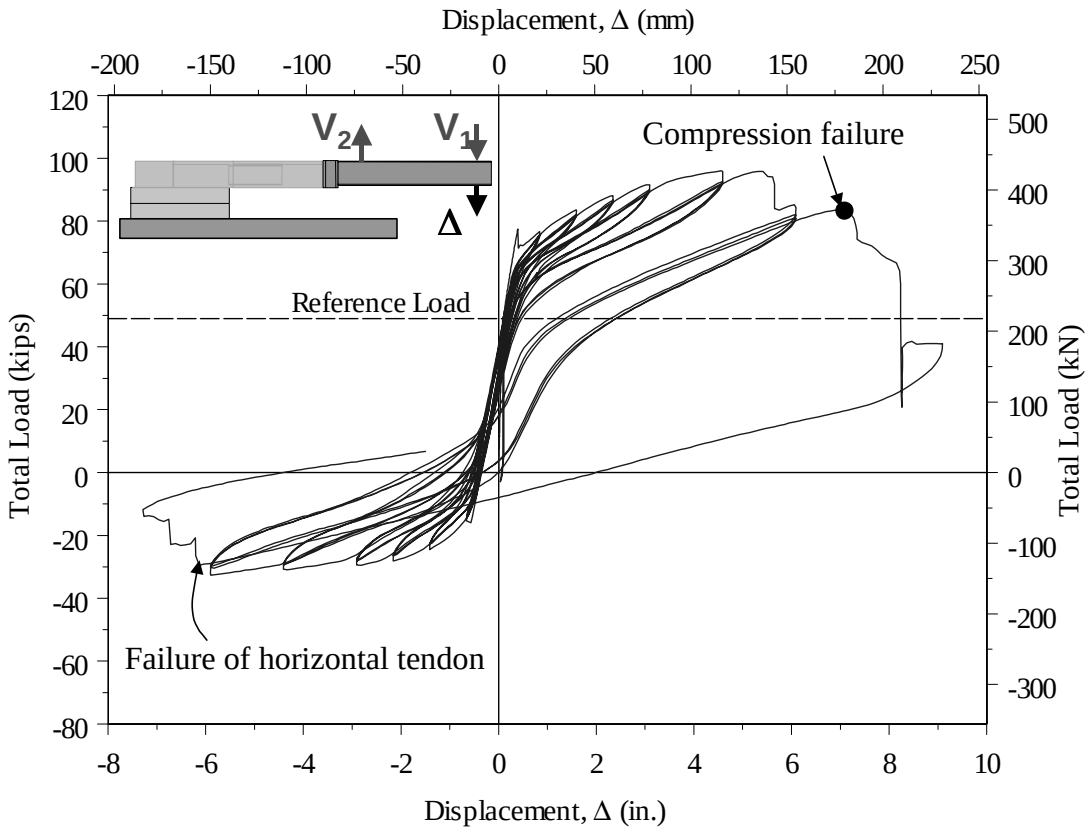


**Figure 6-39 Total load versus displacement of Test Unit 50-INT/50-EXT**

## 6.3 Test Data

A selection of the experimental results is presented here for conciseness. The remaining experimental results can be found in Appendix B. Unlike Phase I test results; the deflection profiles of the Phase II test units are not shown here because there was only one segment-to-segment joint in Phase II experiments. Except in Unit 100-INT-CIP, opening of the joint caused all the nonlinear deformations. The elastic deflections of the remaining portion of the test unit and of the steel beam were negligible compared to vertical deflections caused by the joint opening.

### 6.3.1 Opening of the Joints

Detailed results of joint opening are given in Appendix B. The measured openings of Joint $J_1$ at the top surface of the test units are shown in Figure 6-40 to Figure 6-43 for all test units. The joint opening shown in Figure 6-41 for Unit 100-INT-CIP was measured at the interface between the cast-in-place deck closure joint and the deck of precast Segment No. 1. The positive sign convention for joint opening is also shown in the figures. It should be mentioned that some of the potentiometers used to measure joint openings were removed during the tests to protect them from damage from falling concrete pieces during late stages of the tests. The measured maximum joint openings before failure of the test units were higher than the joint openings shown in Figure 6-40 to Figure 6-43. Test Units 100-INT, 100-EXT and 50-INT/50-EXT did not have any mild reinforcement across the joint, thus the joint opening measured at the top surface was relatively high for these three units with respect to joint openings at the top of Unit 100-INT-CIP. The cast-in-place deck closure joint was reinforced with headed bars; these mild-reinforcing bars controlled the widths of cracks at the top surface of the test unit in the joint vicinity. Instead of having one wide crack, or joint opening, in Units 100-INT, 100-EXT and 50-INT/50-EXT, provision of mild steel reinforcement across the segment-to-segment joint in Unit 100-INT-CIP resulted in occurrence of several cracks. These cracks were closely spaced and had relatively small crack widths.

The measured joint openings at top surface of Units 100-INT and 50-INT/50-EXT were comparable, although the joint openings in Unit 50-INT/50-EXT were slightly higher. With 100% external post-tensioning, the measured maximum joint openings at the top surface were much higher than the measured joint openings for Units 100-INT

and 50-INT/50-EXT. The maximum joint opening at the top surface just before failure of Unit 100-EXT was about 3.25 in. (83 mm).

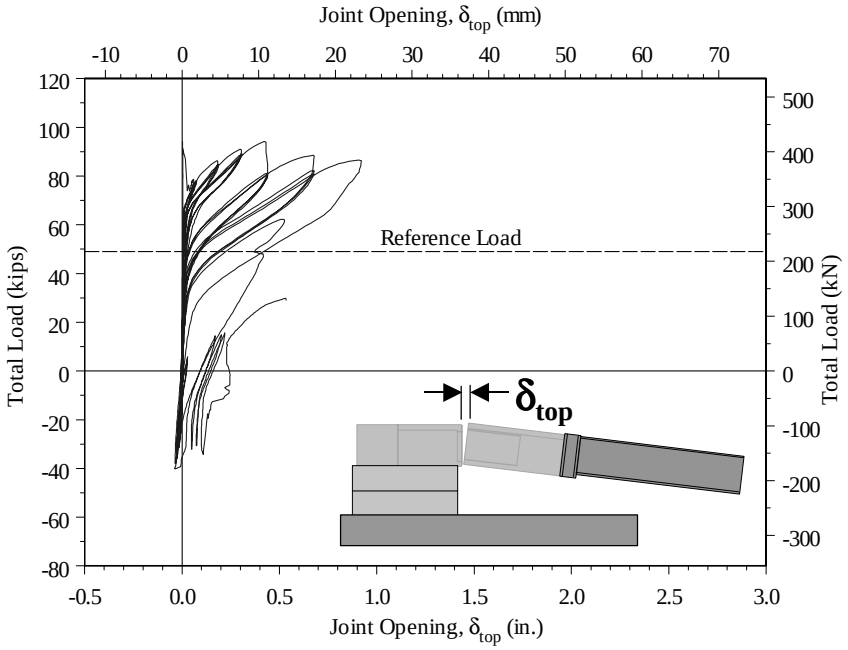


**Figure 6-40 Load versus joint opening at top surface of Unit 100-INT**

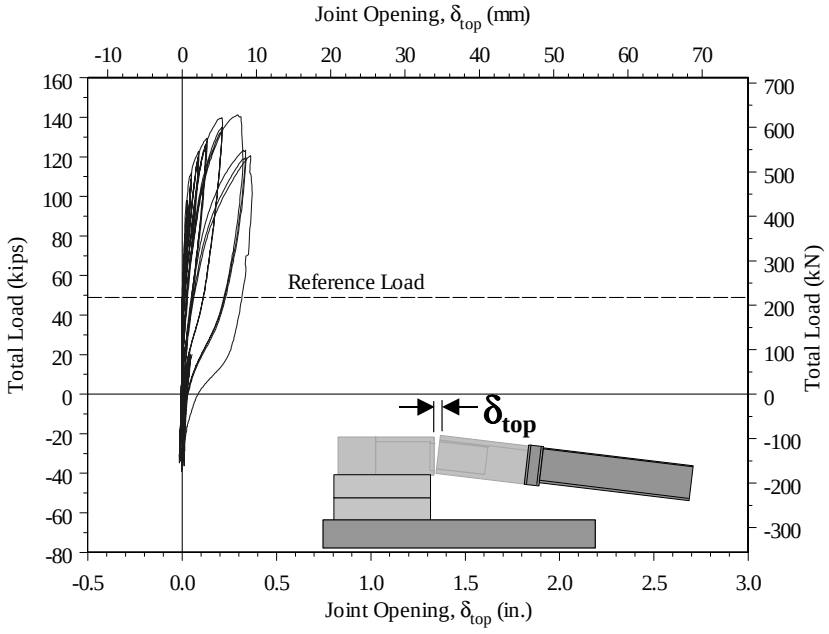


**Figure 6-41 Load versus joint opening at top surface of Unit 100-INT-CIP**

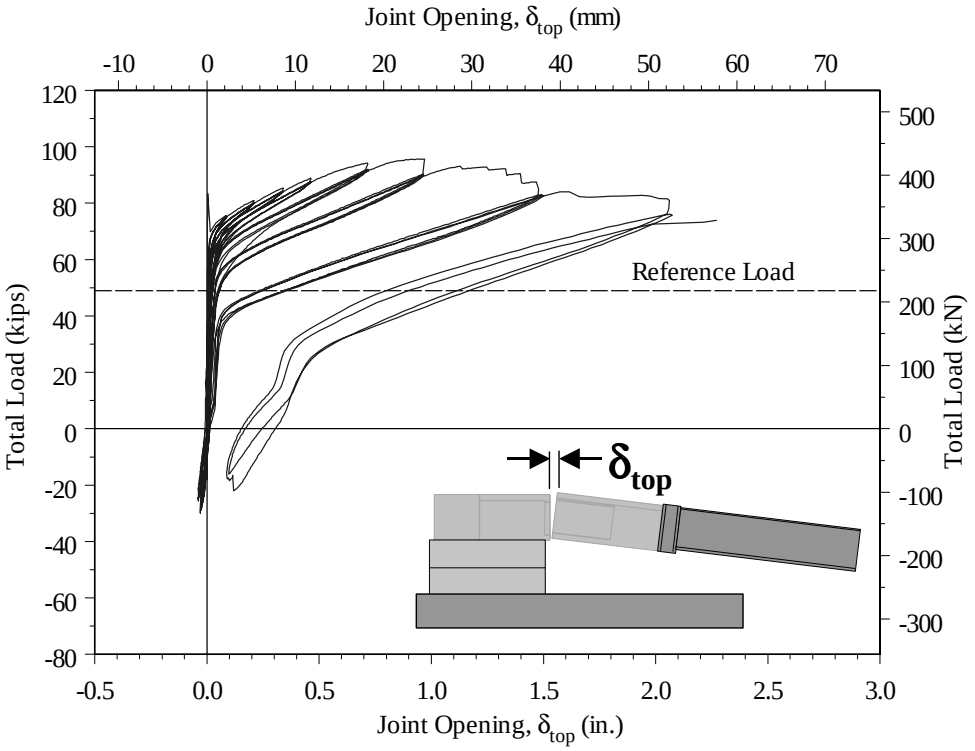


**Figure 6-42 Load versus joint opening at top surface of Unit 100-EXT**

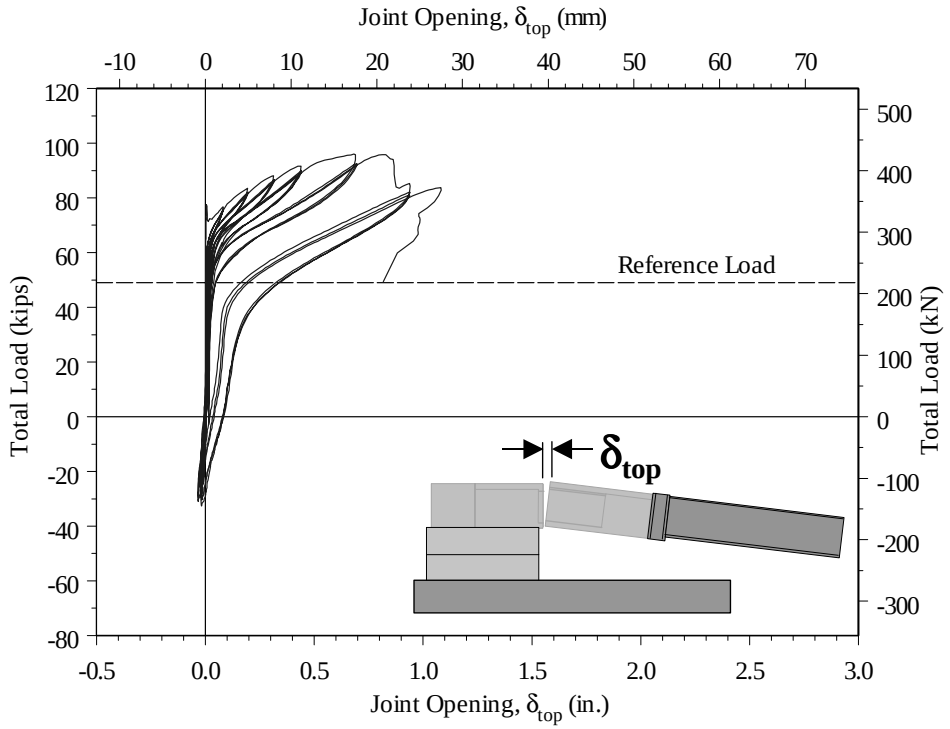


**Figure 6-43 Load versus joint opening at top surface of Unit 50-INT/50-EXT**

The measured opening of Joint $J_1$ at the bottom surface of all test units is shown in Figure 6-44 to Figure 6-47. All test units did not have mild reinforcement across the joint in the bottom slab. Thus, the measured joint openings at bottom surface of all test units were comparable as Figure 6-44 to Figure 6-47 indicate. However the figures show that the maximum measured joint openings in Units 100-INT-CIP and 100-EXT were higher than the measured values of the other test units. The bottom (horizontal) tendon in Unit 100-EXT was external, whereas the same tendon was internally bonded in other test units. This may explain why the joint opening at the bottom surface of Unit 100-EXT was relatively high.

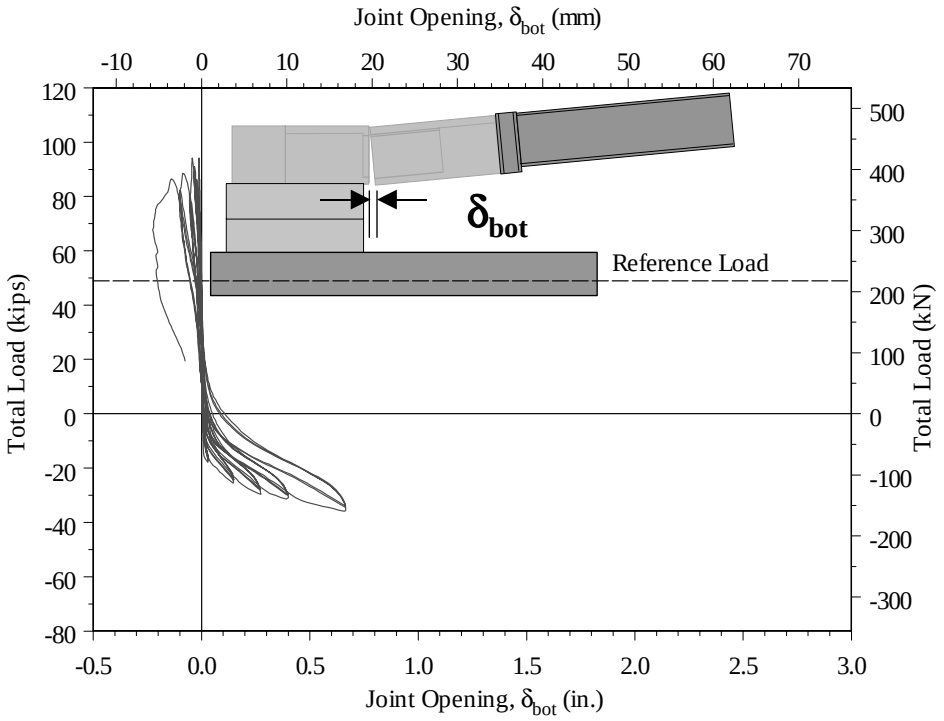


**Figure 6-44 Load versus joint opening at bottom surface of Unit 100-INT**

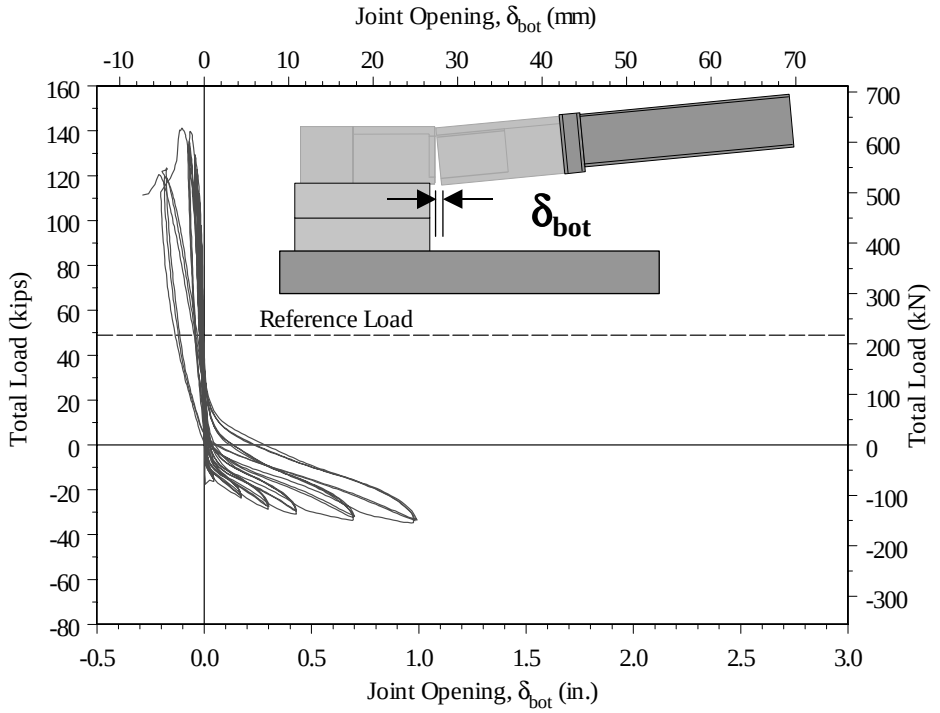


**Figure 6-45 Load versus joint opening at bottom surface of Unit 100-INT-CIP**

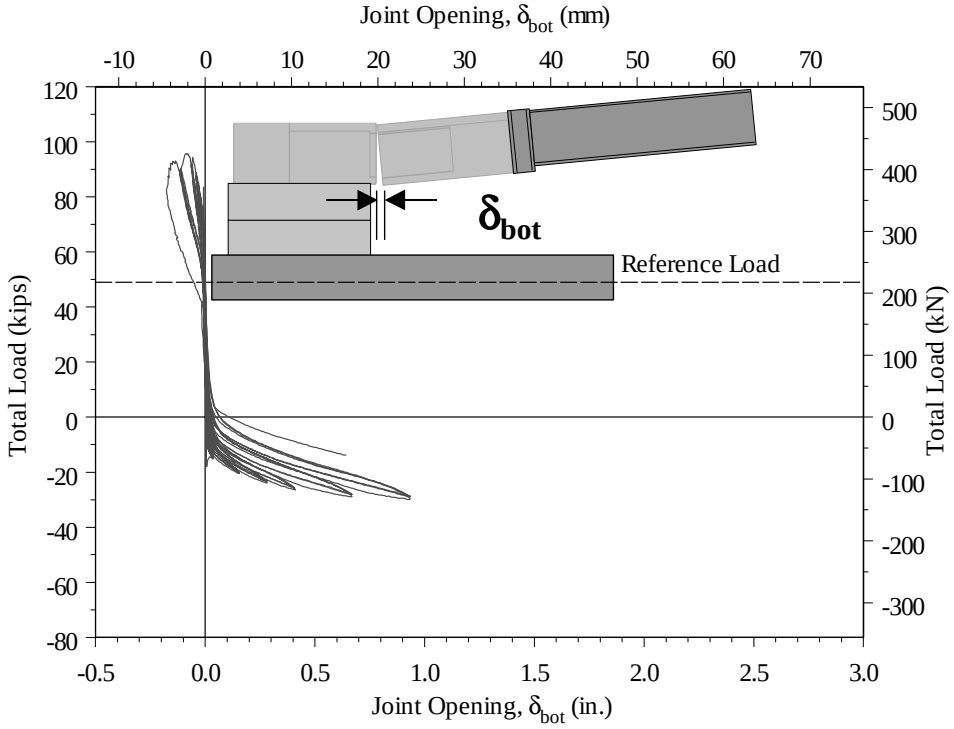


**Figure 6-46 Load versus joint opening at bottom surface of Unit 100-EXT**

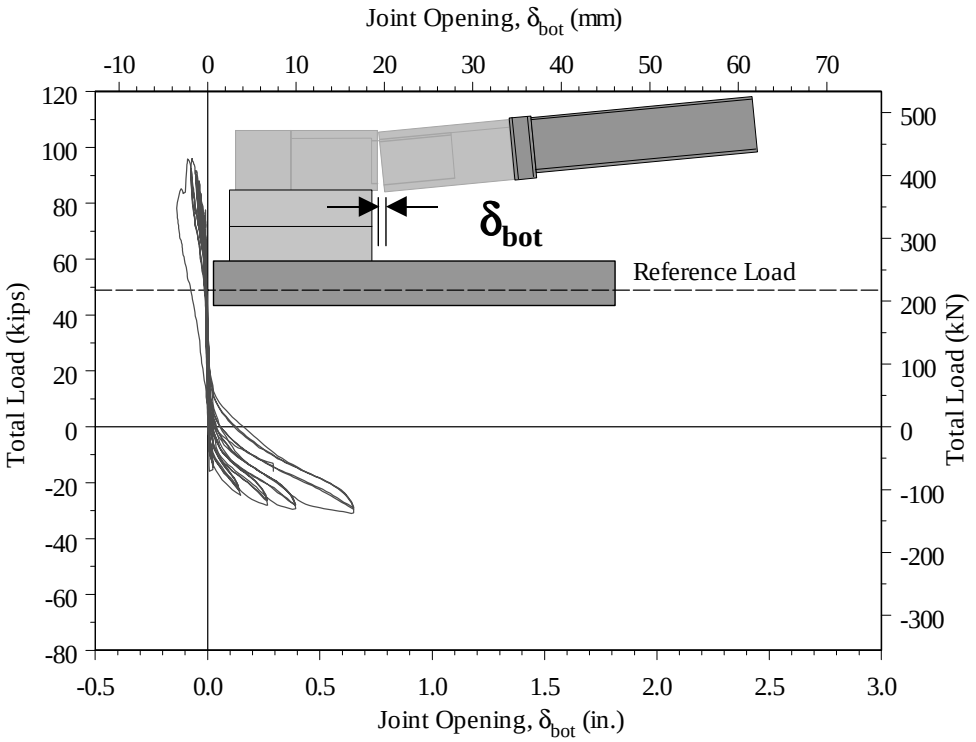


**Figure 6-47 Load versus joint opening at bottom surface of Unit 50-INT/50-EXT**

### 6.3.2 Joint Rotations

As mentioned earlier, all of the nonlinear deformations occurred at Joint $J_1$. Rotations of the joint could be calculated using the measured values of the joint openings at the top and bottom surfaces of the test units. Rotation of the joint was also directly measured by means of inclinometers installed on Segments 1 and 2 in the vicinity of Joint $J_1$. Rotation of Joint $J_1$ was the difference between the measured rotation of Segment 1 (See Figure 5-2) and the measured rotation of Segment 2 (the pier segment). Rotations of Segments 1 and 2 are shown in Appendix B for all test units. It should be mentioned that there was very good correlation between the joint rotations measured from readings of inclinometers and those calculated from the measured joint openings. As mentioned earlier, some of the potentiometers were removed during the test, however the

inclinometers were attached to the test units up to end of testing. Thus the rotations determined from the inclinometer readings are presented in this section.

Figure 6-48 to Figure 6-51 show the bending moments at joint $J_1$ versus the joint rotation. The bending moments plotted in the figures include those due to self-weights of the test units and the steel beam. The positive sign convention is for bending moments that produce tensile stresses in the top surface of the test units. Positive sign convention for joint rotation, $\theta$, is shown in Figure 6-48 to Figure 6-51. Table 6-2 gives the maximum joint rotation measured in both upward and downward loading directions during the tests. Comparison of maximum rotations among the four test units will be discussed later in this chapter.

**Table 6-2 Maximum joint rotations in the Phase II test units**

| Test Unit | Maximum Joint Rotation (rad.) | |
|---|---|---|
| | Downward | Upward |
| 100-INT | 0.021 | -0.040 |
| 100-INT-CIP | 0.015 | -0.052 |
| 100-EXT | 0.050 | -0.045 |
| 50-INT/50-EXT | 0.028 | -0.022 |

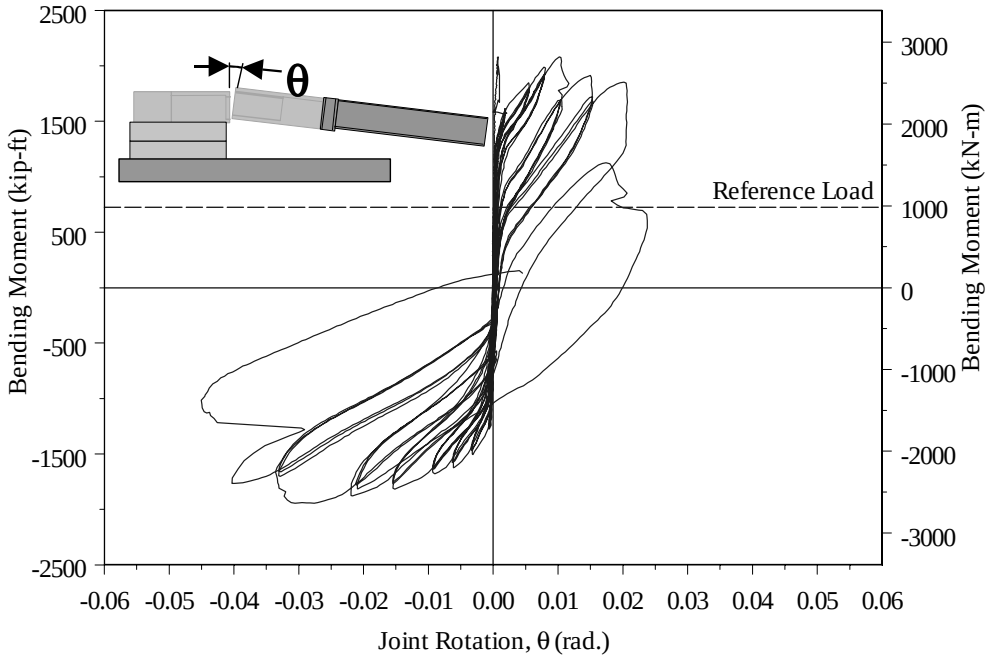


**Figure 6-48 Bending moment versus joint rotation of Test Unit 100-INT**

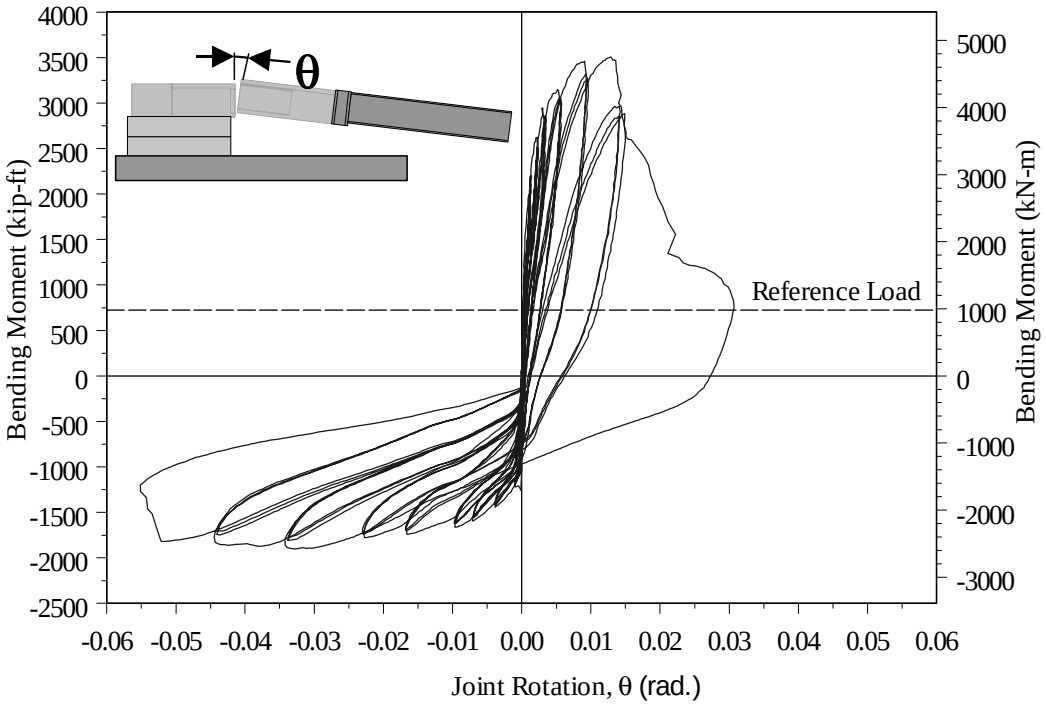


**Figure 6-49 Bending moment versus joint rotation of Test Unit 100-INT-CIP**

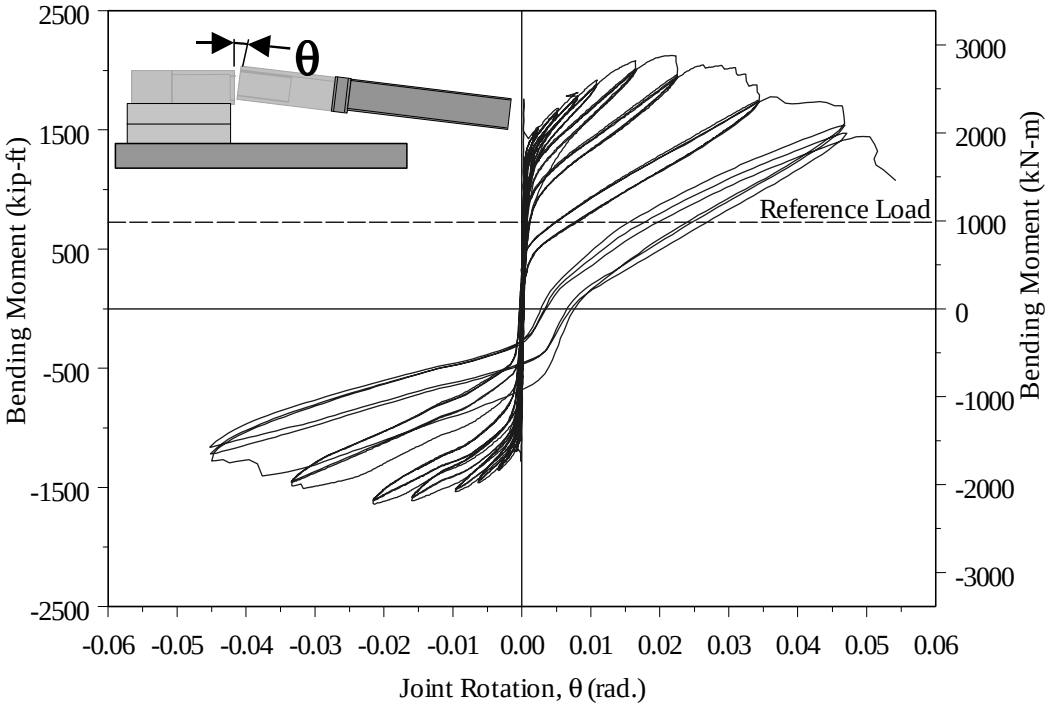


**Figure 6-50 Bending moment versus joint rotation of Test Unit 100-EXT**

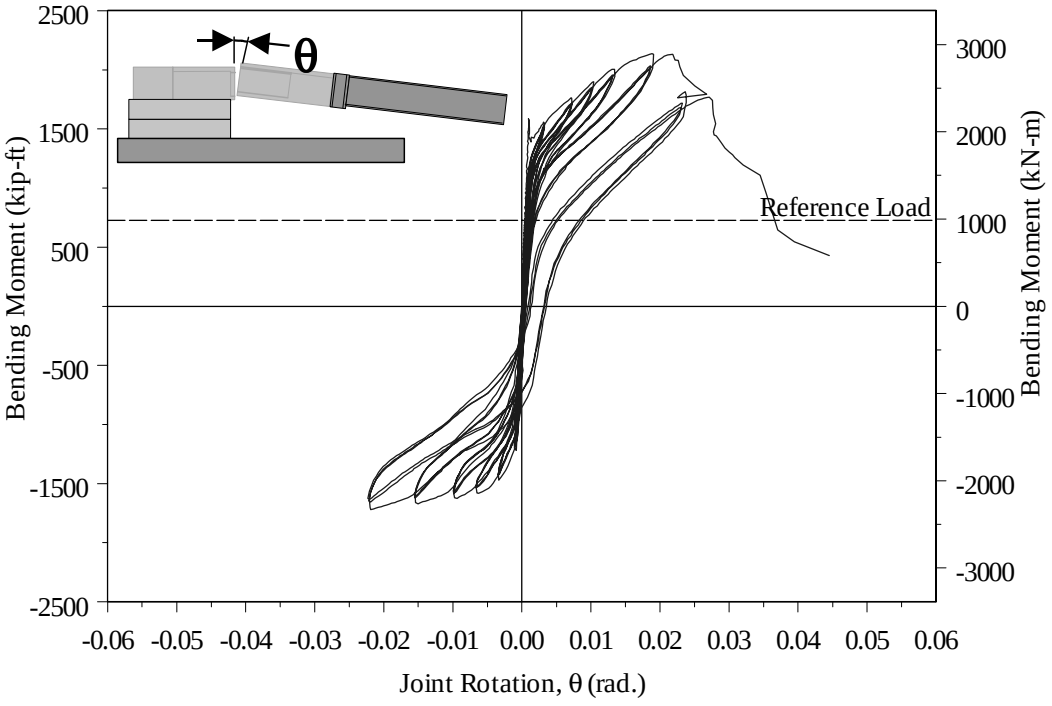


**Figure 6-51 Bending moment versus joint rotation of Test Unit 50-INT/50-EXT**

### 6.3.3 Vertical Slip Between Adjacent Precast Segments

It was essential to measure the vertical slip between the adjacent precast Segments 1 and 2 since Joint $J_1$ was subjected to high bending moments and wide joint openings combined with high shearing forces, especially under downward loading of the test units. Figure 6-52 to Figure 6-55 show the vertical slip measured between Segments 1 and 2 in all test units. In each of these figures, the horizontal axis represents the number of loading cycle (see Figure 5-33) and the vertical axis represents the measured vertical slip values. Also, values of the displacement, $\Delta$, are shown on the corresponding loading cycles in Figure 6-52 to Figure 6-55. The sign convention for vertical slip is shown in the figures and is positive for downward displacement of Segment 1 with respect to Segment 2 (the pier segment).

The figures show that for all test units, there was no considerable vertical slip between the two segments before compression failure of the bottom slab which initially occurred at $\Delta$ = +6.0 in. (152 mm). The figures also show that the vertical slip under downward loading was less than the measured slip during upward loading. This was observed despite the fact that the shearing forces at Joint $J_1$ under downward loading were much higher than the shearing forces at the joint under upward loading, especially for Test Unit 100-INT-CIP. Comparison of Figure 6-52 and Figure 6-55 indicates that the vertical slip had comparable values in test units with 100% internal post-tensioning (Unit 100-INT) and with 50% internal post-tensioning (Unit 50-INT/50-EXT). However, significant vertical slip occurred in Unit 100-INT after compression failure of the bottom slab as shown in Figure 6-52. With 100% external post-tensioning in Unit 100-EXT, less vertical slip was measured between Segments 1 and 2, compared to measured slip values at the

same displacement levels for Units 100-INT and 50-INT/50-EXT. This can be seen by comparison of the measured vertical slip values at Δ = +6.0 in. (152 mm) in Figure 6-54 and in Figure 6-55. The experimental results shown in Figure 6-52 to Figure 6-55 indicate that in all test units, vertical slip between the adjacent precast segments occurred only after flexural failure of the test units (compression failure).

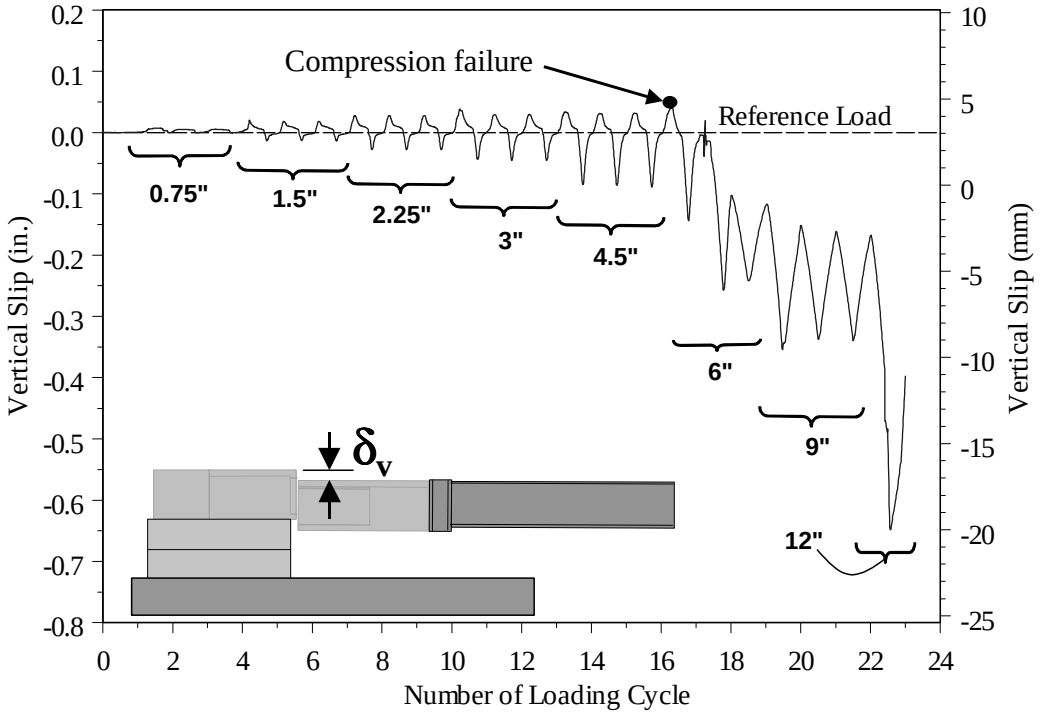


**Figure 6-52 Vertical slip between adjacent precast segments in Unit 100-INT**

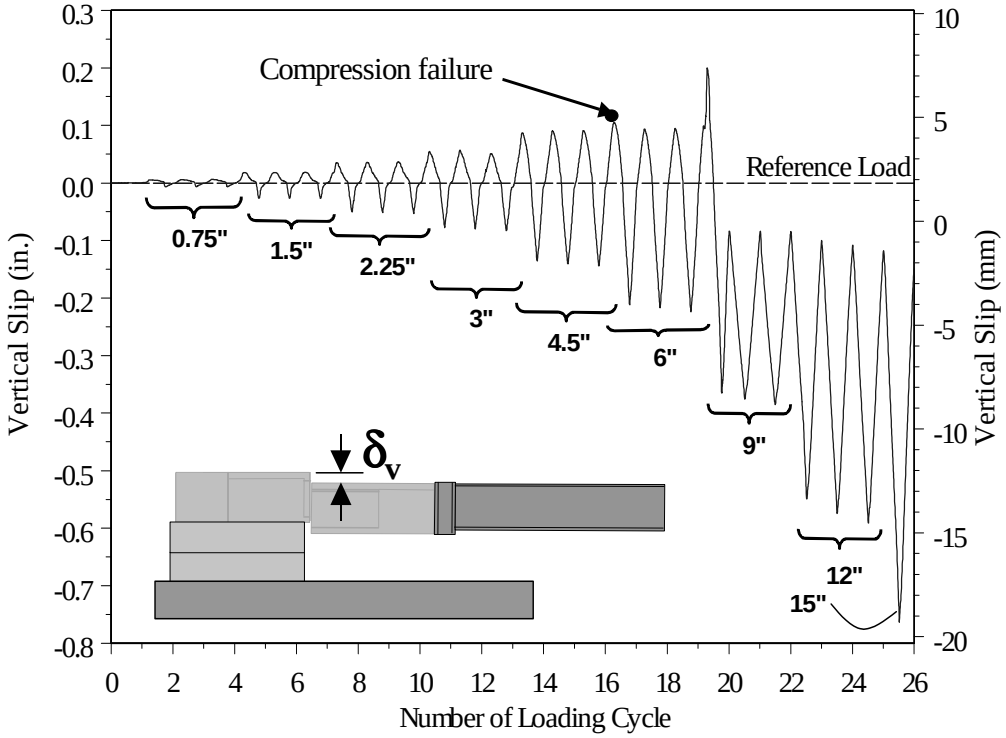


**Figure 6-53 Vertical slip between adjacent precast segments in Unit 100-INT-CIP**

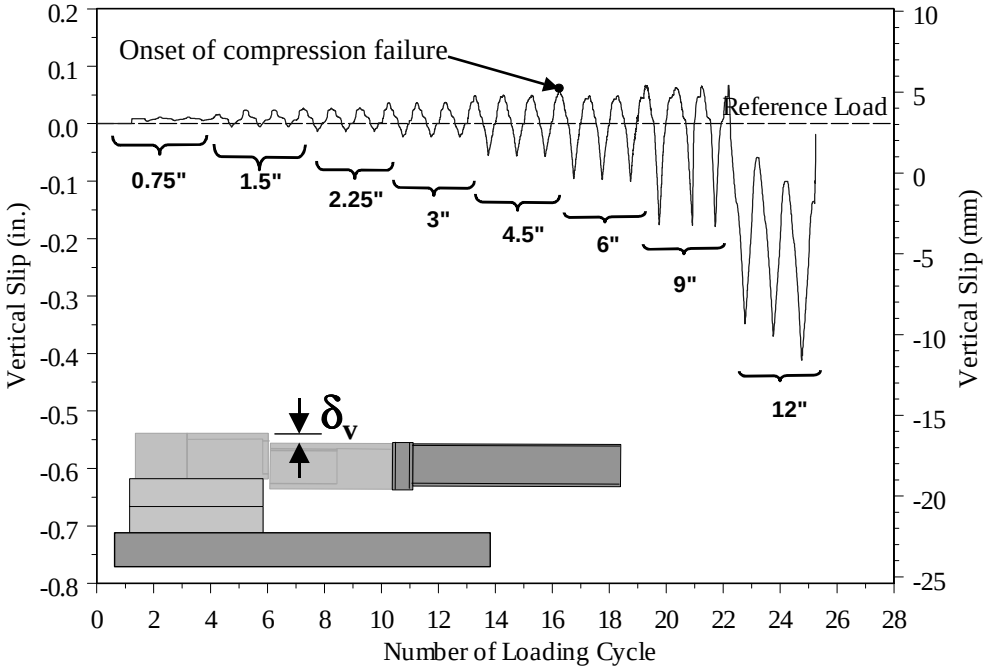


**Figure 6-54 Vertical slip between adjacent precast segments in Unit 100-EXT**

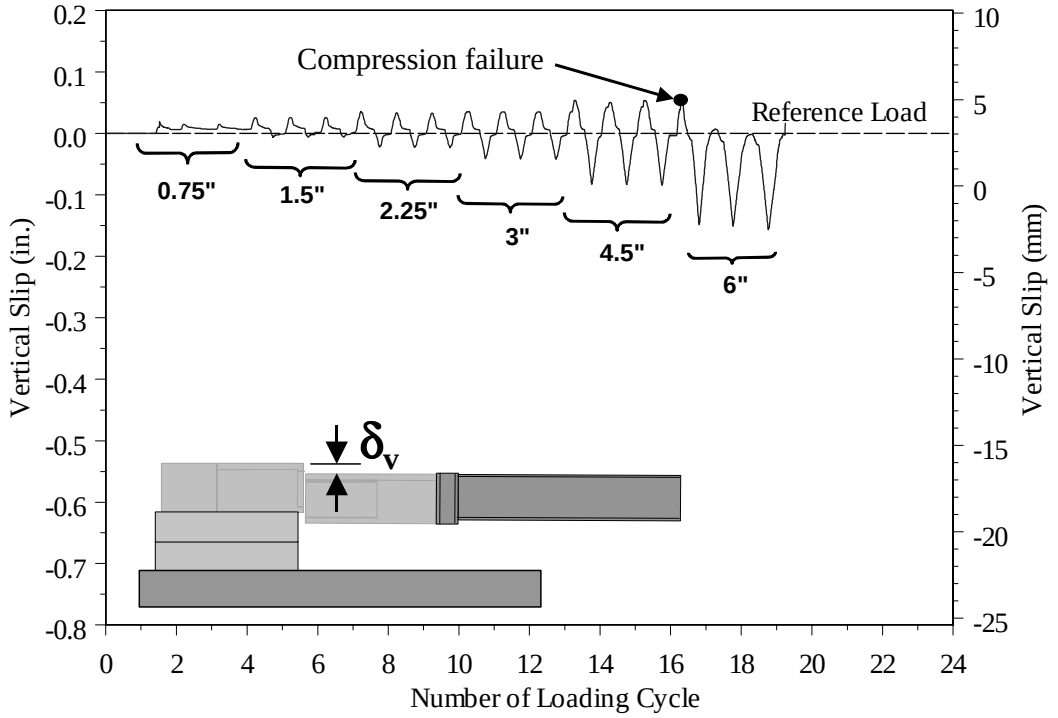


**Figure 6-55 Vertical slip between adjacent precast segments in Unit 50-INT/50-EXT**

### 6.3.4 Strains in Prestressing Steel

Strains were measured at different sections in the internally bonded tendons of all test units (see Figure 5-29). Strains in external tendons were also measured. The tendon strains were measured during post-tensioning of the test units. The tendon strains were also recorded at time intervals between post-tensioning and the day of test. The strain readings gave a good indication of the actual prestressing force at the time of test. It was found that the measured actual prestressing forces were close to those values assumed in design of the test units. Unfortunately, a significant number of strain gages placed on the internally bonded tendons were affected by moisture of the grout. These strain gages were functioning during the test, but it was believed that readings of these gages were not reliable. Unfortunately, all of the strain gages placed on the tendons of Units 100-INT

and 100-INT-CIP were affected by moisture of the grout. The moisture of the grout also affected some of the gages in Unit 50-INT/50-EXT, whereas few other gages survived and could function properly during the test. Some gages also malfunctioned during the test as a result of the high strains in the tendons. Detailed results of tendon strain gages are given in Appendix B.

Figure 6-56 and Figure 6-57 show the history of the strains measured at the location of Joint $J_1$ in the upper and lower tendons of Units 100-EXT, and 50-INT/50-EXT, respectively. The strains are plotted versus the number of loading cycles (see Figure 5-33). Values of the vertical displacement, $\Delta$, are shown in the figures. The yield strain of the tendons is also represented in Figure 6-56 and Figure 6-57 by the horizontal dashed line; the yield strain was determined according to the 0.2% offset yield strain definition.

Figure 6-56 indicates that both of the external upper and lower tendons in Unit 100-EXT yielded and some of the strand wires fractured at higher displacements (see Figure 6-26 and Figure 6-28). It should be mentioned that yielding of the external tendons in Unit 100-EXT occurred during the loading cycle to $\Delta$ = +/-9.0 in. (+/-229 mm).

Figure 6-57 shows that the lower (horizontal) internally bonded tendon reached yield during upward loading to $\Delta$ = -2.25 in. (-57 mm), whereas the upper internally-bonded upper tendon reached yield during downward loading of the test unit to $\Delta$ = +3.0 in. (76 mm). The figure also shows that the external upper tendons of Unit 50-INT/50-EXT did not yield; this was expected and also was observed in Test Unit 50-INT/50-EXT of Phase I (see Section 3.4.4). It should be remembered that the external tendons in Units 100-EXT and 50-INT/50-EXT were not grouted; however the experimental results are applicable to superstructures with external tendons that are grouted after post-tensioning.

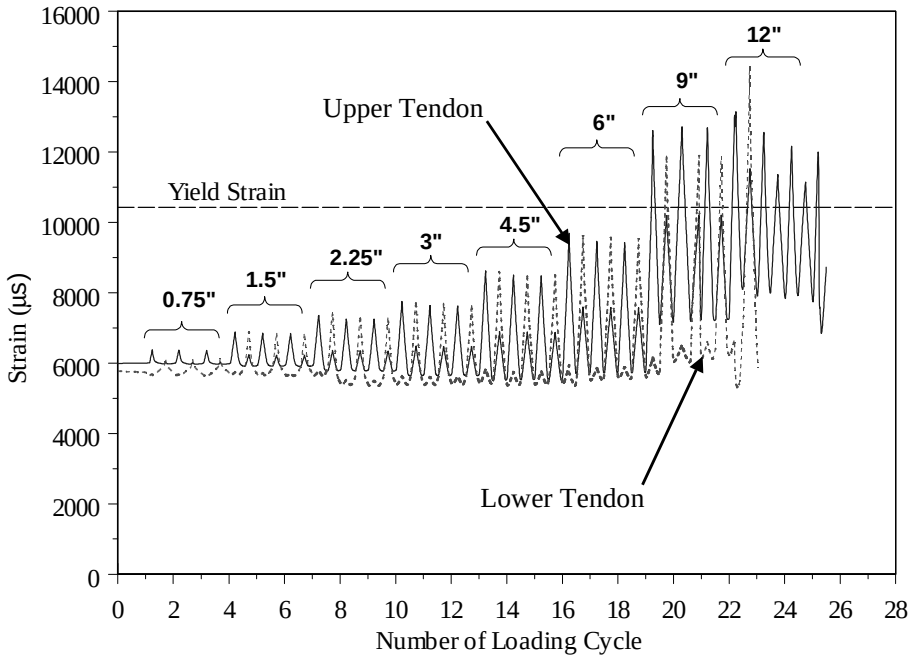


**Figure 6-56 Strains in external prestressing tendons of Test Unit 100-EXT**

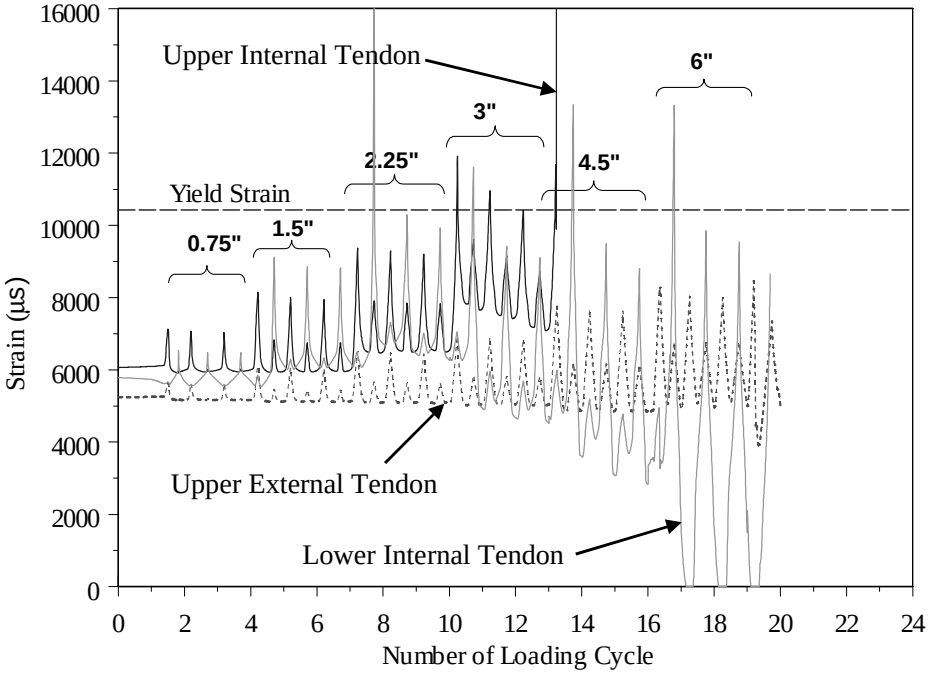


**Figure 6-57 Strains in prestressing tendons of Test Unit 50-INT/50-EXT**

### 6.3.5 Strains in Reinforcement of The Cast-In-Place Closure Joint (Test Unit 100-INT-CIP)

As mentioned in Section 5.5, electrical resistance strain gages were used to measure the strains in the deck longitudinal mild reinforcing bars. Strains were measured in top and bottom reinforcement layers in the deck at the following three locations: (1) interface between the cast-in-place deck closure joint and the precast deck of Segment No. 1, (2) interface between the cast-in-place deck closure joint and the precast deck of Segment No. 2 (pier segment), and (3) inside the cast-in-place deck closure joint at centerline of Joint $J_1$. The results are shown for selected monitored bars in Figure 6-58 to Figure 6-60, respectively.

As mentioned earlier in Section 6.1.2, cracks occurred at the three sections in which strain gages were placed on the mild reinforcement. However, the widest cracks occurred at the interface between the cast-in-place deck closure joint and the precast Segments 1 and 2. The deck reinforcement yielded at these locations during the first displacement cycle to $\Delta$ = +0.75 in. (19 mm) as shown in Figure 6-58 and Figure 6-59. These mild steel-reinforcing bars reached extremely high inelastic strains during the subsequent loading cycles as also shown in Figure 6-58 and Figure 6-59. The deck reinforcing bars overlapped and the cracks had small widths inside the cast-in-place deck closure joint. Thus, the recorded strains inside the cast-in-place deck at the location of Joint $J_1$ were small as shown in Figure 6-60. Figure 6-60 also shows that the deck reinforcement reached relatively high compressive strains under upward loading of the test unit. Despite the high compressive strains in these bars, no buckling occurred.

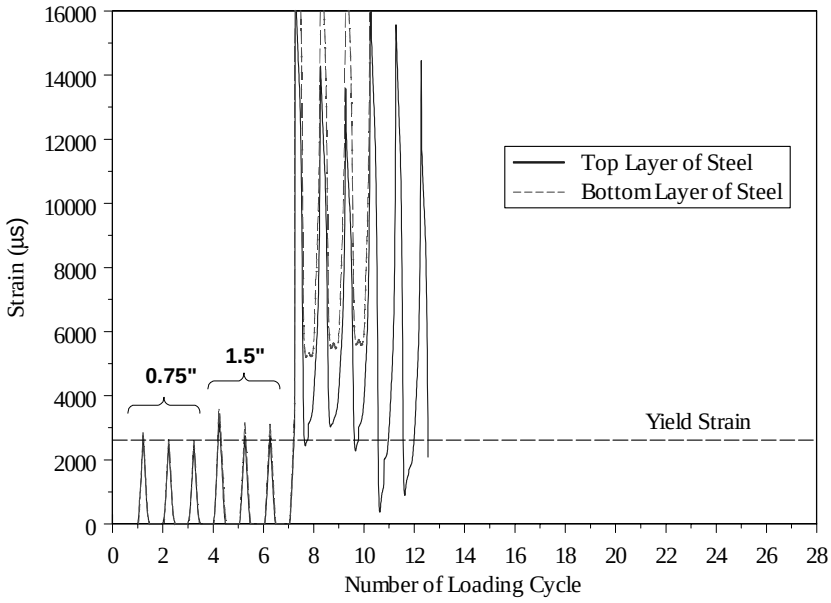


**Figure 6-58 Strains in deck mild reinforcement at the interface between the cast-in-place deck closure joint and precast Segment No. 1 (Unit 100-INT-CIP)**

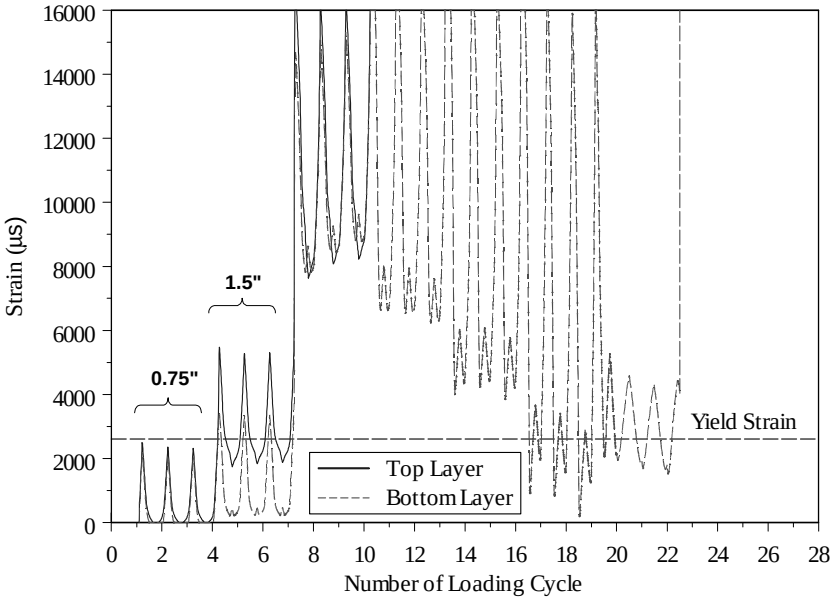


**Figure 6-59 Strains in deck mild reinforcement at the interface between the cast-in-place deck closure joint and precast Segment No. 2 (Unit 100-INT-CIP)**

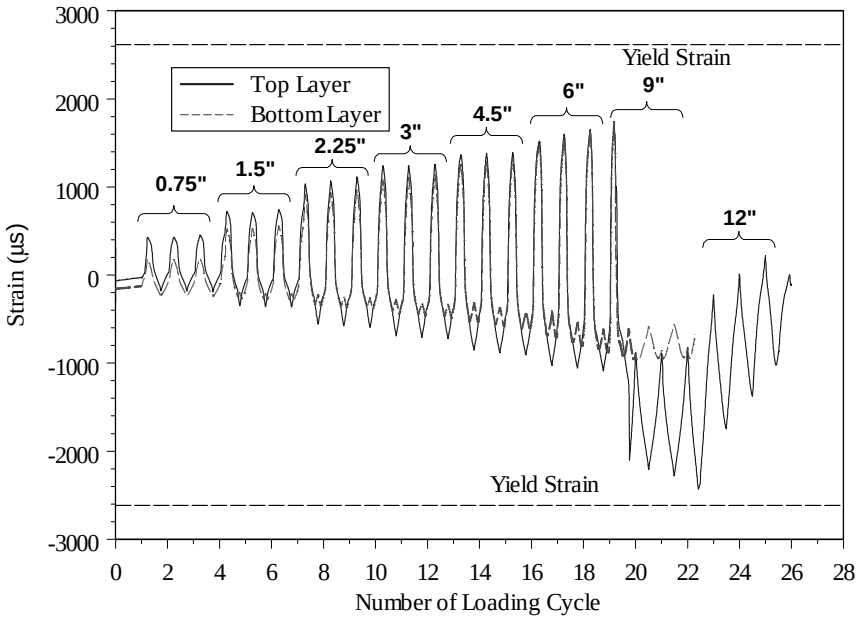


**Figure 6-60 Strains in deck mild reinforcement at the centerline of Joint $J_1$ (Unit 100-INT-CIP)**

## 6.4 Comparison of Experimental Results of Different Test Units

The experimental results of different test units are compared in this section. Two test variables were investigated in the Phase II experimental program. The first variable was the ratio of internal to external post-tensioning and the second variable was provision of cast-in-place deck closure joint between the precast segments. The four experiments can be grouped in two test series. Test Series I includes Units 100-INT, 100-EXT and 50-INT/50-EXT with the test variable being the ratio of internal to external post-tensioning. Test Series II includes Units 100-INT and 100-INT-CIP in which the variable was provision of the cast-in-place (CIP) deck closure joints.

### 6.4.1 Load-Displacement Curves

Figure 6-61 shows the total load versus displacement, Δ, for test units of Series I in which the test variable was the ratio of internal to external post-tensioning (Units 100-INT, 100-EXT and 50-INT/50-EXT). Figure 6-62 is similar to Figure 6-61, but it shows the load-displacement curves for Test Series II units (Units 100-INT and 100-INT-CIP). The envelopes of the total load-displacement curves of all test units are shown in Figure 6-63 for clarity.

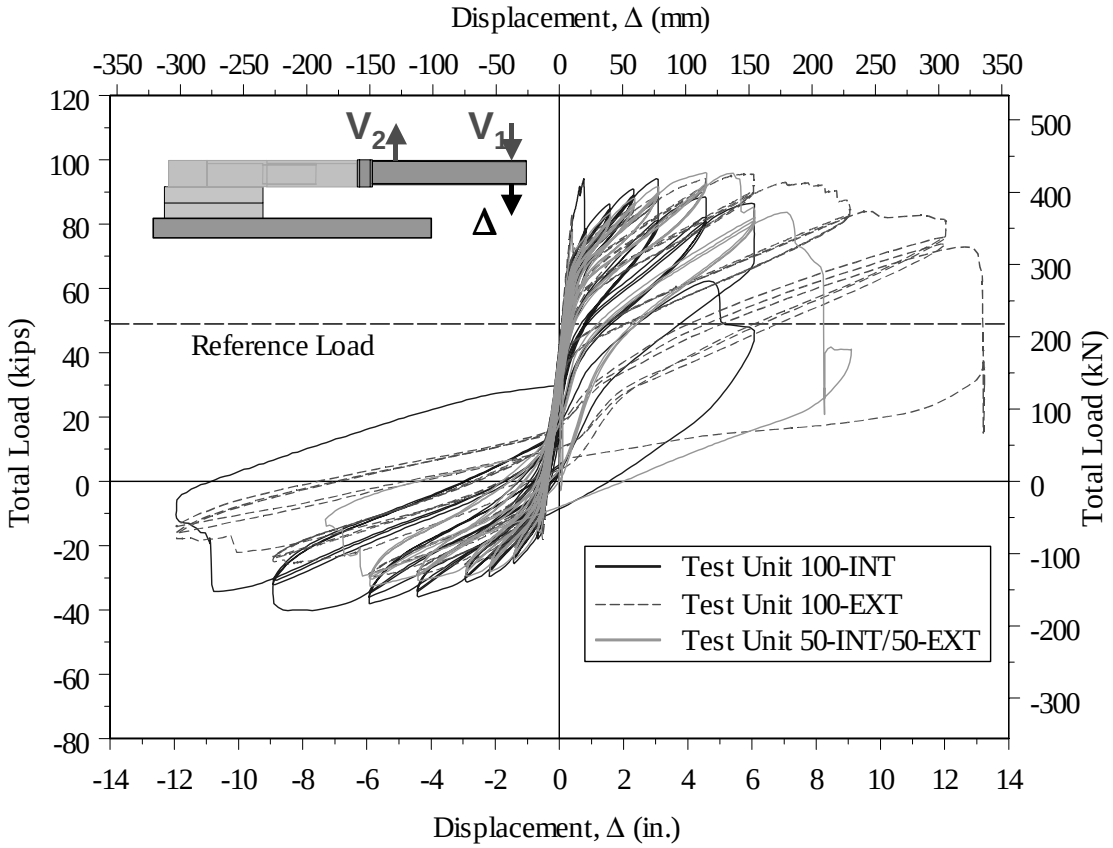


**Figure 6-61 Total load versus displacement of Test Series I units**

Figure 6-61 and Figure 6-63 show that the maximum load carrying capacity was almost equal for all units of Test Series I under downward loading. This can be also seen

from Table 6-1. In the Phase I test units, the maximum load carrying capacity was different among test units with different ratios of internal to external post-tensioning (see Table 3-1). It should be remembered that each of the Phase I test units consisted of six precast segments and the test unit was simply supported at its ends with a span length of 32 ft (9.75 m). The test unit was displaced under downward loading whereas the external tendons in Units 100-EXT and 50-INT/50-EXT of Phase I remained horizontal (see Figure 3-16). Thus the internal moment arm at the midspan section was reduced and the maximum load carrying capacity was reduced as a result of this. The reduction in the internal moment arm at the location of Joint $J_1$ in the Phase II test units with external tendons was insignificant. Thus, the maximum load carrying capacity of Units 100-INT, 100-EXT and 50-INT/50-EXT was almost equal.

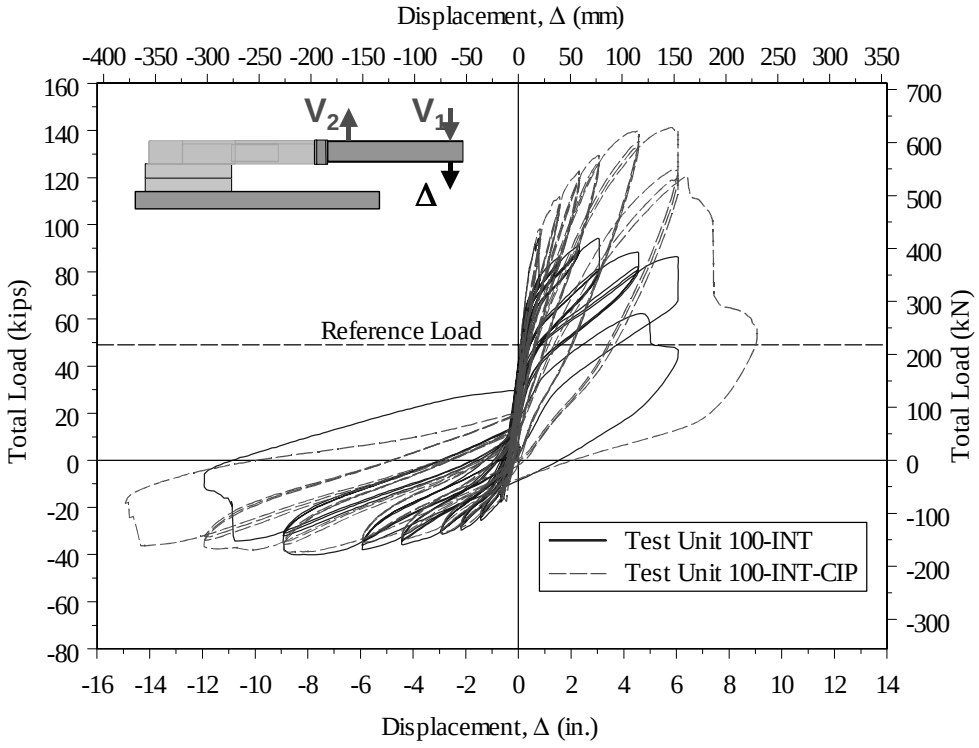


**Figure 6-62 Total load versus displacement of Test Series II units**

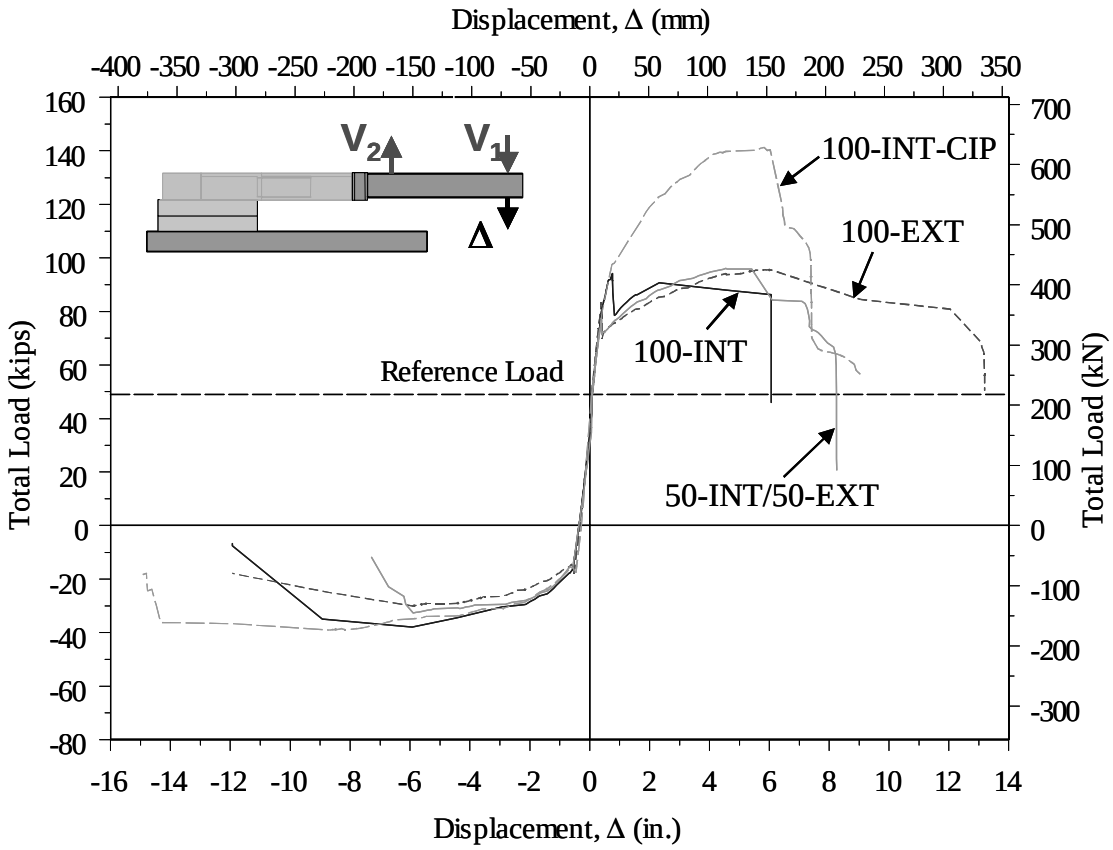


**Figure 6-63 Envelopes of total load versus displacement of the Phase II test units**

Under downward loading, Figure 6-61 and Figure 6-63 show that with 100% external post-tensioning, the ductility and maximum displacement reached before failure were substantially improved. Unit 50-INT/50-EXT with combined internal and external post-tensioning failed at slightly higher displacement than Unit 100-INT with 100% internal post-tensioning. This does not indicate that combination of internal and external post-tensioning would result in higher ultimate displacement than superstructures with 100% internal post-tensioning. It should be remembered that Unit 100-INT had premature concrete crushing in the bottom slab at about 3 in. (76 mm) of downward displacement (see Figure 6-3).

Presence of the reinforced cast-in-place deck closure joint in Unit 100-INT-CIP significantly increased the load carrying capacity under downward loading as can be seen in Figure 6-62 and Figure 6-63, because of the deck mild reinforcement crossing Joint $J_1$; this mild reinforcement could develop their yield strength.

The load carrying capacity under upward loading was comparable in all test units as shown in Figure 6-61 to Figure 6-63. However, test units with 100% internal or 100% external post-tensioning could undergo high displacement before failure and their performance was ductile. Figure 6-61 and Figure 6-63 show that the test unit with combined internal and external post-tensioning (Unit 50-INT/50-EXT) had significantly lower ductility and maximum displacement before failure of the test unit.

Figure 6-62 indicates that provision of the reinforced cast-in-place deck closure joint would improve the energy dissipation capability of the superstructure. This is because of the mild reinforcement crossing the segment-to-segment joint. The effect of the cast-in-place deck closure on the energy dissipation capability can be seen in the hysteresis loops shown in Figure 6-62 under downward loading (i.e. positive values of the displacement $\Delta$).

### 6.4.2 Permanent Residual Displacements

One of the important seismic performance issues is the permanent residual displacement of the superstructure after earthquake occurrence. Residual displacement, $\Delta_r$, were measured for all Phase II test units during the displacement cycle to $\Delta$ = +4.5 in. (114 mm). Figure 6-64 shows the seismic load versus displacement, $\Delta$, during the downward loading portion of the 4.5 in. (114 mm) displacement cycle of all test units. It

should be mentioned that the horizontal axis represents zero seismic load, or in other words it represents the reference load level. The displacement measured during the unloading portion, of any of the curves shown in Figure 6-64, at zero seismic load (i.e. at the reference load level) represents the permanent residual displacement, $\Delta_r$. Values of $\Delta_r$ measured after 4.5 in. (114 mm) maximum displacement of all test units are also given in Table 6-3. The values of $\Delta_r$ for all test units are normalized to the residual displacement of Unit 100-EXT, $\Delta_{ref}$ (= 0.17 in. = 4.3 mm). The ratio $\Delta_r/\Delta_{ref}$ is given in Table 6-3 for all test units. Comparison of the $\Delta_r/\Delta_{ref}$ values given in the table indicates that residual displacements can be minimized by use of 100 external post-tensioning. This is because the strains in external tendons are significantly less than the corresponding strains in internally bonded tendons. Inelastic strains in internally bonded tendons result in loss of the prestressing force, large permanent displacements and joint openings. Comparison of $\Delta_r/\Delta_{ref}$ values given in Table 6-3 for Units 100-INT and 100-INT-CIP also indicates that use of cast-in-place deck closure in segment-to-segment joints close to the piers, in which the deck is subjected to high tensile stresses, will result in high post-earthquake permanent residual displacements. This is because of the high inelastic strains in the mild reinforcement of the cast-in-place deck closure joint under negative bending moments. Negative bending moments are those that produce tensile stresses in the top surface of the superstructure.

It should be remembered that in Phase I, the cast-in-place deck closure joints in Unit 100-INT-CIP reduced the permanent residual displacements compared to Unit 100-INT. However, Test Unit 100-INT-CIP in Phase I failed under positive bending by compression in the deck. The experiments of Phases I and II indicate that in zones where

the cast-in-place deck closure joints are mainly subjected to compressive stresses (i.e. at joints close to midspan of the superstructure), permanent residual displacements will be reduced. However permanent residual displacements will be increase with provision of cast-in-place deck closure joints in zones where the CIP deck closures are subjected to tensile stresses (i.e. at joints close to the columns).

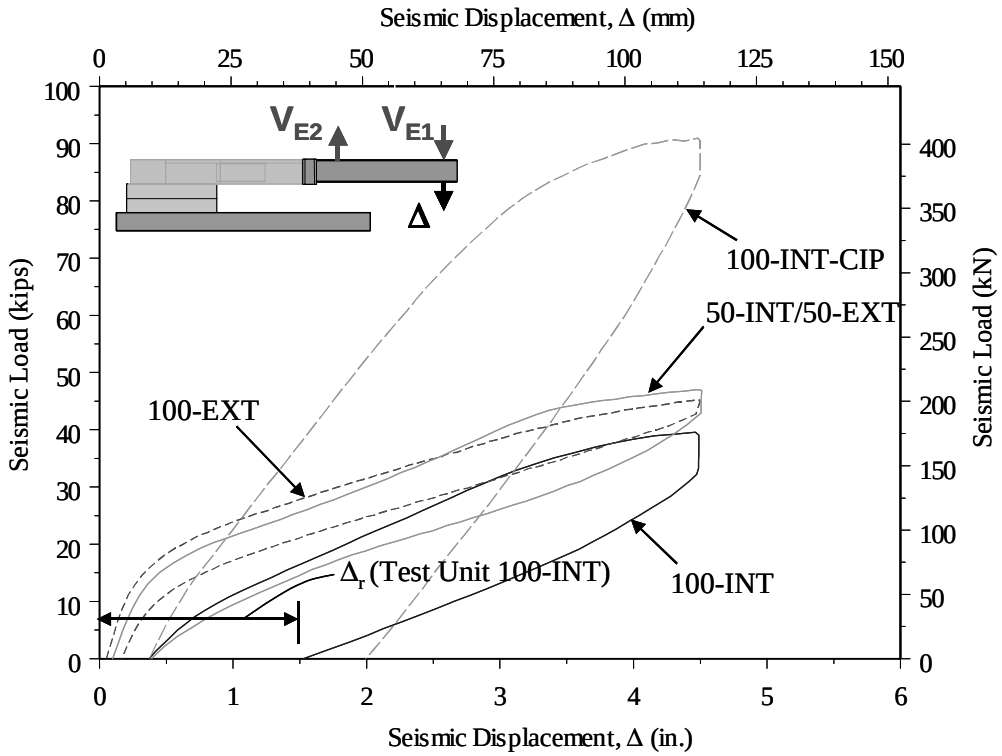


**Figure 6-64 Downward load versus displacement, 4.5 in. (114 mm) cycle only**

**Table 6-3 Residual displacements and damping coefficients of Phase II test units**

| Test Unit | Residual Displacements | | Damping Coefficients | |
|---|---|---|---|---|
| | $\Delta_r$ in. (mm) | $\Delta_r / \Delta_{ref}$ | $\zeta$ (%) | $\zeta / \zeta_{ref}$ |
| 100-INT | 1.53 (38.9) | 9.00 | 4.84 | 2.47 |
| 100-INT-CIP | 1.99 (50.5) | 11.71 | 5.79 | 2.95 |
| 100-EXT | 0.17 (4.3) | 1.00 | 1.96 | 1.00 |
| 50-INT/50-EXT | 0.39 (9.9) | 2.29 | 3.70 | 1.89 |

### 6.4.3 Energy Dissipation and Damping Coefficients

Viscous damping coefficient, ., can be considered as a measure of energy dissipation capability of the test units. The viscous damping coefficient is determined by Eq. (3-1) that relates the area within the hysteresis loop of the 4.5 in. (114 mm) displacement cycle to that of the elastic strain energy. The values of . are given in

Table **6-3**. The viscous damping coefficient for all test units is normalized to the damping coefficient of Unit 100-EXT, $._{ref}$ (= 1.96%).

Table **6-3** also gives values of the ratio $./._{ref}$ for all test units.

Table **6-3** indicates that segment-to-segment joints in superstructures with internally bonded tendons are able to dissipate more energy than joints in superstructures with external tendons. Values of the damping coefficient given in the table also indicate that use of cast-in-place deck closure joints enhances energy dissipation capability, which can also be seen in Figure 6-62.

### 6.4.4 Joint Rotations

Figure 6-65 shows the history of bending moments versus the rotation of Joint $J_1$ for the Test Series I units (Units 100-INT, 100-EXT and 50-INT/50-EXT). Figure 6-66 is similar to Figure 6-65, but it shows the bending moment versus joint rotation for Test Series II units (Units 100-INT and 100-INT-CIP). Values of the maximum joint rotations of all test units are given in Table 6-2. Figure 6-65, Figure 6-66 and the values given in Table 6-2 indicate that the segment-to-segment joints can undergo significant rotations without failure. Test units with 100% internal post-tensioning, and with combined internal and external post-tensioning, had comparable maximum joint rotations before failure. The experimental results of the Phase II units confirm the findings of the Phase I

experiments that 100% external post-tensioning of the superstructure substantially increases the rotational capacity of the segment-to-segment joints.

The maximum rotation of Unit 100-INT-CIP before failure under downward loading was the lowest among all test units. The reinforced cast-in-place deck closure joint substantially increased the stiffness of Unit 100-INT-CIP under downward loading. The maximum bending moment at Joint $J_1$ was extremely high at relatively low rotation (see Figure 6-66). The high bending moment resulted in extremely high compressive force in the bottom slabs and subsequently resulted in compression failure of the bottom slab. The rotational capacity of Unit 100-INT-CIP under downward loading was the highest among all test units (see Figure 6-65 and Figure 6-66).

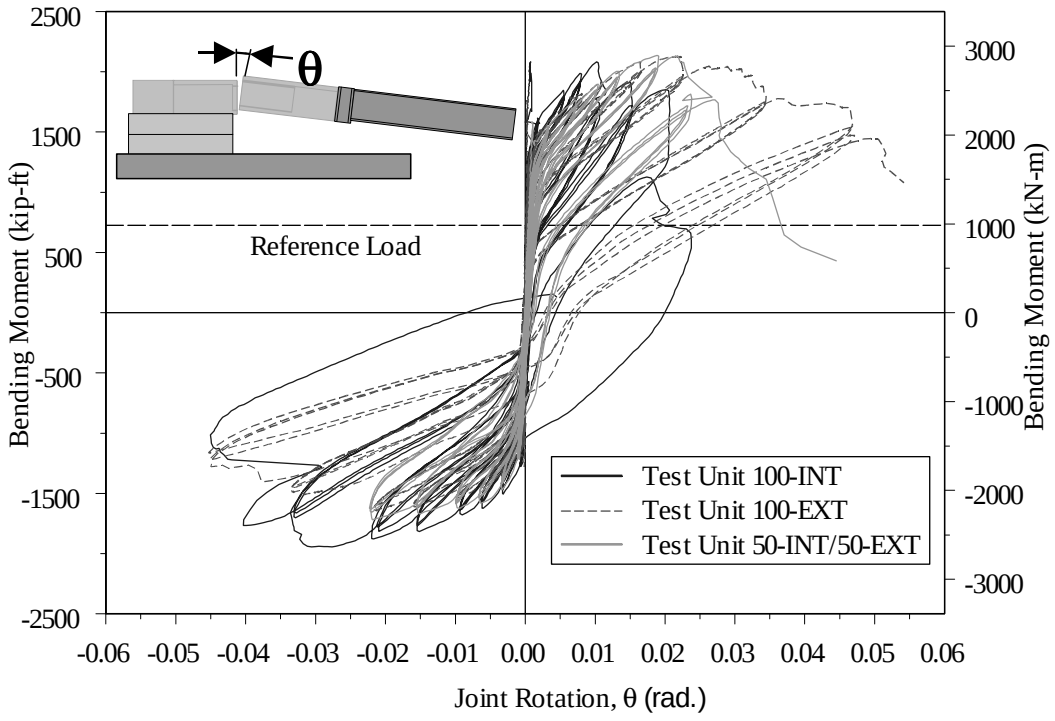


**Figure 6-65 Bending moment versus joint rotation in Test Series I units**

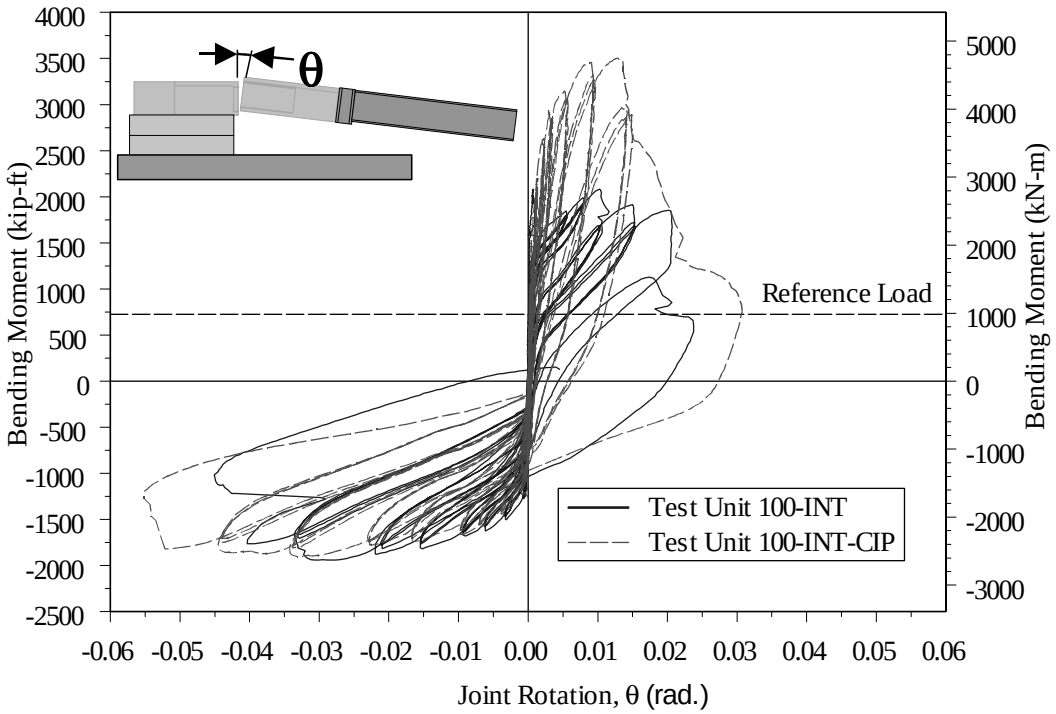


**Figure 6-66 Bending moments versus joint rotation in Test Series II units**

### 6.4.5 Tendon Strains

As mentioned earlier, strain gages placed on the tendons of Test Units 100-INT and 100-INT-CIP were affected by moisture of the surrounding grout. Figure 6-67 shows the variation of the strains measured in the upper tendon (the inclined tendon which represented the harped-shape tendon in the prototype structure); the strains shown in the figure were measured at the location of Joint $J_1$ in Units 100-EXT and 50-INT/50-EXT. Figure 6-67 shows that the internally bonded tendon in Unit 50-INT/50-EXT experienced much higher strains compared to the external tendon of Unit 100-EXT. This was also observed for test Units 100-EXT and 50-INT/50-EXT in Phase I. Figure 6-67 shows that the internally bonded tendon in Unit 50-INT/50-EXT yielded during the 3 in. (76 mm) displacement cycles, whereas the external tendon in Unit 100-EXT yielded during the 9.0 in. (229 mm) displacement cycle. This explains the high value of maximum displacement

before failure of Unit 100-EXT compared to maximum displacement of the other test units.

Figure 6-68 is similar to Figure 6-67, but it shows the strains measured in the horizontal (lower) tendons of Units 100-EXT and 50-INT/50-EXT. It should be remembered that the lower tendons in Unit 100-EXT were external, whereas the lower tendon in Unit 50-INT/50-EXT was internally bonded. The figure shows that the internally bonded tendon in Unit 50-INT/50-EXT yielded at a low displacement compared to the external tendons of Unit 100-EXT. This explains why the lower internally bonded tendon of Unit 50-INT/50-EXT fractured at relatively low upward displacement (about 6.1 in. = 155 mm) compared to the maximum displacement of 11.9 in. (302 mm) in Unit 100-EXT. Again it should be remembered that the external tendons in Units 100-EXT and 50-INT/50-EXT were not grouted after stressing of the tendons.

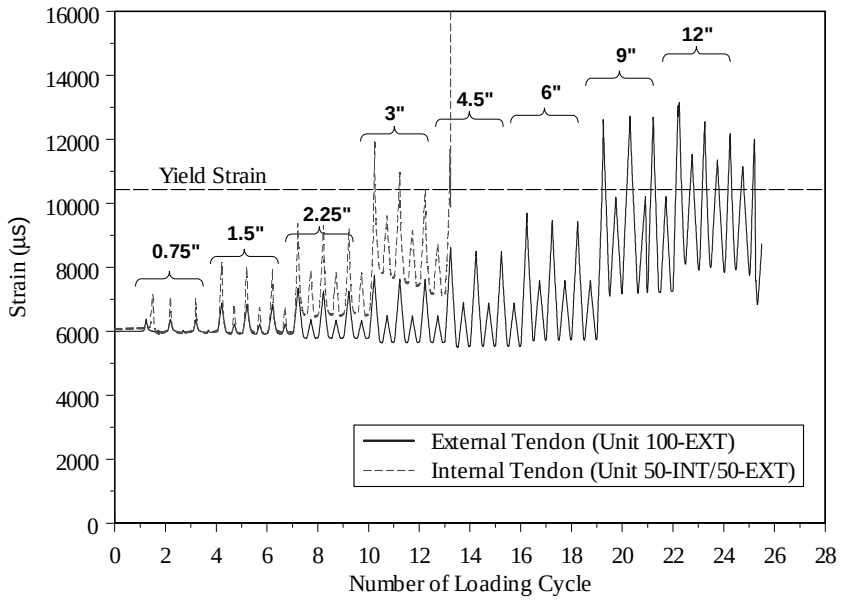


**Figure 6-67 Strains in the inclined (upper) tendons of Units 100-EXT and 50-INT/50-EXT**

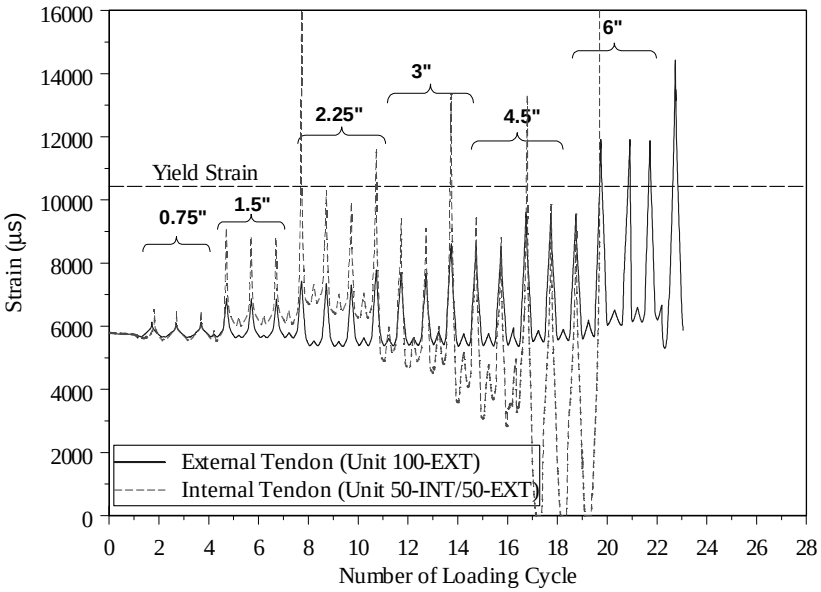


**Figure 6-68 Strains in the horizontal (lower) tendons of Units 100-EXT and 50-INT/50-EXT**

### 6.4.6 Cracking Strength

The concrete cracking strength at joint $J_1$ was determined using the known section properties of the test units, the experimental flexural moments at onset of cracking, or joint opening, and the measured effective prestressing force. Joint $J_1$ in Unit 100-INT opened under downward loading when the concrete reached a relatively high tensile stress of 8.13 $\sqrt{f_c'}$ (psi) [= 0.68 $\sqrt{f_c'}$ (MPa)]. However, the joint opened under upward loading when the concrete at the soffit reached a tensile stress of 4.59 $\sqrt{f_c'}$ (psi) [= 0.38 $\sqrt{f_c'}$ (MPa)]. As in the Phase I tests, opening of the joint occurred by cracking in the concrete cover adjacent to the segment-to-segment joint, rather than by opening of the epoxy bonded joint itself. Joint $J_1$ in Unit 100-INT-CIP opened under upward loading at a concrete tensile stress of 4.75 $\sqrt{f_c'}$ (psi) [= 0.40 $\sqrt{f_c'}$ (MPa)]. Again as in Phase I,

cracking of the top surface in Unit 100-INT-CIP occurred at a concrete tensile stress of about 4.24 $\sqrt{f_c'}$ (psi) [= 0.35 $\sqrt{f_c'}$ (MPa)], which was relatively low considering the continuity of the deck. The onset of cracking occurred in the deck at the interface between the precast concrete and that of the cast-in-place deck closure joint. The relatively weak interface between the precast and cast-in-place concretes resulted in this relatively low cracking strength.

Joint $J_1$ in Unit 100-EXT opened when the concrete reached tensile stresses of 5.50 $\sqrt{f_c'}$ (psi) [= 0.46 $\sqrt{f_c'}$ (MPa)] and 4.87 $\sqrt{f_c'}$ (psi) [= 0.41 $\sqrt{f_c'}$ (MPa)] under downward and upward loading, respectively. Joint $J_1$ in Unit 50-INT/50-EXT opened when the concrete reached tensile stresses of 5.04 $\sqrt{f_c'}$ (psi) [= 0.42 $\sqrt{f_c'}$ (MPa)] and 4.76 $\sqrt{f_c'}$ (psi) [= 0.40 $\sqrt{f_c'}$ (MPa)] under downward and upward loading, respectively.

The above-mentioned results indicate that tensile strength of 3.00 $\sqrt{f_c'}$ (psi) [= 0.25 $\sqrt{f_c'}$ (MPa)], which was recommended based on the results of Phase I (Section 3.4.5), can be conservatively used in design as evidenced by the results of Phase II experiments. Also, for precast segmental bridges with cast-in-place deck closure joints, onset of potential cracks would occur at the interface between concrete of the precast segments and concrete of the deck closure because of the relatively weak interface between the precast and cast-in-place concretes. Based on the experimental results of Unit 100-INT-CIP of Phase II, a concrete cracking strength of 4.00 $\sqrt{f_c'}$ (psi ) [= 0.33 $\sqrt{f_c'}$ (MPa)] is recommended for design, which also agrees with the findings of Phase I (Section 3.4.5).

### 6.4.7 Flexural Moment Capacity

Each test unit had two tendons (see Figure 5-4) and all units failed by compression in the bottom slab under downward loading. The AASHTO Guide Specifications[1] allows use of the strain compatibility provisions of the ACI318 building code[14] to calculate the flexural moment capacity of bridges with bonded tendons. The flexural moment capacities of Units 100-INT and 100-INT-CIP, with internally bonded tendons, were calculated using strain compatibility. The concrete strain at the extreme compression fiber was assumed to be 0.003[14]. The calculated flexural moment capacities of Units 100-INT and 100-INT-CIP were 2235 and 3562 kip-ft (3030 and 4829 kip-in.), respectively.

Under downward loading, the lower tendon was close to the neutral axis and its contribution to the flexural moment capacity was very small; the calculated contribution of the lower tendon to the flexural moment capacity of Units 100-INT and 100-INT-CIP was about 4 and 2 percent, respectively. For simplicity, contribution of the lower tendon to the flexural strength (under downward loading) was ignored and provisions of Section 9.17 of the AASHTO Standard Specifications[5] and Section 11.2 of the AASHTO Guide Specifications[1] (i.e. Eq. 3-2 combined with Eq. 3-3 or Eq. 3-4) were used to calculate the flexural moment capacity of all test units.

The calculated flexural moment capacity of all test units, $M_n$, is given in Table 6-4. The experimental peak flexural moment at midspan, $M_{Test}$, as well as the ratio ($M_{Test}/M_n$) are also given in Table 6-4 for all test units. The stresses in the external tendons at ultimate load were calculated according to provisions of Section 11.2 of the AASHTO Guide Specifications[1], but assuming that the tendon stress could not exceed the yield stress, $f_{py}$ (see Eq. 3-4; $f_{py}$ = 243 ksi = 1676 MPa).

Values of the ratio ($M_{Test}/M_n$) were close to 1.00 for all test units, which agree with the Phase I findings that the flexural moment capacity of precast segmental bridge superstructures can be reasonably estimated using Eqs. 3-2 to 3-4.

The ratio ($M_{Test}/M_n$) was slightly less than 1.00 for Unit 100-INT. As mentioned earlier premature compression failure occurred in the bottom slab of Test Unit 100-INT as a result of concrete segregation in a local zone of the bottom slab (see Section 6.1.1 and Figure 6-3); the weakened slab could not prevent buckling of the longitudinal mild steel bars inside Segment 1 of Unit 100-INT resulting in local compression failure (see Figure 6-3).

**Table 6-4 Experimental and calculated flexural moment capacity of test units (Phase II)**

| Unit | $M_{Test}$ kip-ft (kN-m) | $M_n$ kip-ft (kN-m) | $M_{Test} / M_n$ |
|---|---|---|---|
| 100-INT | 2082 (2823) | 2189 (2967) | 0.95 |
| 100-INT-CIP | 3504 (4750) | 3543 (4804) | 0.99 |
| 100-EXT | 2124 (2880) | 2089 (2833) | 1.02 |
| 50-INT/50-EXT | 2136 (2896) | 2156 (2922) | 0.99 |

# 7 Finite Element Prediction Analyses of Phase II Experiments (Joints Subjected to High Bending Moments and High Shears)

## 7.1 Analysis Model

Detailed 3-D models were developed for each of the four Phase II test Units. These structural tests investigated the behavior of segment-to-segments joints of precast concrete superstructure components near the bent of the prototype structure under severe seismic loading. While Phase I tests examined joint opening and closing behavior under large moment and small shear force, representative of the prototype bridge superstructure at midspan, the Phase II tests modeled both large moment and shear force expected near the bent. As discussed in detail in Chapter 5, dead load and seismic loading were applied by two vertical actuators, placed several feet apart along a cantilever steel loading beam. This design allowed the correct moment and shear forces to be applied to the critical segment-to-segment joint throughout the loading history.

In the analysis model, three-dimensional 8-node solid brick elements were used to model the concrete and truss elements were used to model both bonded and unbonded prestressing steel, as well as to model the steel reinforcement in the cast-in-place (CIP) deck joint. Concrete was modeled as unconfined, utilizing a 3-D plasticity based material model while prestressing steel and rebar were modeled with 1-D plasticity formulation. The concrete compressive strength was assumed to be 5.0 ksi (34.5 MPa) for the finite element analyses. Most of the analyses presented here were performed prior to testing of the test units; thus the actual concrete strengths of the test units were not known when the finite element analyses were performed. The actual concrete compressive strengths (see

Table 5-2) were close to the 5.0 ksi (34.5 MPa) compressive strength assumed in the finite element analyses.

The shape of the stress-strain curve for the 270 ksi (1,862 MPa) prestressing steel has not been measured and thus this behavior had to be assumed. For all of the predictions presented in the following, the Menegotto-Pinto function (Eq. 4-1), used by Collins and Mitchell[13], was incorporated. A rupture strain of 0.04 was assumed at an ultimate stress of 270 ksi (1,862 MPa). The structure was modeled using ½-symmetry as shown in Figure 7-1, which considerably increases the speed of the analysis while decreasing storage requirements on the hard drive. All finite element analyses were performed using the general-purpose computer program ABAQUS[11].

The concrete components, including the footing, were modeled with 3-D brick elements and the loading steel nose was modeled with beam elements, utilizing elastic steel properties. Prior to developing the final prediction models and building the steel nose a detailed model was developed of the loading steel nose. With a small initial offset of the load, it was found that the original steel nose design would develop large stresses and local buckling at the expected ultimate load. Thus the results of this preliminary analysis allowed the test setup to be modified to increase torsional rigidity and to prevent sudden increases in stress resulting in local buckling. The same loading procedure used for the test units was followed in the analyses, producing the same dead loads and the same ratio of moment to shear force.

The critical segment-to-segment joint was modeled using a surface interaction definition[11], which allows two surfaces to move apart from each other and then close again under cyclic loading. For all but the 100% unbonded case (Test Unit 100-EXT),

this resulted in interface sliding from the cyclic analyses (Figure 7-18), at displacements significantly less than measured failure displacements and predicted failure displacements from monotonic analysis. Sliding did not occur in the monotonic analyses because some portion of the two surfaces was always in contact and the rough shear transfer model was used[11]. However, as displacements increased in both loading directions from cyclic analysis the bonded prestressing steel began to yield, causing it to develop compression stresses prior to closing the gap. The most sensitive region of the cyclic loading pattern for slip to occur was when the critical joint had small moment and significant shear force. In all cases this was when the shear slip developed in the cyclic analysis. At this point in the loading the top and bottom tendons were balancing each other's forces. One tendon was in compression and the other was in tension, with the entire surface not in contact. This explains why slip did not occur in the 100 % unbonded cyclic analysis (Test Unit 100-EXT), as the strains remained small through the loading allowing the two surfaces to remain in contact at all times. Most of the results presented in the following are from the monotonic predictions, although some interesting cyclic behaviors are presented of the bonded and unbonded strands.

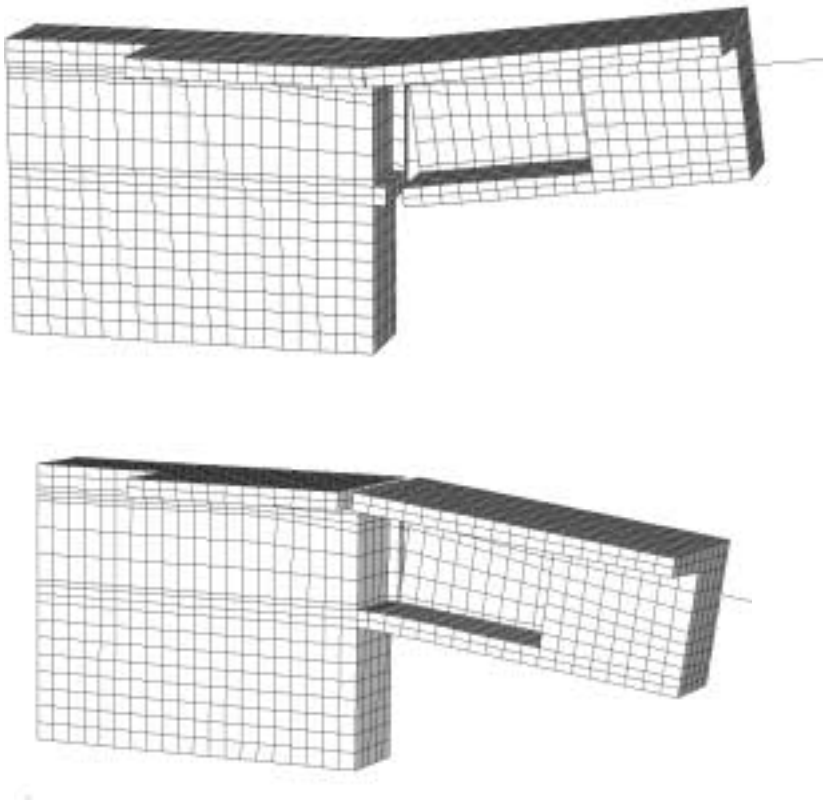

**Figure 7-1 Typical finite element model mesh and deformation modes**

## 7.2 Analysis Results

### 7.2.1 Test Unit 100-INT (100% bonded prestressing steel)

The overall shape of the blind prediction force-deformation results matched the test results very well, in both loading directions (Figure 7-2). In the downward direction (positive displacement) the structure was predicted to fail from crushing of the unconfined bottom flange concrete in the critical joint region at a displacement and seismic shear force of 5.92 inches (150 mm) (Figure 7-2 and Figure 7-10a) and 50.3 kips (224 kN), respectively. In the upward loading direction the bottom bonded prestressing tendon (4 strands) was expected to fracture at a displacement of 7.92 inches (201 mm)

(Figure 7-2 and Figure 7-11b) and associated seismic shear force of 89.7 kips (399 kN). These results were in fairly close agreement with results from a relatively simple moment-curvature analysis using the program ANDRIANNA[15], which gave displacement and seismic shear force capacities in the downward direction of 6.54 inches (166 mm) and 51.5 kips (229 kN), respectively, at a compressive strain of 0.005, and capacities in the upward direction of 5.93 inches (151 mm) and 85.8 kips (382 kN), respectively, due to failure of the bottom strands. Measured and observed results from the test showed that initial crushing of the bottom flange and associated drop in force occurred at about 3 inches (76 mm) of downward displacement, followed by sudden crushing of the bottom flange and severe loss of strength at 6 inches (152 mm) of downward displacement (Figure 7-2).

Initial crushing at 3 inches (76 mm) of displacement is considered somewhat of an anomaly, and occurred to several contributing factors (see Section 6.1.1 and Figure 6-3). The concrete, in a local zone of the bottom slab, did not have the required tensile and compressive strengths to prevent the buckling of the longitudinal bars inside precast Segment 1 in the test unit (see Figure 6-3). As the bars simultaneously buckled out and pushed the cover concrete off, the section size was suddenly reduced, causing the measured drop in force.

This explains why the concrete and buckling bars blew out on the top side of the bottom flange, away from the critical section. Based on section analysis as well as from the more detailed finite element analysis there were very little compression stresses in this region and compression failure was expected only at the critical section. Thus it is reasonable to compare the predicted failure at 5.9 inches (150 mm) of displacement to the

observed complete compression failure of the bottom flange, which occurred at the critical section at 6 inches of displacement (Figure 7-2).

In the upward loading direction the bottom strand was predicted to fail at 7.9 inches (201 mm) of displacement. However, at this displacement level the test unit did not quite reach the force necessary to fracture the strands (as indicated by the difference in measured and predicted forces in Figure 7-2), resulting in compression failure of the deck at about 12 inches (305 mm) of displacement.

From a cyclic analysis the stress and strain responses are given in Figure 7-6 to a displacement of 4.5 inches (114 mm). It is of interest to note that as the strains increased into the nonlinear range the initial prestressing was lost. In fact, the bottom strand went into compression, with almost 100 ksi (690 MPa) compressive stress.

### 7.2.2 Test Unit 50-INT/50-EXT (50% unbonded & 50% bonded prestressing steel)

The second unit tested had 50 % bonded (8 strands) and 50 % unbonded (8 strands) strands in the top tendon, with 4 bonded strands for the bottom tendon. Predicted force-deformation responses in both loading directions matched the test results fairly closely, as were the predicted failure modes and deformations (Figure 7-3). In the downward loading direction the bottom flange was predicted to fail in compression at a displacement of 5.55 inches (141 mm) (Figure 7-3 and Figure 7-12a), which almost exactly matched the observed failure displacement shown in Figure 7-3. In the upward loading direction the bottom tendon was predicted to fail at a displacement of 7.27 inches (185 mm) (Figure 7-3 and Figure 7-13b). As Figure 7-3 shows, two of the four bottom tendon strands were

observed to fail between 6 and 7 inches (152 and 178 mm) of displacement, matching the predicted failure displacement relatively closely.

Compression failure was predicted when the concrete compressive strain exceeded 0.005 across the whole flange width. In the upward loading direction the bottom strand reached the assumed failure stress of 270 ksi (1,862 MPa) (Figure 7-13b) prior to compressive strains reaching 0.005 in the top slab (Figure 7-13a). In the downward loading direction the compressive strains in the bottom slab reached the critical value of 0.005 (Figure 7-12a) prior to rupture of the top bonded tendon (Figure 7-12b). Of course, the top unbonded tendon spread any local deformations over its entire unbonded length, with small increases in strain and stress compared to the bonded tendons (Figure 7-12b). The cyclic prediction results nicely demonstrated this behavior, with only small strain and stress changes for the unbonded strand throughout the loading (Figure 7-7), whereas top and bottom bonded strands had significant variations in strain and stress, with almost identical behavior to the 100 % bonded test unit (100-INT) tendons discussed above (compare Figure 7-6 and Figure 7-7). As discussed previously, this resulted in the loss of the initial prestressing for the bonded strands and small losses for the unbonded strand (Figure 7-7b).

### 7.2.3 Test Unit 100-EXT (100% unbonded prestressing steel)

This test unit with 100 % unbonded tendons was the only test Unit that had an unbonded bottom strand. Prediction and post-test analyses are shown against the measured force-deformation response in Figure 7-4. Post-test analysis results are included here along with the prediction analysis results because in the blind prediction

analysis the bottom, unbonded tendon was inadvertently modeled as bonded. The only change made to the prediction model was to unbond the bottom tendon from the concrete elements over the debonded length. Of interest in this analysis is that in the downward loading direction the force levels from the model were less than measured. This discrepancy was not seen with the analysis of the test units that had bonded prestressing, although there was some difference between predicted and measured force for Unit 50-INT/50-EXT (Figure 7-3). This was probably a consequence of the movement of the tendons in the vertical direction with respect to the test Unit and the resulting slight change in the internal moment arm of the test unit cross section with increased downward displacement.

Compression failure was predicted at 5.50 inches (140 mm) of downward displacement (Figure 7-4 and Figure 7-14a), and this agreed well with the onset of softening observed in the test. However, a sudden compression failure did not occur and was probably because the compression force in the bottom slab was not as high as in the other cases, which had bonded top prestressing steel. Whatever tension force developed in the strand was balanced by compression in the bottom flange. However, very little increase in stress developed in the unbonded tendons as local joint rotations were accounted for by strains that were spread over the entire unbonded length. Once the critical joint opened, the stiffness was much smaller than for the bonded cases, resulting in development of smaller tension and compression forces. Results from cyclic analysis showed that the strains and stresses for the unbonded tendons remained relatively small throughout the loading (Figure 7-8). It was assumed that rupture strain of the tendons is 0.04, and thus the tendons were not close to rupture (Figure 7-8a). However, by 6 inches

(152 mm) of downward displacement the bottom strand had lost about half of its initial presressing force (Figure 7-8b).

In the upward loading direction the post-test analysis did not show any failure to almost 12 inches (305 mm) of displacement (Figure 7-4 and Figure 7-15), whereas the test showed rupture of two strands in the bottom tendon at about 10 inches (25 mm) of displacement.

### 7.2.4 Test Unit 100-INT-CIP (100% bonded with cast-in-place deck joint)

This test was representative of a proposed design of segment-to-segment joints of the new East Span of the San Francisco-Oakland Bay Bridge (SFOBB). The Skyway Structure is being designed with a precast segmental superstructure that contains cast-in-place (CIP) deck joints to provide mild steel reinforcement and continuity across all precast segment joints. Reinforcement was modeled with nonlinear truss elements across the CIP deck joint. As indicated in Figure 7-5, the prediction analysis captured overall force-deformation responses in both loading directions very well. In particular, the large increase in force in the downward loading direction, compared to the other tests, associated with the added mild steel placed across the CIP deck joint was nicely captured in the prediction. Compression failure of the bottom flange was expected at a downward displacement and seismic shear force of 4.44 inches (113 mm) and 98.9 kips (440 kN), respectively (Figure 7-5 and Figure 7-16a). Although the compression failure of the flange was observed at 6 inches (152 mm) of downward displacement (Figure 7-5), the onset of crushing was evident by 4.5 inches (114 mm) of displacement, with horizontal splitting cracks in the bottom flange that extended from the critical section. In the upward

loading direction the bottom strand was expected to rupture at a displacement of 7.60 inches (193 mm) (Figure 7-5 and Figure 7-17b). However, rupture did not occur until 14 inches (356 mm) of displacement.

Cyclic results showed that the mild steel reinforcement in the CIP deck joint reached strains that were larger than the bonded prestressing steel (Figure 7-9). This was due to shorter strain penetration of rebar on either side of the critical joint. However, since mild steel reinforcement had greater strain capacity than prestressing steel, and because tensile strains in the mild steel reinforcement developed in the downward loading direction where compression failure of the bottom flange limited the displacement capacity, the failure mode of rupture of mild steel was not predicted or observed in the test.

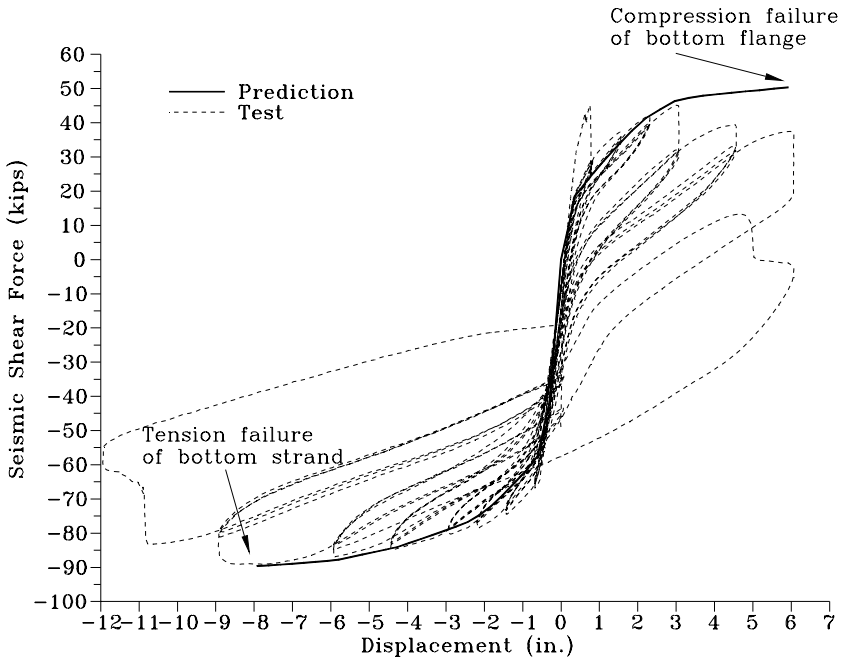


**Figure 7-2 Predicted and measured force-deformation results for 100-INT**

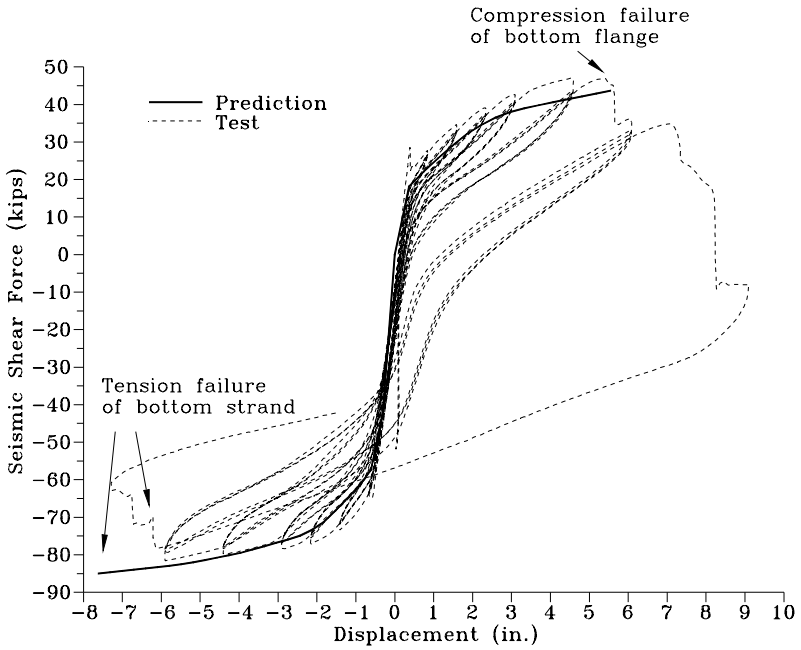


**Figure 7-3 Predicted and measured force-deformation results for 50-INT/50-EXT**

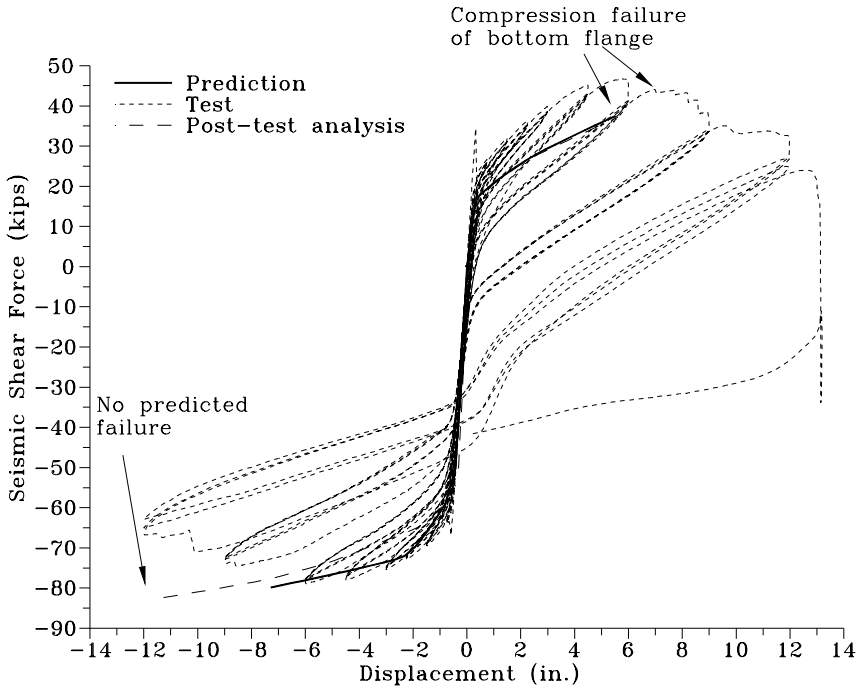


**Figure 7-4 Predicted and measured force-deformation results for 100-EXT**

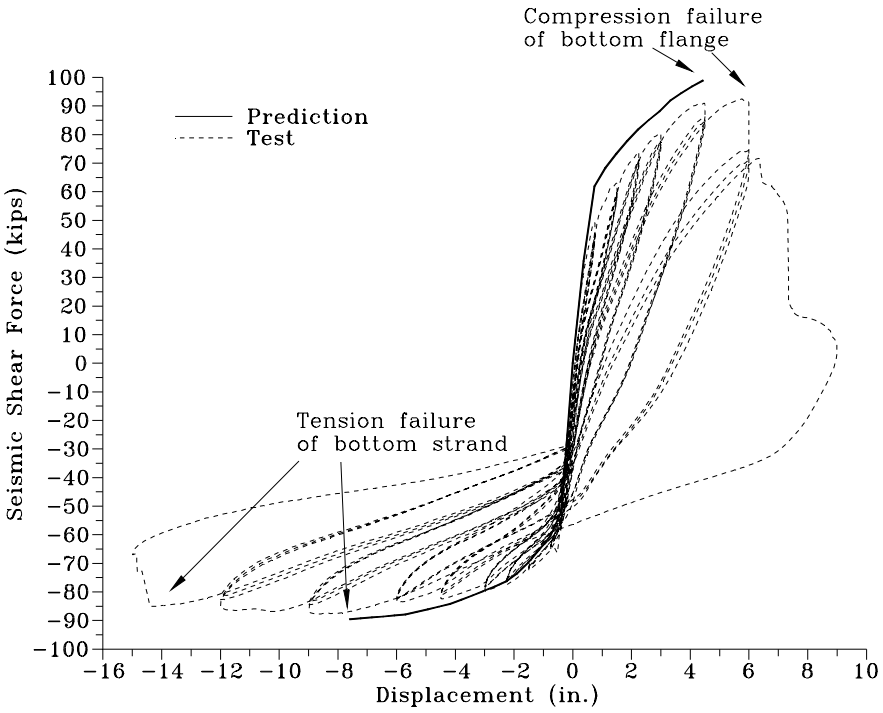


**Figure 7-5 Predicted and measured force-deformation results for 100-INT-CIP**

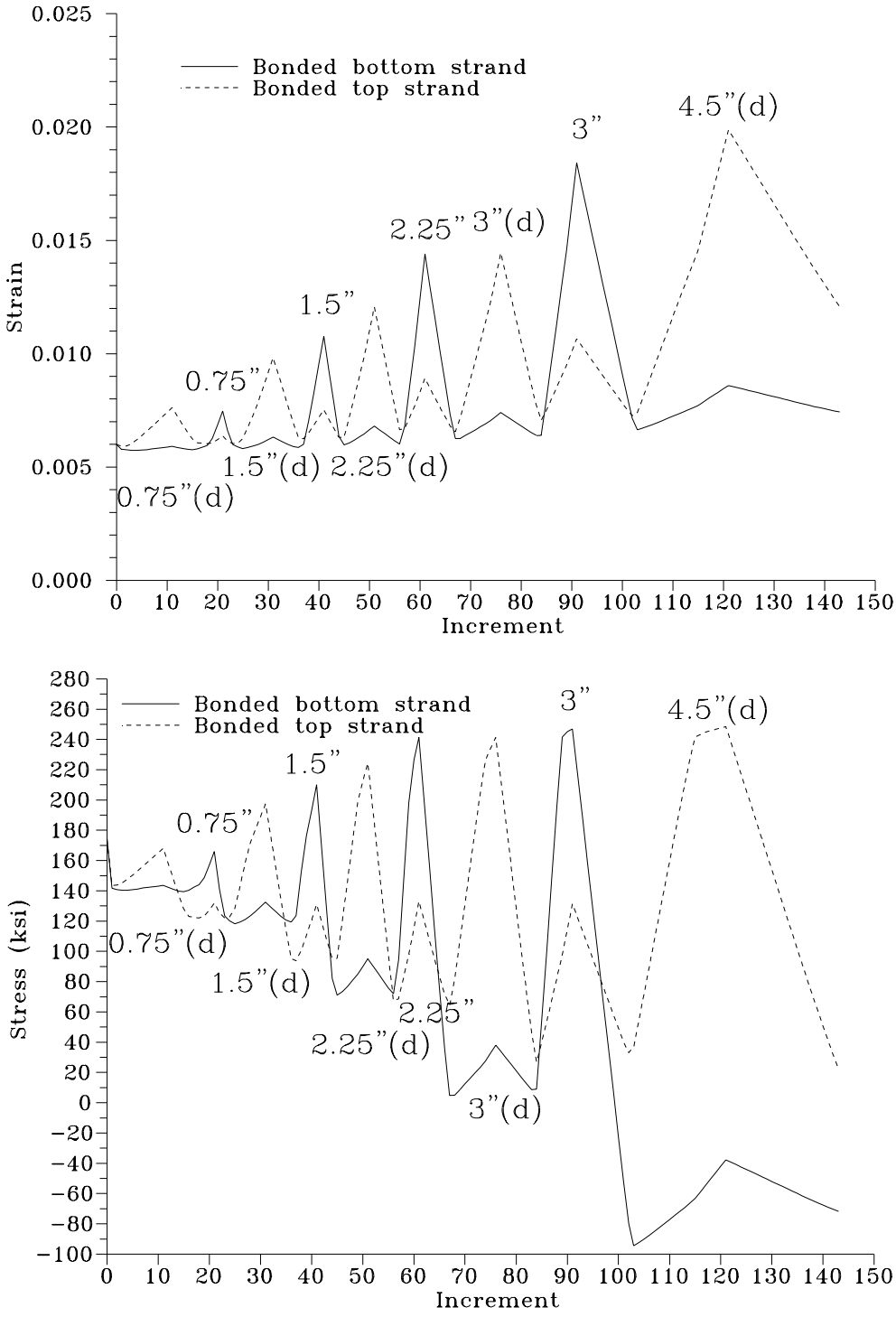


**Figure 7-6 Predicted stress and strain results from cyclic analysis of 100-INT**

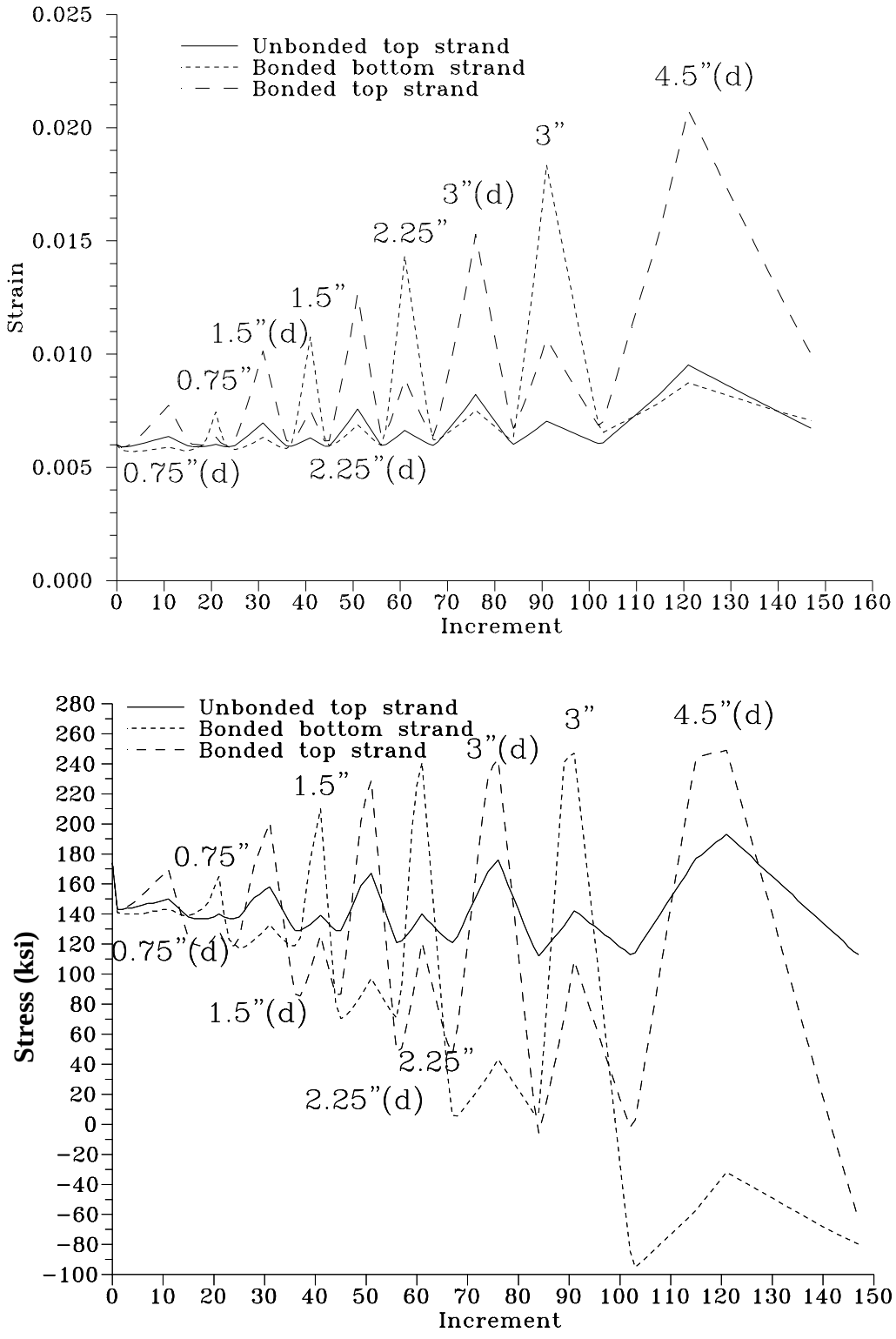


**Figure 7-7 Predicted stress and strain results from cyclic analysis of 50-INT/50-EXT**

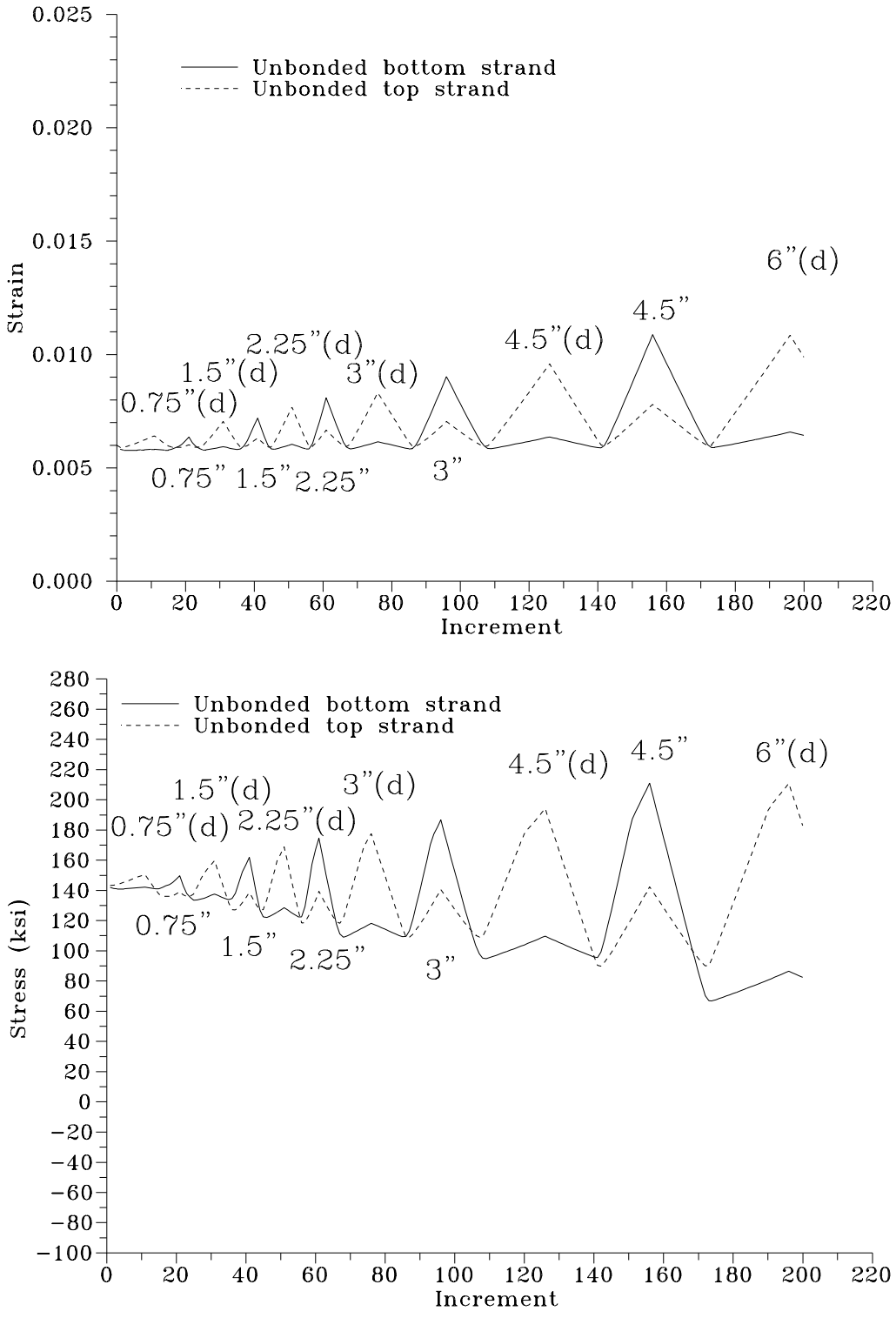


**Figure 7-8 Predicted stress and strain results from cyclic analysis of 100-EXT**

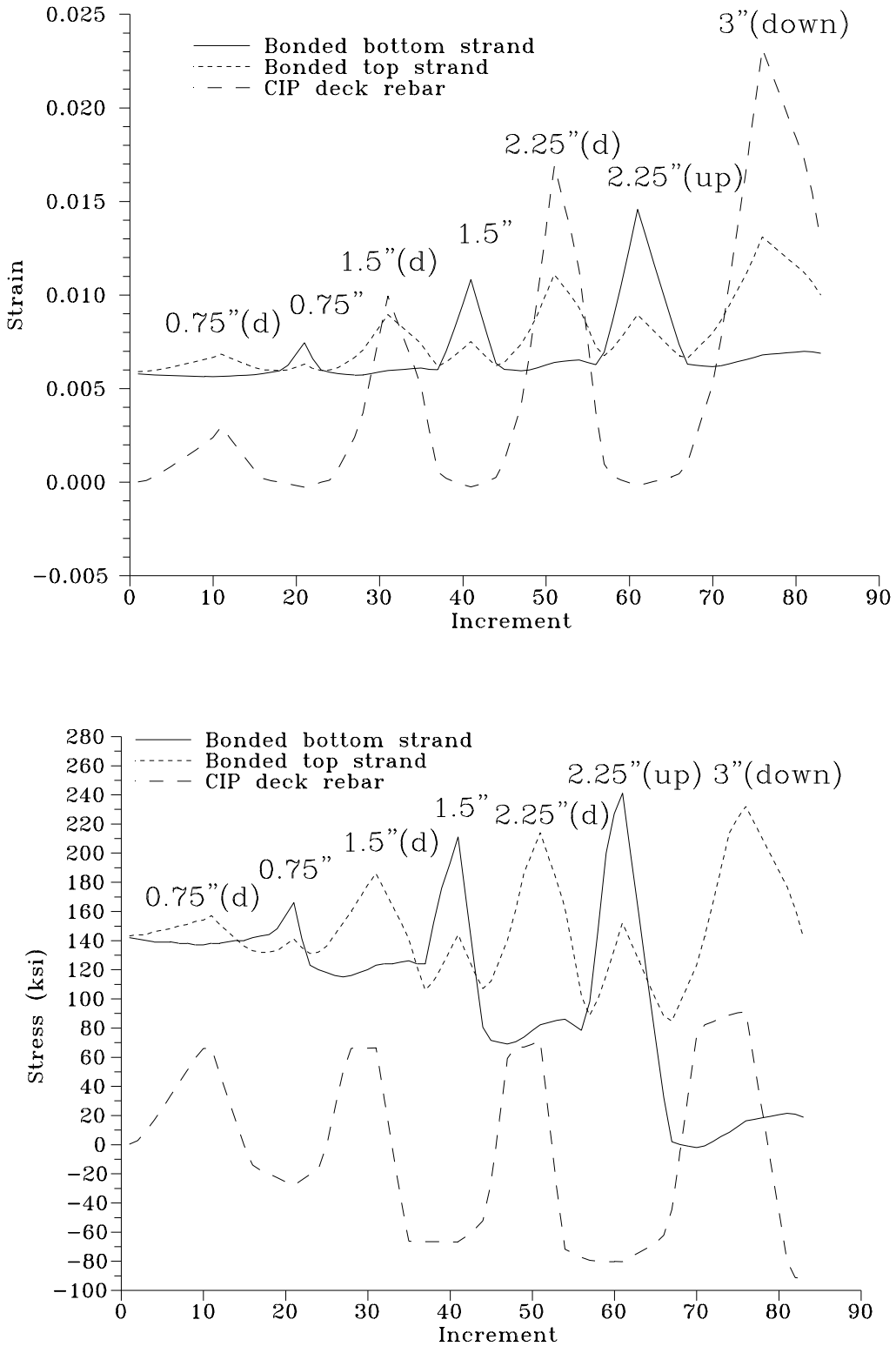


**Figure 7-9 Predicted stress and strain results from cyclic analysis of 100-INT-CIP**

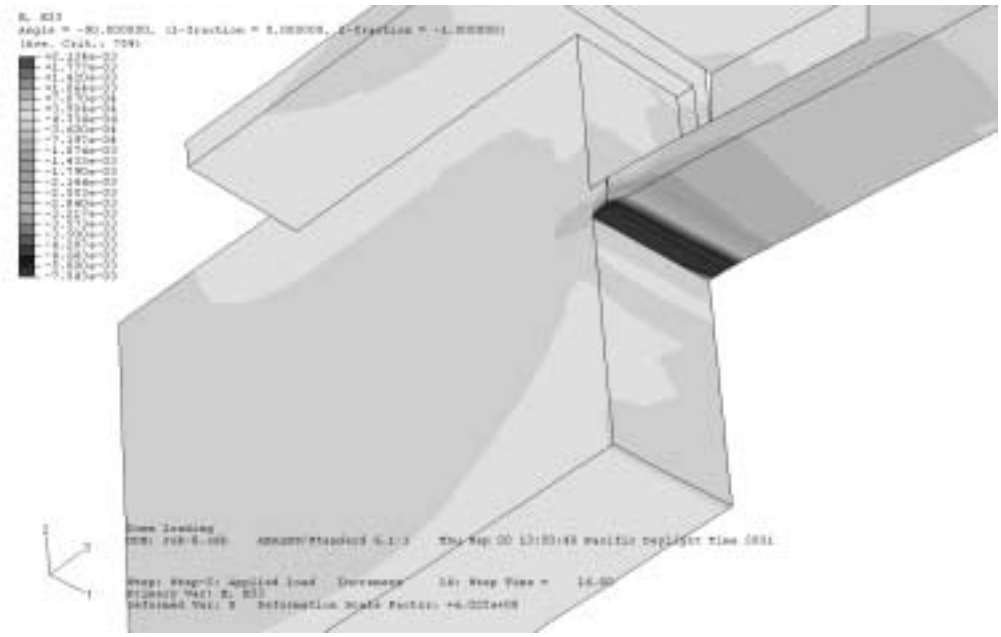

(a) Longitudinal strain contours of concrete (black is compressive strain above 0.005)

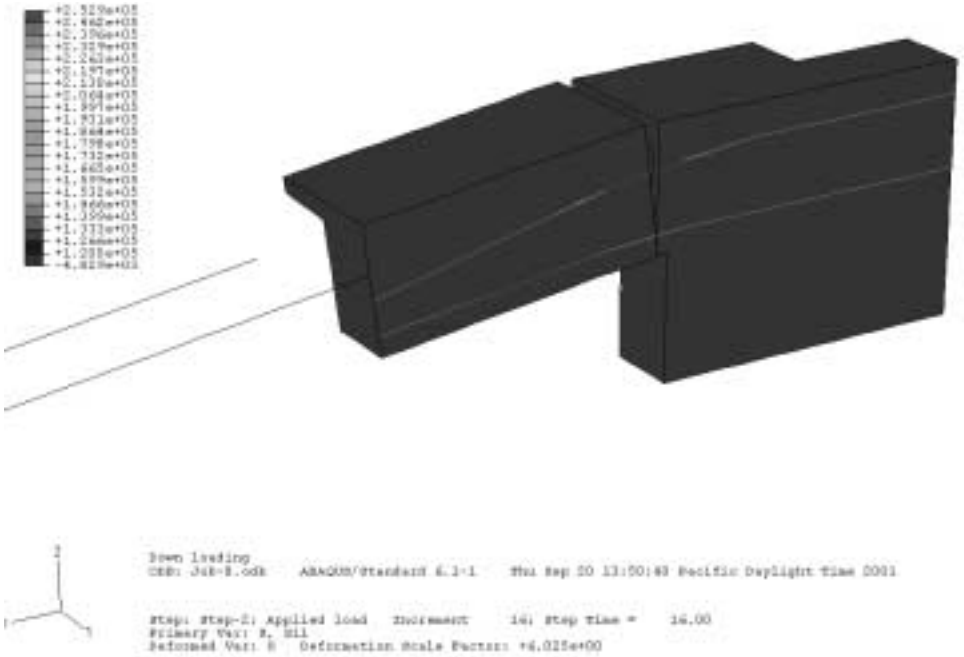


(b) Stress contours of bonded prestressing tendons

**Figure 7-10 Stress and strain contours at failure in the downward direction of 100-INT**

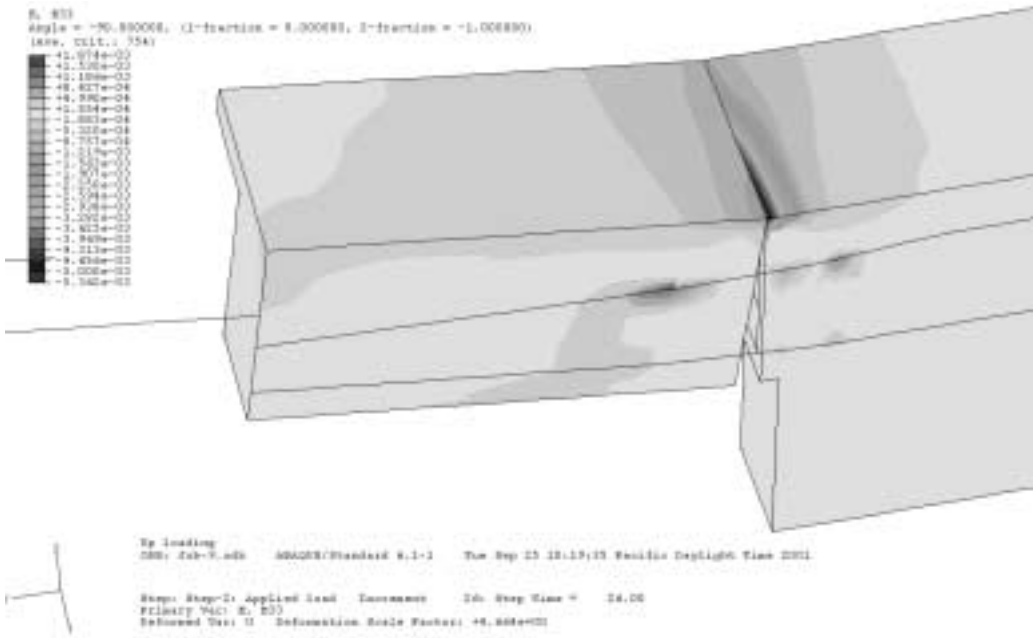

(a) Longitudinal strain contours of concrete (black is compressive strain above 0.005)

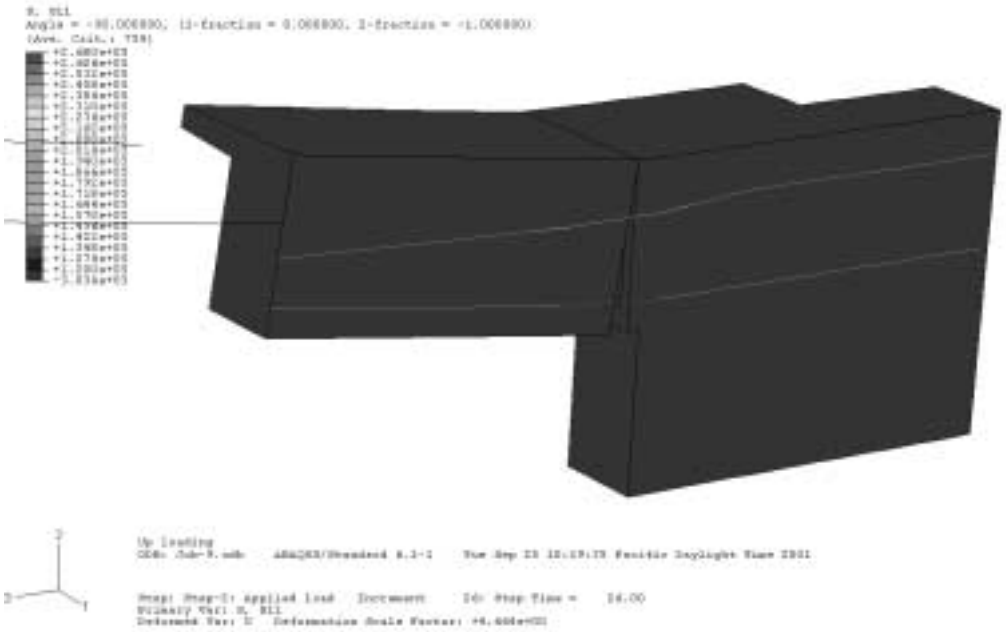

(b) Stress contours of bonded prestressing tendons

**Figure 7-11 Stress and strain contours at failure in the upward direction of 100-INT**

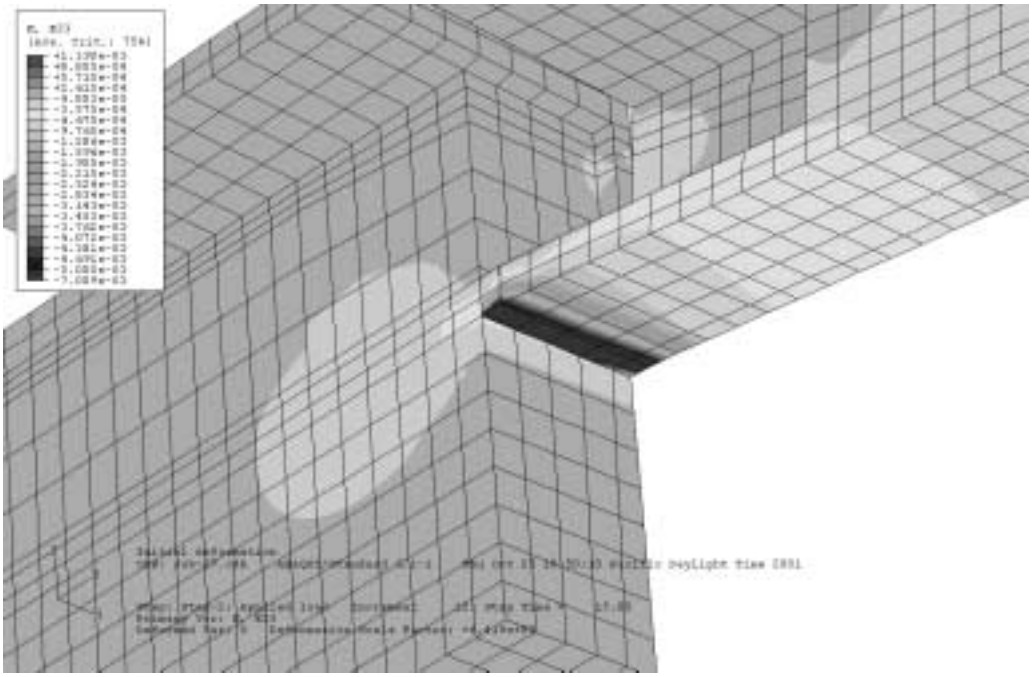

(a) Longitudinal strain contours of concrete (black is compressive strain above 0.005)

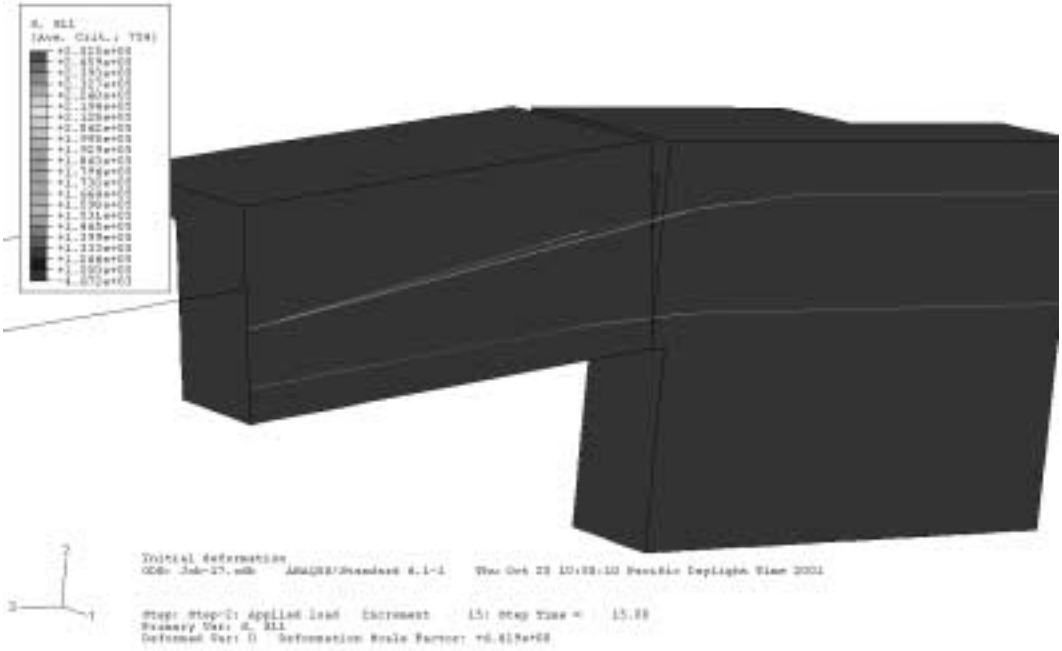

(b) Stress contours of all prestressing tendons, including bonded and unbonded strands

**Figure 7-12 Stress and strain contours at failure in the downward direction of 50-INT/50-EXT**

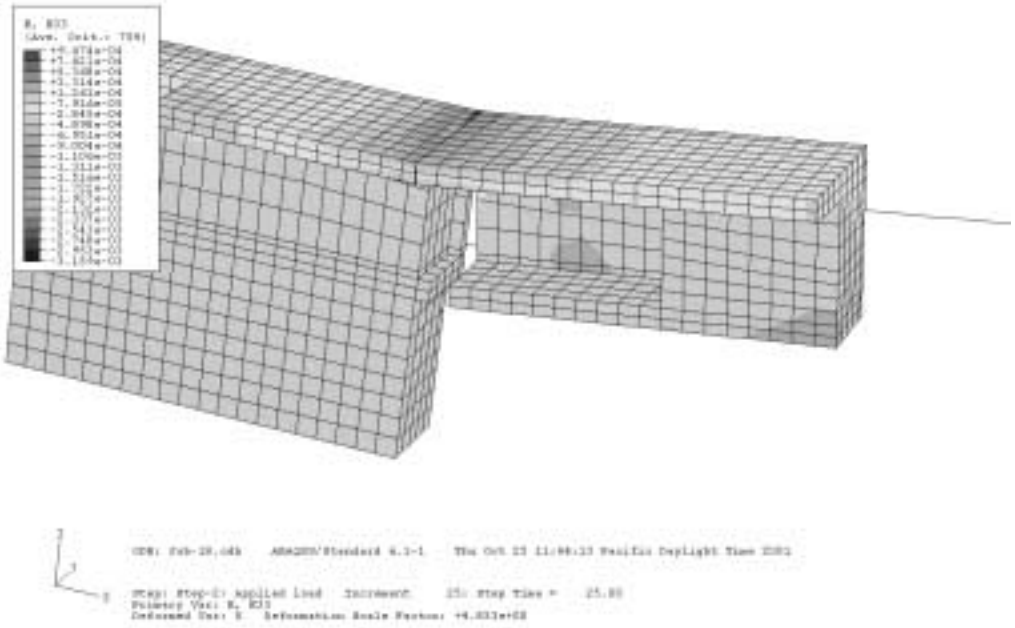

(a) Longitudinal strain contours of the concrete

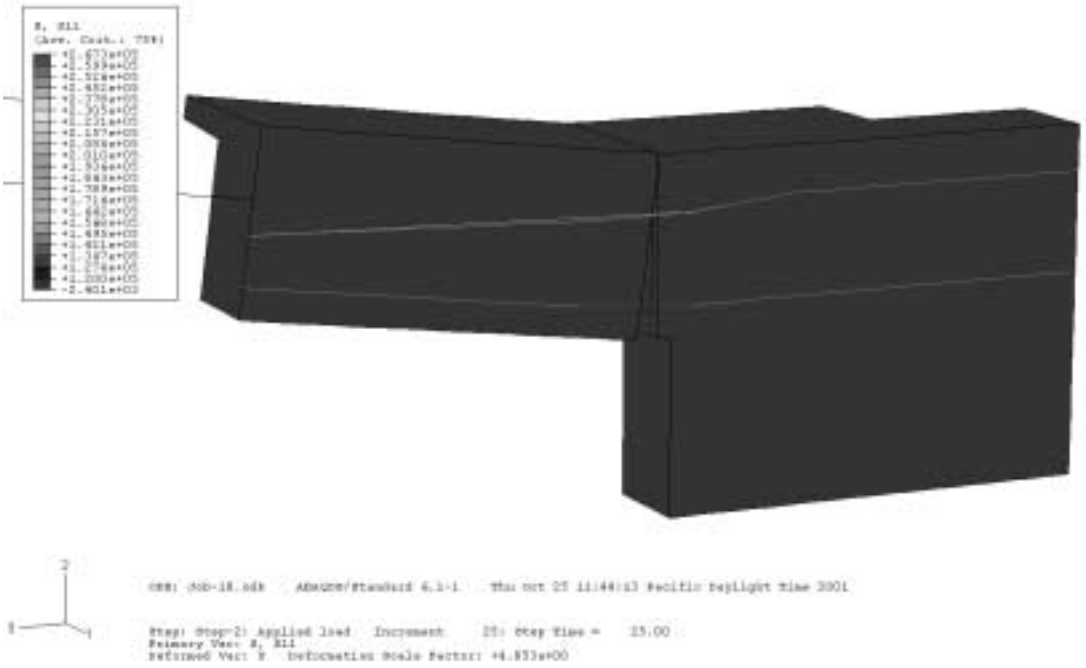

(b) Stress contours of all prestressing tendons, including bonded and unbonded strands

**Figure 7-13 Stress and strain contours at failure in the upward direction of 50-INT/50-EXT**

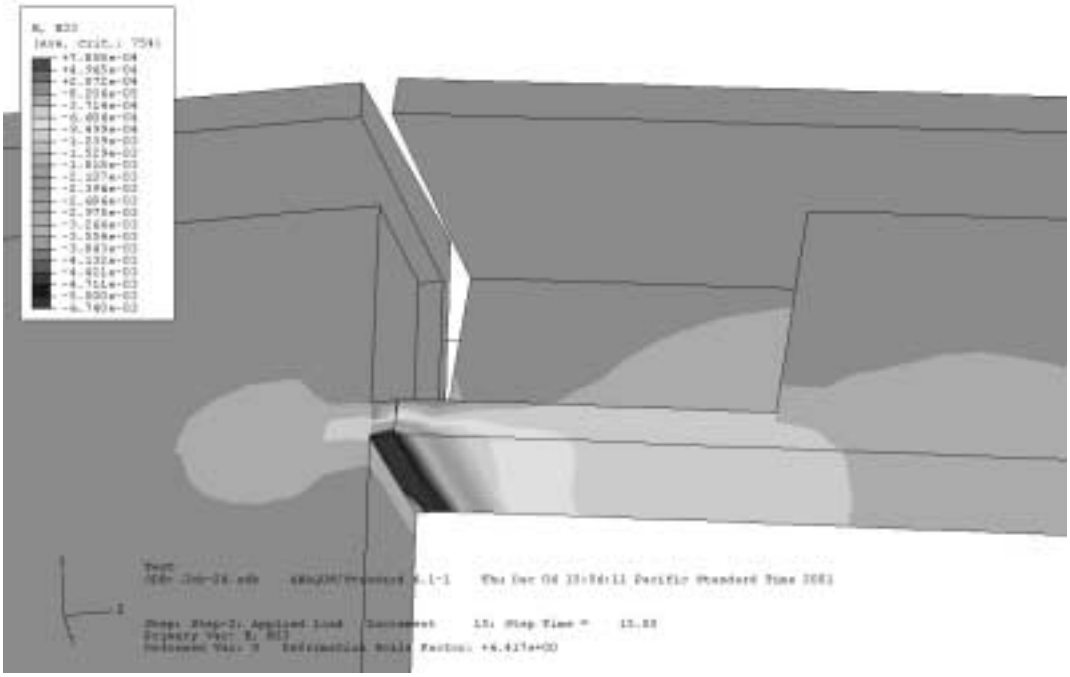

(a) Longitudinal strain contours of concrete (black is compressive strain above 0.005)

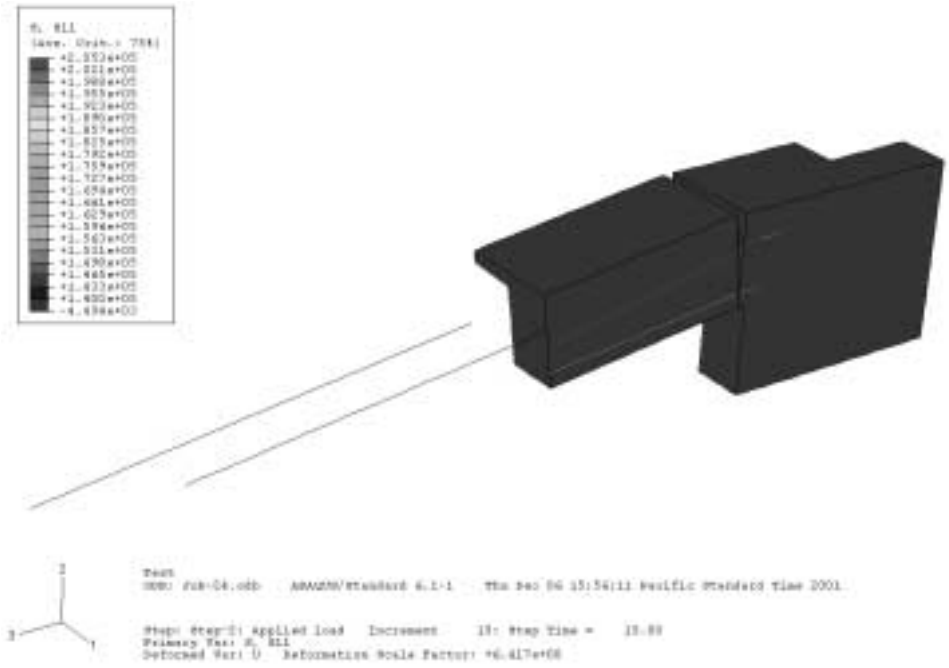

(b) Stress contours of unbonded prestressing tendons

**Figure 7-14 Stress and strain contours at failure in the downward direction of 100-EXT**

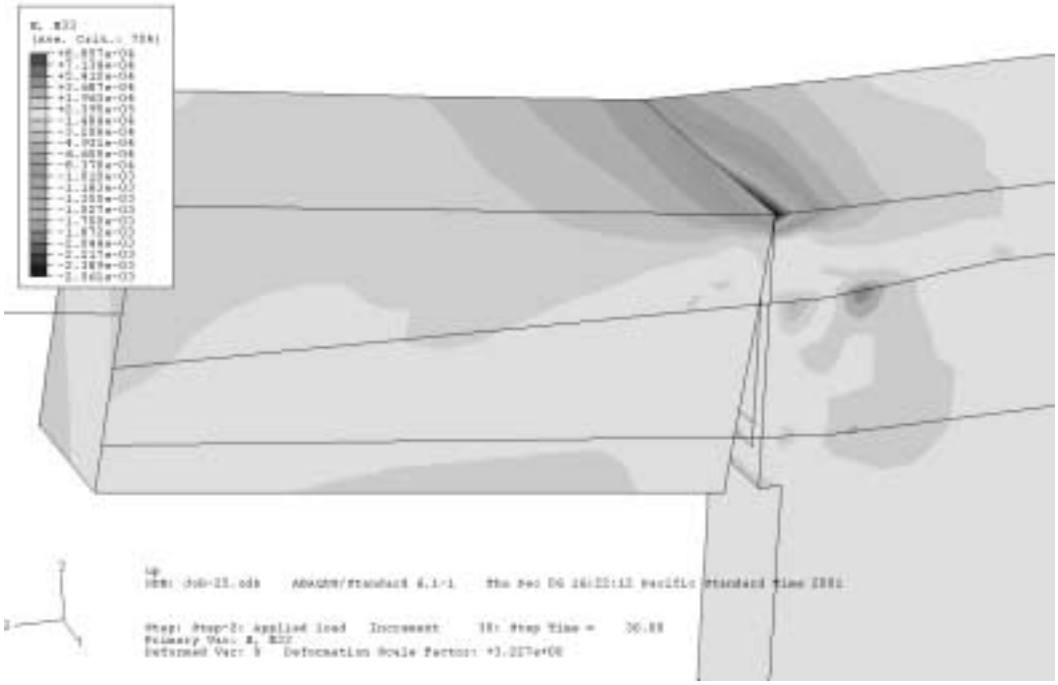

(a) Longitudinal strain contours of the concrete

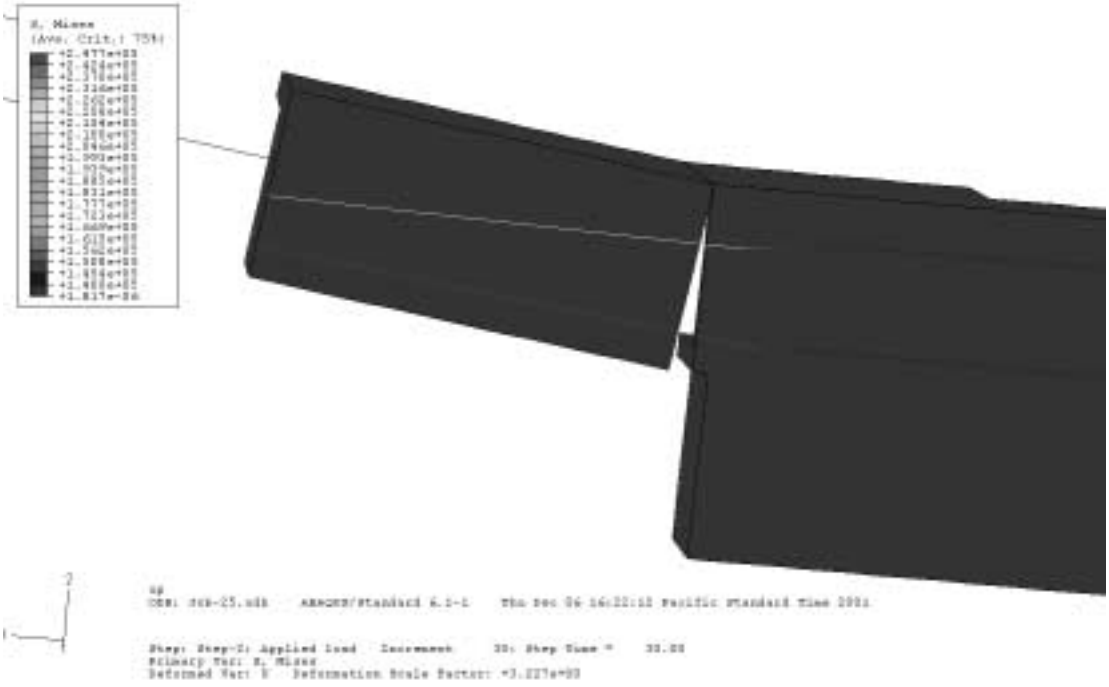

(b) Stress contours of unbonded prestressing tendons

**Figure 7-15 Stress and strain contours at 12” in the upward direction of 100-EXT**

(a) Longitudinal strain contours of concrete (black is compressive strain above 0.005)

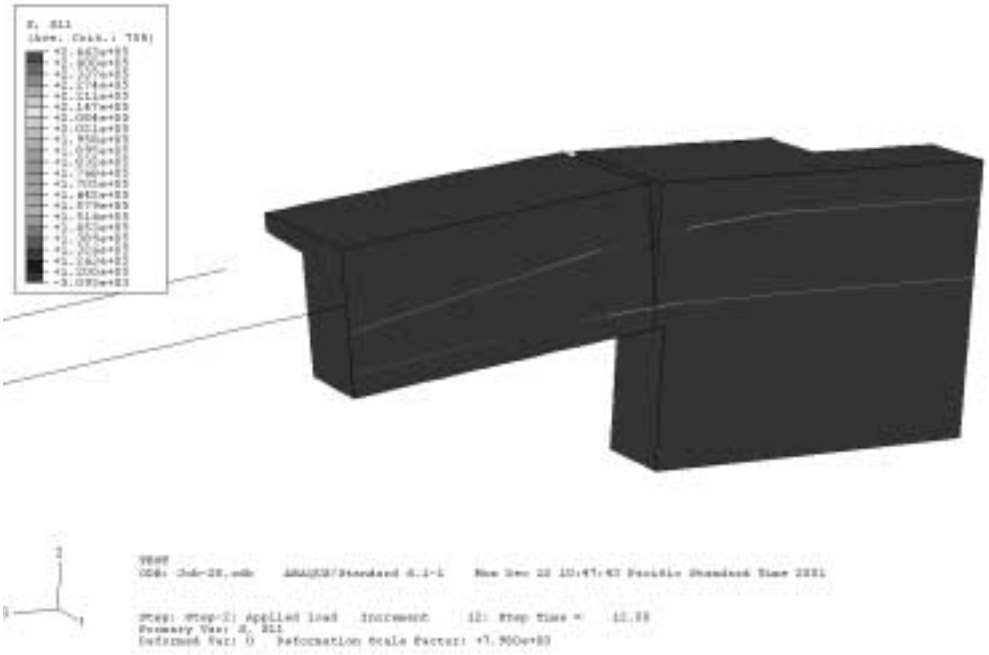

(b) Stress contours of bonded strands

**Figure 7-16 Stress and strain contours at failure in the downward direction of 100-INT-CIP**

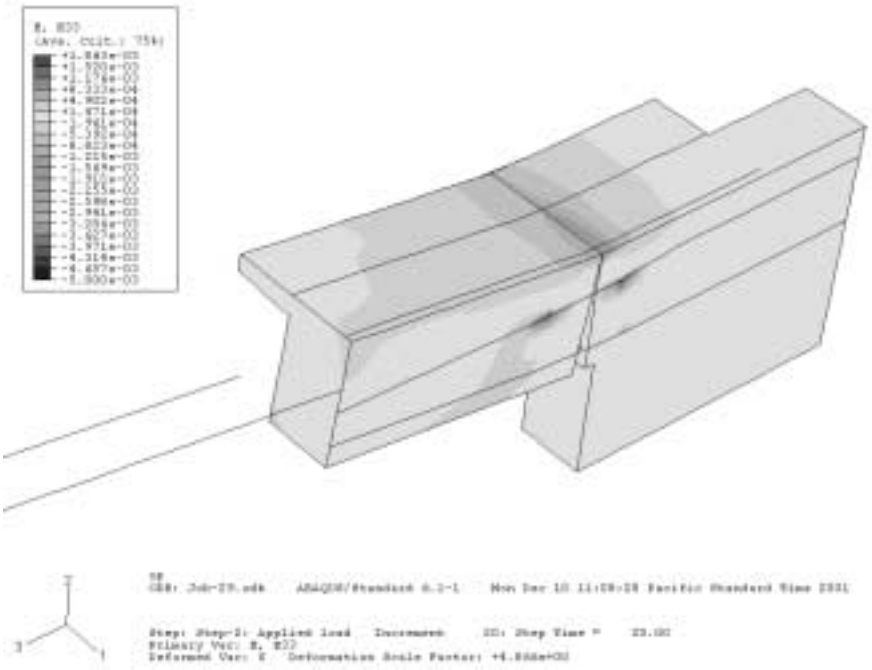

(a) Longitudinal strain contours of the concrete

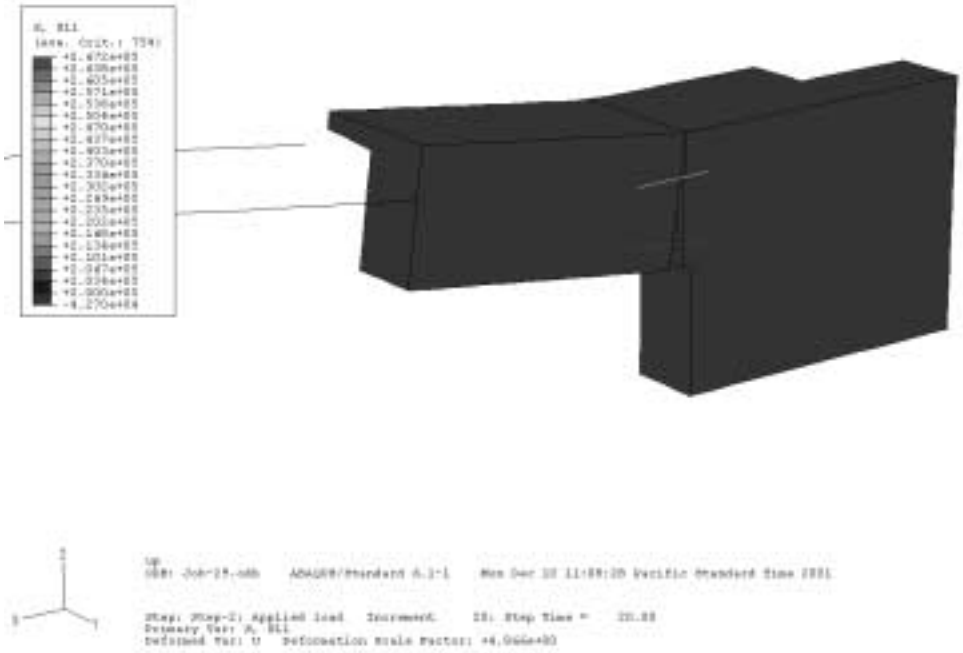

(b) Stress contours of bonded strands

**Figure 7-17 Stress and strain contours at failure in the upward direction of 100-INT-CIP**

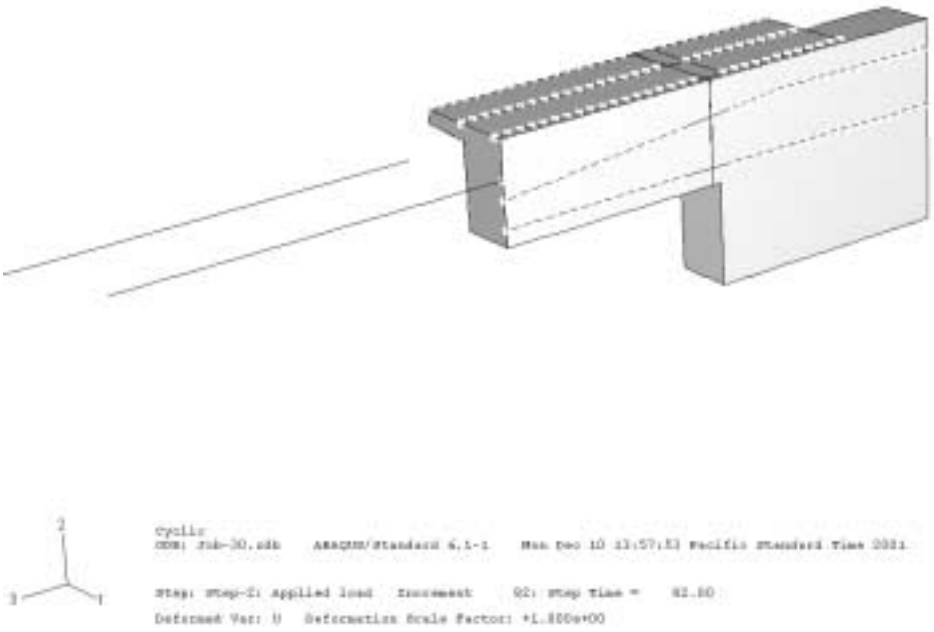

(a) Last increment before failure

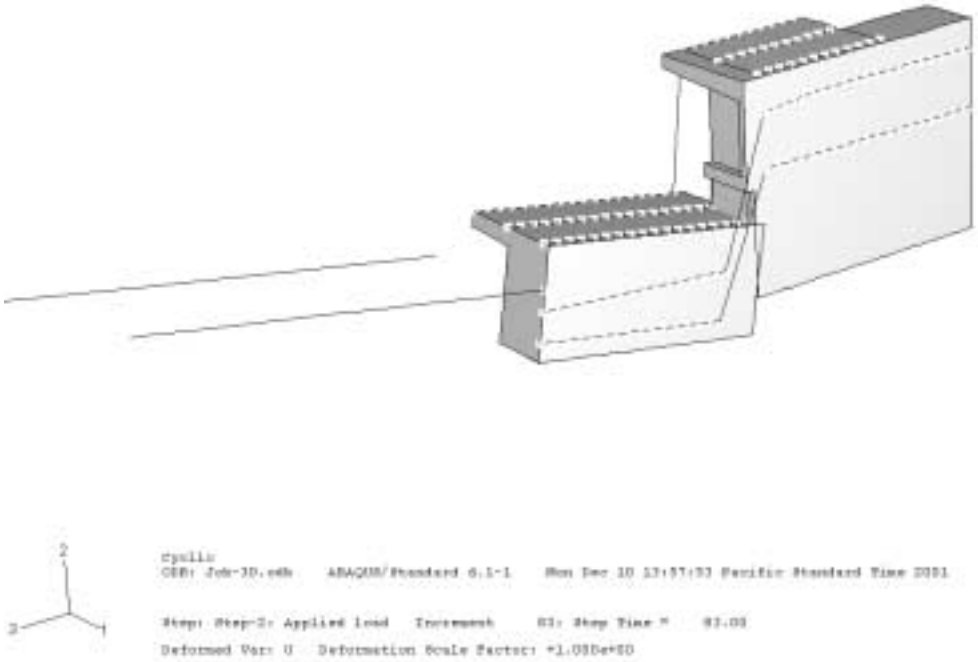

(b) Shear sliding failure

**Figure 7-18 Deformation modes at failure from cyclic analysis of 100-INT-CIP**

# 8 Conclusions

A large-scale experimental research project is currently in progress at the University of California, San Diego (UCSD). This research project consists of the following three phases:

(1) Phase I: To study the seismic performance of segment-to-segment joints with different ratios of internal to external post-tensioning under simulated seismic fully reversed cyclic loading. In this first phase, only superstructure joints close to midspan in regions with high positive flexural moments and low shearing forces were considered.

(2) Phase II: To study the seismic performance of superstructure joints close to the supports in regions of high negative flexural moments combined with high shearing forces.

(3) Phase III: To study the system performance of segmental superstructure and piers under gravity loads combined with seismic forces.

This report presents the research program and results of Phases I and II mentioned above. Thus, the research work presented in this report was concerned about the seismic performance of superstructure segment-to-segment joints. The transfer of forces between the precast superstructure and the bridge column was not in the scope of research of Phases I and II. The major objectives of the research program were to investigate: (1) joint behavior in terms of opening and closure under repeated cyclic loads simulating earthquake effects, (2) development of crack patterns, and (3) modes of failure.

## 8.1 Summary of Phase I Research

The experimental program and the analytical model calibrations of the all tests of Phase I are presented in this report. Phase I consisted of four test units built at a 2/3-scale with respect to a prototype structure. The test variables investigated in Phase I were: (1) ratio of internal to external post-tensioning of the superstructure, and (2) provision of reinforced cast-in-place deck closure joints at the location of precast segment-to-segment joints. Each test unit consisted of six precast segments, which were epoxy bonded. The entire joint surfaces of all test unit were epoxy bonded with no mild reinforcement crossing the joints, except for Test Unit 100-INT-CIP. Test Unit 100-INT-CIP had a reinforced cast-in-place deck closure at the location of each joint, with the web and bottom soffit of the segments epoxy bonded. The cast-in-place deck closure joints in Unit 100-INT-CIP were similar to those in a proposed design for the new East Span Skyway Structure of the San Francisco-Oakland Bay Bridge.

Three-dimensional finite element models of the test units were developed. The models took into account concrete cracking and crushing, opening and closure of segment-to-segment joints and the inelastic characteristics of prestressed and nonprestressed steels. The finite element models were validated with the experimental results. The calibrated analytical models were powerful tools for parameter and design studies that provided useful information, which may be difficult to obtain experimentally. They also provided a better understanding of the observed behavior of segment-to-segment joints. The results will be used to develop a comprehensive global finite element model of bridge structures, which can be used for analytical parametric studies

investigating different superstructure geometry, prestress levels, and seismic input variations.

The first and second test units (Units 100-INT and 100-INT-CIP) were post-tensioned by internally bonded tendons, whereas the third test unit (Unit 100-EXT) was post-tensioned by external tendons. One half of the post-tensioning of the fourth test unit (Unit 50-INT/50-EXT) was achieved by internally bonded tendons, whereas external tendons achieved the other half. All test units were subjected to fully reversed cyclic loads simulating earthquake motions. All test units could undergo significant displacements and joint openings before failure. The first test unit (Unit 100-INT) without mild steel reinforcement in the deck joint failed by rupture of the prestressing tendon, whereas the second test unit (Unit 100-INT-CIP) with mild steel reinforced deck closures failed by buckling of deck rebar and subsequent compression failure of the deck. The third test unit (Unit 100-EXT) with 100% external post-tensioning failed by crushing of the concrete cover of the segment. The last test unit (Unit 50-INT/50-EXT) with combined internal and external post-tensioning failed by rupture of the internally bonded tendon at a lower displacement level compared to the other units.

## 8.2 Summary of Phase II Research

In Phase II, four test units were built at a 2/3-scale with respect to the prototype structure used in design of the phase I test units. The test variables investigated in Phase II were: (1) ratio of internal to external post-tensioning of the superstructure, and (2) provision of reinforced cast-in-place deck closure joints at the location of precast segment-to-segment joints. It was decided to study the seismic performance of one

segment-to-segment joint rather than by having test units with several joints, as was the case for the Phase I test units. The major objective of the Phase II experiments was to investigate the seismic performance of segment-to-segment joints subjected to high flexural moments combined with high shearing forces. The entire joint surfaces of all test units were epoxy bonded with no mild steel reinforcement crossing the joints except for Test Unit 100-INT-CIP, which had a reinforced cast-in-place deck closure at the location of the joint, with the web and bottom soffit of the segments epoxy bonded. Again, the cast-in-place deck closure joint in Unit 100-INT-CIP was similar to that in a proposed design of the new East Span Skyway Structure of the San Francisco-Oakland Bay Bridge. As in Phase I research, three-dimensional finite element models of the test units were developed. The finite element models were validated with the experimental results.

The test matrix of Phase II experiments was identical to the test matrix of Phase I experiments. The first and second test units (Units 100-INT and 100-INT-CIP) were post-tensioned by internally bonded tendons, whereas the third test unit (Unit 100-EXT) was post-tensioned by external tendons. One half of the post-tensioning of the fourth test unit (Unit 50-INT/50-EXT) was achieved by internally bonded tendons, whereas external tendons achieved the other half. All test units were subjected to fully reversed cyclic loads simulating the effects of gravity loads and longitudinal seismic forces. All the test units of Phase II experienced compression failure in the bottom soffit under downward loading. The test units could undergo significant displacements and joint openings before failure. The test unit with 100% internal post-tensioning (Unit 100-INT) and with 100% external post-tensioning (Unit 100-EXT) failed under upward loading by compression in the deck. Some of the strands in Unit 100-EXT also ruptured at high displacement levels

before end of the test. Test Unit with 100% internal post-tensioning and cast-in-place deck closure joint (Unit 100-INT-CIP) failed under upward loading when the strands of the lower tendon ruptured at relatively high displacement. Unlike Unit 100-INT-CIP in Phase I, no buckling occurred in the mild reinforcement of the cast-in-place deck closure joint in Unit 100-INT-CIP of Phase II. The test unit with combined internal and external post-tensioning (Unit 50-INT/50-EXT) failed under upward loading at relatively low displacement, compared to other test units, when strands in the lower prestressing tendon fractured.

## 8.3 Other Issues Related to External Tendons

External tendons in bridges are grouted after post-tensioning for long-term protection of the strands against corrosion. The external tendons in the test units of both Phases I and II were housed in transparent poly-carbon pipes, which were not grouted after stressing of the tendons. The grout of external tendons would crack at relatively low additional loading on the bridge superstructure; thus for all practical purposes, the effect of grout of external tendons on the load carrying capacity and stiffness is commonly ignored. If the external tendons in the test units were grouted, the grout would have been fully cracked during loading the test units to the reference load level; it means before application of fully reversed cyclic displacements (the seismic test). Thus the results of the ungrouted external tendons in Units 100-EXT and 50-INT/50-EXT of both Phase I and II are also applicable to structures with grouted external tendons.

One of the other issues related to use of external tendons in precast segmental bridge superstructures is the vibration of external tendons between the deviators, or

between the anchorage blocks and deviators. The AASHTO Guide Speficications[1] requires that vibration analysis should be performed if the unsupported length of the external tendons exceeds 25 ft (7.62 m). Vibration of external tendons was not in the scope of the research work presented in this report. Based on information obtained from the American Segmental Bridge Institute (ASBI) as well as bridge design engineers, no problems or significant issues have been raised in existing bridges as a result of vibration of the external tendons. However if the unsupported length of external tendons exceeds 25 ft (7.62 m), no deviators may need to be added but simple steel brackets supporting neoprene dampeners can be provided to reduce vibrations of the external tendons. Alternatively, vibration analysis should be performed as required by the AASHTO Guide Specifications[1].

## 8.4 Conclusions of Phase I Research

Based on experimental and analytical results, the following conclusions can be made for precast segmental bridge segment-to-segment joints subjected to high flexural moments combined with low shearing forces (joints close to midspan):

1. Superstructure segment-to-segment joints can undergo significant joint openings without failure.
2. Test units with internally bonded tendons experienced explosive failure by either rupture of the tendons or concrete crushing. With 100 percent external post-tensioning, the failure was ductile. The maximum displacement before failure of the units could be substantially improved by use of 100 percent external post-tensioning.

3. Permanent residual superstructure displacement following an earthquake occurrence can be substantially minimized by use of 100 percent external post-tensioning.
4. Combination of internal and external post-tensioning of precast segmental bridge superstructures is not recommended in high seismic zones.
5. The use of cast-in-place deck closure joints reduces post-earthquake residual displacements of the superstructure and improves the energy dissipation capability. However cast-in-place deck closure joints complicate the precast segmental construction concept. With respect to common precast segmental bridges; construction of precast segmental bridges with cast-in-place deck closures at the segment-to-segment joints would be delayed because of concrete curing time of the cast-in-place deck closure joints, resulting in higher construction costs.
6. Longitudinal reinforcing bars in the cast-in-place deck closure joints tend to buckle due to repeated cyclic loading in compression and tension. These bars tend to buckle and push against the concrete cover in the deck at high displacement levels. Closed stirrups should be used in the deck to confine the longitudinal mild reinforcement in order to prevent their buckling.
7. Seismic response of precast segmental bridge superstructures with cast-in-place closure joints will not differ if headed or hairpin bars are used as longitudinal reinforcement in the closure joints. However headed bars are recommended over bent bars for construction reasons.

8. Finite element analyses showed that under severe earthquake loading, the prestressing force in the internally bonded tendons could diminish under repeated cycling in the inelastic strain range. The analyses also showed losses in the prestressing forces of external tendons, however prestress losses in external tendons were substantially less than prestress losses in internally bonded tendons.
9. The flexural moment capacity of precast segmental bridge superstructures can be reasonably predicted using provisions of the AASHTO Guide Specifications[1] and the AASHTO Standard Specifications for Highway Bridges[5]. Designers should pay attention to the change in geometry and the corresponding change in the distance between the extreme compression fiber and the external tendons.

## 8.5 Conclusions of Phase II Research

Based on experimental and analytical results, the following conclusions can be made for precast segmental bridge segment-to-segment joints subjected to high flexural moments combined with high shearing forces (superstructure joints close to the column):

1. Superstructure segment-to-segment joints can undergo significant joint openings without failure.
2. Test units with internally bonded tendons, or with combined internally bonded and external tendons, experienced explosive failure by concrete crushing. With 100 percent external post-tensioning, the failure was ductile. The maximum displacement before failure of the units could be substantially improved by use of 100 percent external post-tensioning. Test unit with cast-in-place deck closure

joint failed also by compression of the bottom slab; however the failure was not explosive.

3. Permanent residual superstructure displacement following an earthquake occurrence can be substantially minimized by use of 100 percent external post-tensioning.
4. Combination of internal and external post-tensioning in precast segmental bridge superstructures is not recommended in high seismic zones. The test unit with combined internally bonded and external tendons failed at relatively low displacement in the upward loading direction.
5. The use of cast-in-place deck closure joints improves the energy dissipation capability, but complicates the precast segmental construction concept.
6. Vertical slip between the precast segments subjected to high shearing forces does not occur before flexural failure of the superstructure.
7. Finite element analyses showed that under severe earthquake loading, the prestressing force in tendons was reduced under repeated cycling in the inelastic strain range, especially in internally bonded tendons.

## 8.6 Recommendations for Future Research

The following should be done in future research related to seismic performance of precast segmental bridges:

1. Experiments on precast segmental bridge columns should be performed to investigate their seismic performance.

2. Complications associated with the use of cast-in-place deck closure joints should be avoided. An alternative would be provision of strands in the deck; these strands should have very low initial prestressing force. Seismic performance of superstructures with such details should be investigated experimentally.
3. A complete superstructure span should be modeled and tested under combined service loads and seismic forces. The complete span test unit should model the precast segmental superstructure and pier segment, anchorage blocks and deviators (external tendons) and the bridge columns. This superstructure-column system test unit would provide a more realistic representation of bridge structures.
4. The seismic performance of precast segmental bridges built using the balanced cantilever method should be investigated by means of finite element analyses.
5. Extensive nonlinear time-history analyses should be performed on precast segmental bridge superstructures with different geometries and tendon layouts, and constructed using the span-by-span and the balanced cantilever methods, to determine the maximum seismic demands on segment-to-segment joint openings and rotations as well as tendons strains.

Items 2 to 5 in the above list should be investigated at the University of California San Diego (UCSD) in the third phase of the research project on seismic performance of precast segmental bridges. Seismic performance of precast segmental bridge columns (Item 1 in the above list) may also be investigated experimentally in Phase III.

# References


1. AASHTO, *Guide Specifications for Design and Construction of Segmental Concrete Bridges*, 2nd Edition, 1999
2. MacGregor, R.J.G., Kreger, M.E., Breen, J.E. *Strength and Ductility of a Three-span Externally Post-tensioned Segmental Box Girder Bridge Model*, Prepared for the Center for Transportation Research, Research Report 1209-2F, University of Texas at Austin, April 1991.
3. Hindi, A.N.A., Kreger, M.E., Breen, J.E. *Enhancing the Strength and Ductility of Post-tensioned Segmental Box-girder Bridges*, Prepared for the Center for Transportation Research, Research Report 1209-2F, University of Texas at Austin, April 1991.
4. AASTHO-PCI-ASBI, *Segmental Box Girder Standards for Span-by-Span and Balanced Cantilever Construction*, 1997.
5. AASHTO, *Standard Specifications for Highway Bridges*, 13th Edition, 1983.
6. Caltrans, *Bridge Design Aides*, Department of Transportation, State of California, Sacramento, August, 1986.
7. Dowell, R.K., Silva, P.F., Seible, F., *Precast Segmental Bridge Performance in Seismic Zones: Phase I, Test Unit Design*, Progress report submitted to Caltrans, April 2000, 30pp.
8. American Segmental Bridge Institute (ASBI), *Recommended Contract Administration Guidelines for Design and Construction of Segmental Concrete Bridges*, March 1995, pp.109-116.
9. Chopra, A.K., *Dynamics of Structures*, Prentice Hall, Inc., 729 pp.

10. Leuenberger, John, Dowell, R.K., *Performance of Precast Segmental Bridges in Seismic Zones*, ANATECH Corporation, July 2001.
11. Hibbitt, Karlsson & Sorenson, Inc., *ABAQUS-User's Manual*, USA, 1998.
12. ANATECH Corporation, *ANACAP-U User's and Theory Manual*, Version 5.8, 1999.
13. Collins, M.P., Mitchell, D, *Prestressed Concrete Structures*, Response Publication, Canada 1997.
14. ACI Committee 318, *Building Code Requirements for Structural Concrete (ACI318-99) and Commentary (ACI318R-99)*, American Concrete Institute, Farmington Hills, Michigan, 1999, 391 pp.
15. ANATECH Corporation, *ANDRIANNA-User's Guide*, Version 1.0, 1999.

# Appendix A

## Additional Test Data for Phase I

**Tendon Punching Test, Unit 100-INT-CIP**

In an attempt to understand the behavior of the tendon-concrete interaction, punching tests were performed on cross-sections of the tendon near midspan. A total of ten segments were cut from Test Unit 100-INT-CIP, each approximately 5 ¾ in. (146 mm) in length starting at midspan. The segments were inspected using a magnifying device for any obvious signs of debonding of the tendon, no conclusive signs of debonding were found. However debonding would be expected to occur between the internally bonded tendons and the concrete in the vicinity of segment-to-segment joints that would open under seismic events.

The tendon segments were then tested using a SATEC Compression machine. The steel tendon was subjected to an axial load and the punching load at which the tendon was pushed through the duct was recorded. The punching load was expected to be very small if there was debonding present between the tendon and the grout. Also expected with debonding was an increase in punching load in segments away from midspan. However, the debonding consequences were not found during testing. The results of the punching tests are given in Table A-1. Segments 7, 8, and 9 had significant cracks in the concrete surrounding the duct before the punching test; the punching tests were not successful for these segments. The punching load is plotted versus the distance from midspan of Unit 100-INT-CIP in Figure A-1. An example of one cross-section after testing is shown in Figure A-2.

Visual investigation and punching tests on the above-mentioned slices were inconclusive to show that debonding was a major factor in the behavior of test units with

internally bonded tendons. Punching load values were not small and did not increase significantly away from midspan.

**Table A-1 Unit 100-INT-CIP punching test results**

| Cross-section | Length | | Punching Load | |
|---|---|---|---|---|
| # | in. | mm | kips | kN |
| 1 | -- | -- | -- | -- |
| 2 | 5.63 | 142.88 | 13.13 | 58.41 |
| 3 | 5.75 | 146.05 | 12.79 | 56.89 |
| 4 | 5.75 | 146.05 | 13.01 | 57.87 |
| 5 | 5.25 | 133.35 | 12.43 | 55.29 |
| 6 | 6.25 | 158.75 | 14.78 | 65.74 |
| 7 | 5.38 | 136.53 | 5.38* | 23.93* |
| 8 | 6.38 | 161.93 | 10.55* | 46.93* |
| 9 | 6.88 | 149.23 | 7.01* | 31.18* |
| 10 | 5.75 | 146.05 | 17.02 | 75.71 |

* Data is to be discarded; the duct and tendon moved as one unit due to large preexisting cracks in the concrete

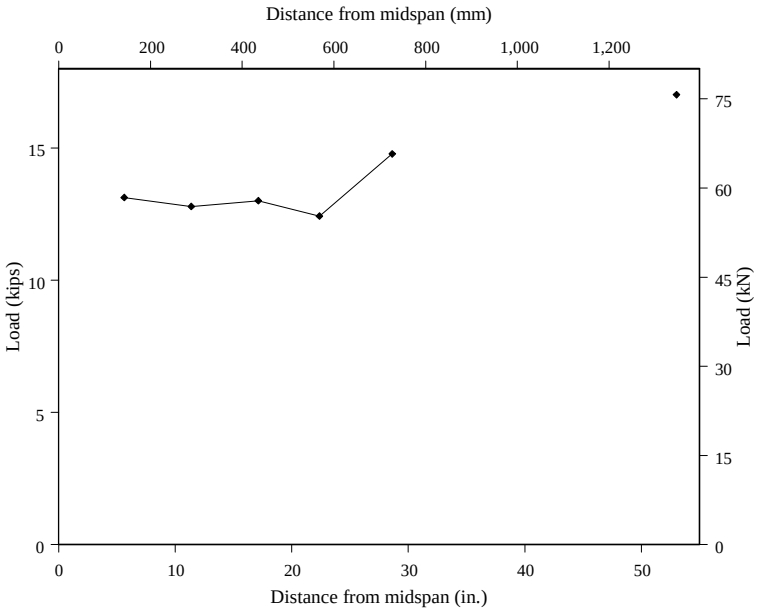


**Figure A-1 Punching test results for Unit 100-INT-CIP**


**Figure A-2 Example of tendon cross-section for Unit 100-INT-CIP**

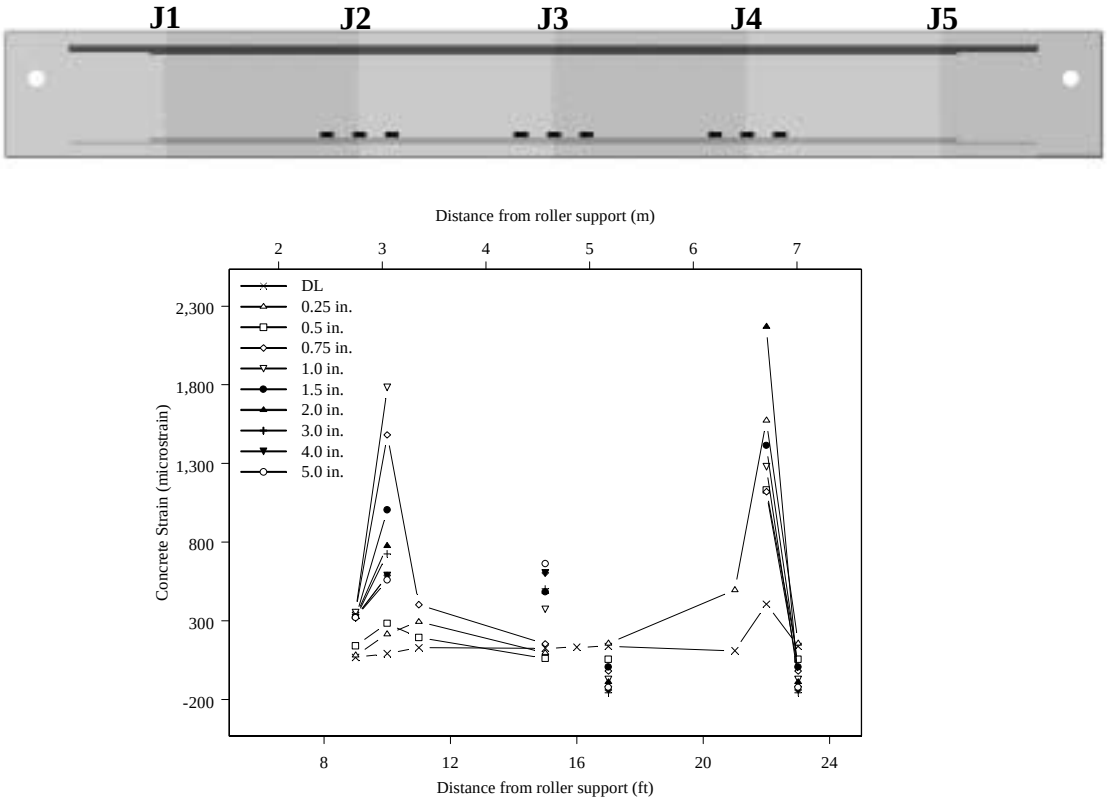


**Figure A-3 Longitudinal concrete strains at PT level, downward loading; Unit 100-INT**

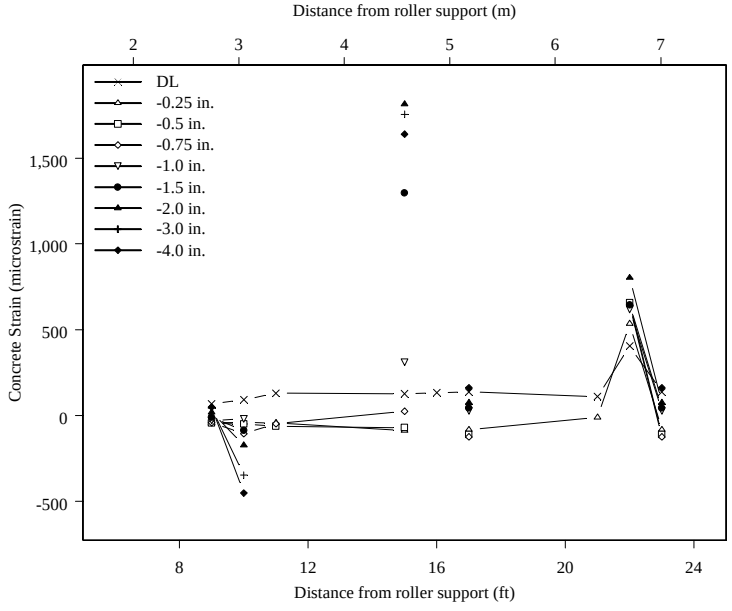


**Figure A-4 Longitudinal concrete strains at PT level, upward loading; Unit 100-INT**

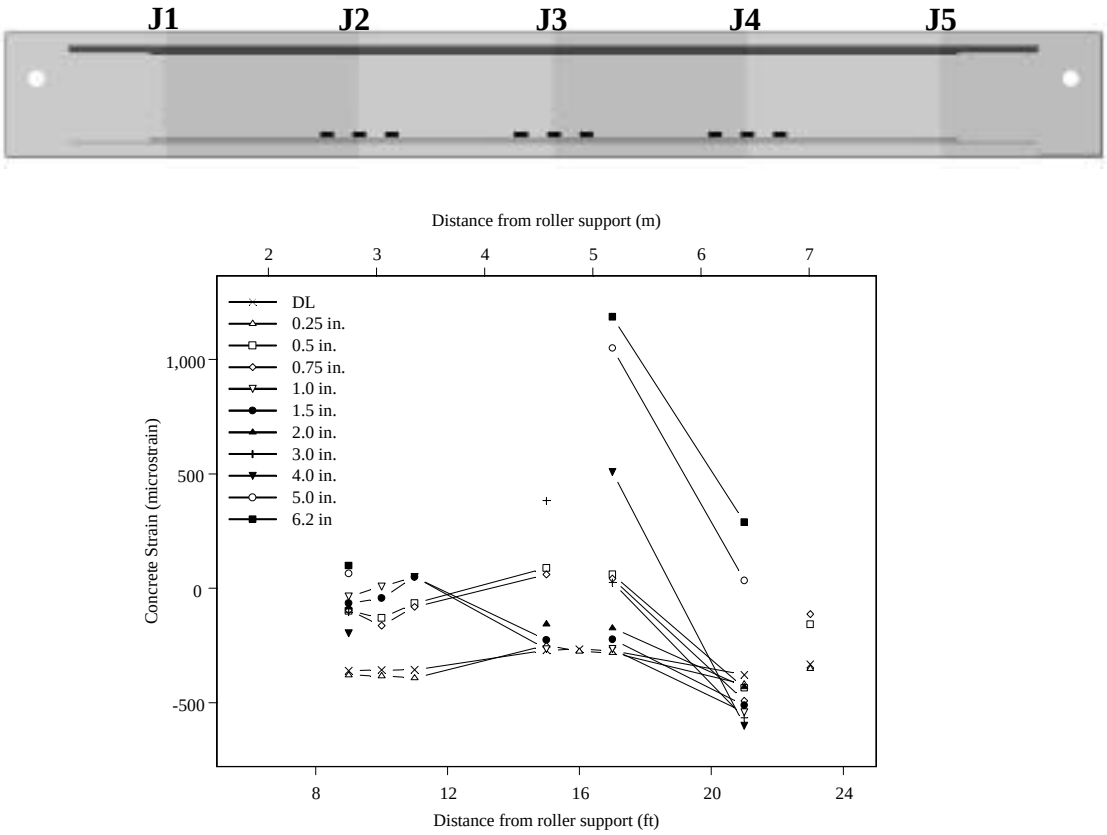


**Figure A-5 Longitudinal concrete strains at PT level, downward loading; Unit 100-INT-CIP**

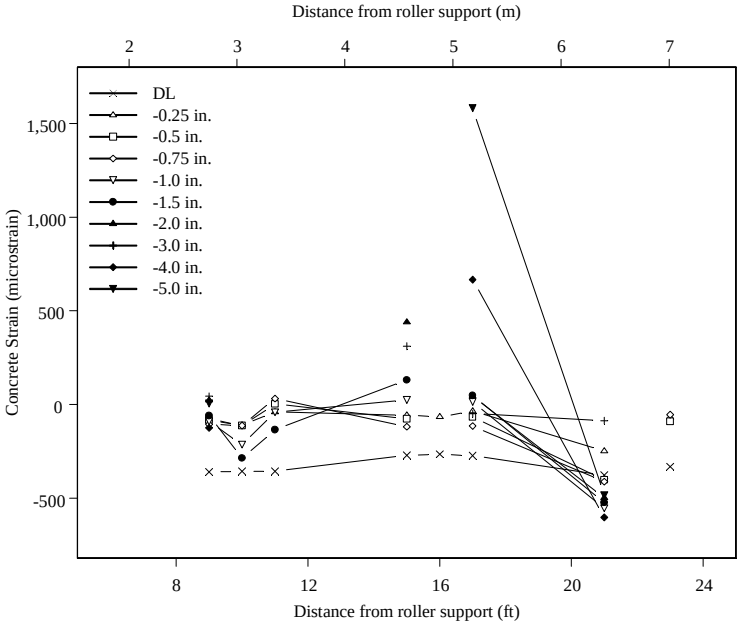


**Figure A-6 Longitudinal concrete strains at PT level, upward loading; Unit 100-INT-CIP**

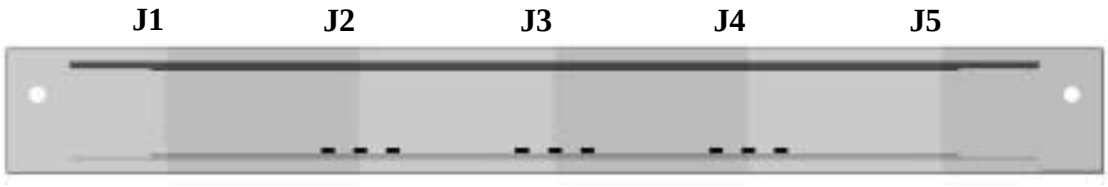


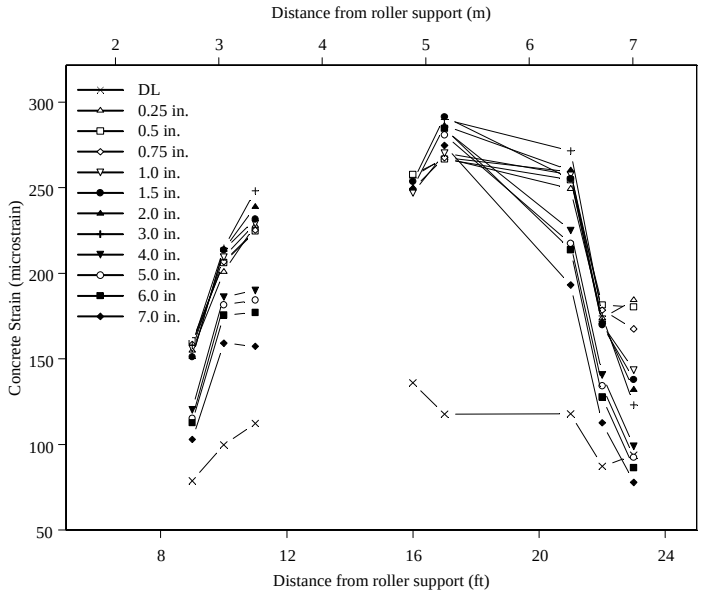


**Figure A-7 Longitudinal concrete strains at PT level, downward loading; Unit 100-EXT**

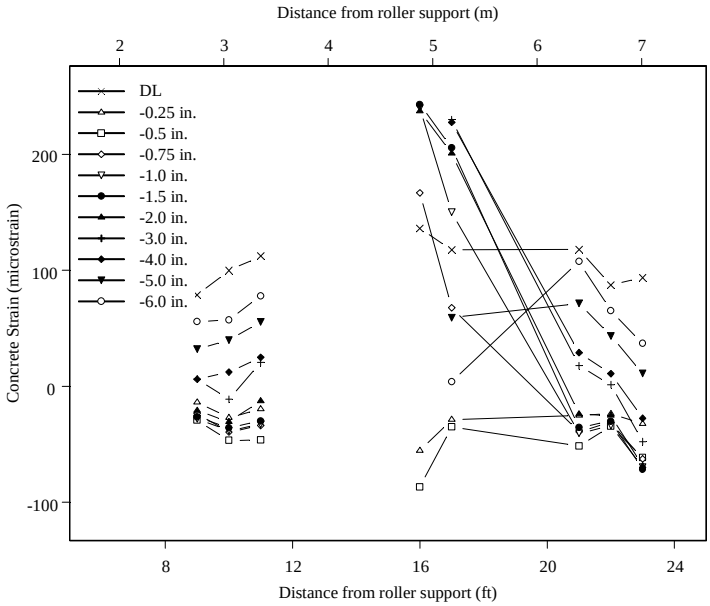


**Figure A-8 Longitudinal concrete strains at PT level, upward loading; Unit 100-EXT**

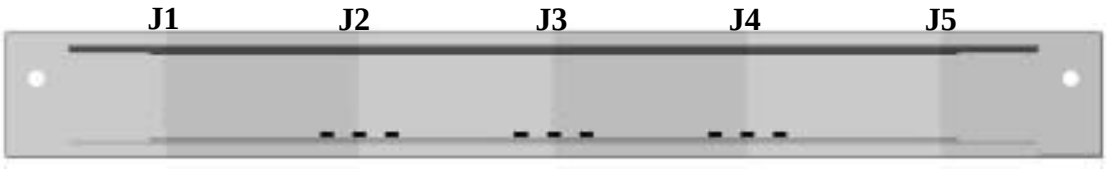


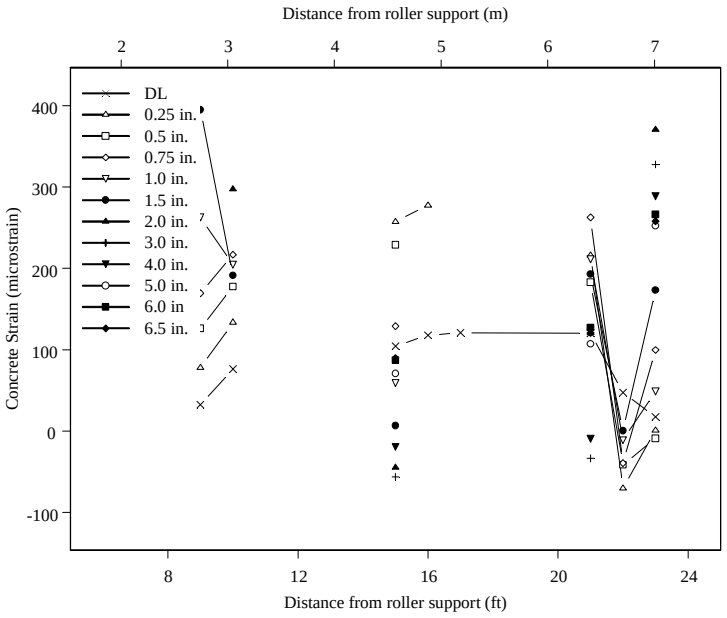


**Figure A-9 Longitudinal concrete strain at PT level, downward loading; Unit 50-INT/50-EXT**

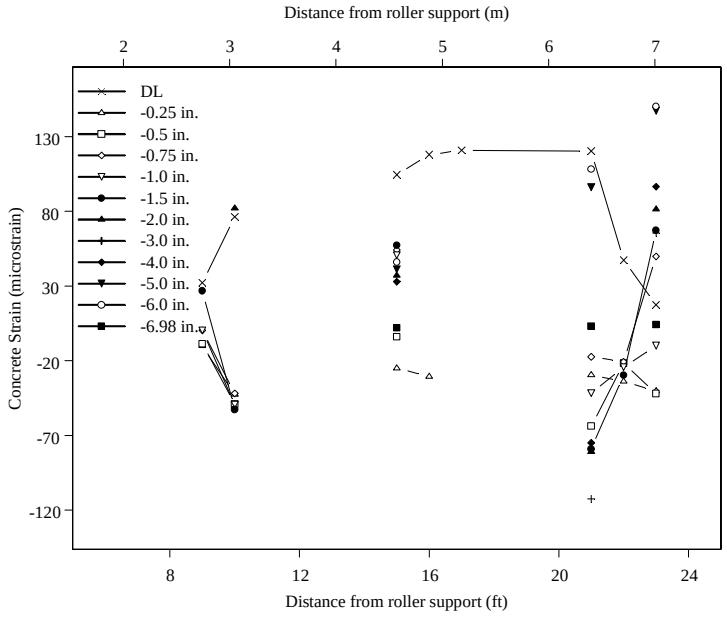


**Figure A-10 Longitudinal concrete strain at PT level, upward loading; Unit 50-INT/50-EXT**

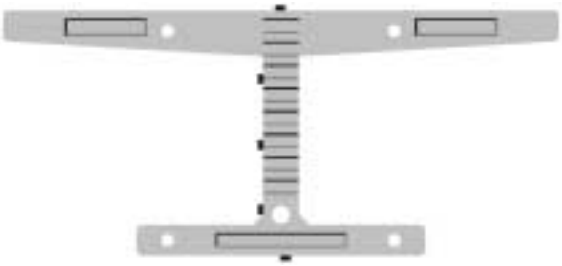

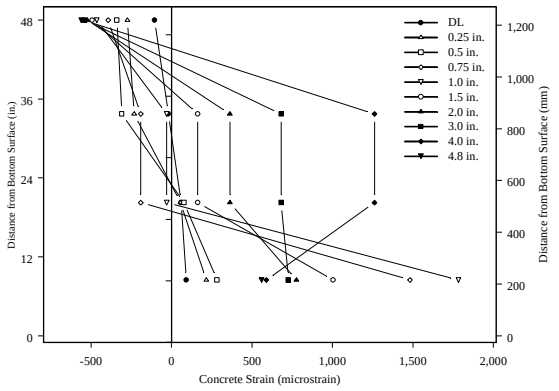


(a) Joint J2, downward loading

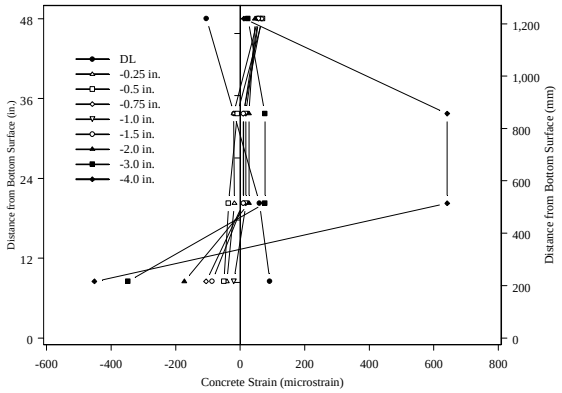


(b) Joint J2, upward loading

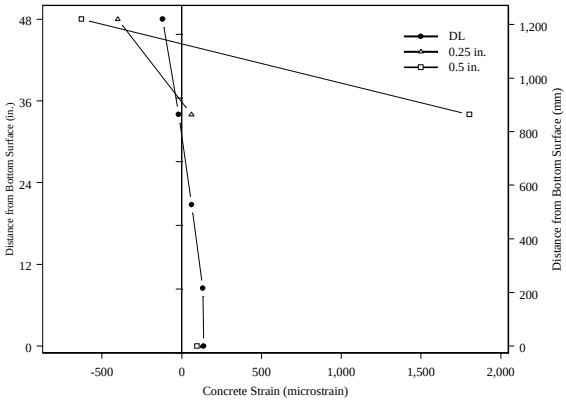


(c) Joint J3, downward loading

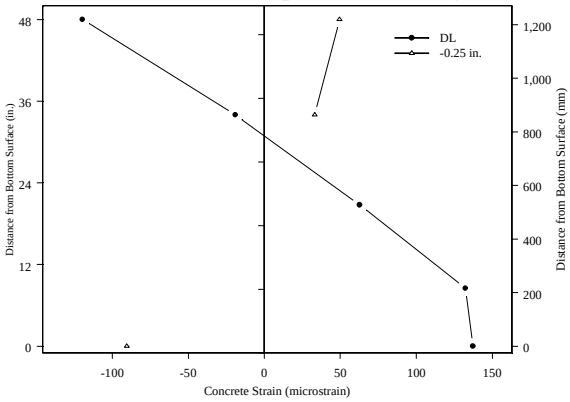


(d) Joint J3, upward loading

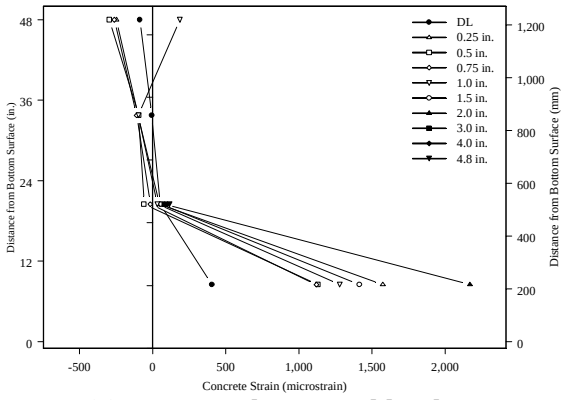


(e) Joint J4, downward loading

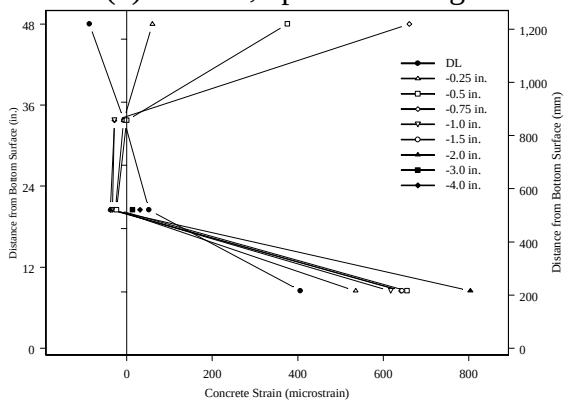


(f) Joint J4, upward loading

**Figure A-11 (a-f) Vertical concrete strain profiles, Unit 100-INT**

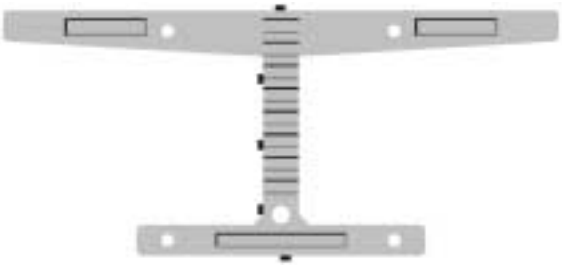

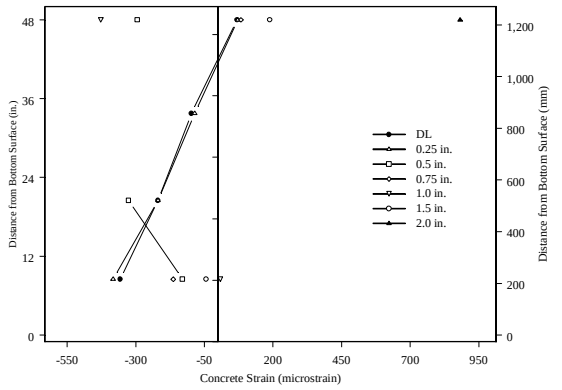


(a) Joint J2, downward loading

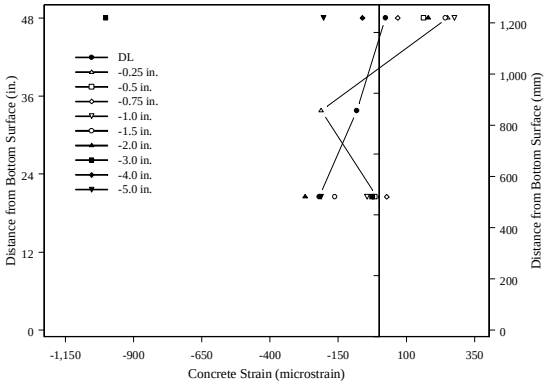


(b) Joint J2, upward loading

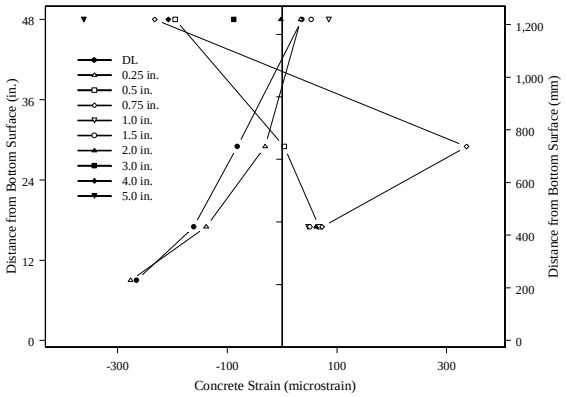


(c) Joint J3, downward loading

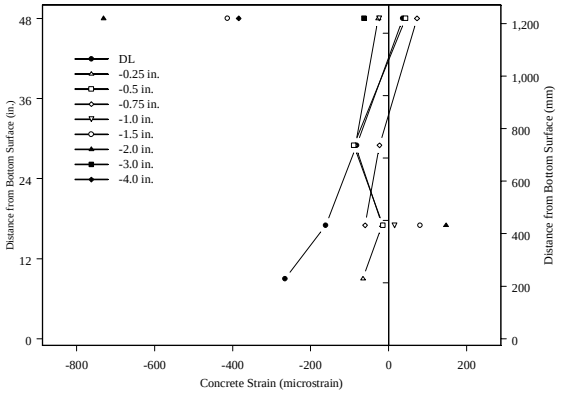


(d) Joint J3, upward loading

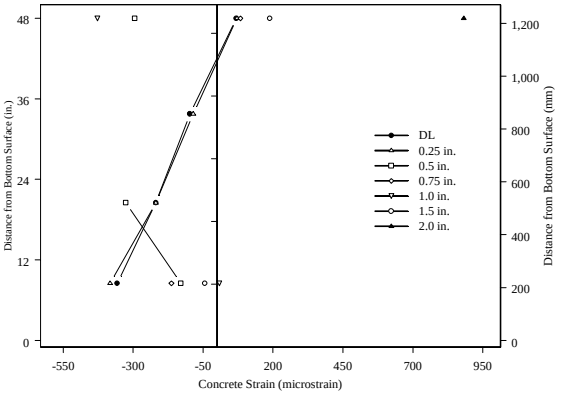


(e) Joint J4, downward loading

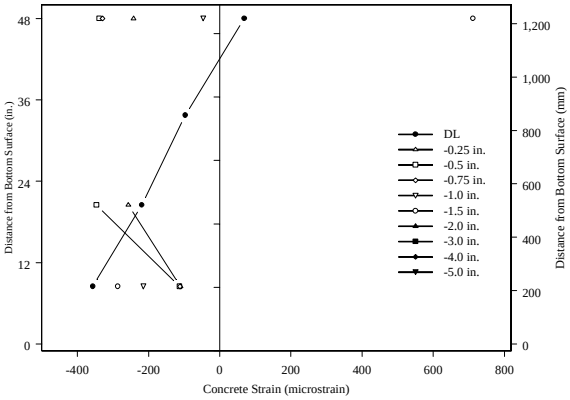


(f) Joint J4, upward loading

**Figure A-12 (a-f) Vertical concrete strain profiles; Unit 100-INT-CIP**

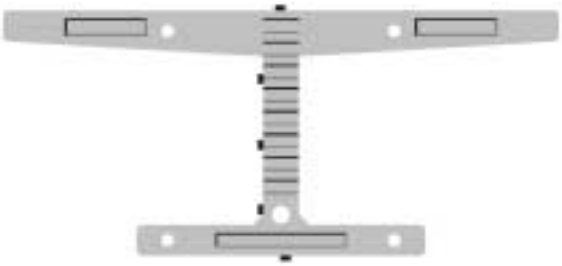

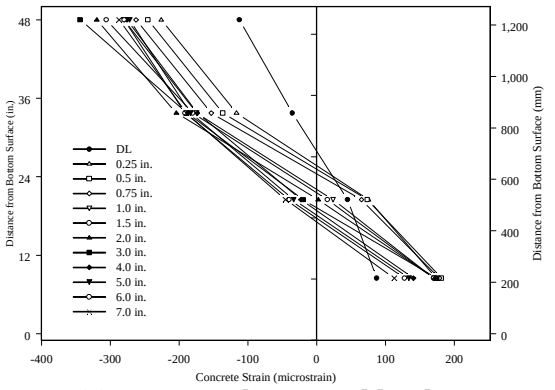


(a) Joint J2, downward loading

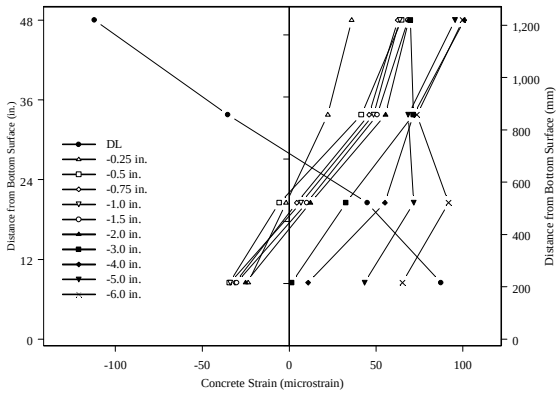


(b) Joint J2, upward loading

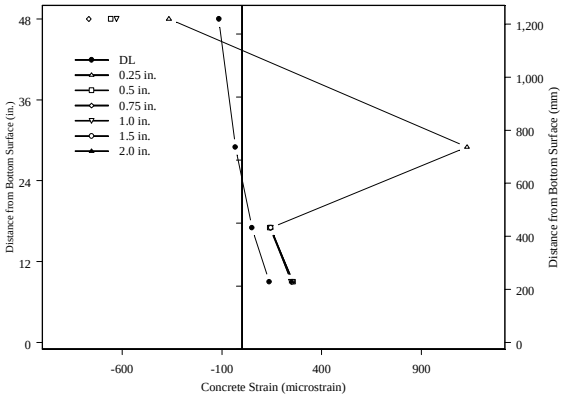


(c) Joint J3, downward loading

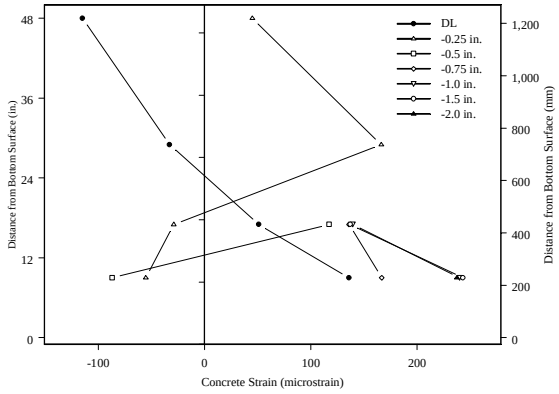


(d) Joint J3, upward loading

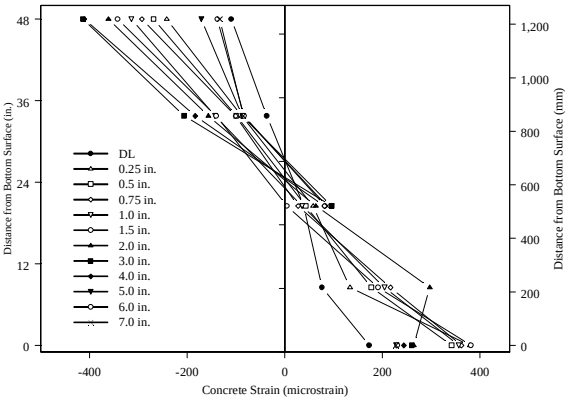


(e) Joint J4, downward loading

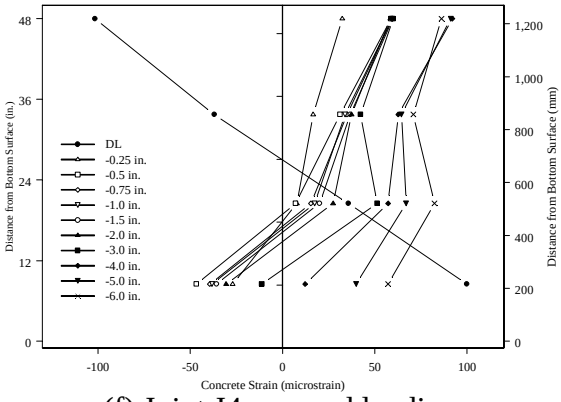


(f) Joint J4, upward loading

**Figure A-13 (a-f) Vertical concrete strain profiles; Unit 100-EXT**

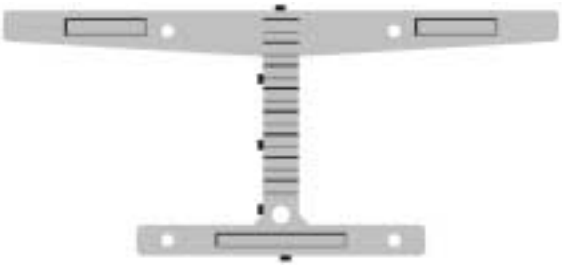

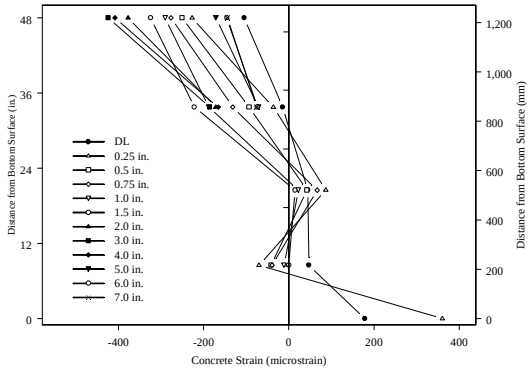


(a) Joint J2, downward loading

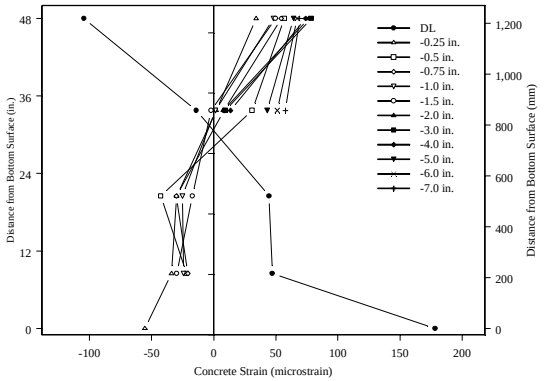


(b) Joint J2, upward loading

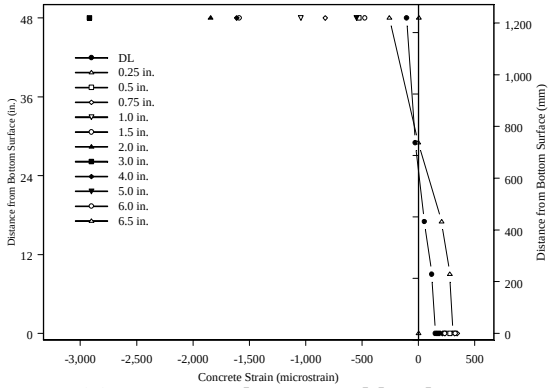


(c) Joint J3, downward loading

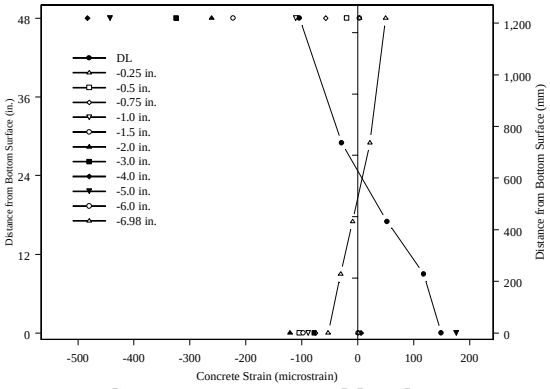


(d) Joint J3, upward loading

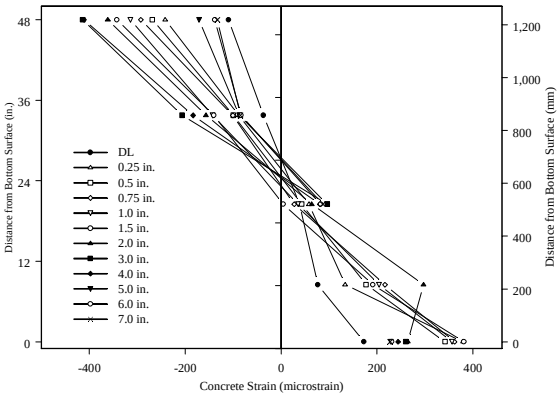


(e) Joint J4, downward loading

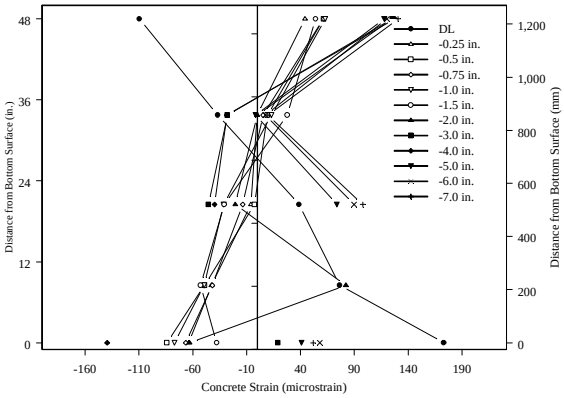


(f) Joint J4, upward loading

**Figure A-14 (a-f) Vertical concrete strain profiles; Unit 50-INT/50-EXT**

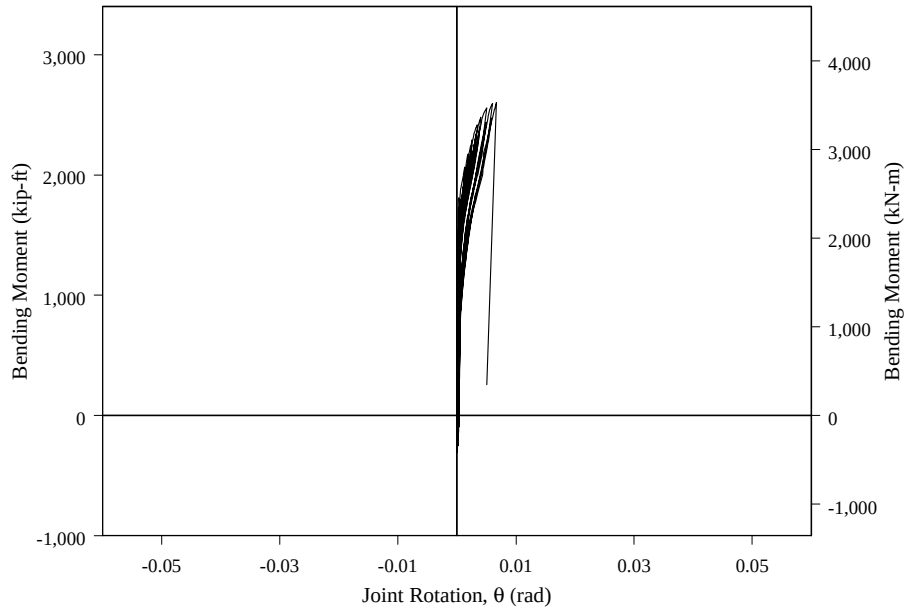


**Figure A-15 Joint J4 rotation versus bending moment; Unit 100-INT**

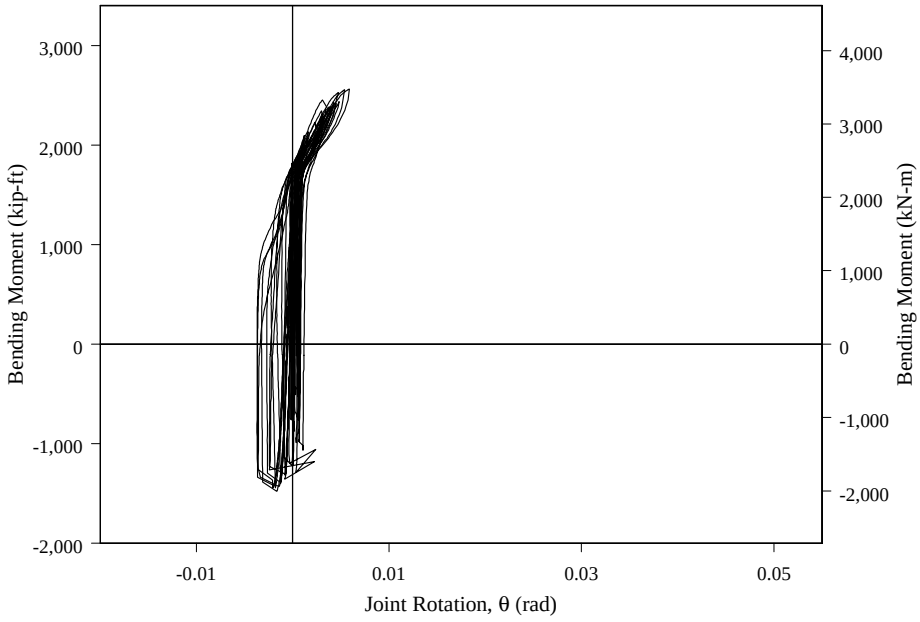


**Figure A-16 Joint J2 rotation versus bending moment; Unit 100-INT-CIP**

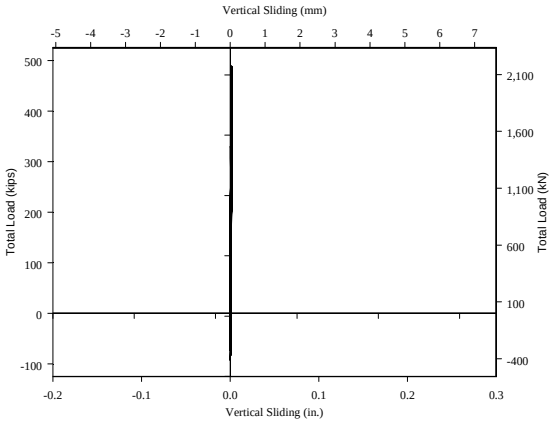


(a) Joint J1

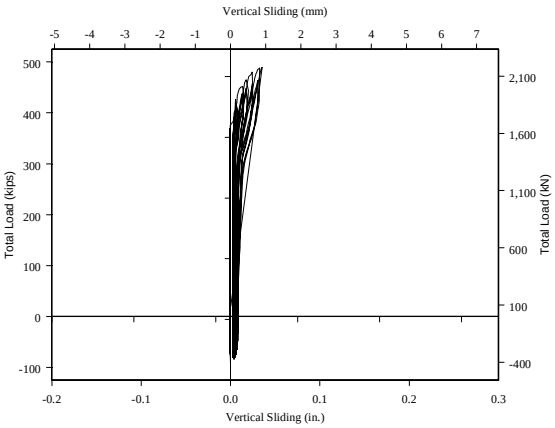


(b) Joint J2

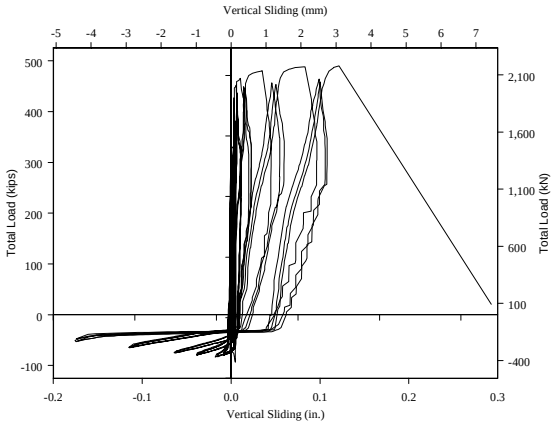


(c) Joint J3

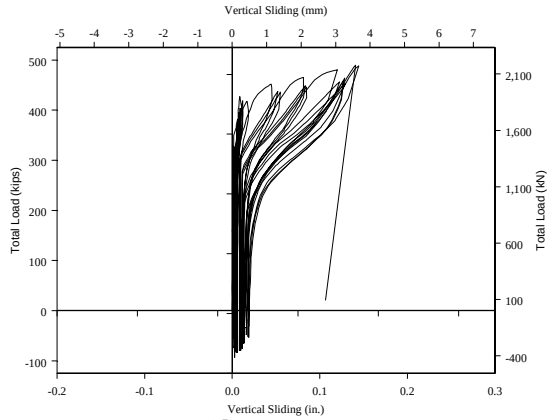


(d) Joint J4

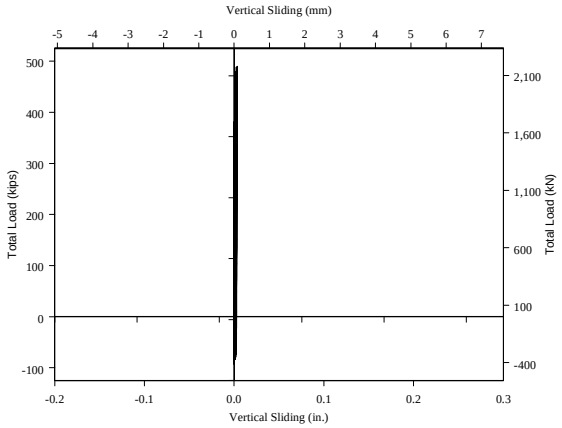


(e) Joint J5

**Figure A-17 (a-e) Vertical sliding between segments; Unit 100-INT**

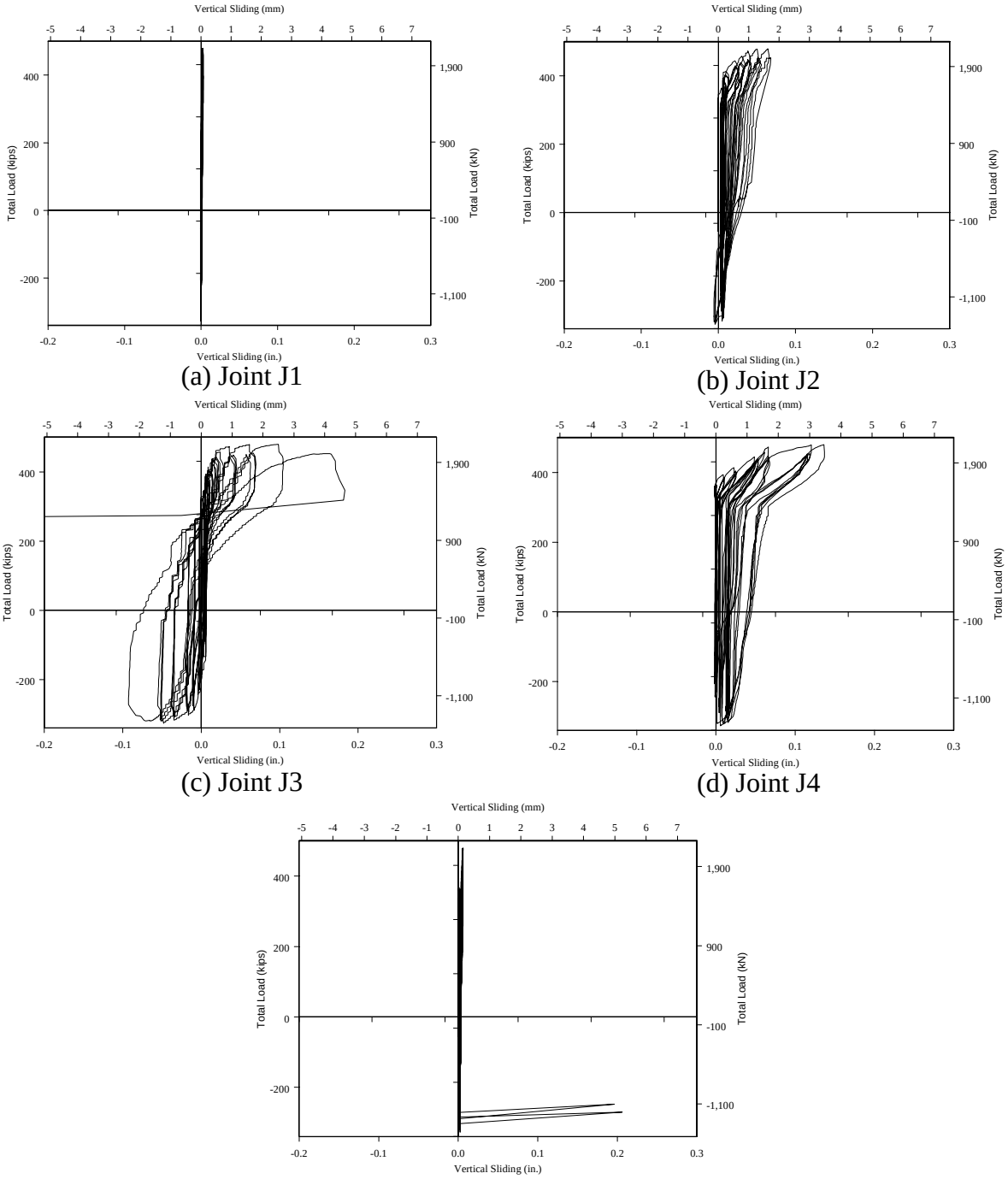


(a) Joint J1

(b) Joint J2

(c) Joint J3

(d) Joint J4

(e) Joint J5

**Figure A-18 (a-e) Vertical sliding between segments; Unit 100-INT-CIP**

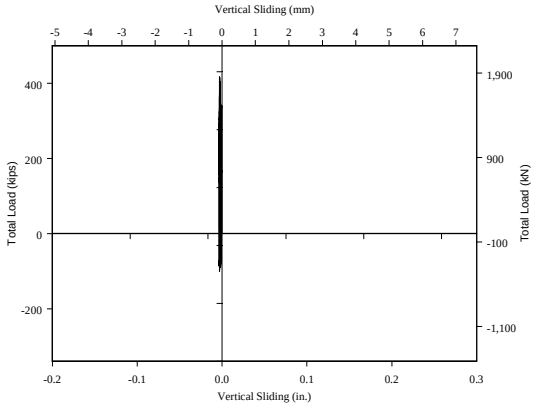


(a) Joint J1

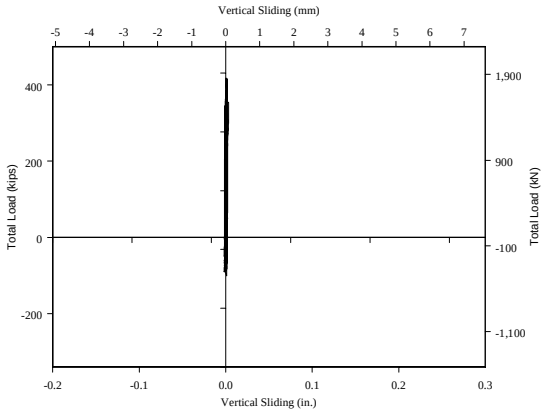


(b) Joint J2

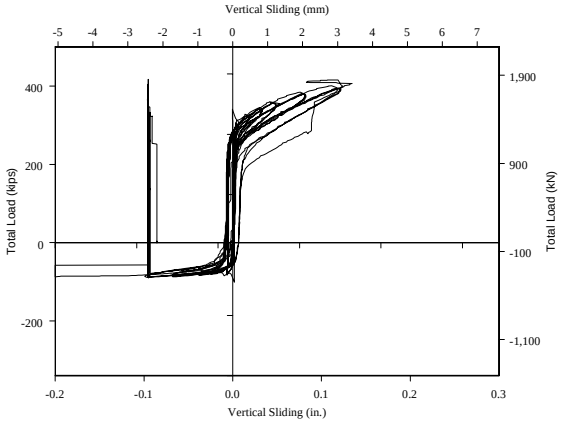


(c) Joint J3

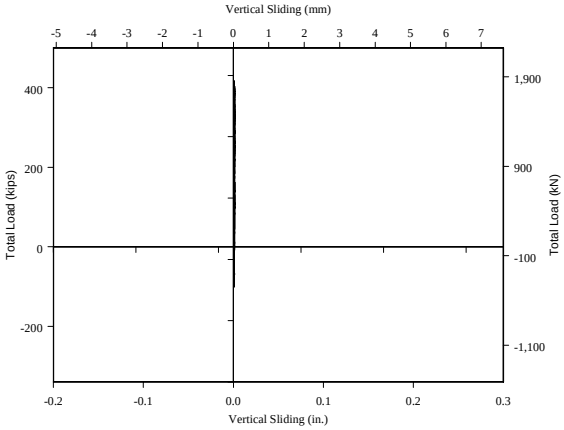


(d) Joint J4

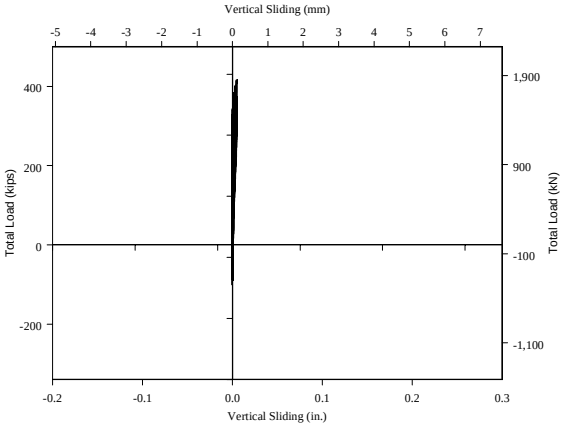


(e) Joint J5

**Figure A-19 (a-e) Vertical sliding between segments; Unit 100-EXT**

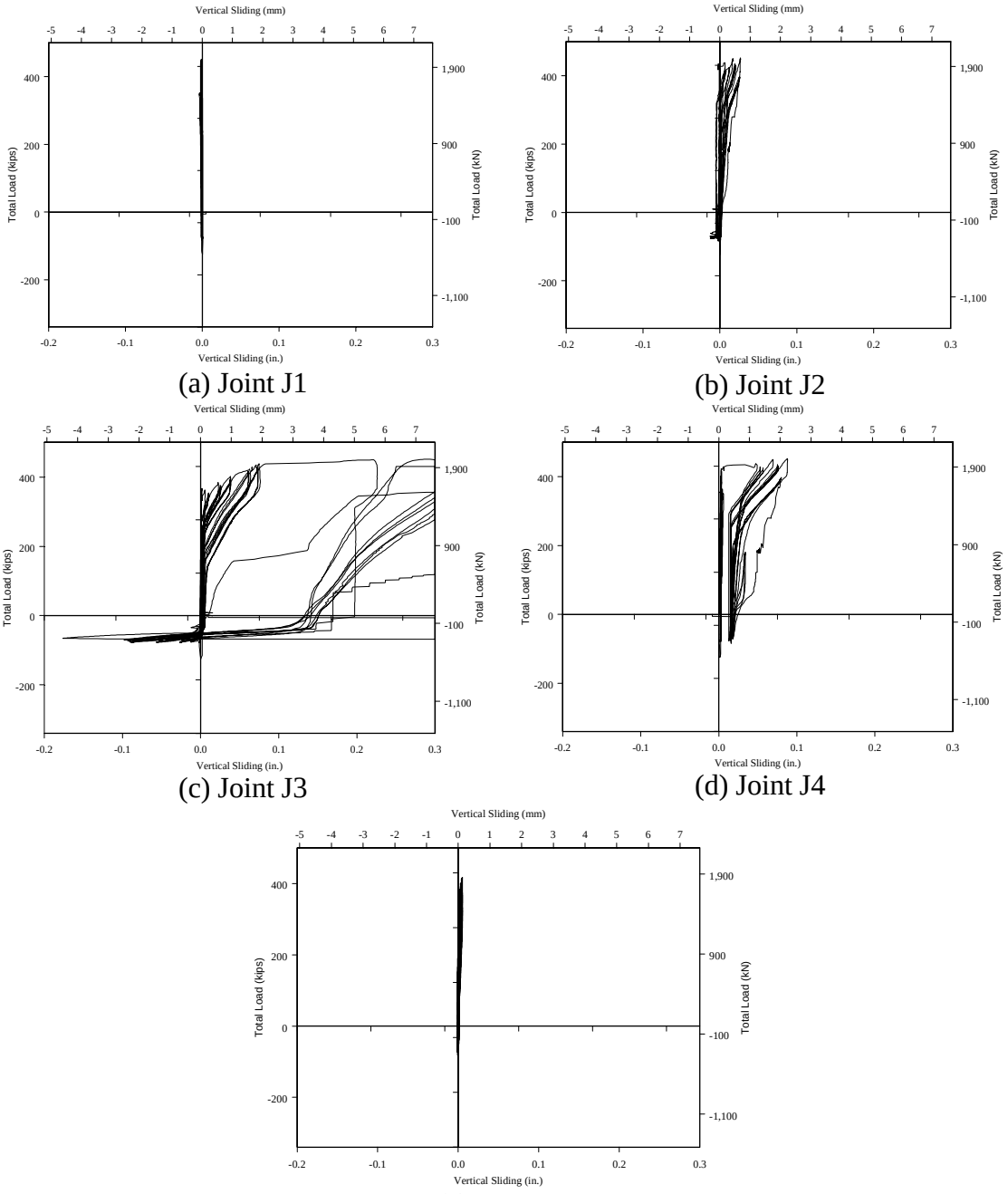


(a) Joint J1

(b) Joint J2

(c) Joint J3

(d) Joint J4

(e) Joint J5

**Figure A-20 (a-e) Vertical sliding between segments; Unit 50-INT/50-EXT**

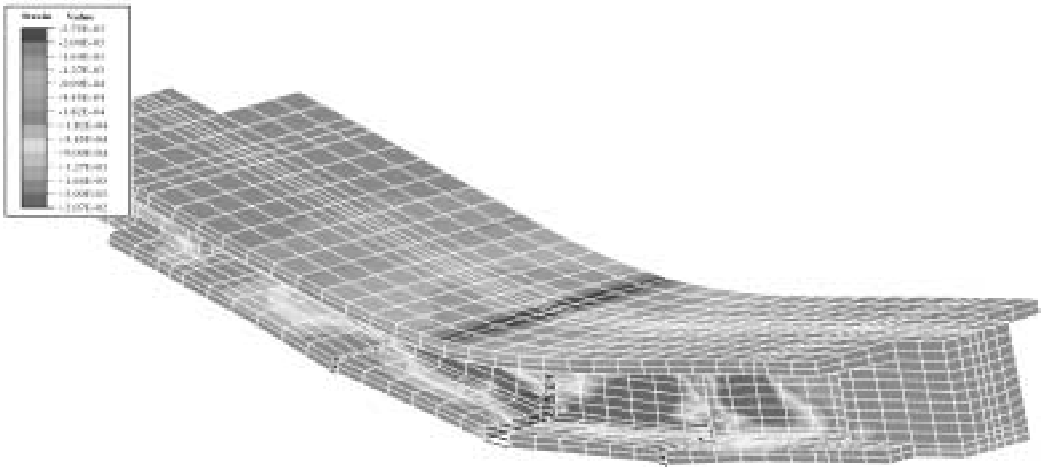

**Figure A-21 Longitudinal concrete strain contour at 4 in. (102 mm) down for Unit 100-INT (finite element analysis)**

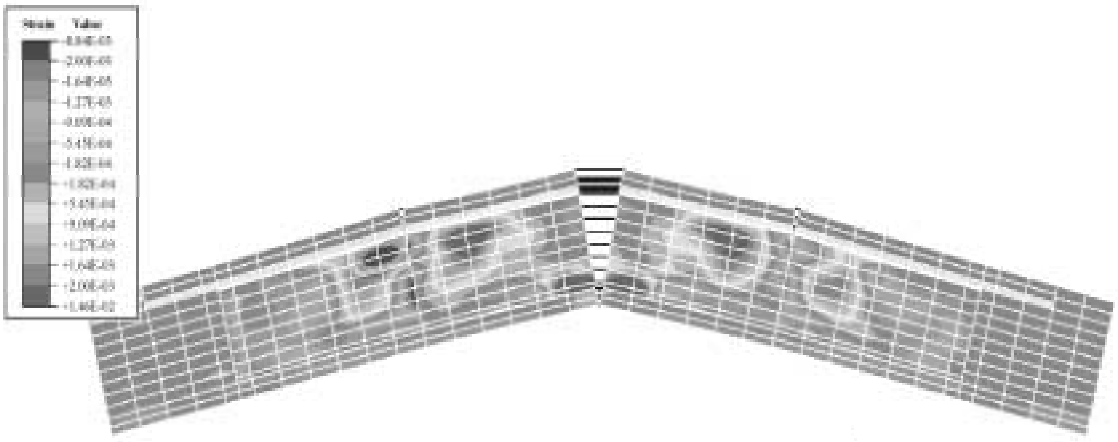

**Figure A-22 Longitudinal concrete strain contours at 4 in. (102 mm) up for Unit 100-INT (finite element analysis)**

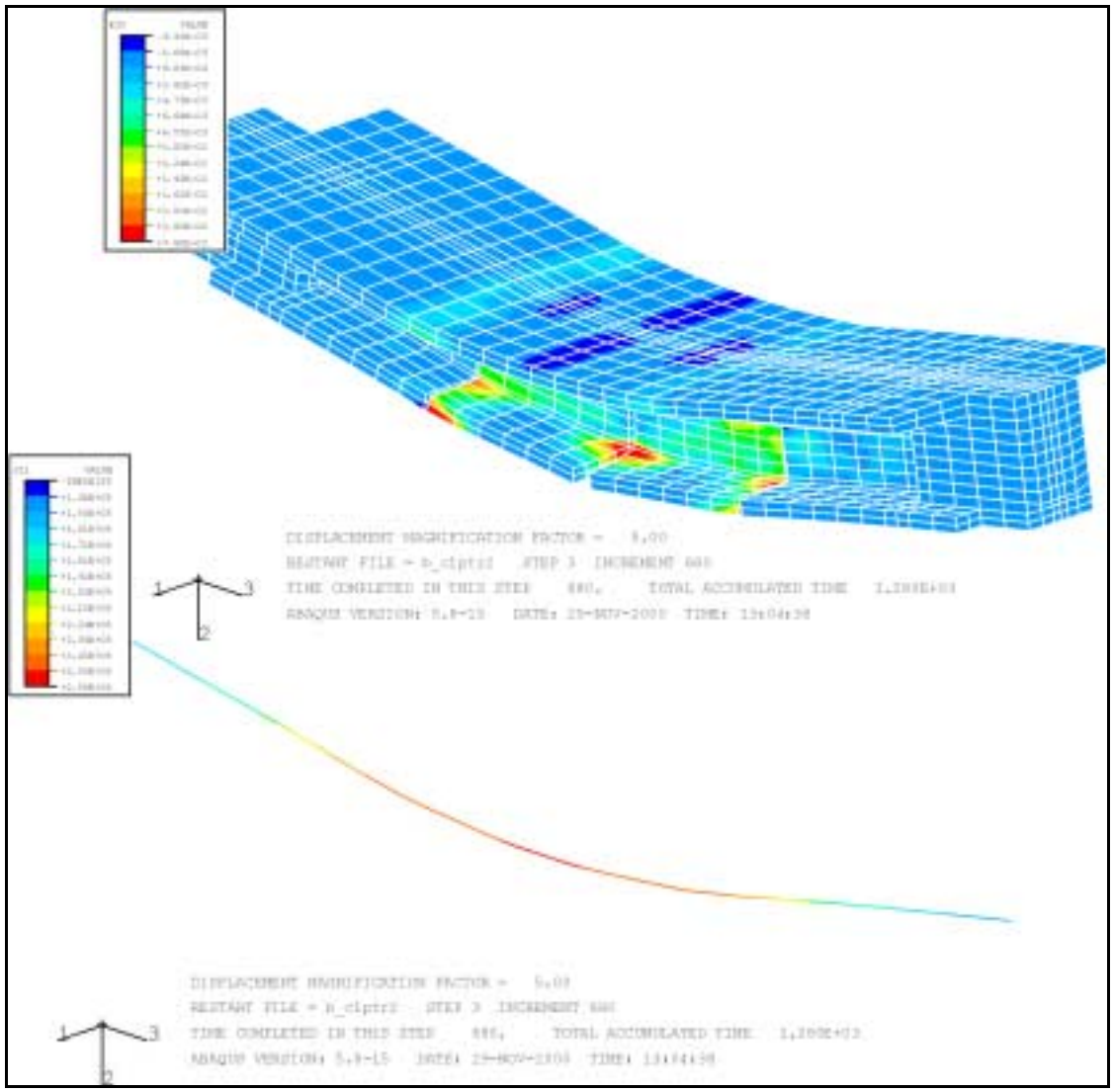

**Figure A-23 Longitudinal concrete strain contours and stress contours of bonded tendon at 6 in. (152 mm) down for Unit 100-INT-CIP (finite element analysis)**

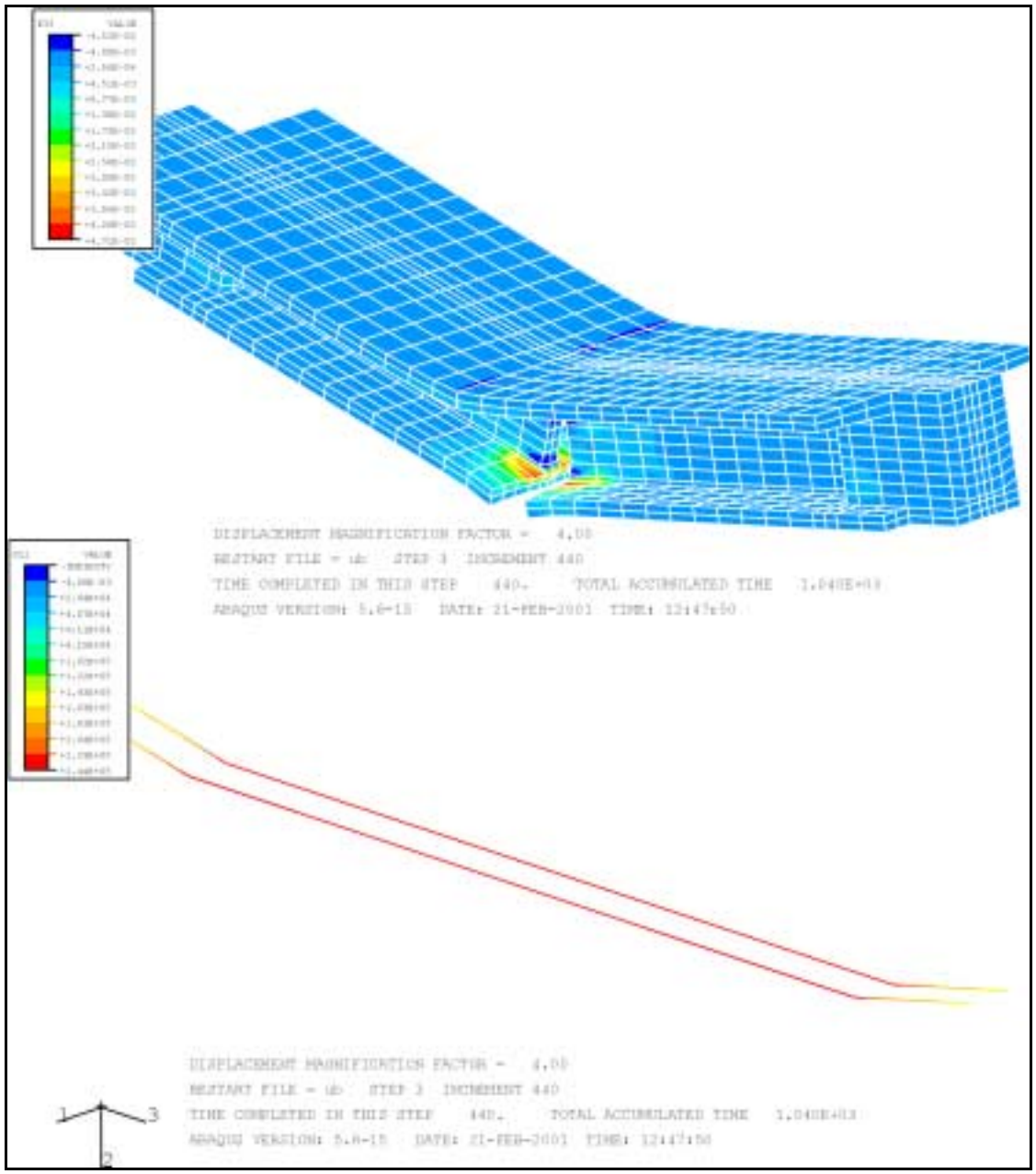

**Figure A-24 Longitudinal concrete strain contours and stress contours of unbonded tendon at 9 in. (229 mm) down for Unit 100-EXT (finite element analysis)**

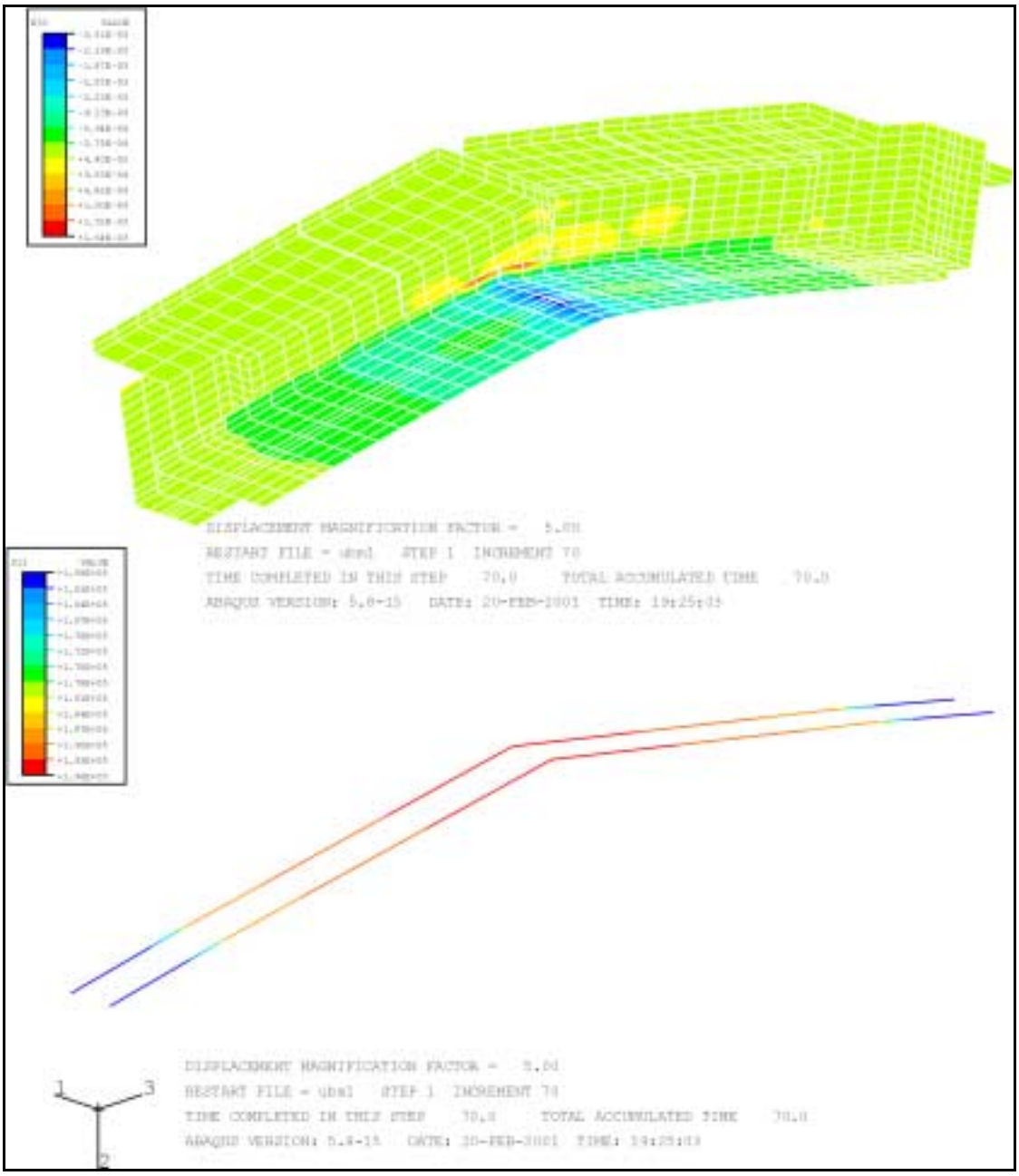

**Figure A-25 Longitudinal concrete strain contours and stress contours of unbonded tendon at 6 in. (152 mm) up for Unit 100-EXT (finite element analysis)**

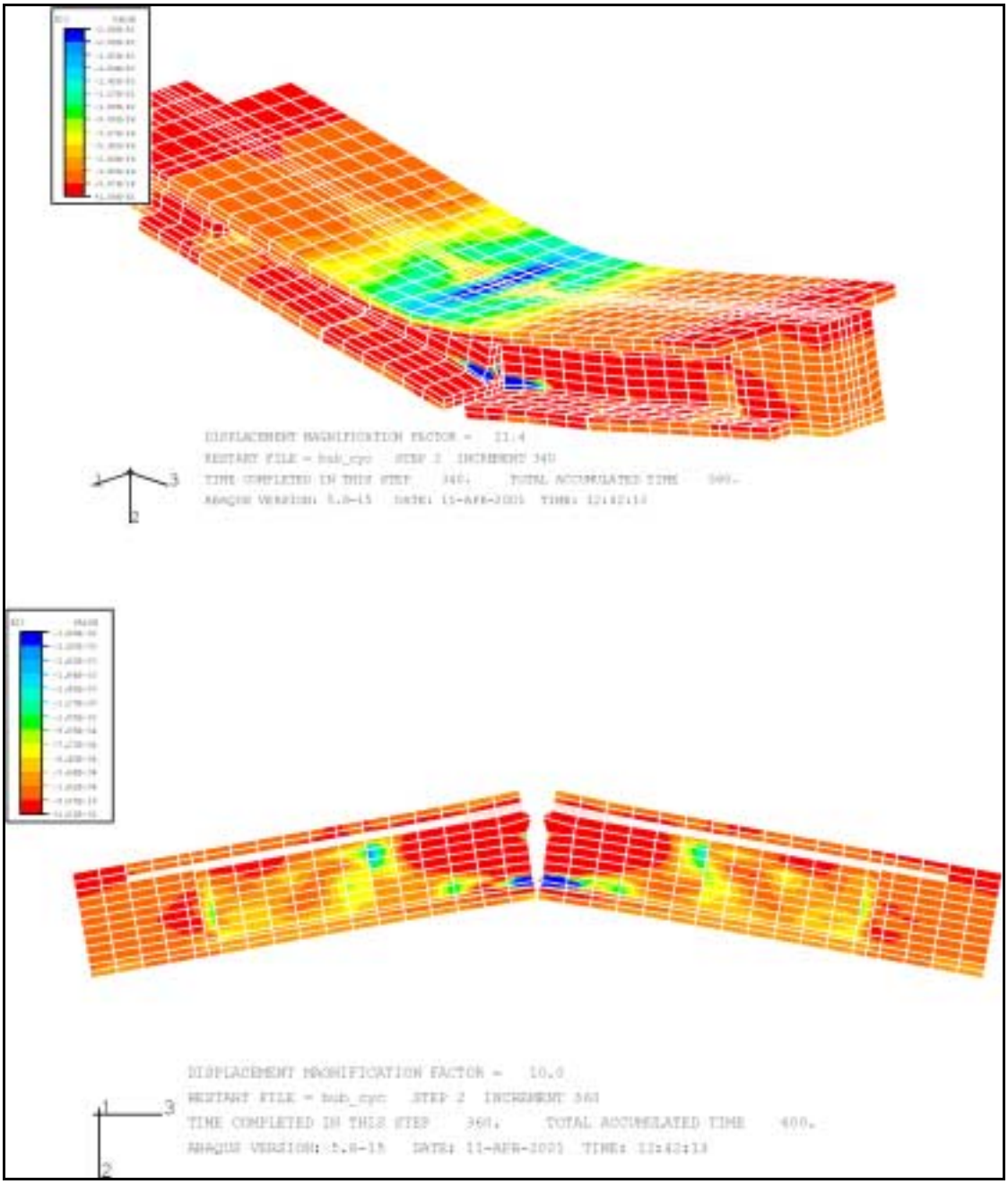

**Figure A-26 Longitudinal concrete strain contours at 4 in. (102 mm) both up and down for Unit 50-INT/50-EXT (finite element analysis)**

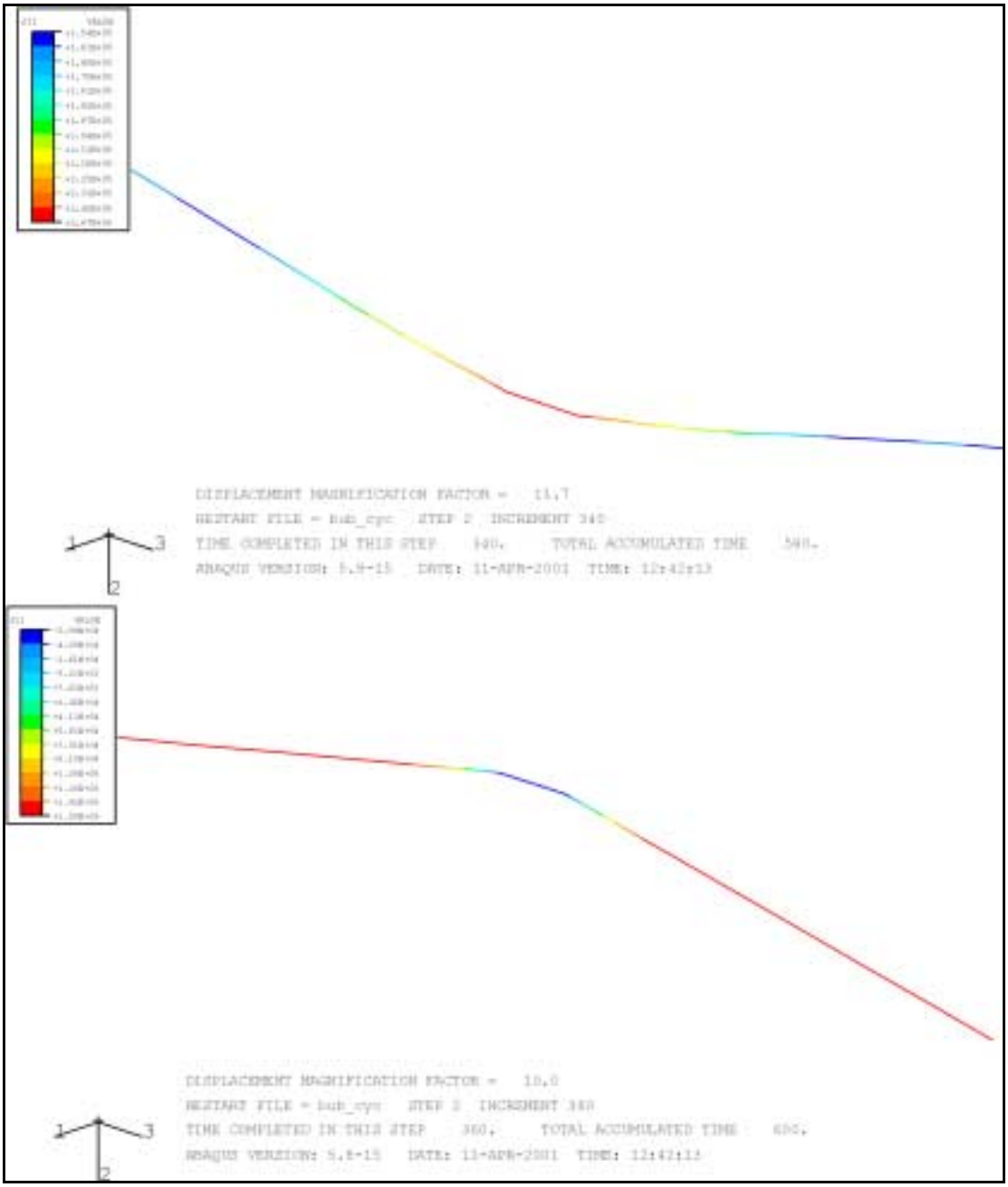

**Figure A-27 Stress contours of bonded tendon at 3 in. (76.2 mm) up and down for Unit 50-INT/50-EXT (finite element analysis)**

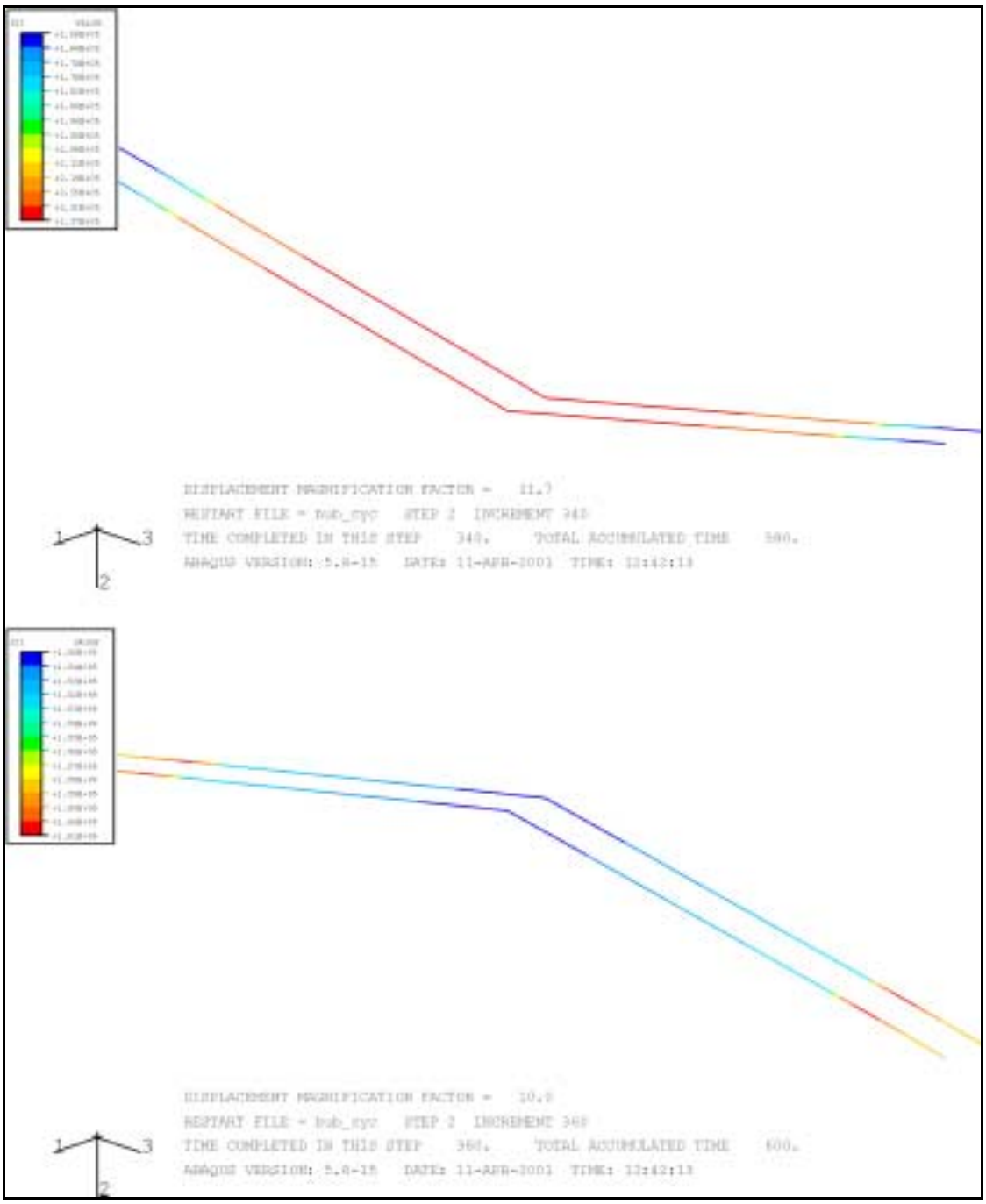

**Figure A-28 Stress contours of unbonded tendon at 3 in. (76.2 mm) down and up for Unit 50-INT/50-EXT (finite element analysis)**

# Appendix B

## Additional Experimental Results of Phase II Tests

Only a selection of the experimental results of the Phase II tests is presented in Chapter 6 of this report for conciseness. More experimental results are given in this appendix. The results shown in this appendix for each test unit include the following:

1. Total load versus total displacement.
2. Seismic load ($V_{E1}$ - $V_{E2}$; see Figure 5-32) versus seismic displacement.
3. Load-displacement cycle at 4.5 in. (114 mm) maximum displacement. The load-displacement curve at this displacement level was used to calculate the energy dissipation capability and equivalent viscous damping of different test units.
4. Measured opening of Joint $J_1$ at the top and bottom surfaces of the test units. Joint openings measured approximately at elevations of the upper and lower prestressing tendons are also presented in this appendix.
5. Rotations of the precast segments and of the segment-to-segment joint.
6. Openings of the joint between the steel loading beam and the test unit. The figures presented in this appendix indicate that no joint opening or relative vertical slip occurred between the steel beam and the test units.
7. Vertical displacement of the test units at different sections.
8. Measured strains in the prestressing tendons. Unfortunately, most of the strain gages placed on the prestressing tendons of Test Units 100-INT and 100-INT-CIP malfunctioned before the test. The tendon strains measured for Test Units 100-INT and 100-INT-CIP were believed to be not reliable because of problems with the strain gages.

Additional data given in this appendix include the concrete strains measured during testing of Unit 100-INT and the strains measured in the reinforcement of the cast-in-place

deck closure joint in Unit 100-INT-CIP. In the figures of this appendix, the seismic force is the total applied actuator force during the second stage of the test (seismic test). Thus the seismic load = $V_{E1}$ - $V_{E2}$ (see Figure 5-32 for definition of $V_{E1}$ and $V_{E2}$). The total shear at Joint $J_1$ at the reference load level should be added to the seismic force to determine the total shearing force at Joint $J_1$ during the test. This additional force consisted of 49 kips (218 kN) (see Figure 5-31), in addition to a 32 kips (142 kN) force resulting from the self-weights of the steel beam and the test unit. Thus the total shearing force at Joint $J_1$ is the seismic force shown in the figures of this appendix in addition to a shearing force of 81 kips (360 kN) (shearing force at the reference load level).

In some of the figures presented in this appendix, the measured displacements, joint openings or strains are plotted versus the number of loading cycle. The first loading cycle was from zero load up to the reference load level (applied actuator forces at reference load level are shown in Figure 5-31). Subsequent loading cycles represented the displacement cycles during the seismic test. In the figures presented in this appendix, the number of loading cycles corresponds to the number of loading cycle shown in Figure 5-33.

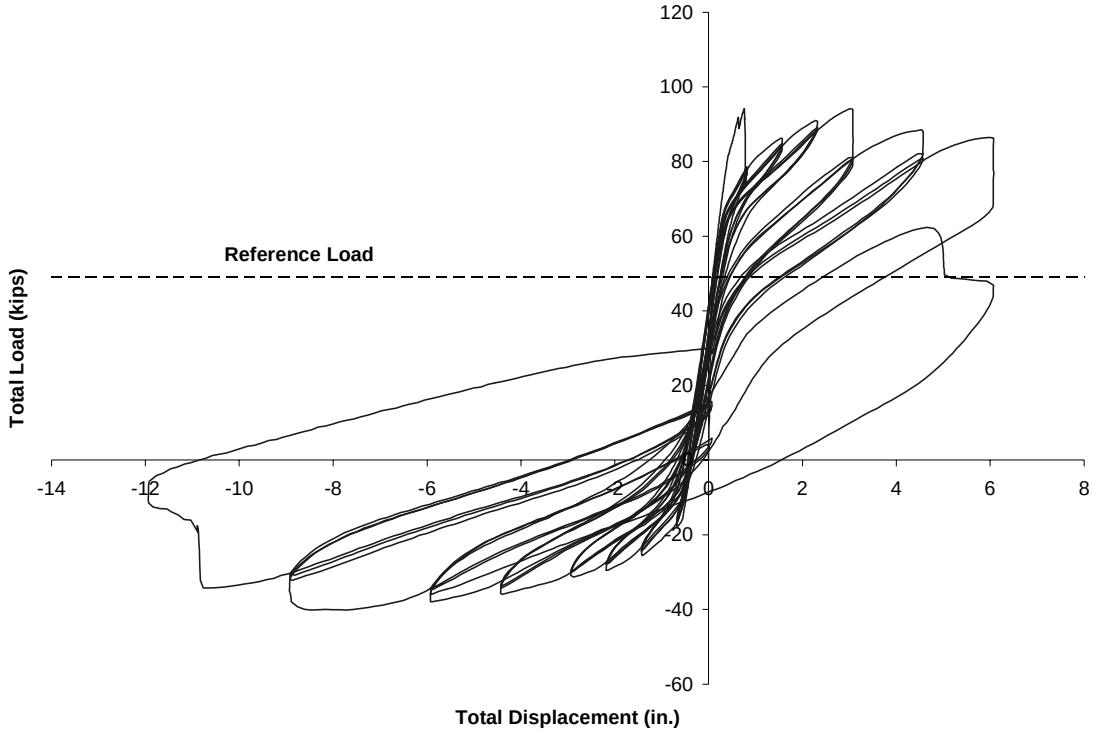


**Figure B-1 Total load versus total displacement at cantilever tip (Unit 100-INT)**

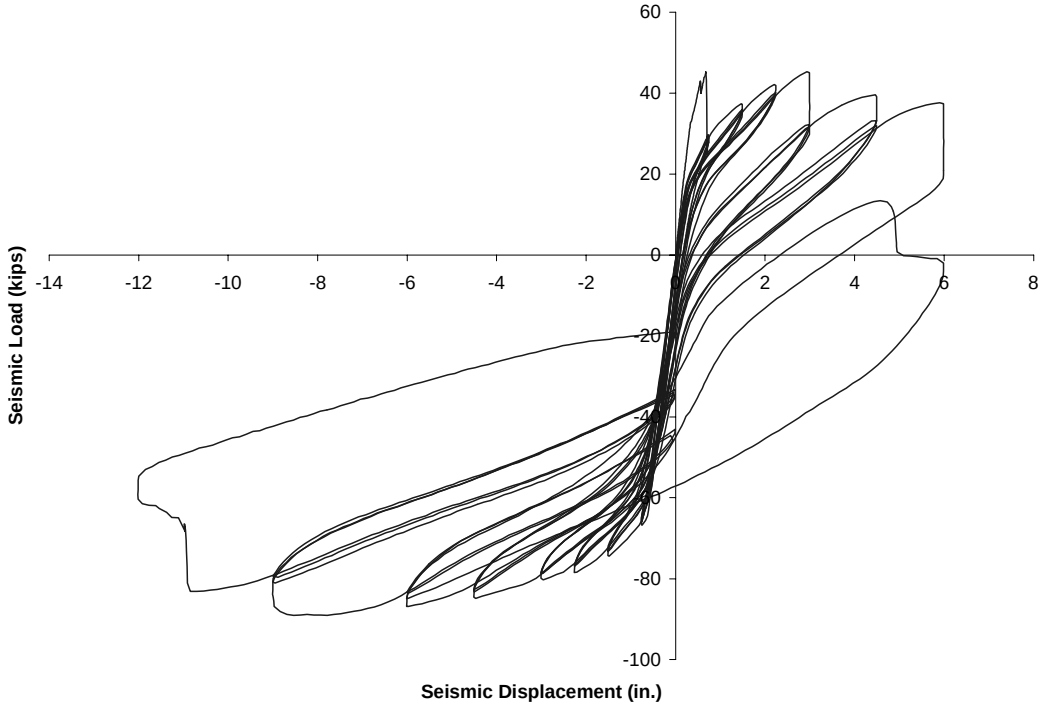


**Figure B-2 Seismic load versus seismic displacement at cantilever tip (Unit 100-INT)**

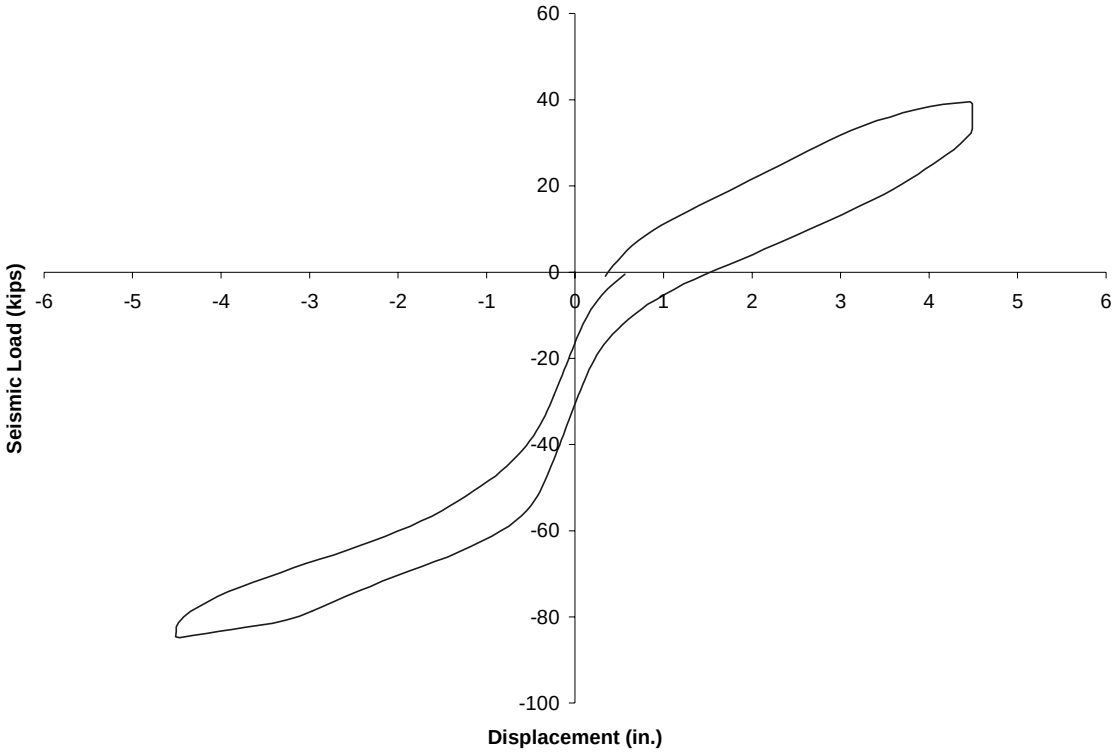


**Figure B-3 Seismic load-displacement for Unit 100-INT at 4.5 in. (114 mm)**

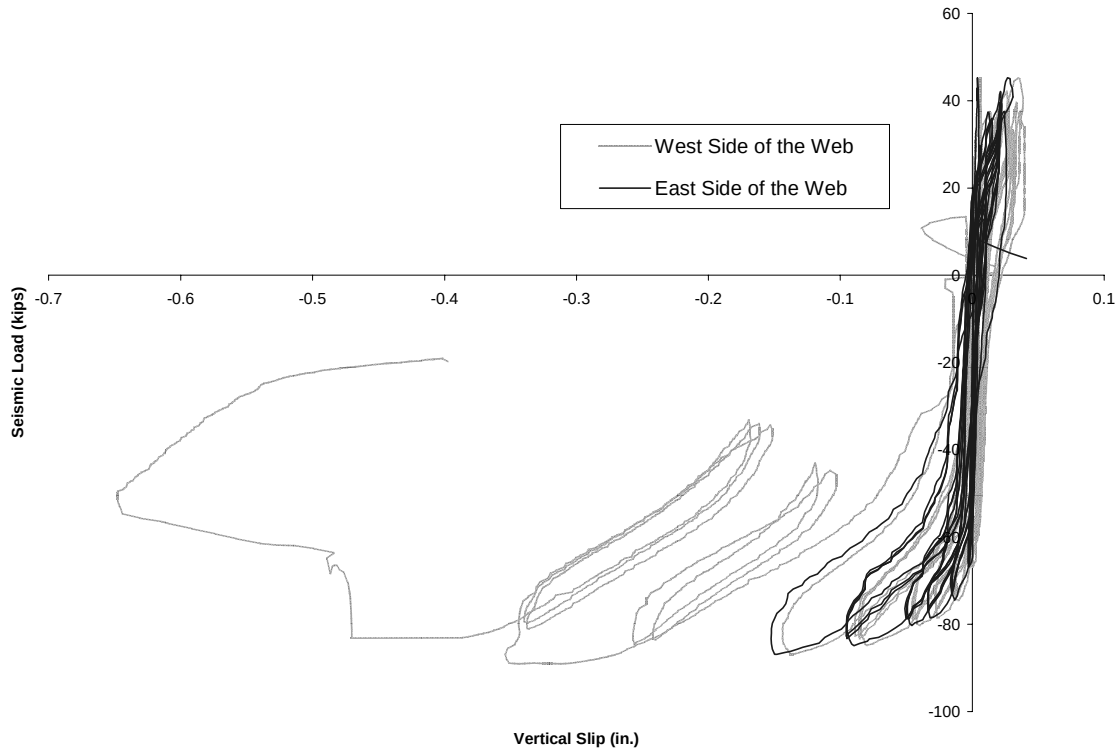


**Figure B-4 Load versus vertical slip between Segments 1 and 2 (Unit 100-INT)**

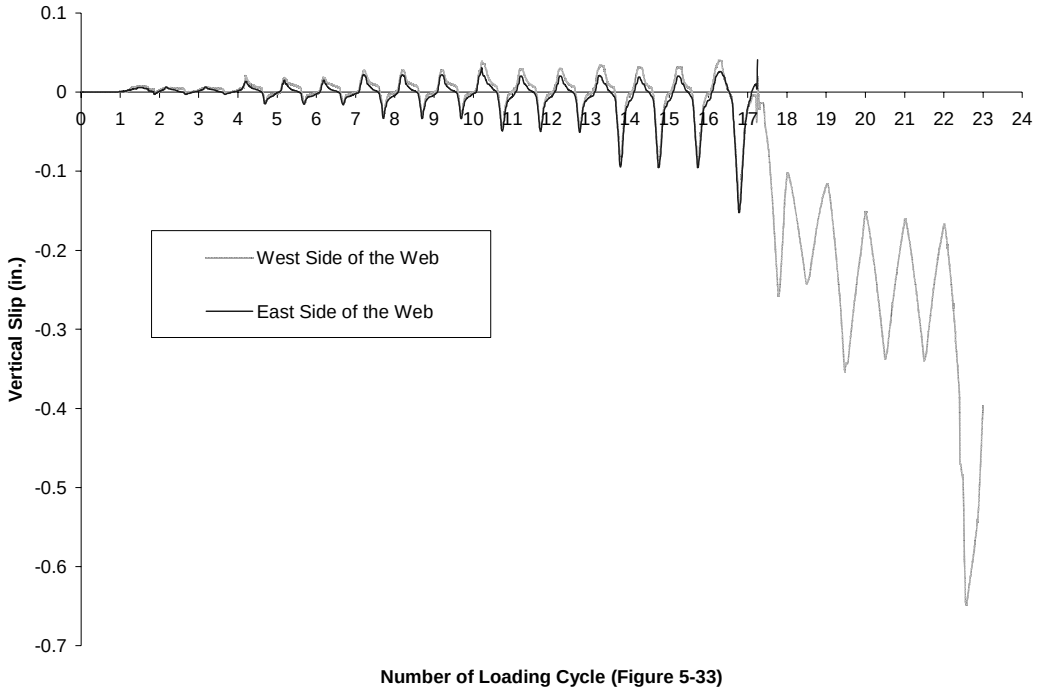


**Figure B-5 History of vertical slip between Segments 1 and 2 (Unit 100-INT)**

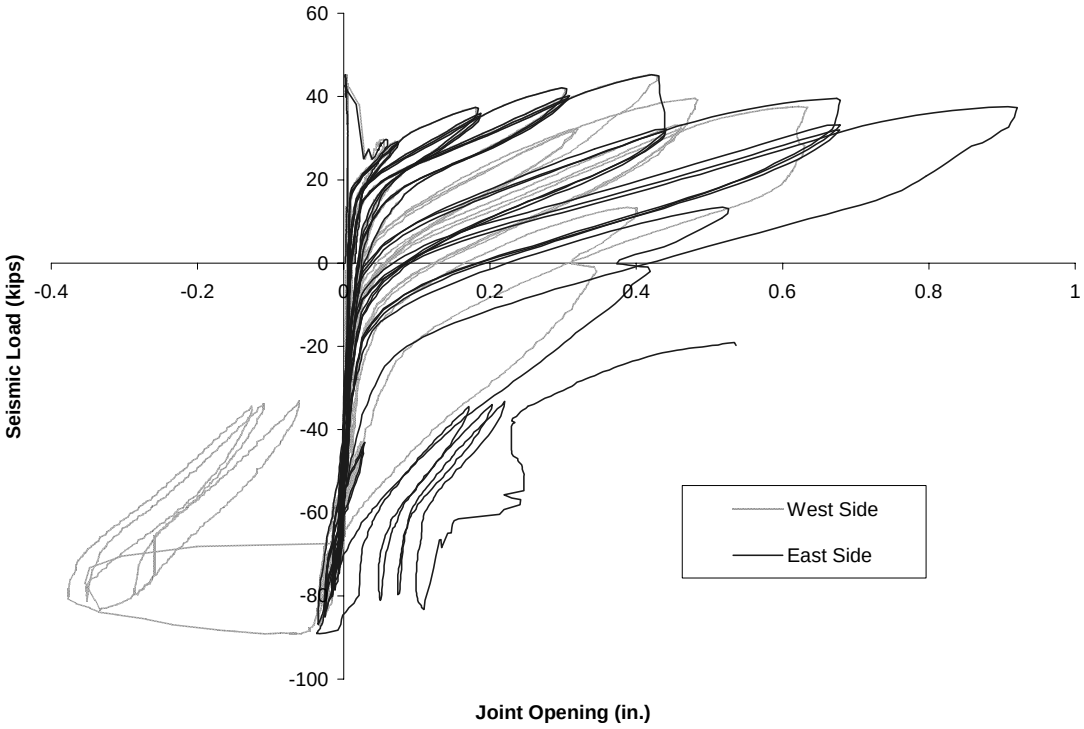


**Figure B-6 Load versus opening of Joint $J_1$ at top surface (Unit 100-INT)**

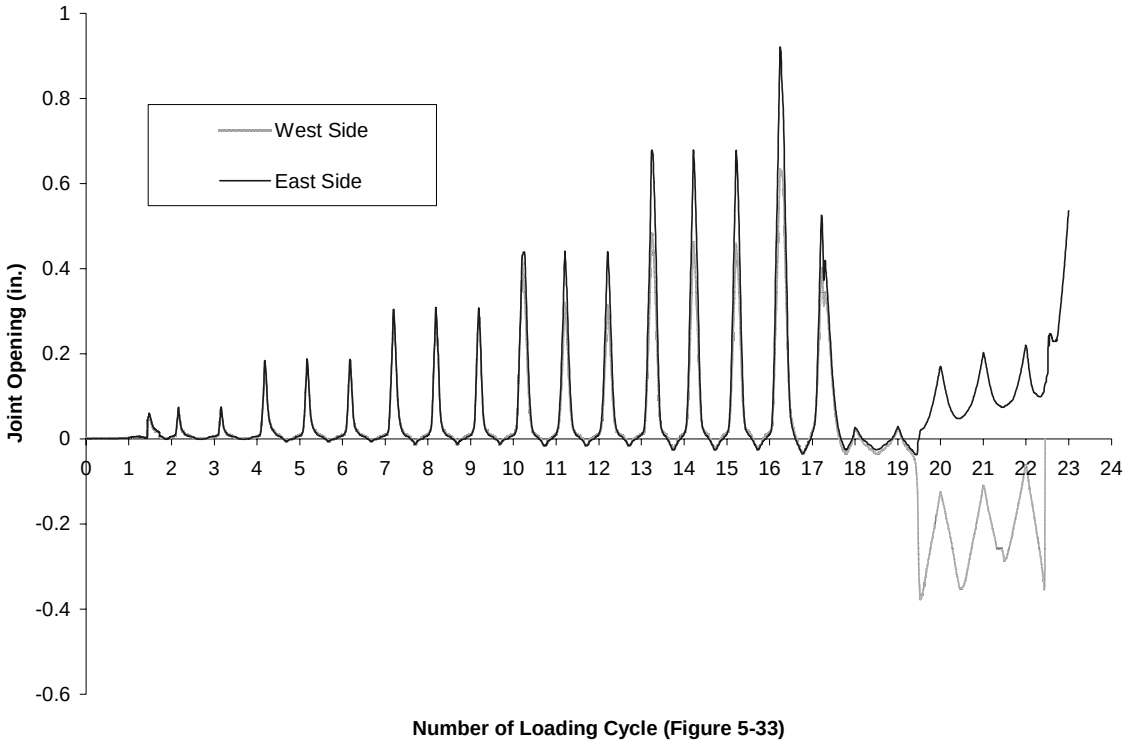


**Figure B-7 History of opening of Joint $J_1$ at top surface (Unit 100-INT)**

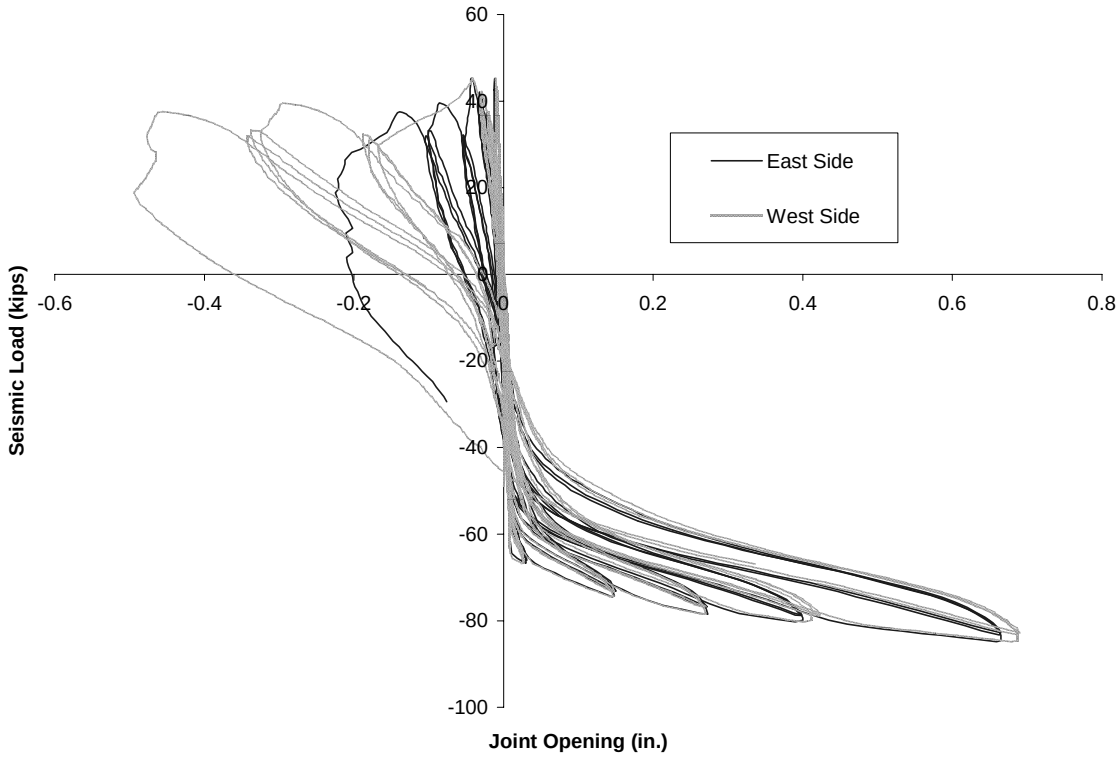


**Figure B-8 Load versus opening of Joint $J_1$ at bottom surface (Unit 100-INT)**

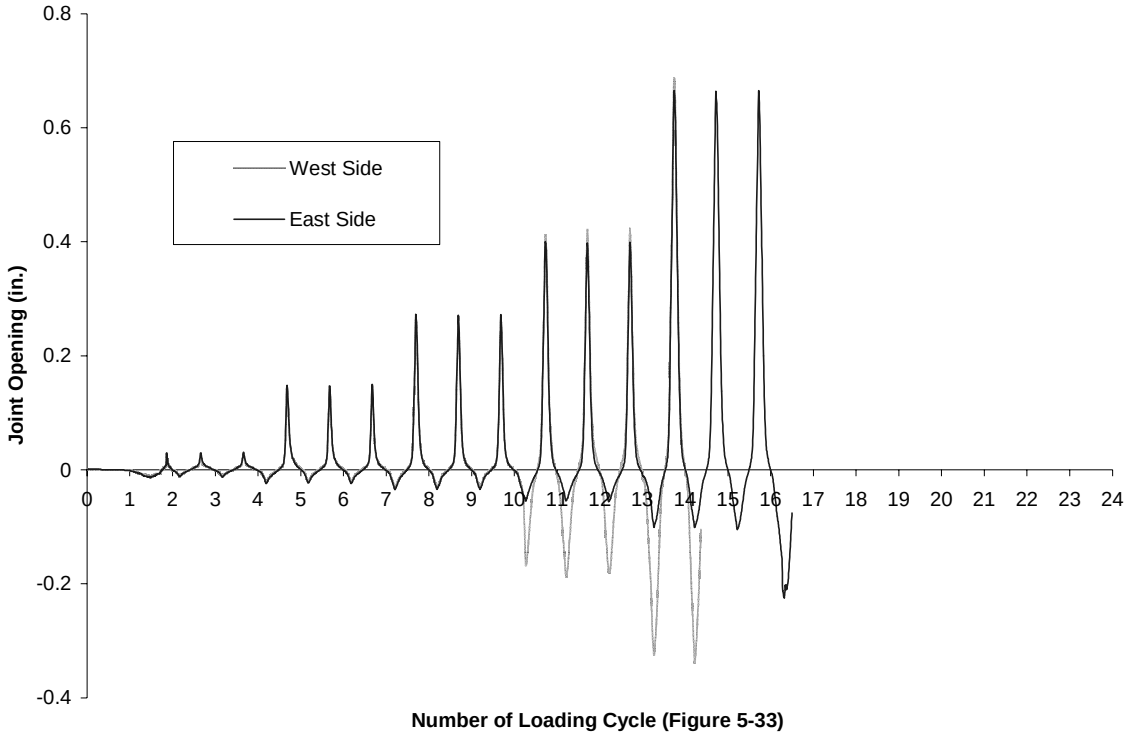


**Figure B-9 History of opening of Joint $J_1$ at bottom surface (Unit 100-INT)**

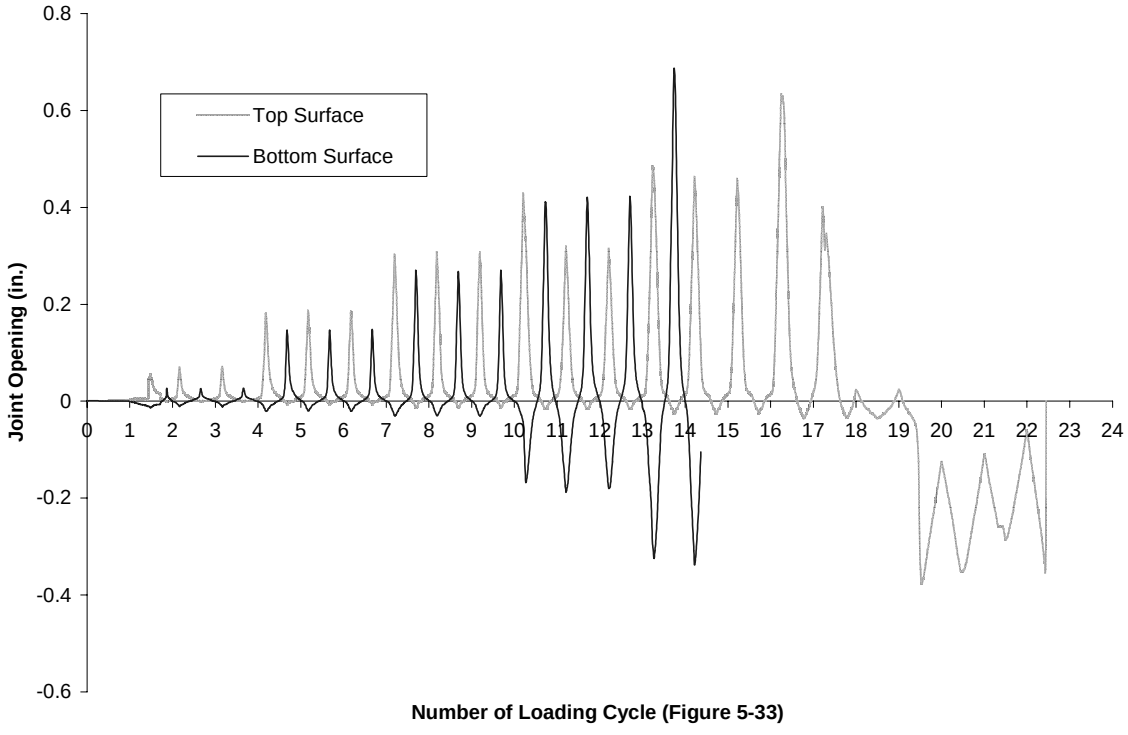


**Figure B-10 Load versus joint opening measured on the West Side of Unit 100-INT**

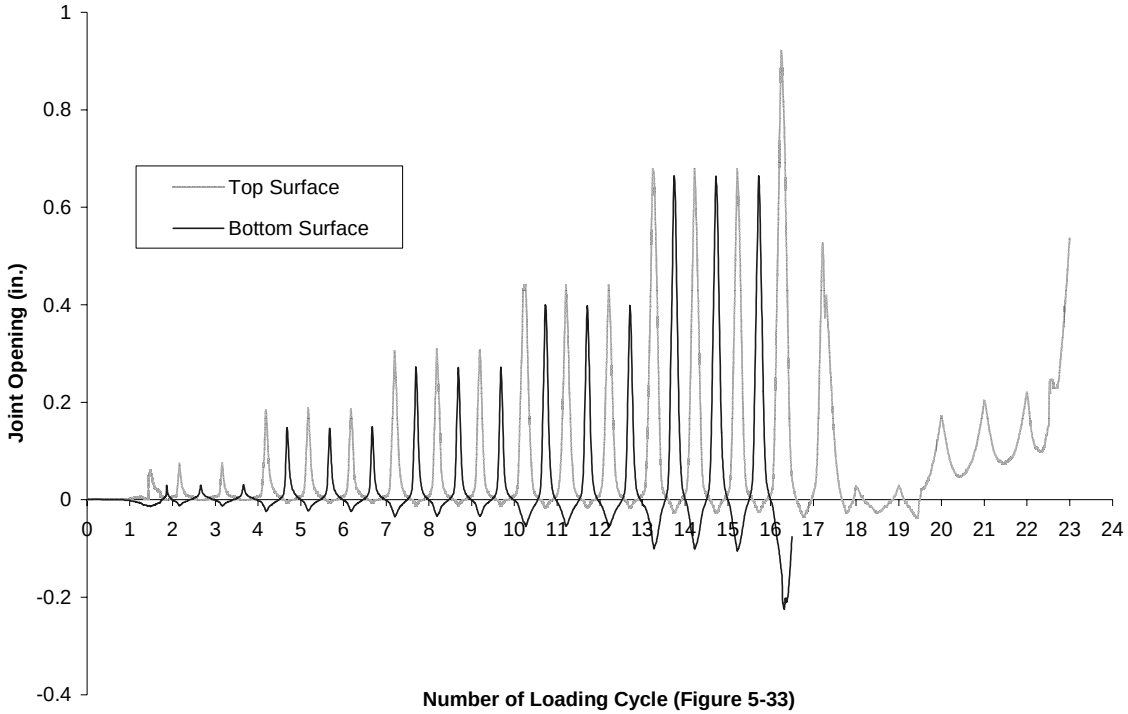


**Figure B-11 Load versus joint opening measured on the East Side of Unit 100-INT**

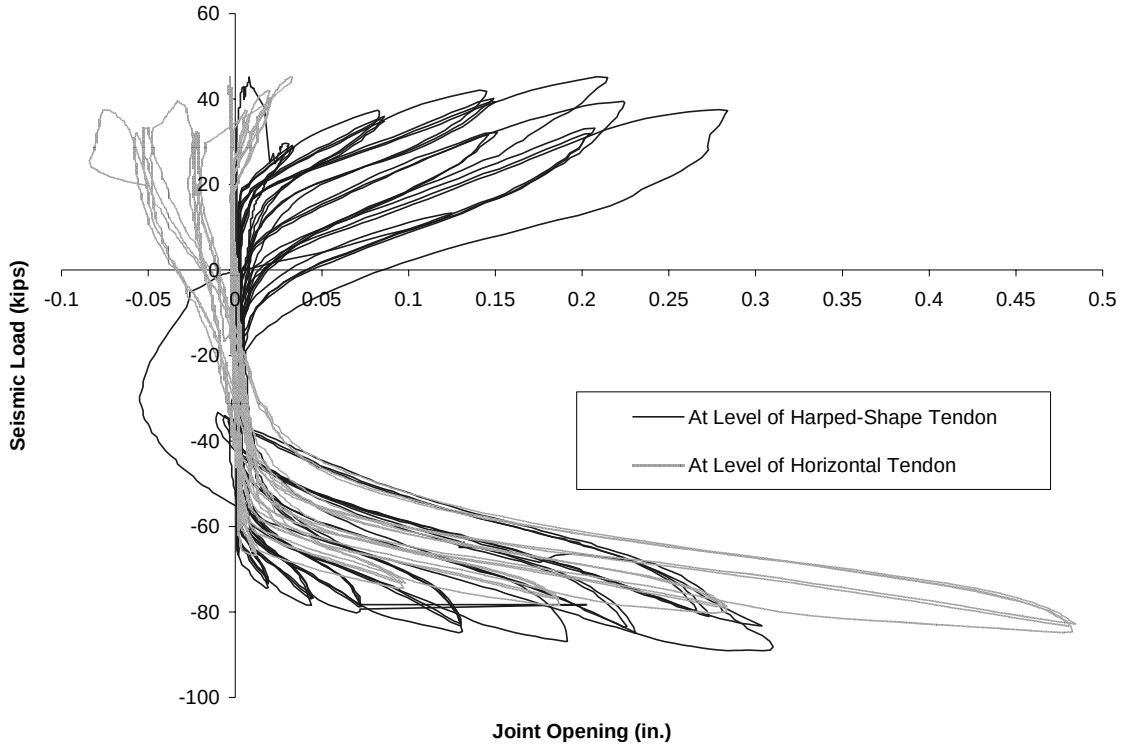


**Figure B-12 Load versus joint openings measured approximately at elevations of the prestressing tendons (Unit 100-INT)**

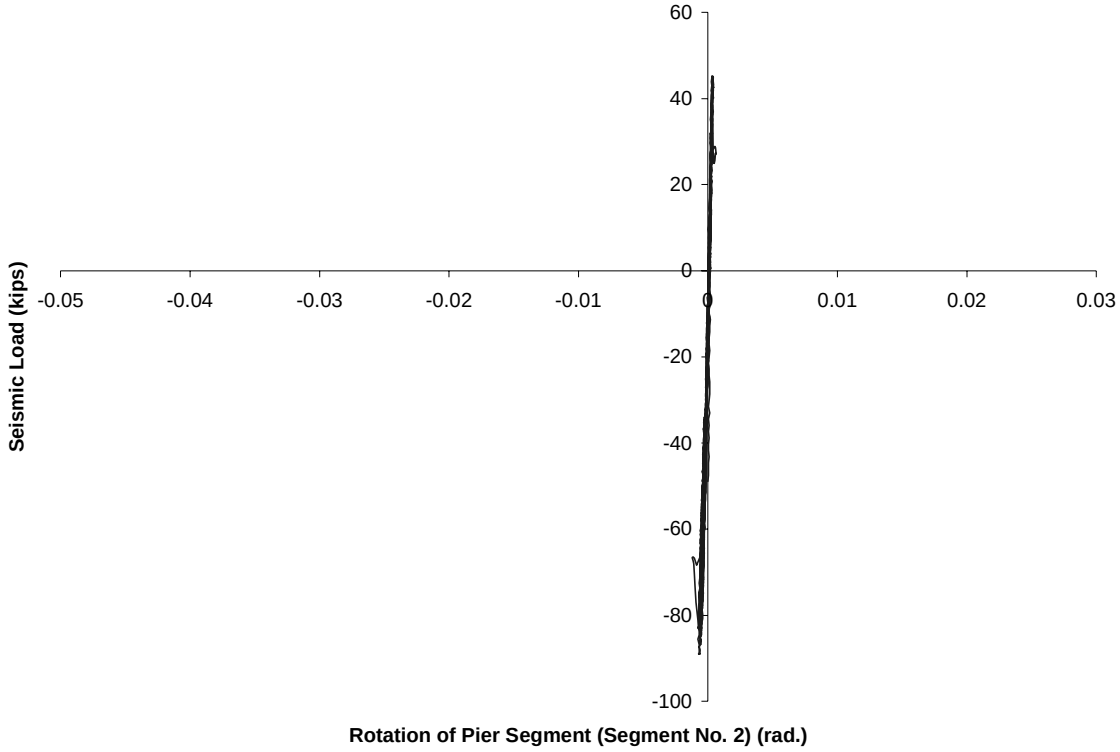


**Figure B-13 Load versus rotation of Segment No. 2 in Unit 100-INT**

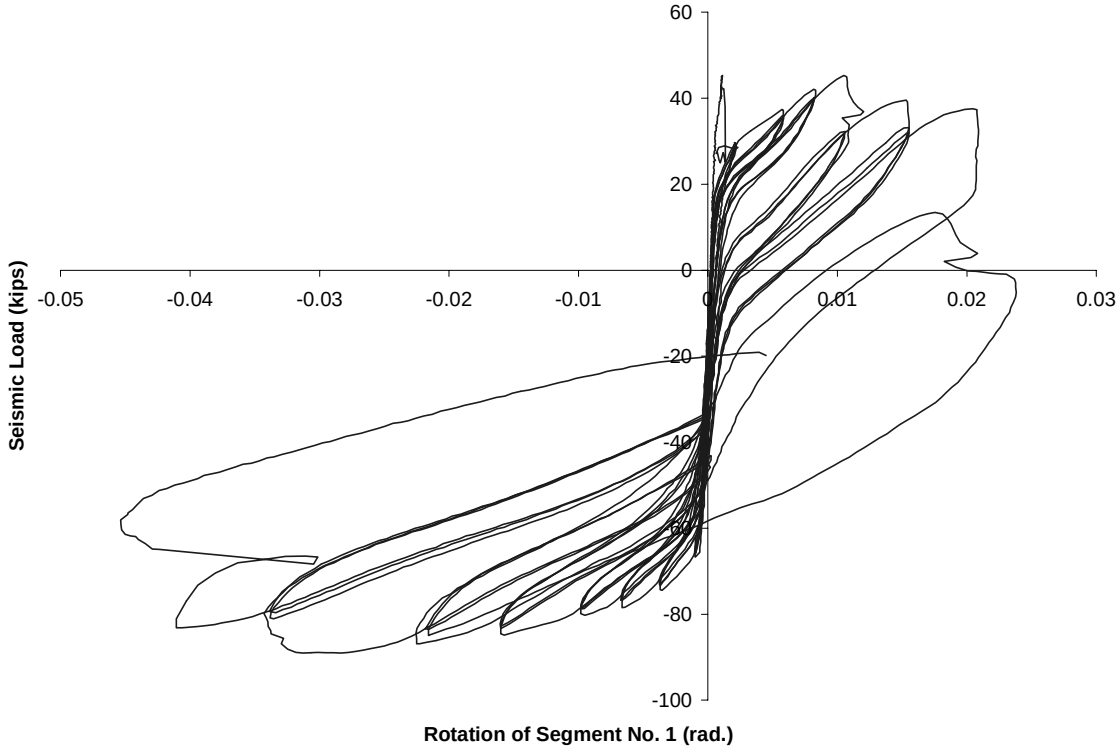


**Figure B-14 Load versus rotation of Segment No. 1 in Unit 100-INT**

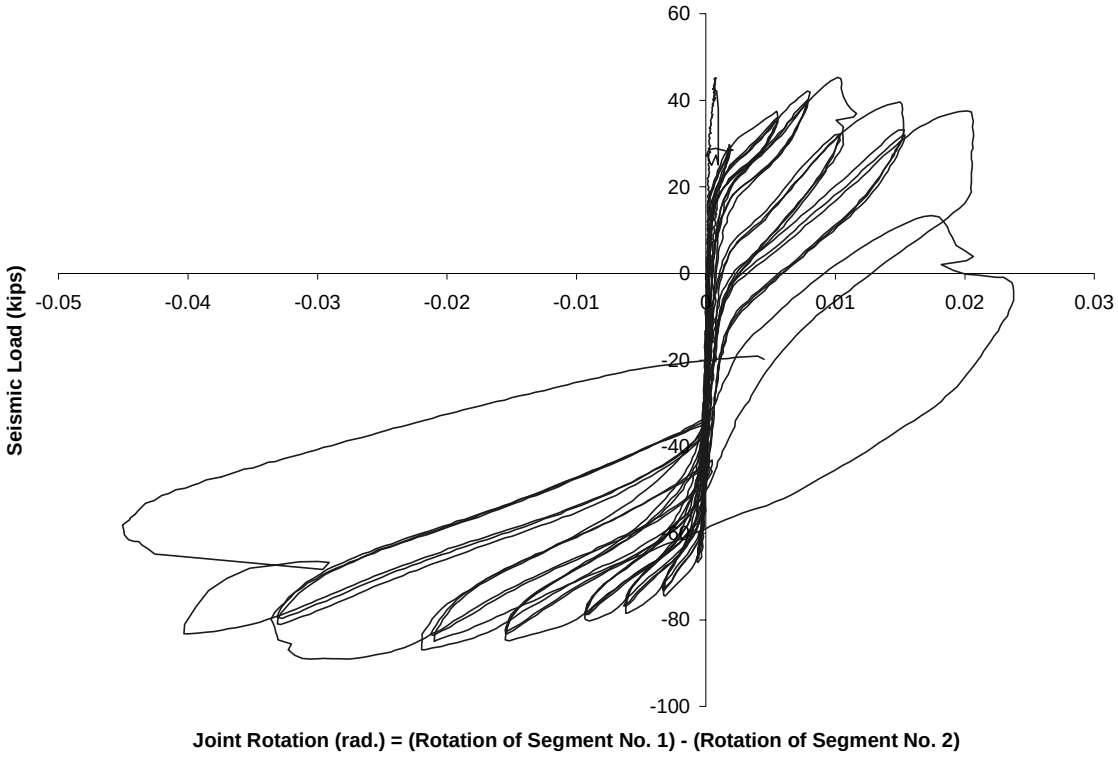


**Figure B-15 Load versus rotation of Joint $J_1$ in Unit 100-INT**

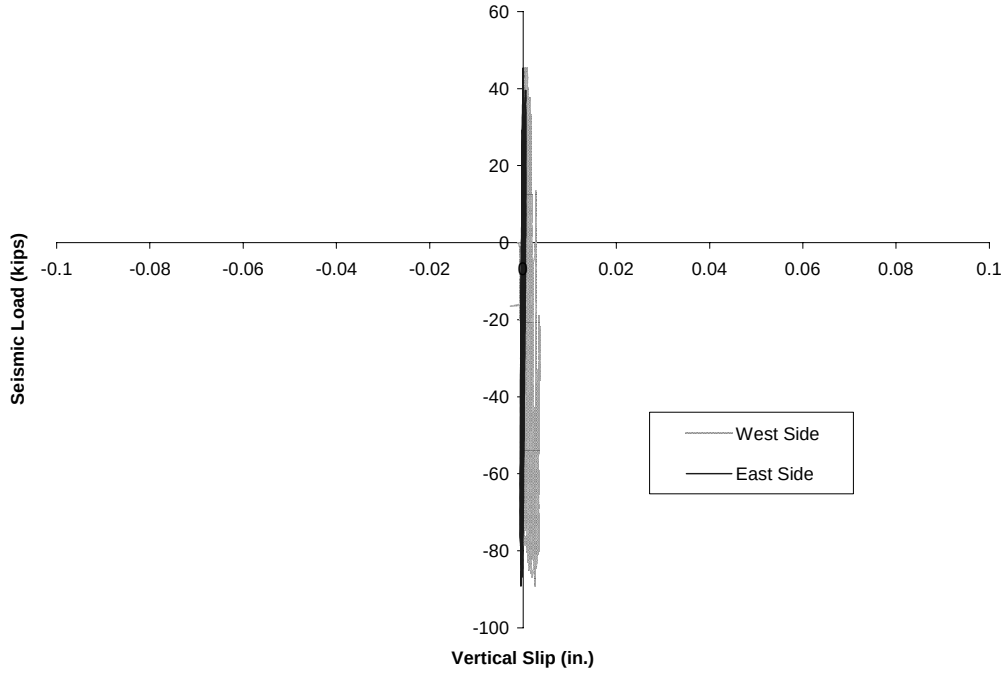


**Figure B-16 Vertical slip between Test Unit 100-INT and the steel loading beam**

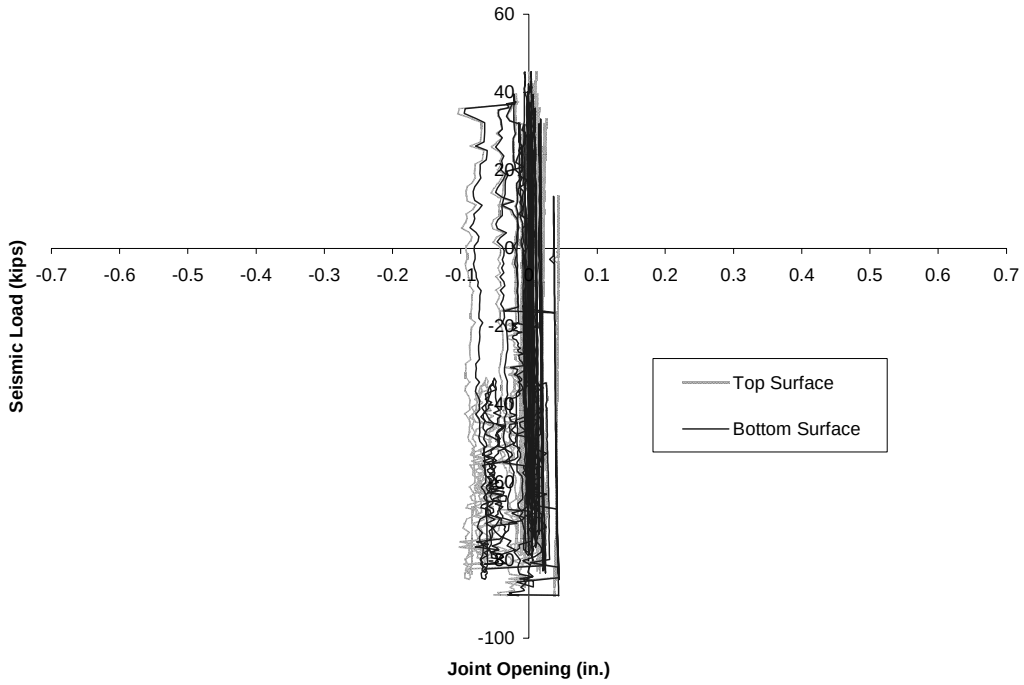


**Figure B-17 Opening of the joint between Test Unit 100-INT and the steel loading beam**

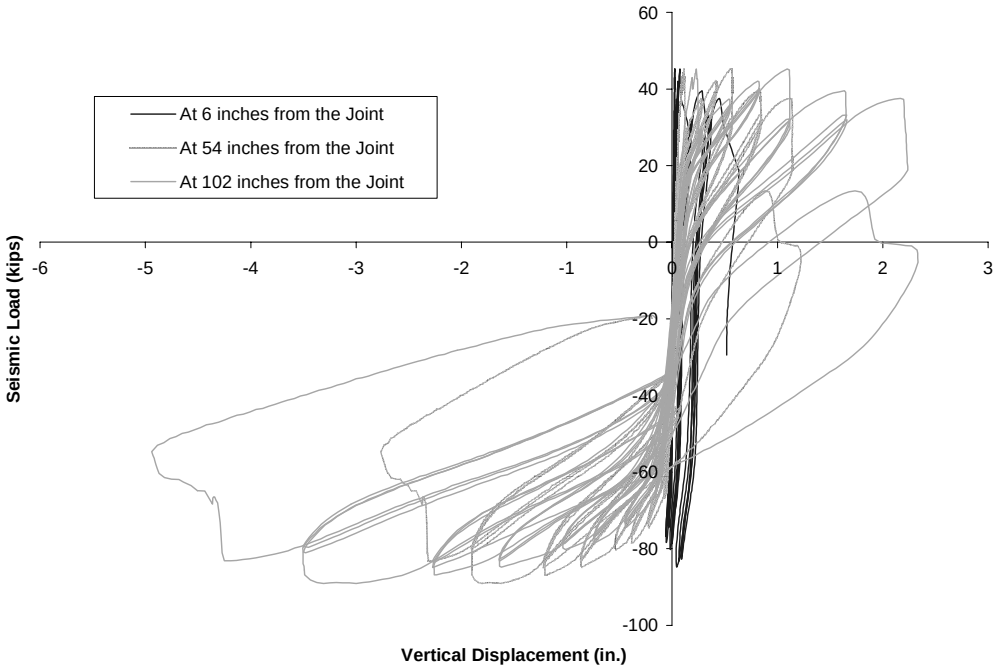


**Figure B-18 Load versus vertical displacement at different sections in Unit 100-INT**

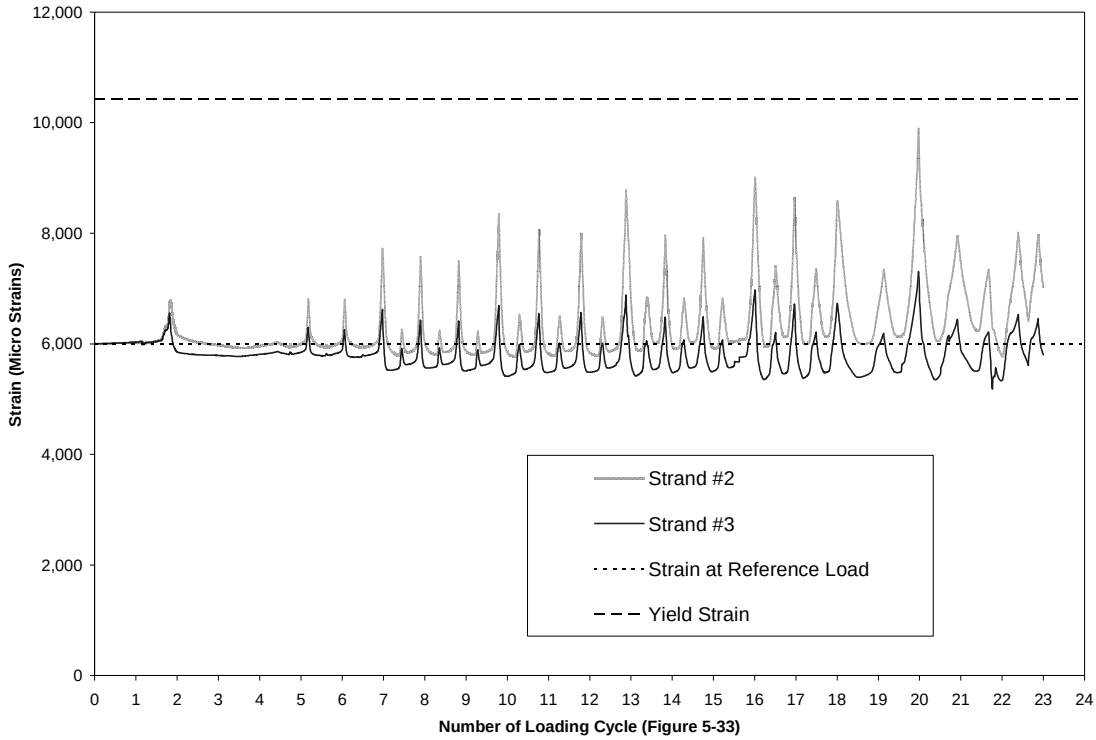


**Figure B-19 Strain in upper tendon of Unit 100-INT at Section A (see Figure 5-29)**

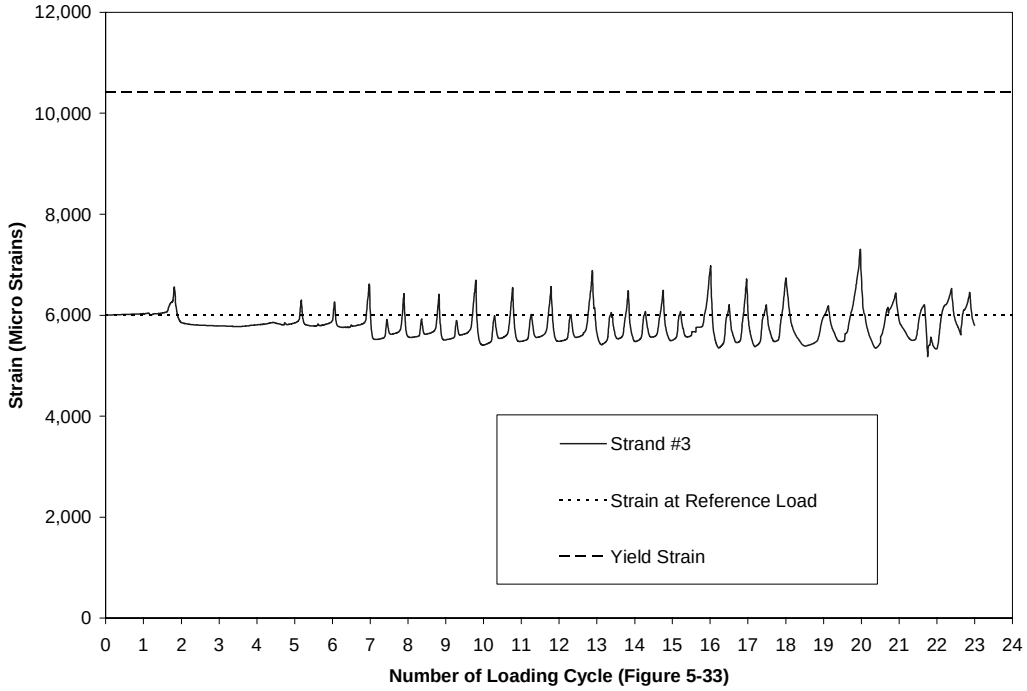


**Figure B-20 Strain in upper tendon of Unit 100-INT at Section A (see Figure 5-29) (Strand #3)**

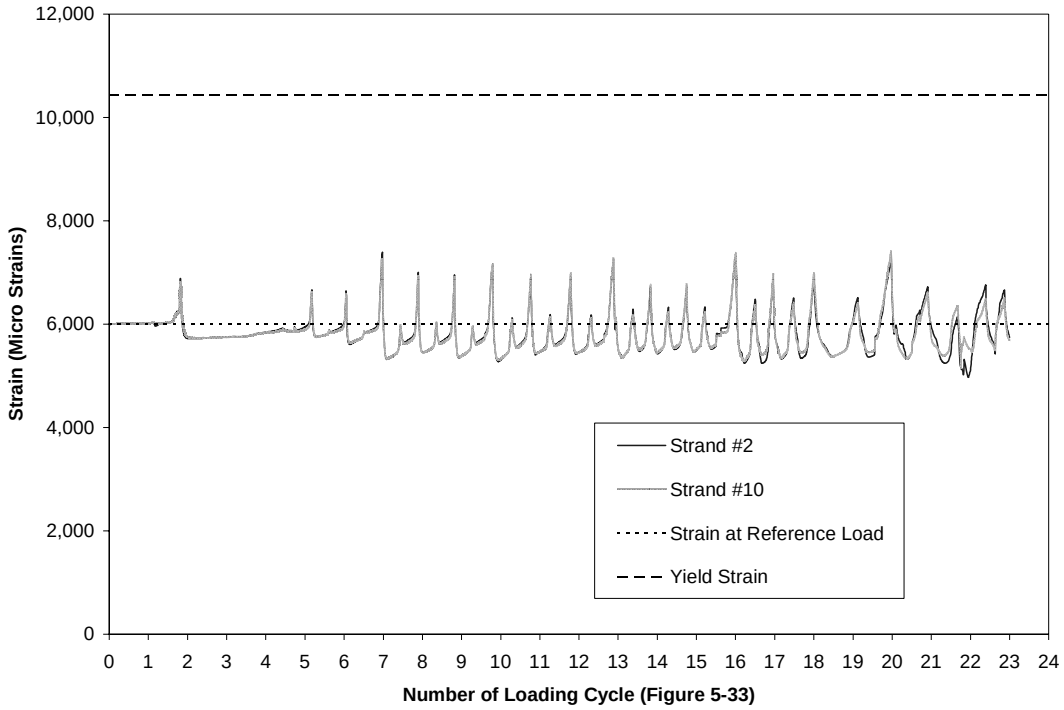


**Figure B-21 Strain in upper tendon of Unit 100-INT at Section B (see Figure 5-29)**

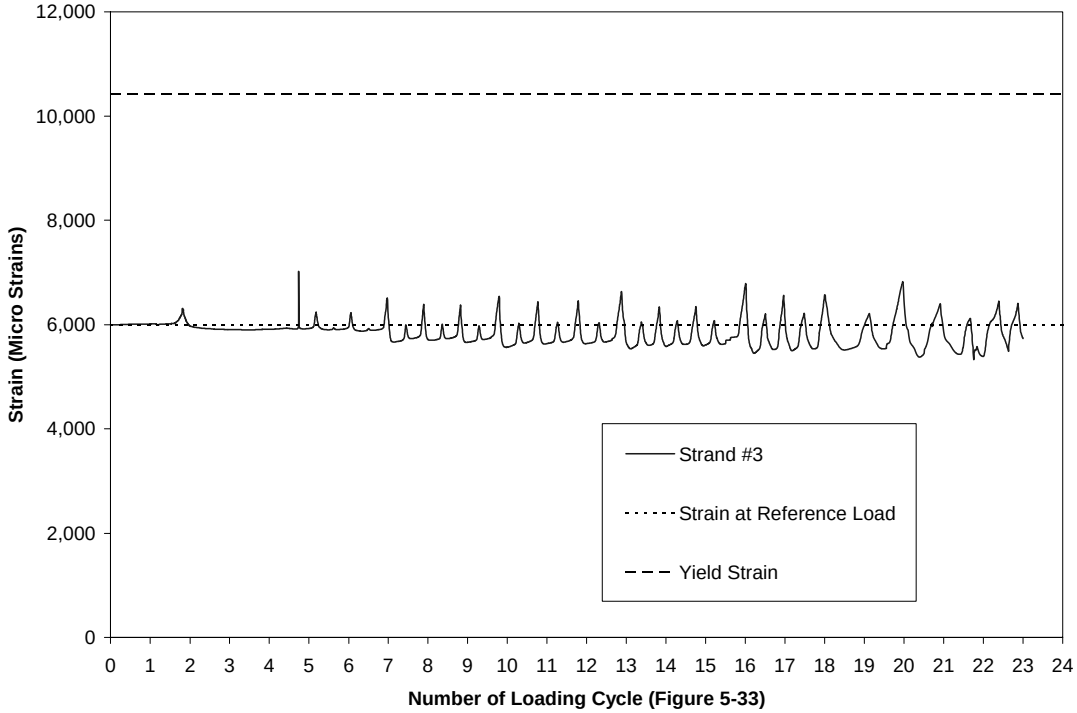


**Figure B-22 Strain in upper tendon of Unit 100-INT at Section C (see Figure 5-29)**

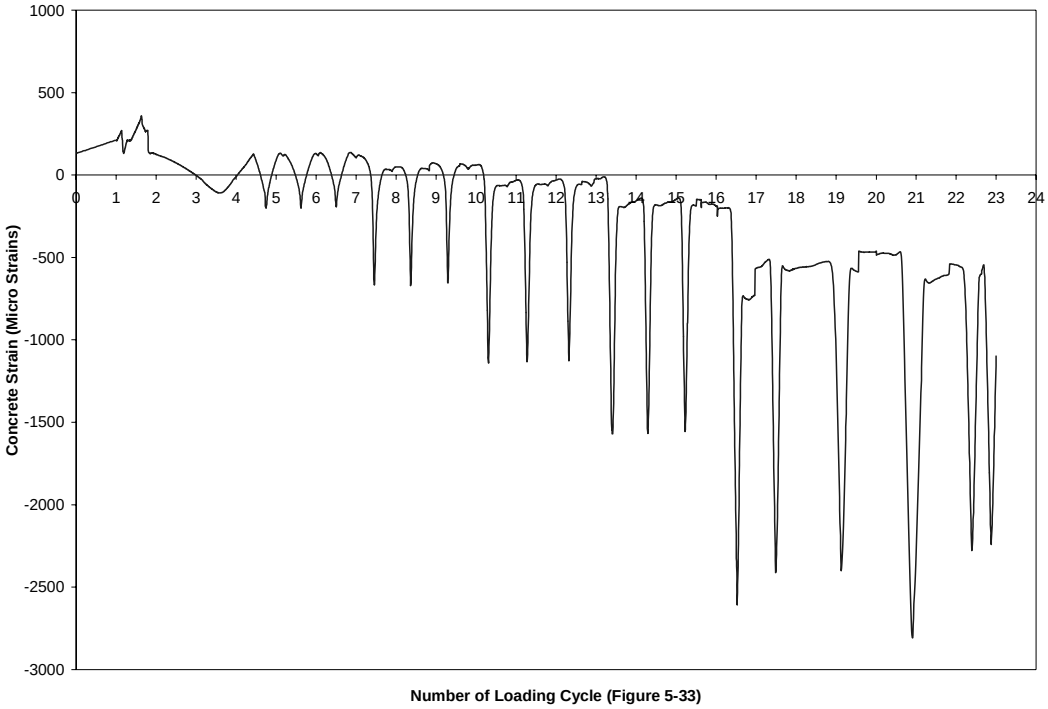


**Figure B-23 Concrete strain measured in top surface at Joint $J_1$ (Unit 100-INT)**

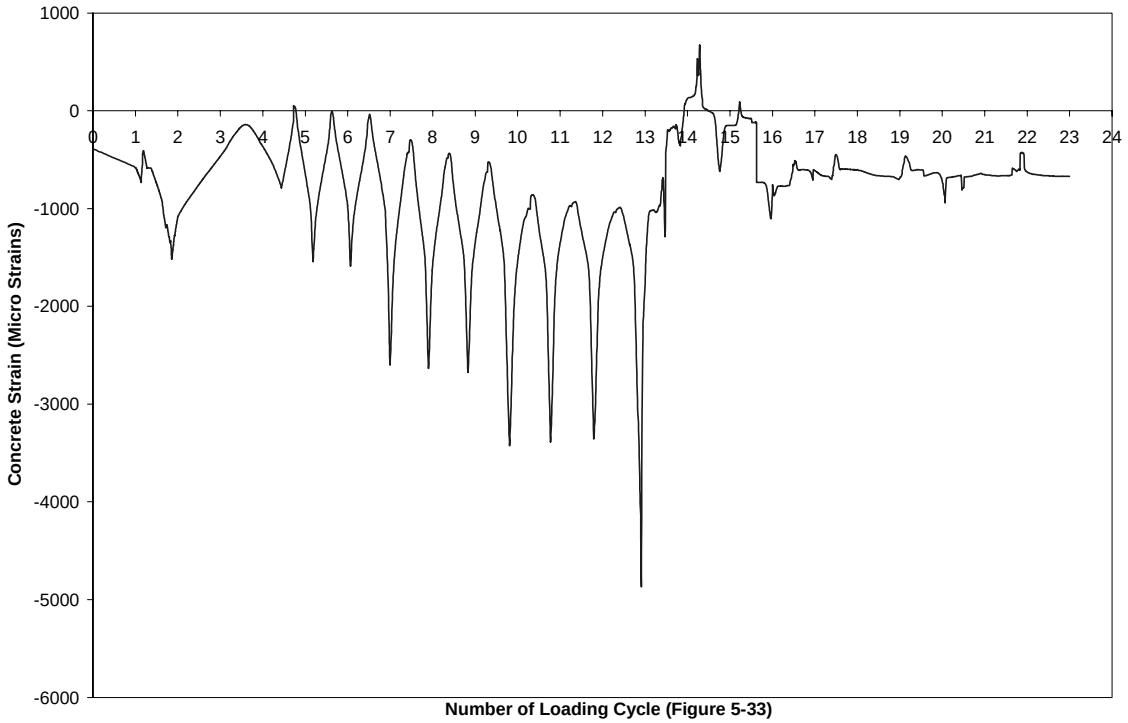


**Figure B-24 Concrete strain measured in bottom surface at Joint $J_1$ (Unit 100-INT)**

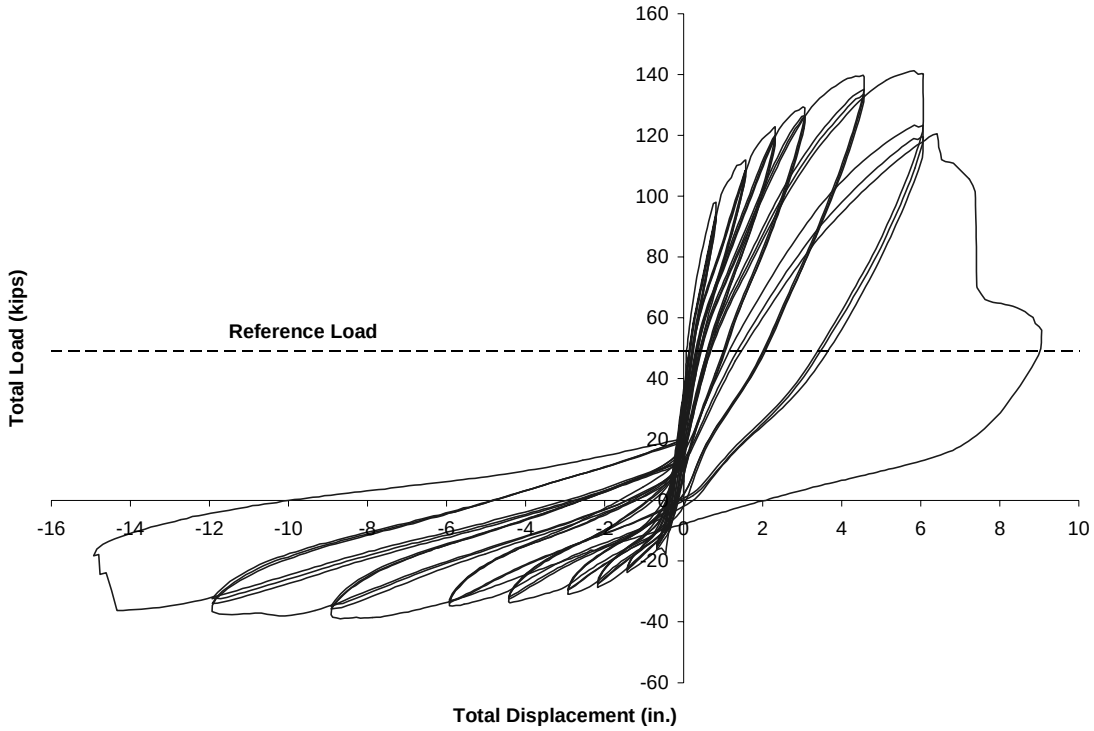


**Figure B-25 Total load versus total displacement at cantilever tip (Unit 100-INT-CIP)**

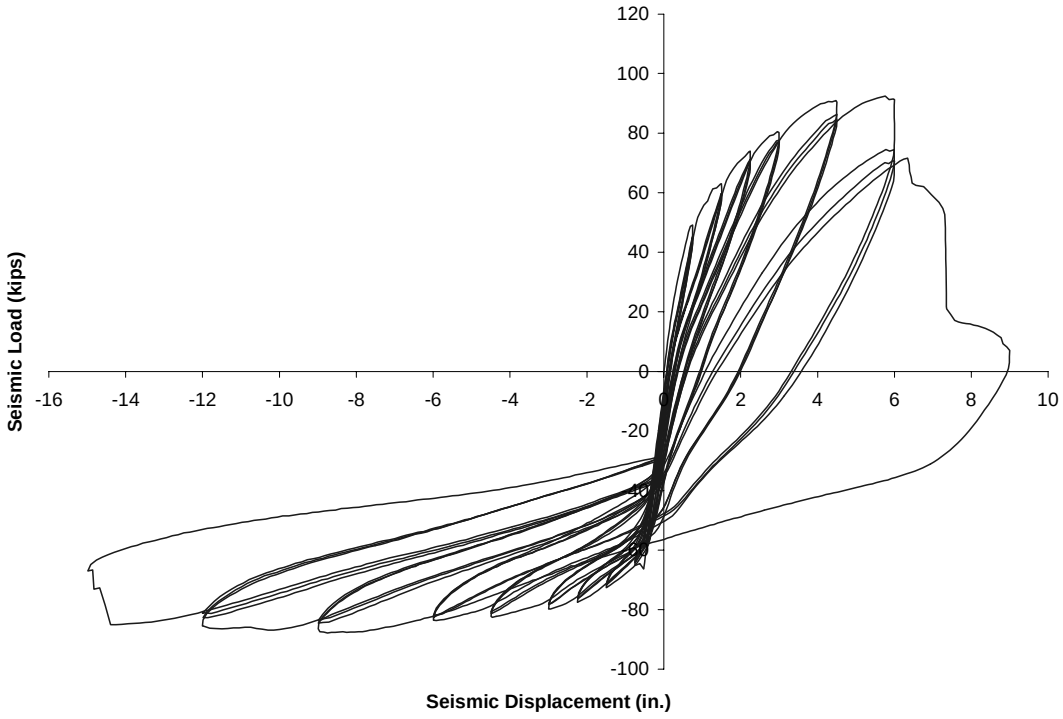


**Figure B-26 Seismic load versus seismic displacement at cantilever tip (Unit 100-INT-CIP)**

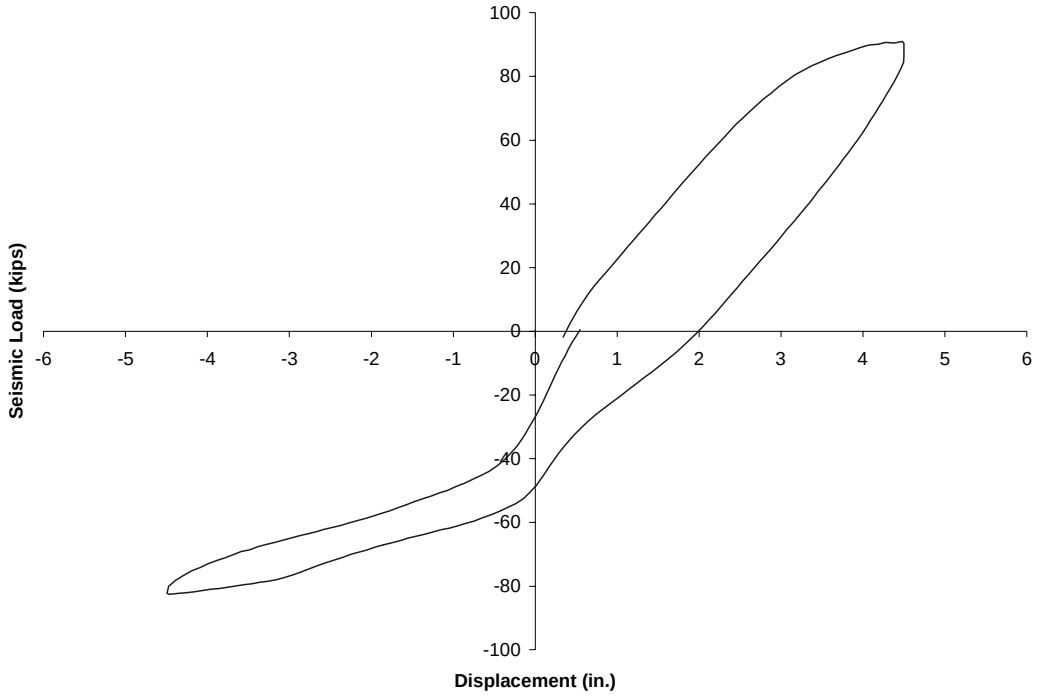


**Figure B-27 Seismic load-displacement for Unit 100-INT-CIP at 4.5 in. (114 mm)**

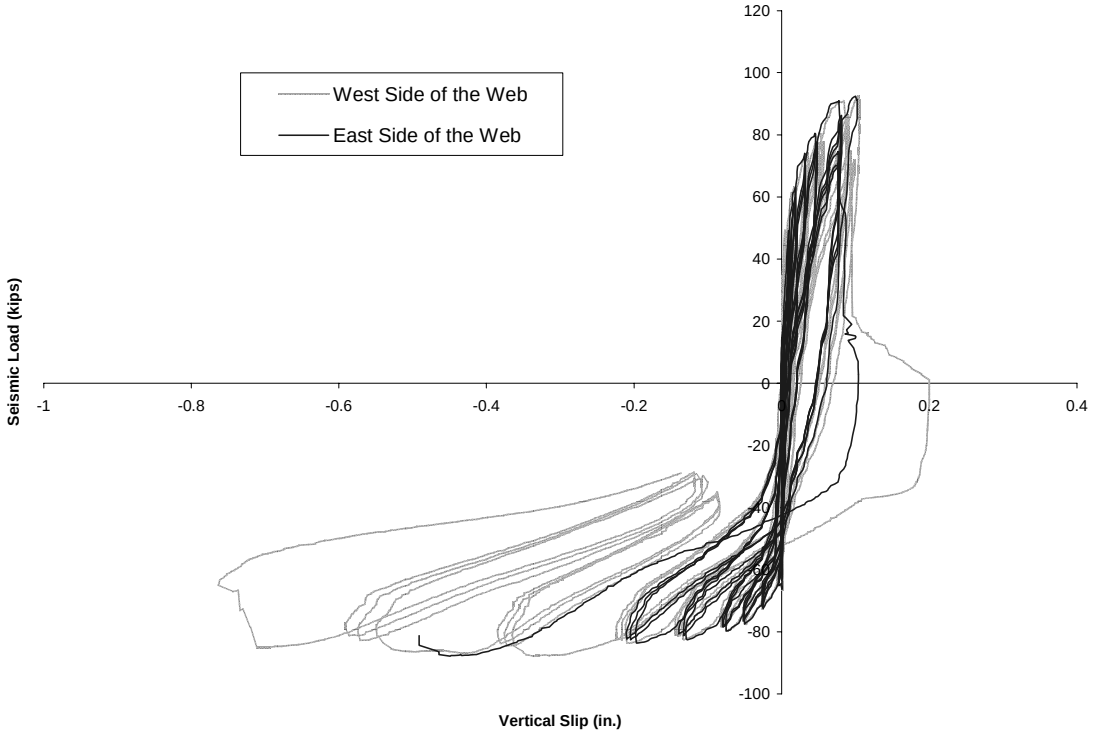


**Figure B-28 Load versus vertical slip between Segments 1 and 2 (Unit 100-INT-CIP)**

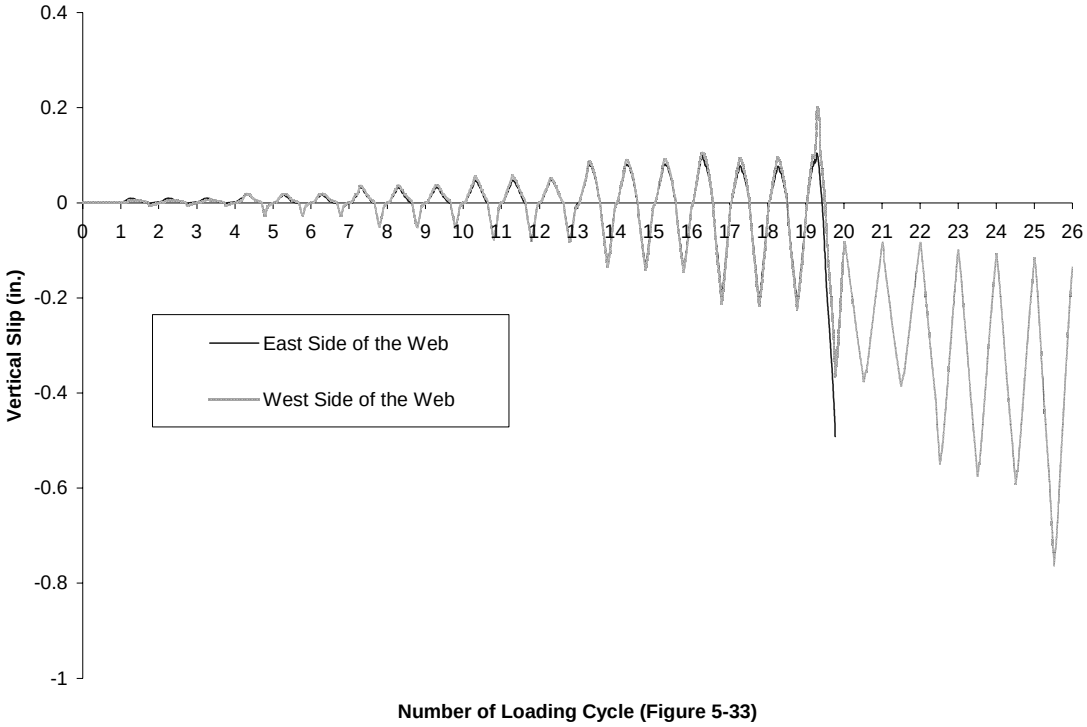


**Figure B-29 History of vertical slip between Segments 1 and 2 (Unit 100-INT-CIP)**

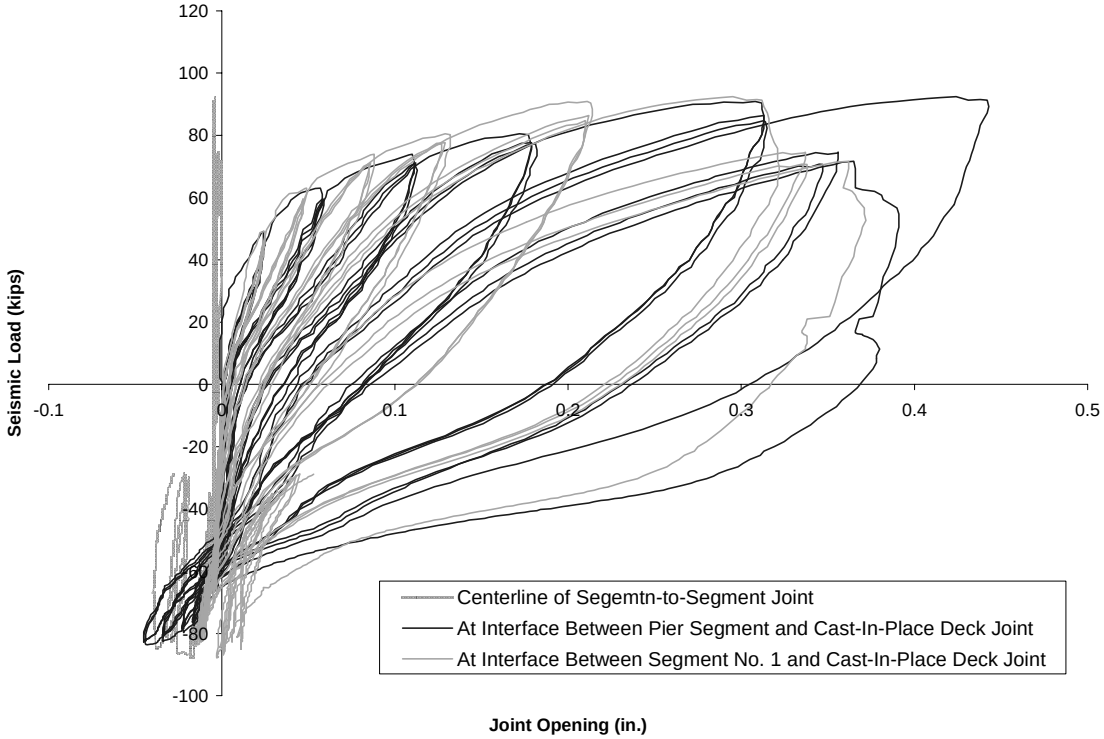


**Figure B-30 Load versus opening of Joint $J_1$ at top surface (Unit 100-INT-CIP)**

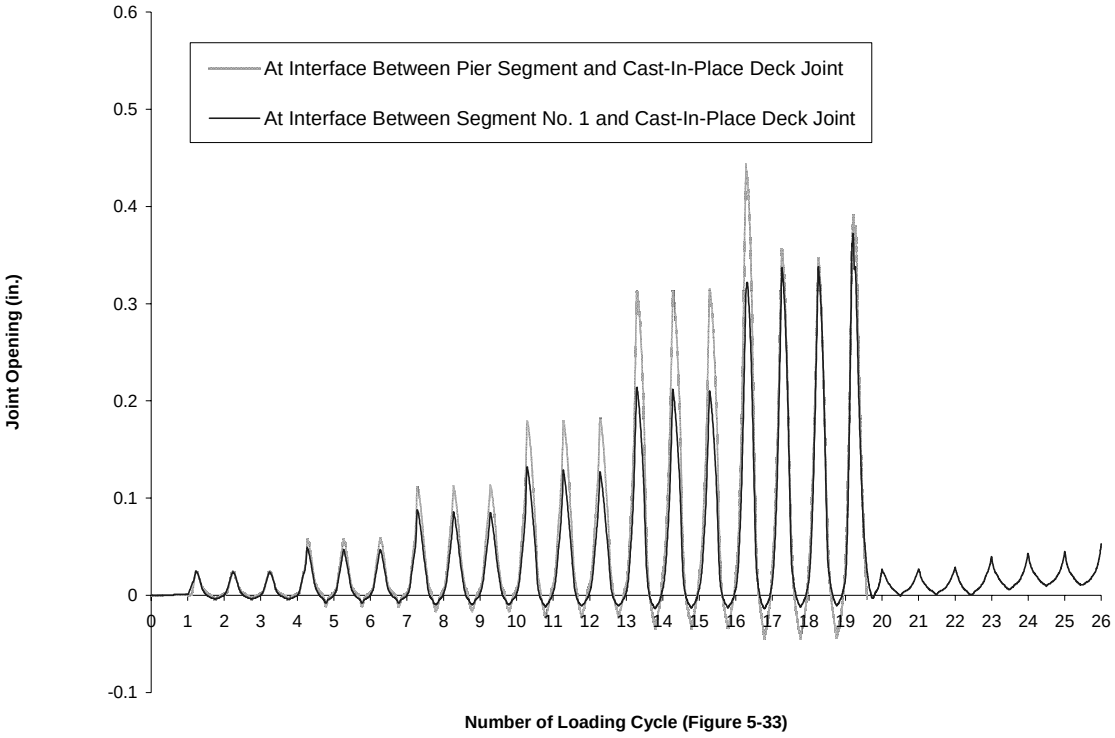


**Figure B-31 History of opening of Joint $J_1$ at top surface (Unit 100-INT-CIP)**

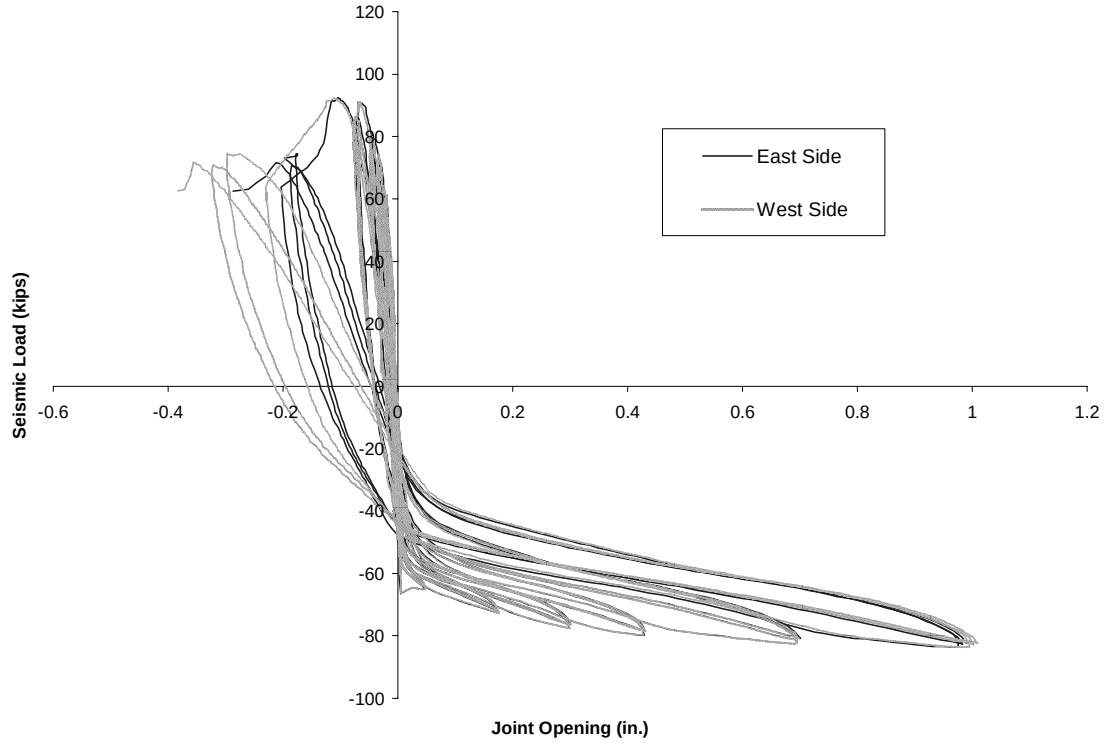


**Figure B-32 Load versus opening of Joint $J_1$ at bottom surface (Unit 100-INT-CIP)**

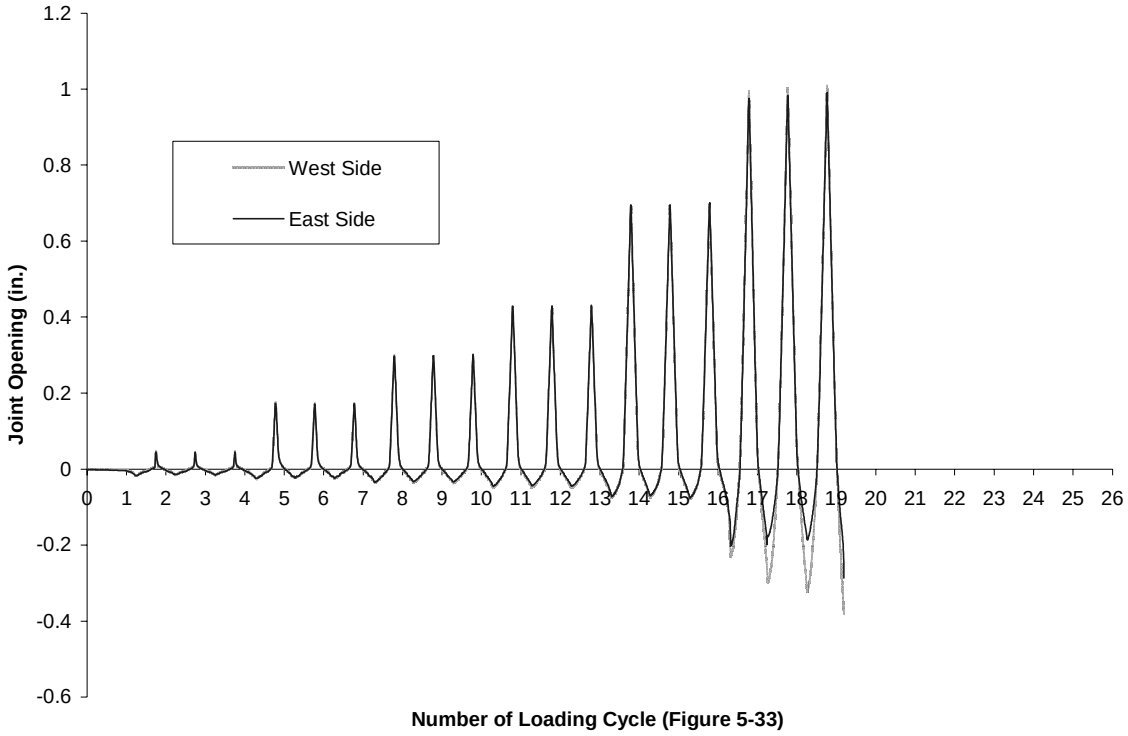


**Figure B-33 History of opening of Joint $J_1$ at bottom surface (Unit 100-INT-CIP)**

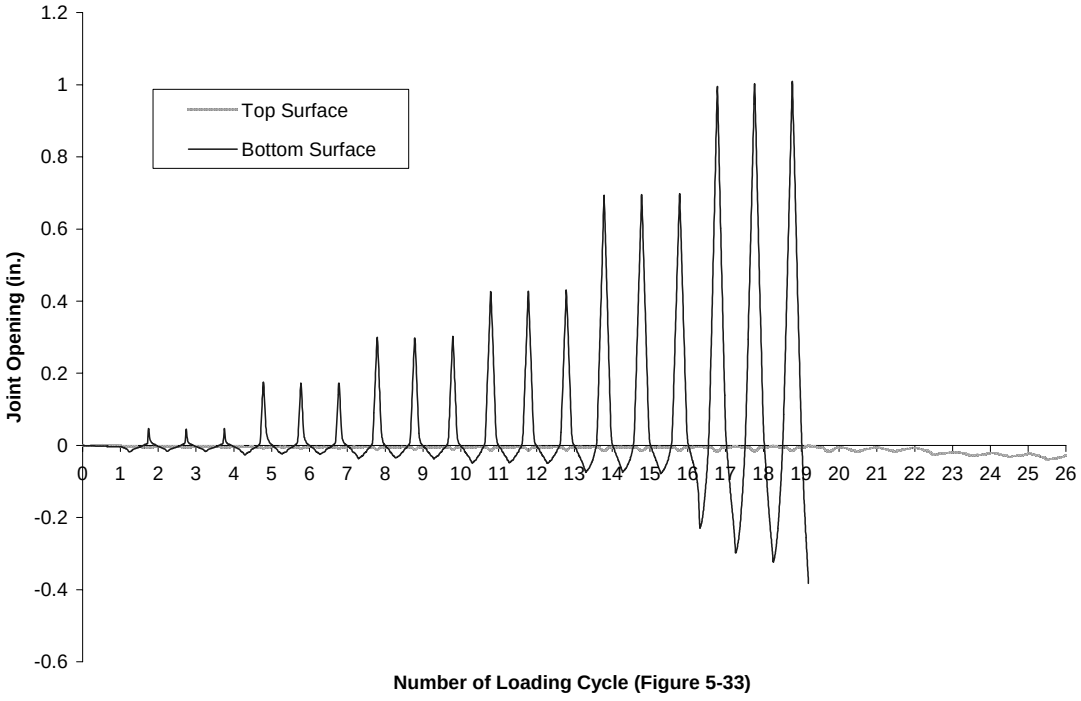


**Figure B-34 Load versus joint opening measured on the West Side of Unit 100-INT-CIP**

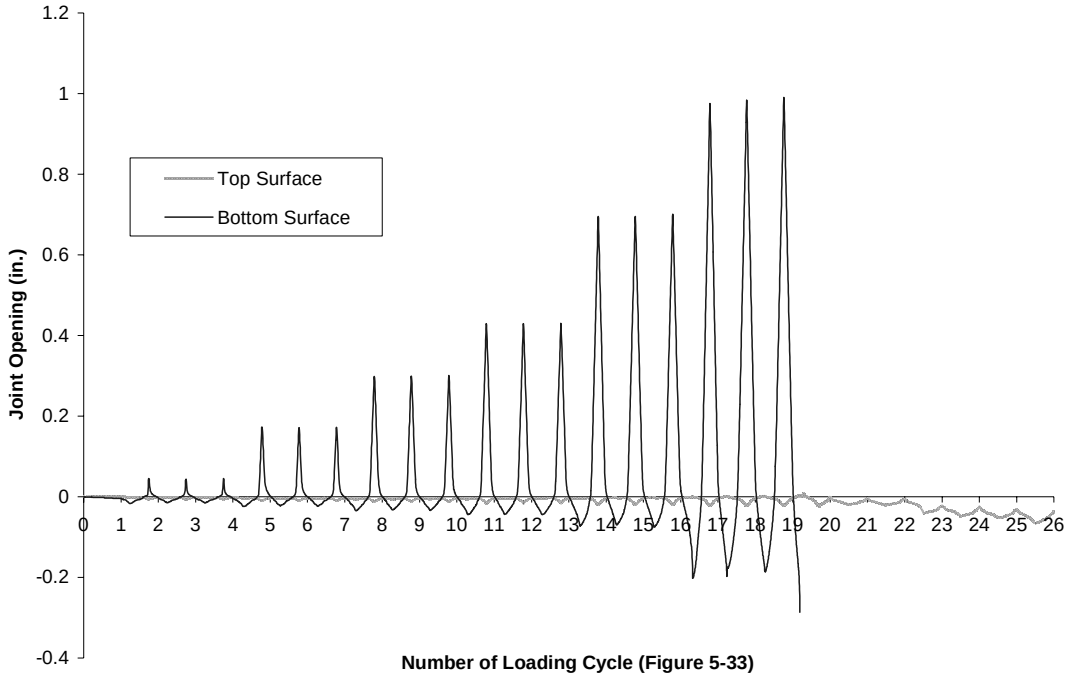


**Figure B-35 Load versus joint opening measured on the East Side of Unit 100-INT-CIP**

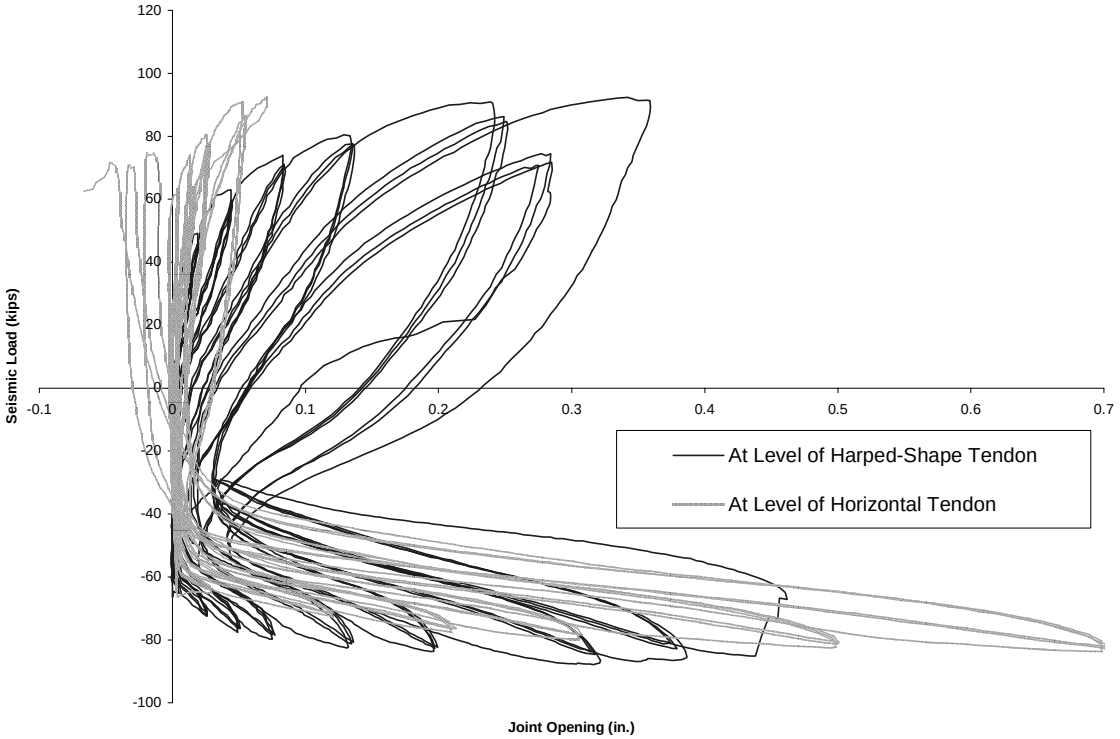


**Figure B-36 Load versus joint openings measured approximately at elevations of the prestressing tendons (Unit 100-INT-CIP)**

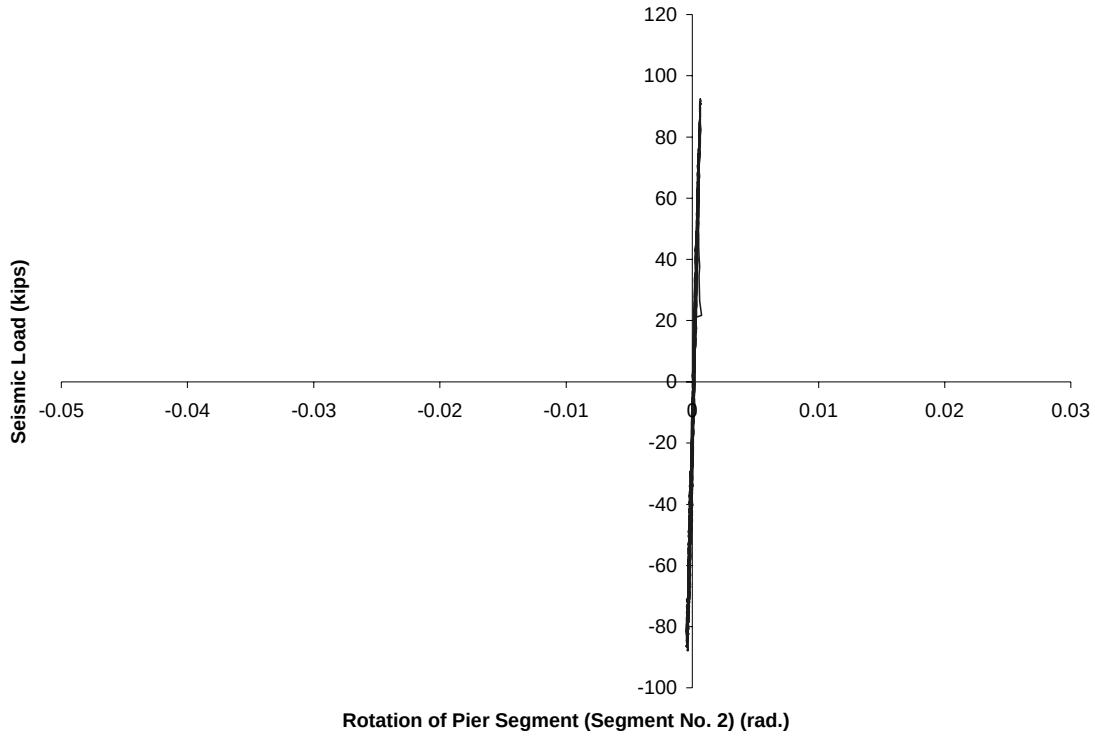


**Figure B-37 Load versus rotation of Segment No. 2 in Unit 100-INT-CIP**

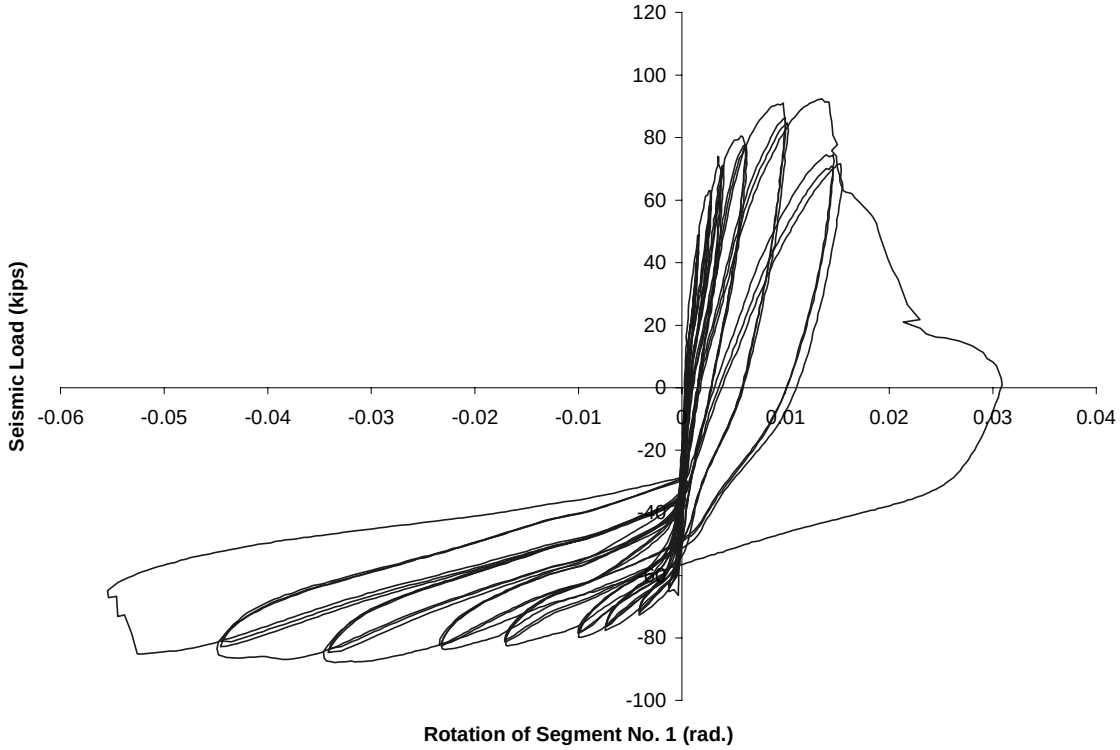


**Figure B-38 Load versus rotation of Segment No. 1 in Unit 100-INT-CIP**

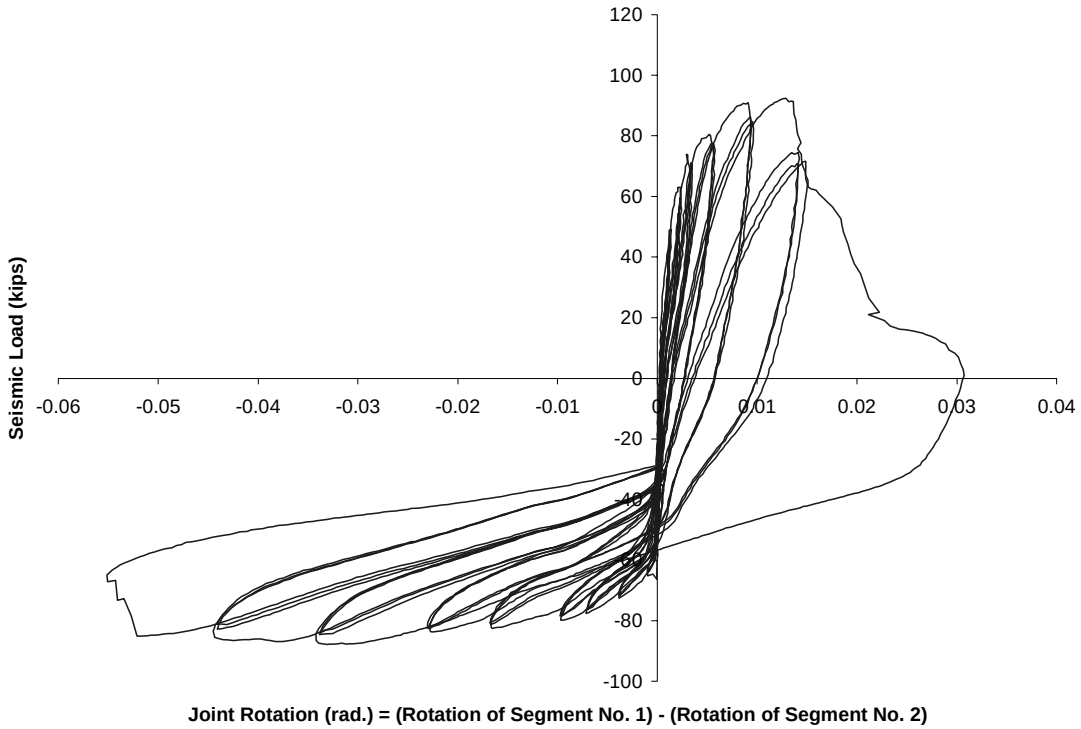


**Figure B-39 Load versus rotation of Joint $J_1$ in Unit 100-INT-CIP**

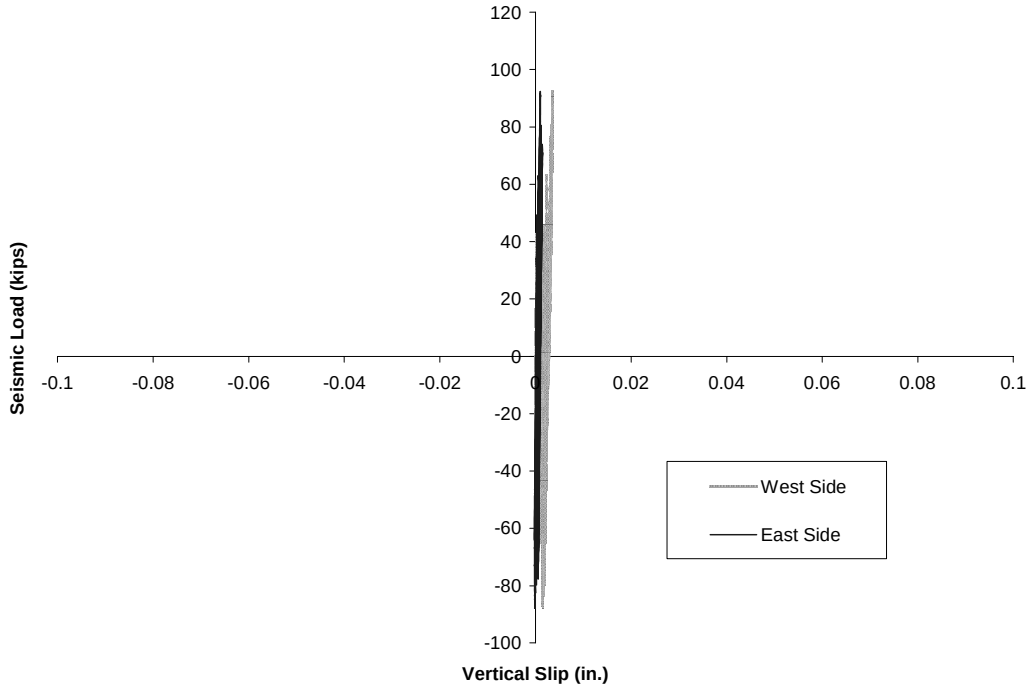


**Figure B-40 Vertical slip between Test Unit 100-INT-CIP and the steel loading beam**

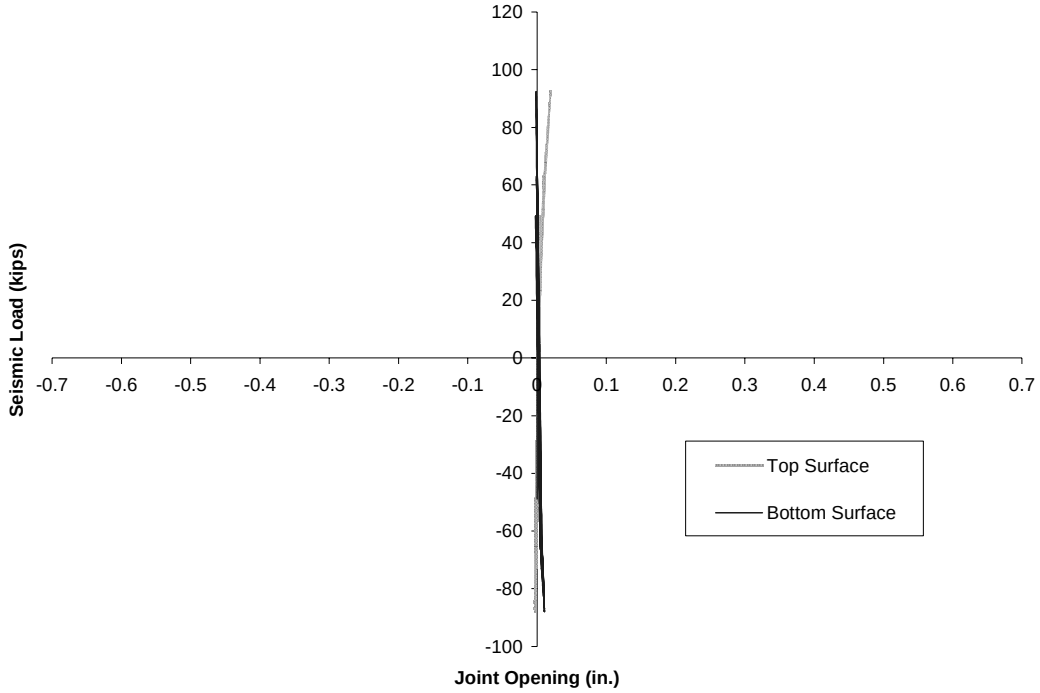


**Figure B-41 Opening of the joint between Test Unit 100-INT-CIP and the steel loading beam**

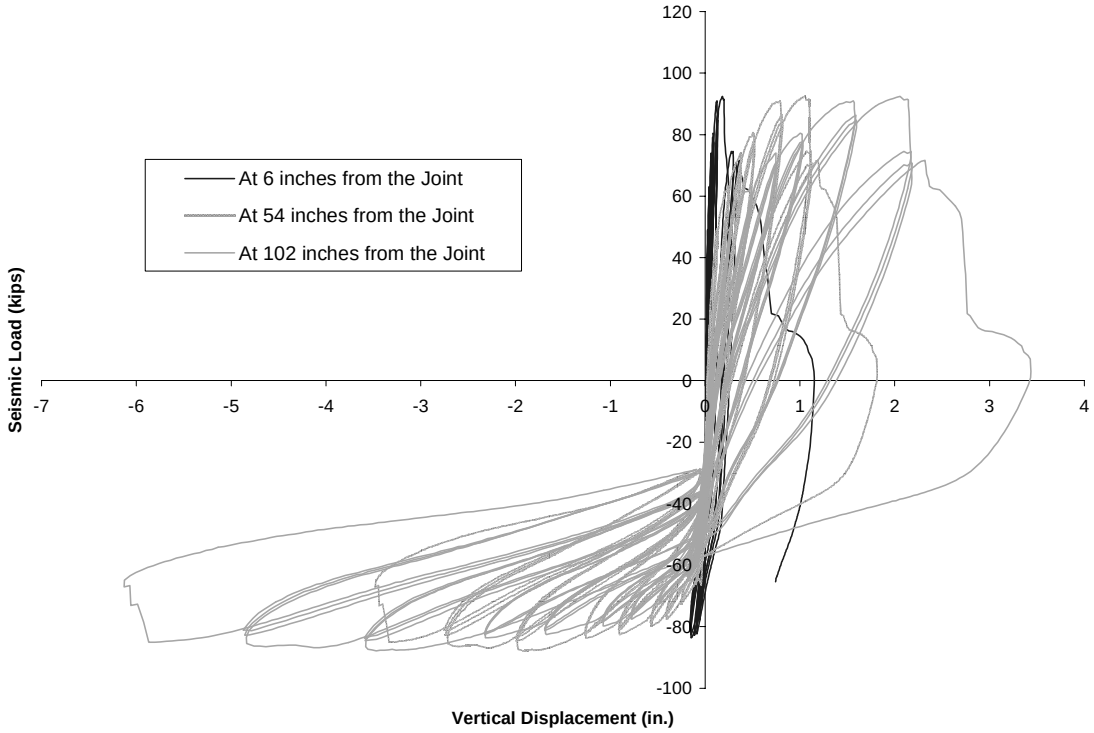


**Figure B-42 Load versus vertical displacement at different sections in Unit 100-INT-CIP**

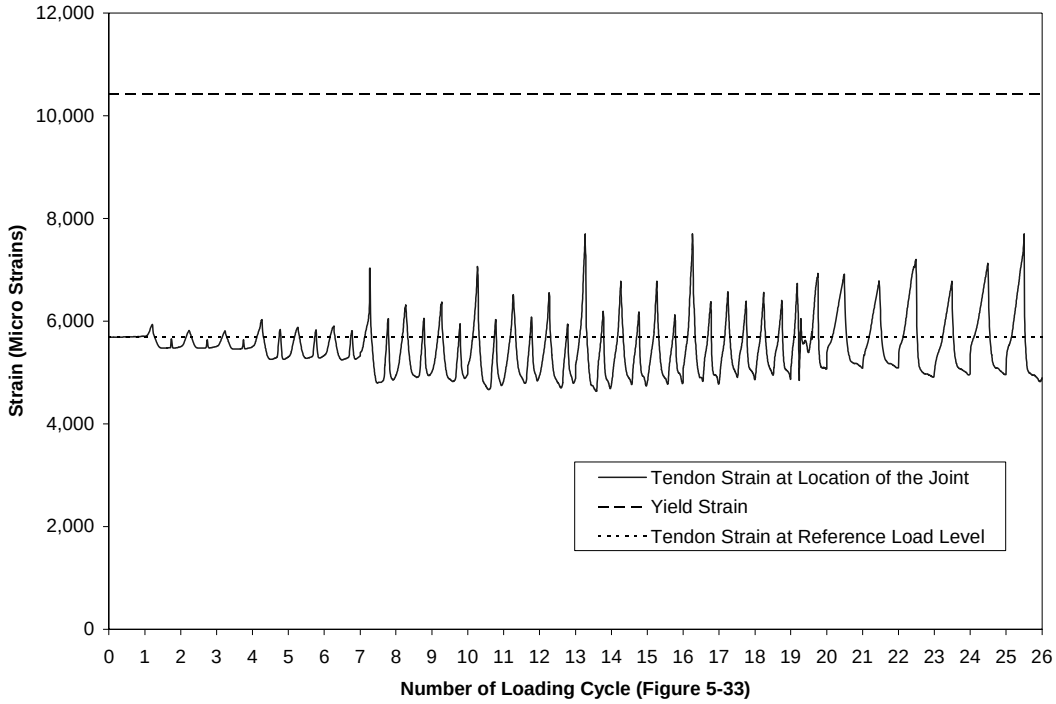


**Figure B-43 Strain in upper tendon of Unit 100-INT-CIP at Section A (see Figure 5-29)**

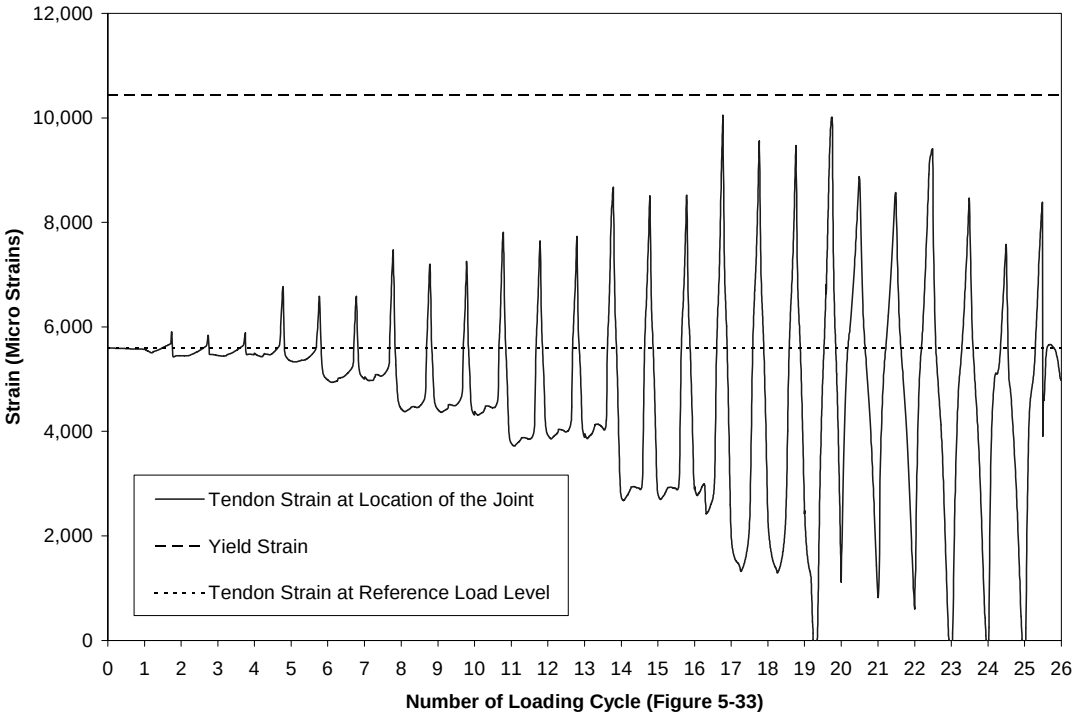


**Figure B-44 Strain in lower tendon of Unit 100-INT-CIP at Section A (see Figure 5-29)**

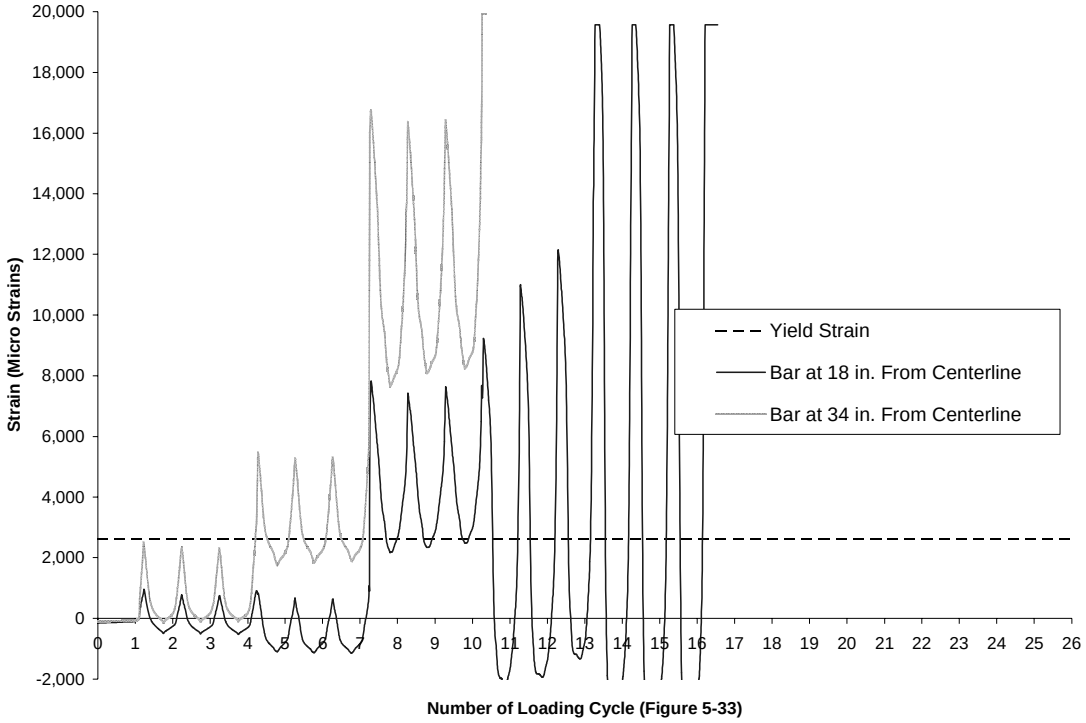


**Figure B-45 Strain in top layer of deck mild reinforcement of Unit 100-INT-CIP at Section E (see Figure 5-30)**

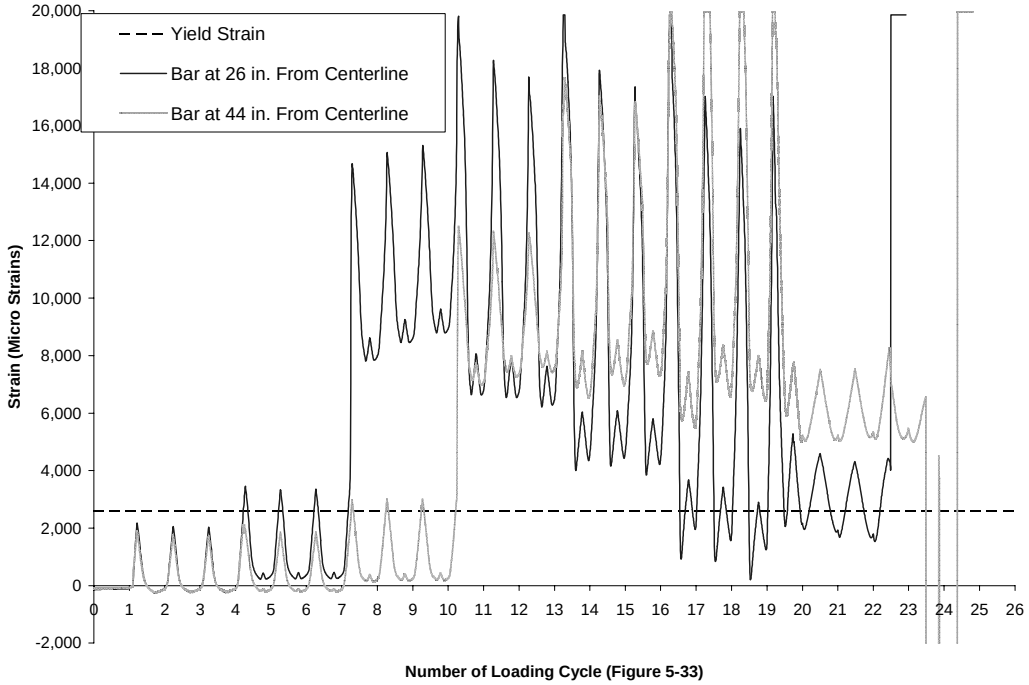


**Figure B-46 Strain in bottom layer of deck mild reinforcement of Unit 100-INT-CIP at Section E (see Figure 5-30)**

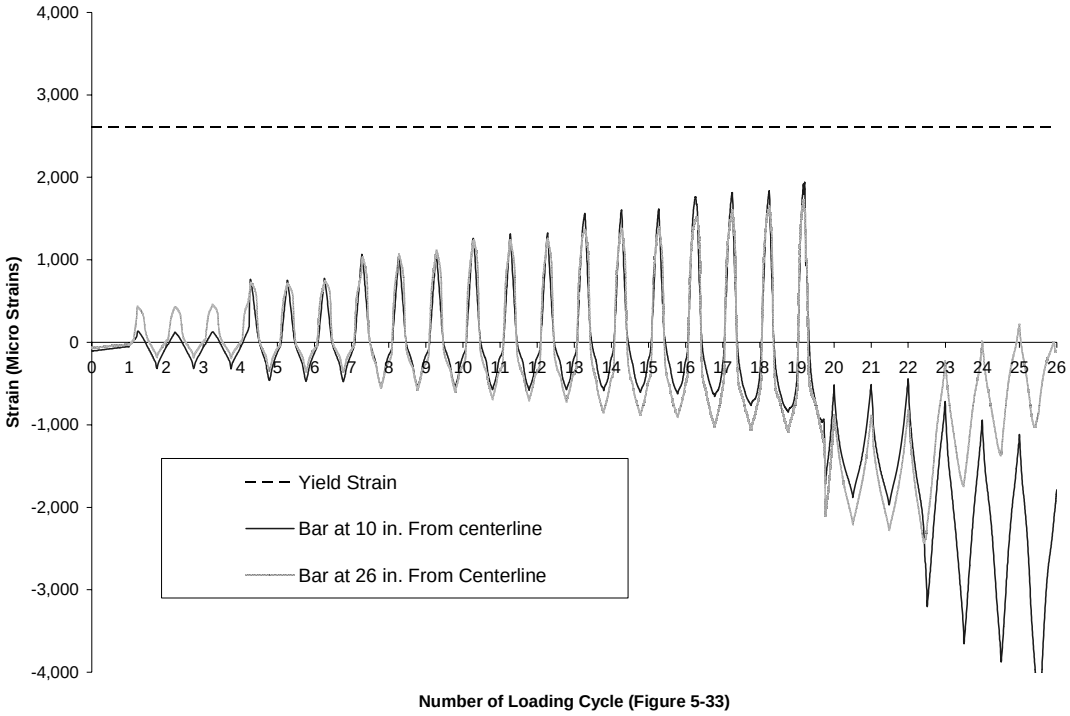


**Figure B-47 Strain in top layer of deck mild reinforcement of Unit 100-INT-CIP at Section F (see Figure 5-30)**

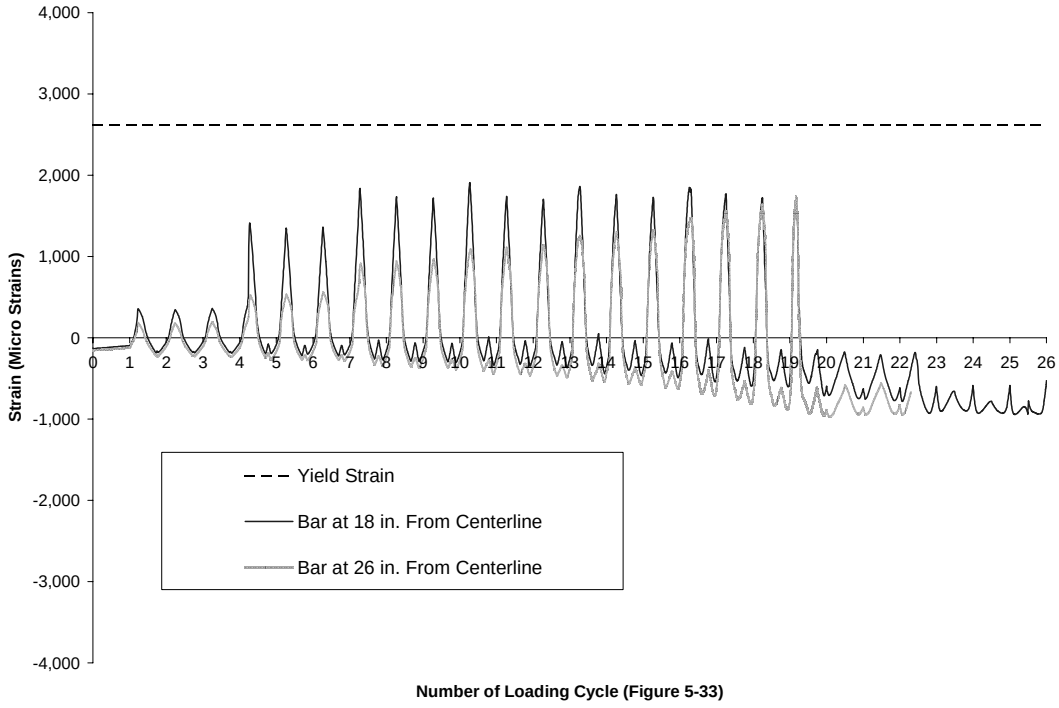


**Figure B-48 Strain in bottom layer of deck mild reinforcement of Unit 100-INT-CIP at Section F (see Figure 5-30)**

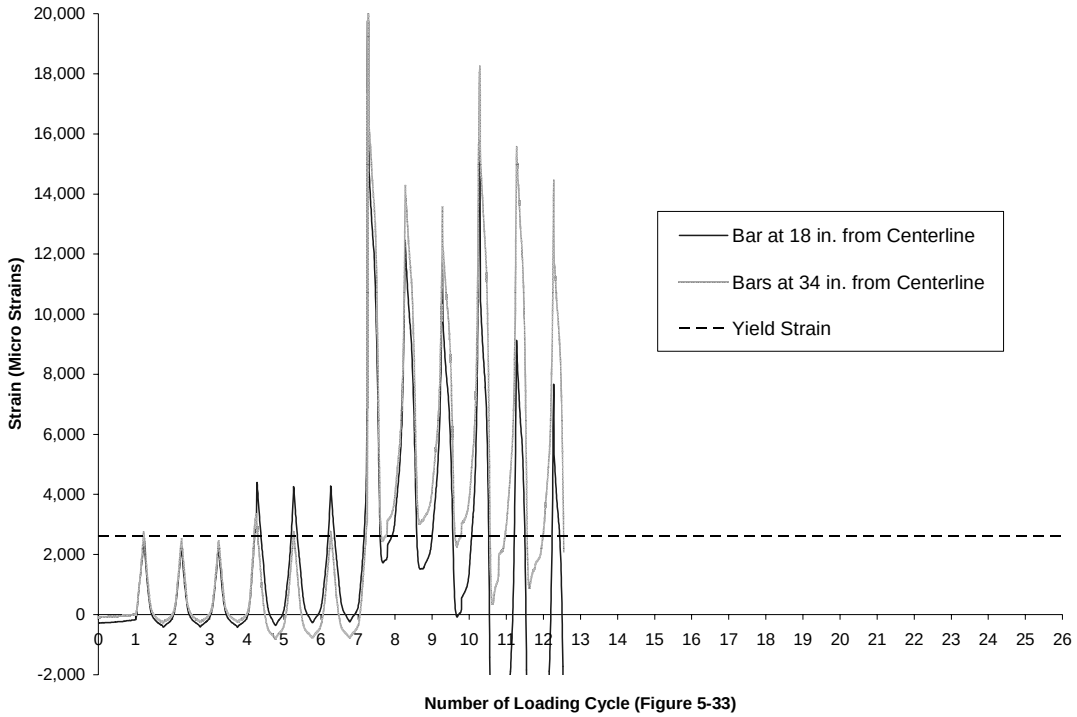


**Figure B-49 Strain in top layer of deck mild reinforcement of Unit 100-INT-CIP at Section G (see Figure 5-30)**

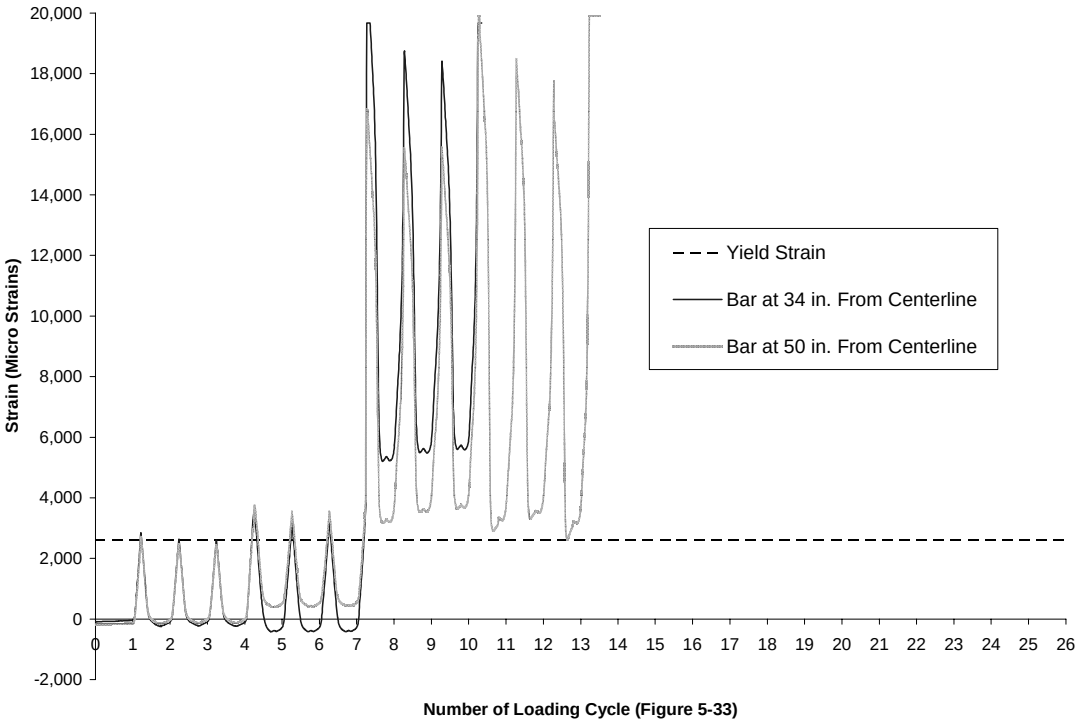


**Figure B-50 Strain in bottom layer of deck mild reinforcement of Unit 100-INT-CIP at Section G (see Figure 5-30)**

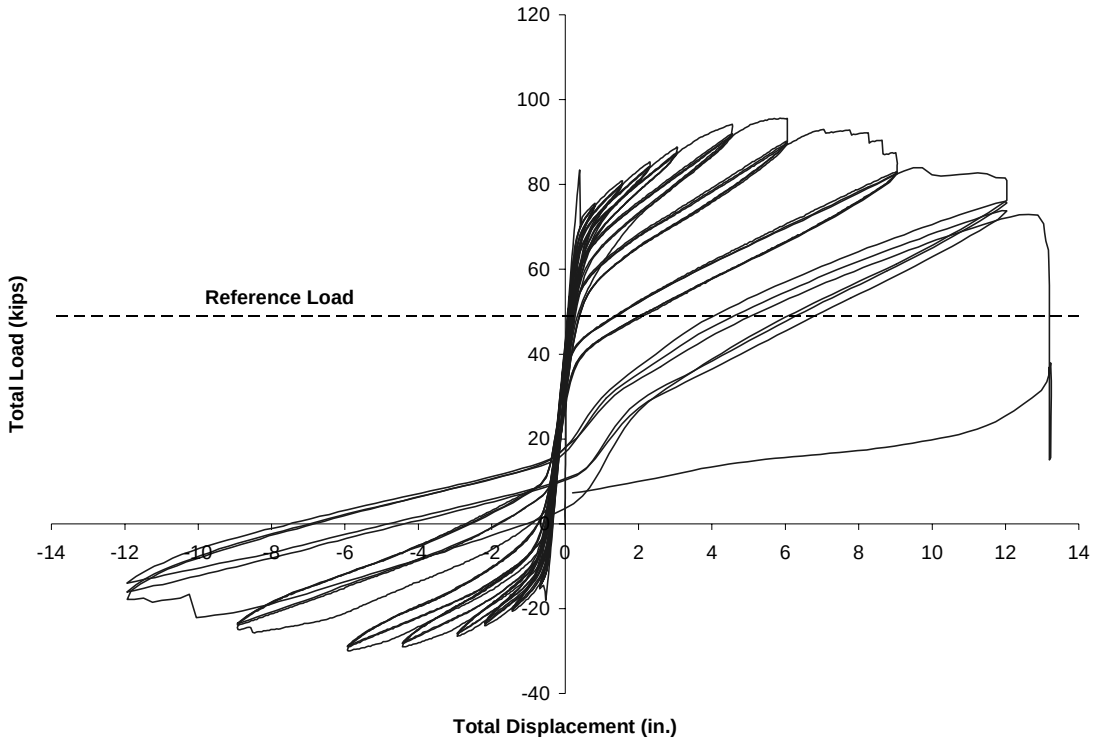


**Figure B-51 Total load versus total displacement at cantilever tip (Unit 100-EXT)**

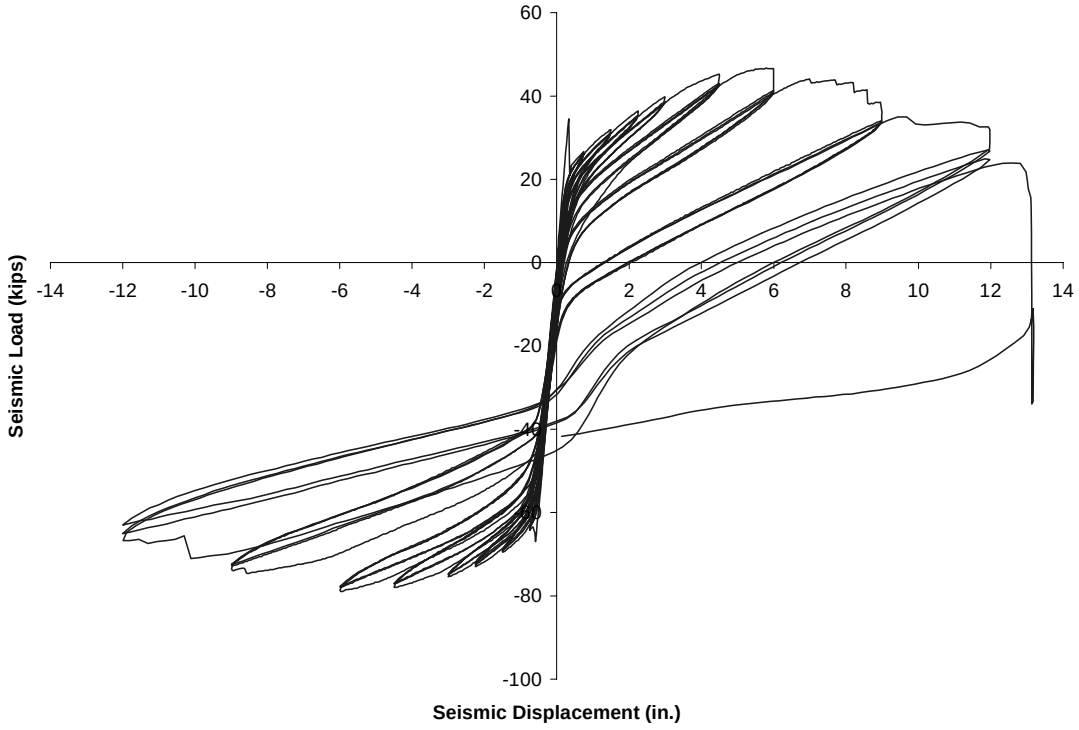


**Figure B-52 Seismic load versus seismic displacement at cantilever tip (Unit 100-EXT)**

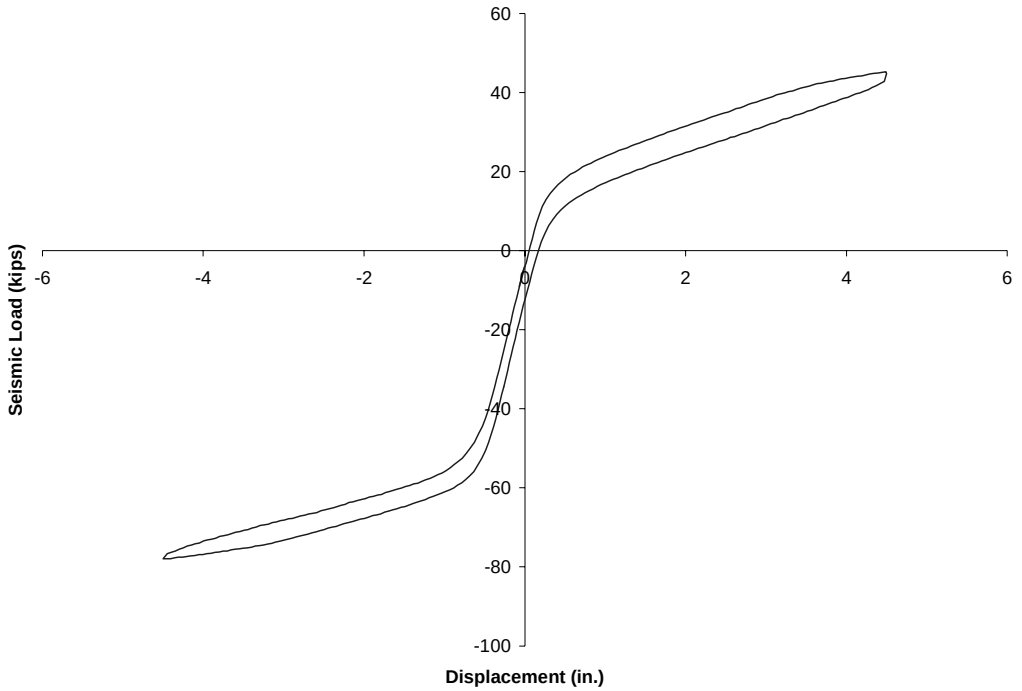


**Figure B-53 Seismic load-displacement for Unit 100-EXT at 4.5 in. (114 mm)**

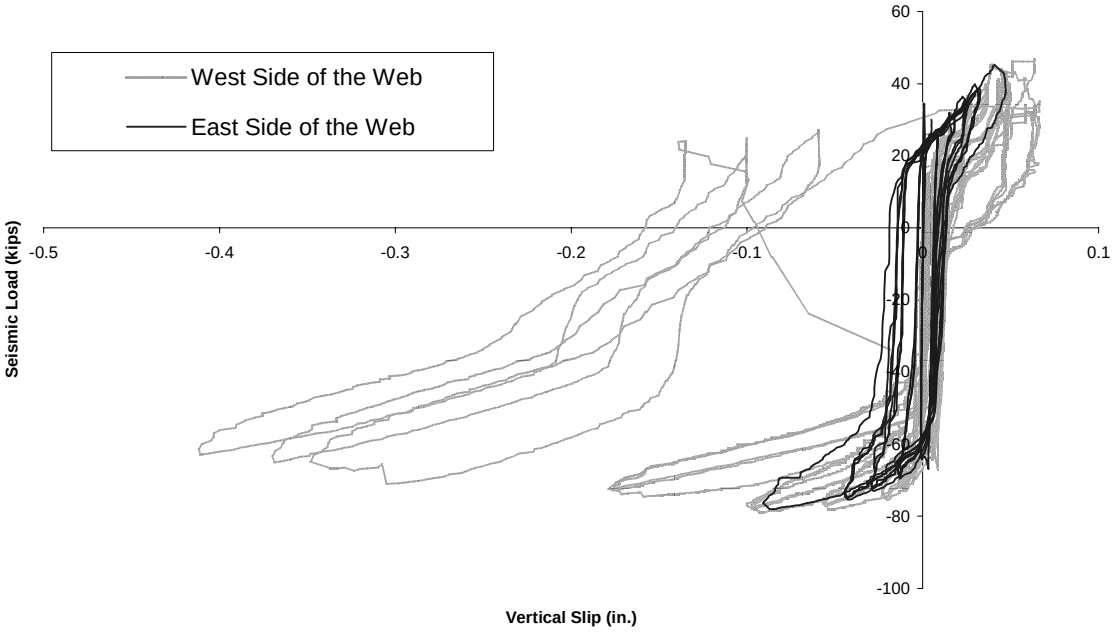


**Figure B-54 Load versus vertical slip between Segments 1 and 2 (Unit 100-EXT)**

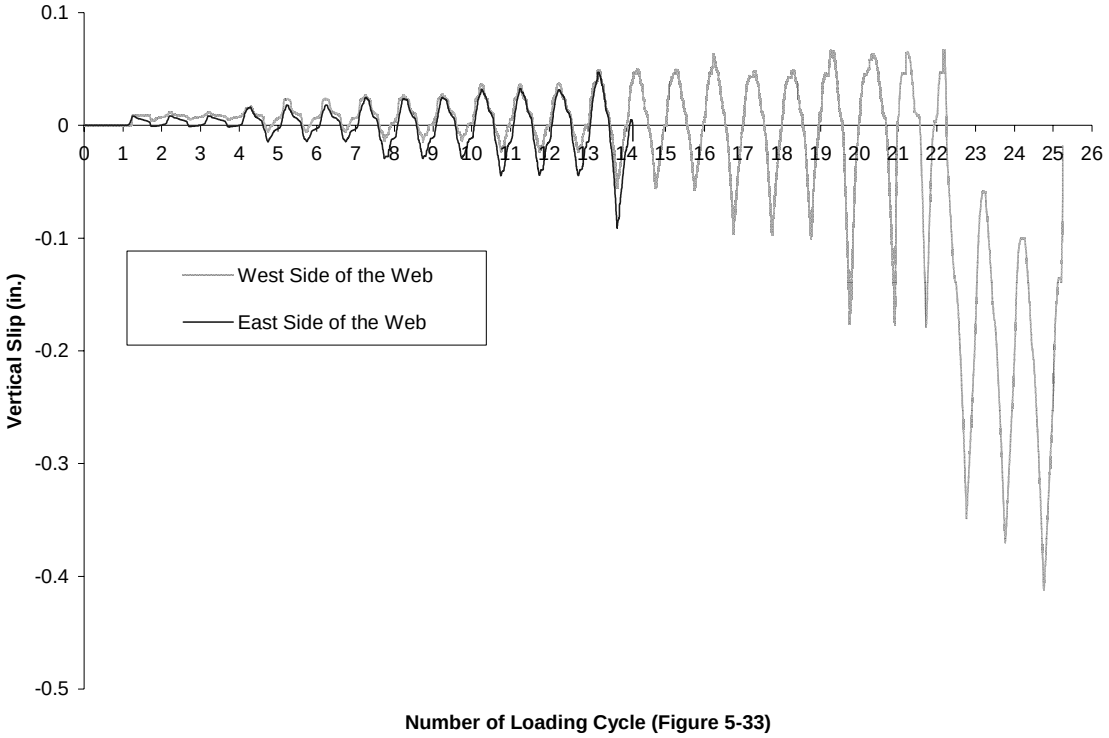


**Figure B-55 History of vertical slip between Segments 1 and 2 (Unit 100-EXT)**

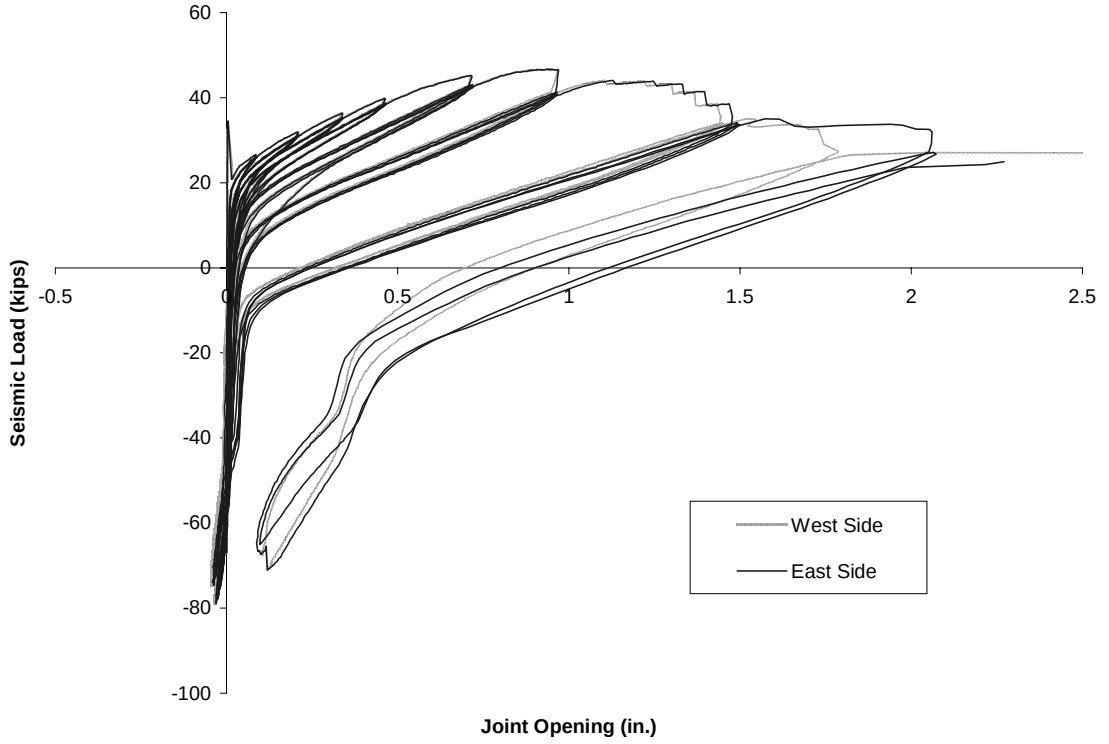


**Figure B-56 Load versus opening of Joint $J_1$ at top surface (Unit 100-EXT)**

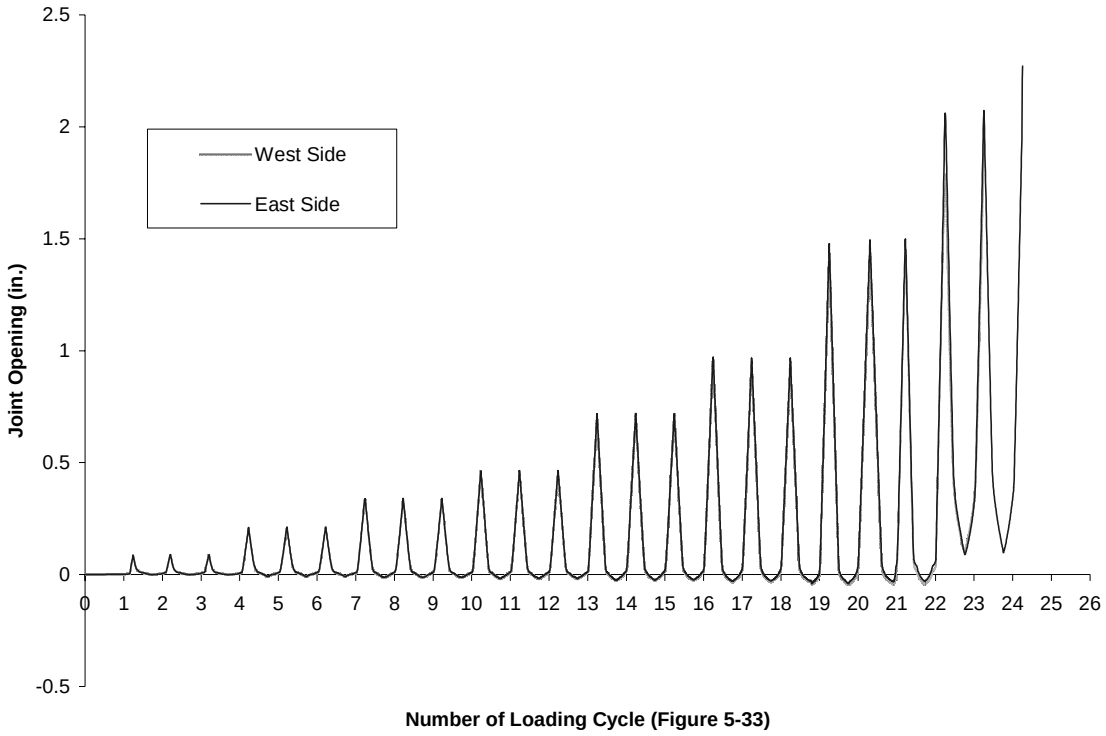


**Figure B-57 History of opening of Joint $J_1$ at top surface (Unit 100-EXT)**

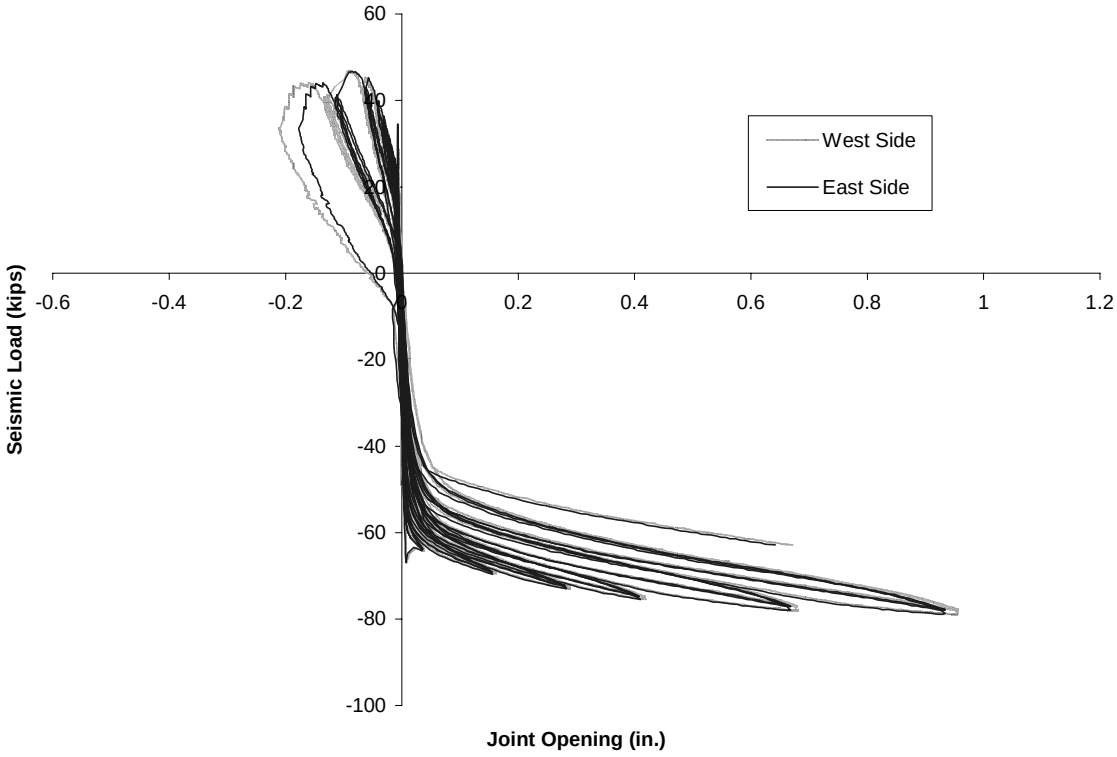


**Figure B-58 Load versus opening of Joint $J_1$ at bottom surface (Unit 100-EXT)**

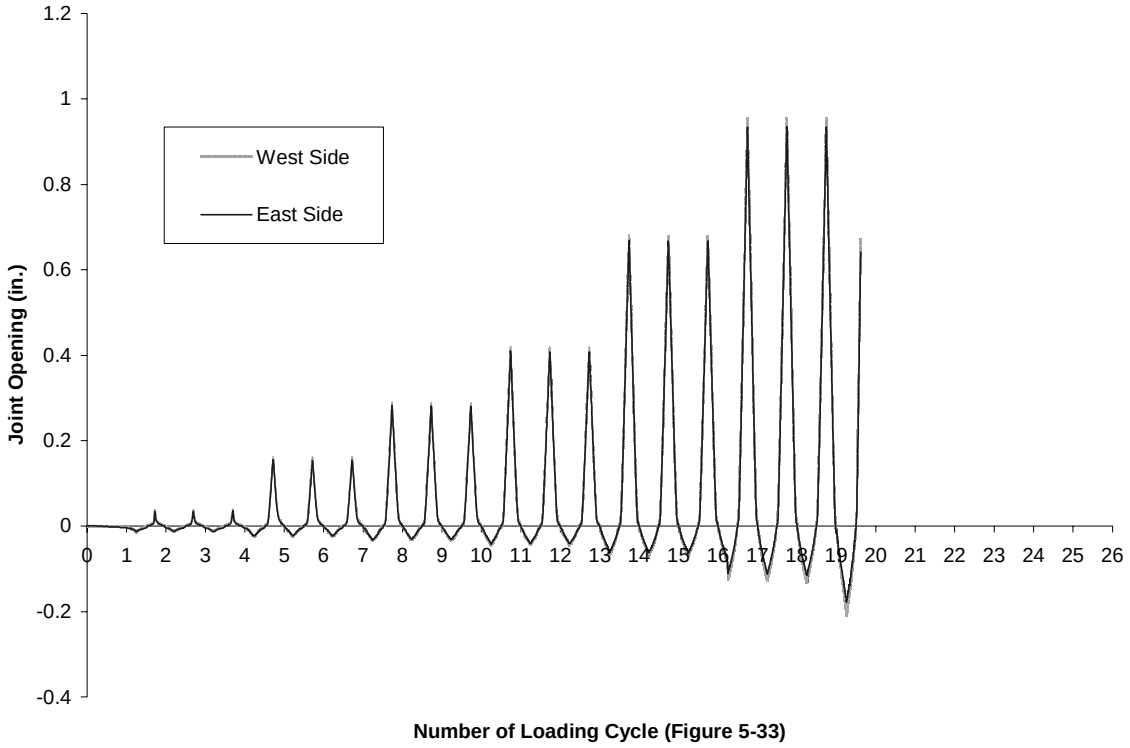


**Figure B-59 History of opening of Joint $J_1$ at bottom surface (Unit 100-EXT)**

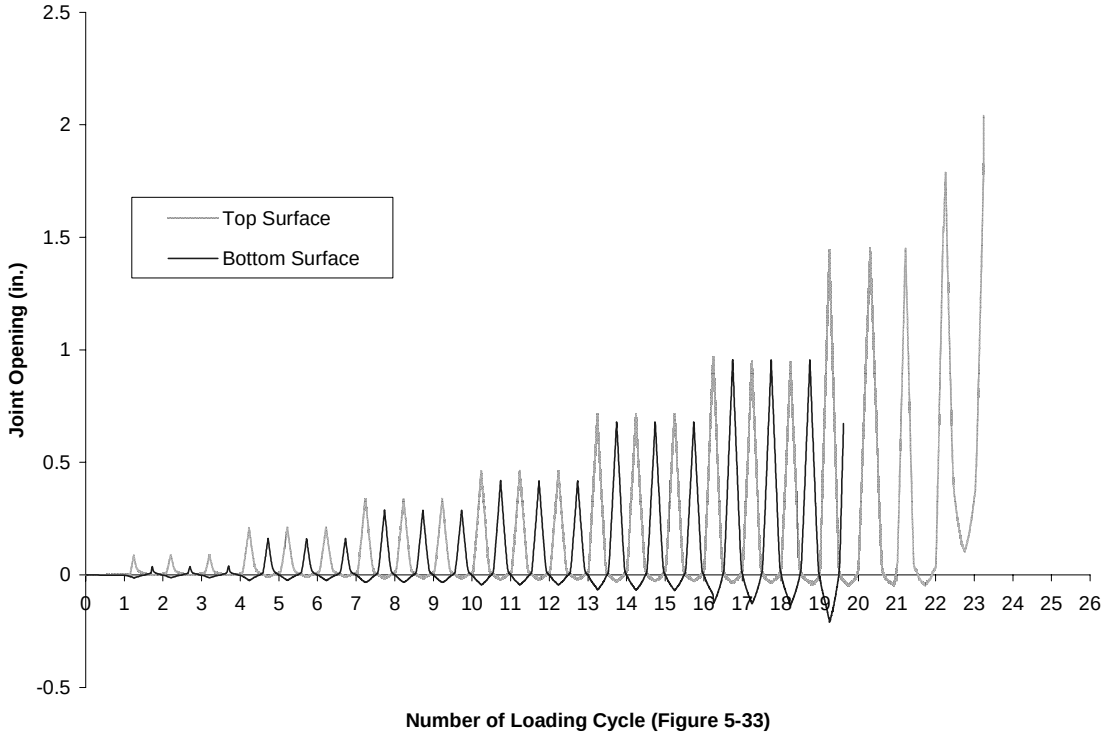


**Figure B-60 Load versus joint opening measured on the West Side of Unit 100-EXT**

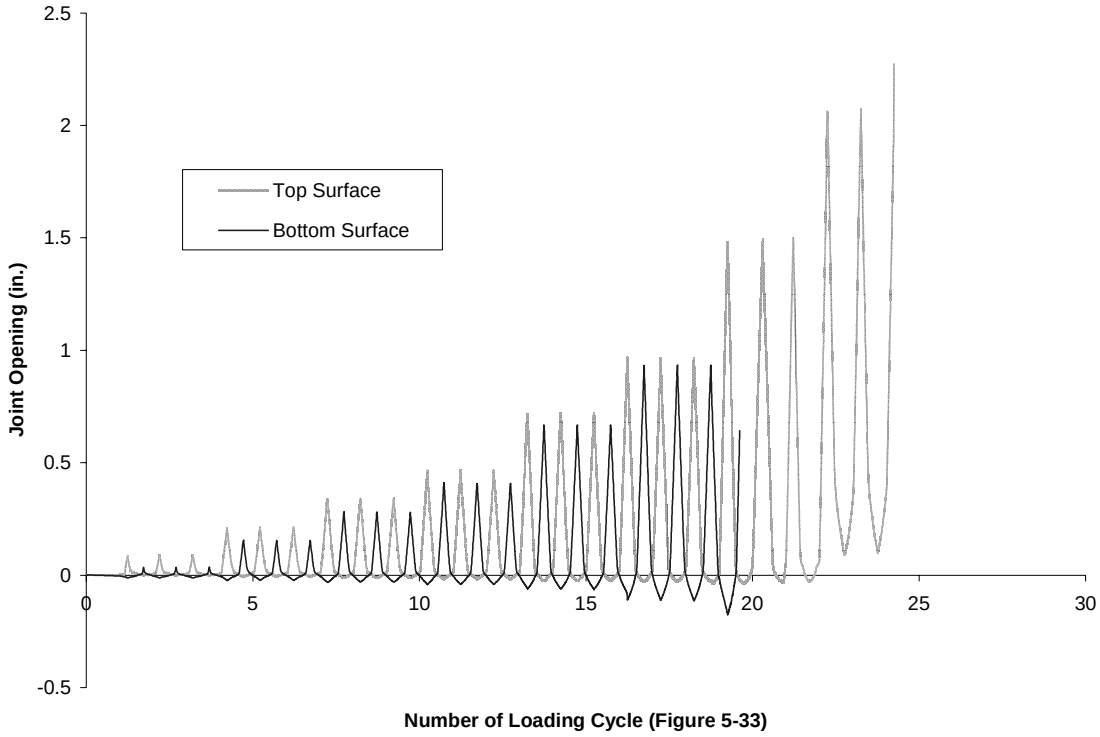


**Figure B-61 Load versus joint opening measured on the East Side of Unit 100-EXT**

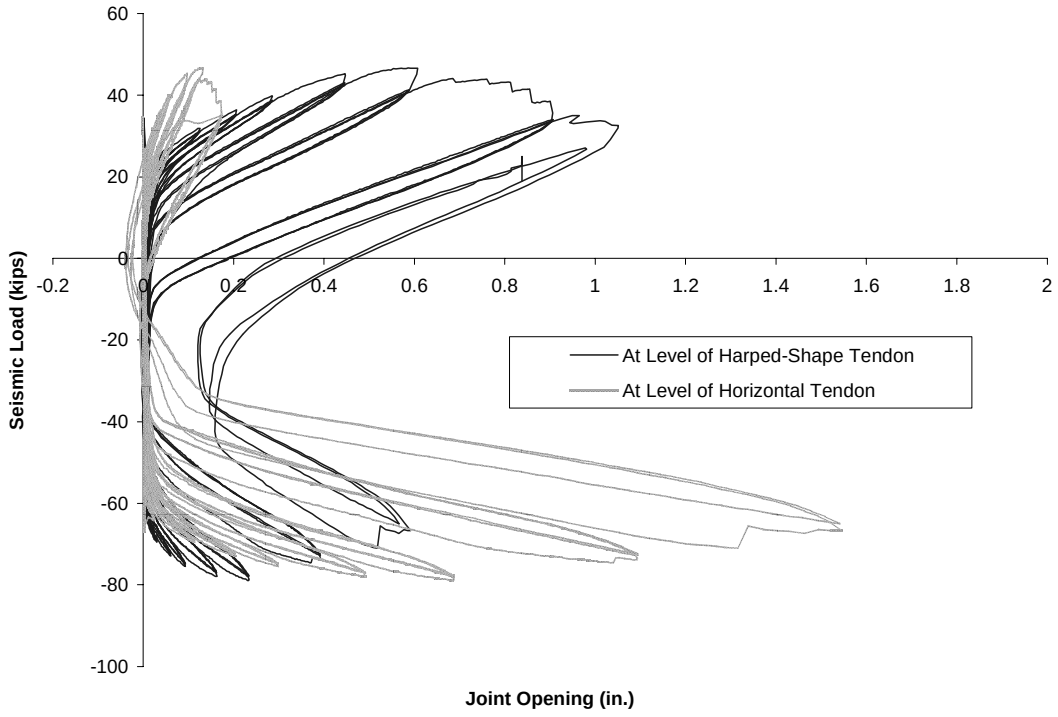


**Figure B-62 Load versus joint openings measured approximately at elevations of the prestressing tendons (Unit 100-EXT)**

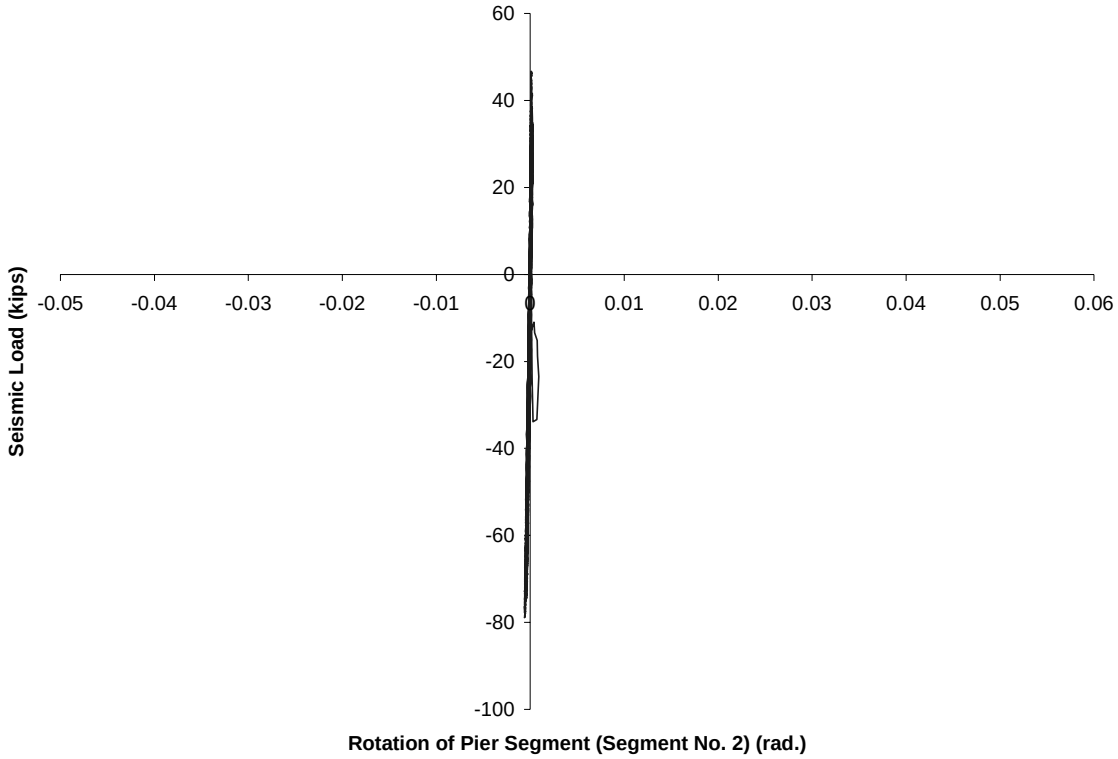


**Figure B-63 Load versus rotation of Segment No. 2 in Unit 100-EXT**

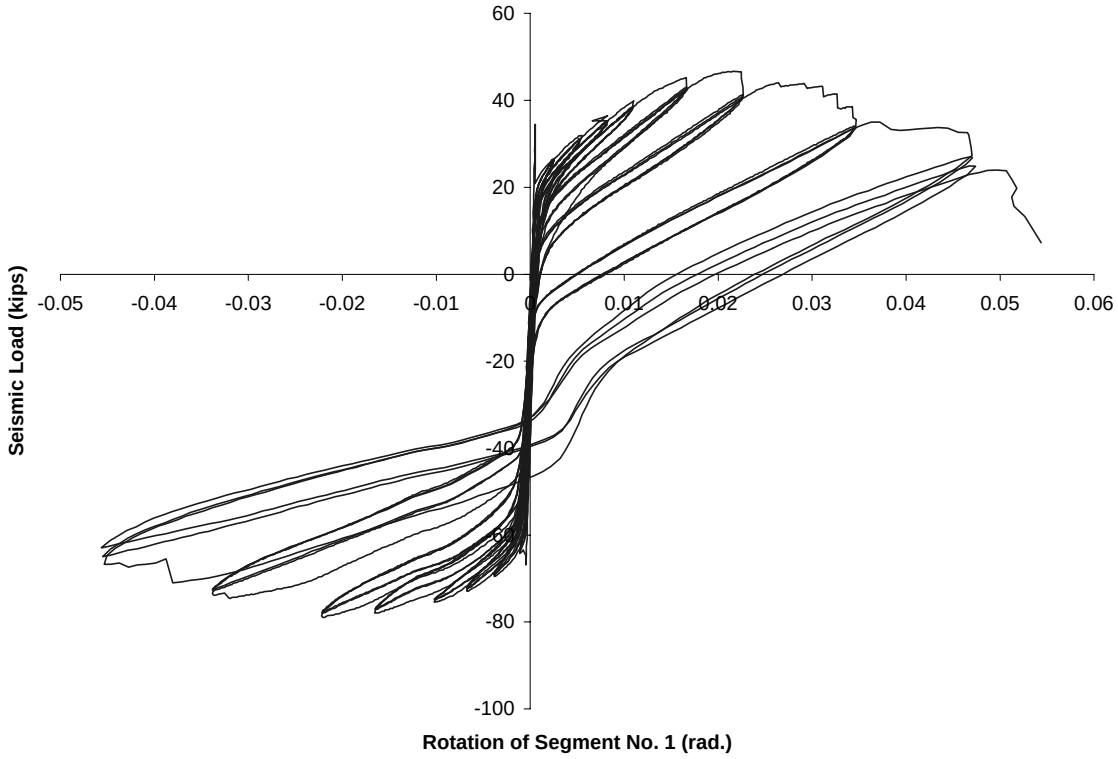


**Figure B-64 Load versus rotation of Segment No. 1 in Unit 100-EXT**

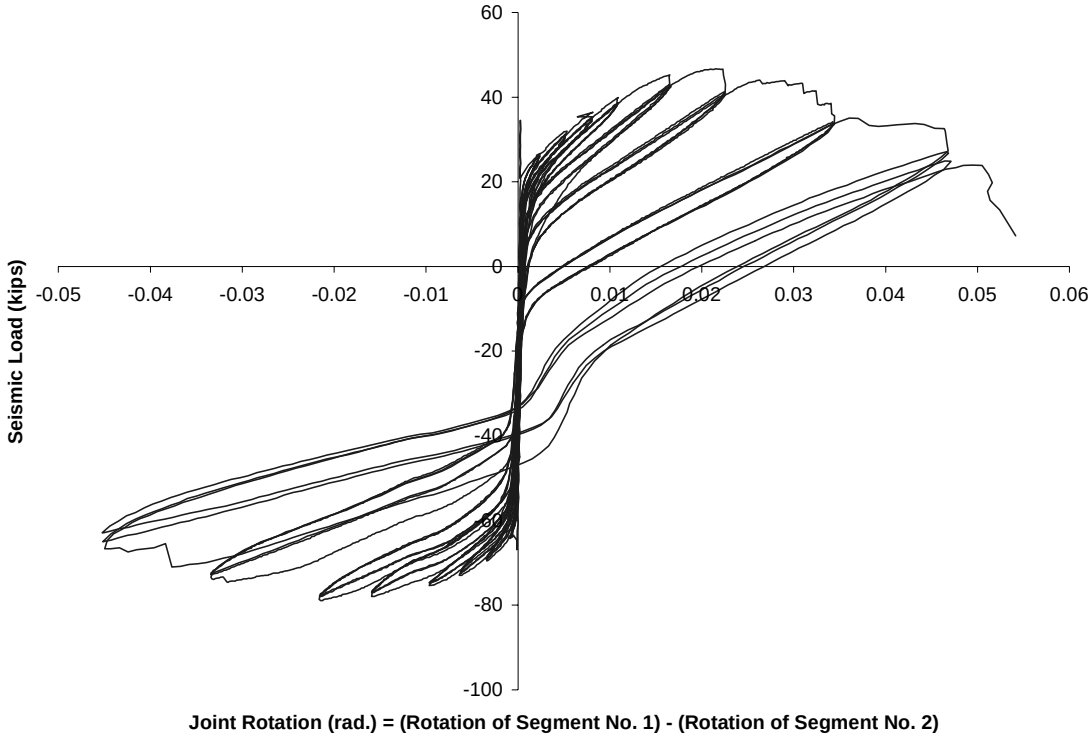


**Figure B-65 Load versus rotation of Joint $J_1$ in Unit 100-EXT**

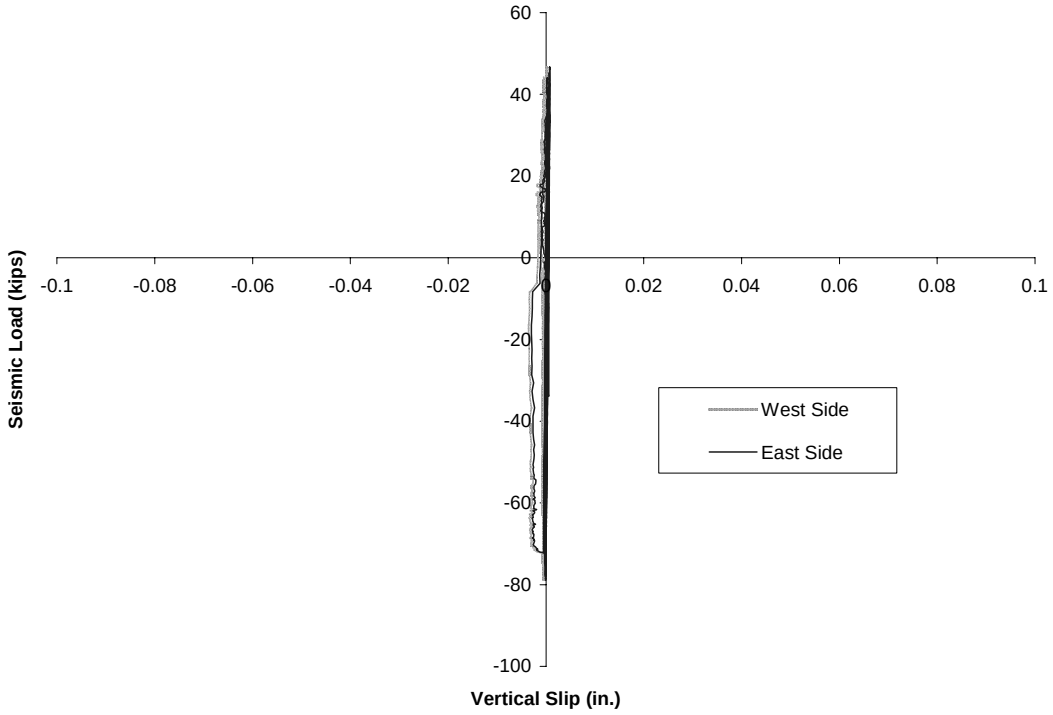


**Figure B-66 Vertical slip between Test Unit 100-EXT and the steel loading beam**

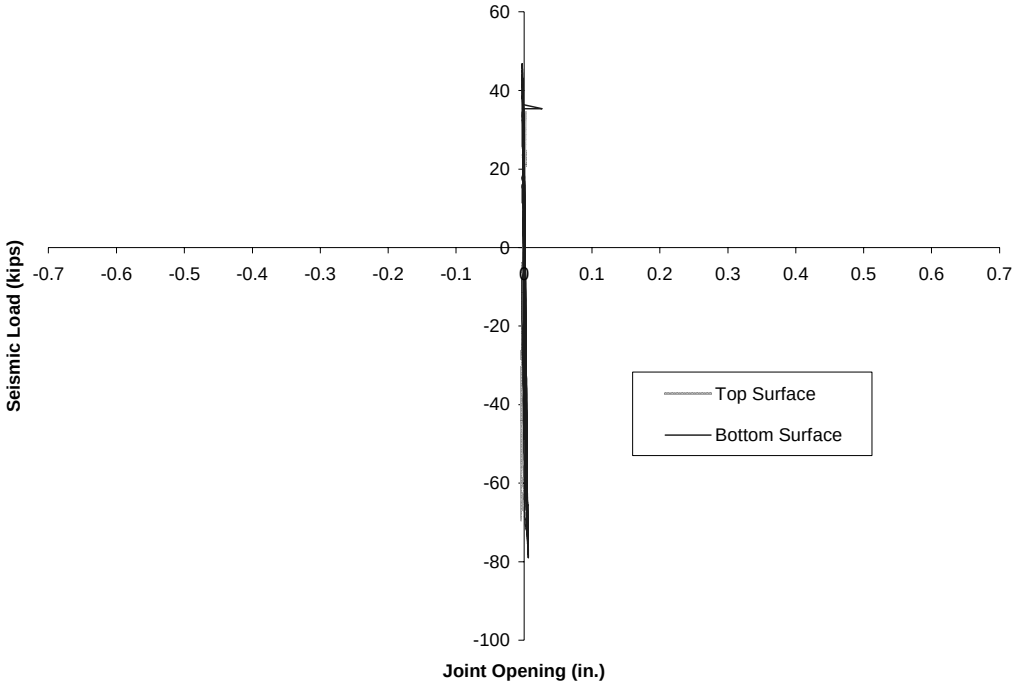


**Figure B-67 Opening of the joint between Test Unit 100-EXT and the steel loading beam**

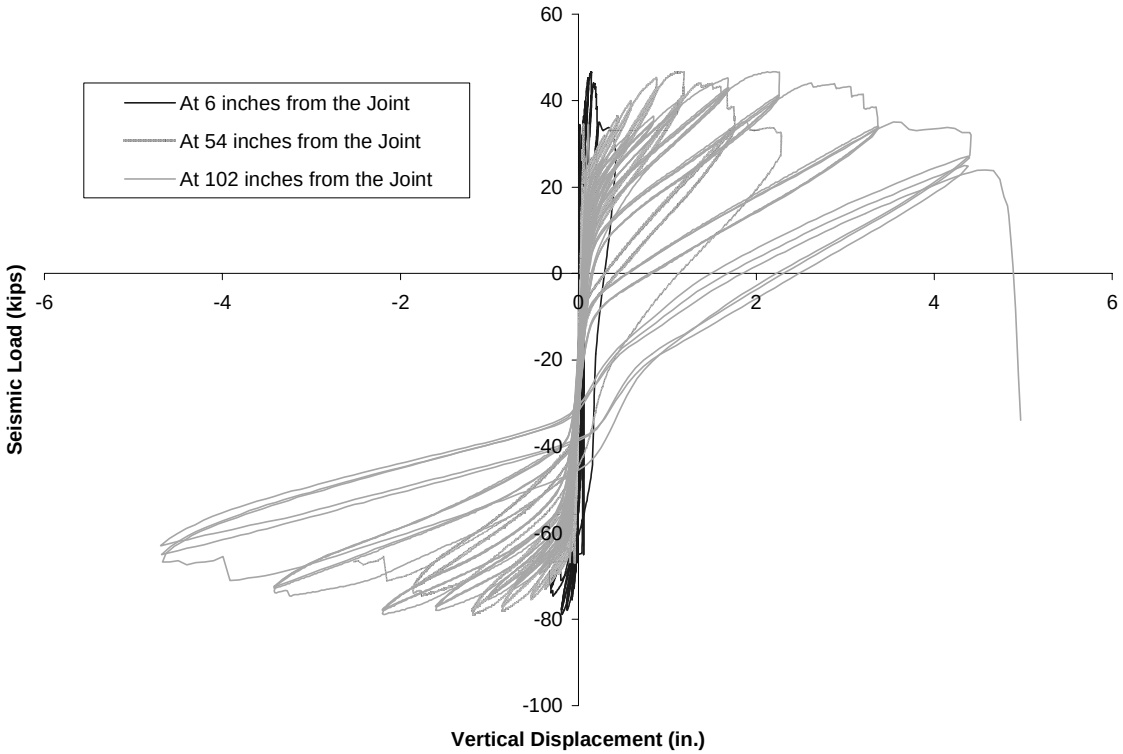


**Figure B-68 Load versus vertical displacement at different sections in Unit 100-EXT**

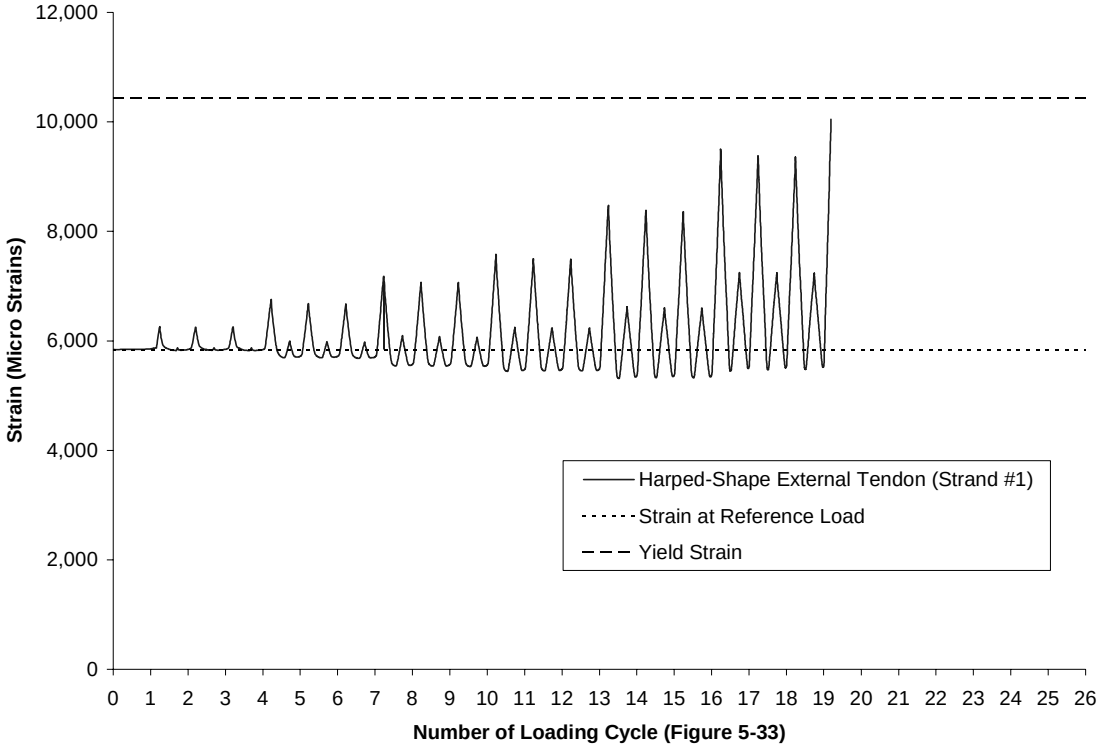


**Figure B-69 Strain in upper tendon of Unit 100-EXT (East Side Tendon)**

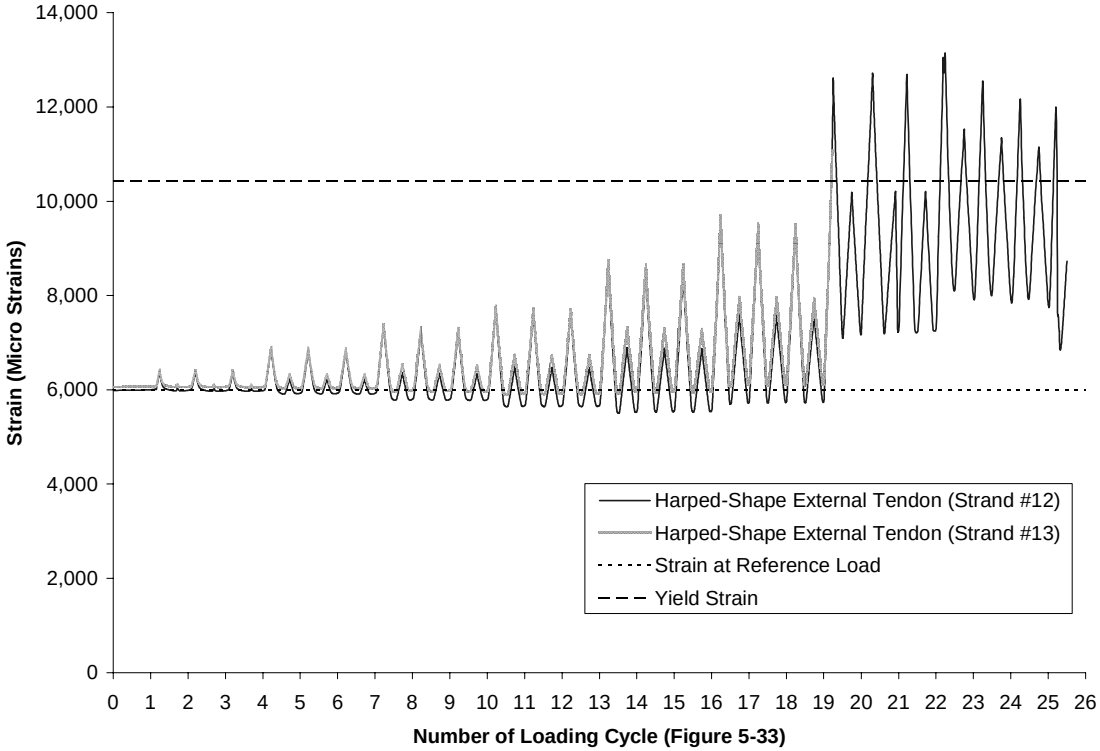


**Figure B-70 Strain in upper tendon of Unit 100-EXT (West Side tendon)**

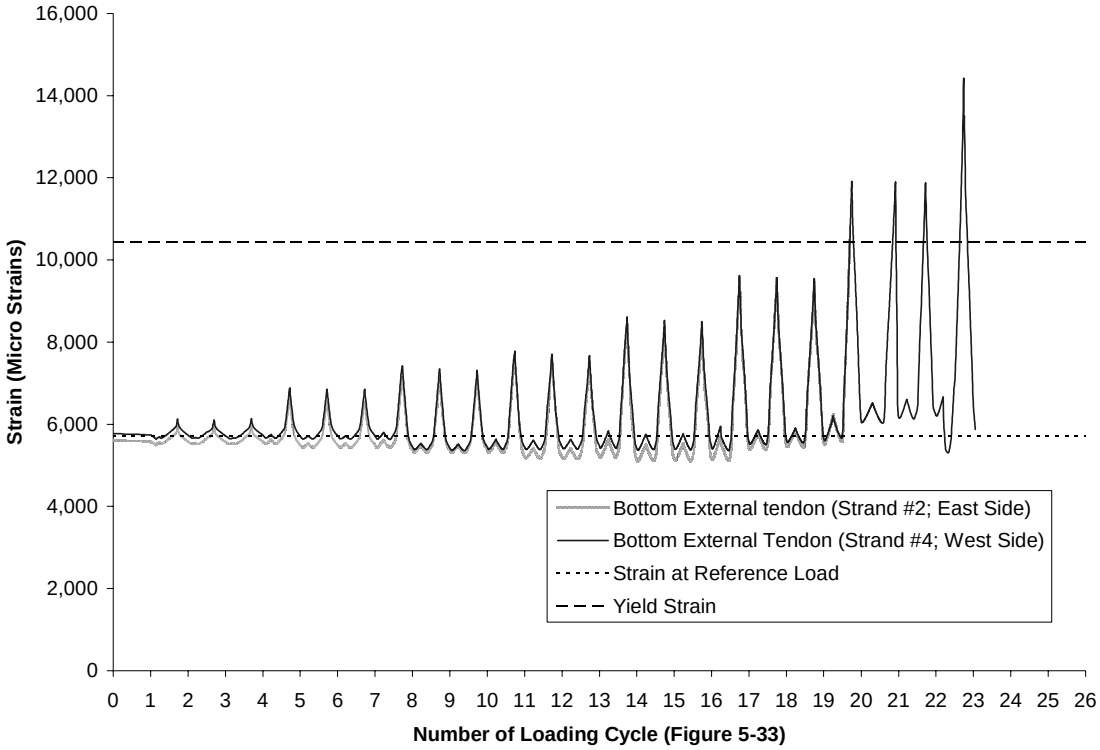


**Figure B-71 Strain in lower tendon of Unit 100-EXT**

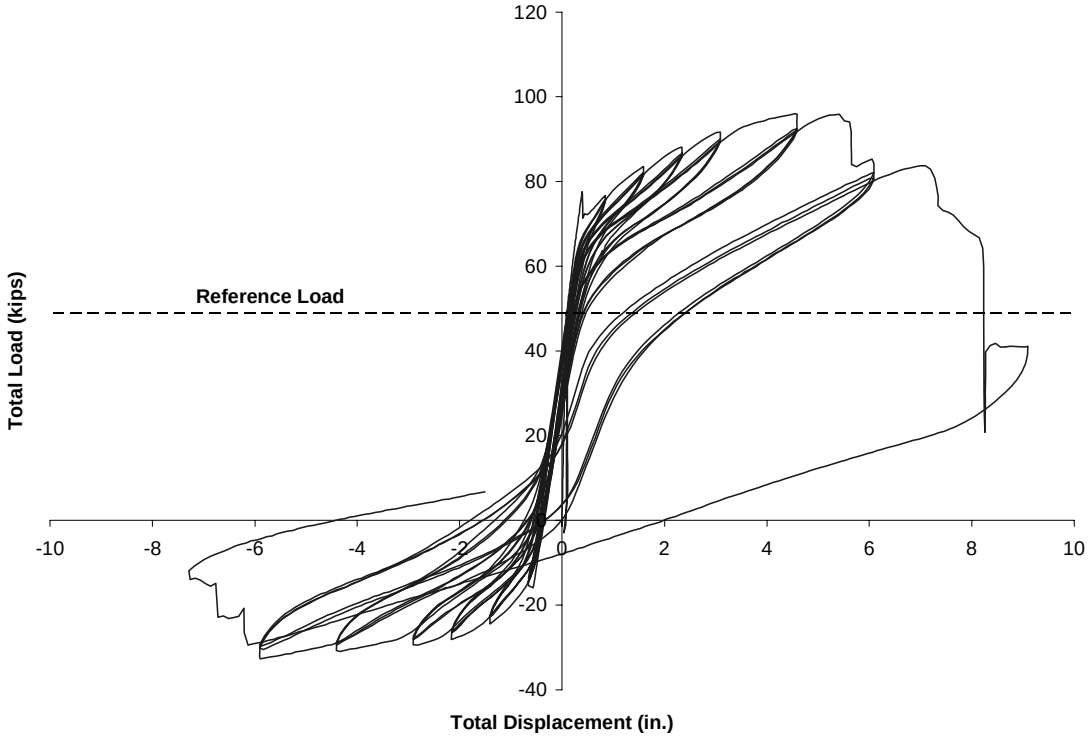


**Figure B-72 Total load vs. total displacement at cantilever tip (Unit 50-INT/50-EXT)**

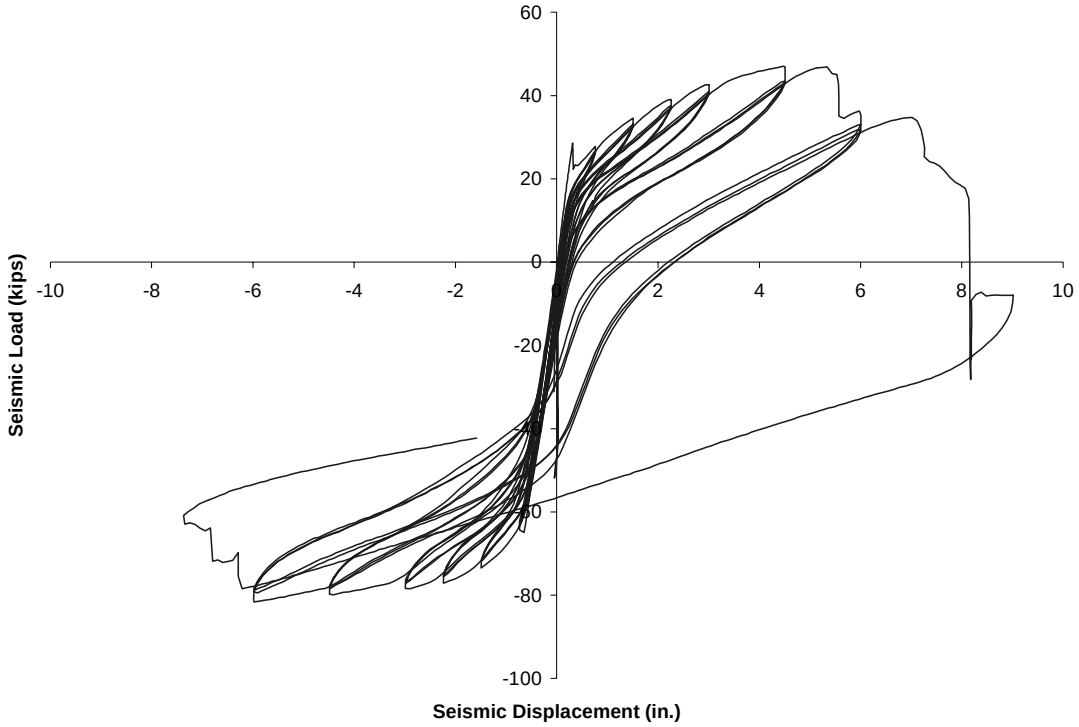


**Figure B-73 Seismic load vs. seismic displacement at cantilever tip (Unit 50-INT/50-EXT)**

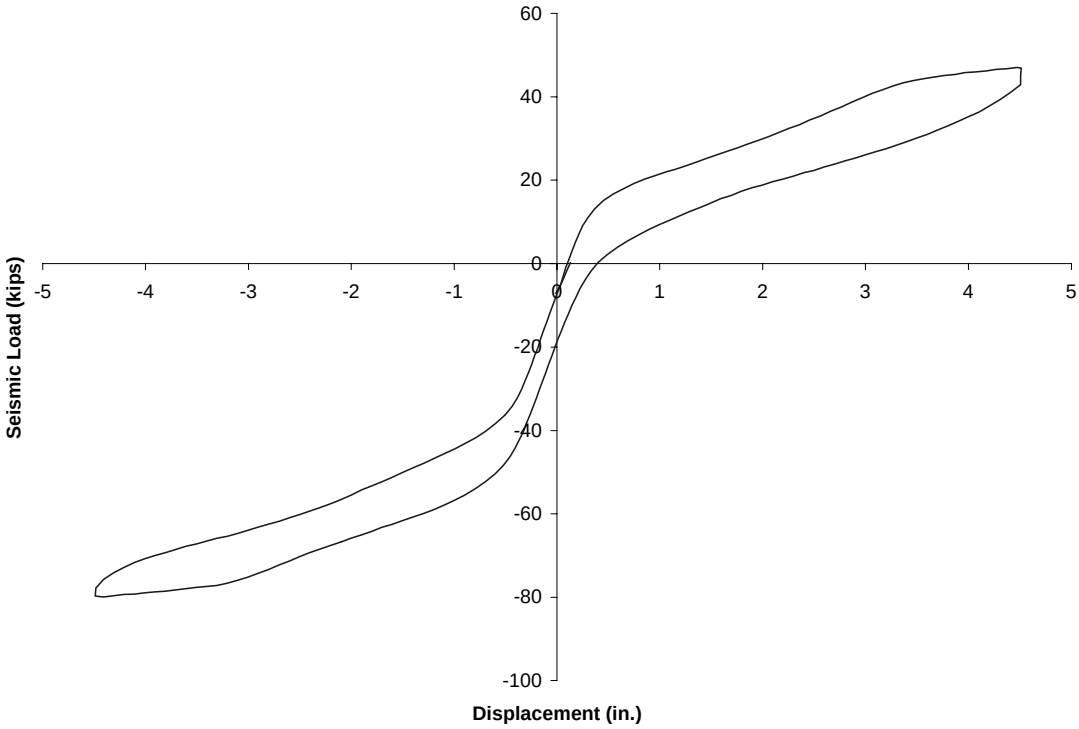


**Figure B-74 Seismic load-displacement for Unit 50-INT/50-EXT at 4.5 in. (114 mm)**

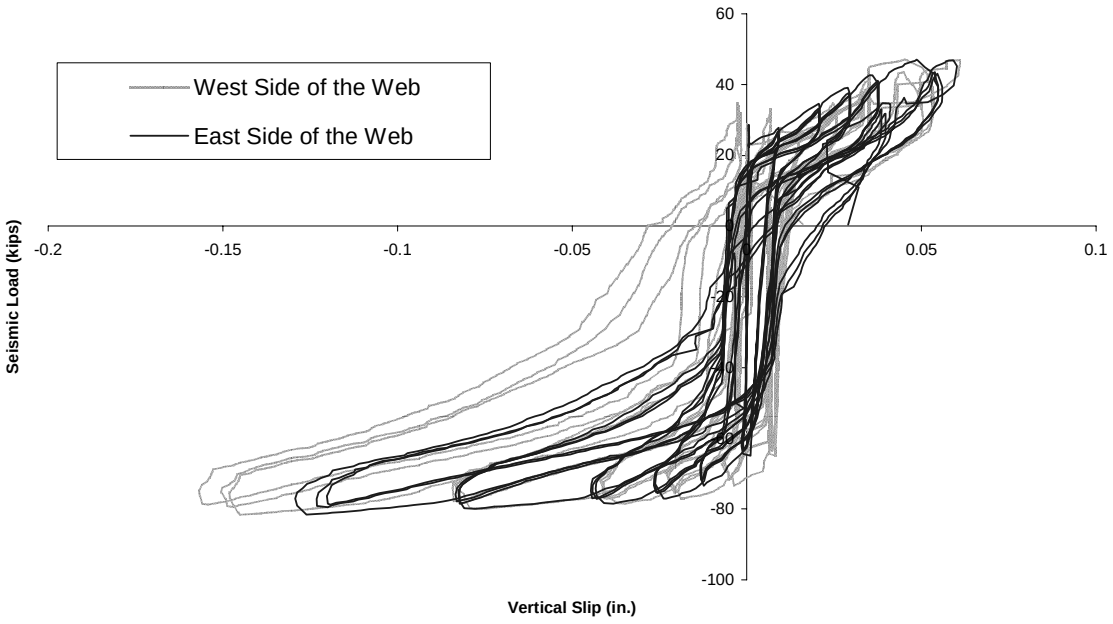


**Figure B-75 Load vs. vertical slip between Segments 1 and 2 (Unit 50-INT/50-EXT)**

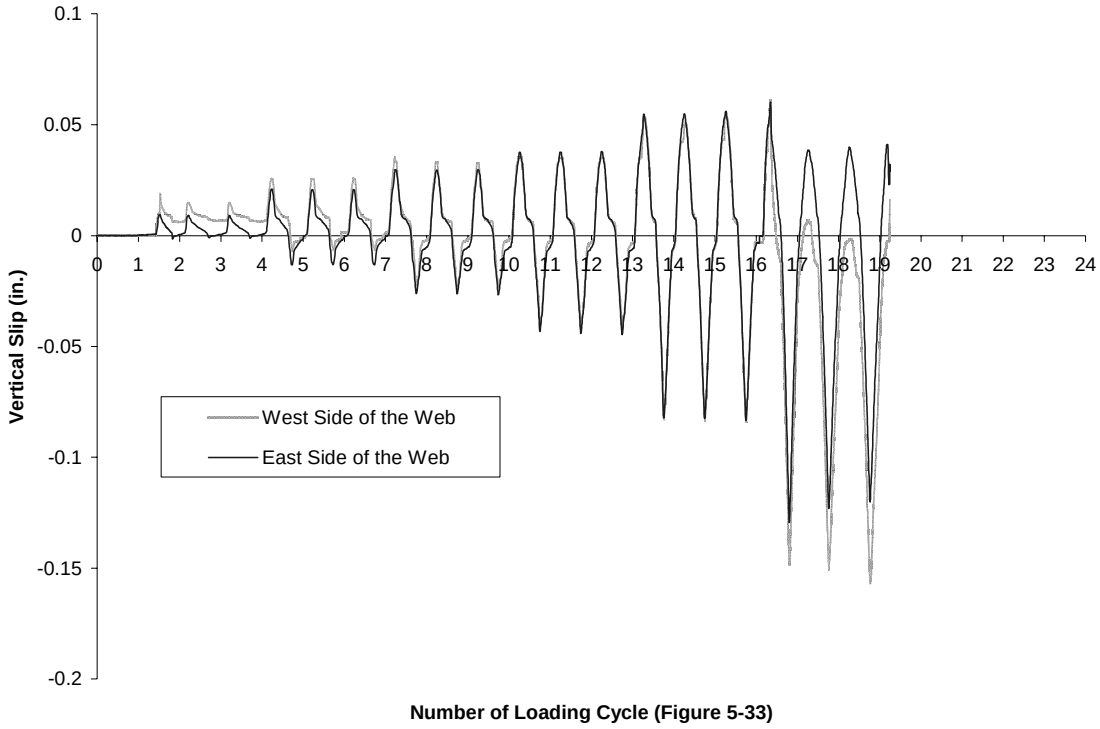


**Figure B-76 Vertical slip between Segments 1 and 2 (Unit 50-INT/50-EXT)**

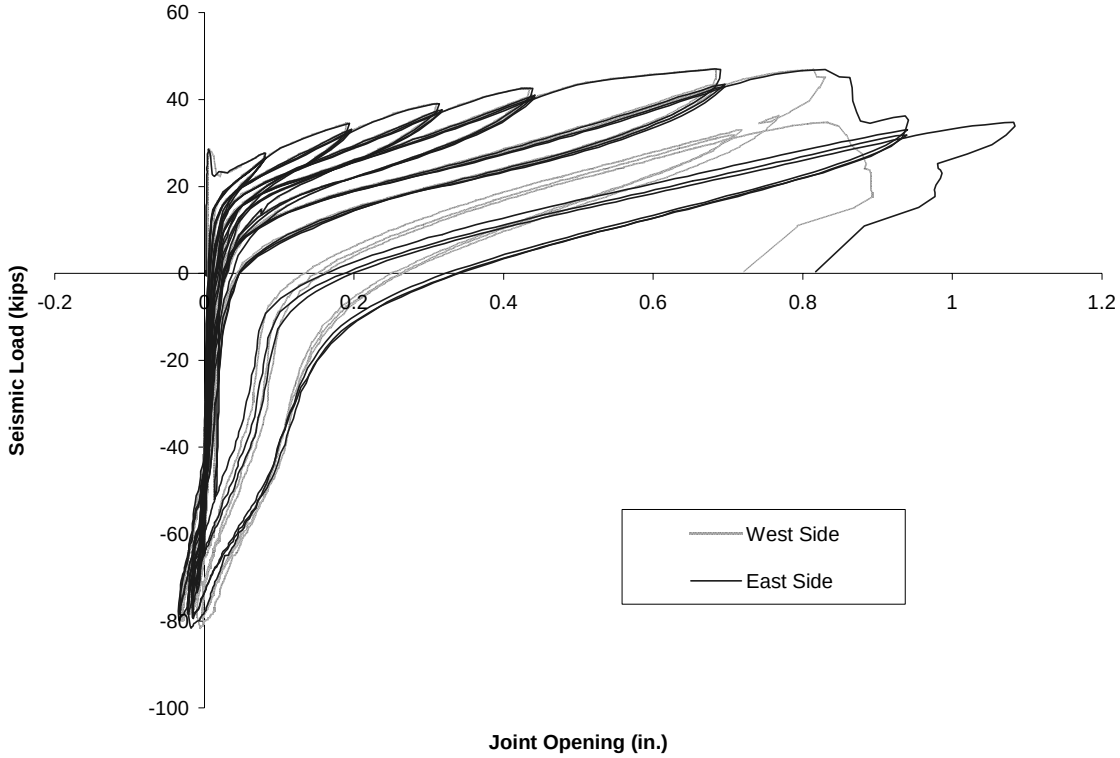


**Figure B-77 Load vs. opening of Joint $J_1$ at top surface (Unit 50-INT/50-EXT)**

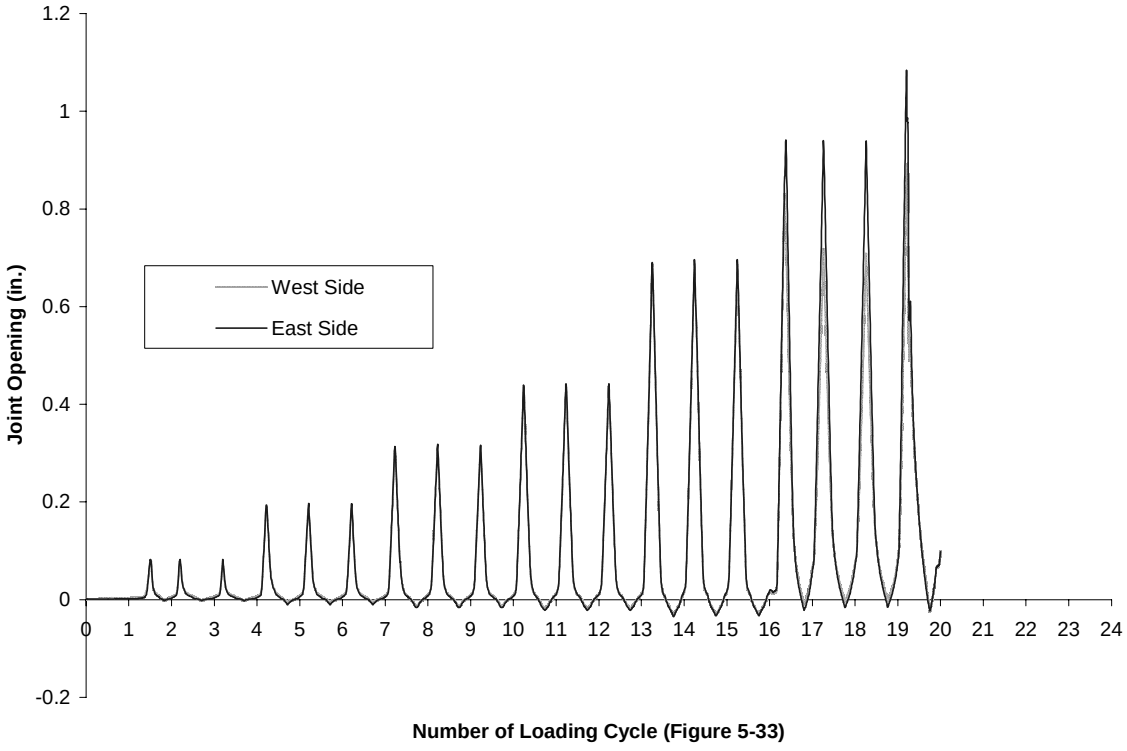


**Figure B-78 History of opening of Joint $J_1$ at top surface (Unit 50-INT/50-EXT)**

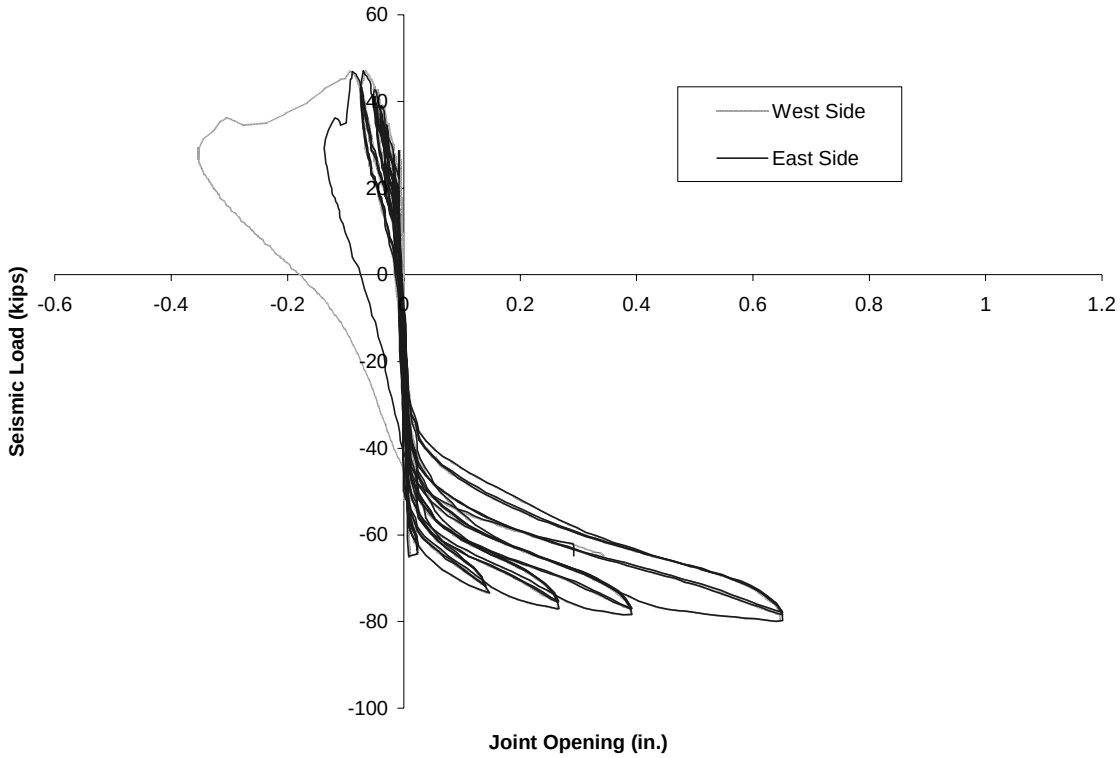


**Figure B-79 Load vs. opening of Joint $J_1$ at bottom surface (Unit 50-INT/50-EXT)**

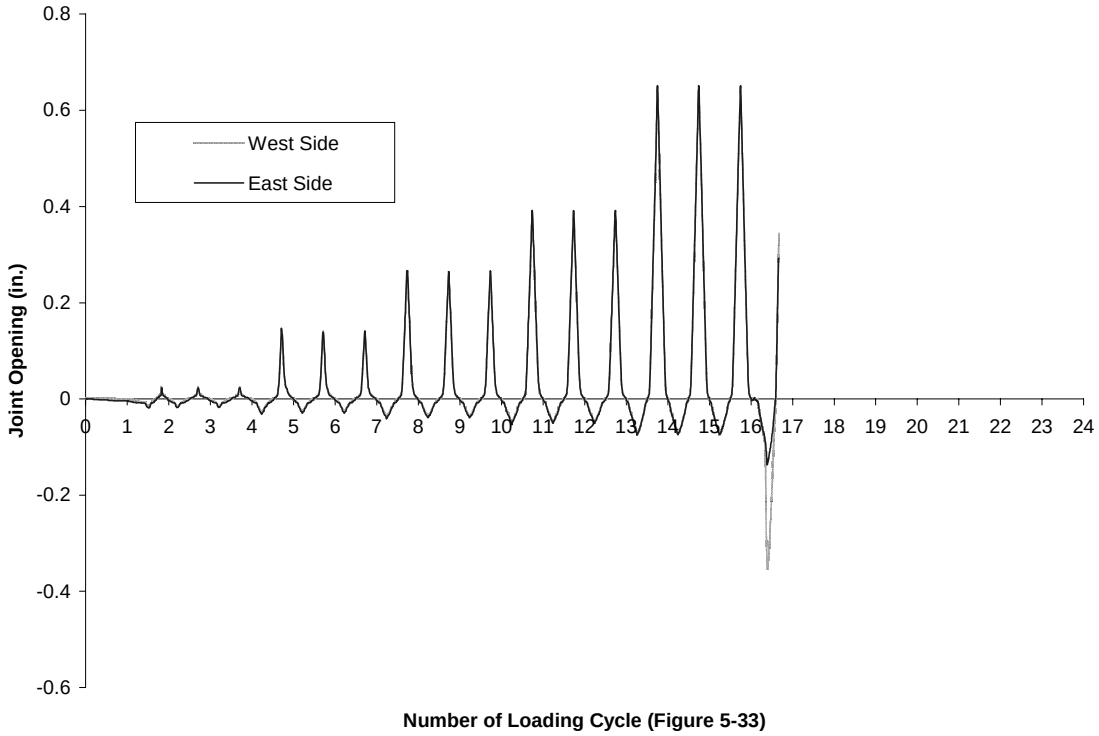


**Figure B-80 History of opening of Joint $J_1$ at bottom surface (Unit 50-INT/50-EXT)**

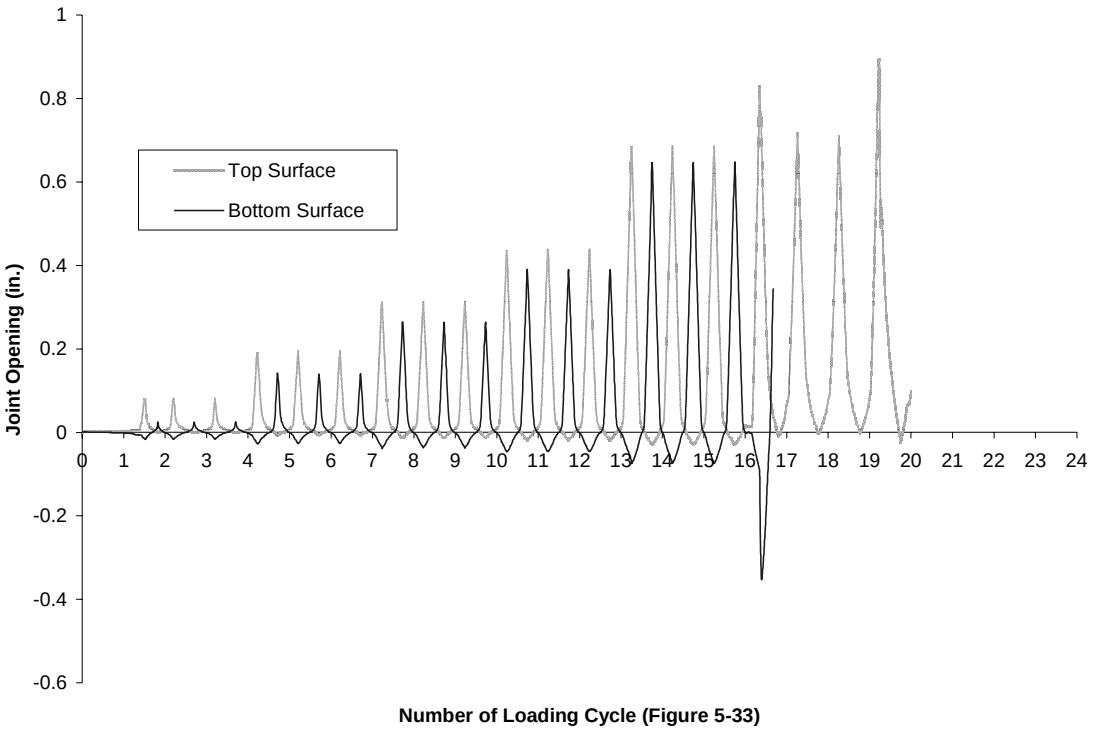


**Figure B-81 Load versus joint opening measured on the West Side of Unit 50-INT/50-EXT**

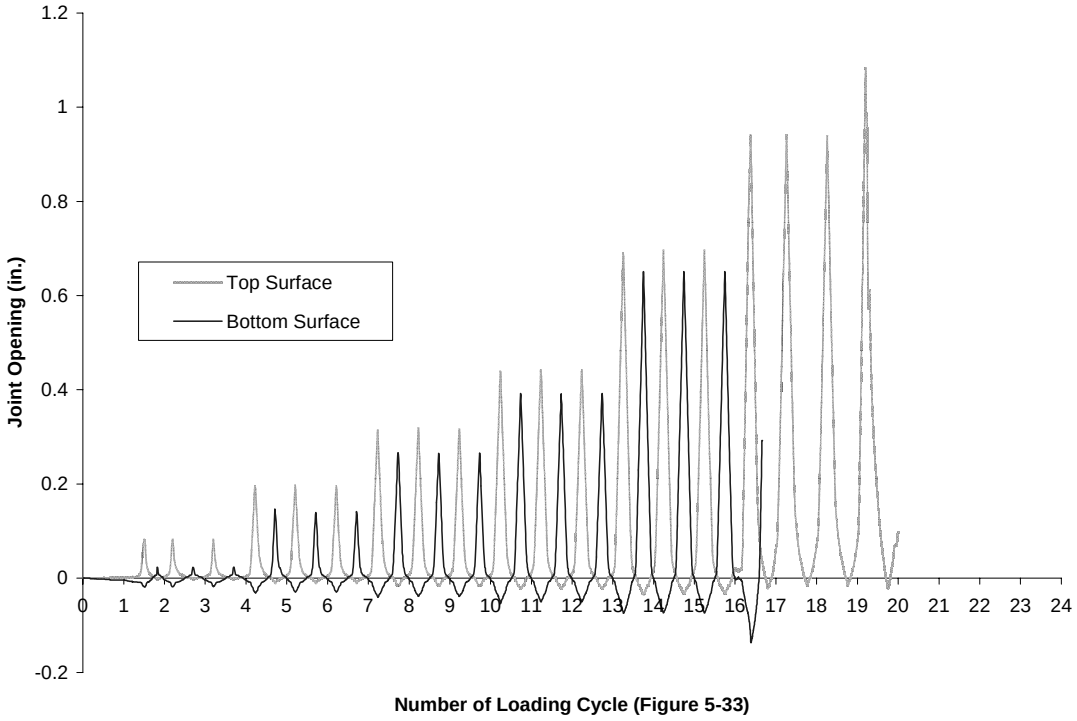


**Figure B-82 Load versus joint opening measured on the East Side of Unit 50-INT/50-EXT**

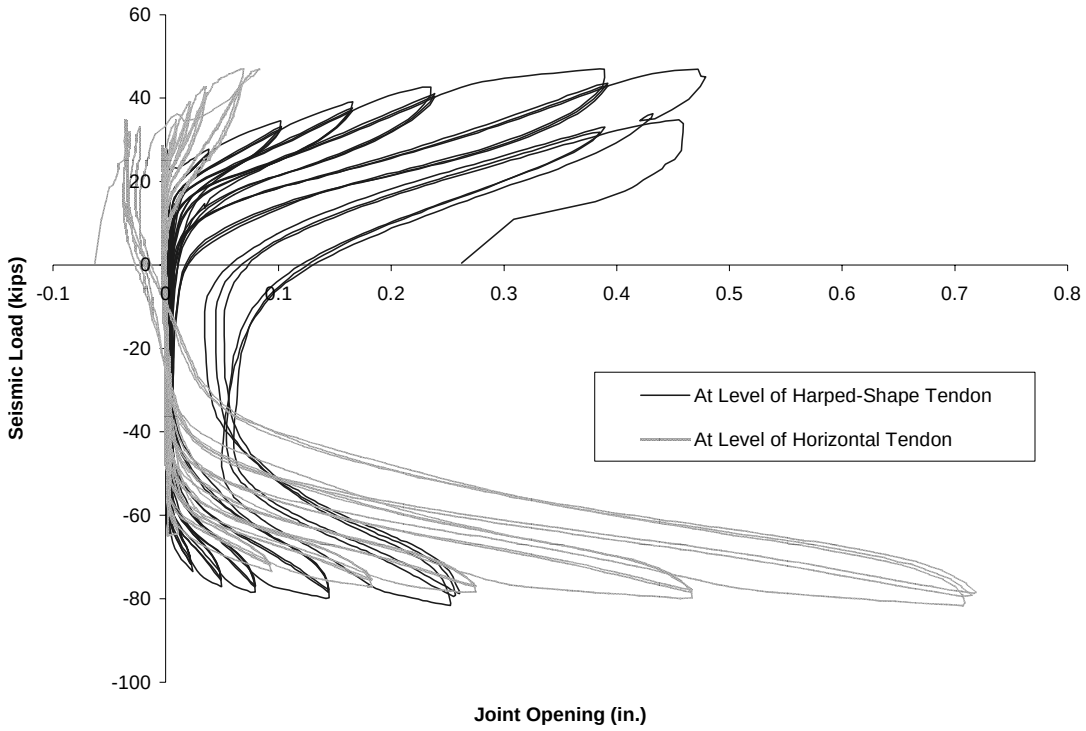


**Figure B-83 Load versus joint openings measured approximately at elevations of the prestressing tendons (Unit 50-INT/50-EXT)**

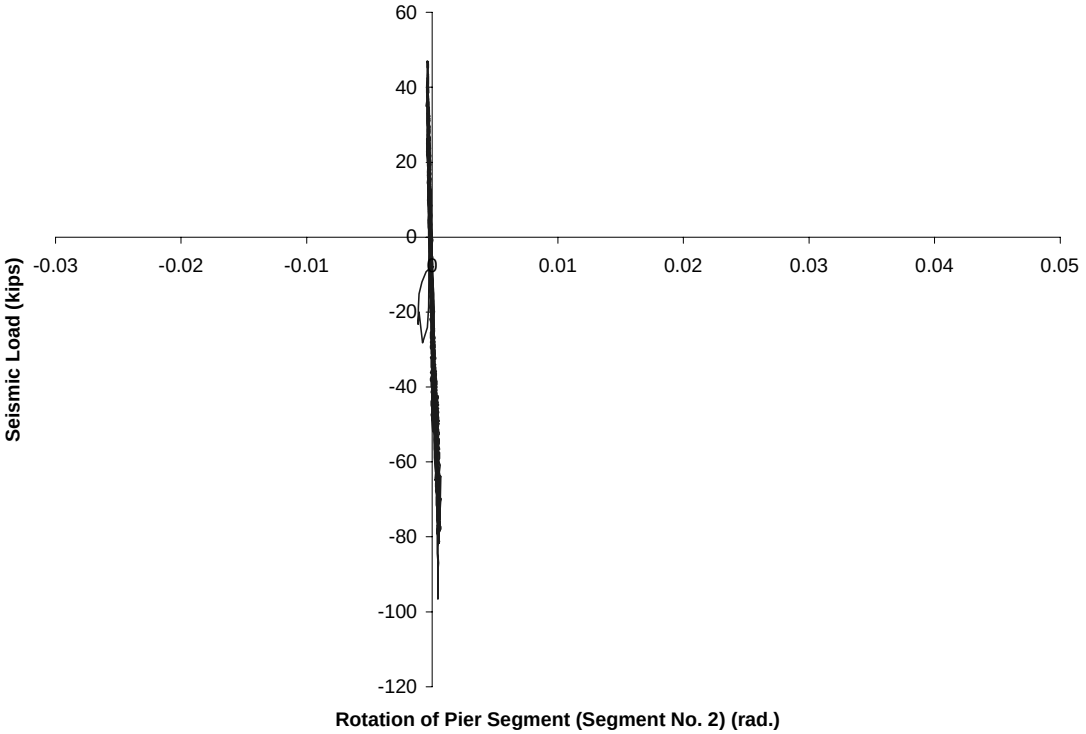


**Figure B-84 Load versus rotation of Segment No. 2 in Unit 50-INT/50-EXT**

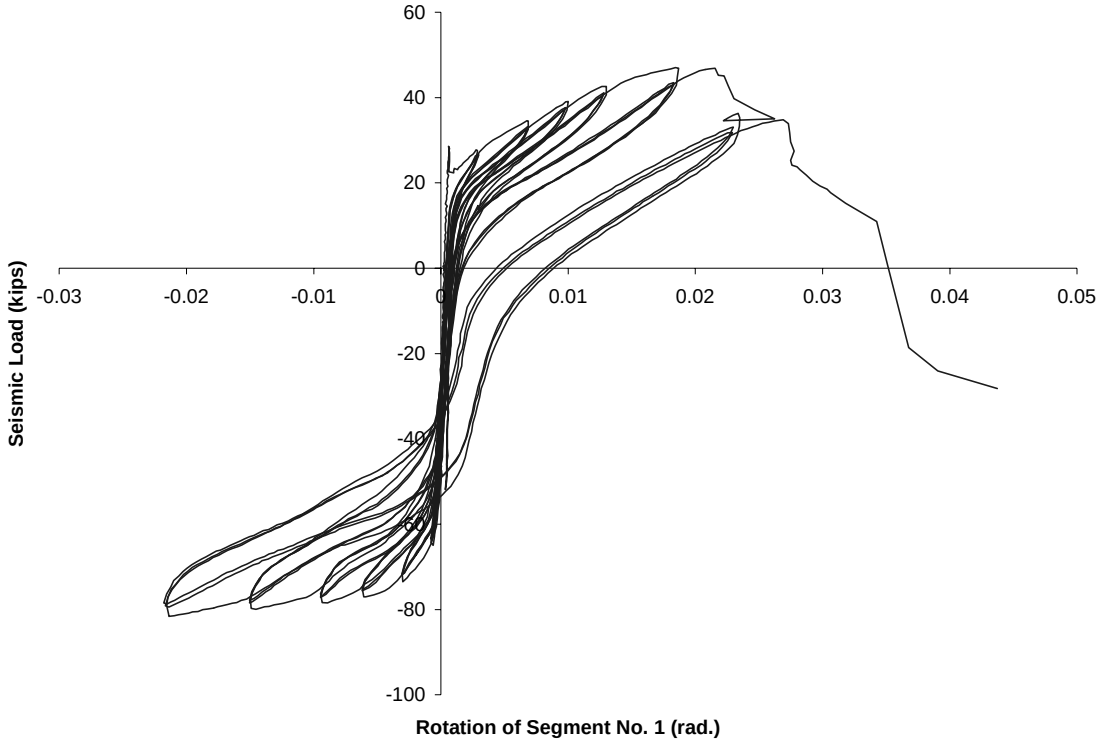


**Figure B-85 Load versus rotation of Segment No. 1 in Unit 50-INT/50-EXT**

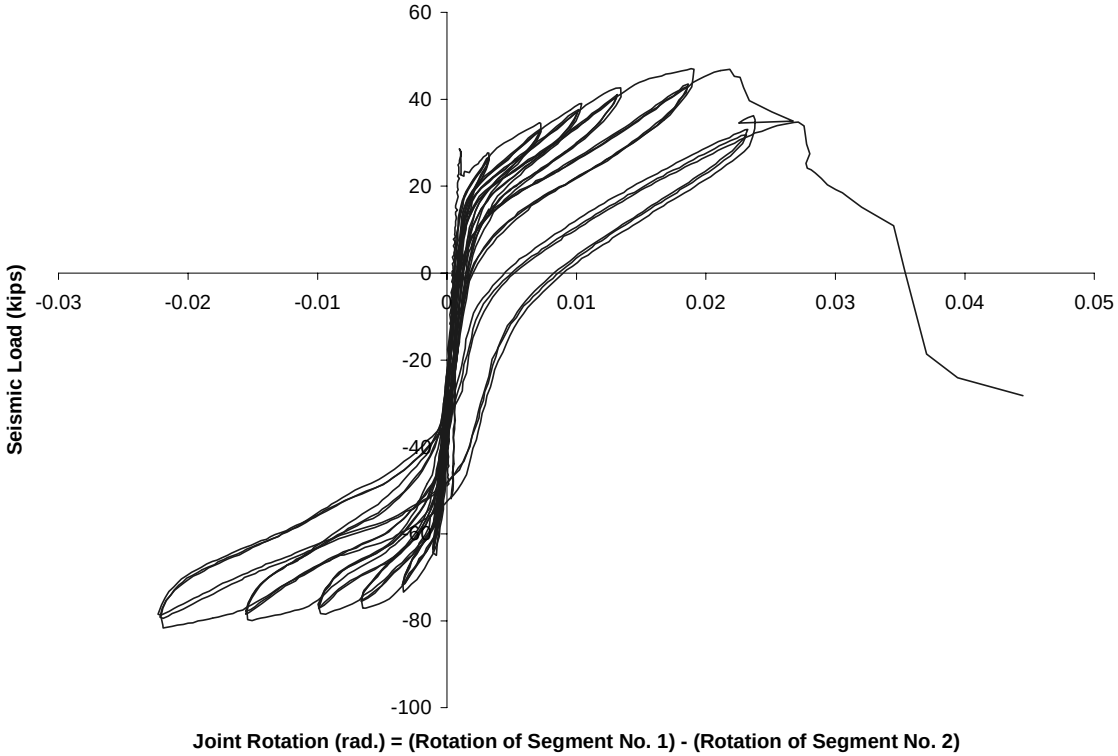


**Figure B-86 Load versus rotation of Joint $J_1$ in Unit 50-INT/50-EXT**

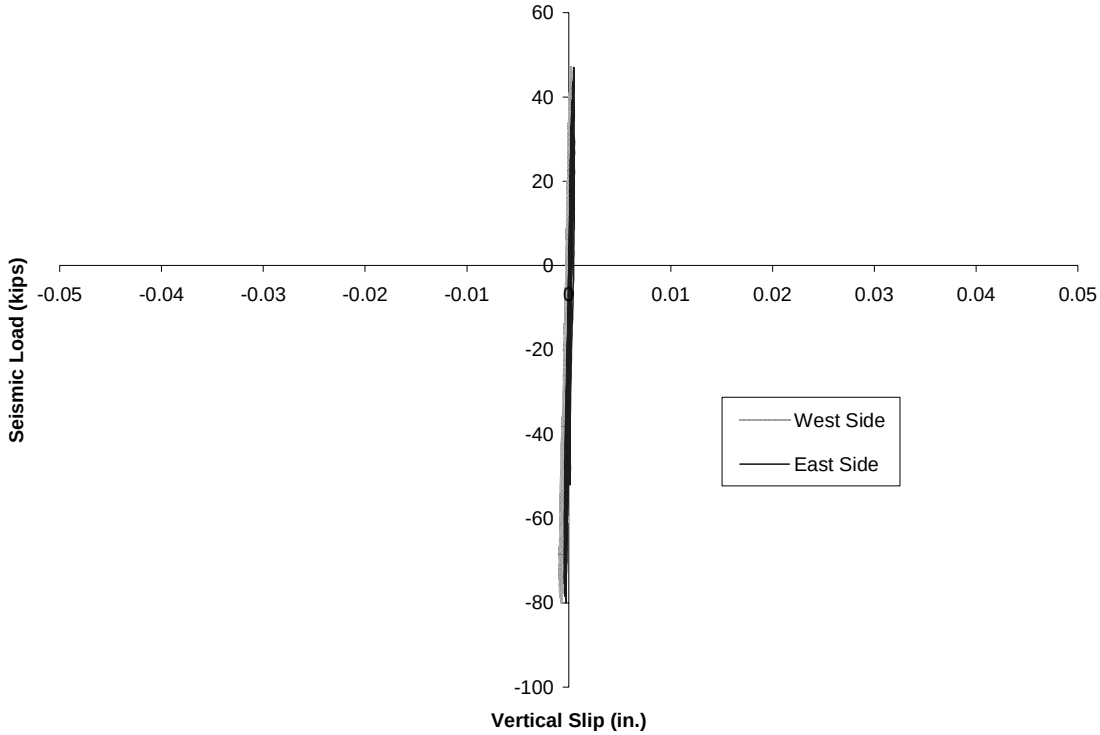


**Figure B-87 Vertical slip between Unit 50-INT/50-EXT and the steel loading beam**

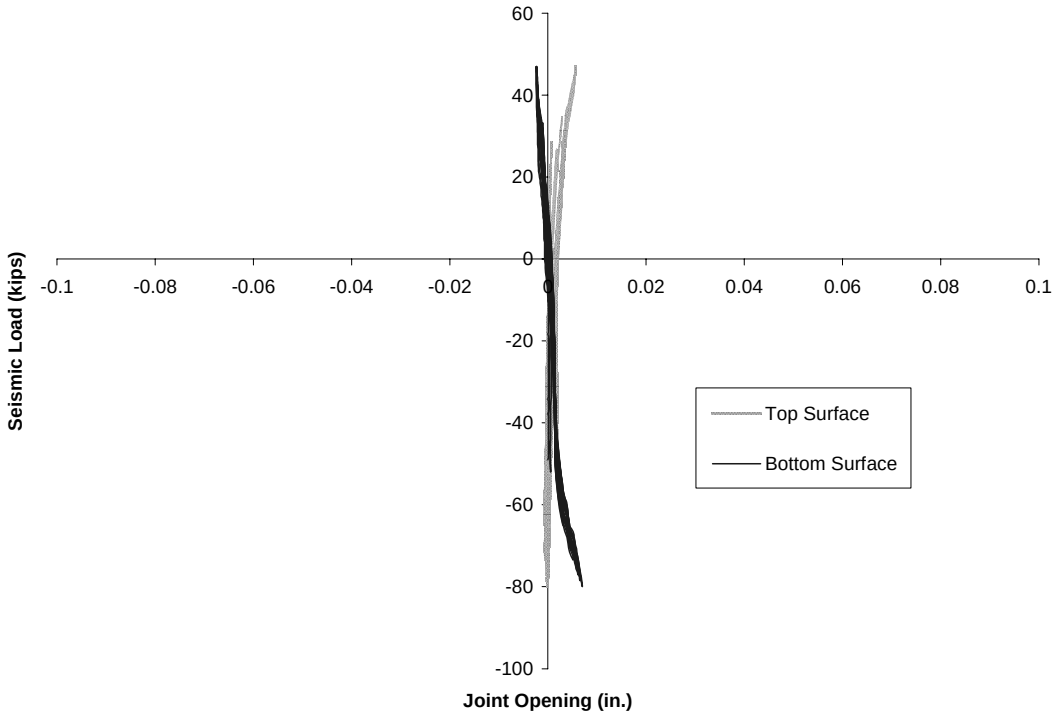


**Figure B-88 Joint opening between Unit 50-INT/50-EXT and the steel loading beam**

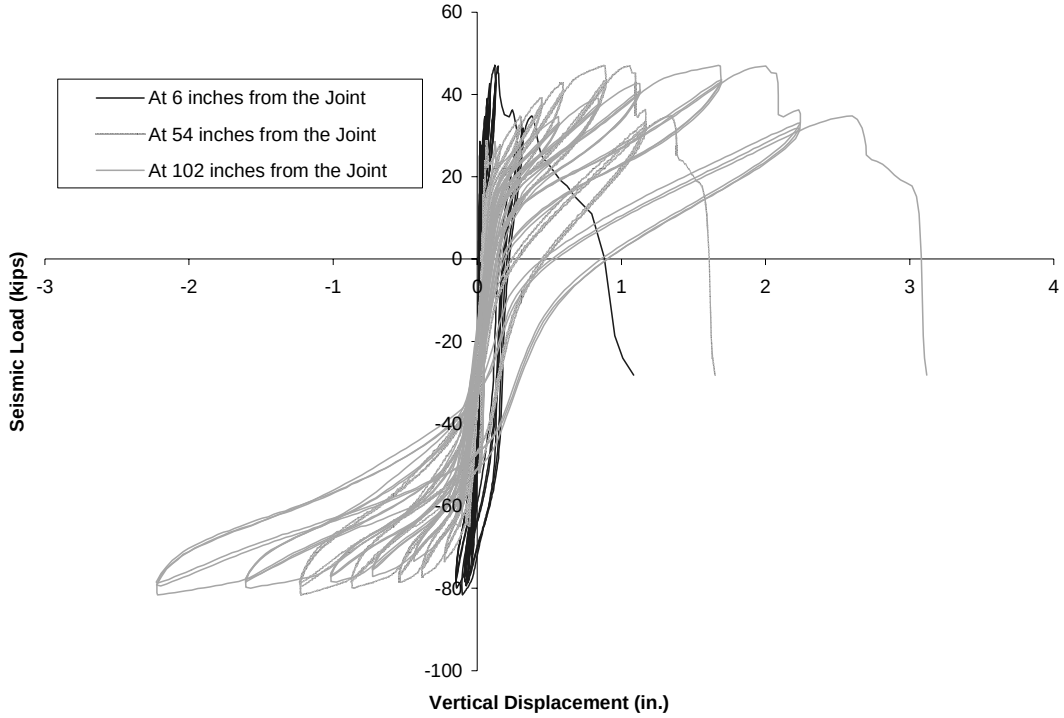


**Figure B-89 Load versus vertical displacement at different sections in Unit 50-INT/50-EXT**

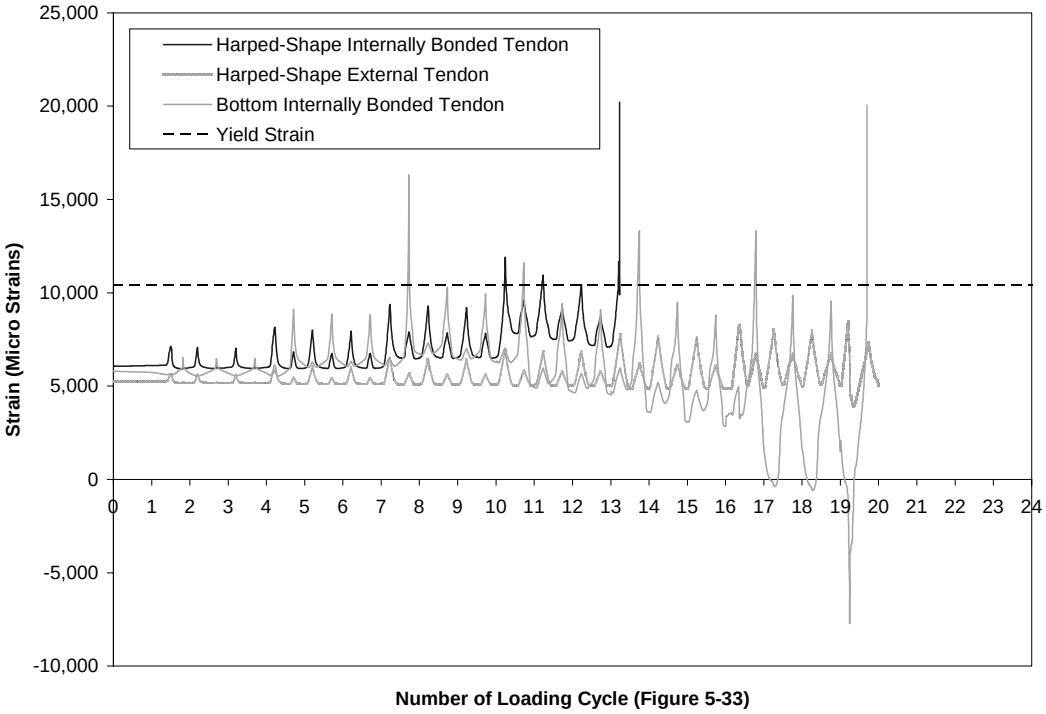


**Figure B-90 Strain in prestressing tendons of Unit 50-INT/50-EXT at location of Joint $J_1$ (Section B in Figure 5-29)**